General Disclaimer

One or more of the Following Statements may affect this Document

- This document has been reproduced from the best copy furnished by the organizational source. It is being released in the interest of making available as much information as possible.

- This document may contain data, which exceeds the sheet parameters. It was furnished in this condition by the organizational source and is the best copy available.

- This document may contain tone-on-tone or color graphs, charts and/or pictures, which have been reproduced in black and white.

- This document is paginated as submitted by the original source.

- Portions of this document are not fully legible due to the historical nature of some of the material. However, it is the best reproduction available from the original submission.

Produced by the NASA Center for Aerospace Information (CASI)

DAC-623305

CR 73281

FACILITY FORM 602

N69-14761
(ACCESSION NUMBER) (THRU)

328 1
(PAGES) (CODE)

CR 73281 03
(NASA CR OR TMX OR AD NUMBER) (CATEGORY)

MCDONNELL DOUGLAS ASTRONAUTICS COMPANY

MCDONNELL DOUGLAS CORPORATION

NOVEMBER 1968

PARAMETRIC STUDY OF SPACE POWER SYSTEMS
FINAL REPORT

NOVEMBER 1968

DAC-62305

Volume III-Power Subsystem Parametric Data

A.D. TONELLI
STUDY MANAGER
ADVANCE SECONDARY POWER SYSTEMS BRANCH

APPROVED BY

K.H. HOUGHTON, CHIEF
ADVANCE BIOTECHNOLOGY & POWER DEPARTMENT
RESEARCH AND DEVELOPMENT DIRECTORATE

STUDY PERSONNEL
R.S. COFFIN
J.V. COGGI
J.J. DEANE
S.D. DIAMOND
J.M. FRANK
R.H. RIEDEL
A.M. TAYLOR
H. WEINER

PREPARED FOR
NATIONAL AERONAUTICS AND SPACE ADMINISTRATION
MISSION ANALYSIS DIVISION – OART
MOFFETT FIELD, CALIFORNIA 94035
CONTRACT NAS2-4482

MCDONNELL DOUGLAS ASTRONAUTICS COMPANY
WESTERN DIVISION

MCDONNELL DOUGLAS CORPORATION

PRECEDING PAGE BLANK NOT FILMED.

ABSTRACT

This volume presents the parametric data that were used in performing the Parametric Study of Space Power Systems. The information contained in this volume includes parametric data on power conversion subsystems, energy sources, heat rejection subsystems, power conditioning subsystems, energy storage, power distribution subsystems, and integration of the power system with the space vehicle. The parametric data are the baseline or reference data that were used in calculating the characteristics such as mass, volume, area, cost, and reliability of the various power systems, subsystems, and major components.

PRECEDING PAGE BLANK NOT FILMED.

ACKNOWLEDGMENTS

The following organizations were contacted in connection with obtaining information for this report.

Batteries

The Electric Storage Battery Company
Exide Missile and Electronics Division
Raleigh, North Carolina

Electrochimica Corporation
Menlo Park, California

Whittaker Corporation
Power Sources Division
Denver, Colorado

Brayton Cycle

Aerojet-General Corporation
Nucleonics Division
San Ramon, California

AiResearch Manufacturing Company
Division of The Garrett Corporation
Los Angeles, California

Fuel Cells

Electro-Optical Systems, Inc.
Pasadena, California

General Electric Company
Defense Programs Division
Los Angeles, California

Isotope Fuel Block

Aerojet-General Corporation
Nucleonics Division
San Ramon, California

MHD

Avco-Everett Research Laboratories
Everett, Massachusetts

General Electric Company
Philadelphia, Pennsylvania

The Jet Propulsion Laboratory
California Institute of Technology
Pasadena, California

Power Conditioning

NASA-OART
Space Power and Electric Power Division
Washington, D. C.

Rankine Cycle

Aerojet-General Corporation
Von Karman Center
Azusa, California

General Electric Company
Nuclear Materials and Propulsion Operation
Cincinnati, Ohio

NASA-OART
Space Power and Electric Power Division
Washington, D. C.

Sundstrand Aviation Company
Rockford, Illinois

Reactors (Nuclear)

Aerojet-General Corporation
El Monte, California

Aerojet-General Corporation
Nucleonics Division
San Ramon, California

General Electric Company
Space Science Laboratory
Philadelphia, Pennsylvania

Solar Cells

Heliotek Division
Textron Electronics Incorporated
Sylmar, California

Hoffman Electronics Corporation
Solar Products Department
El Monte, California

Hughes Aircraft Company
Los Angeles, California

Ion Physics Corporation
Burlington, Massachusetts

The Jet Propulsion Laboratory
California Institute of Technology
Pasadena, California

Texas Instruments Incorporated
Dallas, Texas

TRW Systems
Power Systems Division
Redondo Beach, California

Solar Concentrators

Goodyear Aerospace Corporation
Akron, Ohio

NASA Langley Research Center
Langley Station
Hampton, Virginia

Thermoelectric

Hittman Associates, Inc.
Baltimore, Maryland

Thermionics

General Electric Company
Nuclear Thermionic Power Operation
Atomic Products Division
Pleasanton, California

General Electric Company
Research Laboratory
Schenectady, New York

NASA-Lewis Research Center
Thermionic System Section
Cleveland, Ohio

Radio Corporation of America
Electronic Components and Devices
Lancaster, Pennsylvania

CONTENTS

		LIST OF FIGURES	xi
		LIST OF TABLES	xxi
Section 1		INTRODUCTION	1
Section 2		SCALING LAWS AND DATA CORRELATION TECHNIQUES	5
	2.1	Scaling Laws	5
	2.2	Statistical Growth Projection Techniques	6
	2.3	Exponential Growth Projection Technique	8
	2.4	Hyperbolic Correlation Factor	8
	2.5	Least-Squares Polynomial Fit	10
Section 3		SECONDARY POWER SUBSYSTEM PARAMETRIC DATA	15
	3.1	Power Conversion Subsystems	16
	3.2	Energy Sources	196
	3.3	Heat Rejection Subsystems	247
	3.4	Power Conditioning Subsystems	261
	3.5	Power Distribution Subsystems	277
	3.6	Power System Integration with the Space Vehicle	281
	3.7	Supporting Data	286
	3.8	References for Section 3	295

PRECEDING PAGE BLANK NOT FILMED.

FIGURES

1-1	Major Power Subsystems	2
2-1	Basis for Projecting State of the Art Curves	7
2-2	Example Component Performance	9
2-3	Example Component Size Correlation Factor	9
3-1	Solar Cell Array Power Conversion Subsystem	19
3-2	Solar Cell Types	21
3-3	Solar Cell Array Power System Schematics	22
3-4	Solar Cosmic Ray Events and Sunspot Numbers	28
3-5	Terrestrial Geomagnetic Field Cutoff Effects on Solar Flare Protons	29
3-6	Terrestrial Trapped Electrons (Ee>0.5 MEV)	30
3-7	Terrestrial Trapped Protons (E_p > 3 MEV)	31
3-8	The Effect of Protons on Solar Cell Power Output	32
3-9	The Effect of Electrons on Solar Cell Power Output	33
3-10	Simulated Meteoroid Damage to Solar Cells	34
3-11	Ultra-Violet Exposure Damage to Silicon Solar Cells	35
3-12	Thermal Cycle Induced Power Loss in Silicon Solar Cells	36
3-13	Thermal Cycle Induced Power Loss in Thin-Film CdS Solar Cells	37
3-14	Projection Thermal Cycle Threshold Damage for Solar Cells	38
3-15	Solar Cell Panel Tilt Angle Tolerance Levels	39
3-16	Projection-Array Absorptivity (Cell-Side) ~Silicon Solar Cells	40
3-17	Array Shape Factors for Planetary Radiation	41
3-18	Projection--Silicon Solar Cell Failure Rates	42

3-19	Thin Film Solar Cell Failure Rates	43
3-20	The Effect of Cell Temperature on Solar Cell Efficiency	44
3-21	Projection--Silicon Solar Cell Conversion Efficiency	45
3-22	Projection--Thin-Film CdS Solar Cell Conversion Efficiency	46
3-23	Projection--Silicon Solar Cell Packing Factors	47
3-24	Projection--Thin Film CdS Solar Cell Packing Factors	48
3-25	Projection--Silicon Solar Cell Module Packing Factors	49
3-26	Projection--Assembly Loss Factor, Silicon Solar Cell Arrays	50
3-27	Projection--Assembly Loss Factor, Thin-Film CdS Solar Cell Arrays	51
3-28	Projection--Panel Specific Weight--Thin-Film Cadmium Sulfide and Silicon Solar Cells	52
3-29	Projection--Solar Cell Array Thicknesses	53
3-30	Projection--Silicon Solar Cell Panel Costs	54
3-31	Projection--Thin Film CdS Solar Cell Panel Costs	55
3-32	Structure and Deployment Mechanisms	56
3-33	Solar Cell Arrays--Panel Deflection Coefficient Projection	57
3-34	Projection--Solar Cell Array Deployment Mechanism Failure Probability	58
3-35	Solar Cell Array--Orientation System Specific Mass	59
3-36	Projection--Solar Cell Array Orientation Drive and Controls Failure Rate	60
3-37	Thermoelectric Modules	63
3-38	SiGe Converter Efficiency, %	64
3-39	Pb-Te Thermoelectric Converter Efficiency	65
3-40	Segmented Pb-Te to SiGe Converter Efficiency	66
3-41	Projected Improvement in Thermoelectric Converter Efficiency	67
3-42	PbTe Thermoelectric Converter Specific Weight (Data based on Reference 1)	68
3-43	SiGe Thermoelectric Converter Specific Mass	69
3-44	PbTe-SiGe Converter Specific Mass	70

3-45	Thermoelectric Converter Degradation	71
3-46	Thermoelectric Converter Production Cost Projection	72
3-47	Thermionic Conversion Subsystem Array	74
3-48	Projection of Thermionic Converter Efficiency	77
3-49	Projection of Thermionic Converter Power Density	78
3-50	Projection of Thermionic Converter Voltage	79
3-51	Projection of Thermionic Converter Cost	80
3-52a	Projection of Thermionic Converter Mass	81
3-52b	Variation of Thermionic Converter Efficiency Versus Collector Temperature	82
3-52c	Thermionic Converter Life Projection	83
3-53	Typical H_2-0_2 Fuel Cell Power Conversion Subsystem	85
3-54	Typical Fuel Cell Element Configurations	86
3-55	Projection of Fuel Cell Terminal Voltage	88
3-56	Projection of Fuel Cell Terminal Voltage Degradation	89
3-57	Projection of Fuel Cell Current Density	90
3-58	Projection of Fuel Cell Subsystem Parasitic Losses	92
3-59	Projection of Fuel Cell Specific Mass	93
3-60	Projection of Fuel Cell Subsystem Density	94
3-61	Projection of Fuel Cell Element Mean Time Before Failure	95
3-62	Projection of Fuel Cell Module Production Costs	96
3-63	Storable Reactant Fuel Cell Reformer/Decomposer Characteristic	97
3-64	Storable Fuel Cell Reformer/Decomposer Mean Time Before Failure	98
3-65	Battery Cell Assembly	102
3-66	Battery Module and Battery	102
3-67	Energy Storage Subsystem	103
3-68	η_d ~ Battery Depth of Discharge ~ Percent	107
3-69	Projection--Battery Cycle Life	108

3-70	Charge Acceptance of Secondary Batteries	109
3-71	Charge Rates of Secondary Batteries	110
3-72	Projection Minimum Battery Charge Time	111
3-73	Projection--Battery Cell Failure Rates	112
3-74	Energy Density of Secondary Batteries	113
3-75	Volumetric Energy Density of Secondary Batteries	114
3-76	Energy Density Correction Factor for Primary AGZN Batteries Automatically-Activated	115
3-77	Projection--Battery Specific Costs	116
3-78	Battery Charge Regulator Efficiency	117
3-79	Battery Charge Regulator Efficiency	118
3-80	Battery Charge Regulator Operational Characteristics (Projected)	119
3-81	Power Level Correction Factor for Battery Charge Regulator Specific Mass	120
3-82	Brayton Cycle Power Conversion Module	122
3-83	Effect of Temperature Ratio on Turbine and Compressor Efficiency	125
3-84	Brayton Cycle Subsystem Compression Ratios	126
3-85	Brayton Cycle Optimum Turbine Exit Pressure (N/CM^2)	127
3-86	Projection of Brayton Cycle Turbine Inlet Temperature	128
3-87	Projection of CRU Lifetime	130
3-88	Projection of Component Specific Masses for Brayton Cycle Power Conversion Unit	131
3-89	Projection of Production Costs for Brayton Cycle Power Conversion Unit Components	132
3-90	Projection of MTBF For Brayton-Cycle Power Conversion Unit Components	133
3-91	Projection of Density for Brayton-Cycle Power Conversion Unit	134
3-92	Typical Mercury or Alkali Metal Rankine Cycle Module	136
3-93	Projection--Mercury Rankine Turboalternator (CRU) - Specific Mass	140
3-94	Power Level Correction Factor For Mercury Rankine Turboalternator Specific Mass	141

3-95	Projection--Mercury Rankine Boiler Specific Mass	142
3-96	Power Level Correction Factor for Mercury Rankine Boiler Specific Mass	143
3-97	Projection Mercury Rankine Condenser Specific Mass	144
3-98	Projection Mercury Rankine Accessories Specific Mass	145
3-99	Power Level Correction Factor for Mercury Rankine Accessories Specific Mass	146
3-100	Specific Cost of Mercury Rankine Cycle Equipment	147
3-101	Projection of Mercury Rankine Component Failure Rates	148
3-102	Projection of Mercury Rankine Power Conversion Module Wearout Life	149
3-103a	Projection--Mercury Rankine Turbine Efficiency	150
3-103b	Power Level Correction Factor for Mercury Rankine Turbine Efficiency	151
3-104	Projection of Maximum Turbine Inlet Temperature - Mercury Rankine	152
3-105	Mercury Rankine Turbine Inlet Enthalpy	153
3-106	Projection of Alkali Metal Rankine Cycle Turboalternator Specific Mass	154
3-107	Alkali Metal Rankine Cycle Turboalternator Factor for Specific Mass	155
3-108	Projection of Alkali Metal Rankine Boiler Specific Mass	156
3-109	Alkali Metal Rankine Boiler Specific Mass Factor	157
3-110	Projection of Alkali Metal Condenser Specific Mass	158
3-111	Alkali Metal Rankine Condenser Specific Mass Correction Factor	159
3-112	Projection Alkali Metal Rankine Accessories Specific Mass	160
3-113	Alkali Metal Rankine Accessories Specific Mass Factor	161
3-114	Projection of Alkali Metal Rankine Component Failure Rate	162

3-115	Specific Cost of Alkali Metal Rankine Cycle Accessories	163
3-116	Projection of Alkali Metal Rankine Power Conversion on Module Wearout Life	164
3-117	Projection of Alkali Metal Rankine Cycle Maximum Turbine Inlet Temperature	165
3-118	Maximum Alkali Metal Turbine Inlet Temperature Factor Versus Power Level	166
3-119	Specific Cost of Alkali Metal Rankine Cycle Components	167
3-120	Deleted	168
3-121	Typical Organic Rankine Cycle Module	169
3-122	Organic Rankine Cycle Boiler Mass	172
3-123	Organic Cycle Turbo-Alternator Mass	173
3-124	Organic Cycle Condenser Mass	174
3-125	Organic Cycle Regenerator Mass	175
3-126	Organic Cycle Accessory Mass	176
3-127	Mass Correction Factor For Organic Rankine Cycle Components	177
3-128	Failure Rates of Accessories (Organic Rankine Cycle)	178
3-129	Failure Rates of Organic Rankine Cycle Components	179
3-130	Projection Boiler and Condenser Failure Rates - (Organic Rankine)	180
3-131	Specific Cost of Component - Organic Rankine Cycle	181
3-132a	Organic Cycle Turbine Efficiency	182
3-132b	Correction Factor For Turbine Efficiency (Organic Rankine Cycle)	183
3-133	Projection of Organic Rankine Cycle Power Conversion Module Wearout Life	184
3-134	Projection Turbine Inlet Temperature Trend (Organic Rankine Cycle)	185
3-135	Chemical Dynamic Subsystem Module Schematic	187
3-136	Projection, Chemical Dynamic PCU Module Specific Mass	189
3-137	Production Cost of Chemical Dynamic Module	190
3-138	Projection of Chemical Dynamic Power Conversion Module Failure Rate	191

3-139	Projection of Chemical Dynamic Power Conversion Module Wearout Life	192
3-140	Projection of Chemical Dynamic Specific Reactant Consumption	193
3-141	Chemical Dynamic Power Conversion Specific Mass Factor	194
3-142	Deleted	195
3-143	U-Z_rH_x (SNAP-8 Type) Reactor Subsystem	198
3-144	Reactor Assembly Data for Minimum Weight Shadow Shielded Configurations (DAC-59213) May 1966	199
3-145	Preliminary Coolant Loop Weight vs Reactor Power NaK $\Delta T = 200°F$	200
3-146	Space Power Reactor Outlet Temperature vs. Calendar Year	201
3-147	Projected Reactor Failure Rate and Lifetime	203
3-148	Projected Nuclear Reactor Cost	204
3-149	Representative Single Source Radioisotope System Installation	206
3-150	Fuel Block Design	210
3-151	Conceptual Design of a $^{238}PuO_2$ Fuel Capsule	210
3-152	Projected Temperature Capability of Isotope Fuels	211
3-153	Projected Isotope Cost	213
3-154	Projected Isotope Availability (Preliminary)	214
3-155	Nuclear Reactor Shield Configurations (Reference 5)	217
3-156	Instrument Shield Weight vs. System Parameters (Extracted From Reference 5)	218
3-157	Shadow Shield Weight As a Function of Reactor and Shield Parameters (Extracted from Reference 2)	219
3-158	Typical Isotope Shield Arrangement	220
3-159	Neutron Dose Rates from LiH-Shielded Isotopic Power Sources of Plutonium-238 as a Function of Penetration Depth of Shielding Material. Center of source to dose point separation distance = 100 cm. Abstracted from Ref. 7	221

3-160	Neutron Dose Rates from LiH-Shielded Isotopic Power Sources of Curium-244 as a Function of Penetration Depth of Shielding Material. Center of source to dose point separation distance = 100 cm. Abstracted from Ref. 7.	222
3-161	Bremsstrahlung Dose Rates from Uranium-Shielded Isotopic Power Sources of Strontium-90 (Strontium Titanate). Center of source to dose point separation distance = 100 cm. Abstracted from Ref. 7.	223
3-162	Gamma Dose Rates from Uranium-Shielded Isotopic Power Sources of Cobalt-60. Center of source to dose point separation distance = 100 cm. Specific activity of source = 75 curies per gram of cobalt. Abstracted from Ref. 7.	224
3-163	Projection - Nuclear Shield Reliability (LiH)	226
3-164	Projection - Nuclear Shield Cost	227
3-165	Solar Concentrator Heat Source Subsystem	228
3-166	Projection Solar Concentrator Specific Mass	231
3-167	Projected Boiler-Absorber Specific Mass	232
3-168	Projection Specific Mass of Solar Concentrator Subsystem Accessories	233
3-169	Projection of Failure Rate of Solar Concentrator Subsystem Components	234
3-170	Projection of Failure Rate-Solar Concentrator Subsystem Accessories	235
3-171	Specific Production Cost of Solar Concentrators	236
3-172	Specific Production Cost,Solar Boiler Absorber	237
3-173	Cost of Solar Concentrator Subsystem Accessories	238
3-174	Cost of Heat Storage Material-Solar Heat Source	239
3-175	Solar Concentrator - Absorber Efficiency versus Temperature	240
3-176	Projection of Solar Concentrator Subsystem Wearout Life	241
3-177a	Two-Phase (Subcritical) Storage with Vapor Delivery	244
3-177b	Supercritical Cryogenic Fluid Storage	245
3-178	Specific Weight Reactant Supply	246
3-179a	Cost of Reactant System Tankage	248
3-179b	High-Pressure Gas Storage - Gas Supply Subsystem Diagram	249
3-179c	Projected Failure Rate for Reactant Supply Subsystems	251

3-180	Single Phase and Condensing Radiator Configuration	252
3-181	Typical Radiator Configuration	252
3-182	Typical Radiator Mass To Area Ratios (Armored Tube - Fin Module Only)	257
3-183	Canned Rotor Pump Mass (Lithium Coolant Conditions)	258
3-184	Electromagnetic Pump Mass (AC Induction)	259
3-185	Trends in Radiator Structure Production Costs	260
3-186	Power Conditioning Subsystem for DC Source	262
3-187	Power Conditioning Subsystem for AC Source	263
3-188	Projection of DC - AC Inverter Specific Mass	266
3-189	Projection of DC Voltage Converter Specific Mass	267
3-190	Projection of Efficiency of DC Voltage Converters	268
3-191	Projection of Efficiency of DC - AC Inverters	269
3-192	Projection of Power Conditioning Equipment Production Costs	270
3-193	Projection of MTBF for Power Conditioning Equipment	271
3-194	Projection of Density of Power Conditioning Equipment	272
3-195	Projection of Transformer Specific Mass	273
3-196	Transformer Mass Correction Factor	274
3-197	Projection of Rectifier Specific Mass	275
3-198	Projection of Efficiency of Rectifiers	276
3-199	Power Distribution Weight Correction Factor	280
3-200	Specific Mass of Shroud	282
3-201	Nuclear Reactor Power System Design Concept	284
3-202	Power System - Mission Phases for Costing Model	287
3-203	Power Conversion Module DTI&Q Cost	290
3-204	Power Conversion Module DTI&Q Cost	291
3-205	Radiator Module DTI&Q Cost	292
3-206	Heat Source DTI&Q Costs	293
3-207	Interstage/Shroud & Boom and Power Conditioning Distribution Equipment DTI&Q Cost	294

TABLES

2-1	Projection and Correlation Methods	5
3-1	Improvement Indexes	15
3-2	Solar Cell Array Power Conversion Subsystem	18
3-3	Model Solar Flare Characteristics	23
3-4	Meteoroid Flux, Mass, and Velocity Constants	24
3-5	Meteoroid Damage Ratio	24
3-6	Meteoroid Particle Mass Limits	24
3-7	Solar Cell Ultraviolet Exposure Damage	25
3-8	Planetary Characteristics	25
3-9	Solar Cell Panel Thermophysical Properties	25
3-10	Assumed Panel Geometry	26
3-11	Packing Factors for Solar Cell Panels	26
3-12	Power Prediction Tolerance	26
3-13	Direct Losses	26
3-14	Structure/Deployment Mechanism Characteristics	27
3-15	Orientation Drive Characteristics	27
3-16	Thermoelectric Power Conversion Subsystems Briefing Chart	62
3-17	Thermionic Power Conversion Subsystem Briefing Chart	75
3-18	Fuel Cell Power Conversion Subsystem Briefing Chart	87
3-19	Battery Power Conversion Subsystem Briefing Chart	100
3-20	Battery Charge Time Limits	105
3-21	Battery Discharge Time Limits	105
3-22	Space Battery Voltage Efficiency	105
3-23	Battery Cell Operational Requirements (Assumed)	106
3-24	Battery Charge Regulator Characteristics	106

3-25	Brayton-Cycle Power Conversion Subsystem Briefing Chart	123
3-26	Mercury Rankine Power Conversion Subsystem Briefing Chart	138
3-27	Alkali Metal Rankine Power Conversion Subsystem Briefing Chart	139
3-28	Organic Rankine Cycle Conversion Subsystem Briefing Chart	171
3-29	Chemical Dynamic Power Conversion Subsystem Briefing Chart	188
3-30	Nuclear Reactor Heat Source Subsystem Briefing Chart	197
3-31	Isotope Heat Source Subsystem Briefing Chart	205
3-32	Radioisotopic Power Fuel Data	207
3-33	Shielding (Reactor and Isotope) Briefing Chart	215
3-34	Solar Concentrator Heat Source Subsystem Briefing Chart	229
3-35	Reactant Storage Subsystems Briefing Chart	243
3-36	Chemical Properties of Reactants	250
3-37	Candidate Radiator Armor Material Properties (Room Temperature)	254
3-38	Heat Rejection Subsystems Briefing Chart	255
3-39	Summary of Heat Rejection Subsystem Component Failure Rate Data	256
3-40	Power Conditioning Components Briefing Chart	261
3-41	Power Conditioning Subsystems Briefing Chart	264
3-42	Power Distribution Subsystem Briefing Chart	278
3-43	Power Distribution Subsystem Weights	279
3-44	Vehicle Interstage and Shroud Briefing Chart	283
3-45	Briefing Chart Deployment Boom	285

Section 1
INTRODUCTION

This volume, Volume III, is one of four volumes which present the results of the NASA Parametric Study of Space Power Systems conducted by McDonnell Douglas Astronautics Company-Western Division (MDAC-WD) for the Mission Analysis Division - OART under Contract NAS2-4482. The title of the final reports are as follows:

Title	Volume No.	Report No.
Summary	I	DAC-62303
Technical Report	II	DAC-62304
Power Subsystem Parametric Data	III	DAC-62305
Computer Manual		
Book 1 - Power Subsystem Analysis	IV	DAC-62306
Book 2 - Program Operation	IV	DAC-62307

The objective of the study is to provide a computer program and supporting documentation which permits the prediction of space power system characteristics (such as mass, volume, area, cost, and reliability) as a function of mission parameters (such as mission duration, launch date, trajectory, power load profile, and nuclear radiation levels). The various power subsystems that have been investigated in the study are shown in Figure 1-1.

The final report contains the state-of-the-art and parametric data, analysis, logic networks, system design data, and recommendations. The report contains tables, diagrams, curves, and drawings in sufficient detail to explain the methodology of the power system analysis. The computer program code

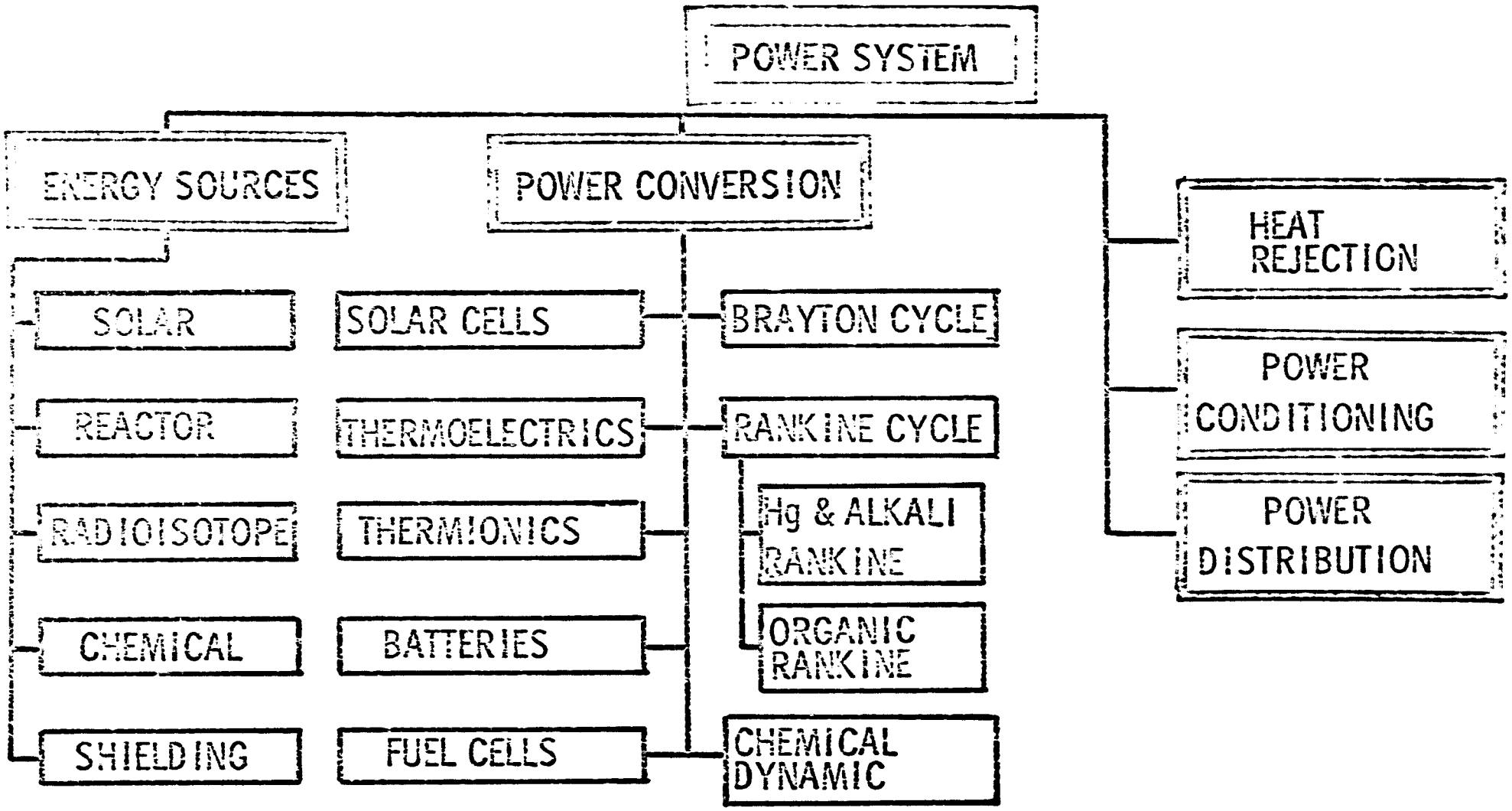

Figure 1-1. Major Power Subsystems

code is written in Fortran IV, Version 13 for use on the IBM 7094 computer. The programmer's manual contains (1) a synopsis of each program and the principal techniques involved in coding; (2) flow diagrams describing the structure of each program; and (3) description of input and output variables, data cards, and symbolic names.

This volume contains (1) a description of the scaling laws and data correlation techniques that were employed in the study for projecting and correlating the characteristics and performance data of the power system components; (2) power subsystem schematics and briefing charts indicating the nominal range of values of the subsystem evaluation parameters such as power levels, specific weight, specific area, specific volume, specific cost and reliability; and (3) graphical plots of the component characteristics that were used in the study and are incorporated in the computer program in the form of block data.

PRECEDING PAGE BLANK NOT FILMED.

Section 2
SCALING LAWS AND DATA CORRELATION TECHNIQUES

2.1 SCALING LAWS

The major parameters (called characteristics) that are usually used in performing power system tradeoff studies and sensitivity analysis are mass; solar cell, radiator or solar concentrator area; volume; reliability; and cost. In addition to the power system characteristics, the thermodynamic state-point data, cycle performance, and physical size of the components are also useful. The basic parametric and design data that are used in this study were obtained from published reports, physical principles, empirical data, results of detailed power system studies, hardware programs, and the use of detailed power subsystem computer programs. Two basic analytical methods are used in the study to correlate the data and are dependent on the type of correlation that is desired. The first and primary method is the growth projection method that determines the characteristics or performance of a major component as a function of calendar year to 2000. The second method of correlating the data uses a correlation function or factor that determines the curve to draw through a large number of data points or extrapolates data to a family of curves based on size or power level.

The methods and techniques for projecting and correlating the characteristics and performance data are given in Table 2-1 and are described in subsequent paragraphs.

Table 2-1
PROJECTION AND CORRELATION METHODS

Growth Projection Technique	Correlation Function Technique
Statistical growth projection	Hyperbolic correlation factor
Exponential growth projection	Least-squares polynomial fit

2.2 STATISTICAL GROWTH PROJECTION TECHNIQUES

The statistical growth projection technique has been developed to provide a coherent rationale for estimating performance parameters at any future date. The growth projection technique is based on the assumption that all performance parameters have limiting values. The Carnot cycle limit on thermal efficiencies is one example of a limiting value. The slope of the growth projection curve for a particular parameter at any date is assumed to be proportional to the difference between the parameter at that date and the limiting value of the parameter or mathematically

$$\frac{df(t)}{dt} = \frac{1}{\tau}[f(\infty) - f(t)] . \qquad (2-1)$$

The solution of Equation 2-1 is

$$f(t) = f(\infty) + \left[f(t_i) - f(\infty)\right]e^{-(t-t_i)/\tau} \qquad (2-2)$$

where:

$f(t)$ = value of projected parameter at time t (□t points), e.g., efficiency in Figure 2-1

$f(\infty)$ = limiting value of the project parameter (□a points) after 2000

$f(t_i)$ = value of parameter at start of projection 1965 to 1968 (□i points)

t_i = initial time, years

τ = time constant, years

A summary of the procedures used in determining the projection curves for the characteristics and/or performance of the power subsystem (using the nomenclature as shown in Figure 2-1) is:

1. Establish and plot the present and historical data points, and establish the minimum and maximum limits (□i points) for the performance parameter of present power systems.

2. Establish the minimum and maximum limits for the ultimate performance parameter (asymtotic values) of the system at some time after 2000 as determined by theoretical or practical limits (□a points).

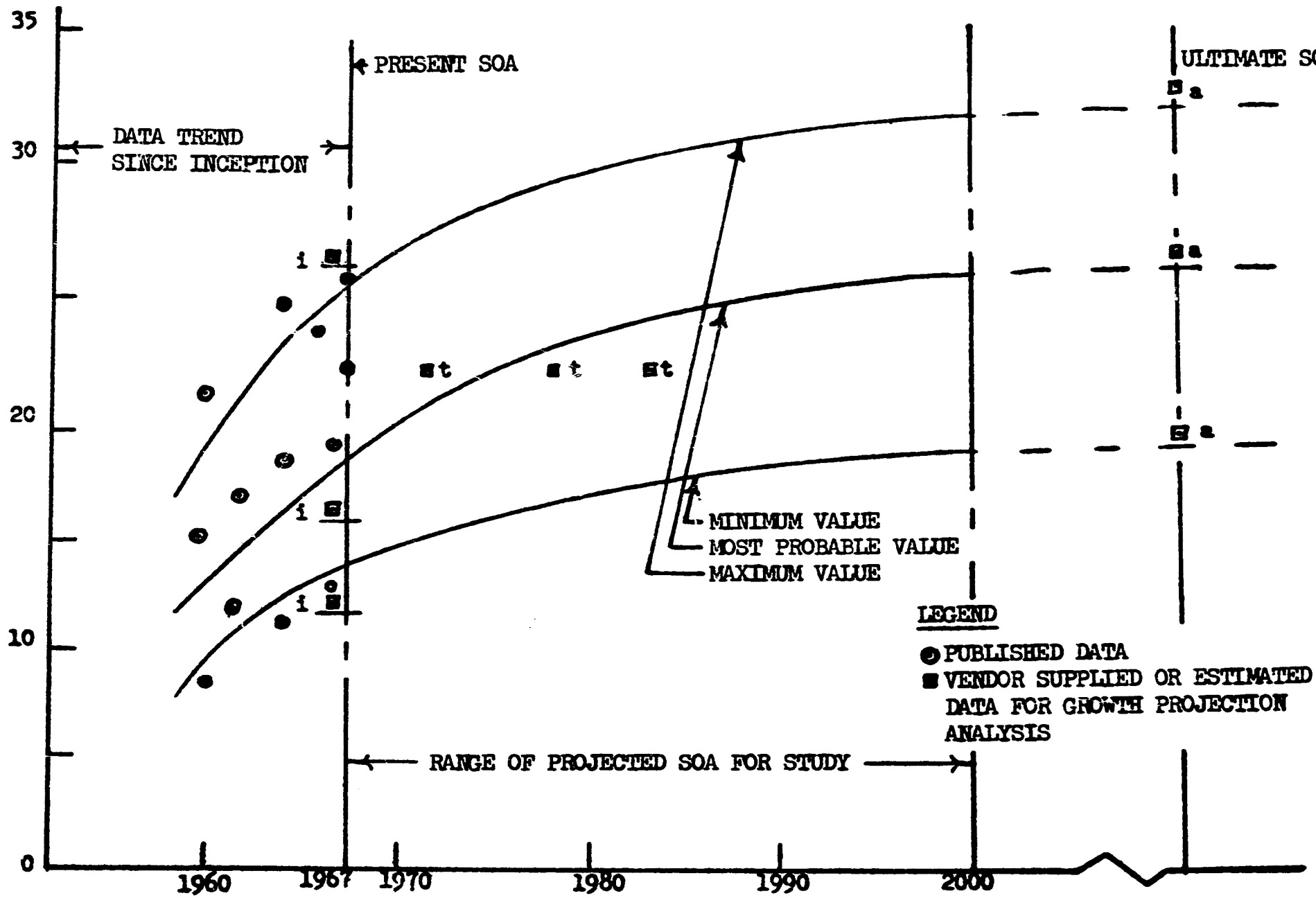

Figure 2-1 Basis for Projecting State of the Art Curves

3. Determine the minimum, the most likely, and the maximum time intervals (□t points) required to progress from the most likely initial value to the most likely point in the asymptotic distribution.

4. With the above data, the minimum value, most probable value, and maximum value curves can be developed by use of the statistical growth projection computer program, which assumes a distribution for data scatter and establishes an exponential relationship for each of the curves. Only the most probable value curve is plotted and used in the study subject to the nomenclature in Section 3.

The statistical growth projection technique is used to obtain 10 sets of data points that determine the shape of the growth projection curve and the 10 data points are stored in block data arrays for use in calculating the power system characteristics and performance by interpolation.

2.3 EXPONENTIAL GROWTH PROJECTION TECHNIQUE

The exponential growth projection technique is a simplified version of the statistical growth projection technique and uses the same equation for determining the projected values of the parameter. The main advantage of the exponential growth projection technique is (1) that only three data points are required to determine the shape of the curve as compared to nine data points for the statistical growth projection technique, and (2) the value that is needed to perform the power system calculation is obtained directly by solving the exponential growth projection equation as compared to interpolation between the data points stored in the block data arrays for the statistical growth projection technique. The three required data points are the initial value of the parameter in the 1965 to 1968 time period, an intermediate value of the parameter in 1970 to 1975 time period, and the asymptotic value of the parameter in the post 2000 time period.

2.4 HYPERBOLIC CORRELATION FACTOR

Certain components such as turbines, compressors, pumps, and power conditioning equipment have characteristic performance curves that vary as a function of size or power level as shown in Figure 2-2. The variation or scaling law that relates the effect of size or power level to the component performance normally follows a hyperbolic function (F_c) as shown in

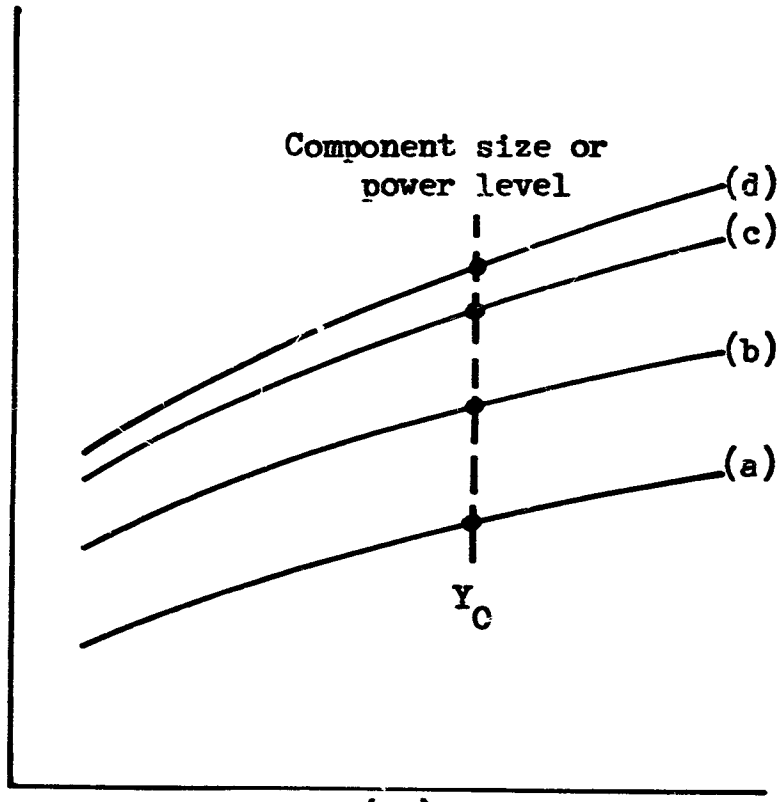

Figure 2-2. Example Component Performance

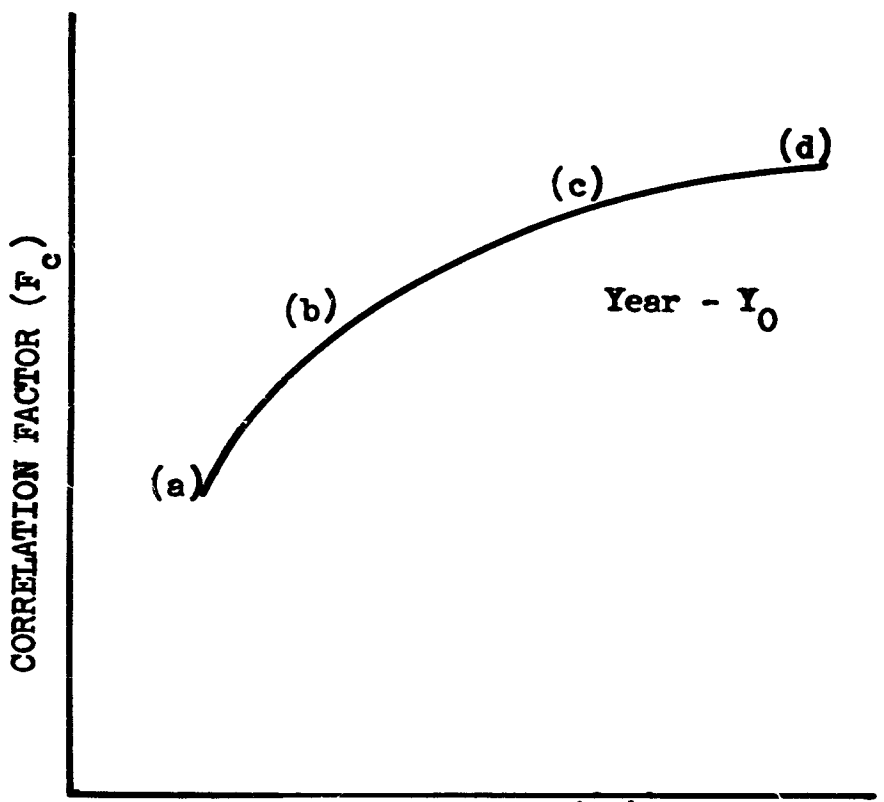

Figure 2-3. Example Component Size Correlation Factor

Figure 2-3. In the analysis, the parametric data for certain components have been plotted as a function of calendar year for a single performance parameter or power level (such as 10-kW turboalternator assembly). The product of the correlation factor (F_c) for year Y_o and the power level of interest and the value of the baseline curve (a) produces an estimate of the value that is needed in the calculation. Where limited data are available, this technique has been used in the analysis to plot a full set of characteristic or performance curves over the range of the parameter that is of interest in the study.

2.5 LEAST-SQUARES POLYNOMIAL FIT

Another method of correlating the data is through the use of a least-squares polynomial fit. This approach is used to correlate the design data for the solar cell/battery and primary battery power subsystems. The basis of the correlation is given below.

Consider a set containing (N) pairs of data points (Y_i, X_i), Y_i being the dependent variable. Associated with each data point is a positive weighing value (W_i). The least-squares polynomial fit to these data is expressed in the form:

$$Y = \sum_{J=1}^{M} C_J X^{(J-1)} \qquad (2-3)$$

where:

Y = dependent variable

X = independent variable

C_J = polynomial coefficients

M = maximum number of polynomial coefficients

The residual of each data point (Y_i, X_i) is defined as:

$$r_i \left[= \sum_{J=i}^{M} C_J X_i^{(J-1)} \right] - Y_i \qquad (2\text{-}4)$$

The weighted sum of the squares of the residuals is then:

$$S = \sum_{i=1}^{N} (W_i r_i)^2 \qquad (2\text{-}5)$$

The principle of least squares asserts that the best approximation to the polynomial coefficients (C_J) is the set for which the sum of the squares of the residuals is a minimum. Necessary conditions for a minimum (S) are the set of partial differential equations (called the "normal" equations).

$$\frac{\partial S}{\partial C_J} = 0 \qquad (2\text{-}6)$$

where:

$$J = 1, 2, 3\ 4, \ldots\ldots M\ .$$

Combining Equations 2-4 and 2-5 and performing the operation indicated by Equation 2-6 yields the general form of the normal equation:

$$\sum_{i=1}^{N} W_i Y_i X_i^{(K-1)} = \sum_{J=1}^{M} \left\{ \sum_{i=1}^{N} W_i C_J X_i^{(J-1)} X_i^{(K-1)} \right\} \qquad (2\text{-}7)$$

where:

$$K = 1, 2, 3, 4 \ldots\ldots M\ .$$

As an example of the use of Equation 2-7 we illustrate the normal equations for a linear fit (M=2) to data having a weighting value of 1 (W_i=1). These normal equations are:

$$\sum_{i=1}^{N} Y_i = NC_1 + C_2 \sum_{i=1}^{N} X_i \tag{2-8}$$

$$\sum_{i=1}^{N} Y_i X_i = C_1 \sum_{i=1}^{N} X_i + C_2 \sum_{i=1}^{N} X_i^2 \tag{2-9}$$

To determine the strength of the least-squares polynomial fit, the statistical analysis outlined below is performed.

For an infinite population of data points (Y_i, X_i), the standard deviation is given by:

$$\sigma = \sqrt{\left(\frac{1}{N}\right) \sum_{i=1}^{N} Y_i^2 - \left[\left(\frac{1}{N}\right) \sum_{i=1}^{N} Y_i\right]^2} \tag{2-10}$$

For a small, finite population, the standard error of estimate is:

$$S_{tda} = \sqrt{\frac{S}{N} \left(\frac{N-1}{N-2}\right)} \tag{2-11}$$

and hence, the coefficient of correlation, a measure of the goodness of fit, is given by

$$C_{ca} = \sqrt{1 - \left(\frac{S_{tda}}{\sigma}\right)^2} \tag{2-12}$$

where:

$$0 \leq C_{ca} \leq 1$$

In statistical terms, a coefficient of correlation ≥ 0.5 is considered a strong correlation between the dependent and independent variable.

Section 3
SECONDARY POWER SUBSYSTEM PARAMETRIC DATA

This section contains the parametric data collected for the analysis of the various subsystems examined in this study. A thorough survey of the parametric and design data of all the major components, subsystems, and power systems was beyond the scope of the study. For some components, a complete set of parametric data is not available. To complete the set of parametric data (mass, area, volume, reliability, and cost), engineering estimates were made by power system manufacturers (in response to questionnaires) and the study team members. Because of differences of opinion in the state of the art between different power system specialists, the block data array storage technique permits the power system specialist to adjust or upgrade the data according to his specifications. To enable the reader to understand the growth projection trends and the basic assumptions that were used in drawing the curve(s), an improvement index label is shown with each projection curve or family of curves. The improvement index (II) label and its meaning are presented in Table 3-1.

Table 3-1
IMPROVEMENT INDEXES

Improvement Index	Definition
II-A	Product improvement through manufacturing technology or new material development
II-B	Current level of effort of research and development or system development programs
II-C	Significantly expanded research and development or system development programs
II-D	Assumed value; based on lack of adequate published engineering data

The power system consists of five major subsystems. The subsystems include the energy source subsystem, the power conversion subsystem, the heat rejection subsystem, the power conditioning subsystem, and the power distribution subsystem. The following major subsystem categories have been analyzed and are programmed:

1. Energy Source Subsystem
   - A. Solar
   - B. Nuclear reactor
   - C. Radioisotope
   - D. Chemical
   - E. Shielding
2. Power Conversion Subsystem
   - A. Solar cells
   - B. Thermoelectrics
   - C. Thermionics
   - D. Batteries
   - E. Fuel cells
   - F. Brayton cycle
   - G. Rankine cycle
   - H. Chemical dynamic
3. Heat Rejection Subsystem
   - A. Single phase
   - B. Condensing
   - C. Direct radiating
4. Power Conditioning Subsystem
   - A. AC conditioning
   - B. DC conditioning
5. Power Distribution Subsystem
   - A. AC distribution
   - B. DC distribution

3.1 POWER CONVERSION SUBSYSTEMS

Various types of power conversion subsystems have been proposed and investigated for the generation of electrical power for space vehicles. The parametric and design data of the various conversion subsystems are presented in the following sections.

3.1.1 Solar Cells (Silicon and Thin-Film CdS) Conversion Subsystem

Solar cells have been designed and successfully operated in space for power ranges from a few hundred milliwatts to over a kilowatt. Development is proceeding in sizes up to 50-kW power output. Solar cell power systems are light in weight, simple, and reliable in operation. Their major disadvantage is a degree of sensitivity to the space environment (particle radiation, thermal radiation, micrometeoroids, and lack of ability to generate power in the dark). The major operational characteristics of the solar cell array power subsystem are given in Table 3-2. Two types of solar cells are considered: the single-crystal silicon cell and the thin-film cadmium sulfide (CdS) cell. The silicon cell has been in use on operational solar cell arrays since 1957 and has been constantly upgraded in performance and environmental resistance. Thin-film cells are presently being developed and hold future promise for low-cost, lightweight solar cell array. They are presently limited in application because of low efficiency and difficulties in quality control during manufacturing processes.

Silicon solar cells are presently available in large quantities (2,000,000 cells/year) in the following sizes: 1 by 2 cm, 2 by 2 cm, and 2 by 6 cm. Other sizes being developed include: 3 by 3 cm, 1 by 30 cm, and 2 by 30 cm. Present operational solar cells range from 0.406 to 0.507 mm (16 to 20 mils) in thickness. In the near future cells of 0.203 to 0.305 mm (8 to 12 mils) will be available. Ultimately 0.101-mm (4-mil) cells are expected to be in general use; however, they have a lower efficiency. Thin-film CdS solar cells in large quantities (10,000 cells/year) are available only in 7.62 by 7.62 cm (3 by 3 in.) sizes. Future developments may lead to cells up to 15.25 by 15.25 cm (6 by 6 in.) size.

The complete subsystem that uses solar cells for power conversion is defined as the solar cell array power conversion subsystem, or simply array. The major components of a solar cell array power conversion subsystem are: (1) solar cell panels, (2) deployment drive and controls, and (3) orientation drive and control. The interactions between these components is shown in Figure 3-1. A solar cell panel consists basically of cell modules attached to the supporting panel structure. The module, as shown in Figure 3-1, is defined as that portion of the panel containing the solar cells, cover glass,

Table 3-2

SOLAR CELL ARRAY POWER CONVERSION SUBSYSTEM

Item	Value
Identification	
Applicable energy source	Solar Energy,
Conversion equipment	Solar Cells, Silicon and Thin Film CdS
Heat rejection subsystem	Passive
Major components	Solar Cell Panel Deployment Drive and Control Orientation Drive and Control
Vehicle-Mission Application Range	
Useful power level	Milliwatts - 1,000 kW
Duration of mission	0 to 5 years
Types of spacecraft	Manned, unmanned orbital interplanetary between heliocentric ranges equivalent to Mercury to Jupiter
Status	
State of the art (1967)	5 to 40 watts/kg
Availability of support subsystems	Adequate
Special problems	Reduction of cell and cover glass weight Ionizing particle radiation temperature extremes and thermal shock Array deployment and orientation
Subsystem Characteristics at 1AU (1967)	
Range of specific weight	5 to 40 watts/kg
Range of specific area	90 to 110 watts/m^2
Range of specific volume	500 to 800 watts/m^3
Range of specific production costs	$200 to $900/watt
Range of reliability	0.95 to 0.99
Performance Data	
Range of solar cell efficiency	
Silicon cells	10 to 14%
Thin-film CdS cells	4 to 8%
Range of operating temperatures	
Silicon cells	75° to 450°K
Thin-film CdS cells	75° to 370°K

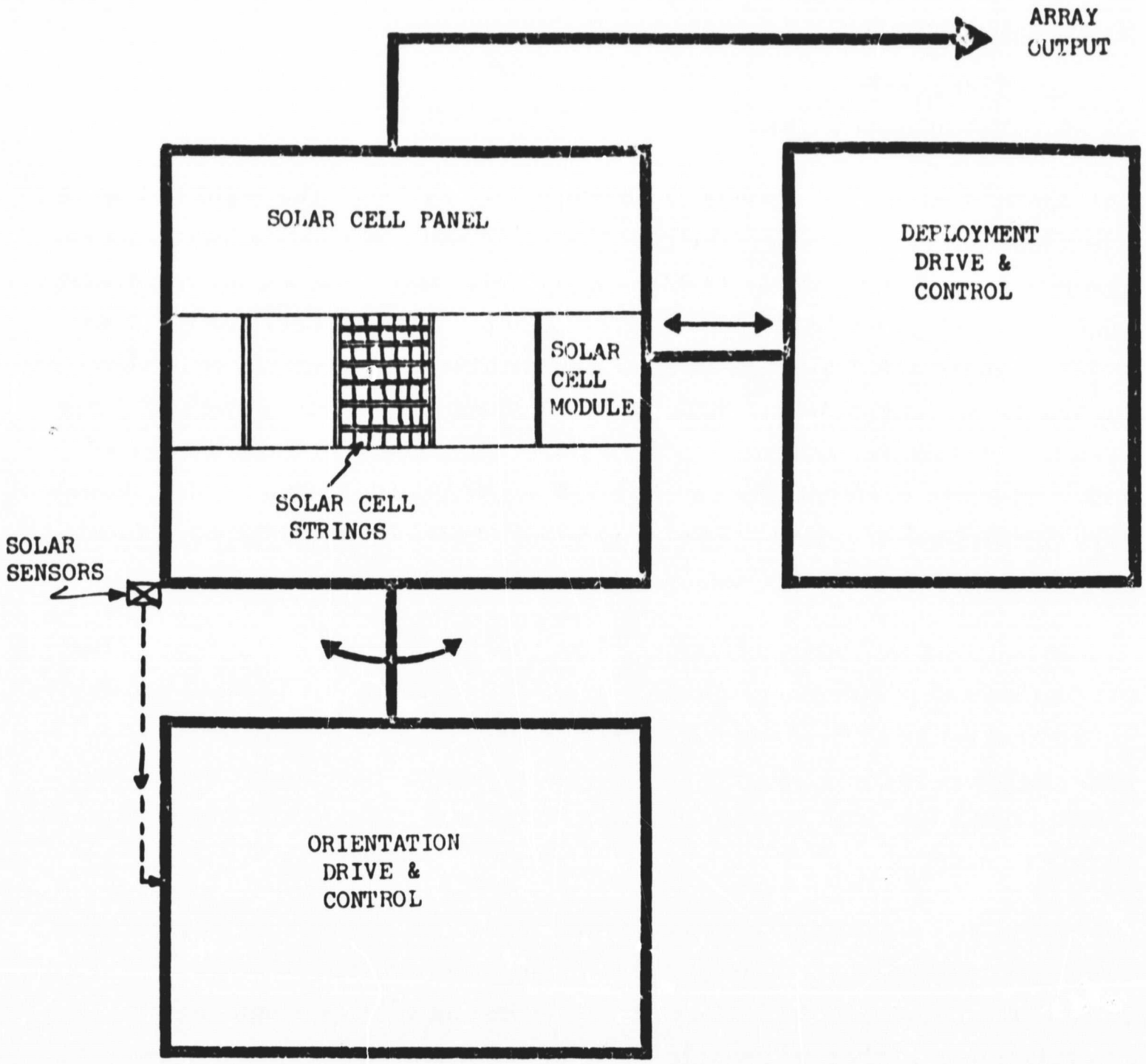

Figure 3-1 Solar Cell Array Power Conversion Subsystem

interconnections, and substrate. The module contains solar cells arranged in the various parallel-series combinations to obtain the required output voltage and current as well as reliability. These arrangements of cells in parallel are defined as the solar cell strings. Typical examples of silicon and thin-film CdS solar cells are shown in Figure 3-2. Panels that can be investigated include:

1. Flat panels
2. Cylindrical panels

The application of these panels is shown in Figure 3-3. The rigid flat-panel type (Figure 3-3b) is being fabricated by all of the solar cell array vendors. The panel is made up of one or more subpanels folded into a compact arrangement for stowage during launch. After launch, the subpanels are unfolded and the panels are deployed. A flexible flat panel or rollup array is shown in Figure 3-3a. These panels differ from rigid panels mainly in the technique used for deployment and making them stiff. They are still being evaluated with respect to performance and mission application. Rollup arrays, however, have the distinct advantage of being easily stowed during launch and of undergoing repeated deployment and stowage cycles during a mission.

Thinner and lighter weight solar cells will be used as the technology of their production and performance characteristics is developed. Lighter substrates will therefore be used for mounting the cells. As a result, differences between panel specific weights for rigid and flexible panels will disappear. These trends are indicated in the state-of-the-art parametric data presented in this section.

An example of a cylindrical panel is shown in Figure 3-3c. The cylindrical panel has been used extensively on many unmanned Earth satellites (SYNCOM, INTELSAT, Applications Technology Satellite) as well as a number of interplanetary probes (Pioneer). Cylindrical panels have been designed for up to 1-kW power output. Because the cylindrical panels usually form an integral part of the satellite structure, they may be fixed in space or rotate along the cylinder axis. The major disadvantage of cylindrical panels is their higher weight (as compared to flat panels) for a given power output.

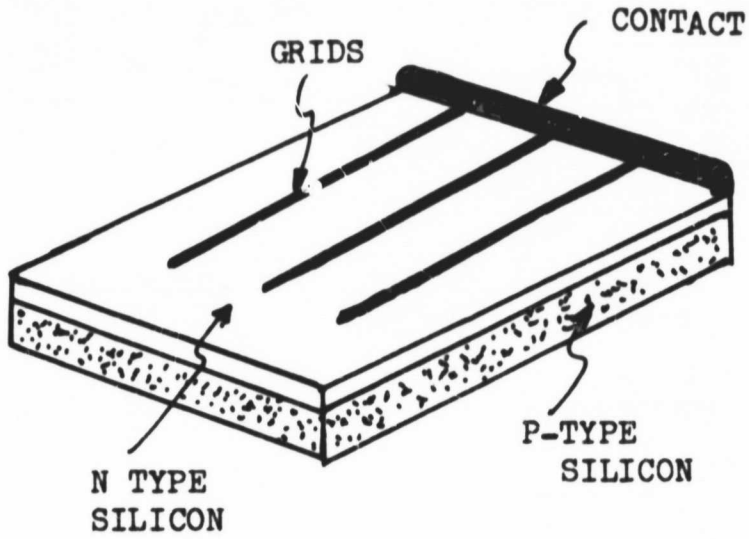

N/P SILICON SOLAR
CELL

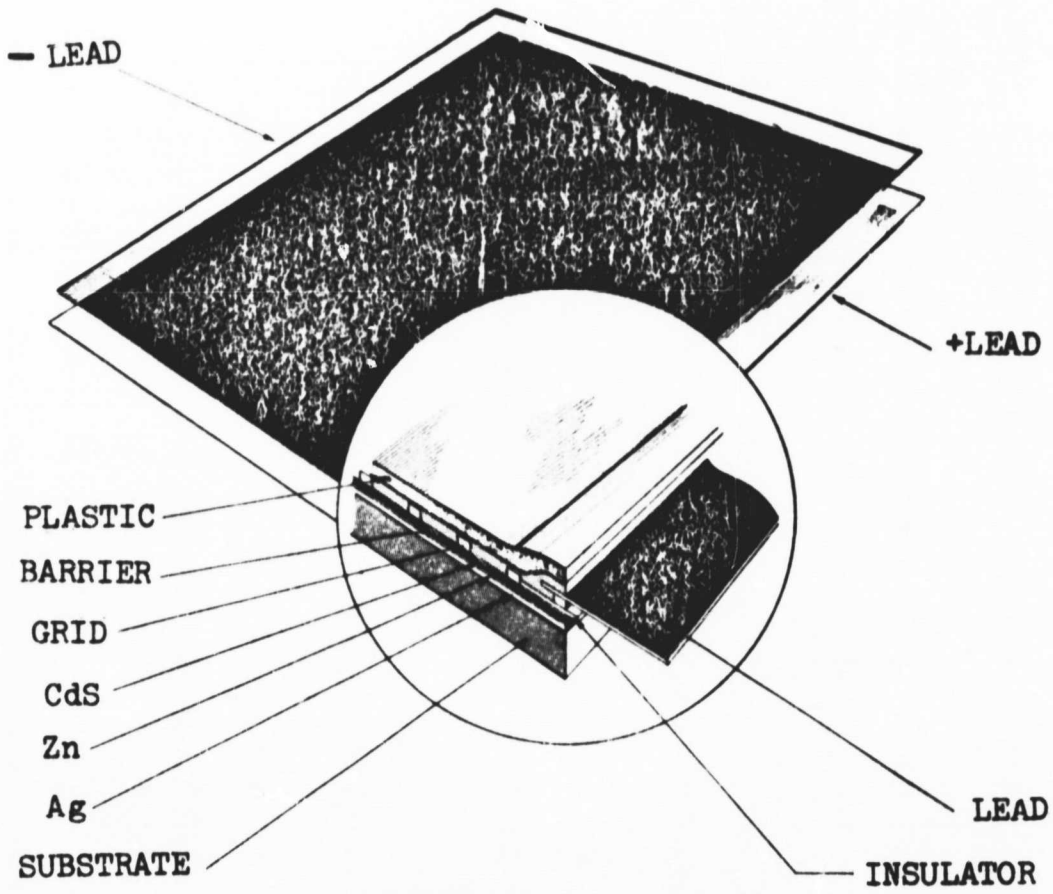

THIN-FILM
CdS

SOLAR CELL

Figure 3-2 Solar Cell Types

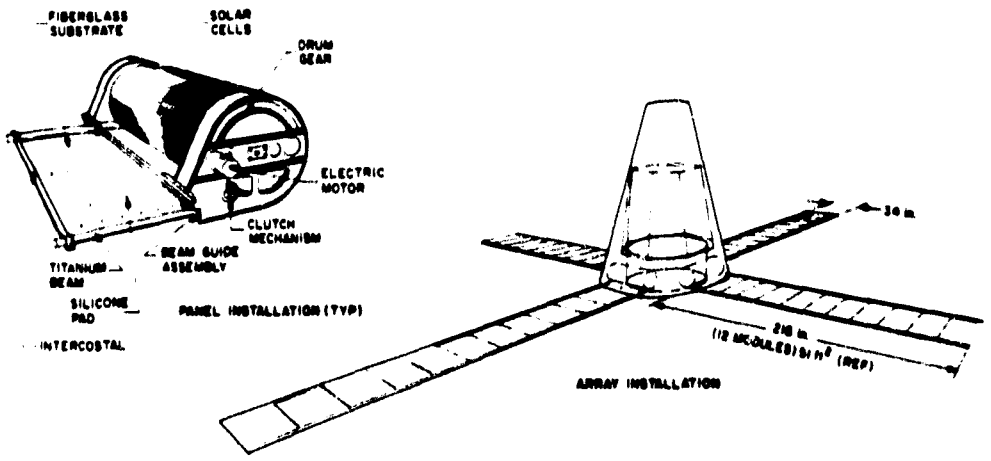

a. Flexible Flat Panel ~ Collapsible Beam Rigidization

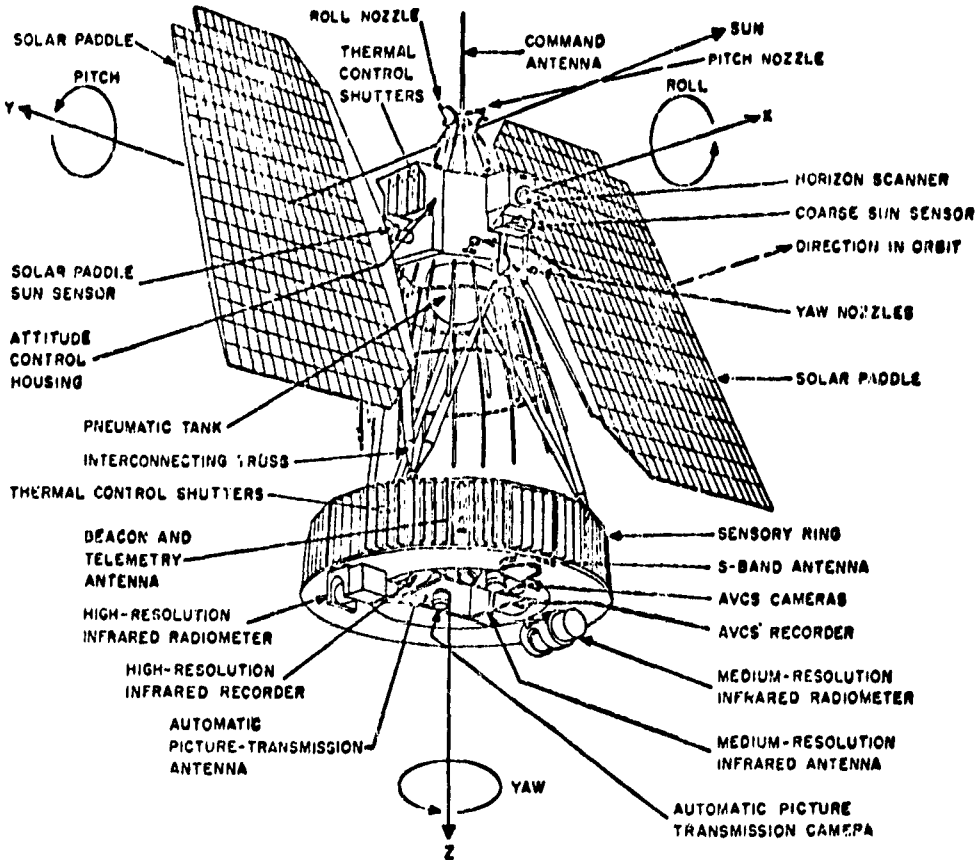

b. Rigid Flat Panel on Nimbus 2 Spacecraft

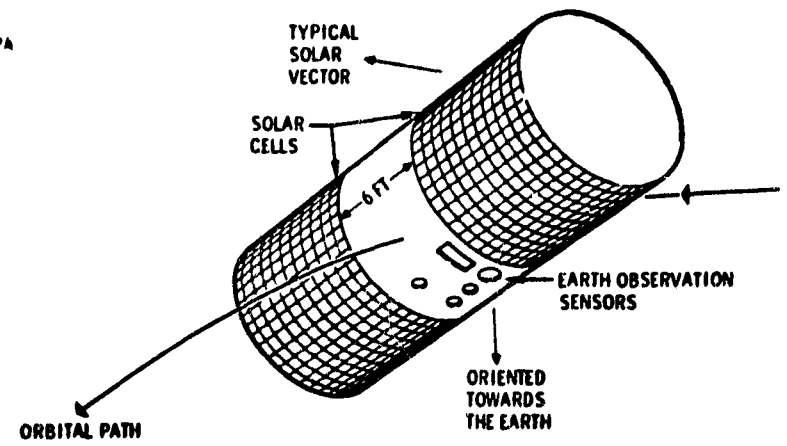

c. Cylindrical Panel

Figure 3-3 Solar Cell Array Power System Schematics

The other portions of the array shown in Figure 3-1 are the deployment and the orientation subsystems. The deployment drive and control erects a geometrically stable configuration of the solar array on the spacecraft. It is generally used only once for unmanned missions. Future manned missions, however, may require repeated deployment and stowage of the solar cell array. The function of the orientation drive and control system is to maintain the desired angle between the panels and the incoming solar radiation (without violating the structural integrity of the array). Solar aspect sensors are usually attached to some portion of the panels and are part of the orientation system.

Data on the characteristics and performance of the major components of the solar cell array subsystem are given in Tables 3-3 through 3-15 and Figures 3-4 through 3-36. Environmental models and their effects on solar cells are shown in Tables 3-3 through 3-9 and Figures 3-4 through 3-36. These are followed by tabular and graphical data for panels, structure/deployment mechanisms, and the orientation drive and controls. It should be noted that the panel structure and deployment mechanism are combined in terms of operational characteristics and performance.

Table 3-3

MODEL SOLAR FLARE CHARACTERISTICS
(November 1960 Event)

Item	Value	Reference
Average rate of occurrence during solar, maximum	1 flare/year	35, 36, 37
Average rate of occurrence during solar, minimum	0.2 flare/year	35
Integrated proton flux	$\frac{9.0 \times 10^{10} \text{ protons}}{\text{cm}^2/\text{event}}$ (>3 MeV)	36

Table 3-4

METEOROID FLUX, MASS, AND VELOCITY CONSTANTS

Particle Mass Limits	Particle Source	Heliocentric Distance Constants C_R	C_{R1}	C_{R2}	C_{R3}	Mass Constant C_M	Velocity Constant C_V	Reference
$<10^{-2.2}$ g	Cometary	-1.0	-13.56	0.0	0.0	-1.00	20.0	34
$>10^{-2.2}$ g	Cometary	-1.0	-14.29	0.0	0.0	-1.34	20.0	(D. E. Evans)
~	Asteroidal	0.0	-21.00	8.0	-1.43	-0.91	15.0	33
~	Cometary	0.0	-14.44	0.0	0.0	-1.34	30.0	(J. M. Deerwester)

Table 3-5

METEOROID DAMAGE RATIO

Cell Type	Ratio of Actual/Simulated Meteoroid Energy Fluence for Equal Solar Cell Damage	Reference
Silicon	0.295	29
Thin-film CdS	0.295	30

Table 3-6

METEOROID PARTICLE MASS LIMITS

Limit	Mass	Reference
Upper	1.0×10^{-8} g/particle	29, 30
Lower	1.0×10^{-12} g/particle	29, 30

Table 3-7

SOLAR CELL ULTRAVIOLET EXPOSURE DAMAGE

Cell Type	UV Damage Factor	Reference
Silicon	Figure 3-11	43
Thin-film CdS (Kapton Cover)	1.0	44

Table 3-8

PLANETARY CHARACTERISTICS (Reference 48)

Planet	Planetary Solar Vector (AU)	Planetary Radius (km)	Solar Albedo
Earth	1.0	6,378.16	0.36
Moon	1.0	3,480.0	0.07
Mercury	0.3871	2,420.0	0.06
Venus	0.7233	6,050.0	0.76
Mars	1.5237	3,410.0	0.15
Jupiter	5.2027	71,400.0	0.51
Saturn	9.5388	60,400.0	0.50
Uranus	19.2529	23,500.0	0.66
Neptune	30.0443	22,300.0	0.62
Pluto	39.6409	7,000.0	0.16

Table 3-9

SOLAR CELL PANEL THERMOPHYSICAL PROPERTIES

Property	Silicon Solar Cells	Thin-Film CdS Solar Cells
α_S (solar absorptivity)	Figure 3-16 (1, 4, 7, 10, 11, 13)*	0.74 (49)
$\alpha_{S\epsilon}$ (backside absorptivity for solar albedo)	0.25 (4, 10, 13)	0.52 (49)
α_{ϵ} (direct planetary radiation absorptivity)	0.85 (4)	0.79 (49)
ϵ_C (cellside emissivity)	0.83 (1, 4, 10, 11, 13)	0.89 (49)
ϵ_B (backside emissivity)	0.90 (1, 4, 10, 13)	0.79 (49)

*( ) indicates Reference

Table 3-10

ASSUMED PANEL GEOMETRY

Panel Type	Aspect Ratio	Definition
Flat	1.0	Length/width
Cylindrical	Calculated by computer program	Length/diameter

Table 3-11

PACKING FACTORS FOR SOLAR CELL PANELS

Panel Type	Cell Type	Cell Packing Factor (η_{LC})	Module Packing Factor (η_{LM})
Flat panel	Silicon	Figure 3-23	Figure 3-25
	Thin-film CdS	Figure 3-24	1.0
Cylindrical	Silicon	Figure 3-23	1.0
	Thin-film CdS	Figure 3-24	1.0

Table 3-12

POWER PREDICTION TOLERANCE

Source of Error	Power Factor	Reference
Current measurement tolerance	0.98	13
Voltage measurement tolerance	0.98	13
Efficiency prediction uncertainty	0.97	13

Table 3-13

DIRECT LOSSES

Loss Type	Cell Type	Percent Loss	Reference
Wiring loss	Silicon	5.0	13
	Thin-film CdS	5.0	
Cover glass transmission loss	Silicon	4.0	10
	Thin-film CdS (Kapton covered)	20.0	32

Table 3-14

STRUCTURE/DEPLOYMENT MECHANISM CHARACTERISTICS

Item	Value	Reference
Structural material	Beryllium	
Material density	1.855×10^3 kg/m^3	21
Material modulus of elasticity	27.6×10^{10} N/m^2	21
Fraction of structure/deployment mechanism mass in deployment drive	0.10	
Structure/deployment mechanism specific cost	\$10,000/m^2	

Table 3-15

ORIENTATION DRIVE CHARACTERISTICS

Item	Value	Reference
Average density	4.0×10^3 kg/m^3	
Power requirement, ratio	0.015	10
Specific cost	1,000 \$k/kW	

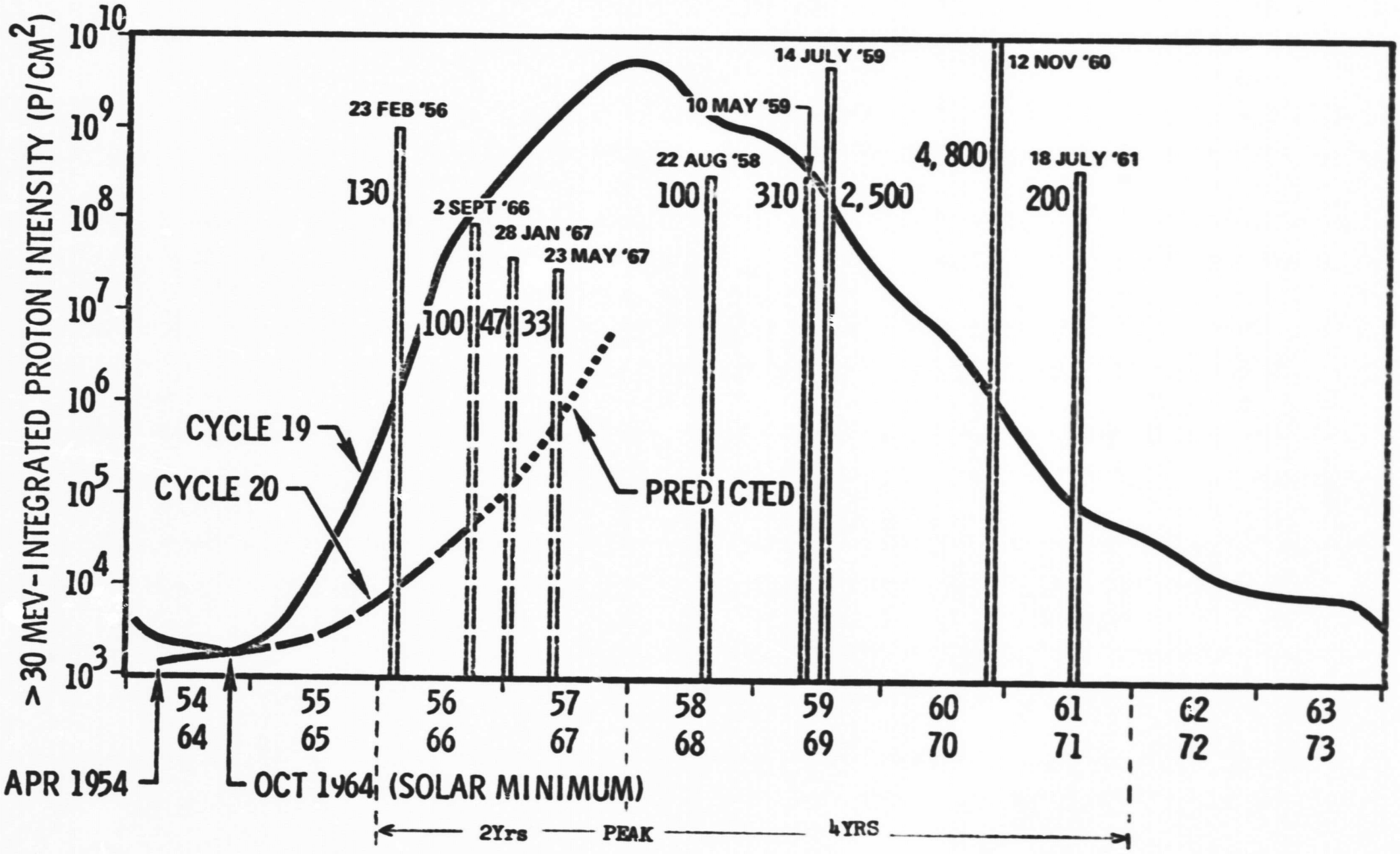

Figure 3-4 Solar Cosmic Ray Events and Sunspot Numbers

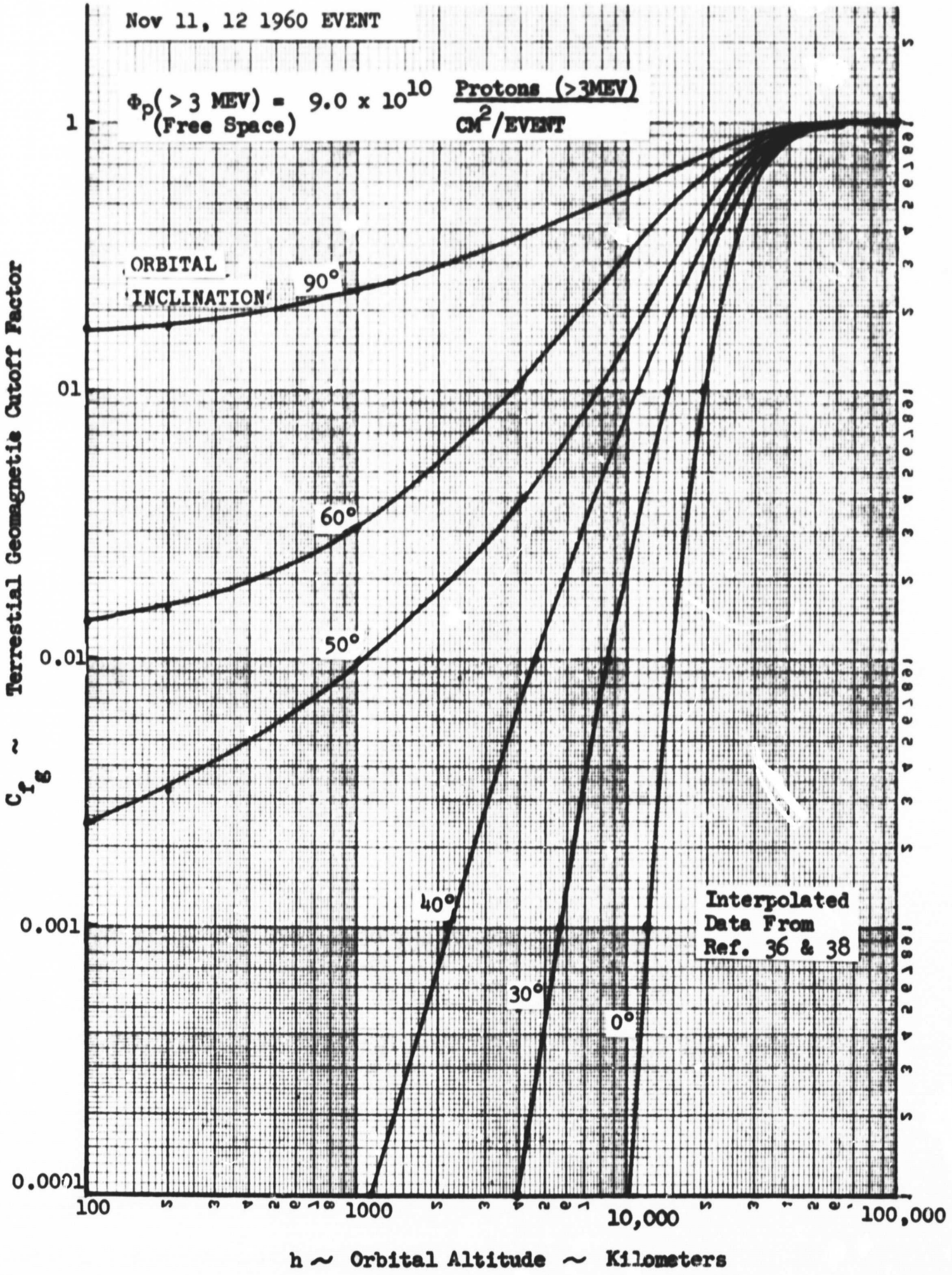

Figure 3-5 Terrestrial Ceomagnetic Field Cutoff Effects on Solar Flare Protons

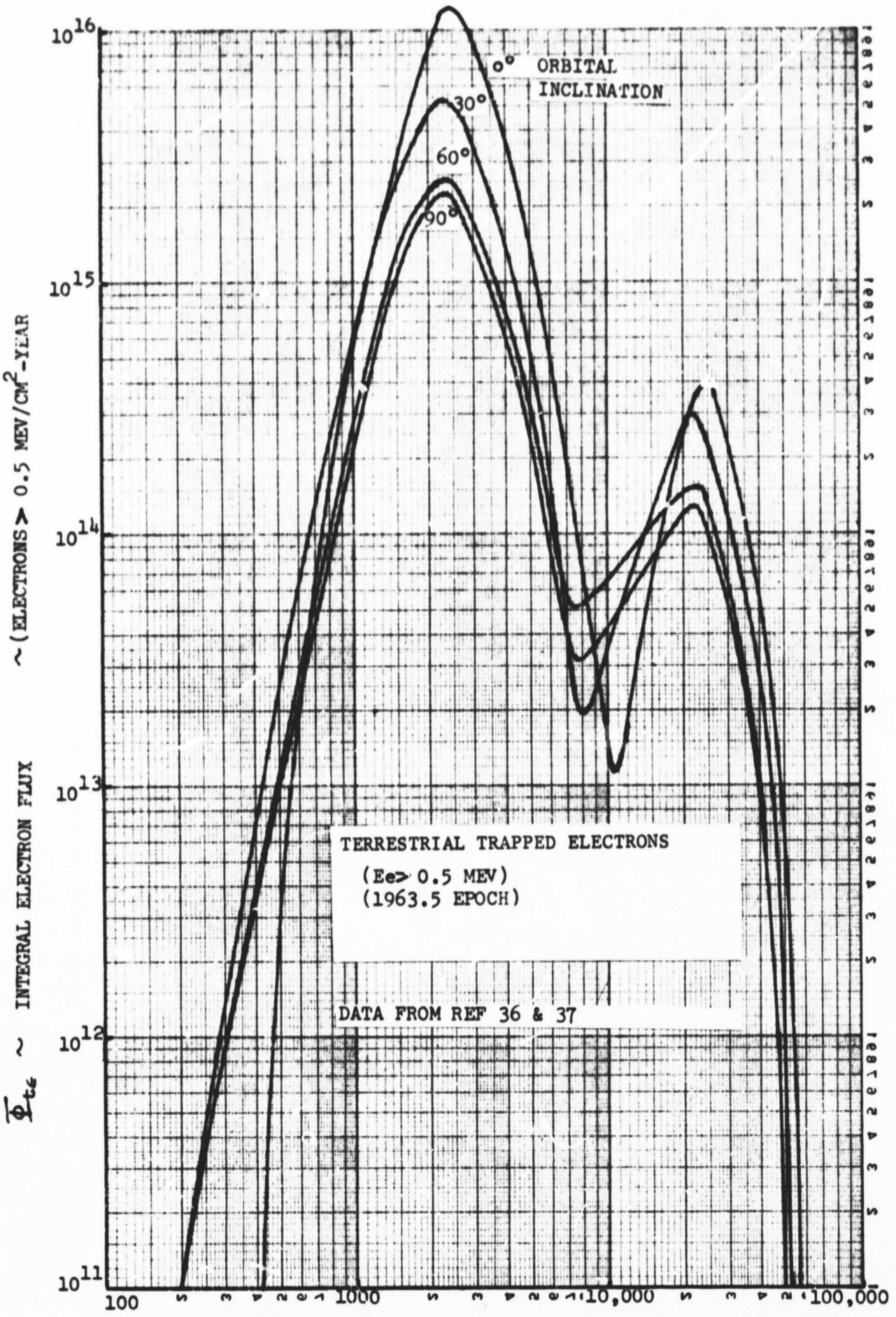
10^{16}
10^{15}
10^{14}
10^{13}
10^{12}
10^{11}
0° ORBITAL INCLINATION
30°
60°
90°
TERRESTRIAL TRAPPED ELECTRONS
(Ee> 0.5 MEV)
(1963.5 EPOCH)
DATA FROM REF 36 & 37
100
1000
10,000
100,000
Φ_{te} ~ INTEGRAL ELECTRON FLUX ~ (ELECTRONS > 0.5 MEV/CM^2-YEAR
h ~ Orbital Altitude ~ Kilometers

Figure 3-6

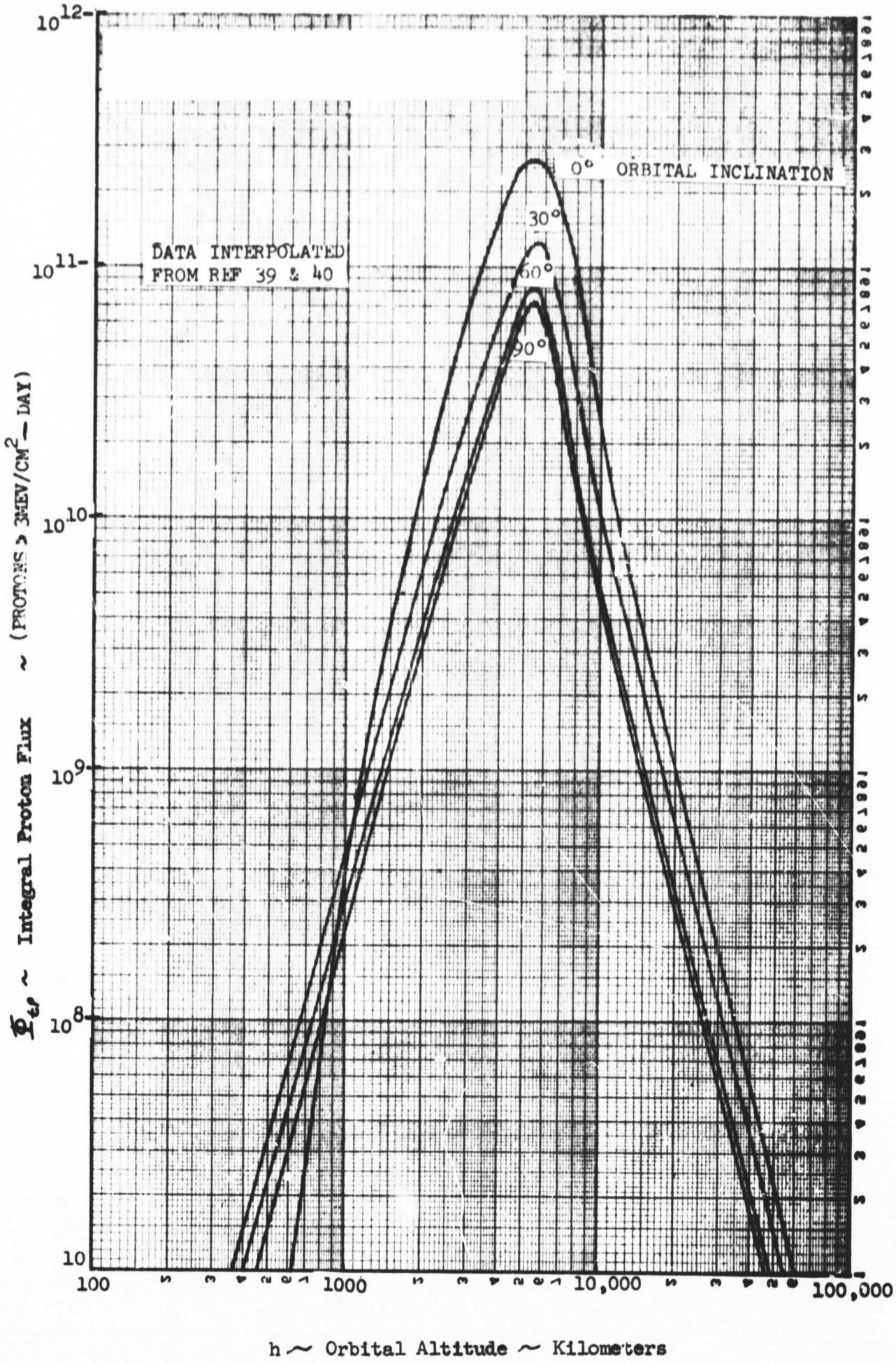

Figure 3-7 Terrestrial Trapped Protons (E_p > 3MEV)

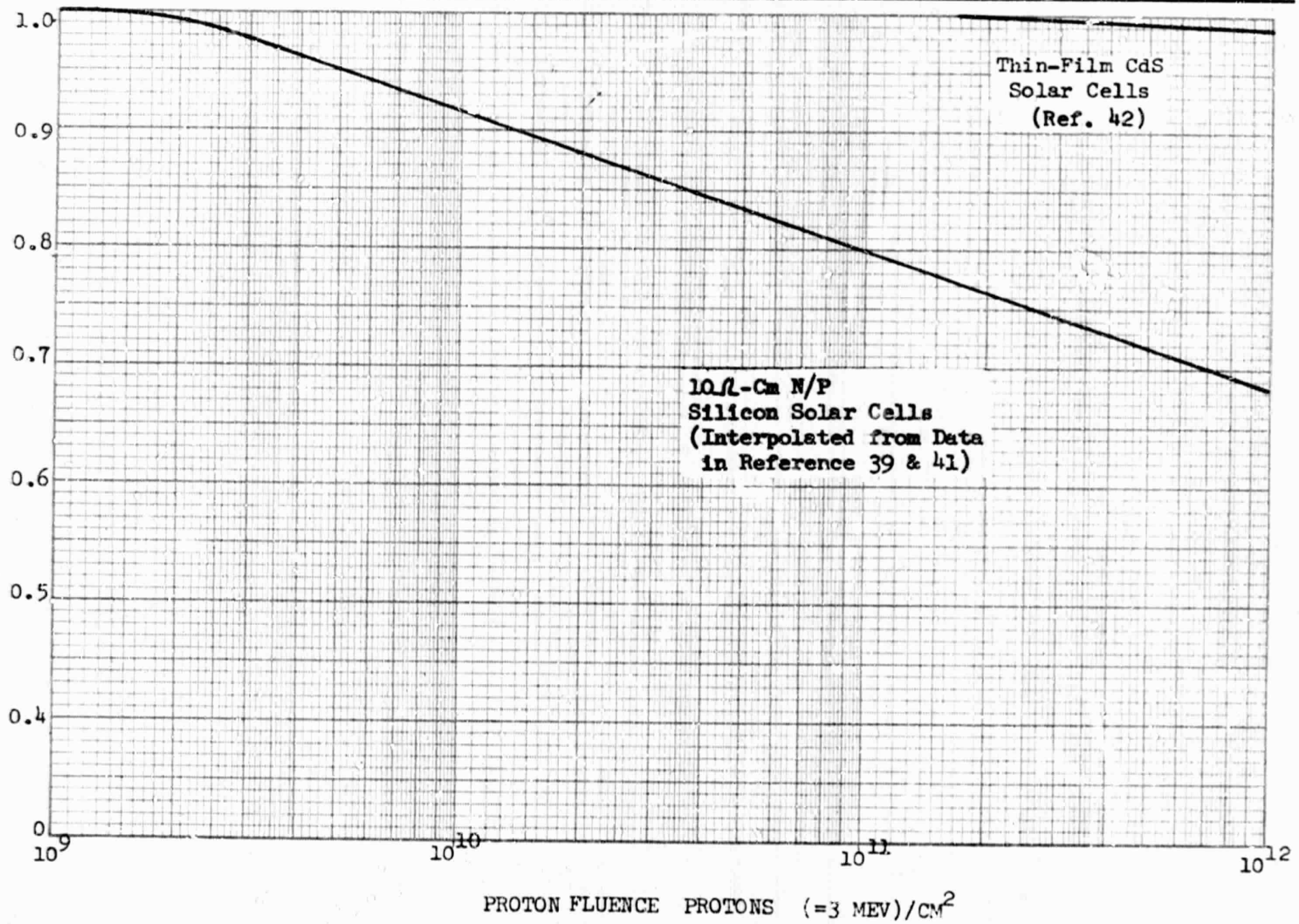

Figure 3-8 The Effect of Protons on Solar Cell Power Output

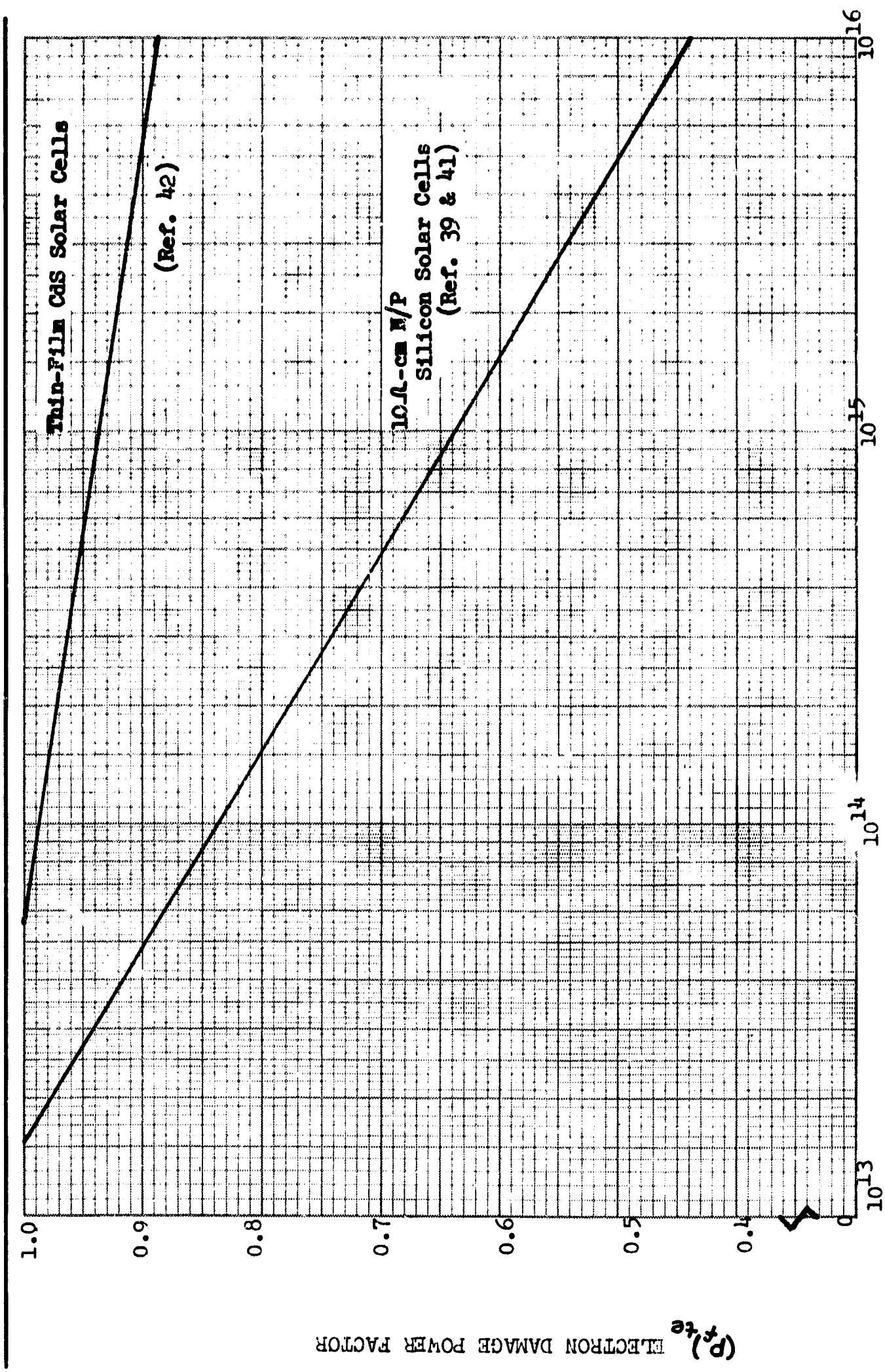

Figure 3-9 The Effect of Electrons on Solar Cell Power Output

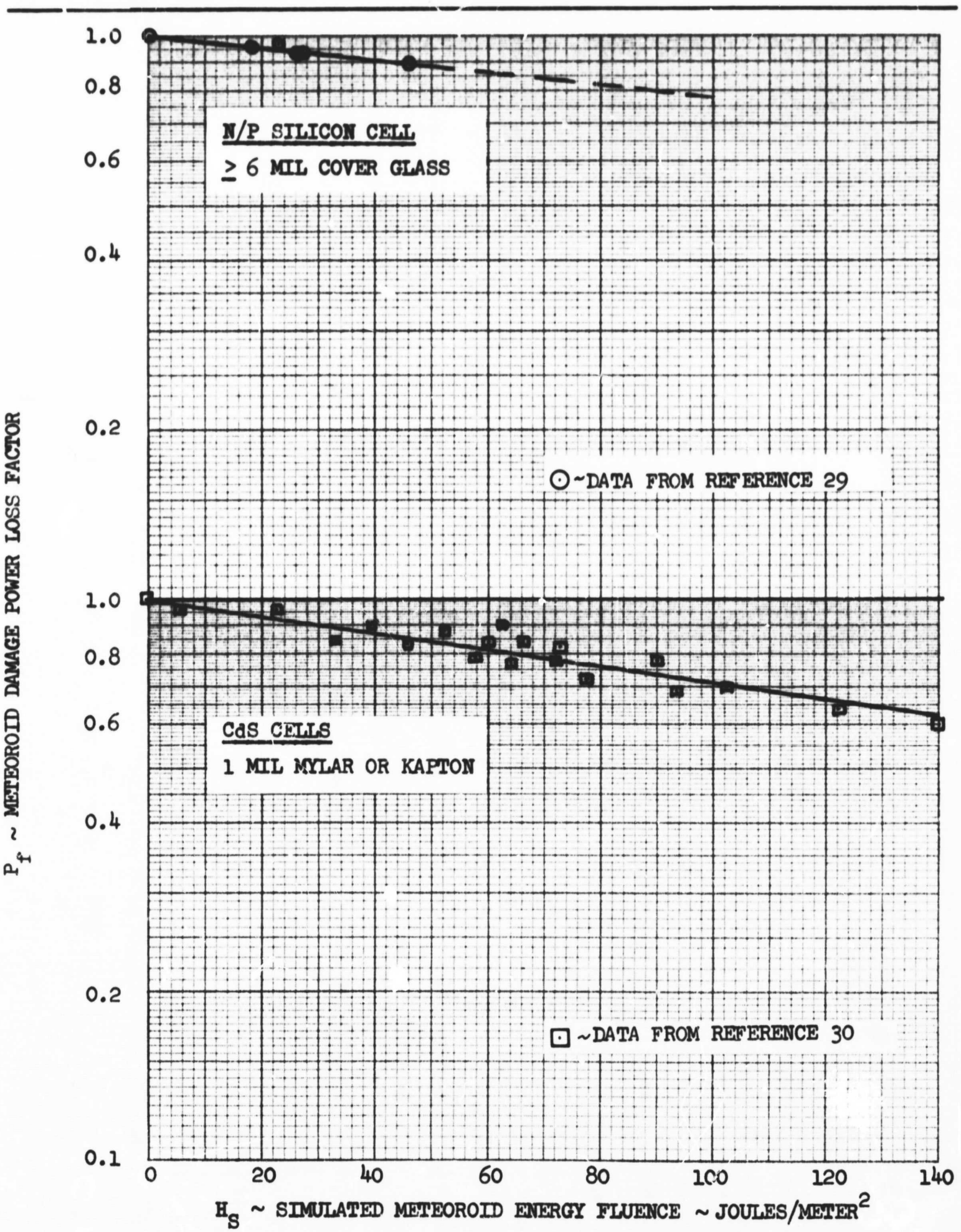

Figure 3-10 .- Simulated Meteoroid Damage to Solar Cells

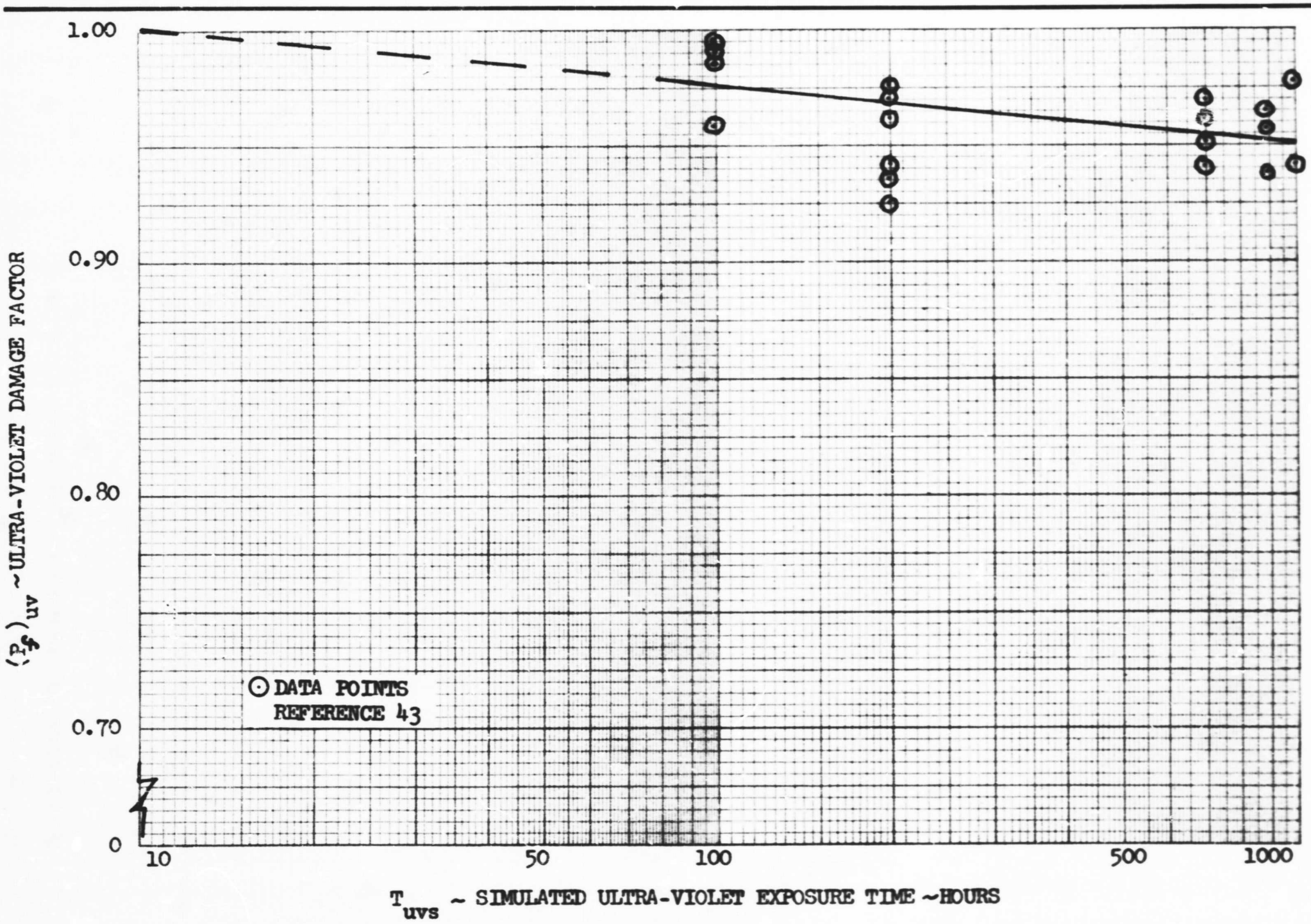

Figure 3-11 Ultra-Violet Exposure Damage to Silicon Solar Cells

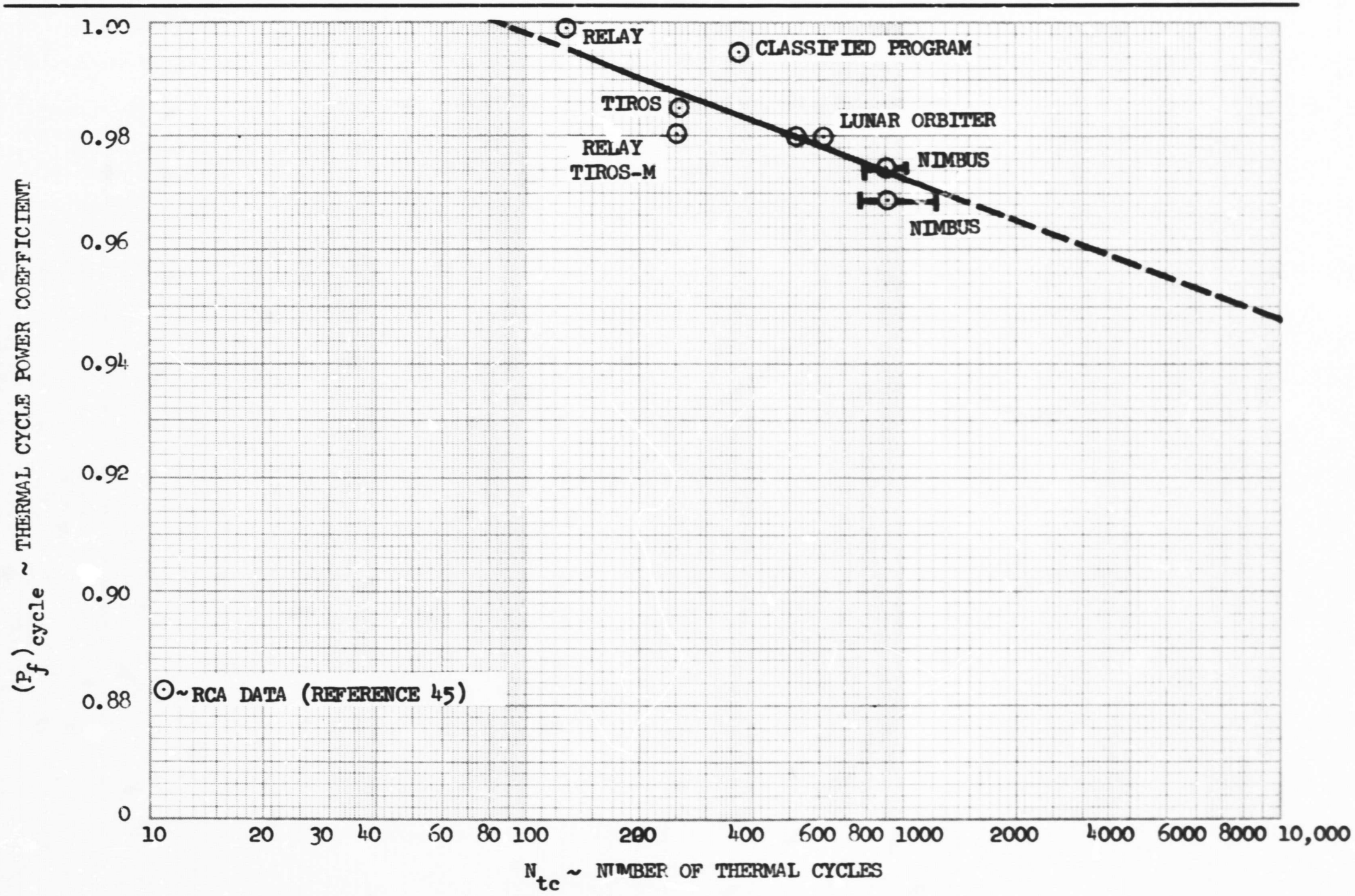

Figure 3-12 Thermal Cycle Induced Power Loss in Silicon Solar Cells

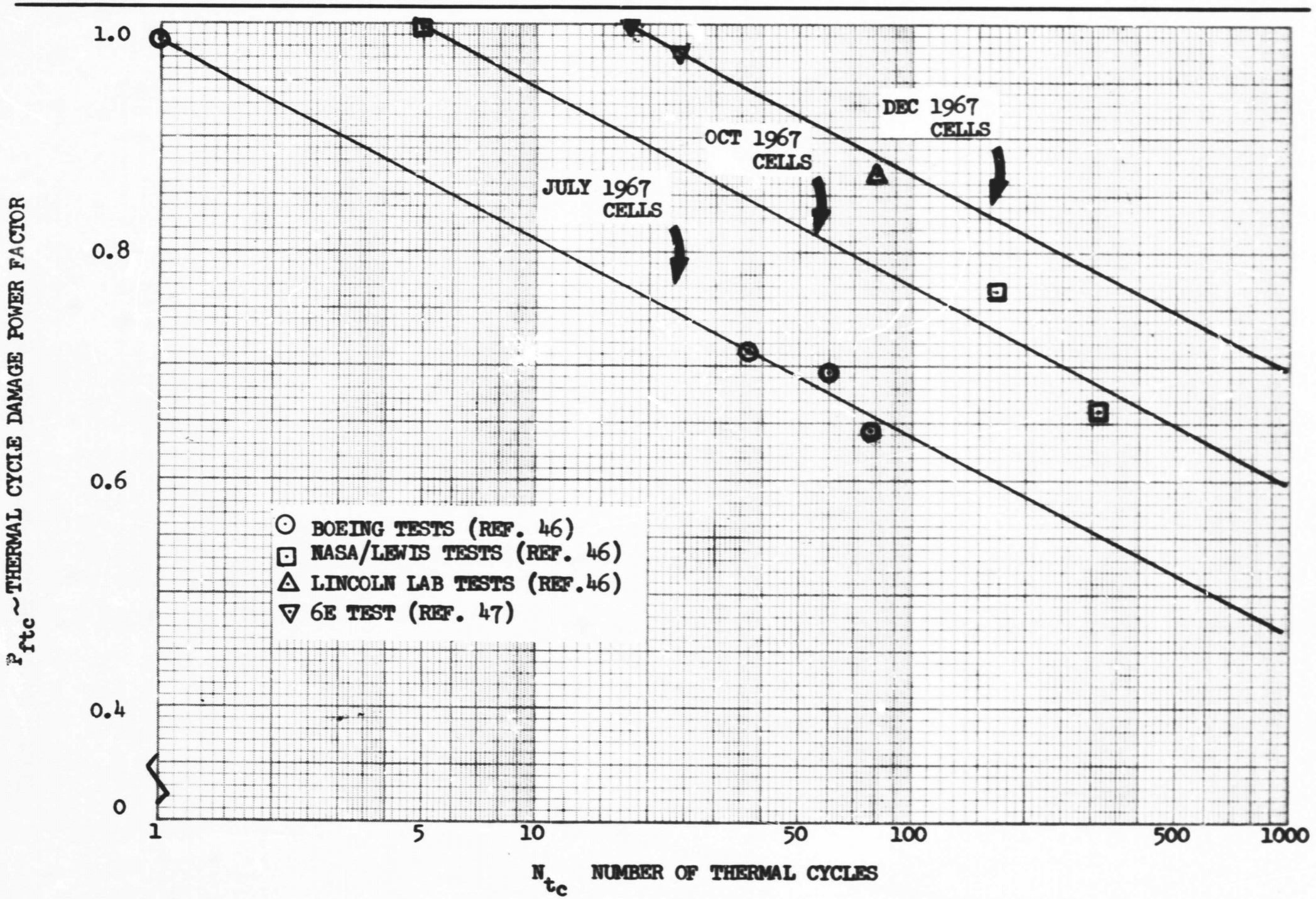

Figure 3-13 Thermal Cycle Induced Power Loss in Thin-Film CdS Solar Cells

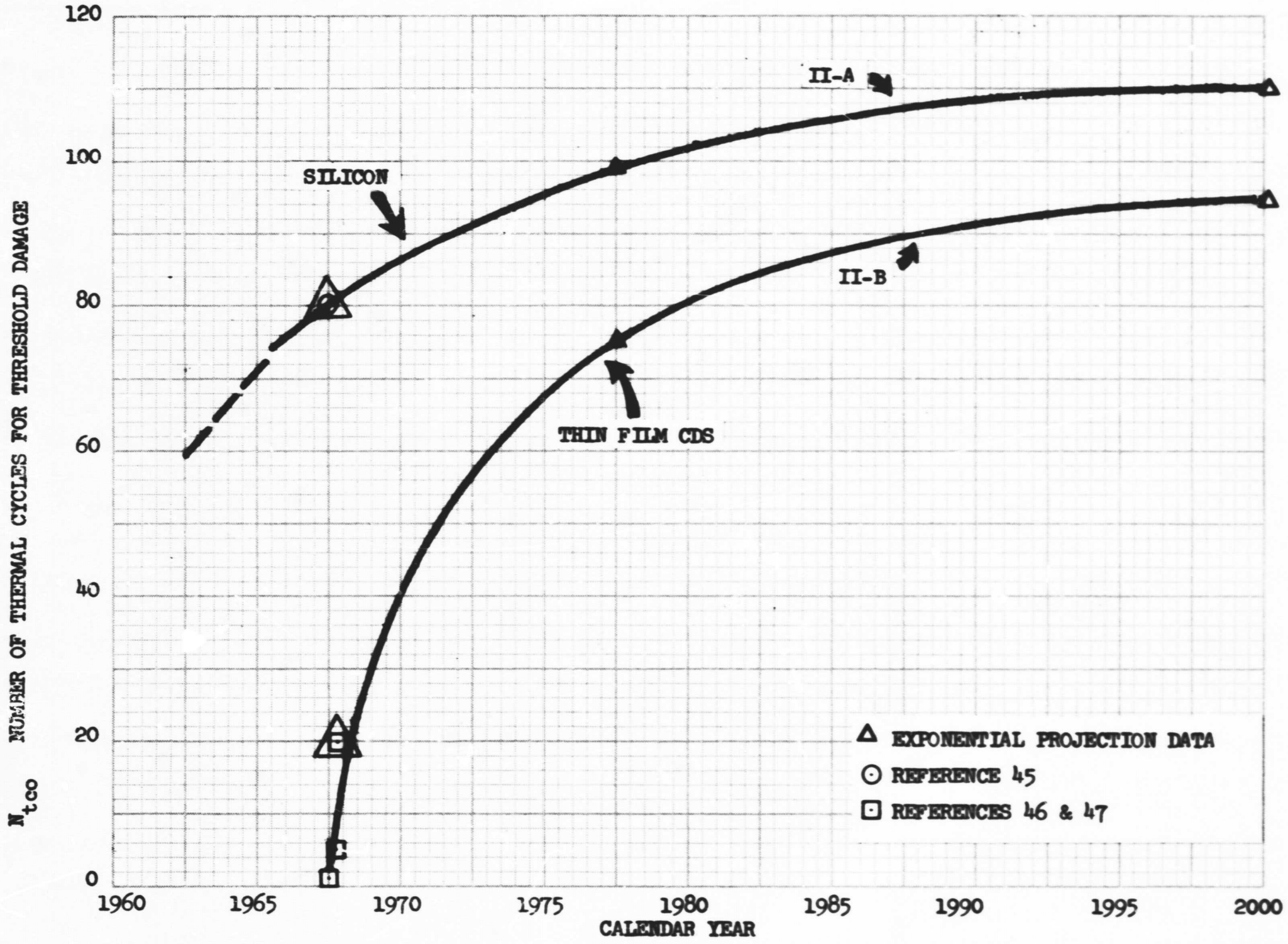

Figure 3-14 Projection Thermal Cycle Threshold Damage for Solar Cells

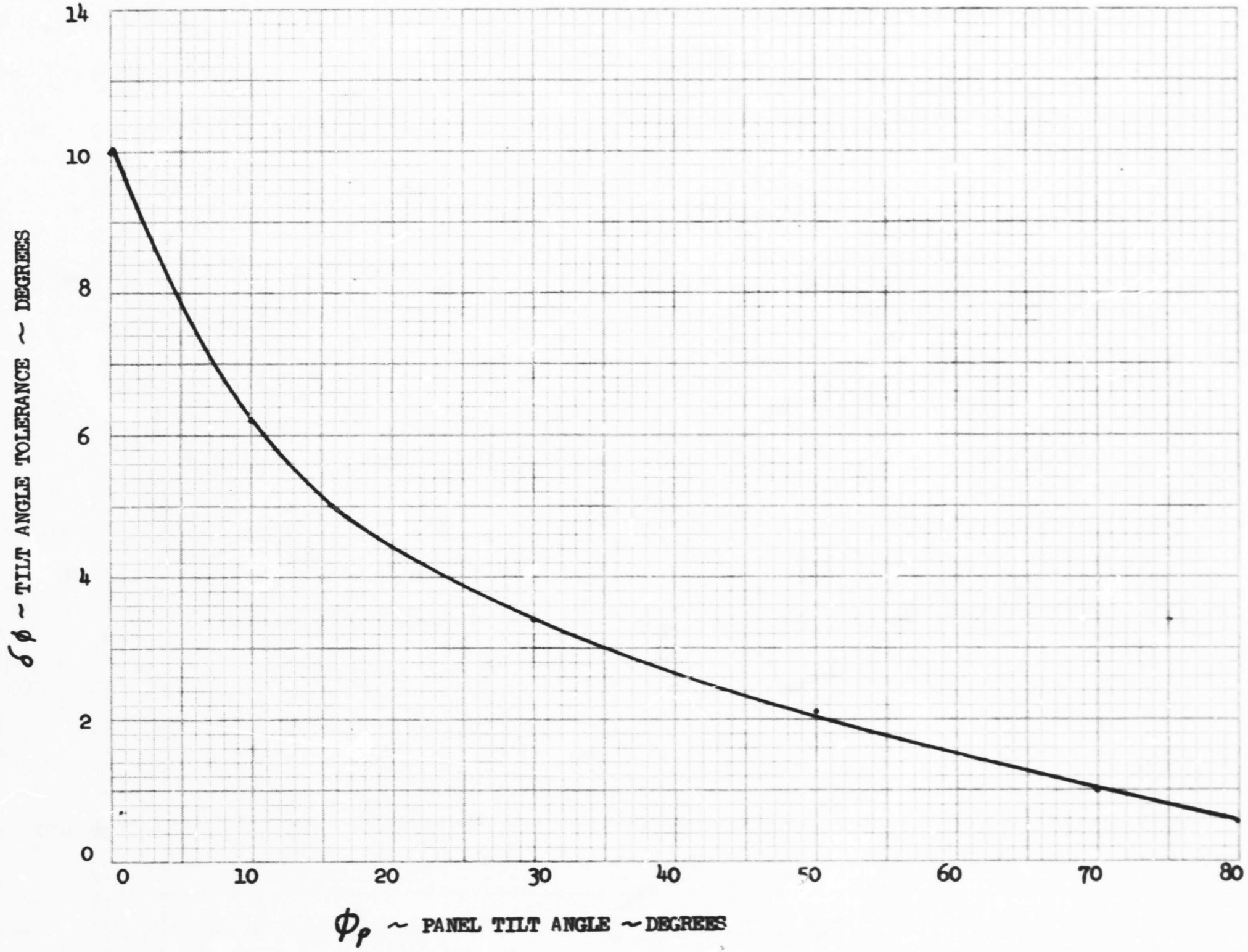

Figure 3-15 Solar Cell Panel Tilt Angle Tolerance Levels

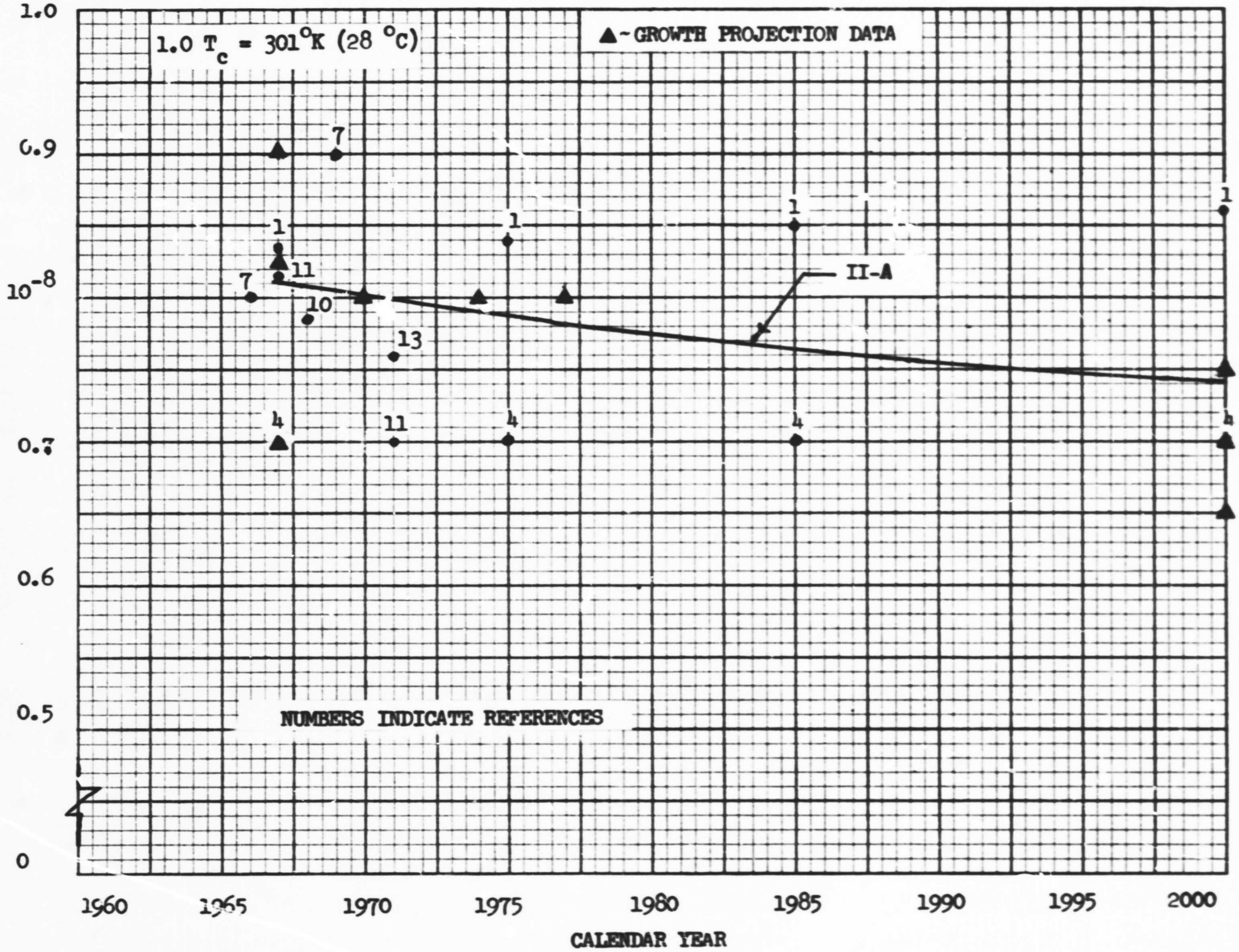

Figure 3-16 Projection ~ Array Absorptivity (Cell-Side) ~ Silicon Solar Cells

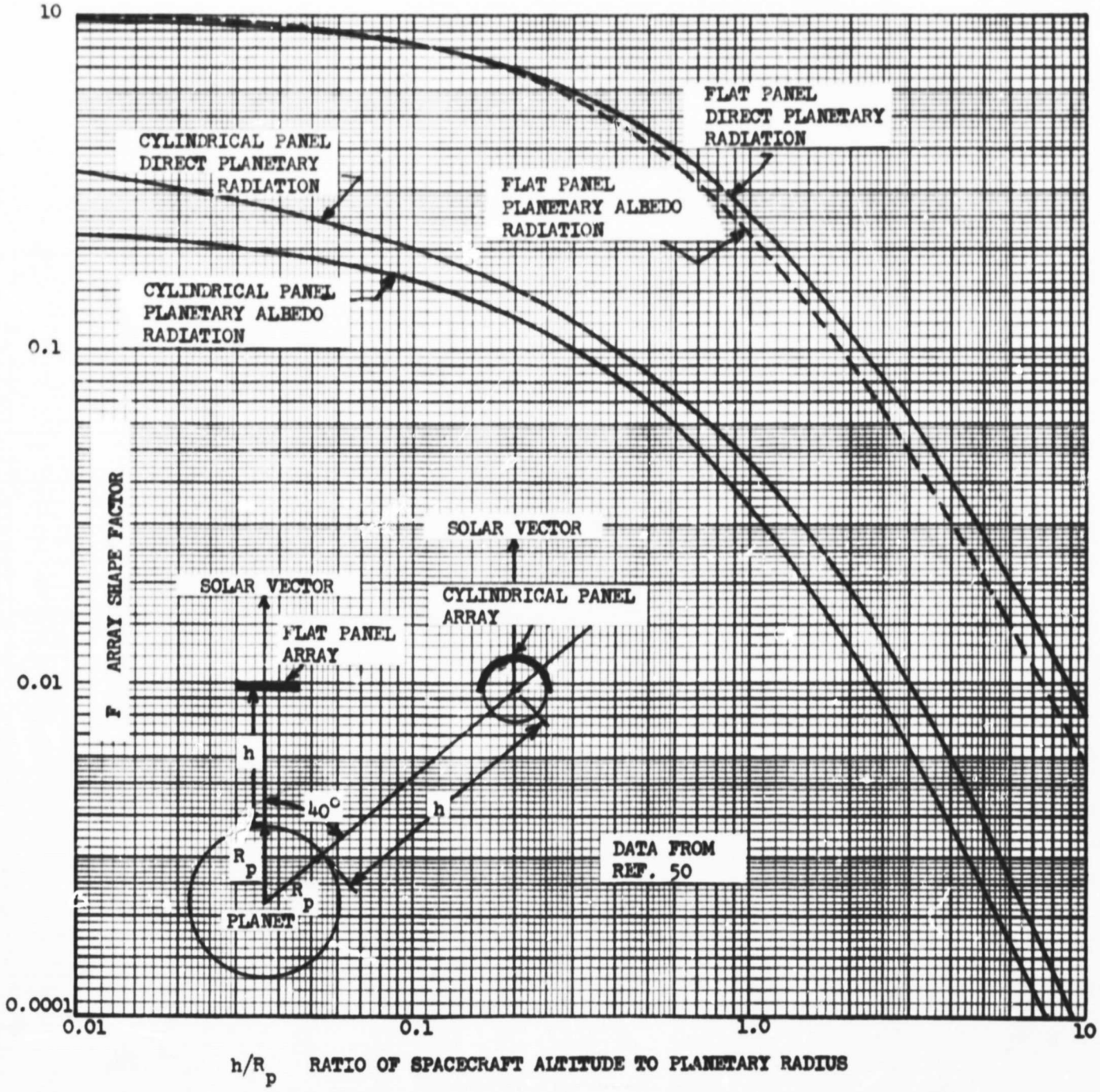

Figure 3-17 Array Shape Factors for Planetary Radiation

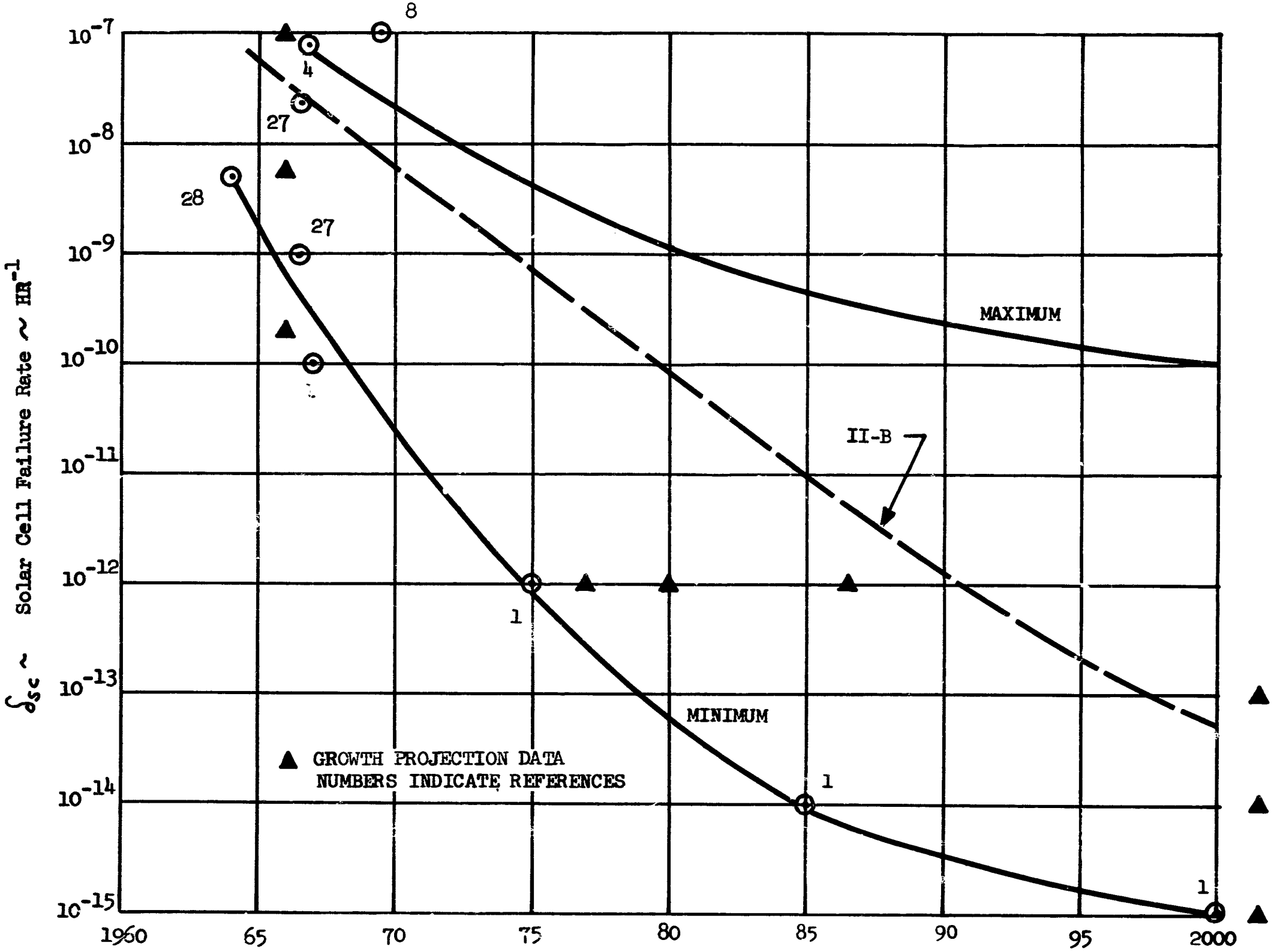

Figure 3-18 Projection -- Silicon Solar Cell Failure Rates

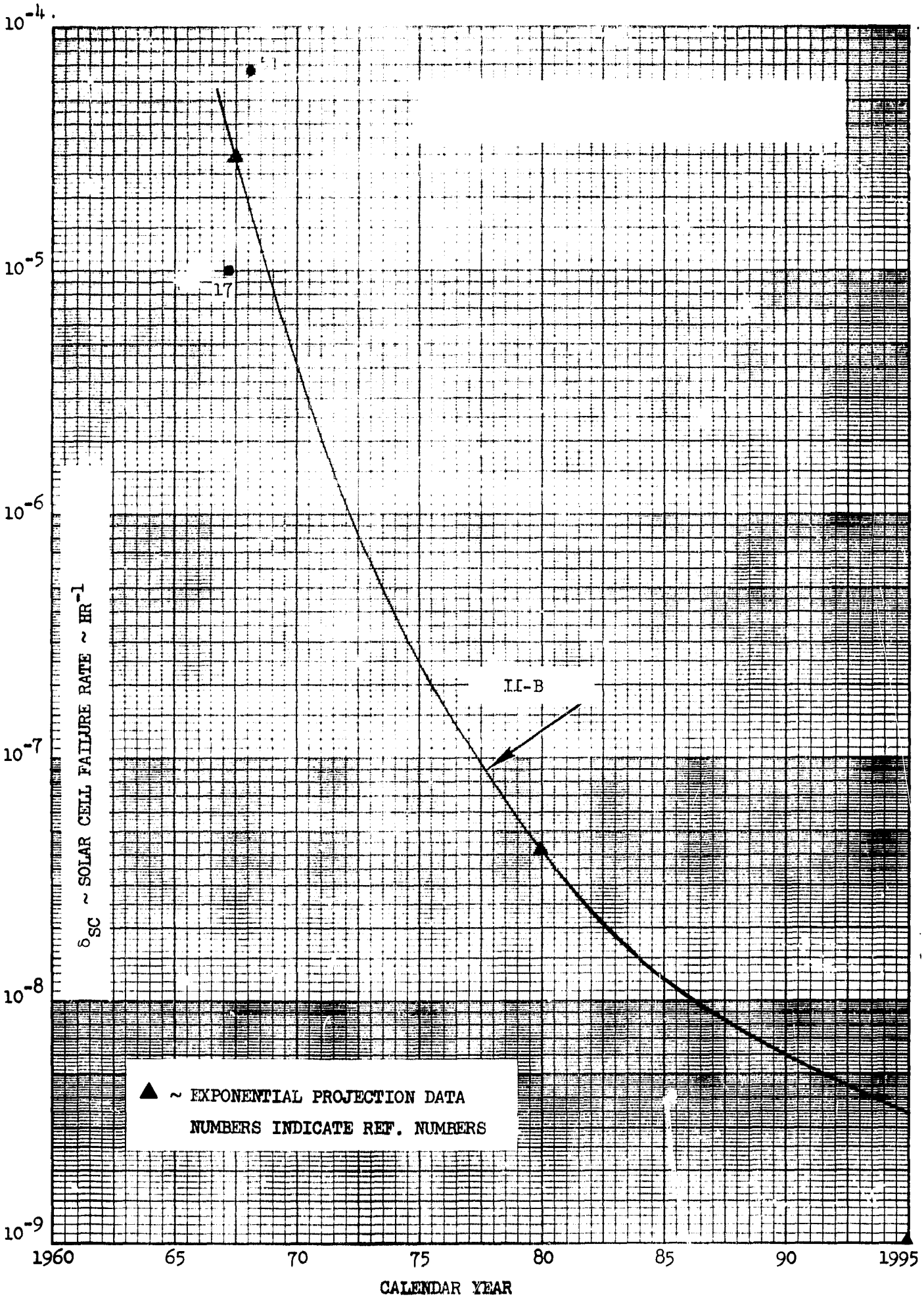

Figure 3-19 Thin Film Solar Cell Failure Rates

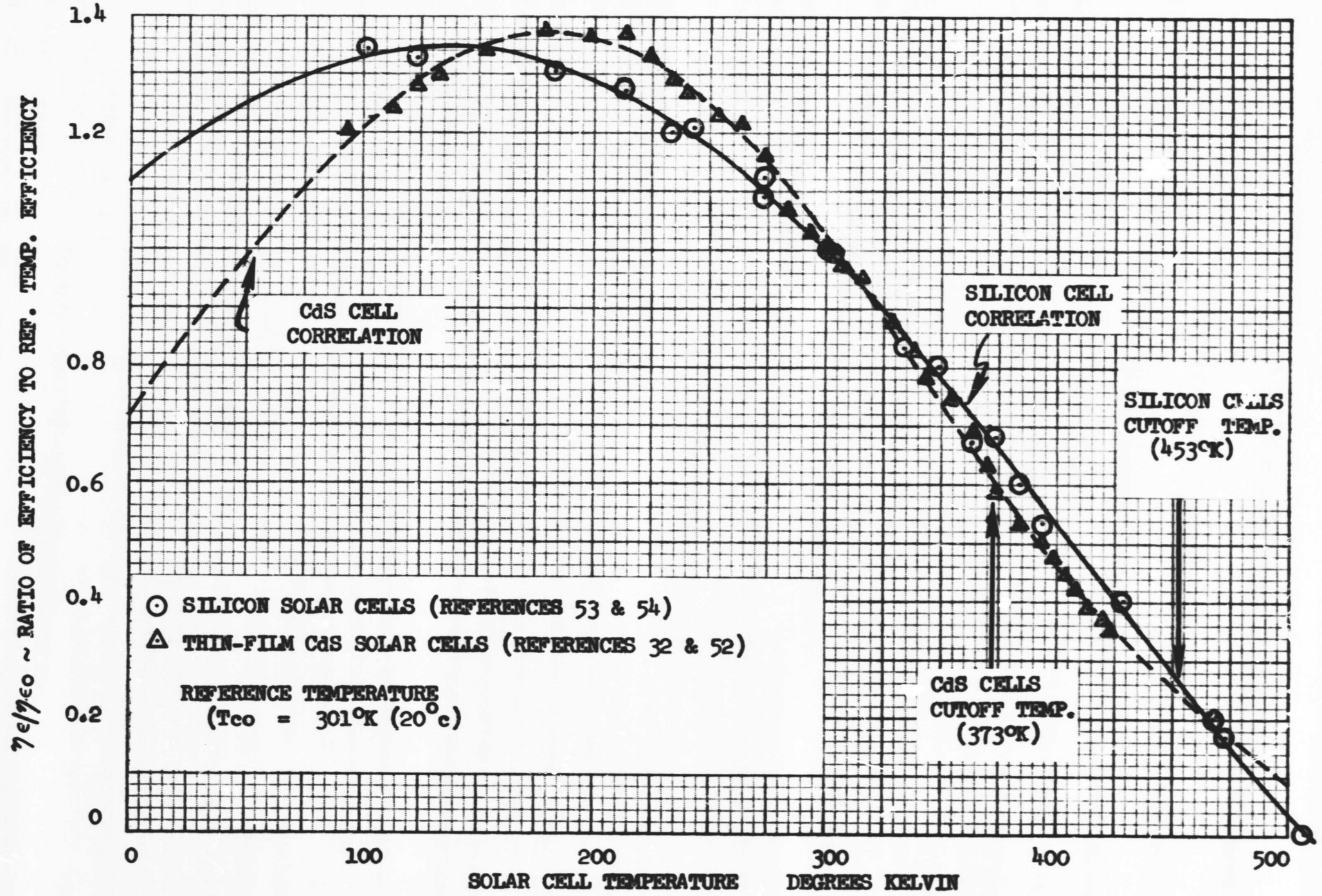

Figure 3-20 The Effect of Cell Temperature on Solar Cell Efficiency

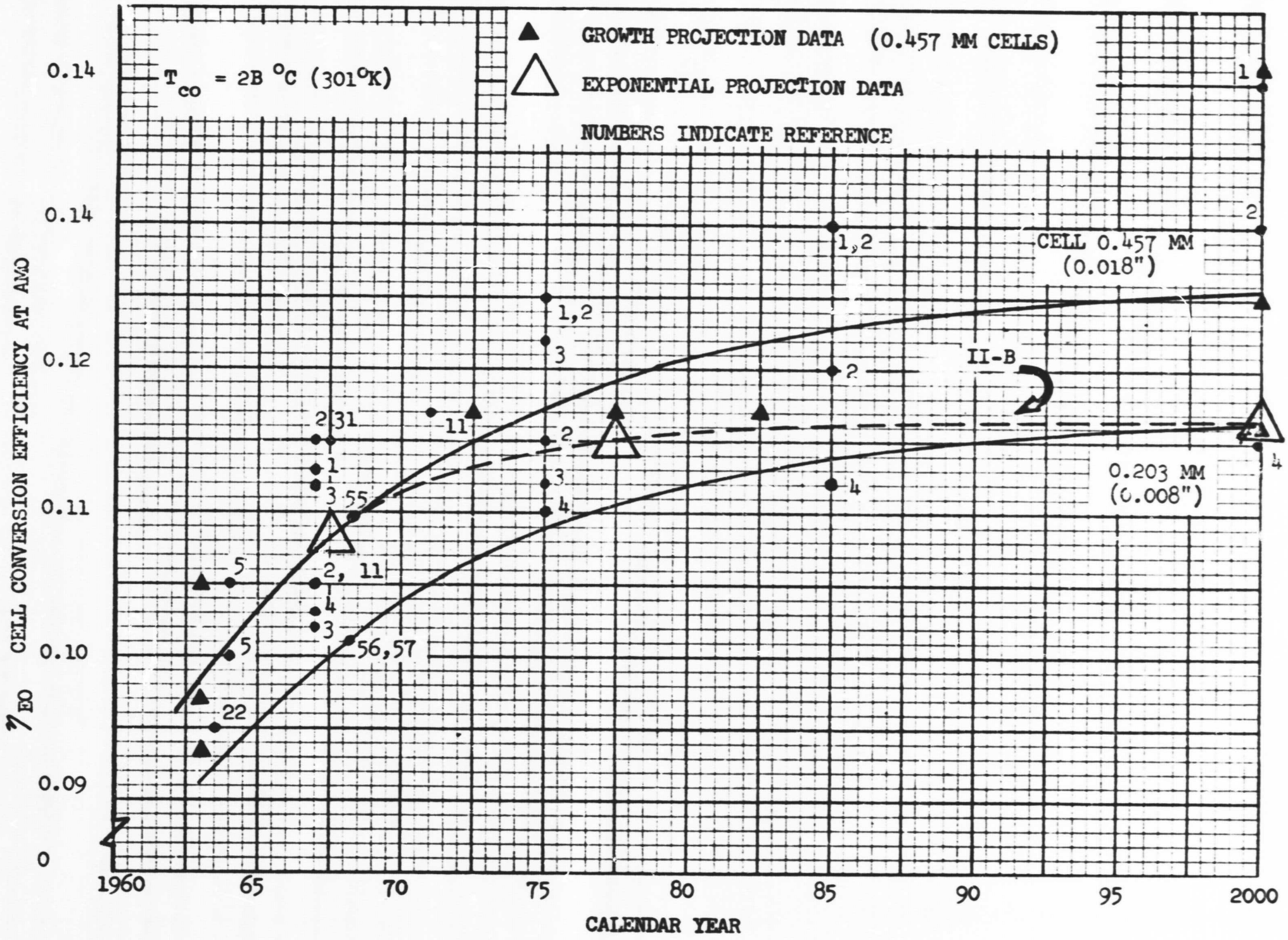

Figure 3-21 Projection -- Silicon Solar Cell Conversion Efficiency

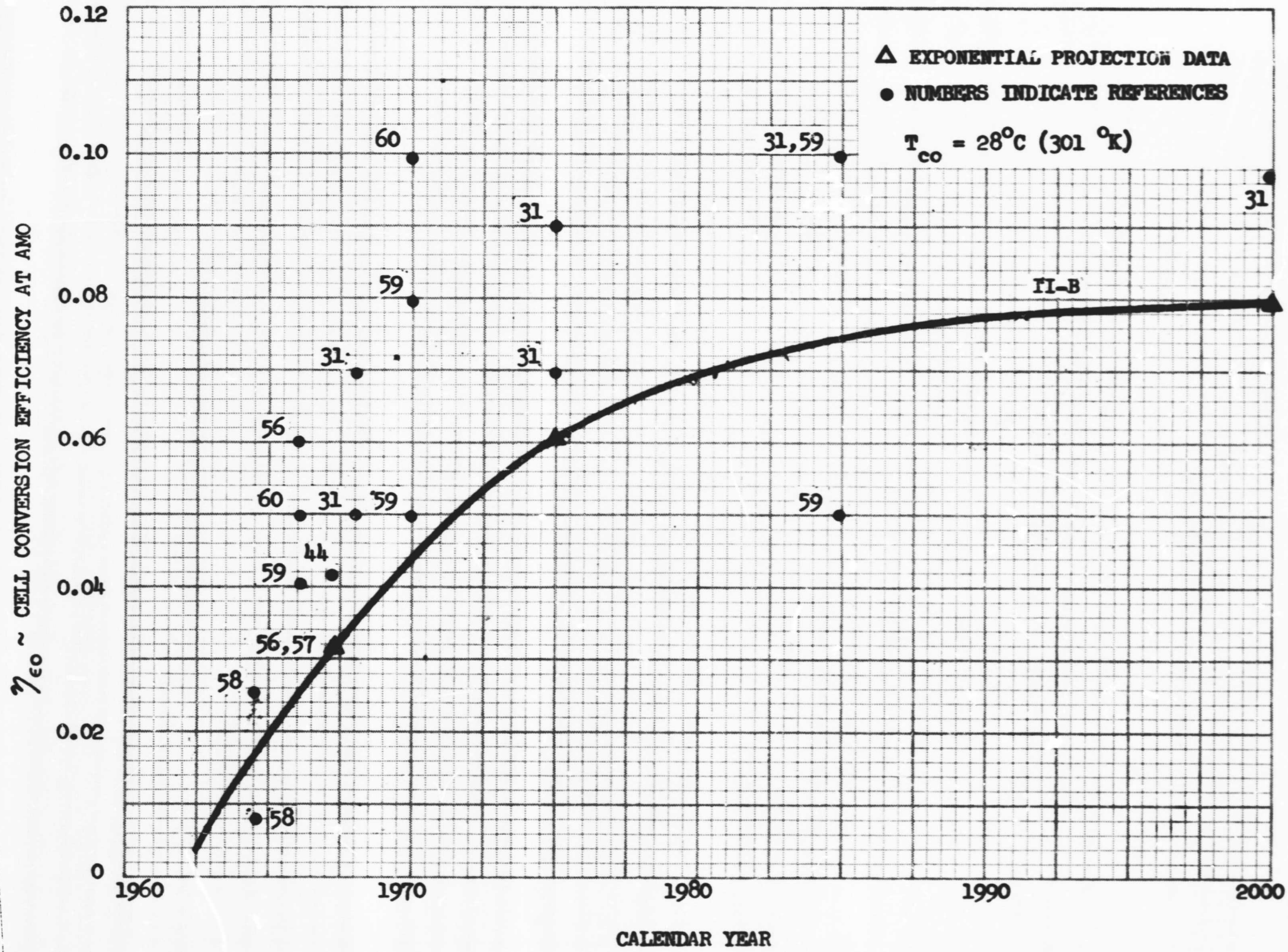

Figure 3-22 Projection - Thin-Film CdS Solar Cell Conversion Efficiency

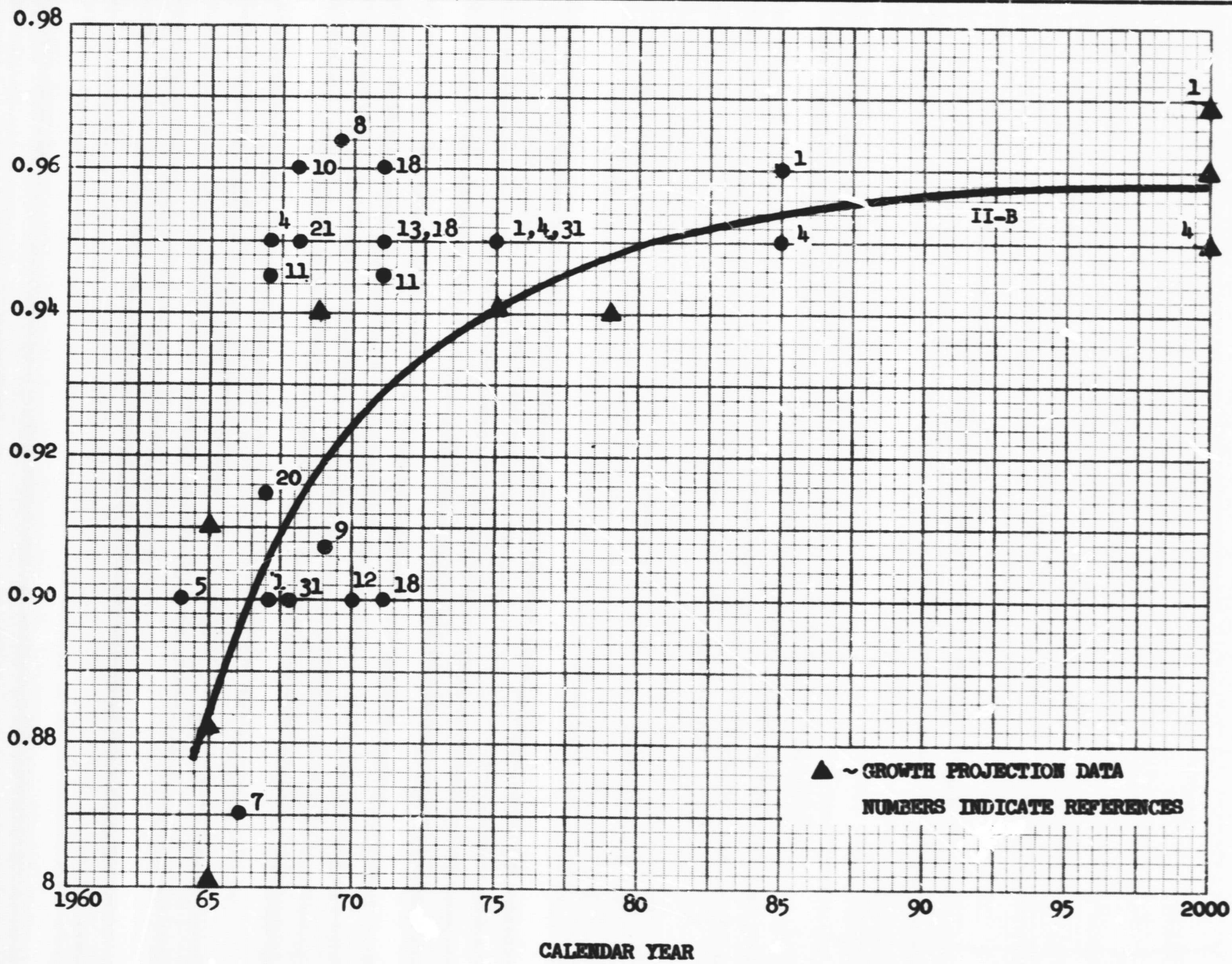

Figure 3-23 Projection -- Silicon Solar Cell Packing Factors

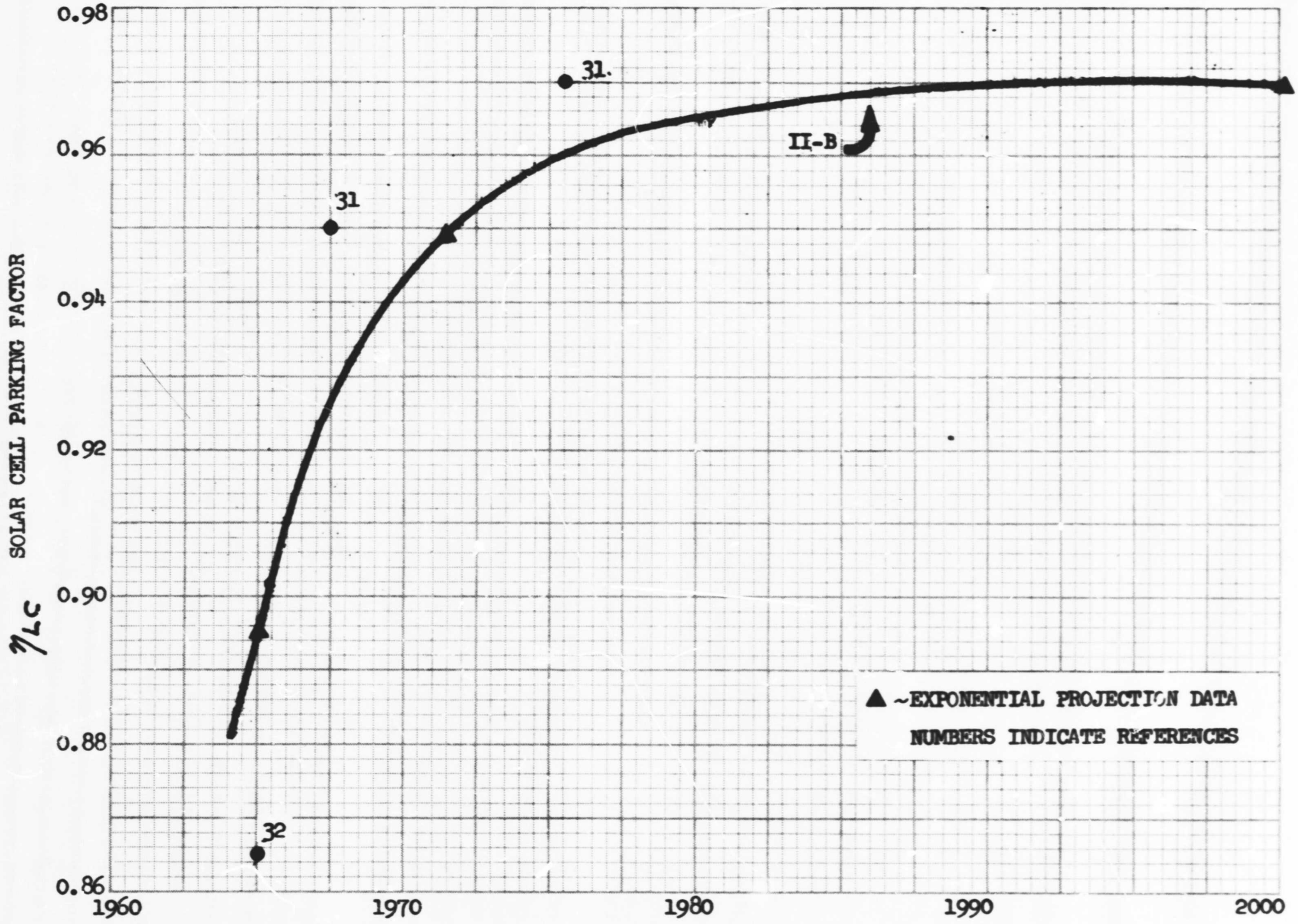

Figure 3-24 Projection - Thin Film CdS Solar Cell Packing Factors

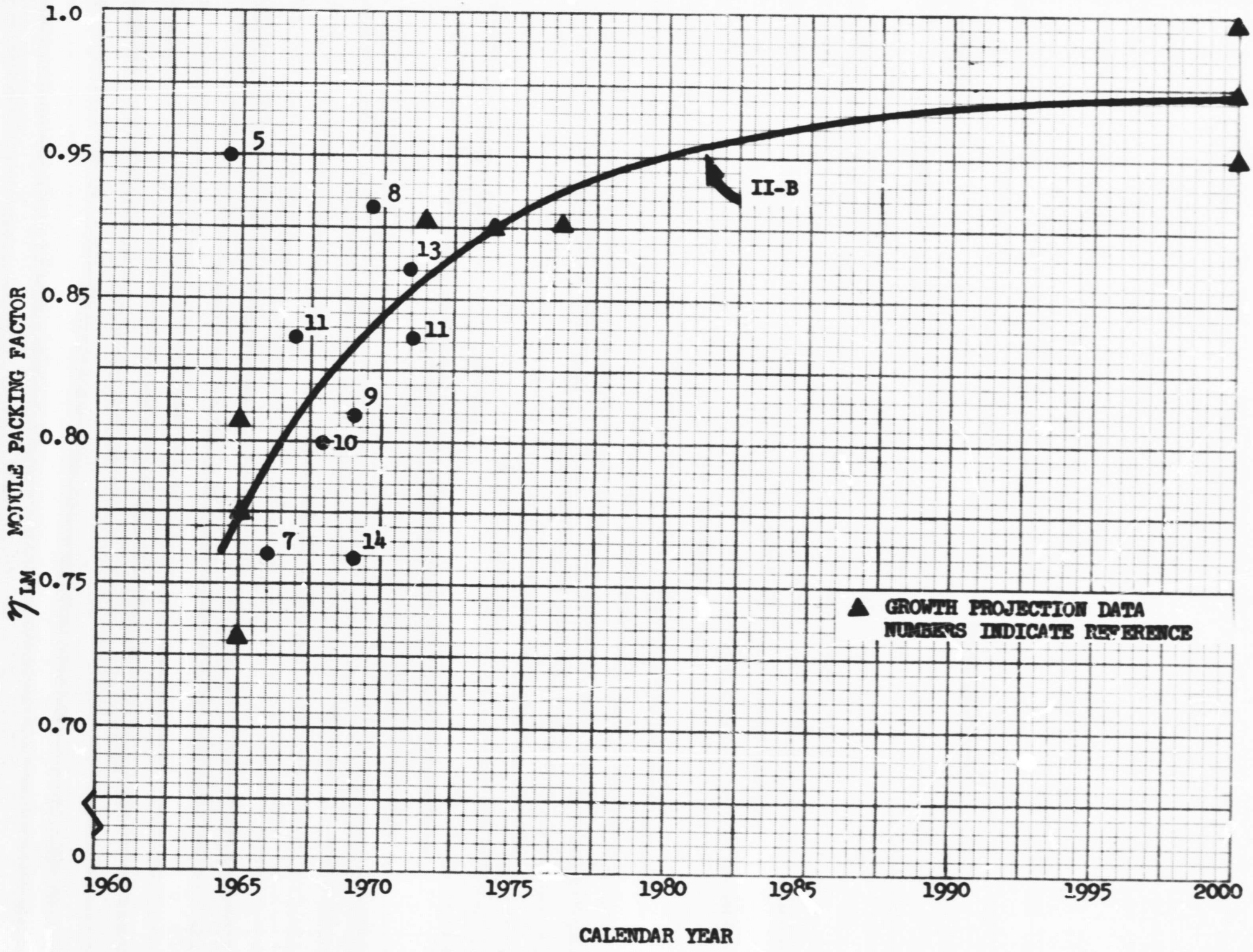

Figure 3-25 Projection - Silicon Solar Cell Module Packing Factors

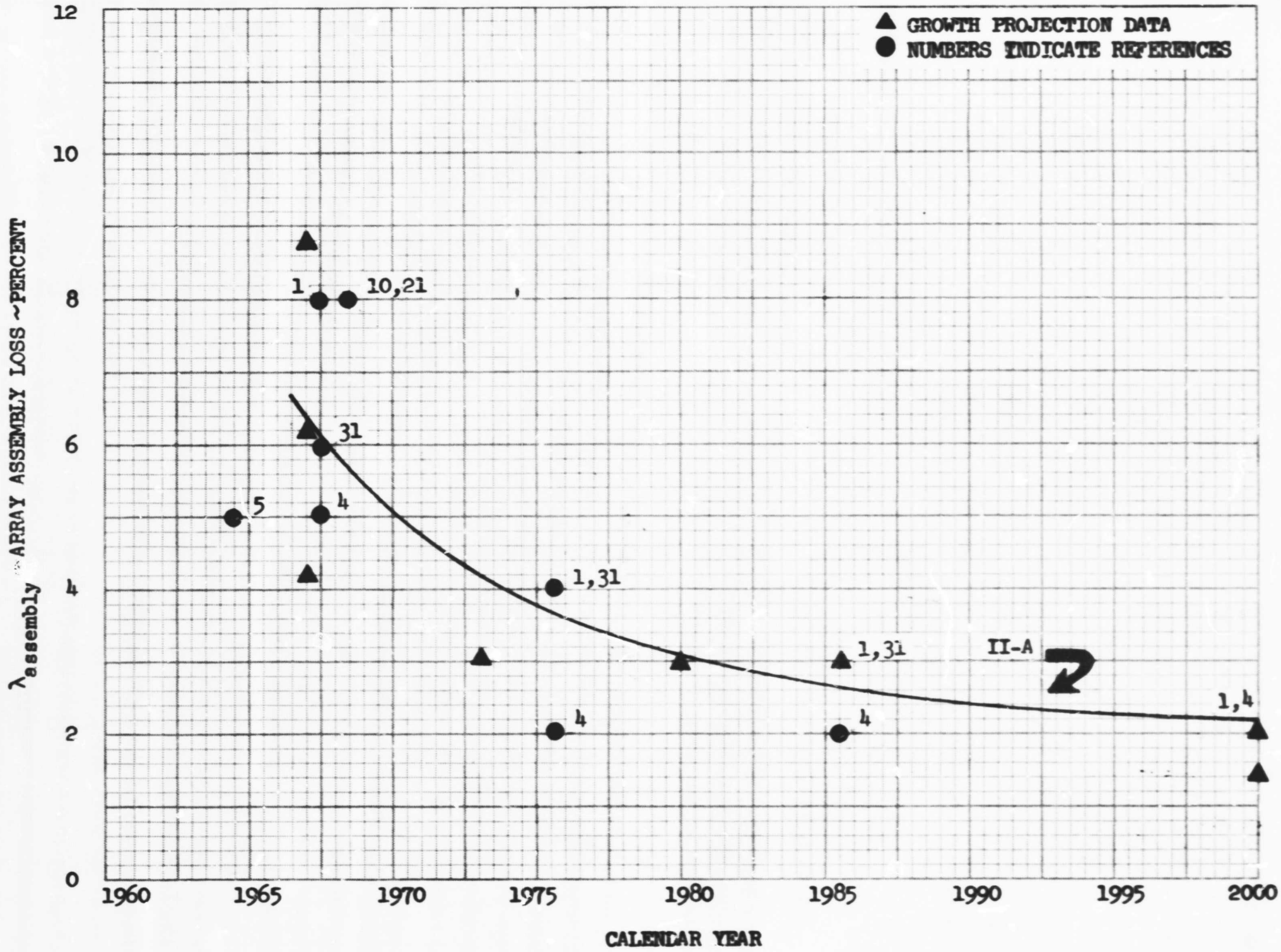

Figure 3-26 Projection - Assembly Loss Factor, Silicon Solar Cell Arrays

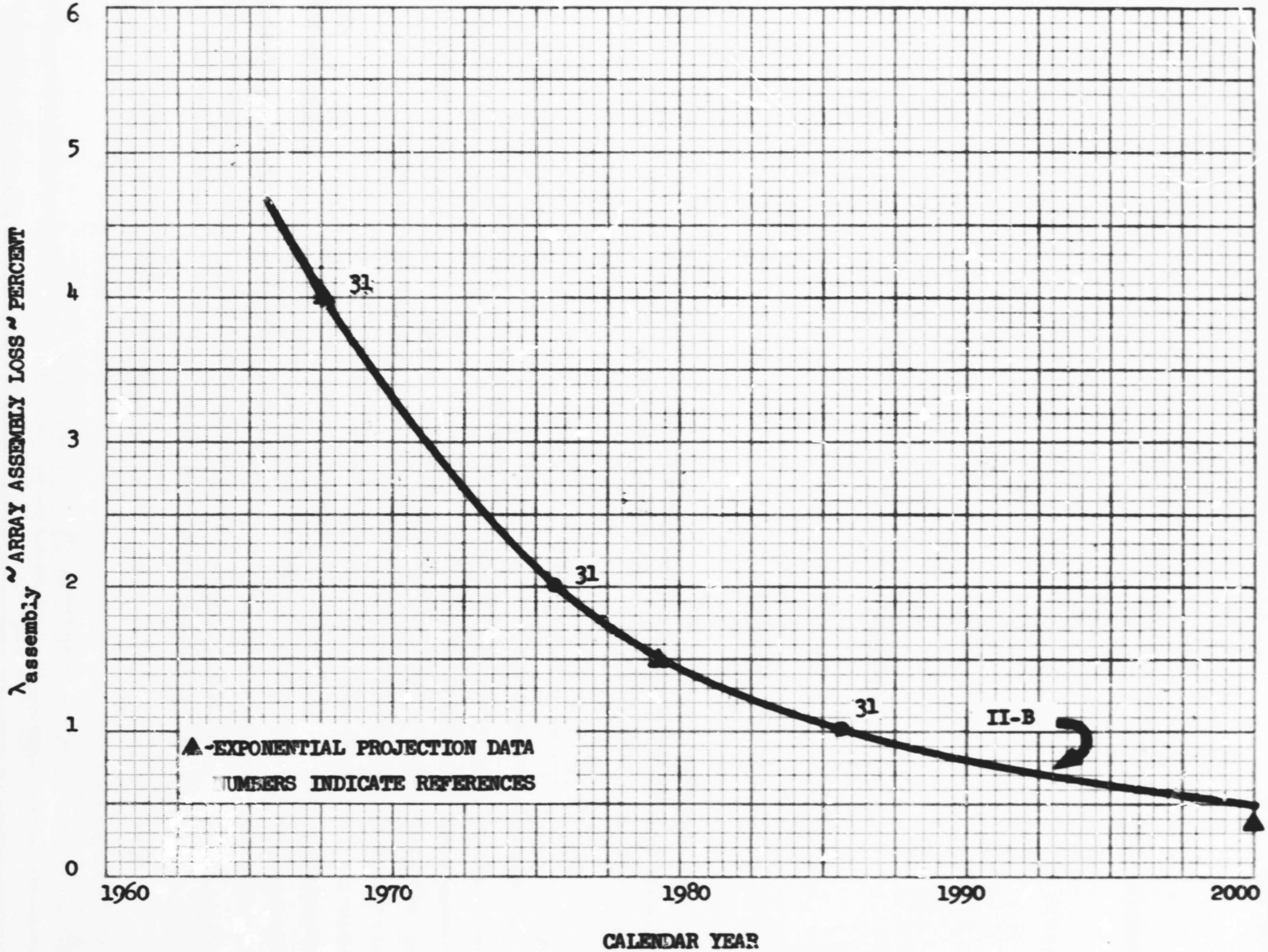

Figure 3-27 Projection - Assembly Loss Factor, Thin-Film CdS Solar Cell Arrays

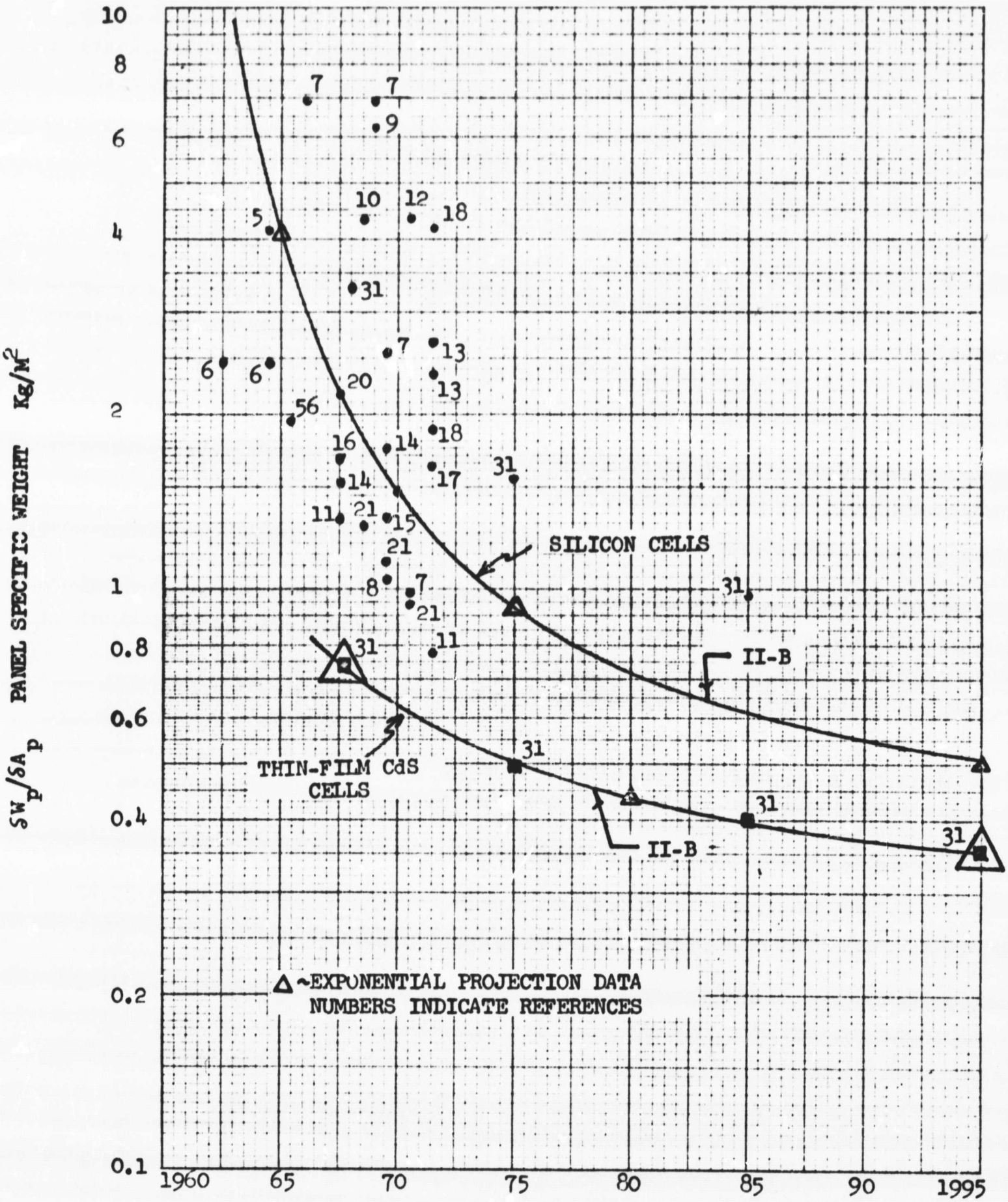

Figure 3-28 Projection -- Panel Specific Weight -- Thin-Film Cadmium Sulfide and Silicon Solar Cells

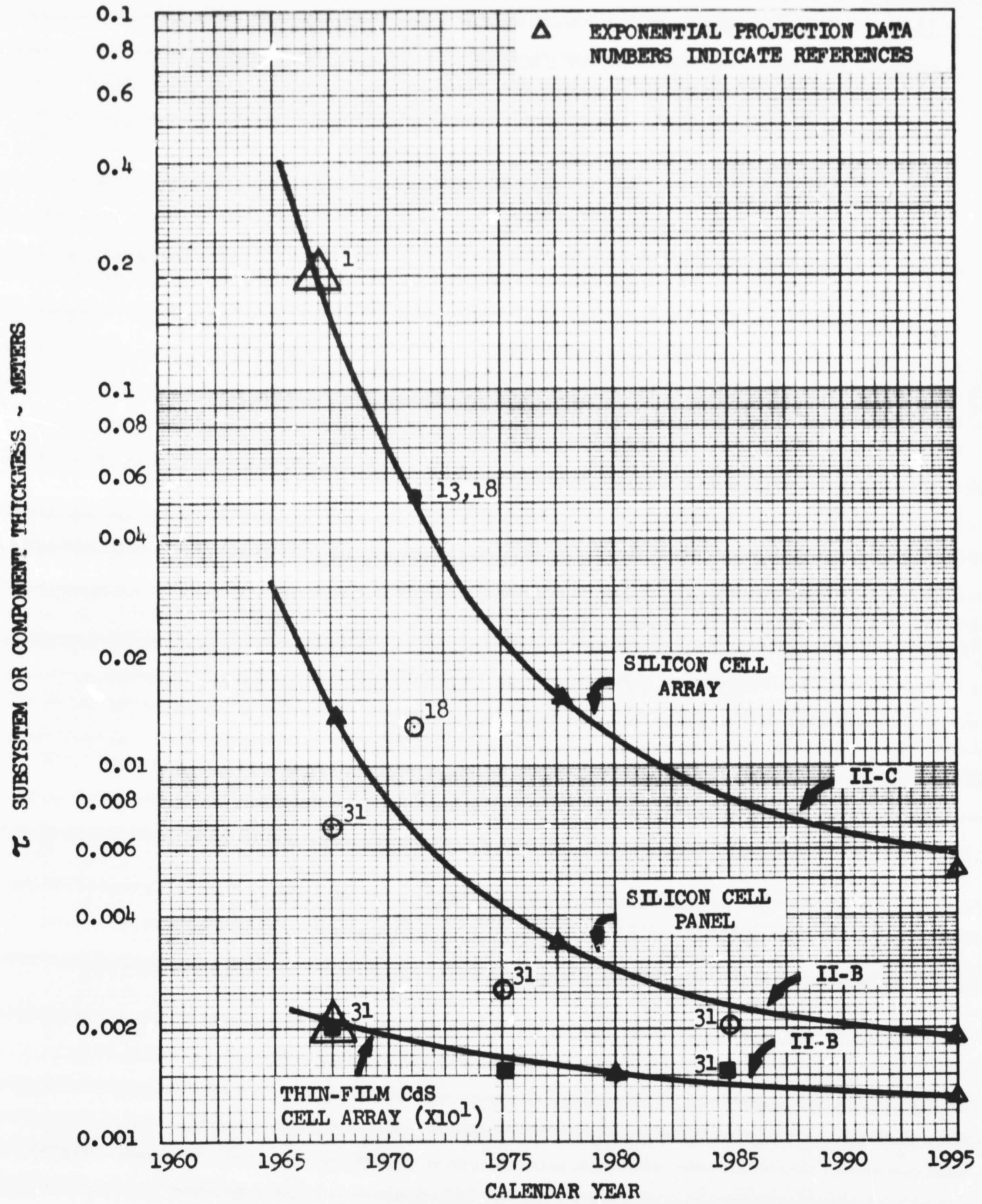

Figure 3-29 Projection - Solar Cell Array Thicknesses

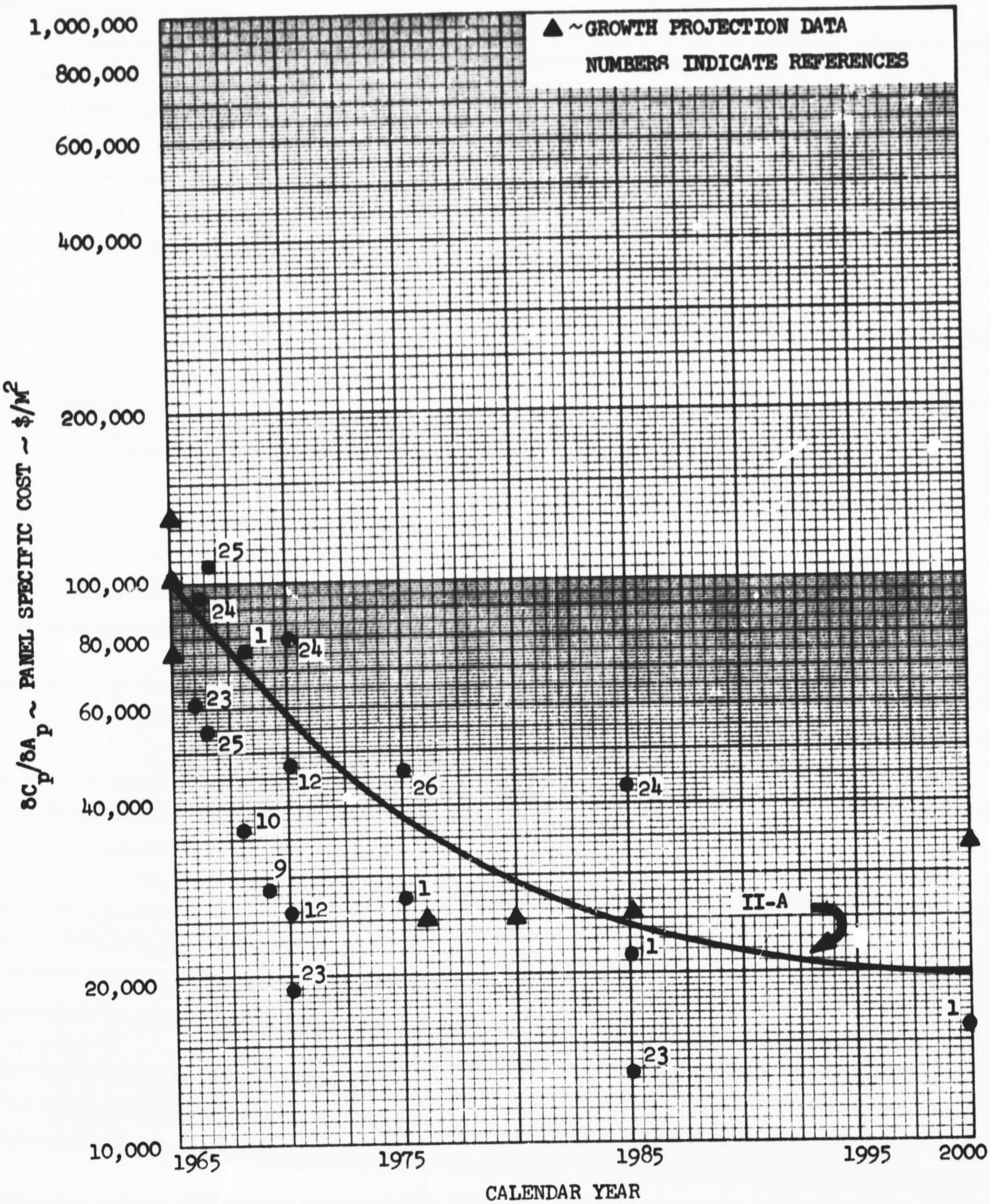

Figure 3-30 Projection - Silicon Solar Cell Panel Costs

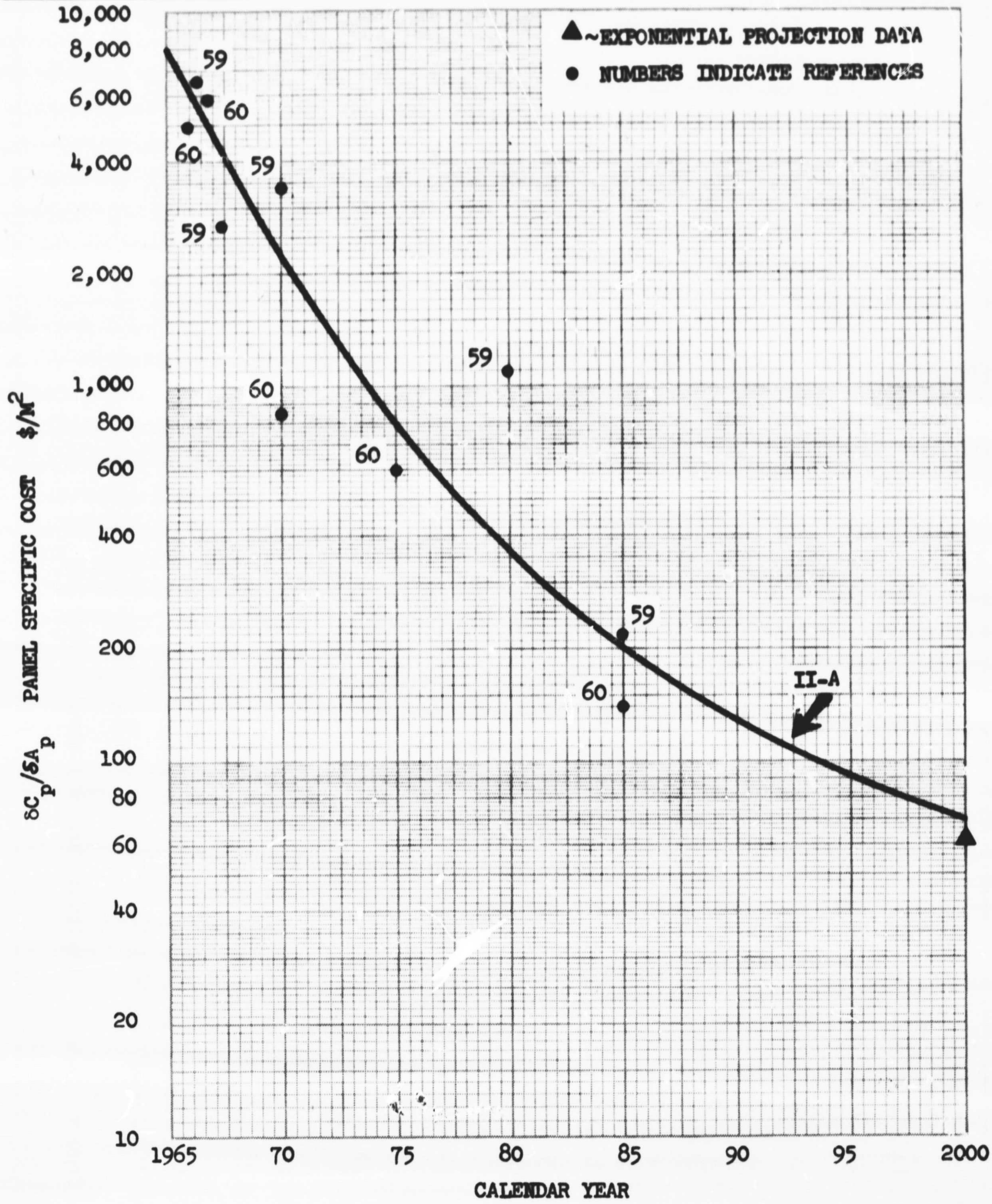

Figure 3-31 Projection Thin Film CdS Solar Cell Panel Costs

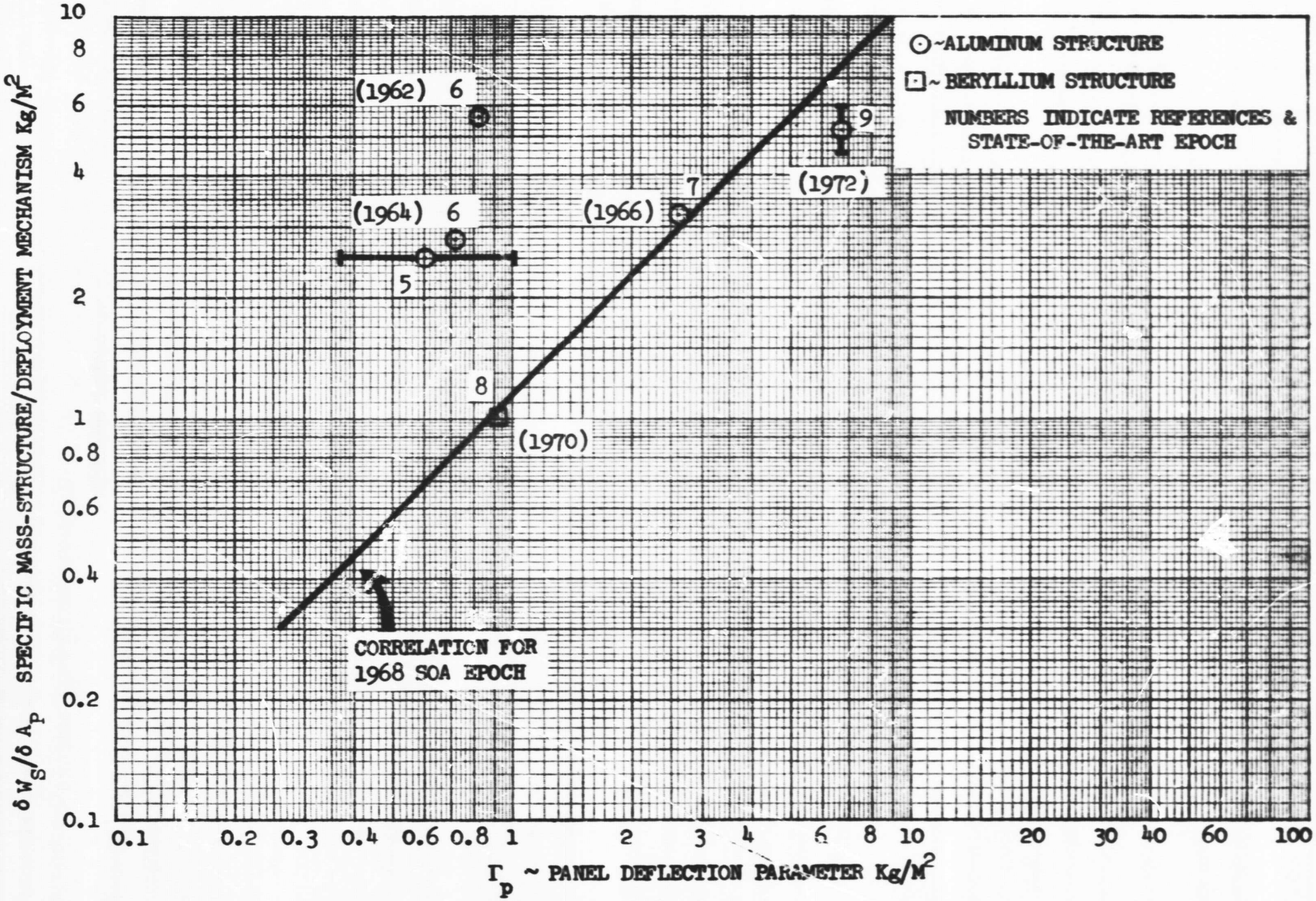

Figure 3-32 Structure and Deployment Mechanisms

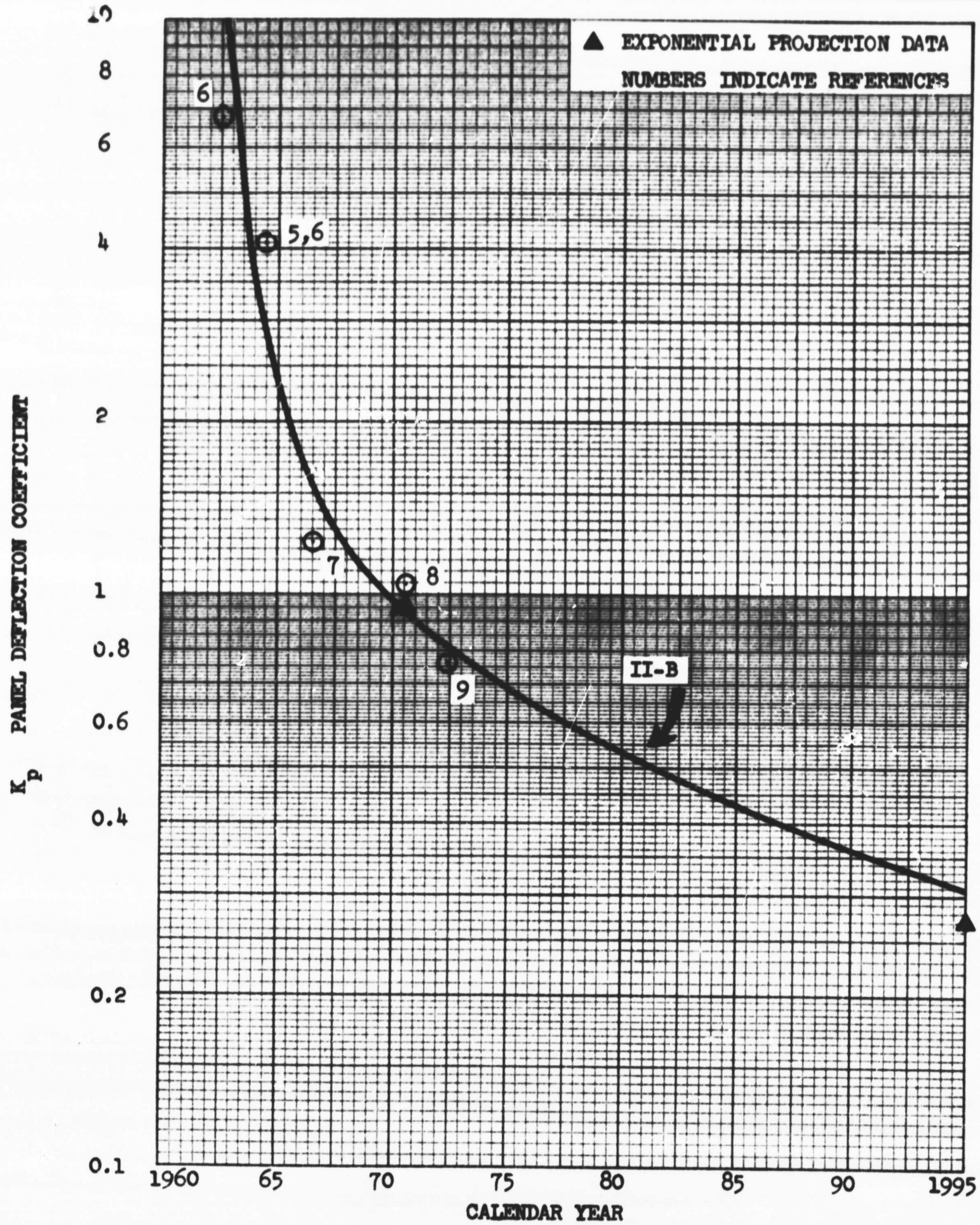

Figure 3-33 Solar Cell Arrays -- Panel Deflection Coefficient Projection

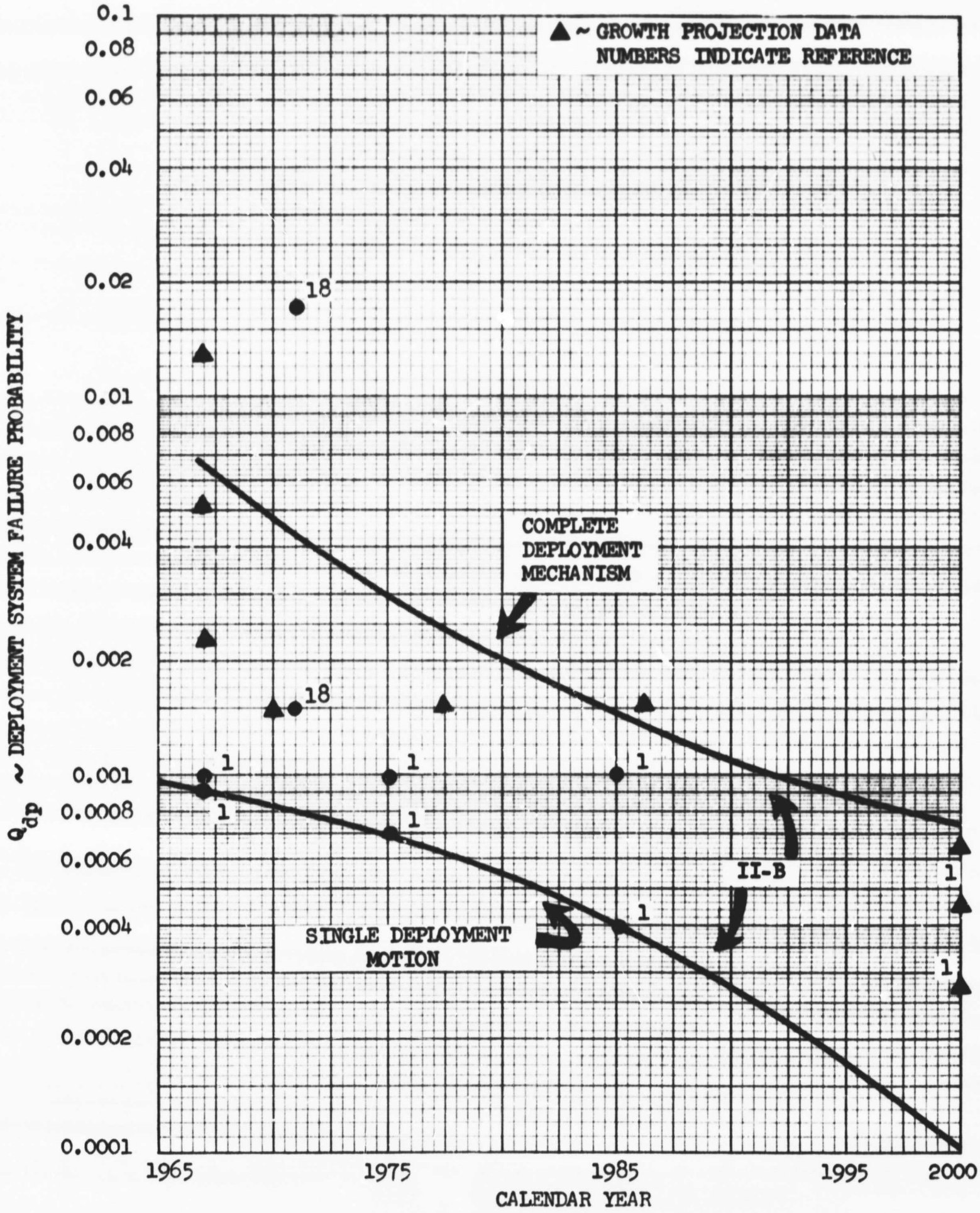

Figure 3-34 - Projection - Solar Cell Array Deployment Mechanism Failure Probability

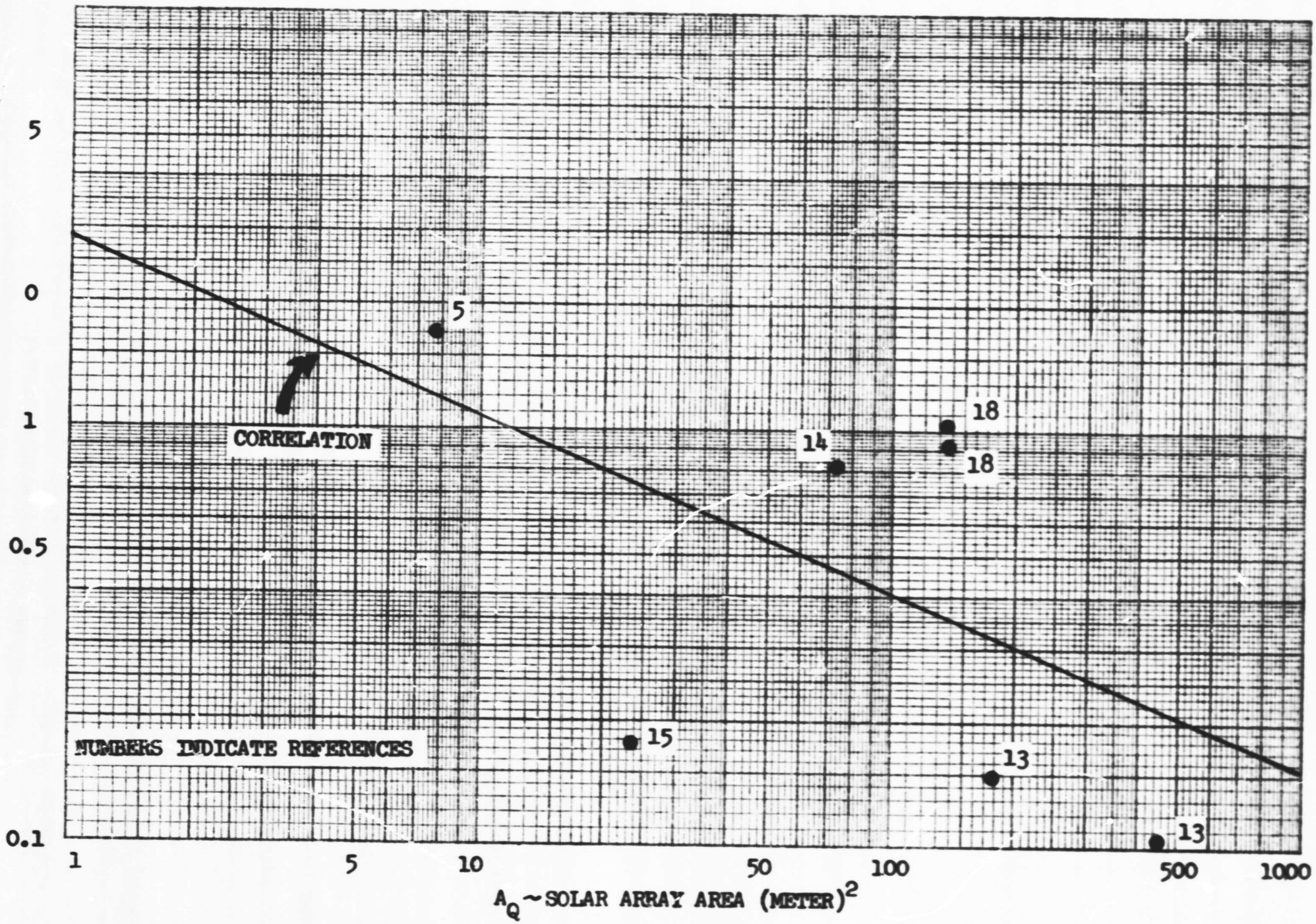

Figure 3-35 Solar Cell Array - Orientation System Specific Mass

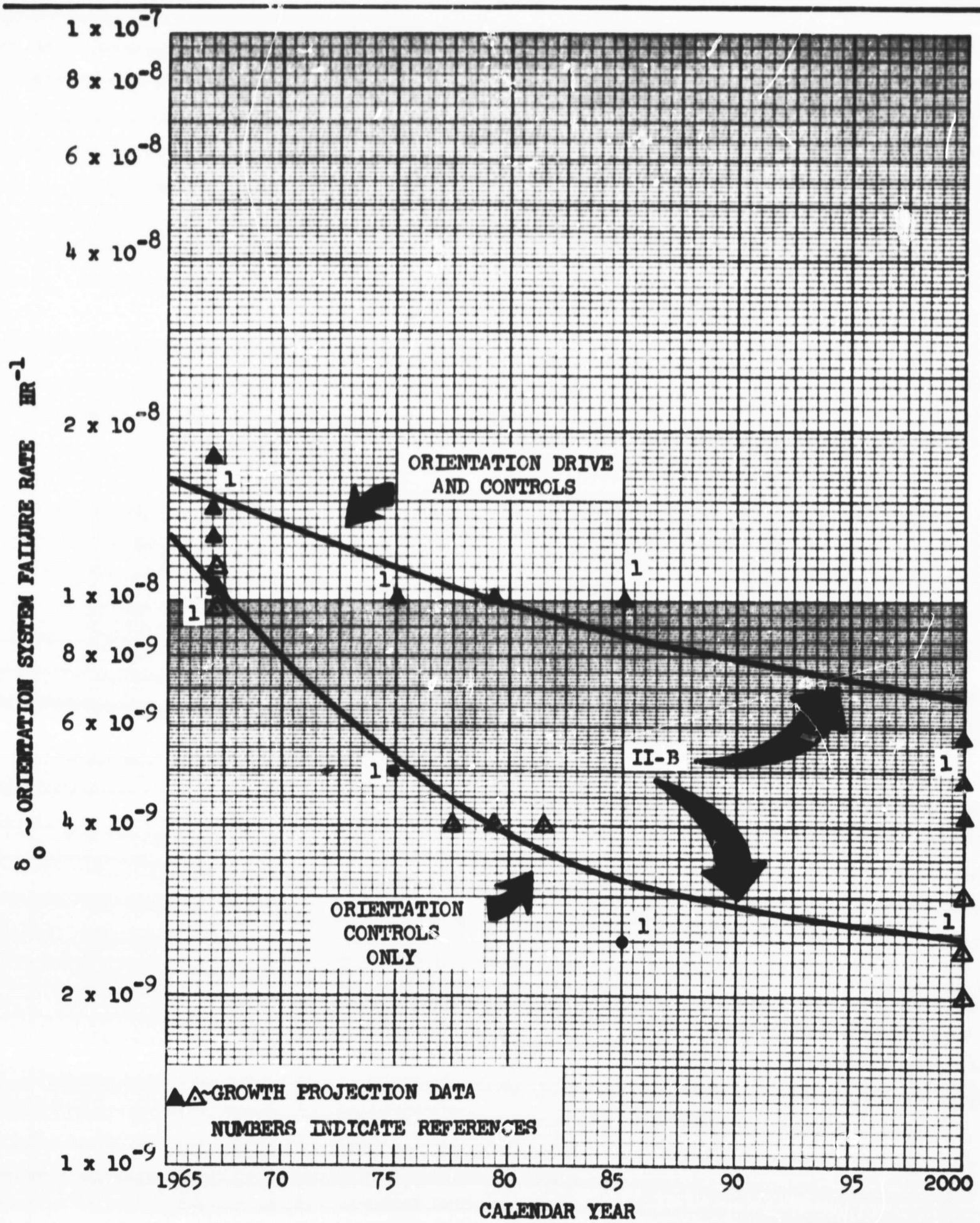

Figure 3-36 Projection -- Solar Cell Array Orientation Drive and Controls Failure Rate

3.1.2 Thermoelectric Conversion Subsystem

The thermoelectric converter is a static energy conversion device which is inherently reliable and compact. The disadvantages include a low conversion efficiency and large radiator area requirement. The three thermoelectric converter materials that are considered in the study include: lead telluride (PbTe), silicon-germanium (SiGe), and the cascaded PbTe-SiGe type converters. The major characteristics of these thermoelectric converters are given in Table 3-16.

The basic thermocouple configuration is shown in Figure 3-37a. Heat enters the hot junction bar in contact with N and P type semiconductors and ionizes pairs of electrons and holes in sufficient quantity to flow to the cold end, producing a potential across the arms of the cold junction. The converter efficiency depends on materials and hot and cold junction temperatures. When the couples are closely packed as with the compact converter configuration of Figure 3-37b, the cold junction is convectively cooled. The direct-radiating couples shown in Figure 3-37c are less closely packed and the space between the couples is used by the couple radiator that conducts heat directly to space from the cold junction. The cascaded PbTe-SiGe converter configuration is shown in Figure 3-37d.

The operating efficiencies of the three converters are shown in Figures 3-38, 3-39, and 3-40. The projected improvement in thermoelectric efficiency is shown in Figure 3-41. The corresponding specific masses of the converters are shown in Figures 3-42, 3-43, and 3-44. The expected degradation over mission life for the converter is shown in Figure 3-45. Figure 3-45 is based on a consensus of the AEC and subcontractors rather than test data. The projected production cost of the thermoelectric converter is shown in Figure 3-46.

Table 3-16

THERMOELECTRIC POWER CONVERSION SUBSYSTEMS BRIEFING CHART

Item	Value	
Identification		
Applicable energy source	Solar, isotope, reactor	
Heat rejection subsystems	Direct radiation, convective loop	
Major components	Converter, voltage control	
Vehicle – mission application range		
Useful power level	1.0W to 50 kW	
Duration of mission	Days to years	
Types of spacecraft	Manned, unmanned, Earth orbiting, interplanetary	
Status		
State of the art	Efficiency 2 to 6% for 5-year life	
Availability of support subsystems	Require isotope heat block and reactor development	
Subsystem Characteristics	Compact Converter	Direct Radiating
Range of efficiency	2 to 10%	2 to 7%
Range of specific weight	5 to 20 kg/kW	10 to 40 kg/kW
Range of specific volume	50 to 1,000 cc/kW	50 to 1,000 cc/kW
Range of specific production cost	$50 to $1,000/kW	$50 to 1,000/kW
Range of reliability	0.99 to 0.999 for 1 year	0.99 to 0.999 for 1 year

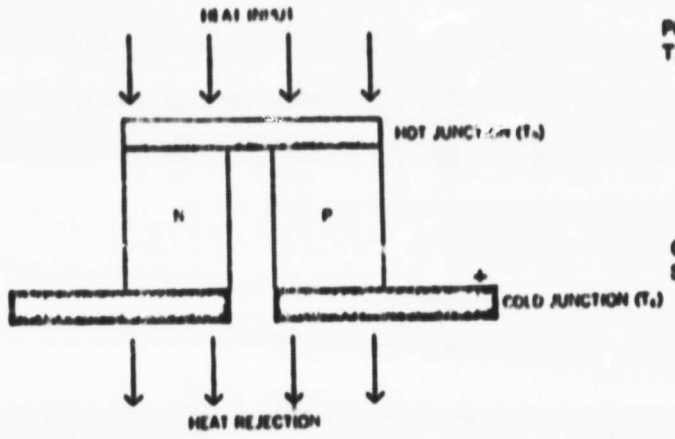

a. Basic Thermoelectric Couple

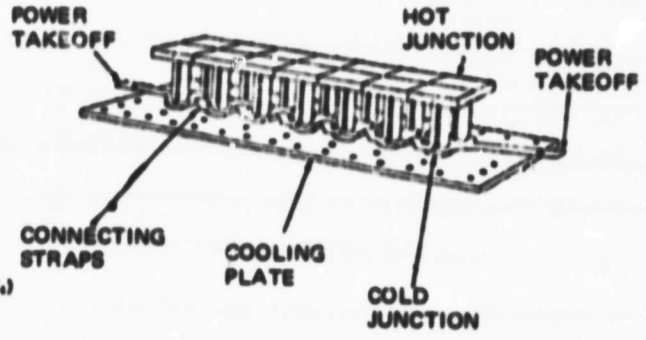

b. Compact Converter Configuration

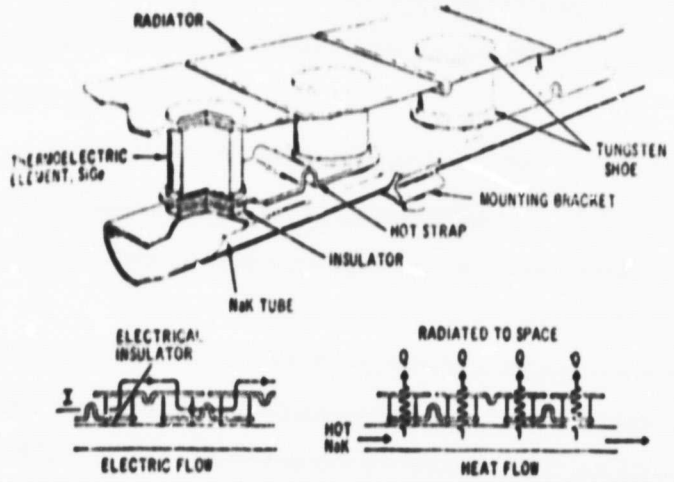

c. Direct-Radiating Thermoelectric Module

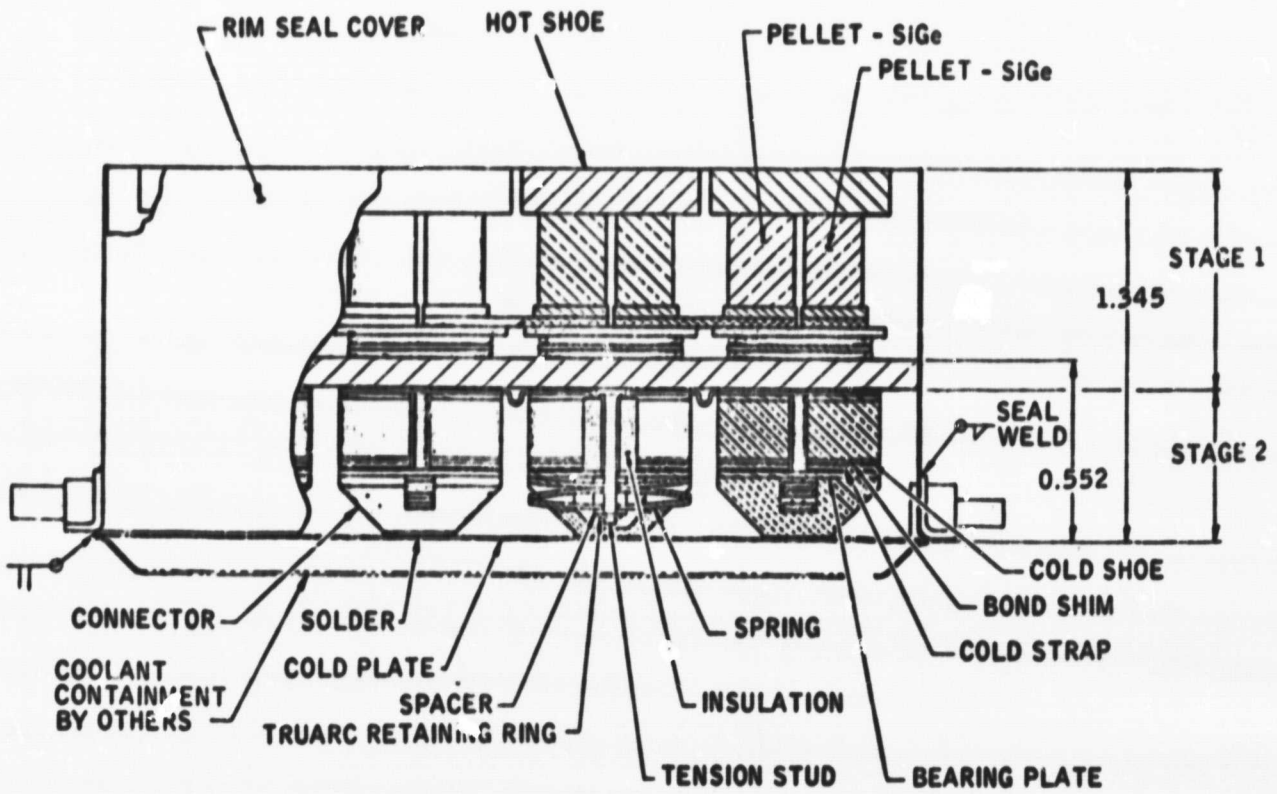

d. CASCADED PbTe-SiGe CASCADED CONFIGURATION

Figure 3-37 Thermoelectric Modules

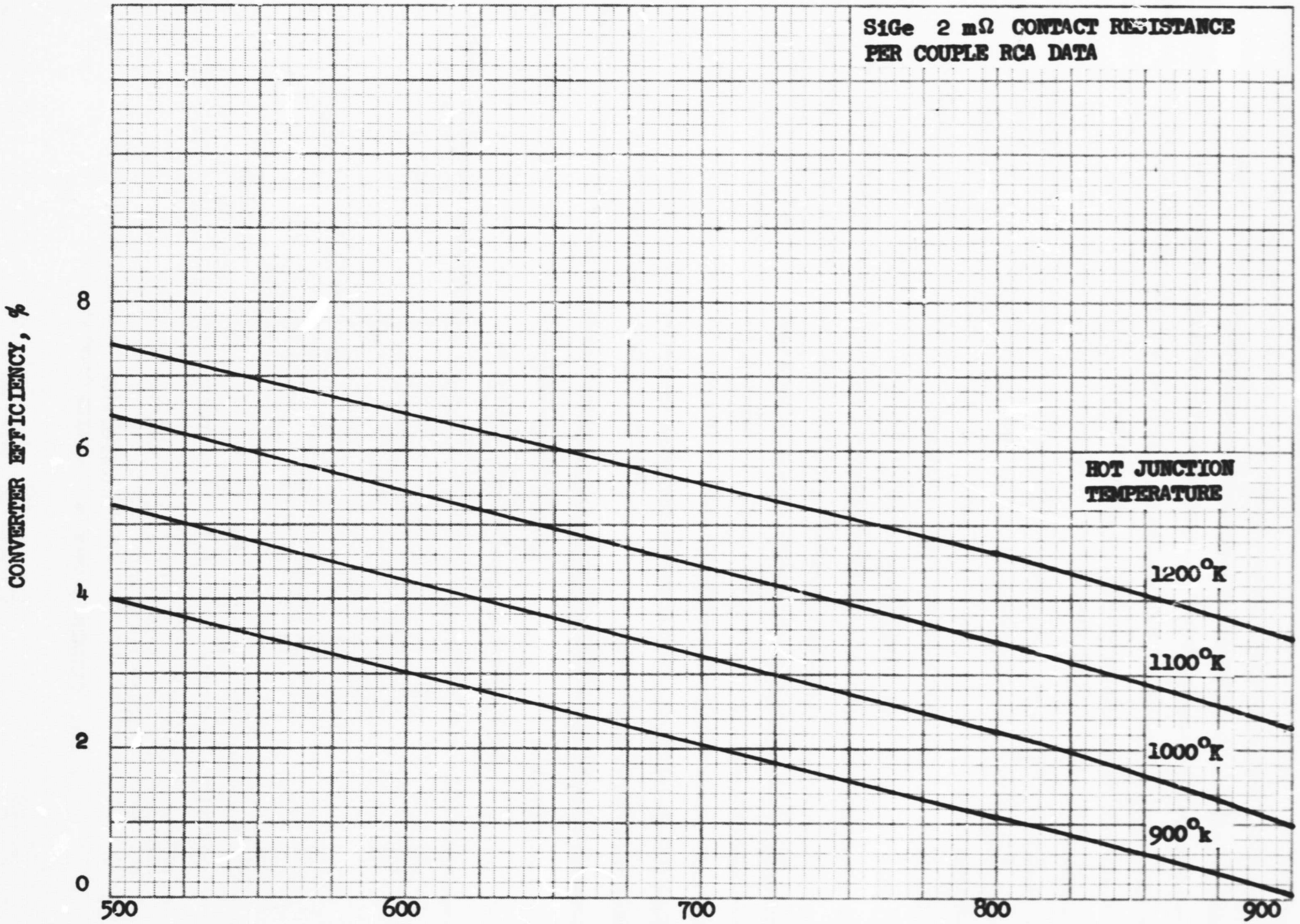

Figure 3-38 SiGe Converter Efficiency, %

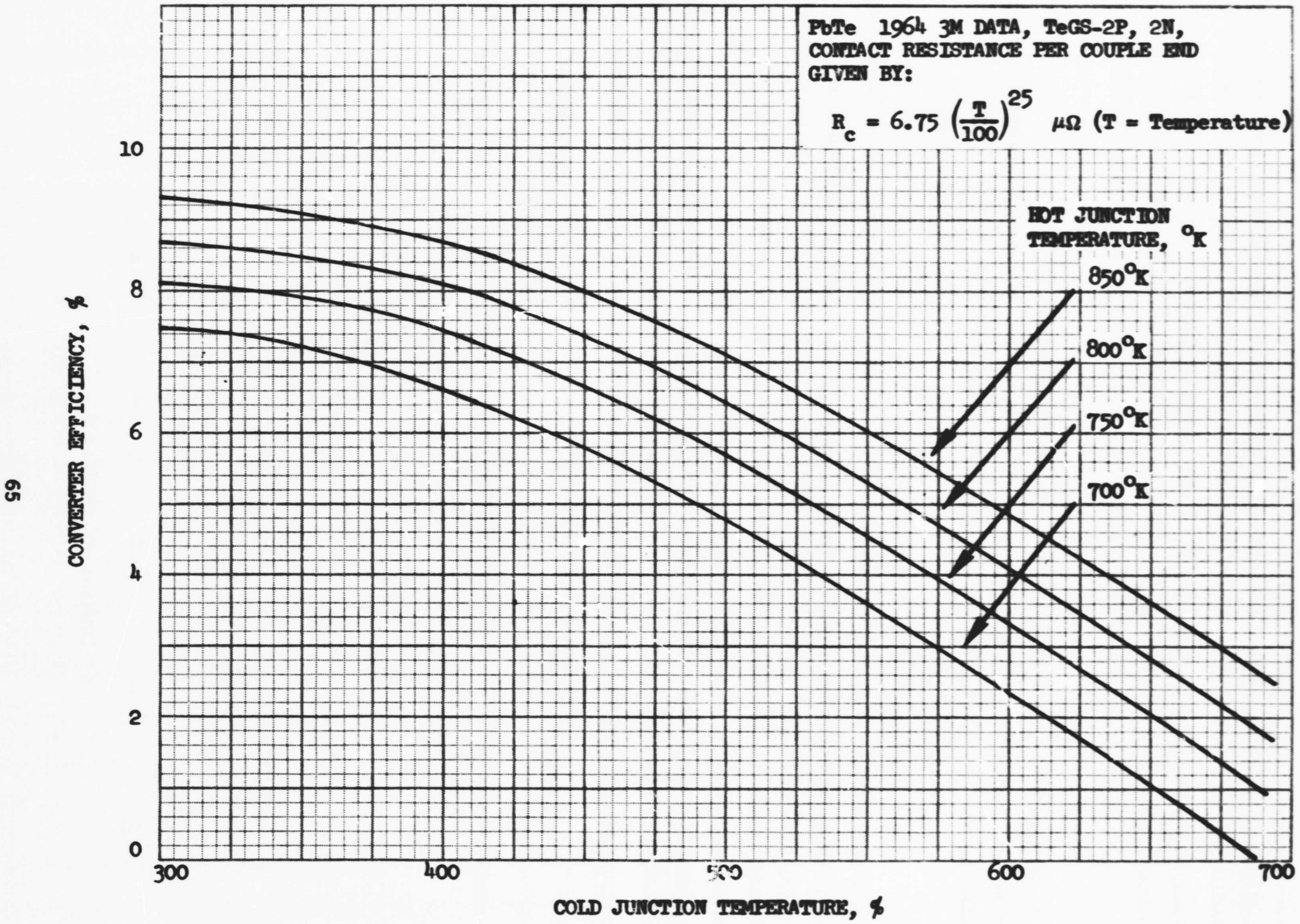

Figure 3-39 Pb-Te Thermoelectric Converter Efficiency

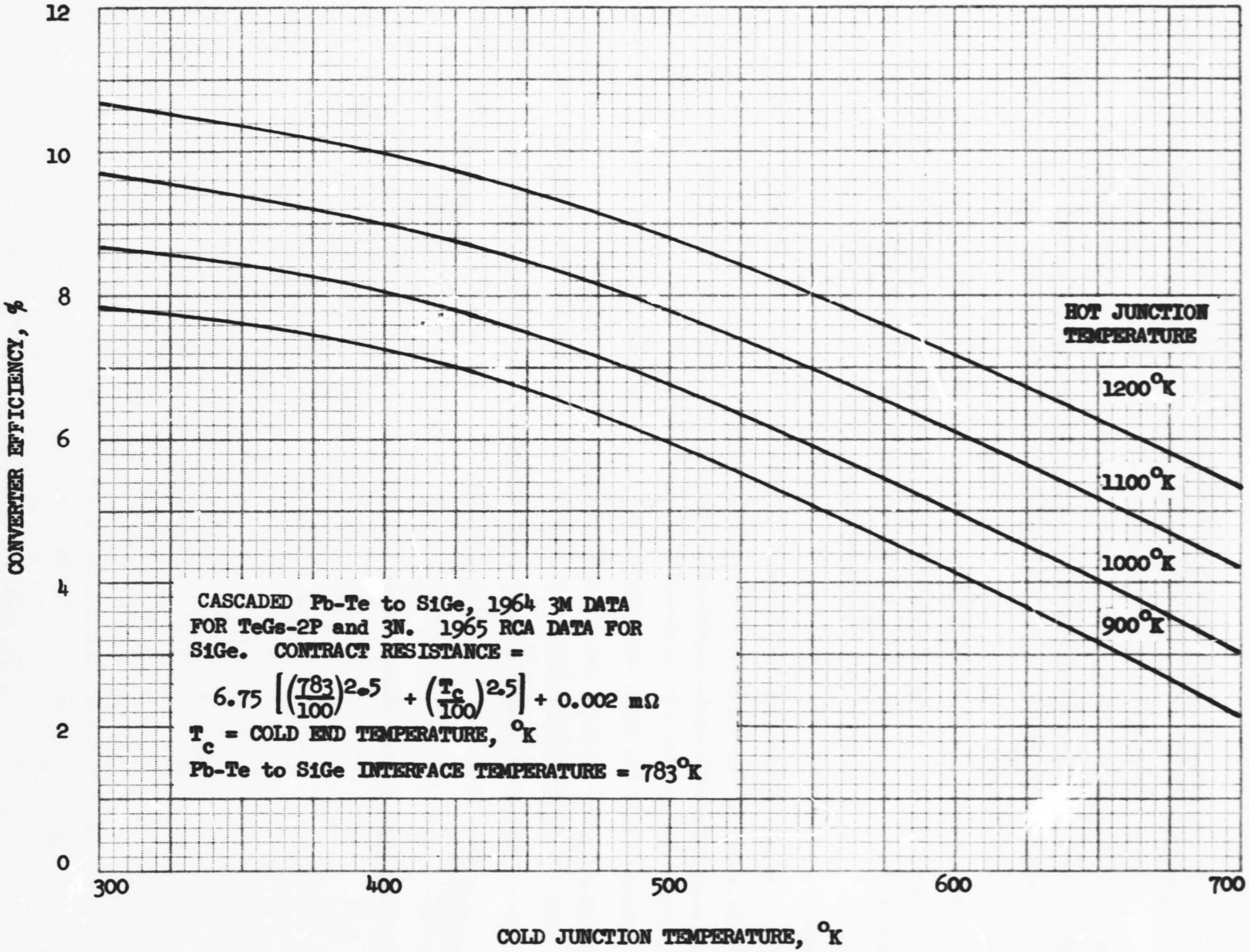

Figure 3-40 Segmented Pb-Te to SiGe Converter Efficiency

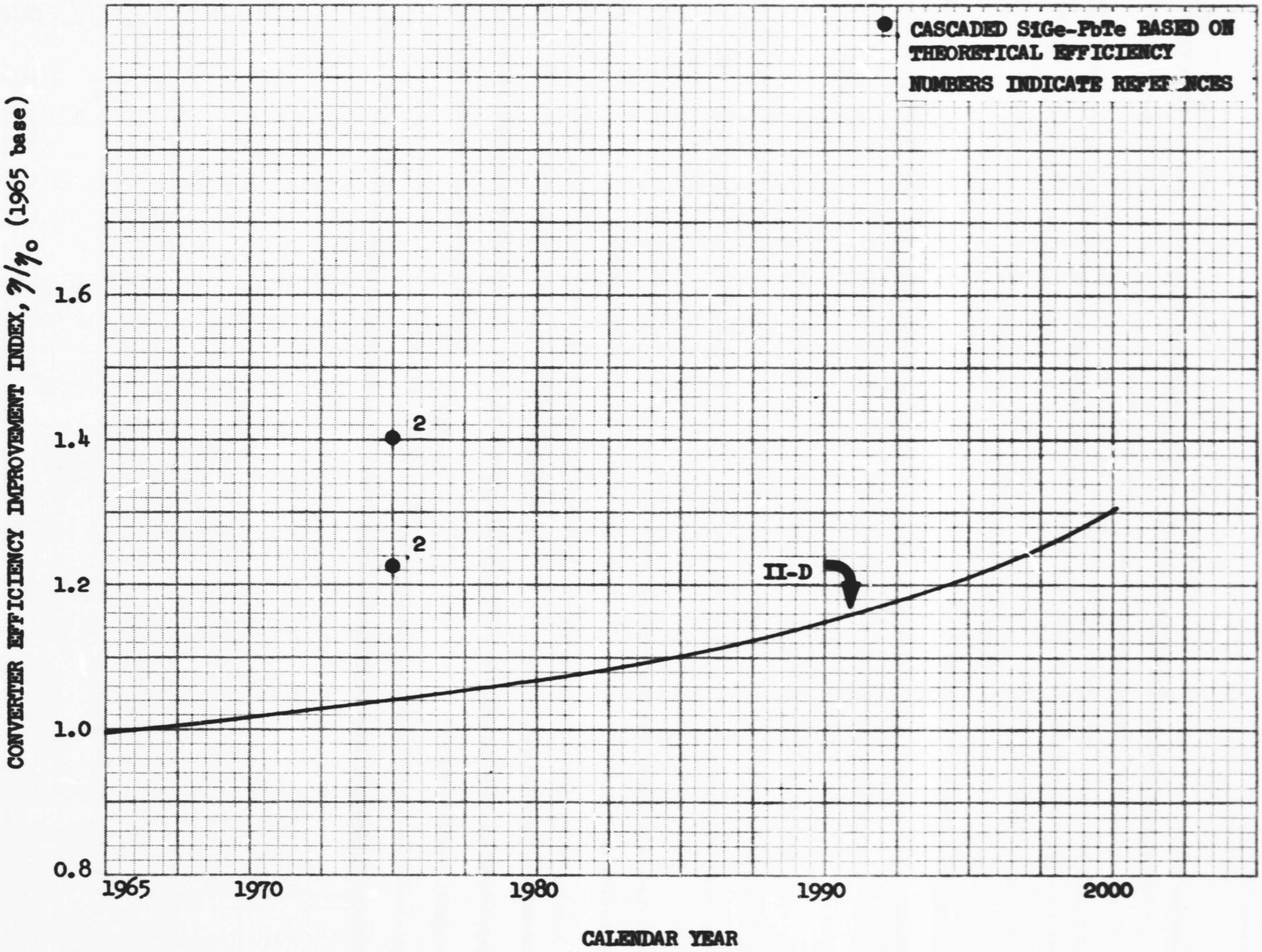

Figure 3-41 Projected Improvement in Thermoelectric Converter Efficiency

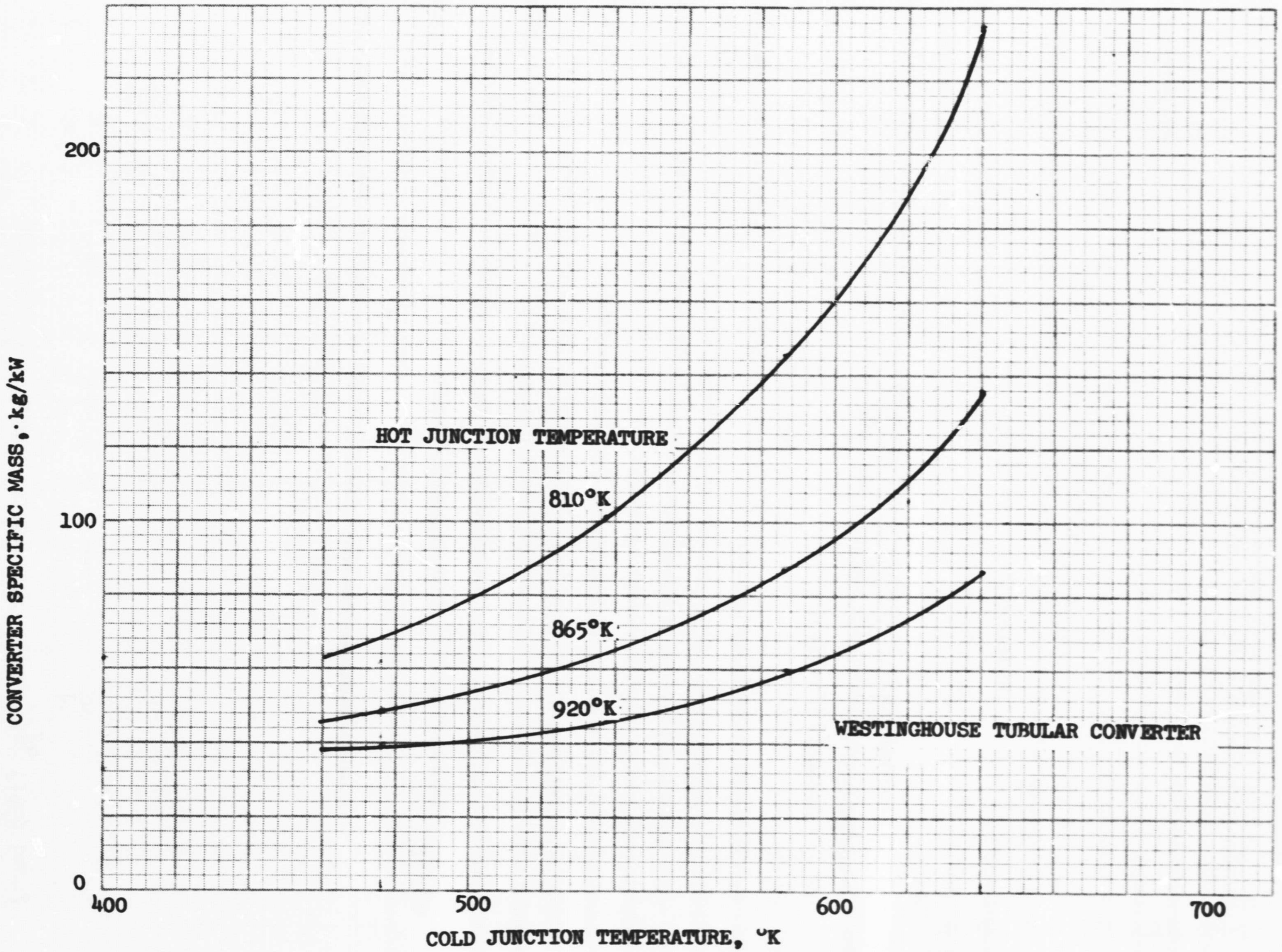

Figure 3-42 PbTe Thermoelectric Converter Specific Weight (Data based on Reference 1)

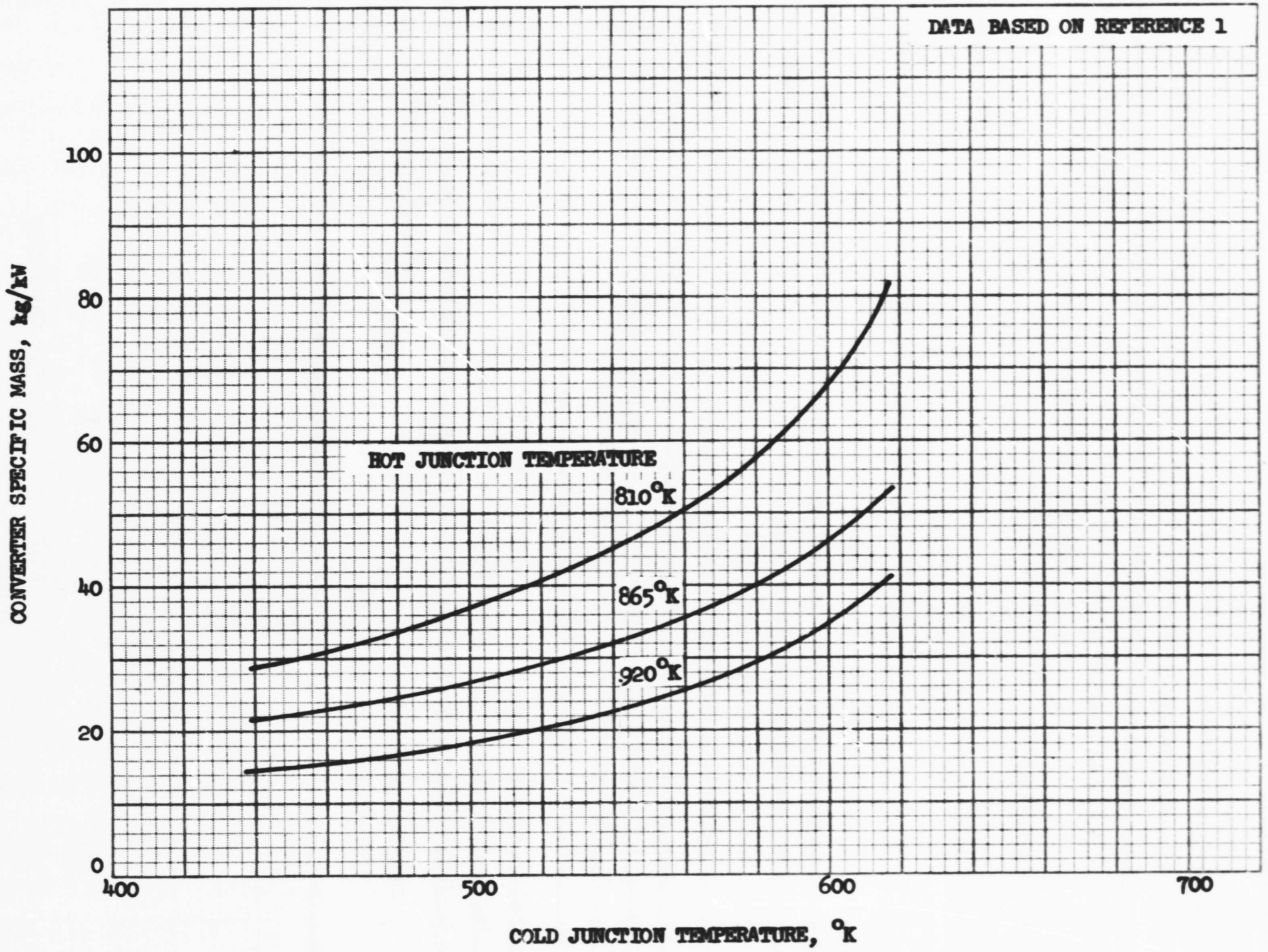

Figure 3-43 Side Thermoelectric Converter Specific Mass

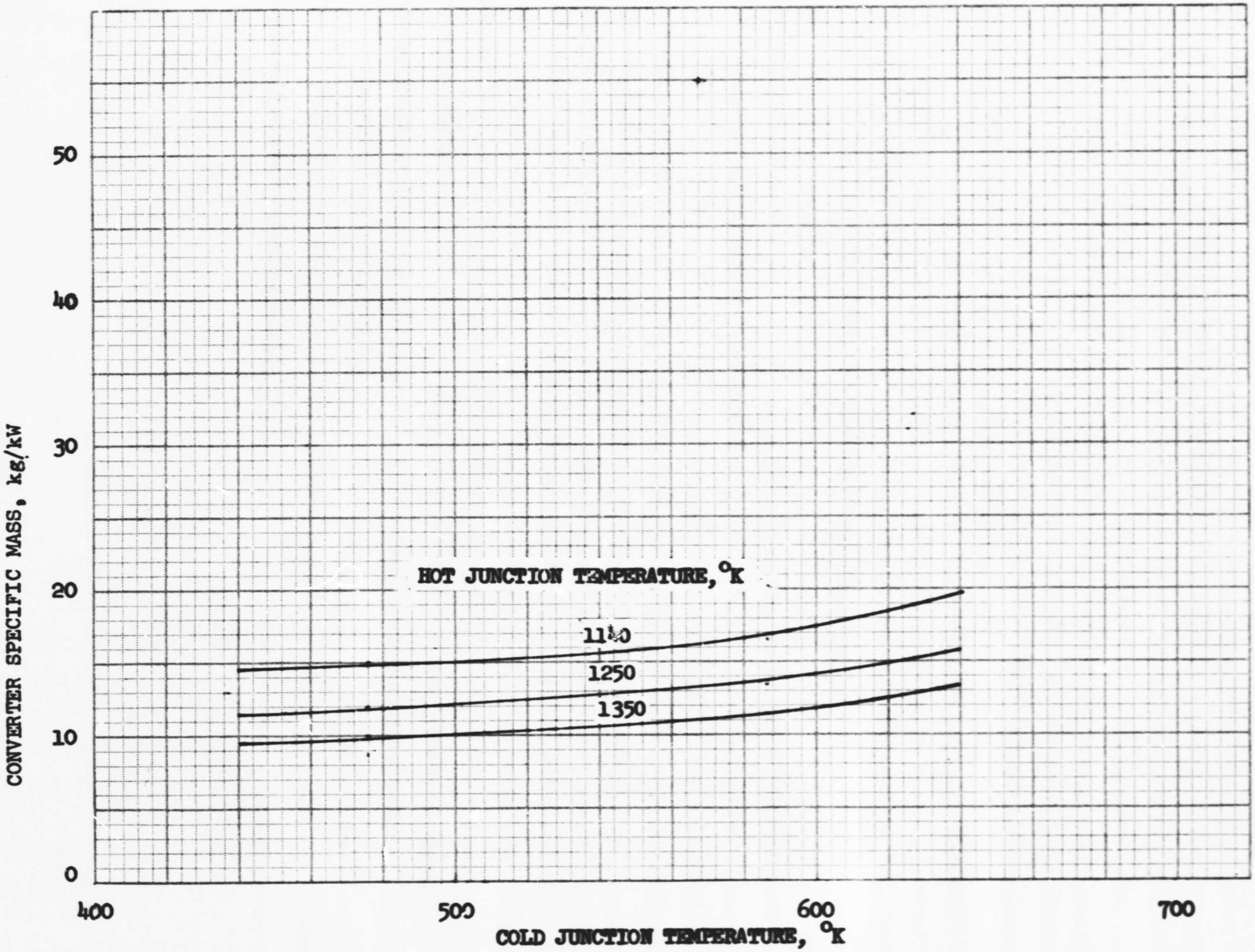

Figure 3-44 PbTe-SiGe Converter Specific Mass

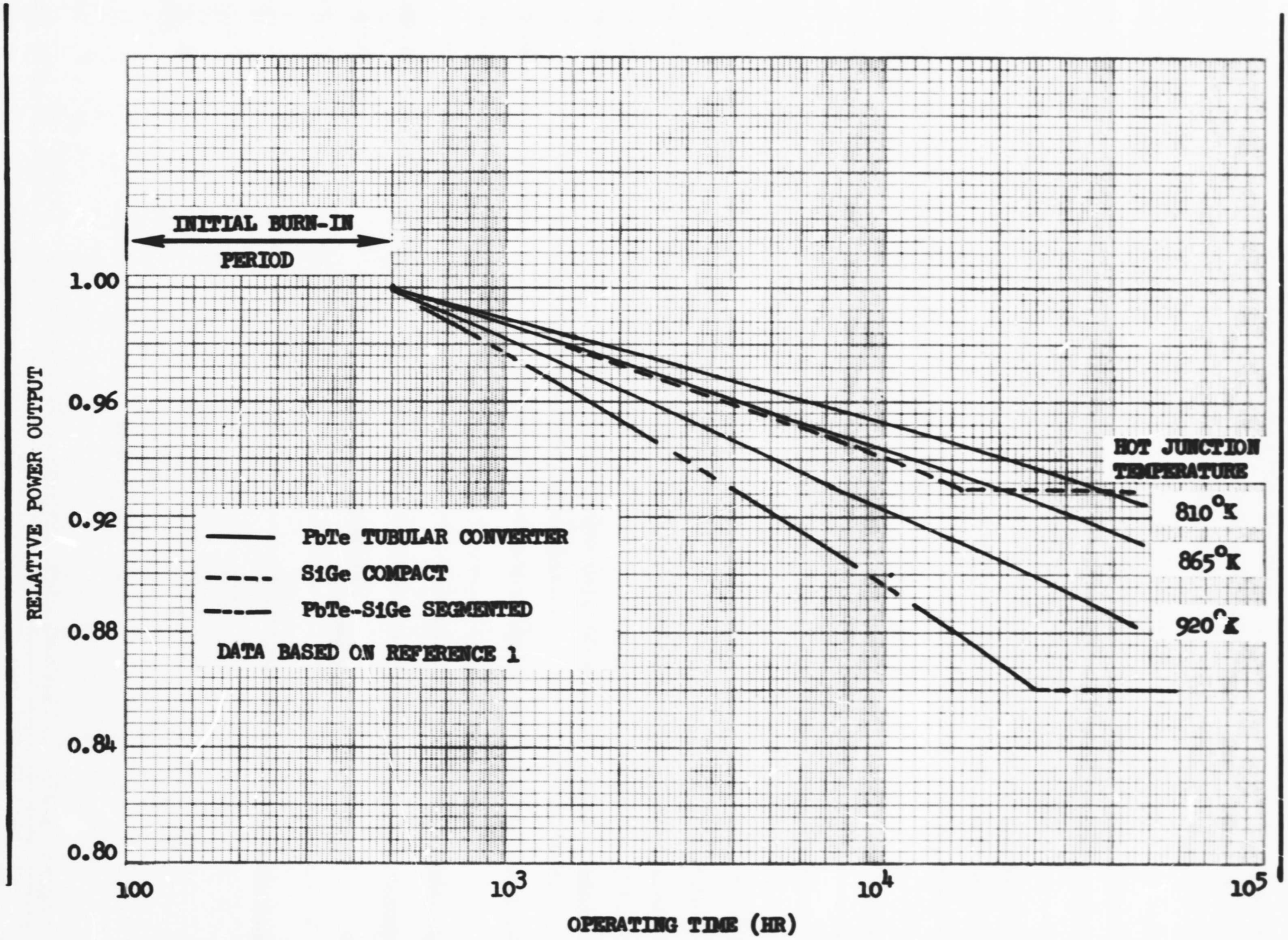

Figure 3-45 Thermoelectric Converter Degradation

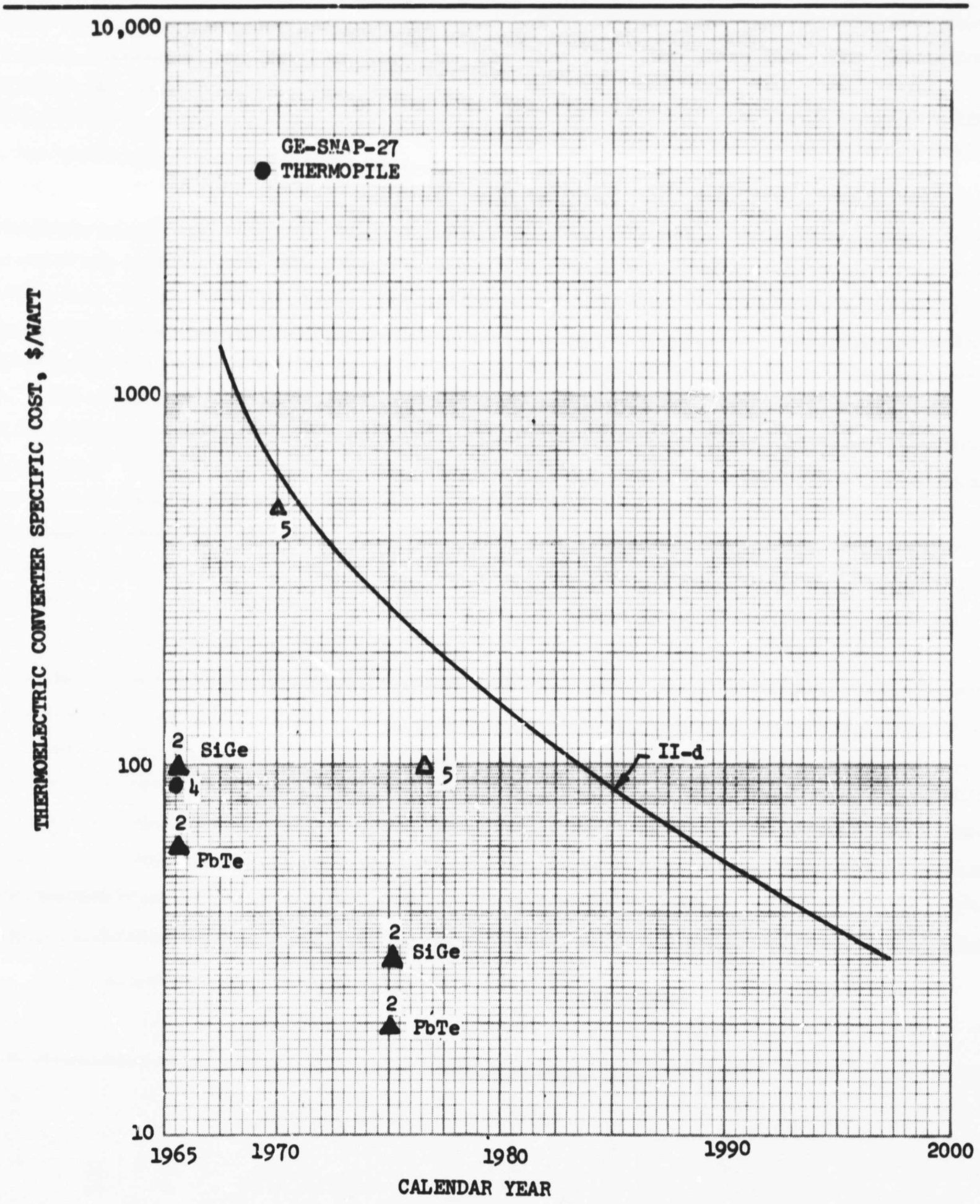

Figure 3-46 Thermoelectric Converter Production Cost Projection

3.1.3 Thermionic Power Conversion Subsystem

The thermionic power conversion subsystem consists of set series-parallel electrically connected thermionic converters, cesium reservoir, and control subsystem. The number and arrangement of the converters is set by the power level, voltage, and reliability requirements. The thermionic converter is a static device made up of two electrodes: the emitter from which electrons are thermionically emitted and the collector which absorbs the electron current. Two leads connect the electrodes to the power terminals. A cesium vapor fills the interelectrode space. The thermionic power conversion subsystem is shown in Figure 3-47. The electrical current flows from the heated emitting surface to the cooler collector surface through the interelectrode space and then from the emitter lead through an electrical load connected to the power terminals of the converter. The typical emitter is made of a refractory metal such as tungsten or rhenium and typically operates at a temperature of 1,600° to 2,200°K. The collector is made of a refractory metal such as molybdenum or niobium. Typical collector temperatures are between 800° and 1,300°K. The cesium vapor in the interelectrode space is held at a pressure of 1 to 10 mm Hg. The cesium is maintained at the desired pressure by connecting the interelectrode space to a cesium reservoir that contains a two-phase mixture of cesium vapor and cesium liquid. The temperature of the reservoir, and therefore the cesium pressure, is thermostatically controlled. The power density of present converters varies between 2 and 20 W/cm^2 with a corresponding 8 to 15% efficiency as the temperature increases from 1,600° to 2,200°K. The converter may receive thermal energy from any energy source such as radioisotopes, nuclear reactor (in-core and out-of-core designs), or a solar concentrator.

The thermionic conversion subsystem status, characteristics, and range of performance data are shown in Table 3-17. The curves of the thermionic power conversion major components or subsystem characteristics and performance data such as mass, area, volume, reliability, cost, efficiency, and temperature are shown in Figures 3-48 through 3-52c.

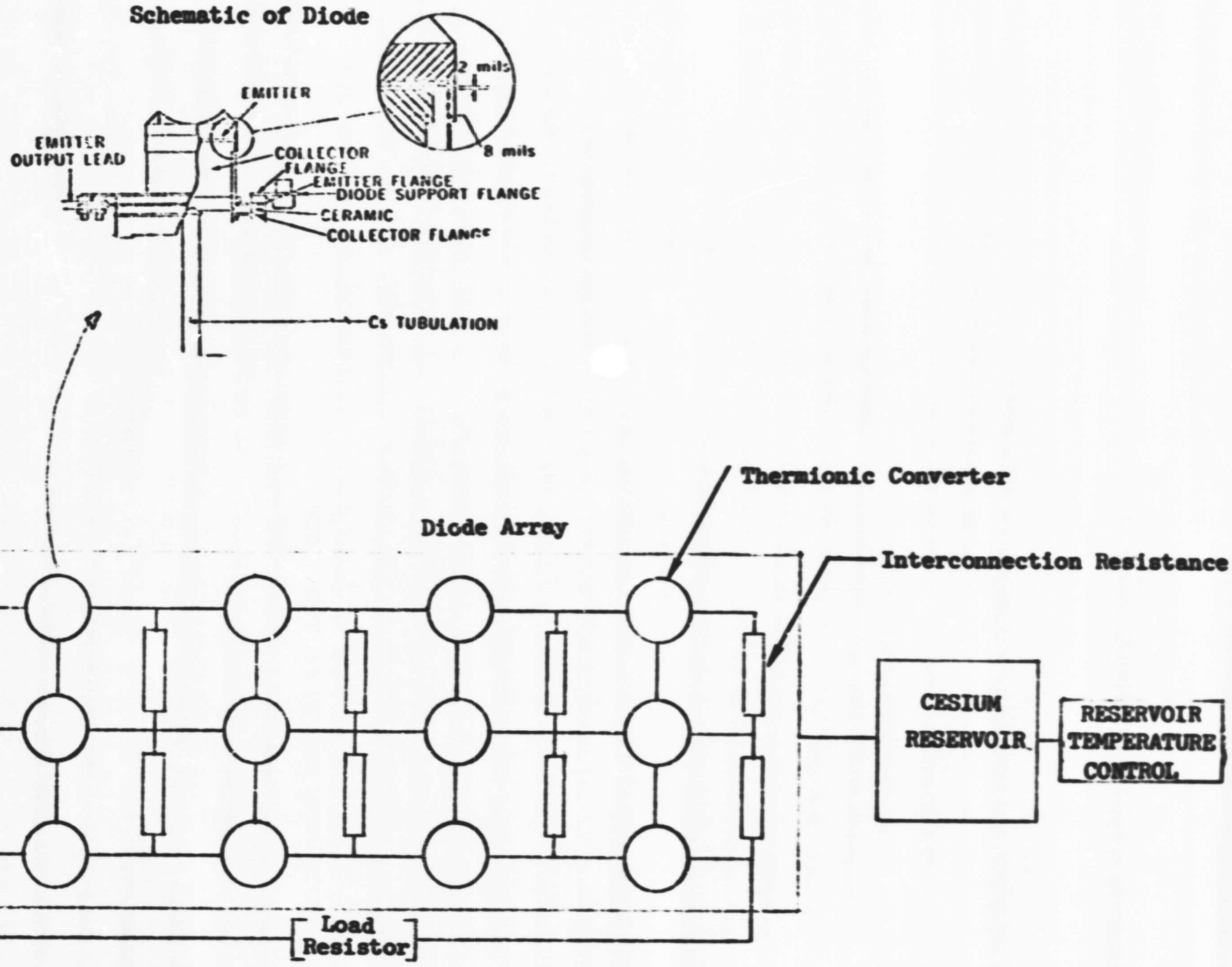

Figure 3-47 Thermionic Conversion Subsystem Array

Table 3-17 (Page 1 of 2)

THERMIONIC POWER CONVERSION SUBSYSTEM BRIEFING CHART

Item	Value
Identification	
Applicable energy source	Solar, isotope, reactor
Heat rejection subsystems	Direct radiation, convection loop, heat pipe
Major components	Diode, cesium reservoir, temperature control
Vehicle--mission application range	
Useful power level	100 watt to megawatt
Duration of mission	Days to years
Types of spacecraft	Manned, unmanned, Earth orbiting, interplanetary
Status	
State of the art	Power output to 20 W/cm^2
	Efficiency 12 to 16%, 3,000-hour MTBF
Availability of support subsystems	Require high-temperature isotope heat block and reactor development
Special problems	Integration of heat source and diodes
	Thermal insulators and electrical conductors
Subsystem characteristics	
Range of specific weight	0.2 to 1 kg/kW
Range of specific area	50 to 500 cm^2/kW
Range of specific volume	50 to 1,000 cc/kW
Range of specific production cost	50 to 5,000,000 $/kW
Range of reliability	0.9 to 0.99 for 1 year

Table 3-17 (Page 2 of 2)

Item	Value
Performance data	
Emitter (cathode) temperature	1,600°to 2,200°K
Collector (anode) temperature	900°to 1,450°K
Diode type	Tungsten-Re emitter and Mo-Ni collector
Range of diode efficiency	12 to 30%
Range of diode power density	2 to 60 W/cm^2

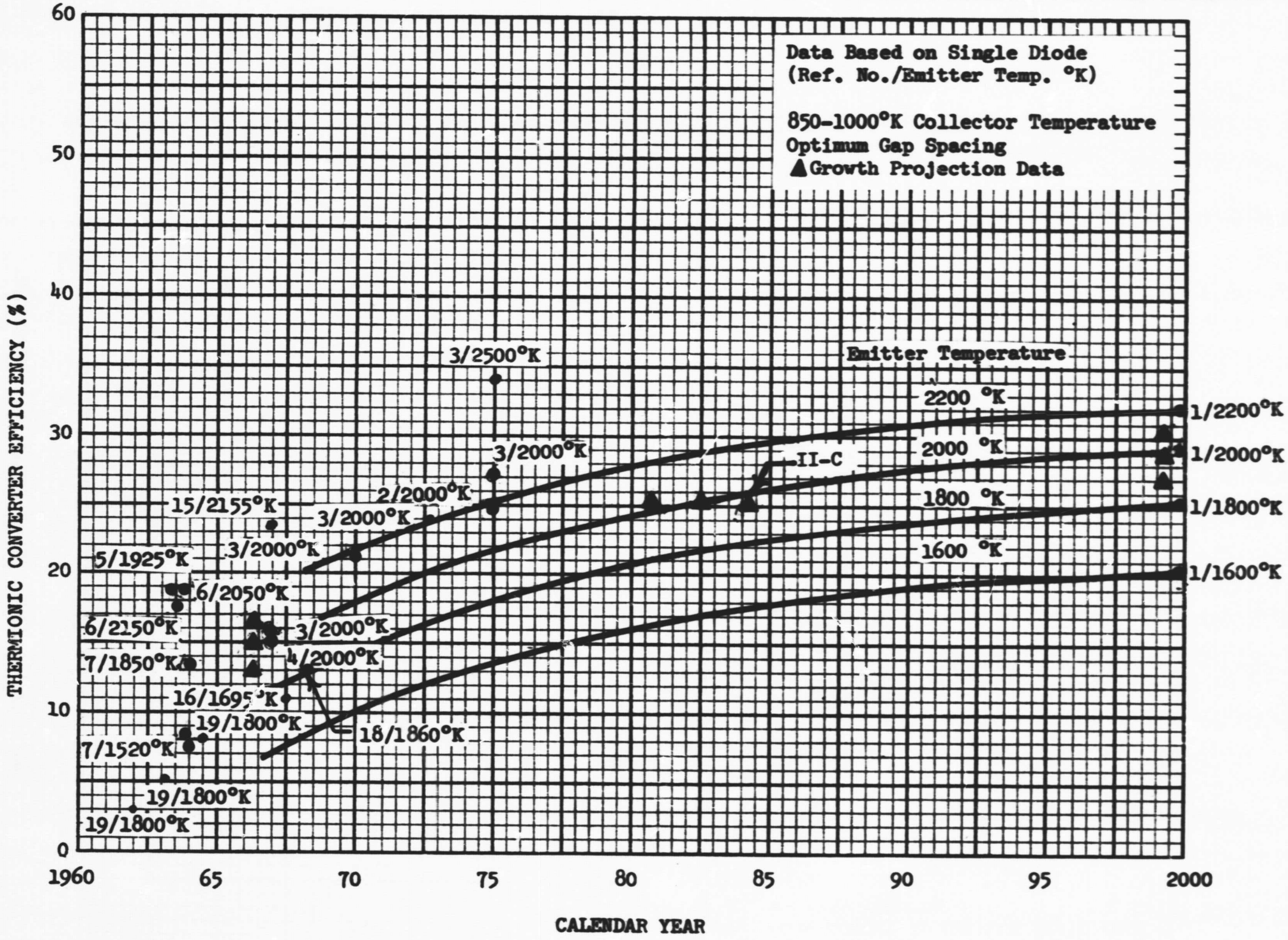

Figure 3-48 PROJECTION OF THERMIONIC CONVERTER EFFICIENCY

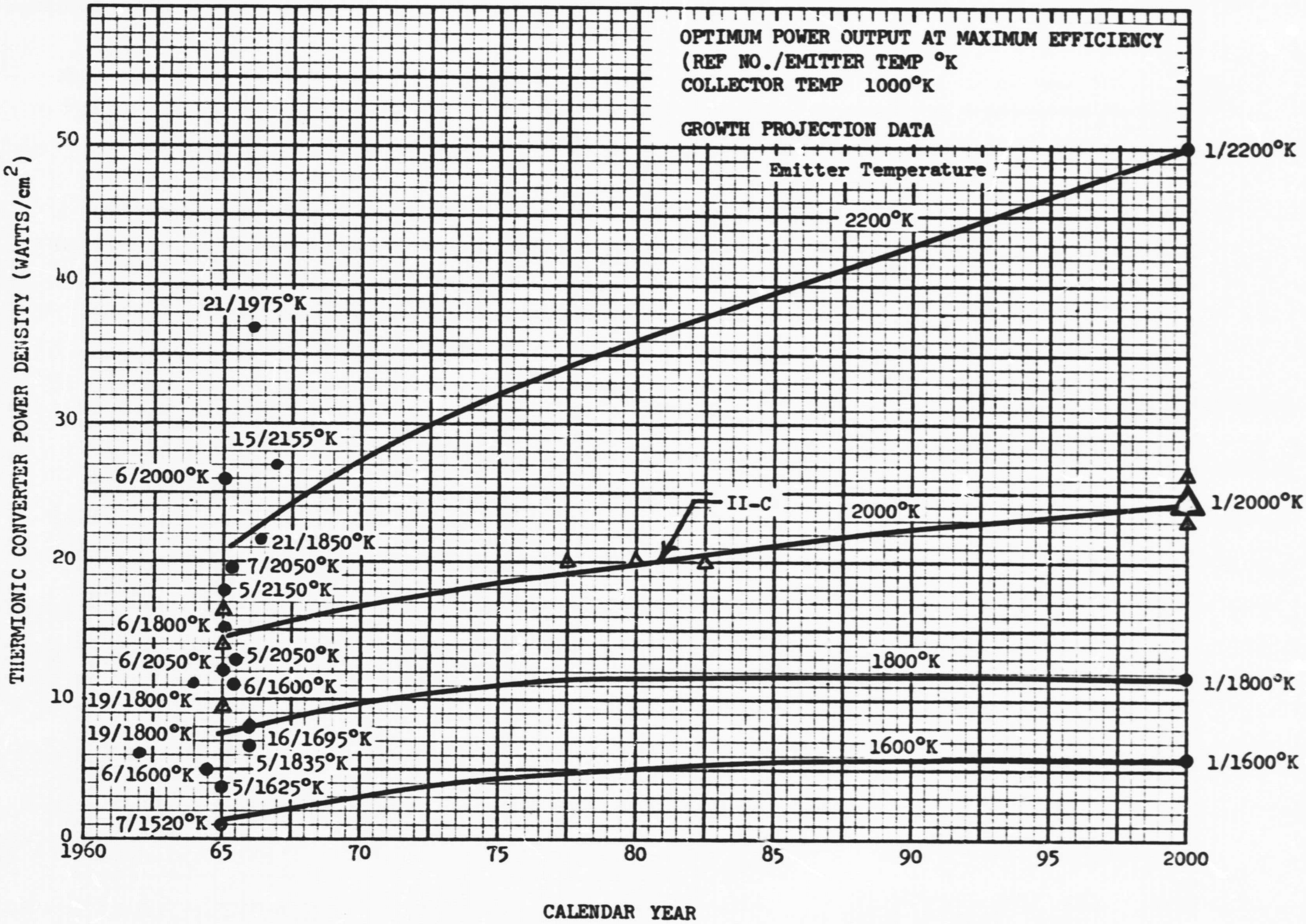

Figure 3-49 - PROJECTION OF THERMIONIC CONVERTER POWER DENSITY

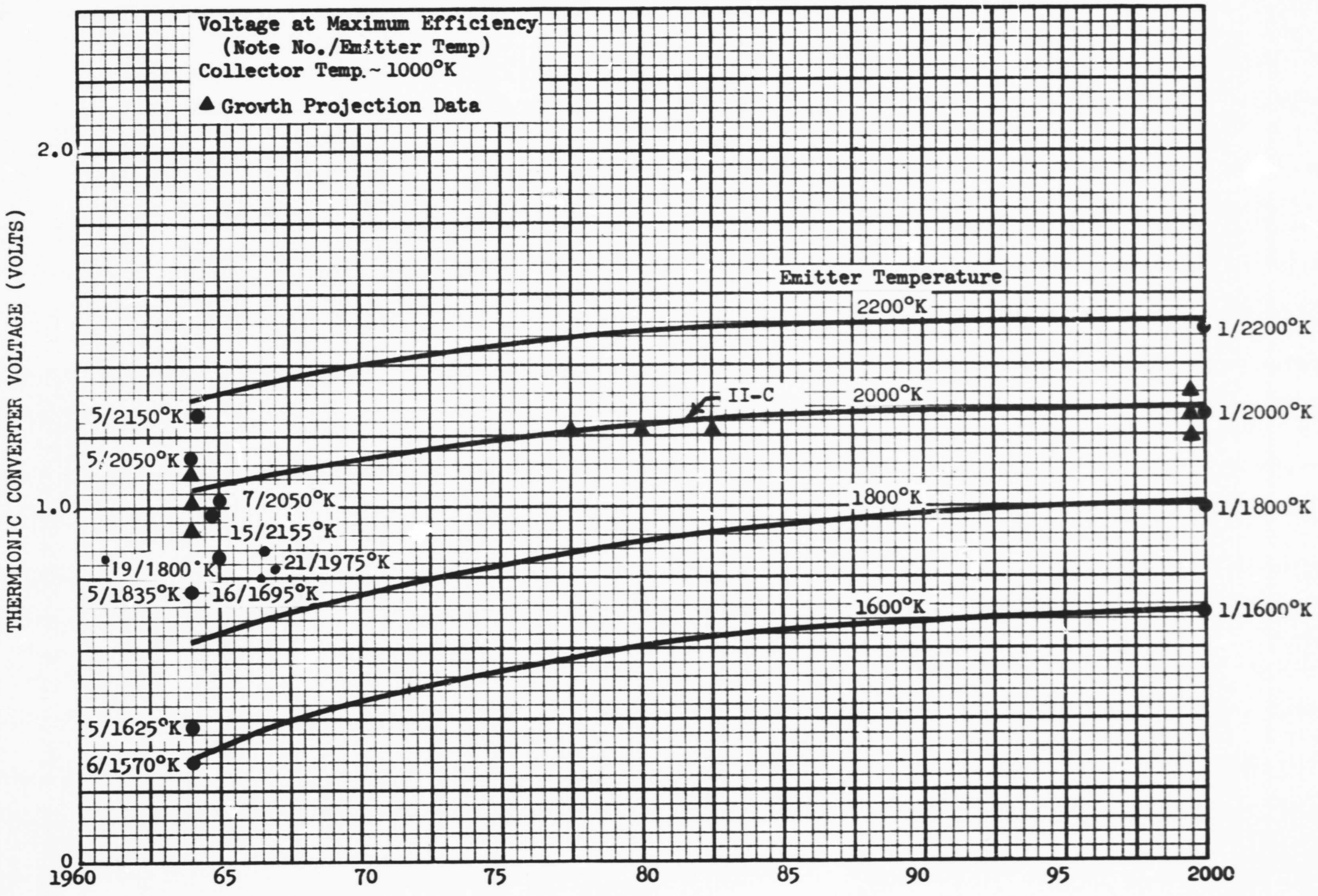

Figure 3-50 - PROJECTION OF THERMIONIC CONVERTER VOLTAGE

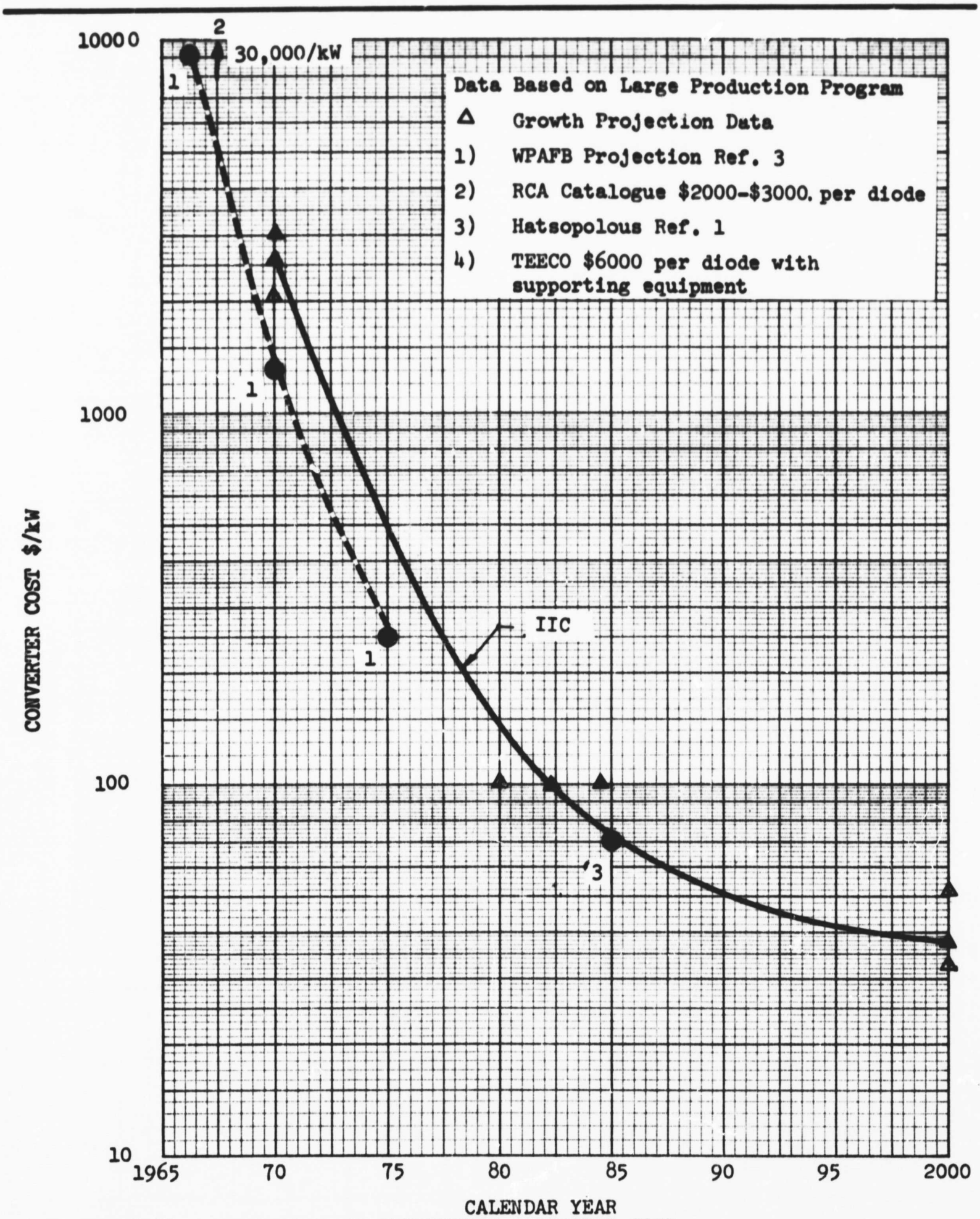

Figure 3-51 - PROJECTION OF THERMIONIC CONVERTER COST

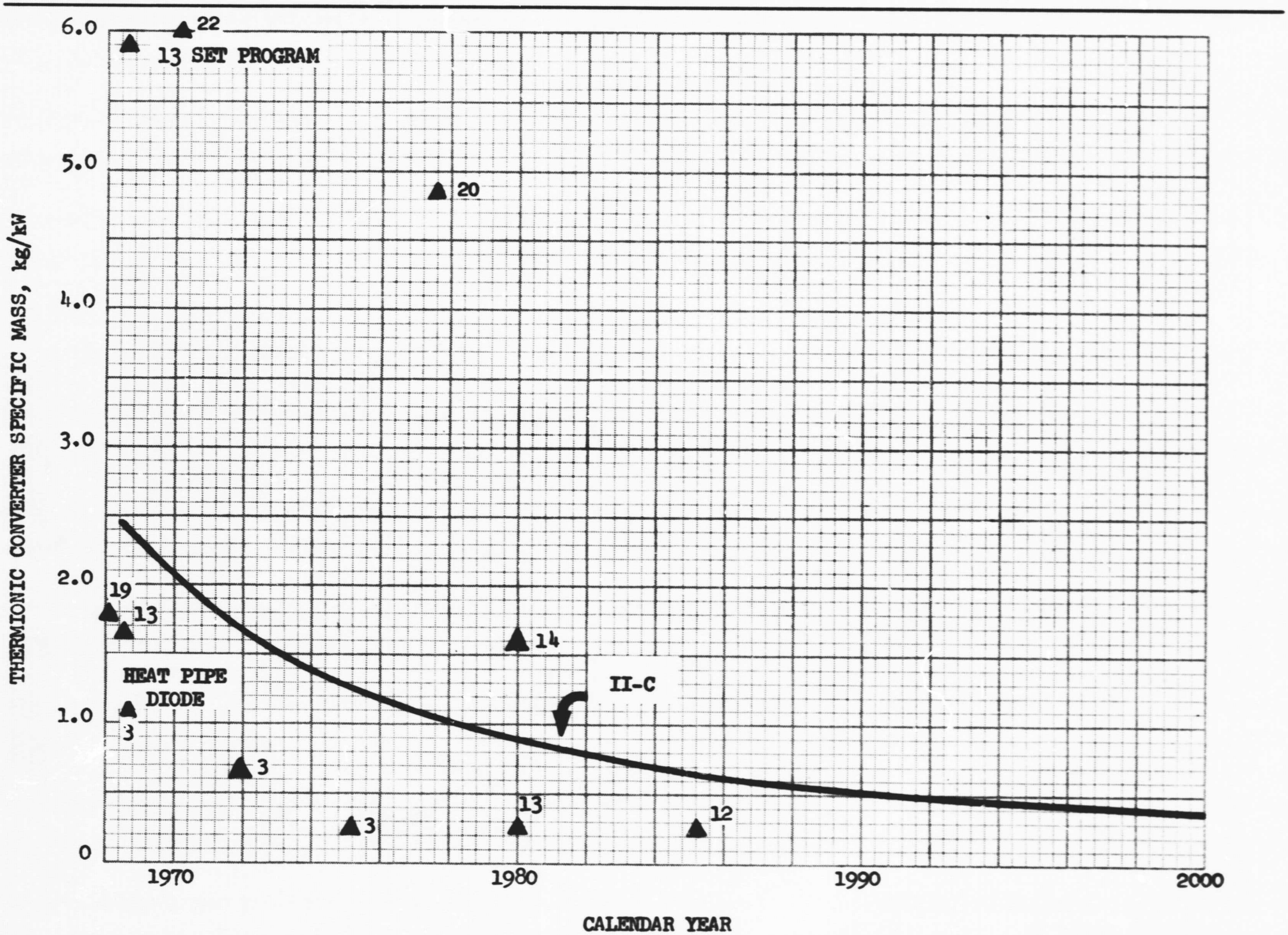

Figure 3-52 a Projection of Thermionic Converter Mass

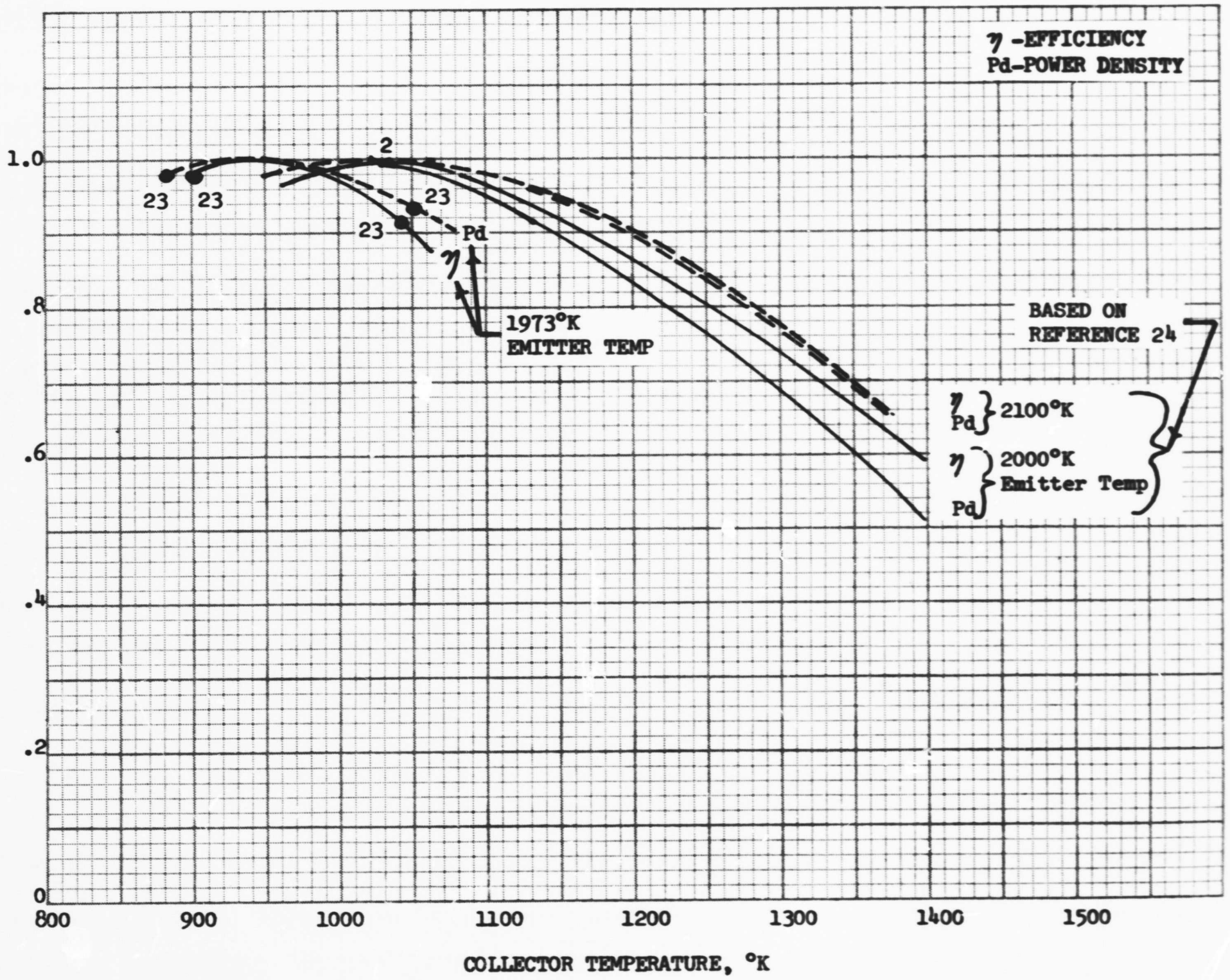

Figure 3-52b Variation of Thermionic Converter Efficiency Versus Collector Temperature

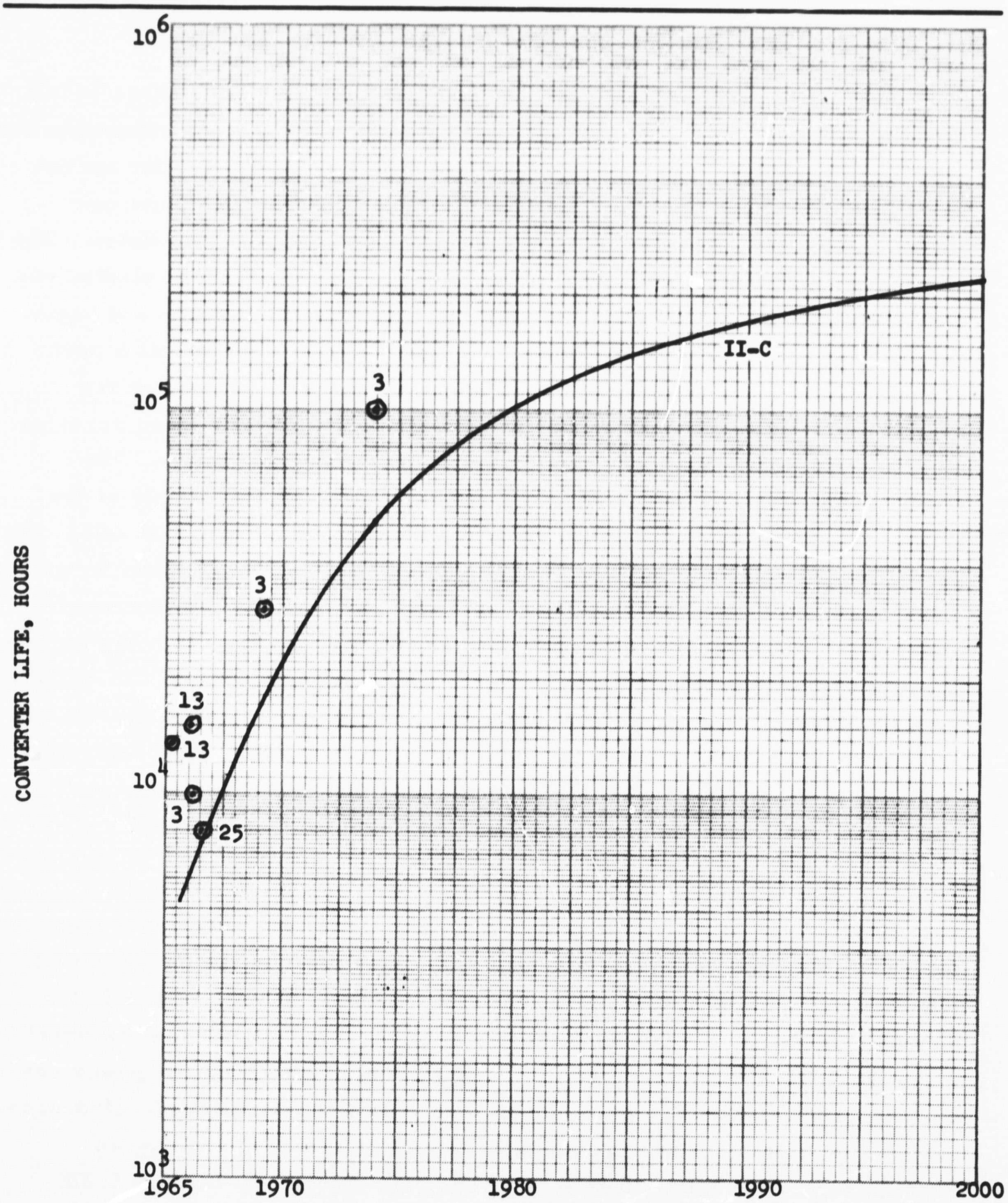

Figure 3-52c Thermionic Converter Life Projection

3.1.4 Fuel Cell Power Conversion Subsystem

Hydrogen-oxygen fuel cell subsystems have received the major share of fuel cell development efforts because of their relative simplicity and theoretically high energy density. Hydrogen-oxygen fuel cells are being used for spacecraft such as Gemini, Apollo, and MOL. The hydrogen-oxygen fuel cell power conversion subsystem consists of one or more fuel cell modules. The fuel cell module consists of the fuel cell elements or electrodes, electrolyte, controls and instrumentation, and the fuel cell housing. Storable and regenerable fuel cell subsystem often use hydrogen-oxygen fuel cells as a part of their subsystem. In these applications, the hydrogen and oxygen are obtained from the decomposition of compounds such as hydrazines, aerozine, nitrogen tetroxide, and hydrocarbons or the electrolysis of water. The storable reactant fuel cell module investigated in the study consists of the reformer-decomposer equipment and a basic hydrogen-oxygen fuel cell. The basic construction of a fuel cell consists of two electrodes separated by an electrolyte. A fuel such as hydrogen is ionized at the anode, producing free electrons. The electrons flow through the external load circuit to the cathode where they are consumed by an oxidant, such as oxygen. Conduction of the ionized hydrogen through the electrolyte completes the electrical circuit. A schematic diagram of a typical H_2-O_2 fuel cell power conversion subsystem is shown in Figure 3-53. The construction of the fuel cell elements or electrodes in the module are shown in Figure 3-54.

Table 3-18 is a briefing chart containing salient facts about fuel cells. Design data used in calculating fuel cell performance are shown in Figures 3-55 to 3-57. The major constraint that tends to restrict the use of present type fuel cells is the rather short operating lifetime (about 1,000 to 2,000 hours). The main incentive for the use of H_2-O_2 fuel cells is the low specific mass (kg/kWe) for short missions. A wider use of fuel cells for power conversion in space vehicles is expected as the lifetime is improved. Hydrogen-oxygen fuel cells consume approximately 0.45 of hydrogen and oxygen reactants for each kilowatt-hour and the lower theoretical limit is 0.286 kg/kWh. The specific mass of a fuel cell module is approximately 36.4 kg/kW. Fuel cell modules will cost from $30,000 to $300,000 for each kilowatt depending on the state of development of the desired hardware.

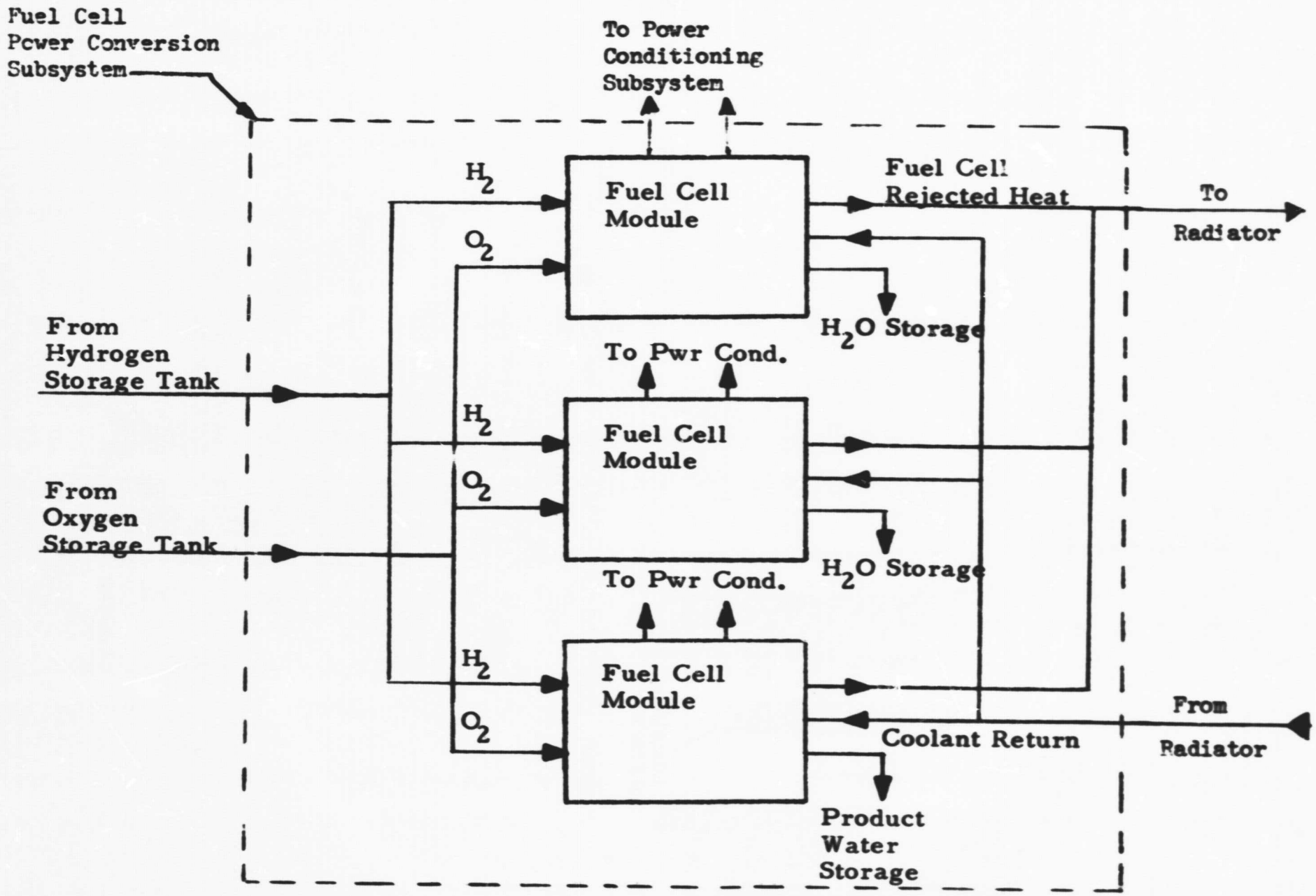

Note: Some fuel cell modules are cooled by direct radiation and have no coolant loop.

Figure 3-53 Typical H_2-O_2 Fuel Cell Power Conversion Subsystem

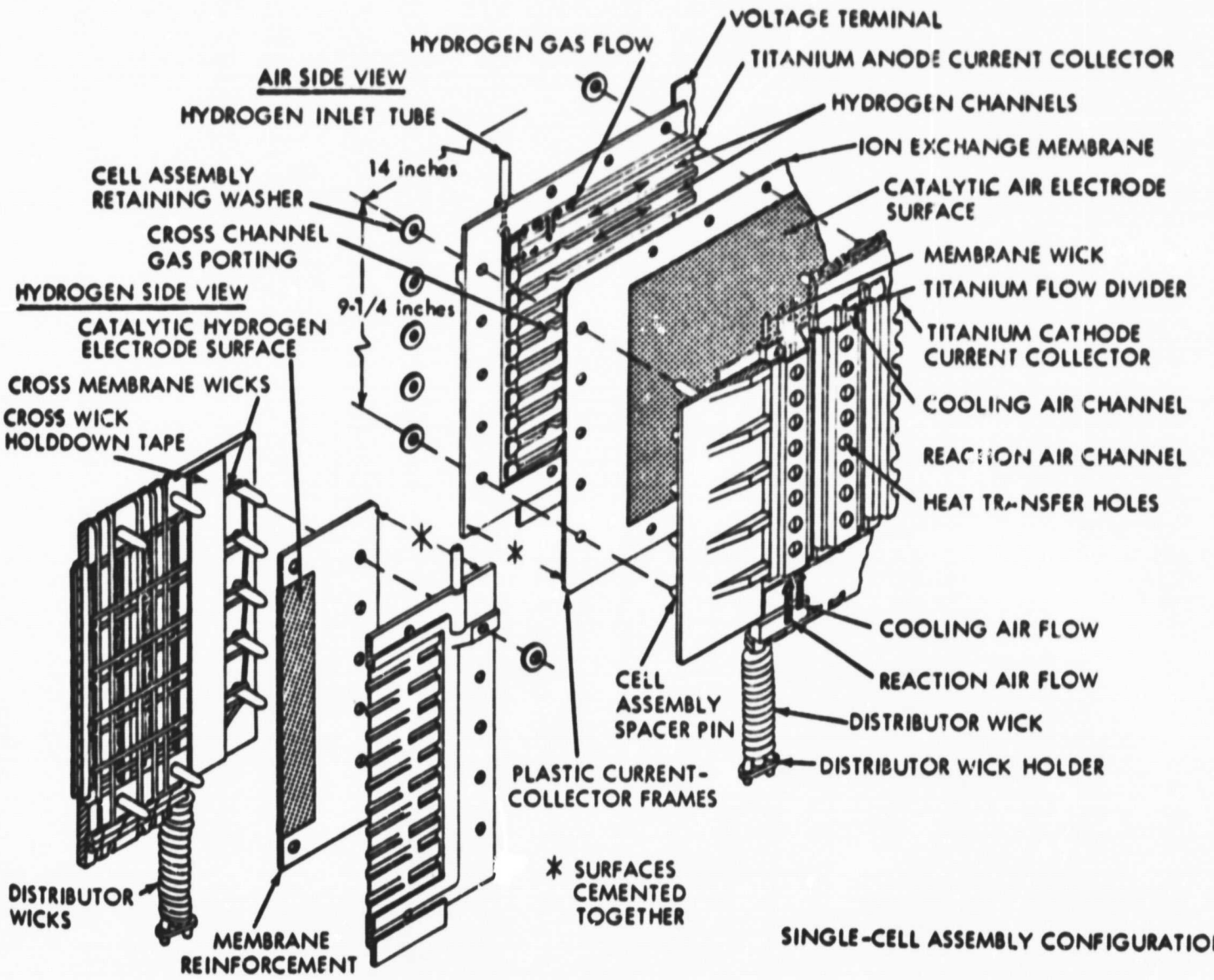

GENERAL ELECTRIC ION EXCHANGE MEMBRANE CELL CONFIGURATION

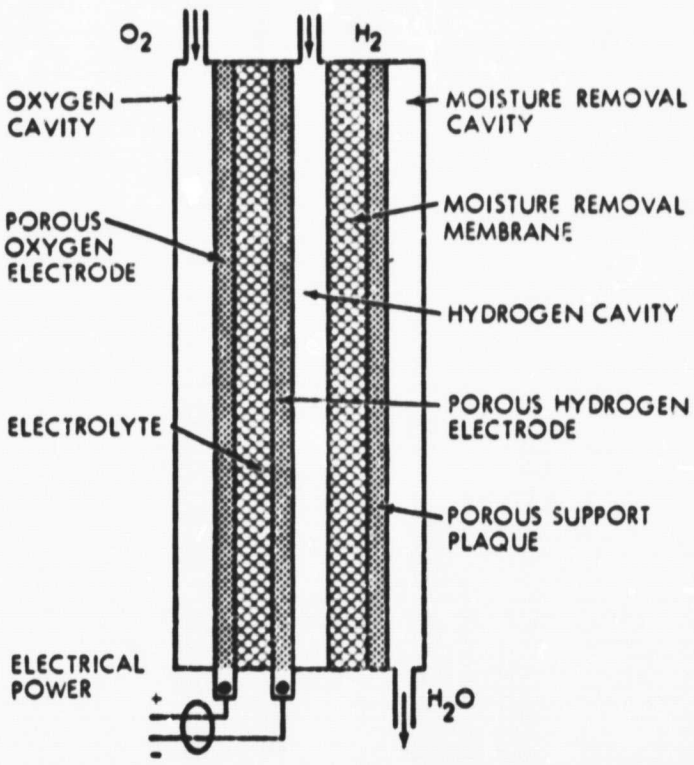

ALLIS CHALMERS ASBESTOS MEMBRANE CELL CONFIGURATION

Figure 3-54 Typical Fuel Cell Element Configurations

Table 3-18

FUEL CELL POWER CONVERSION SUBSYSTEM BRIEFING CHART

Item	Value
Identification	
Applicable energy source	Chemical reactants
Potential heat rejection subsystems	Separate heat transport loop
Major components	Fuel cell module (and reformer-decomposer for storable fuel cells)
Vehicle-Mission Application Range	
Useful power level	50 We to approximately 50 kWe
Duration of mission	1 day to several months
Type(s) of spacecraft	Both manned and unmanned
Status of Module	
State of the art	40 kg/kW, 2,000-hour MTBF for H_2-O_2
Special problems	Electrode and electrolyte degradation
Module Characteristics	
Specific mass	15 to 55 kg/kWe for H_2-O_2 fuel cell 21 to 73 kg/kWe for storable reactant fuel cell (1972)
Specific area	~1 m^2/kWe of radiator area in Earth orbit
Subsystem density	200 to 600 kg/m^3
MTBF	300 to 3,000 hr
Specific cost (production)	$30K to $300K per kW
Performance Characteristics	
Efficiency	55 to 75% H_2-O_2 fuel cell 30% storable reactant fuel cell
Specific fuel consumption	0.43 to 0.53 kg/kWh for H_2-O_2 1.3 to 2.1 kg/kWh for storable fuel cell

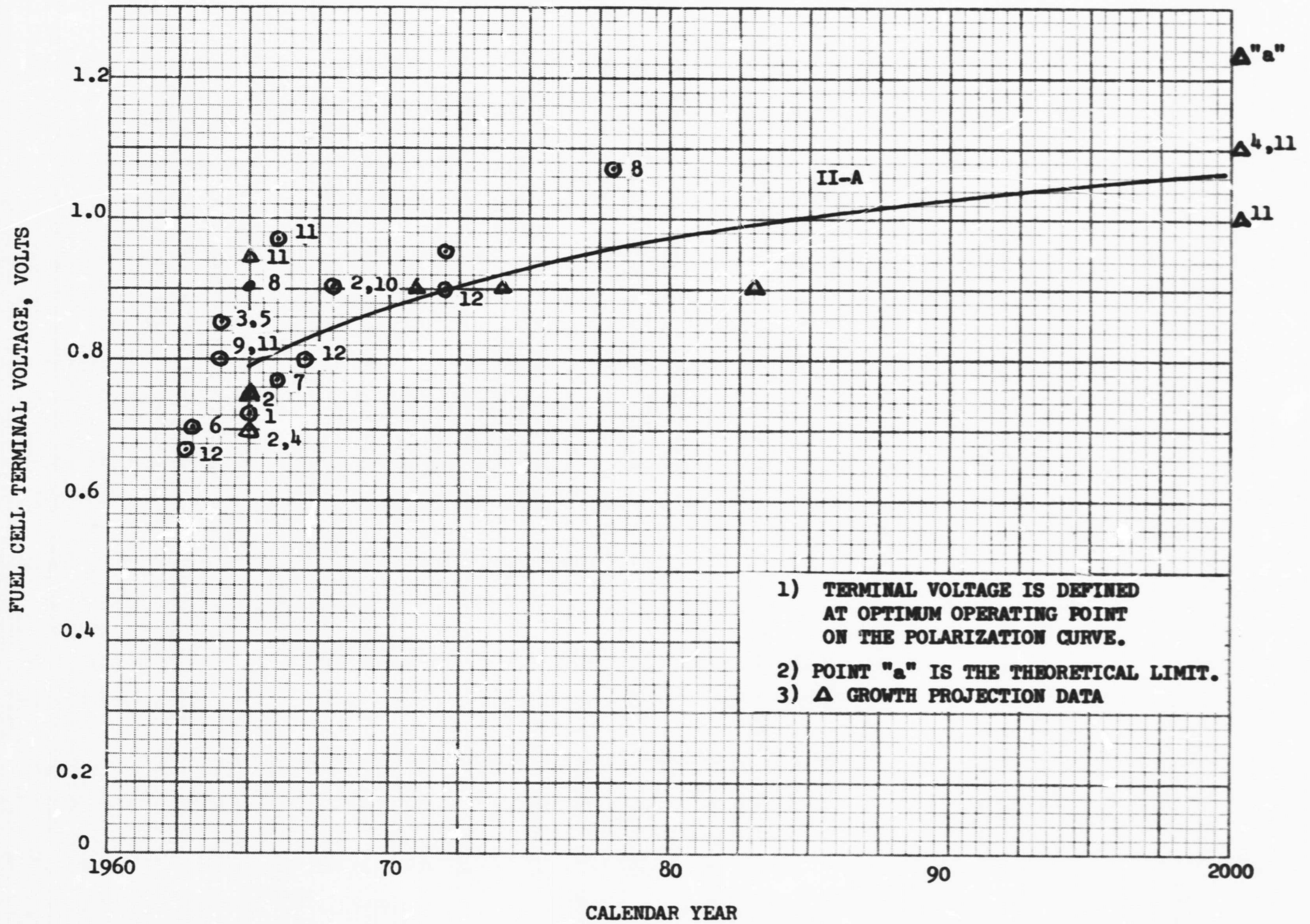

Figure 3-55 Projection of Fuel Cell Terminal Voltage

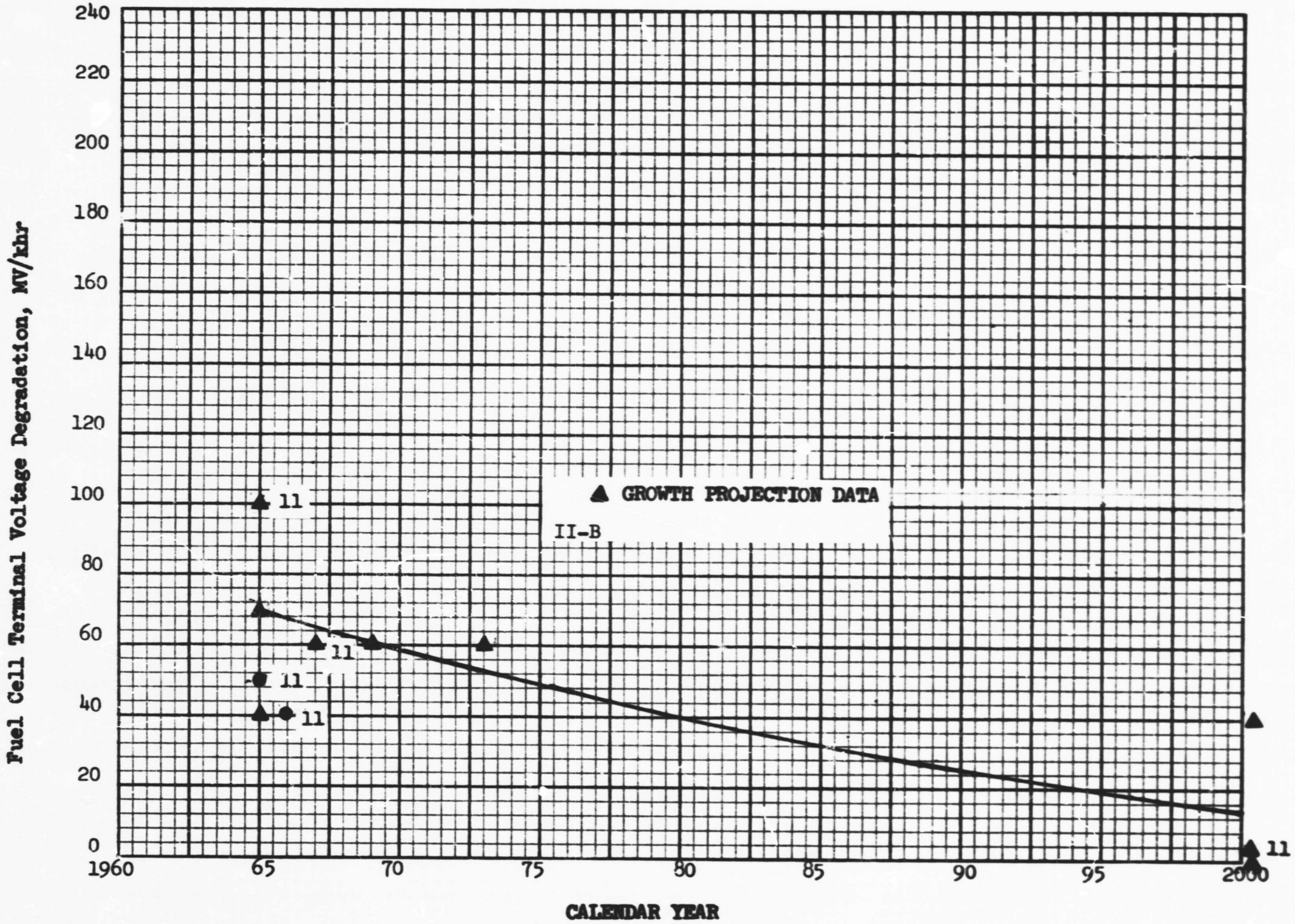

Figure 3-56 **Projection Of Fuel Cell Terminal Voltage Degradation**

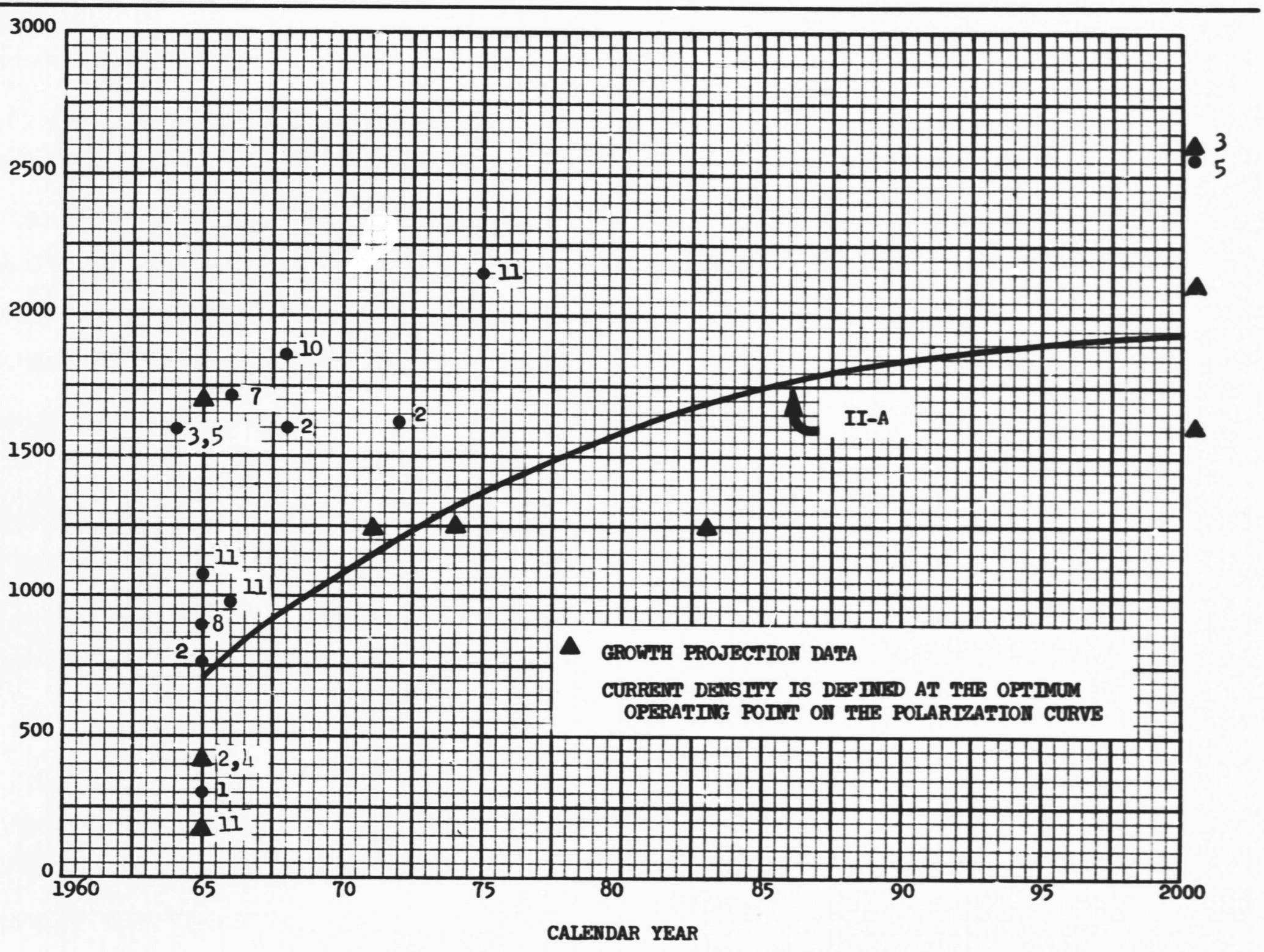

FIGURE 3-57 PROJECTION OF FUEL CELL CURRENT DENSITY

Fuel cell parasitic losses are caused by operation of the control and instrumentation equipment. A projection of parasitic losses in kW/kW is shown in Figure 3-58. Estimates of the specific mass (kg/kW) of a hydrogen-oxygen fuel cell module is shown in Figure 3-59. Figure 3-59 shows a relatively low ultimate specific mass, but indicates that considerable time will elapse before the lower limit can be expected with a practical degree of confidence. The corresponding estimates of density for the fuel-cell and support equipment in kg/m^3 are shown in Figure 3-60.

A projection of the mean time before failure of individual fuel cell elements is shown in Figure 3-61. Random failures in fuel cell elements are often caused by individual cell variations which cause local excess current den-densities and accelerated deterioration. A projection of fuel cell module production cost in $K/kW is shown in Figure 3-62 and the basic parametric data used for the design of the reformer/decomposer equipment for the storable reactant fuel cell module is shown in Figures 3-63 and 3-64.

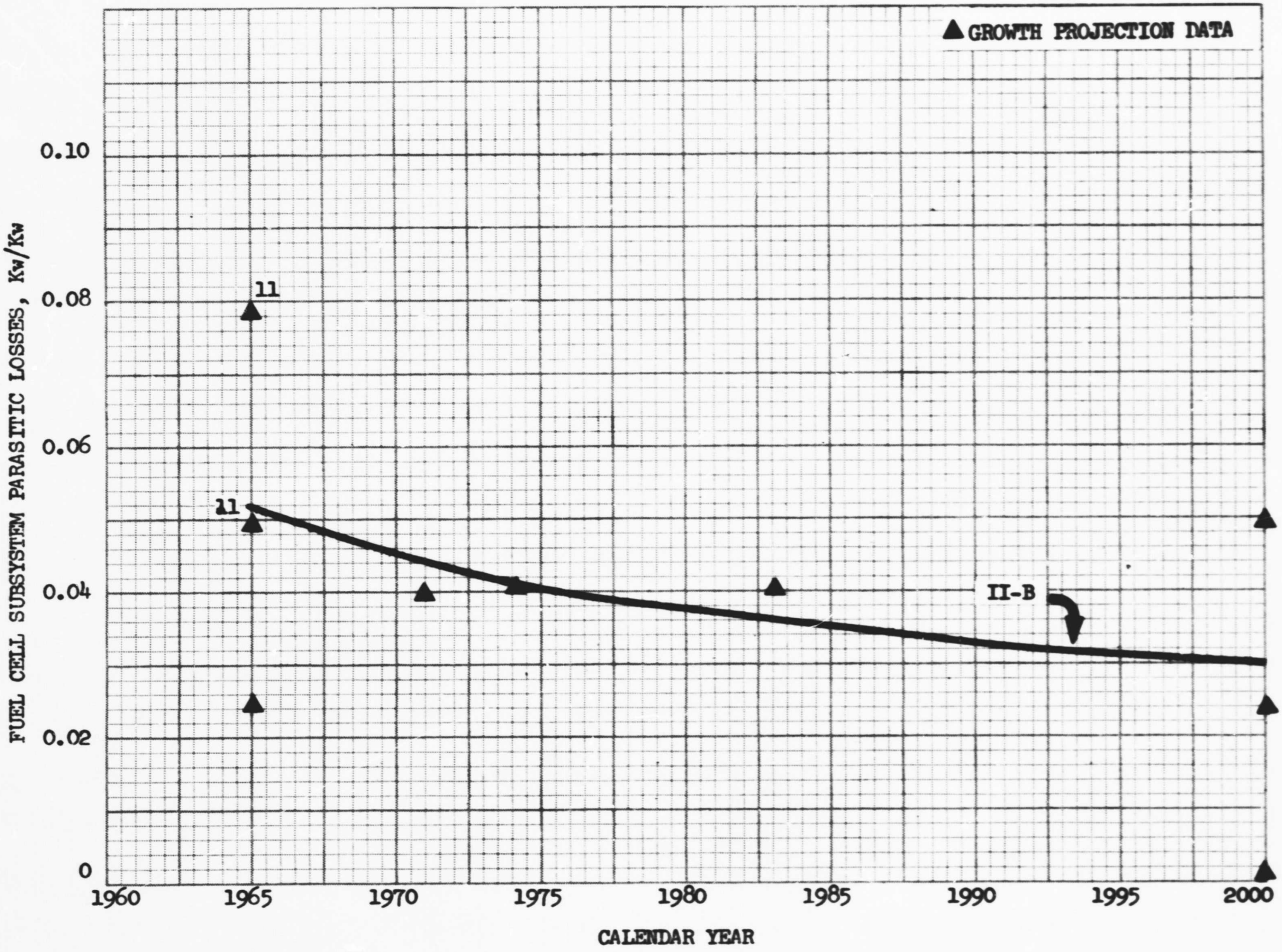

Figure 3-58 Projection of Fuel Cell Subsystem Parasitic Losses

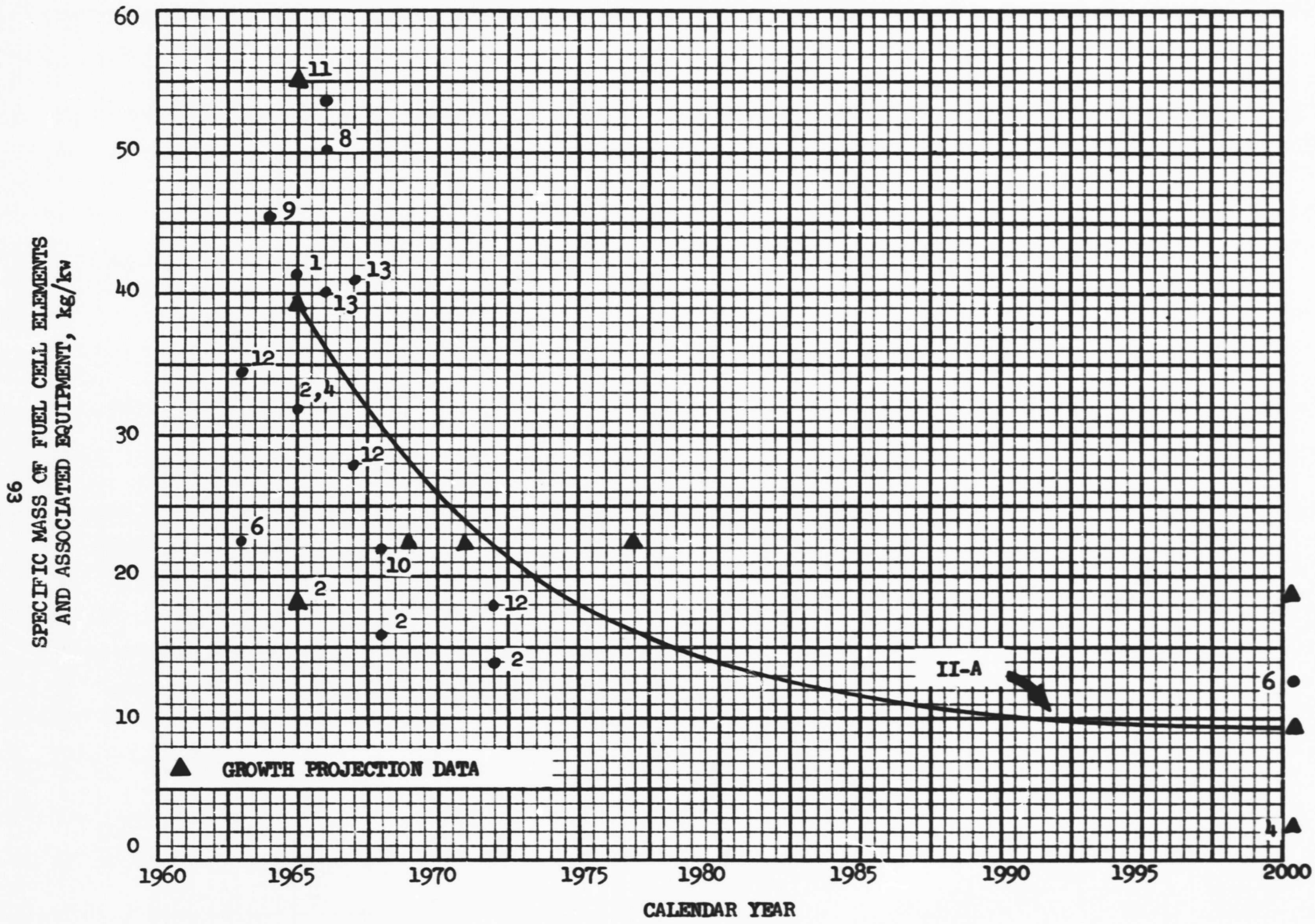

Figure 3-59 Projection of Fuel Cell Specific Mass

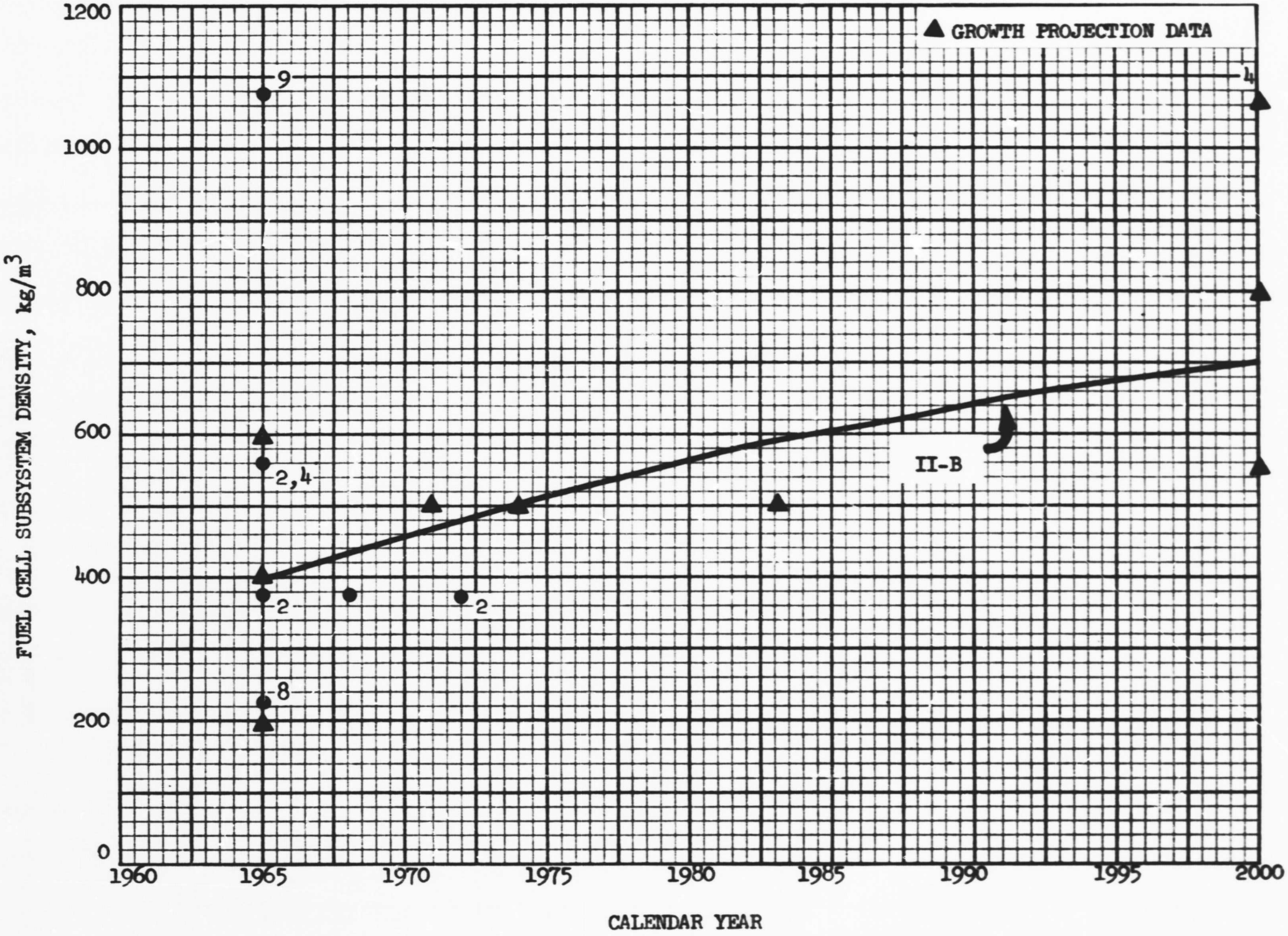

Figure 3-60 Projection of Fuel Cell Subsystem Density

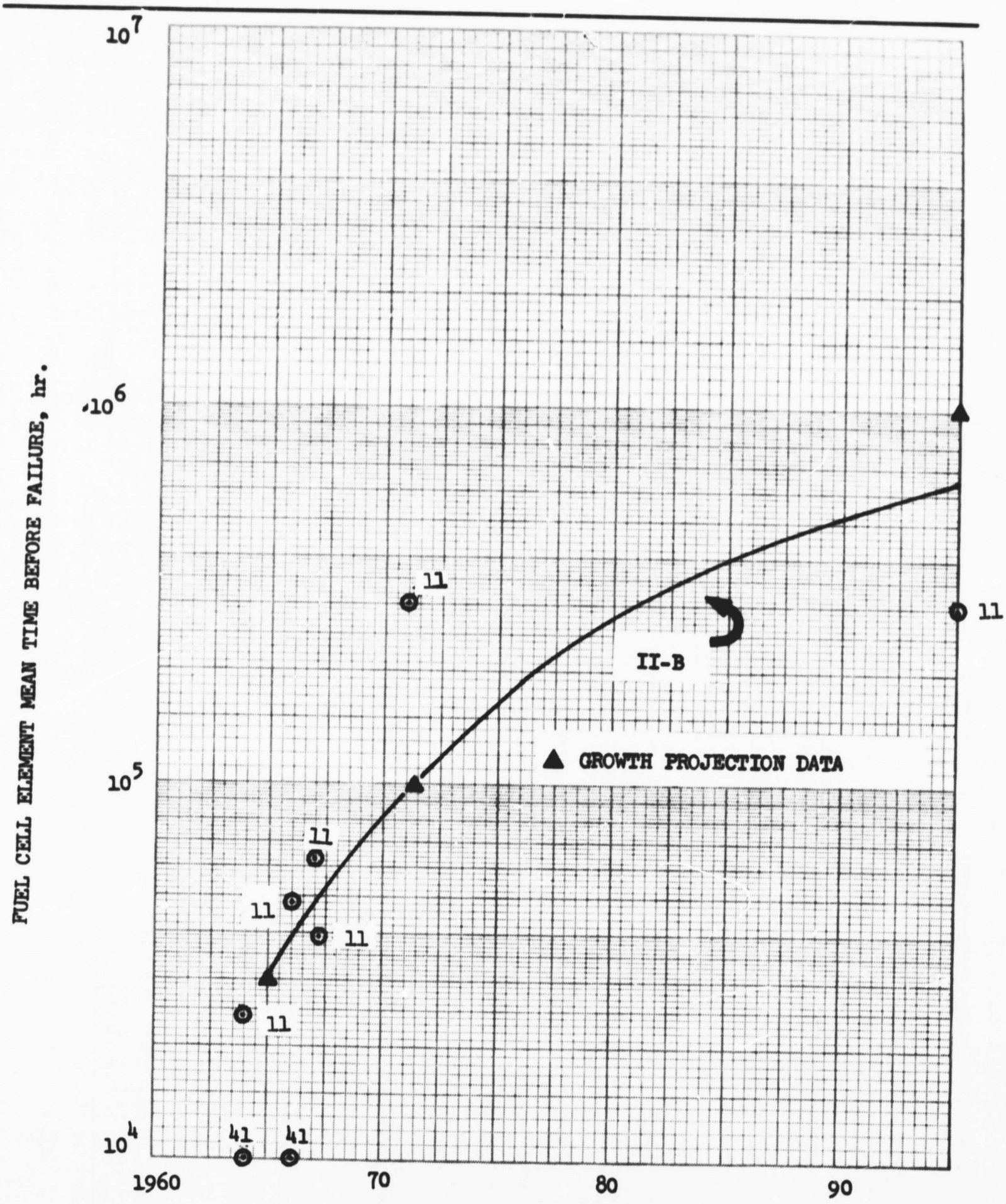

Figure 3-61 Projection of Fuel Cell Element Mean Time Before Failure

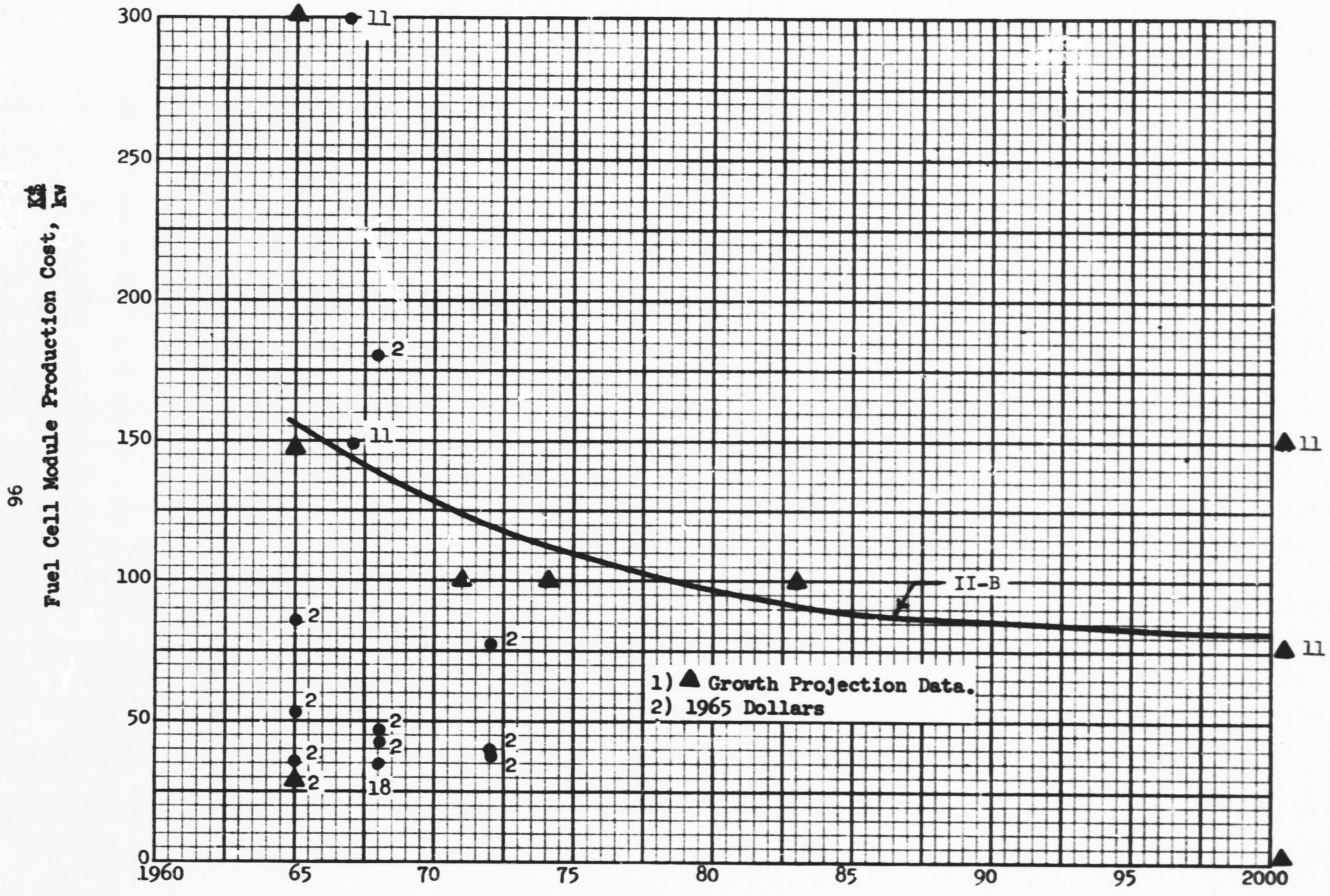

Figure 3-62 Projection of Fuel Cell Module Production Costs

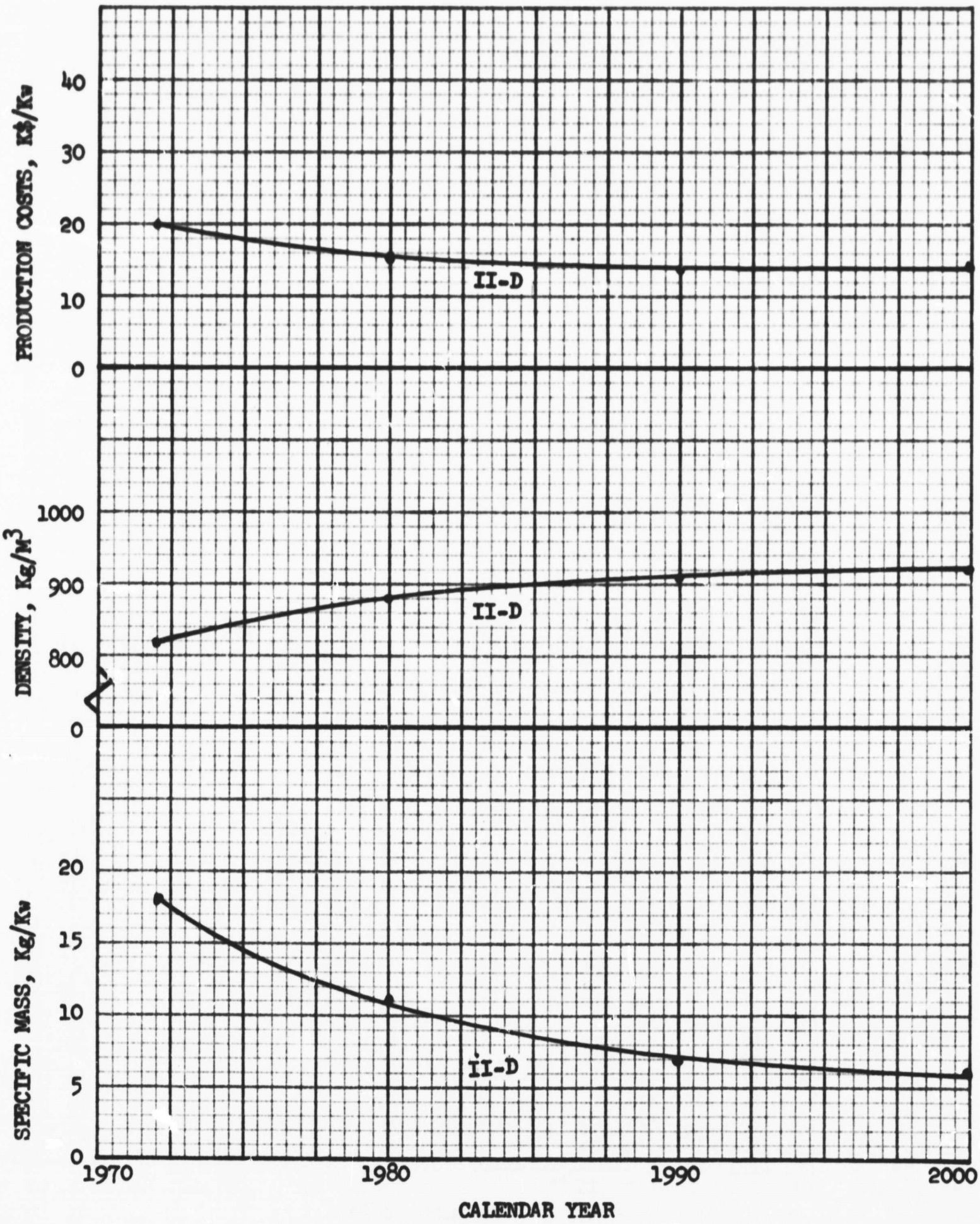

Figure 3-63 Storable Reactant Fuel Cell Reformer/Decomposer Characteristic

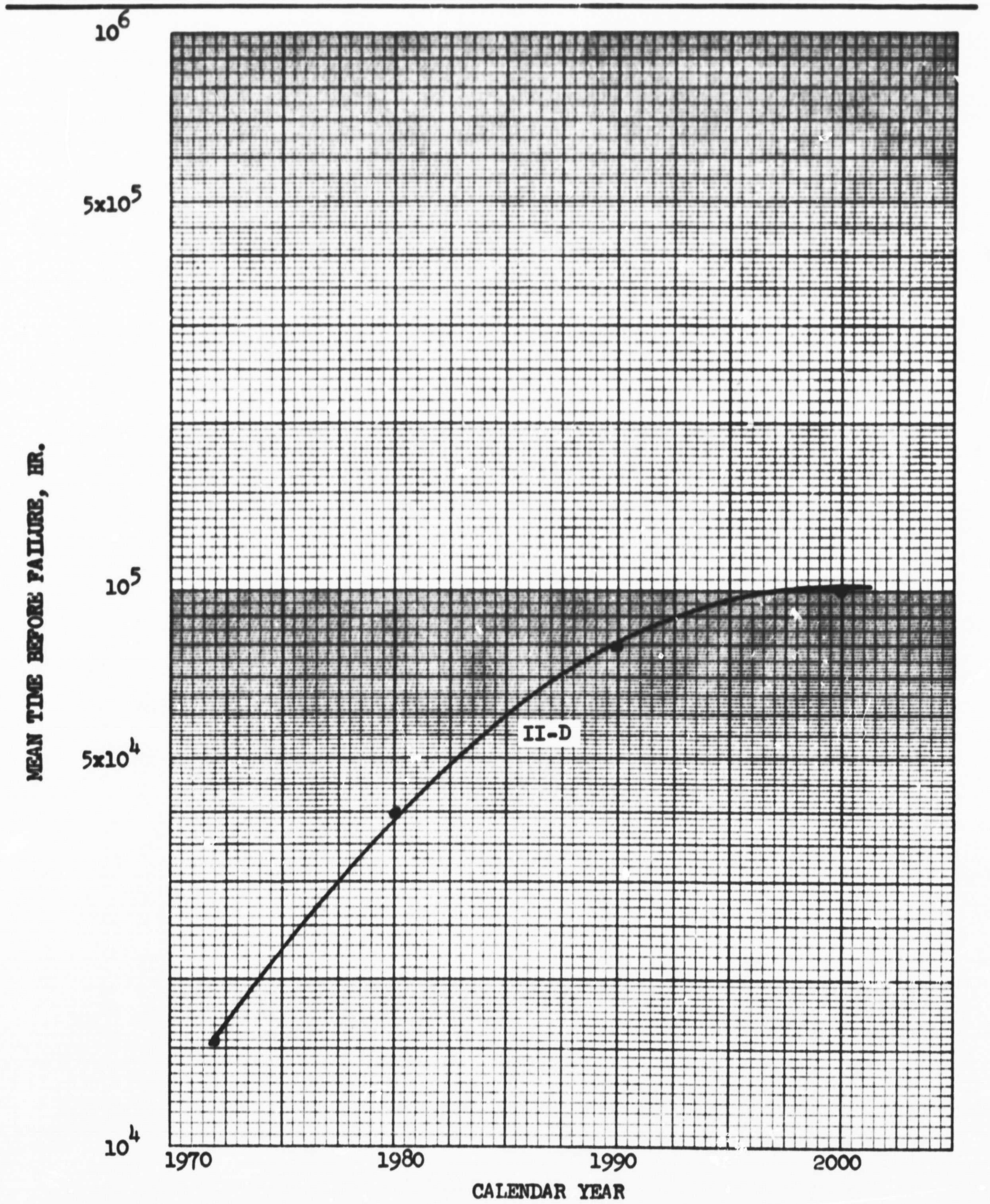

Figure 3-64 Storable Fuel Cell Reformer/Decomposer Mean Time Before Failure

3.1.5 Batteries

Batteries have been used on most of the spacecraft launched by the United States. They have been used as a primary power source on Mercury, early Gemini, Thor, Delta, Atlas, Titan, and Saturn vehicles. Secondary batteries have been used in conjunction with a primary solar cell power subsystem on most of the satellite and space probes. A battery cell shown in Figure 3-65 and is defined as that physical entity yielding the minimum discharge potential of a chemical reduction/oxidation reaction (redox couple). Battery cells up to 100 ampere-hours are presently undergoing development.

Batteries are classified either as primary types that consume the active material and cannot be recharged effectively or as secondary batteries that undergo reversible chemical reactions and can be operated through a number of charge-discharge cycles. Some chemical redox couples can be used as either a primary or secondary type, depending on the design and construction of the battery and the mission requirements. Numerous chemical redox couples have been tested as potential batteries. Many are now undergoing exploratory research for future applications. These systems include such types as the metal-air batteries, thermal batteries, nonaqueous electrolyte batteries, and low-temperature batteries. At this stage of development, however, insufficient data are available for assessing their potential for use in a space power system. For this reason, the batteries investigated will be restricted to those types which have proven themselves in the space program over the past years; for example, the sealed nickel-cadmium, silver-cadmium, and silver-zinc systems. The major operational characteristics of these battery types are given in Table 3-19.

Battery cells are often arranged in series (to increase overall output voltage) or parallel (to increase overall output current) to form battery modules. Battery modules often contain standby cells to improve module reliability. A typical example of a battery module is shown in Figure 3-66a. Modules, in turn, are connected in series until the desired output voltage is achieved. This combination of modules is defined as the battery and is indicated in Figure 3-66b. To attain the necessary output current, batteries are often combined in parallel. This arrangement will be defined as the battery stack

Table 3-19 (page 1 of 2)

BATTERY POWER CONVERSION SUBSYSTEM BRIEFING CHART

Item	Value
Identification	
Applicable energy source	Chemical
Conversion equipment	DC electrical
Potential heat rejection subsystems	Radiator
Major components	Cells, battery modules, charge regulators
Vehicle-Mission Application Range	
Useful power level	10W to 10 kW
Duration of mission	0 to 5 years
Types of spacecraft	Manned, unmanned, orbital, interplanetary
Status (1967)	
State of the art	10W to 3 kW
Availability of support subsystems	Adequate
Special problems	Cycle life, memory effects, charge control, seals, separator materials, gassing
Subsystem Characteristics (1967)	
Range of energy density	
NiCd	25 to 40 Wh/kg
AgCd	40 to 70 Wh/kg
AgZn	55 to 200 Wh/kg
Charge regulator	2 to 100 kg/kW
Range of volumetric energy density	
NiCd	(0.6 to 1) x 10^5 Wh/m^3
AgCd	(0.9 to 1.6) x 10^5 Wh/m^3
AgZn	(1 to 4) x 10^5 Wh/m^3
Range of reliability	0.95 to 0.98 (1 year)
Range of specific costs	$1 to $2/Wh

Table 3-19 (page 2 of 2)

Item	Value
Performance Data (1967)	
Range of coulombic efficiency*	
NiCd	40 to 90%
AgCd	80 to 98%
AgZn	80 to 98%
Range of charge rates**	
NiCd	3 to 24 hr
AgCd	4 to 40 hr
AgZn	4 to 40 hr
Range of cycle life (25% depth of discharge)	
NiCd	5,000 to 16,000 hr
AgCd	3,000 to 9,000 hr
AgZn	100 to 2,500 hr
Range of operating temperature	
NiCd	260° to 310°K
AgCd	260° to 310°K
AgZn	290° to 305°K
Sterilization capacity retention	95% (AgZn)
Range of charge regulator efficiency	70 to 86%

*Coulombic efficiency is the ratio of ampere-hours discharged from the battery to ampere-hours charged into the battery.

**Charge rate is defined as the ratio ampere-hours of battery discharge capacity to the charge current in amperes.

as shown in Figure 3-67a. As indicated in this figure, a charge regulator is necessary to control input and output currents and voltages to the battery stack. The major components of an energy storage subsystem are the battery stack and battery charge regulator. The interactions between these components during charge and discharge are shown in Figure 3-67b.

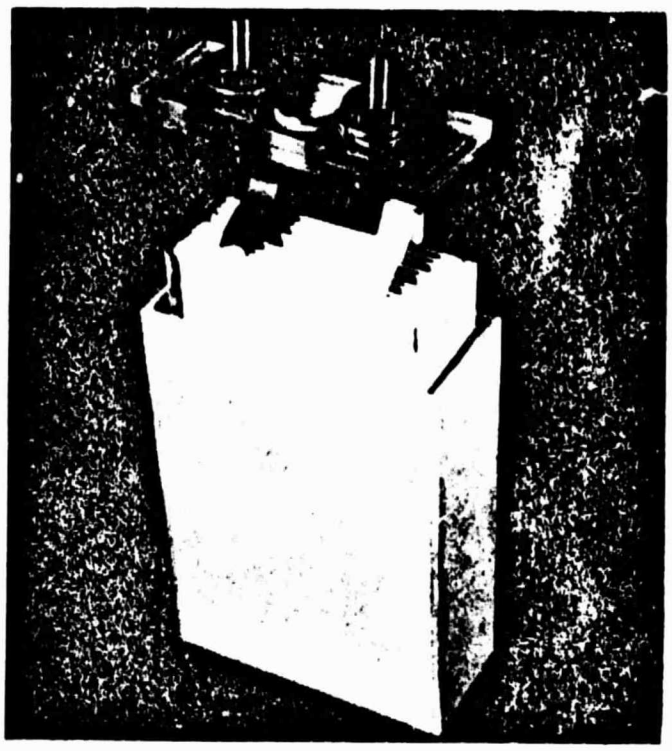

Figure 3-65 Battery Cell Assembly

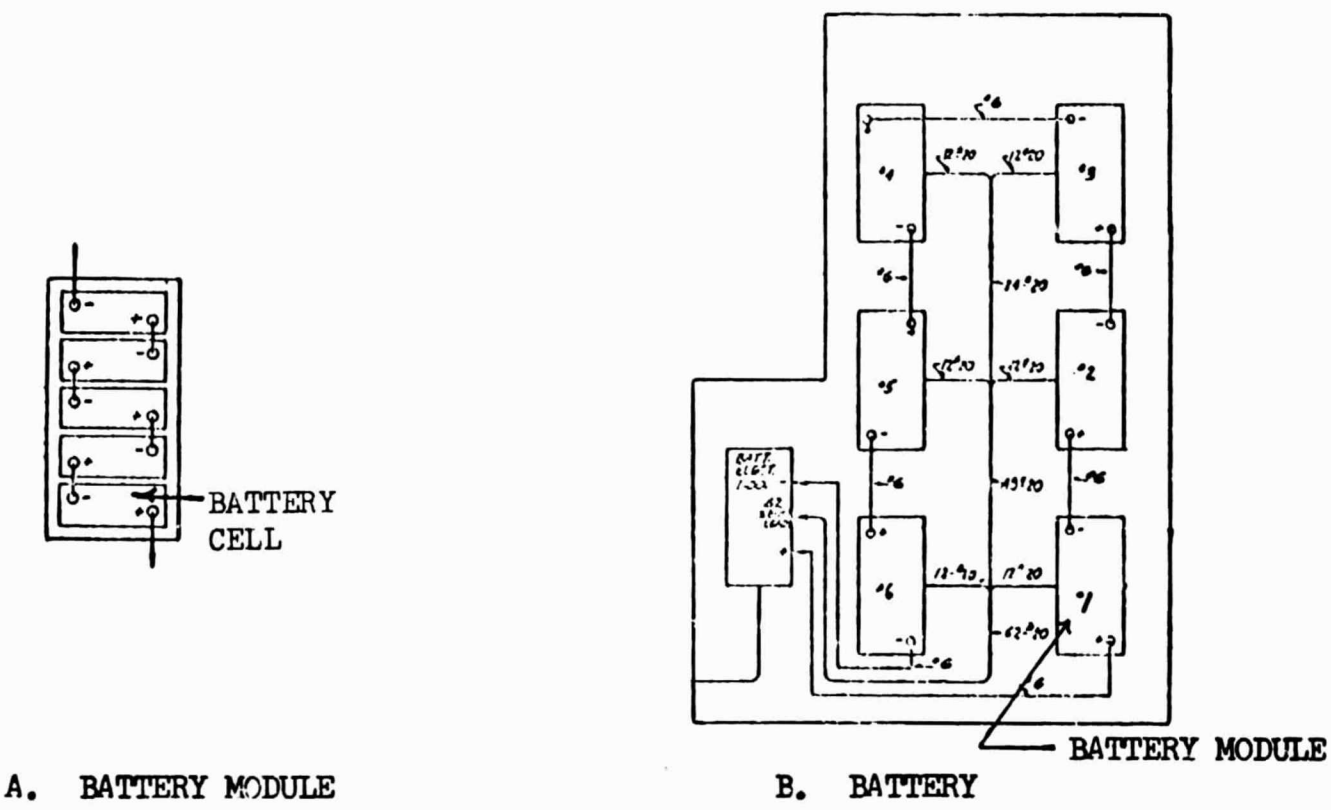

A. BATTERY MODULE B. BATTERY

Figure 3-66 Battery Module and Battery

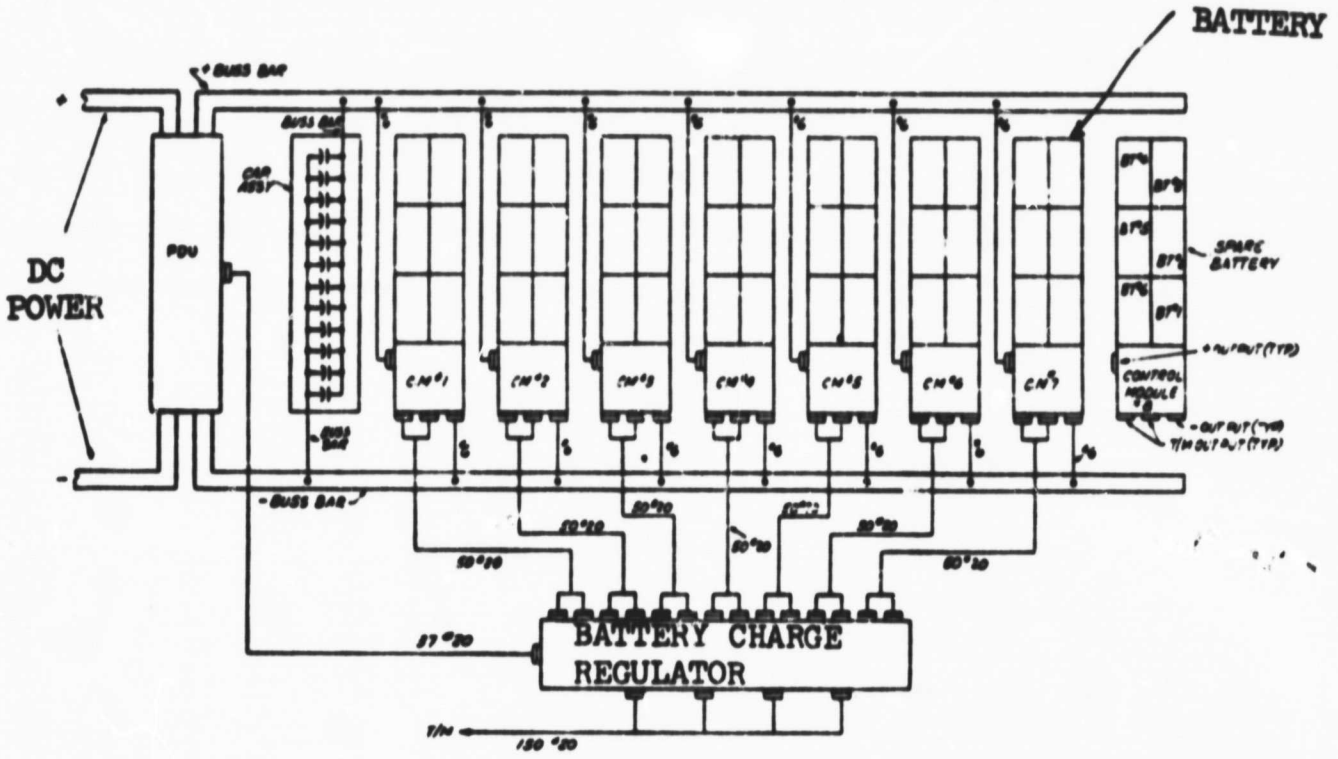

a. BATTERY STACK AND CHARGE REGULATOR

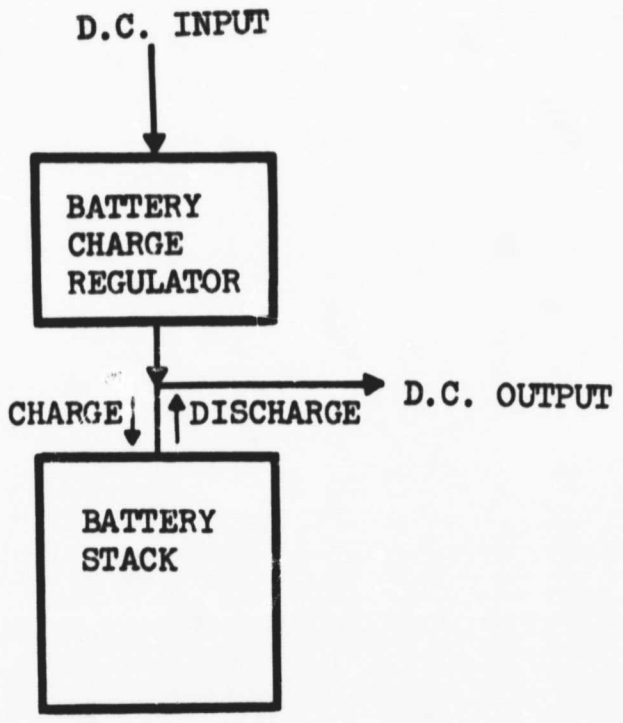

b. SUBSYSTEM SCHEMATIC

Figure 3-67 Energy Storage Subsystem

Data on the characteristics and performance of the major components in the battery subsystem are given in Tables 3-20 through 3-24 and Figures 3-68 through 3-81. The data presented are stored in the computer program block data subprogram. With state-of-the-art projections, the growth projection program is used to generate the curves. Parametric data, on the other hand, are correlated with a least-squares approximation leading to curves of regression.

Table 3-20

BATTERY CHARGE TIME LIMITS

Battery Type	Minimum Charge Time (ampere-hr/ampere)	Maximum Charge Time (ampere-hr/ampere)
NiCd	Figure 3-72	24.0 (Reference 4)
AgCd	Figure 3-72	40.0 (Reference 4)
AgZn	Figure 3-72	40.0 (Reference 4)

Table 3-21

BATTERY DISCHARGE TIME LIMITS

Battery Type	Minimum Discharge Time (ampere-hr/ampere)	Reference
NiCd	0.25	9
AgCd	0.25	9
AgZn	0.25	9

Table 3-22

SPACE BATTERY VOLTAGE EFFICIENCY

System	Average Charge Potential (volts)	Average Discharge Potential (volts)	Voltage Efficiency	Reference
NiCd	1.50	1.20	0.800	3, 11
AgCd	1.50	1.10	0.735	3, 11
AgZn	1.90	1.50	0.790	3, 11

Table 3-23

BATTERY CELL OPERATIONAL REQUIREMENTS (ASSUMED)

Item	Value
Voltage regulation	±10%
Reliability	0.999

Table 3-24

BATTERY CHARGE REGULATOR CHARACTERISTICS

Item	Value	Reference
Specific production cost at 1 kWe	$1.5 K	Power conditioning subsystem data
Mean time between failure	1.0×10^4 hour	

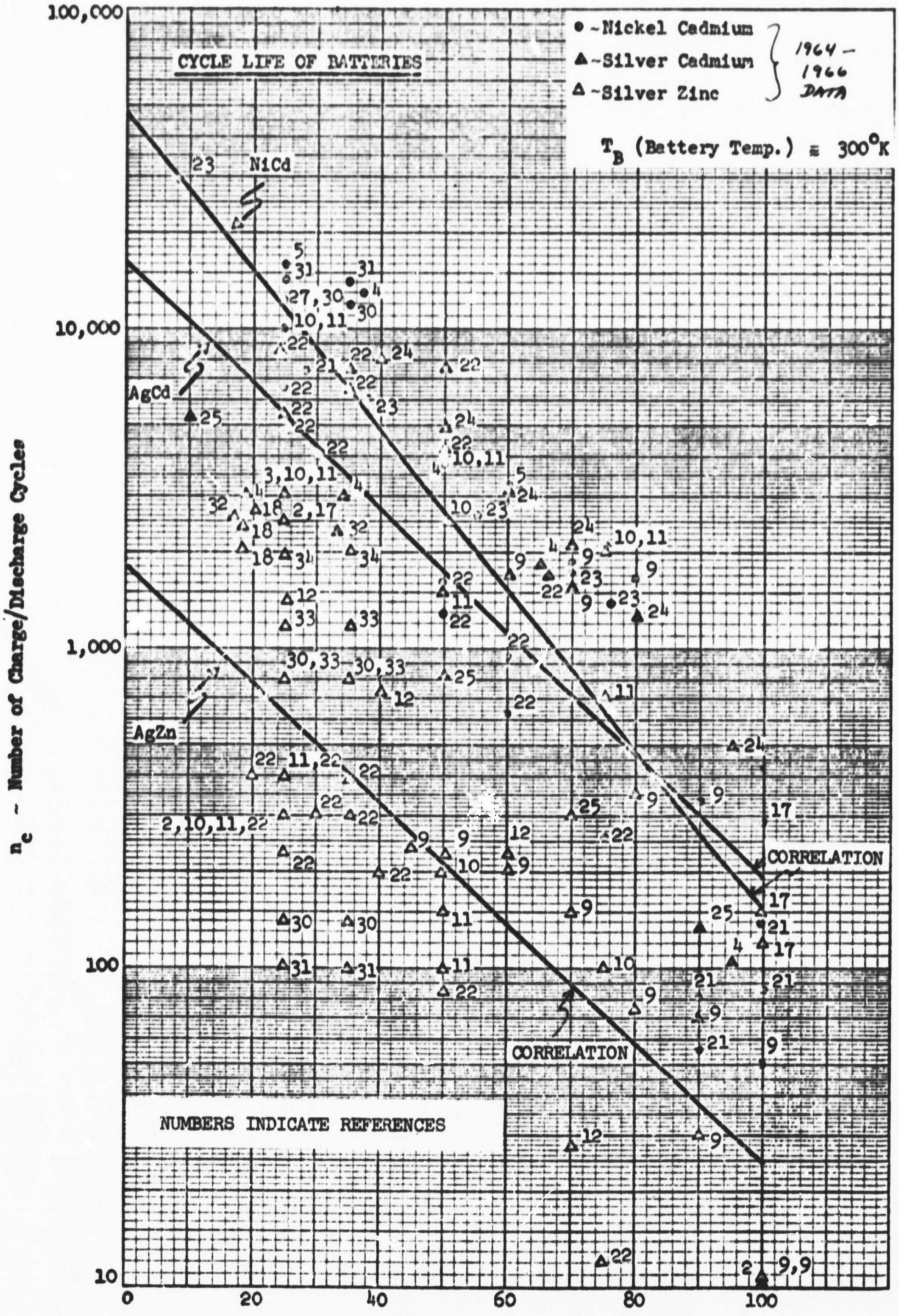

Figure 3-68 η_d - Battery Depth of Discharge - Percent

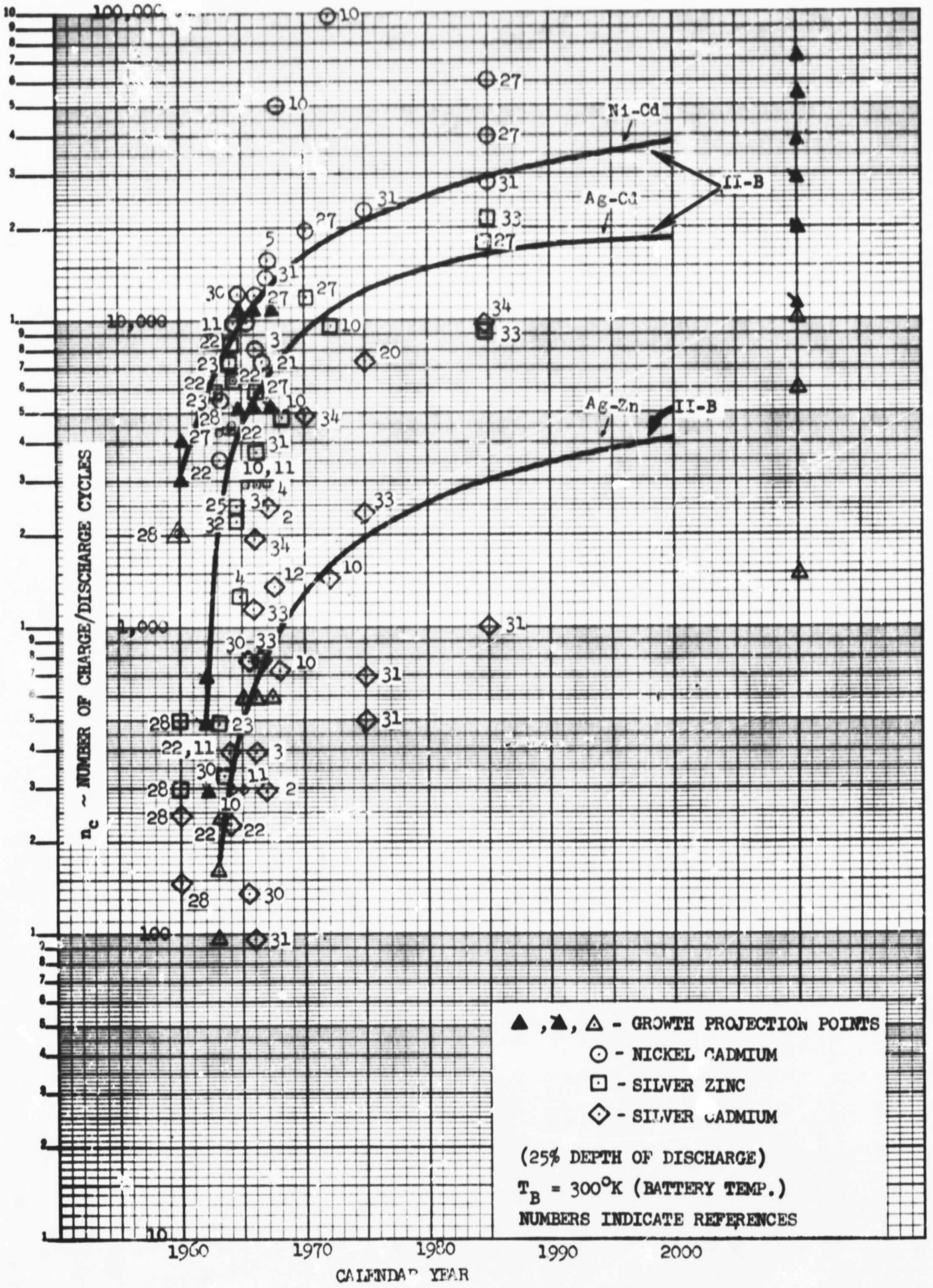

Figure 3-69 Projection - Battery Cycle Life

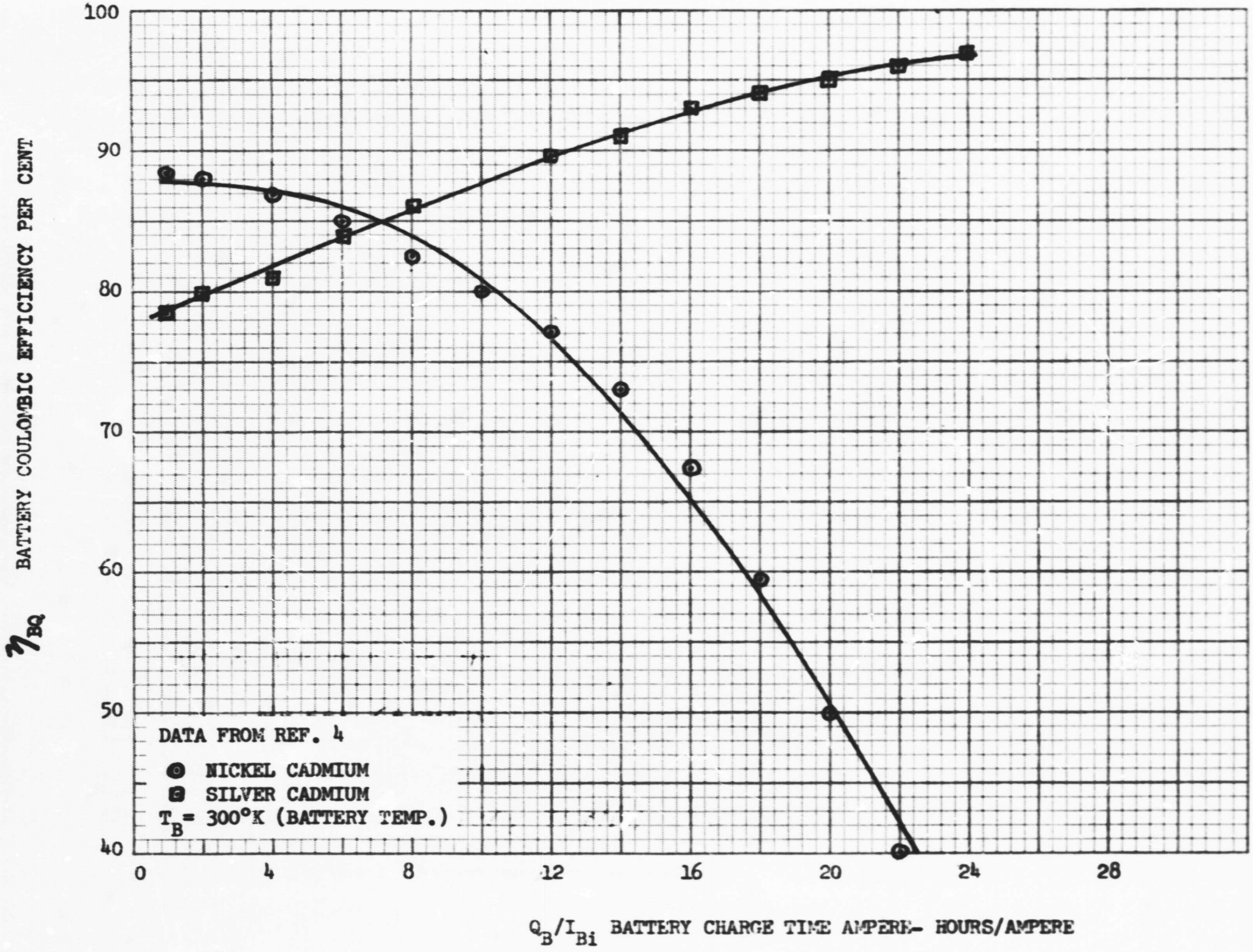

FIGURE 3-70 Charge Acceptance of Secondary Batteries

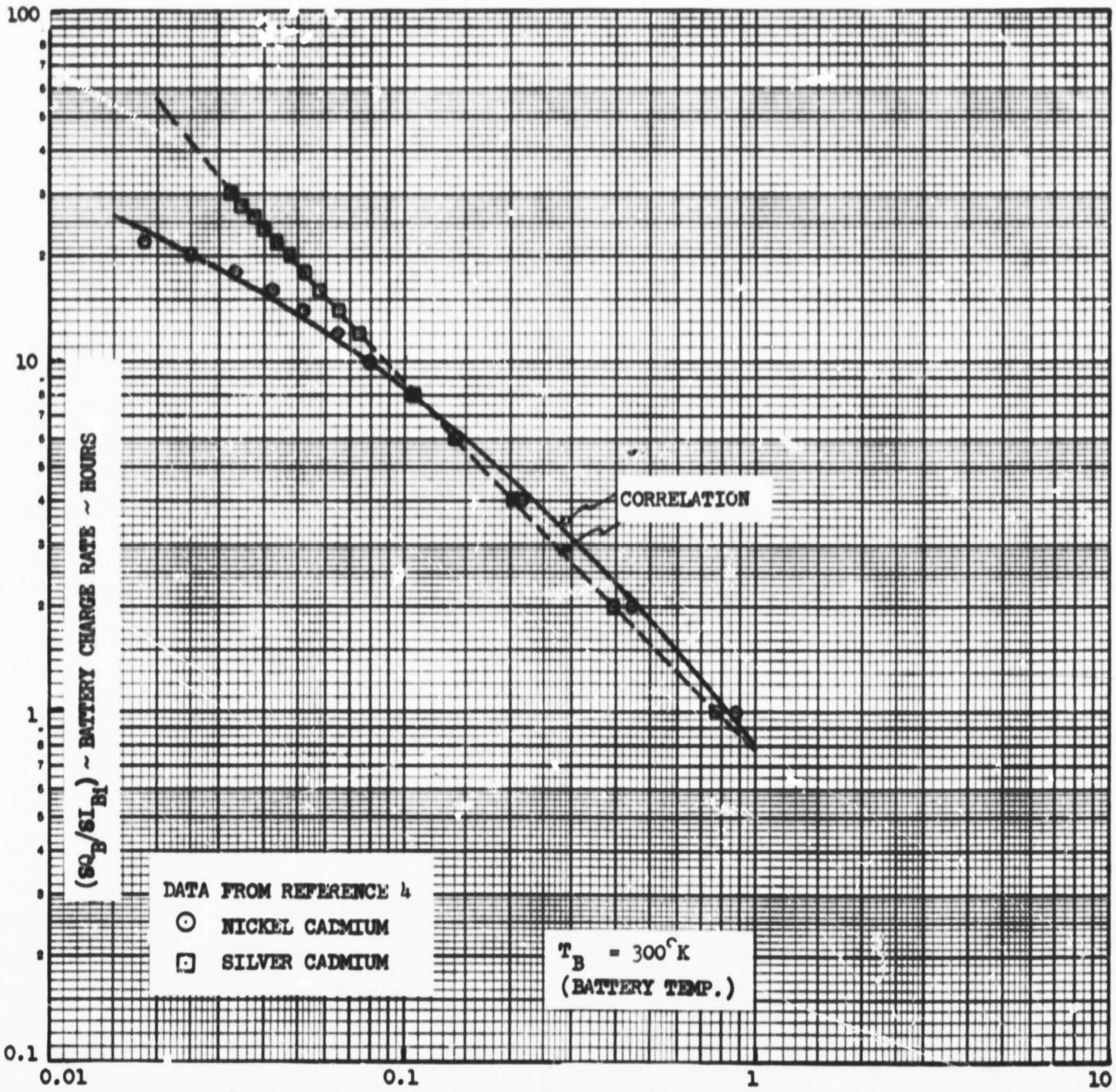

Figure 3-71 Charge Rates of Secondary Batteries

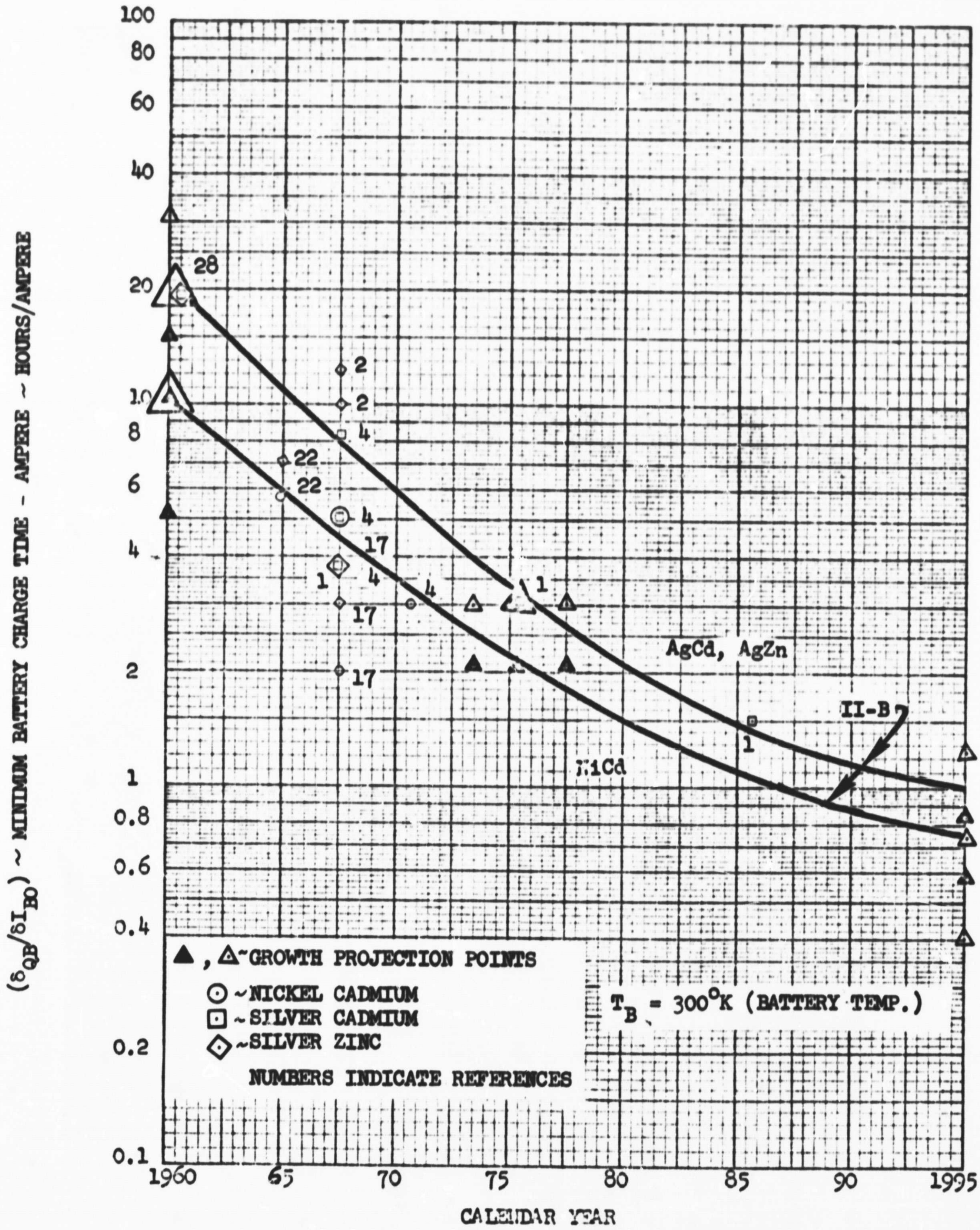

Figure 3-72 - Projection Minimum Battery Charge Time

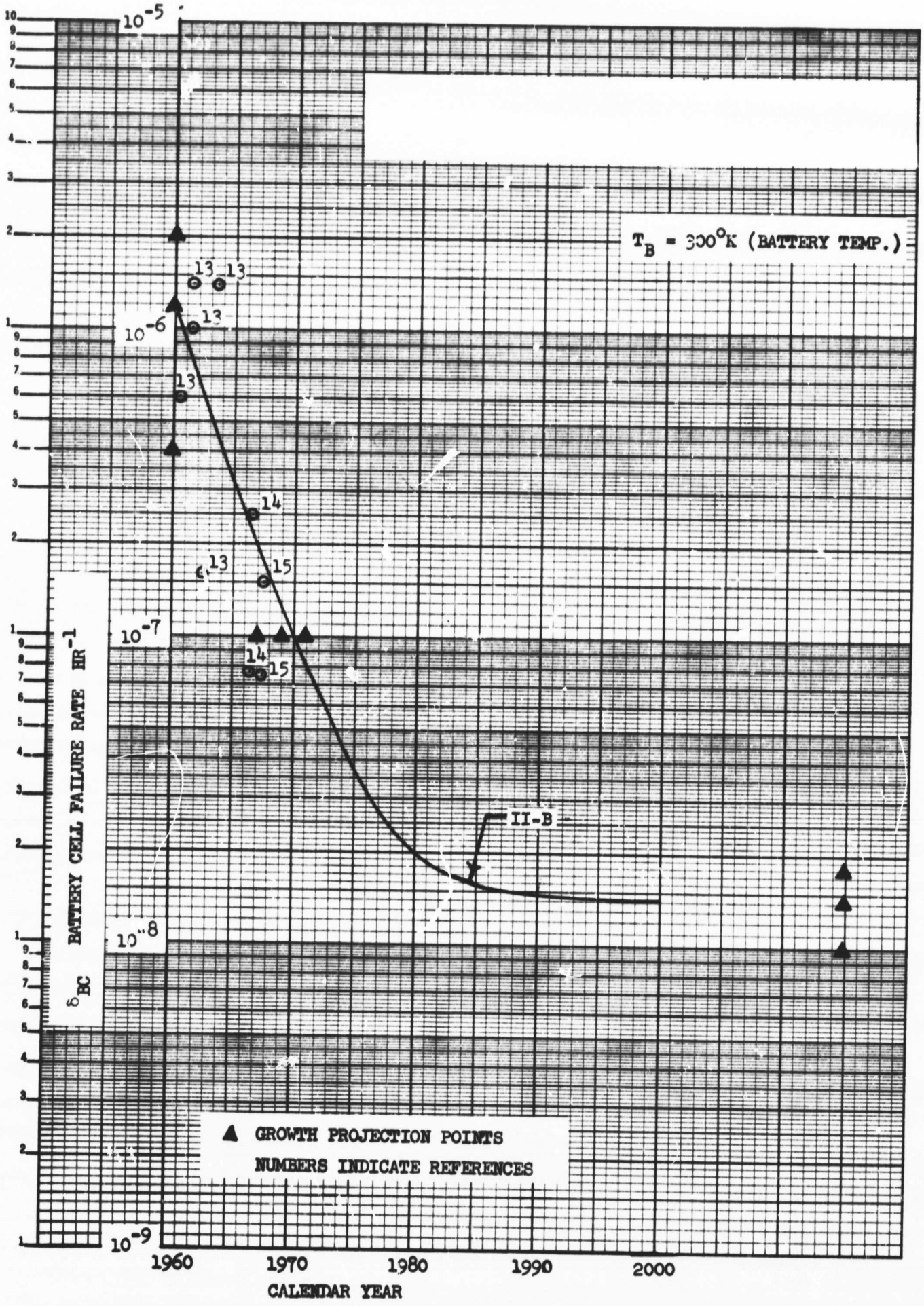

Figure 3-73 Projection -- Battery Cell Failure Rates

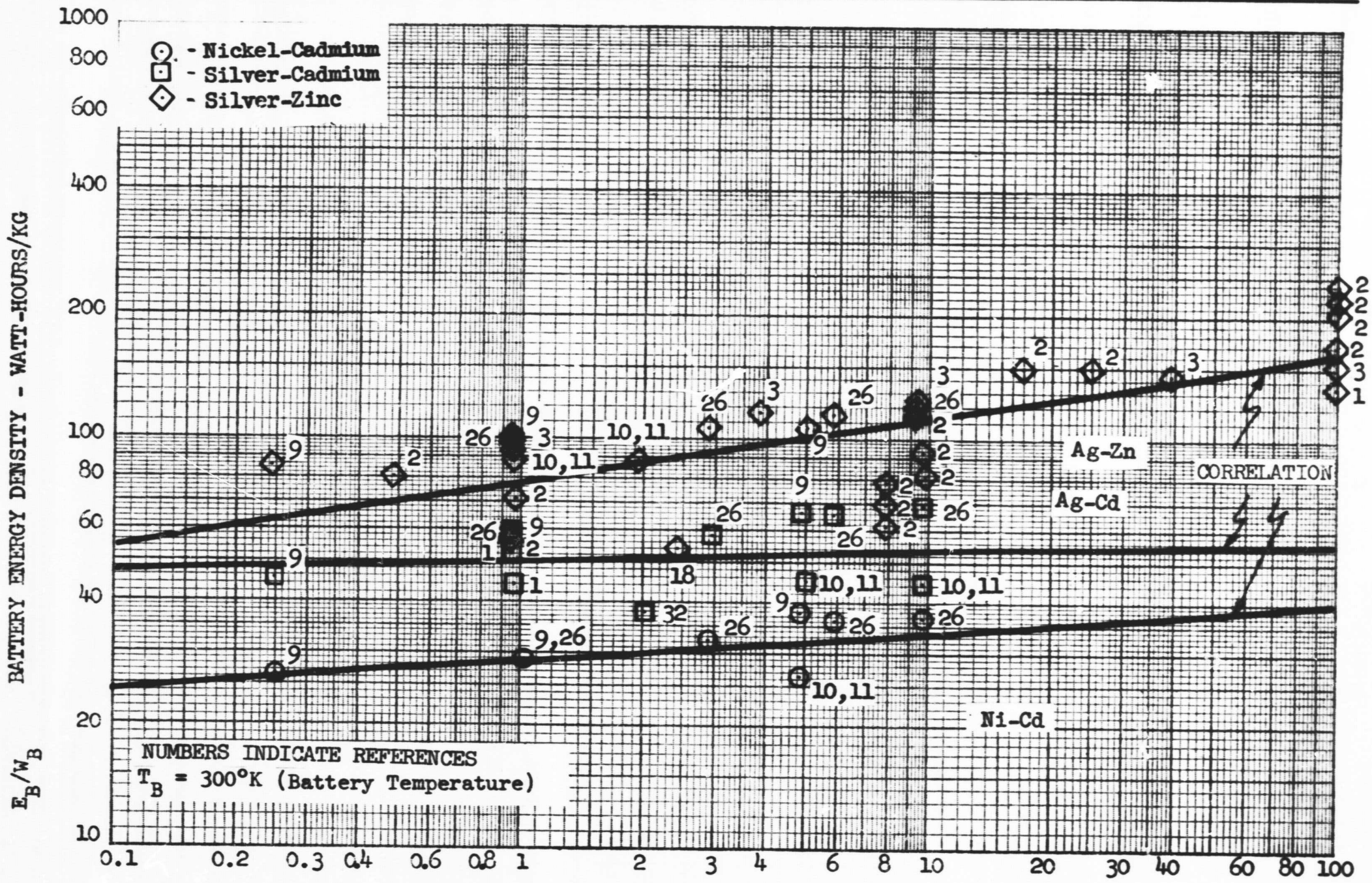

Figure 3-74 - ENERGY DENSITY OF SECONDARY BATTERIES

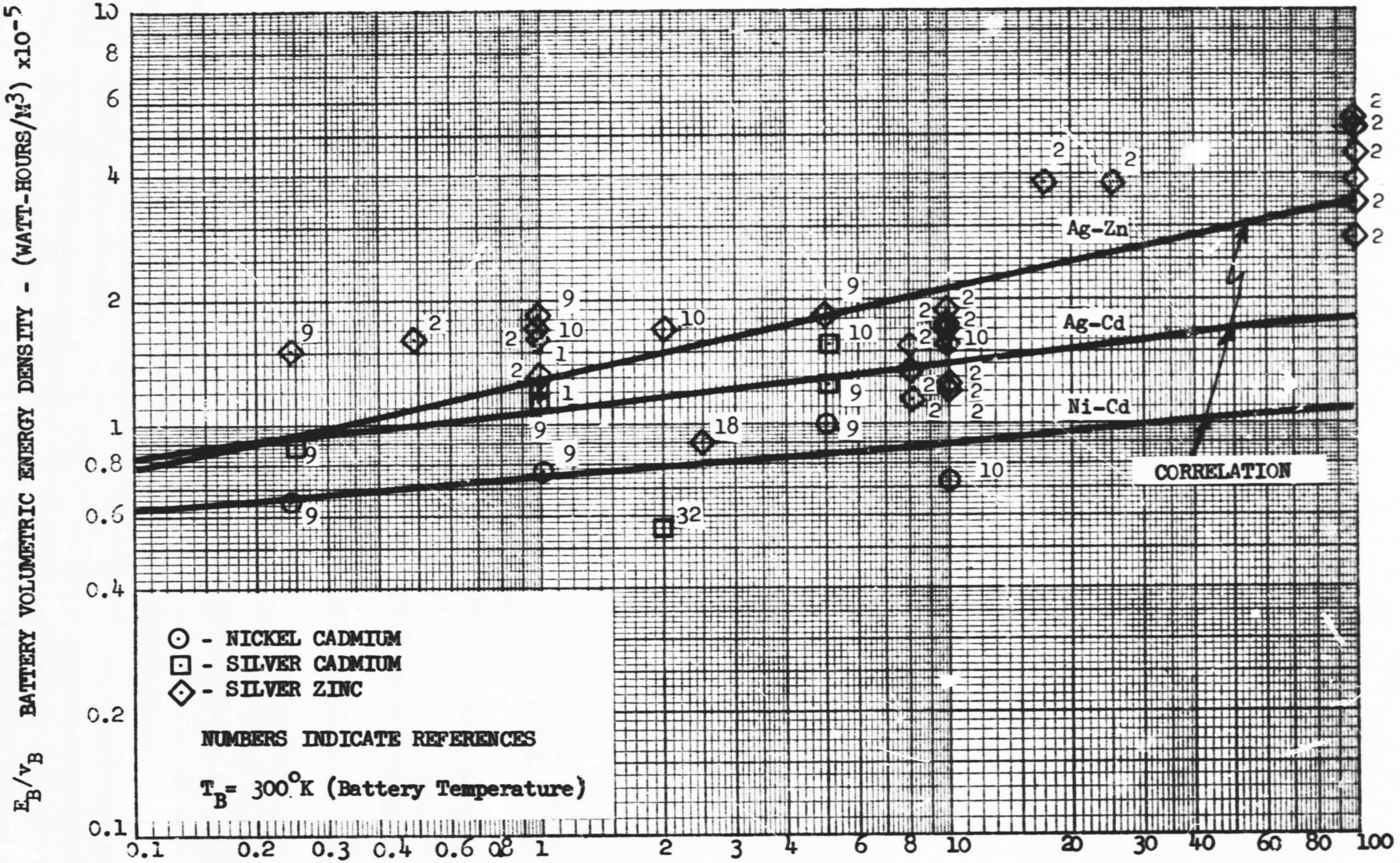

Figure 3-75 Volumetric Energy Density of Secondary Batteries

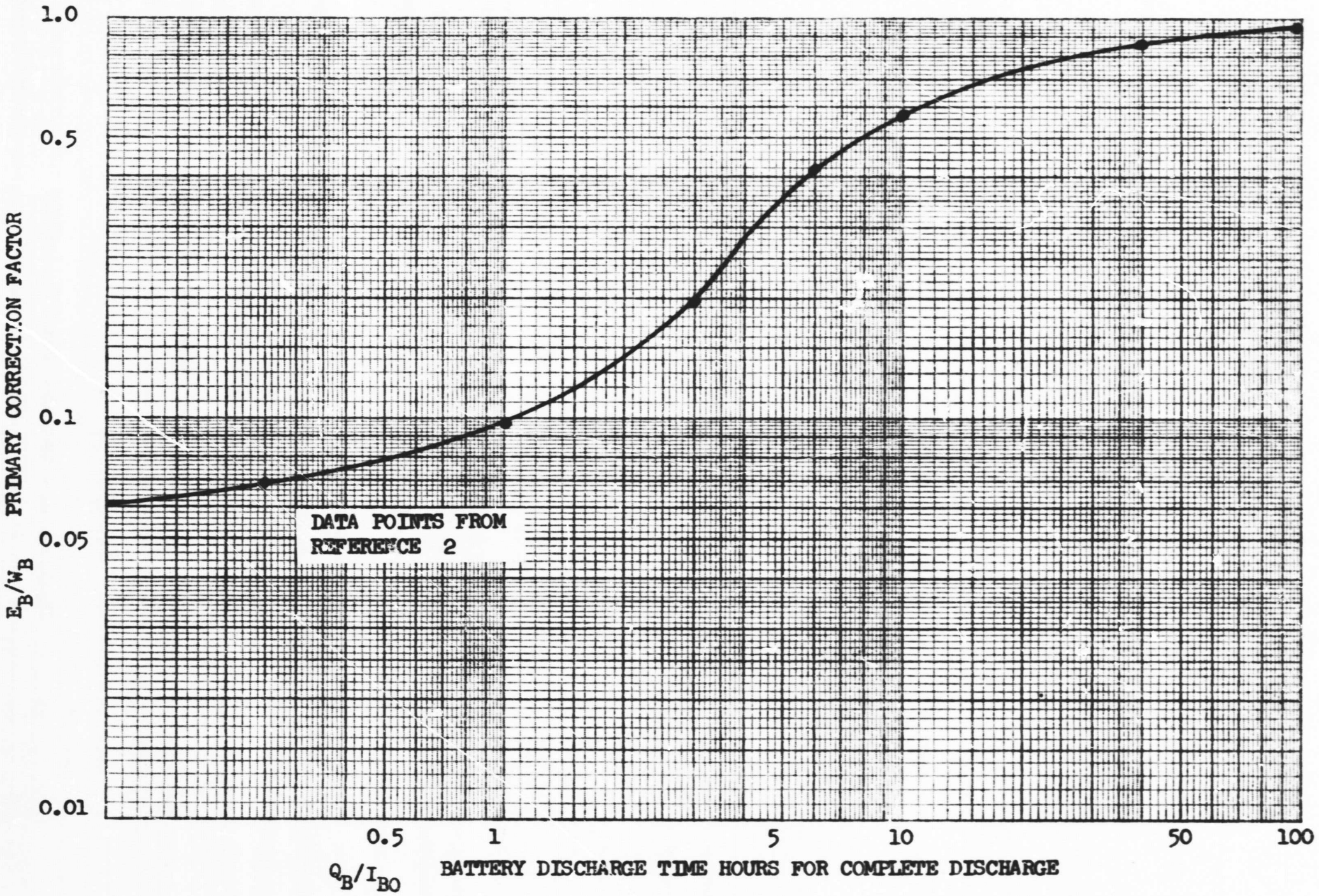

Figure 3-76 Energy Density Correction Factor for Primary AGZN Batteries Automatically - Activated

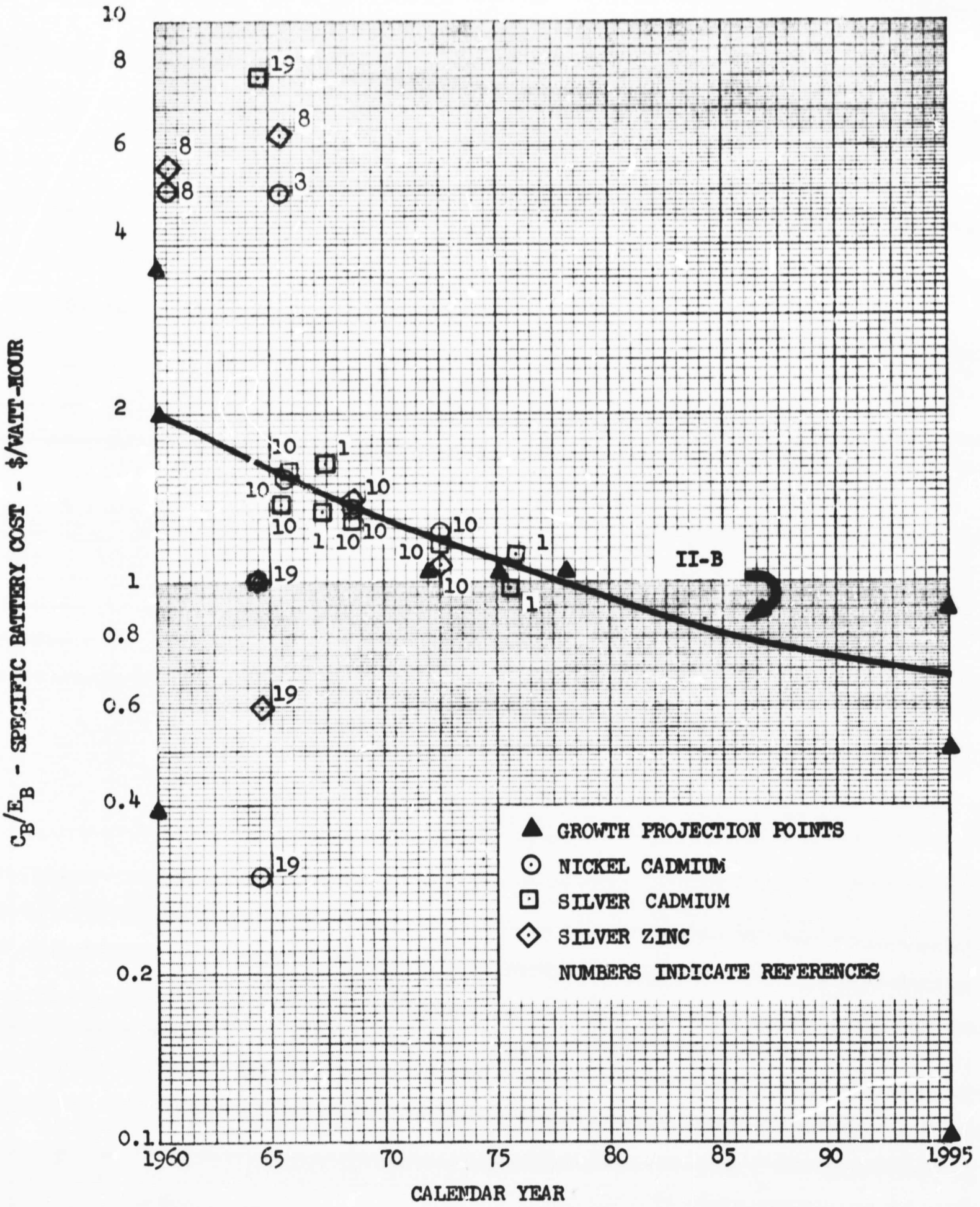

Figure 3-77 Projection - Battery Specific Costs

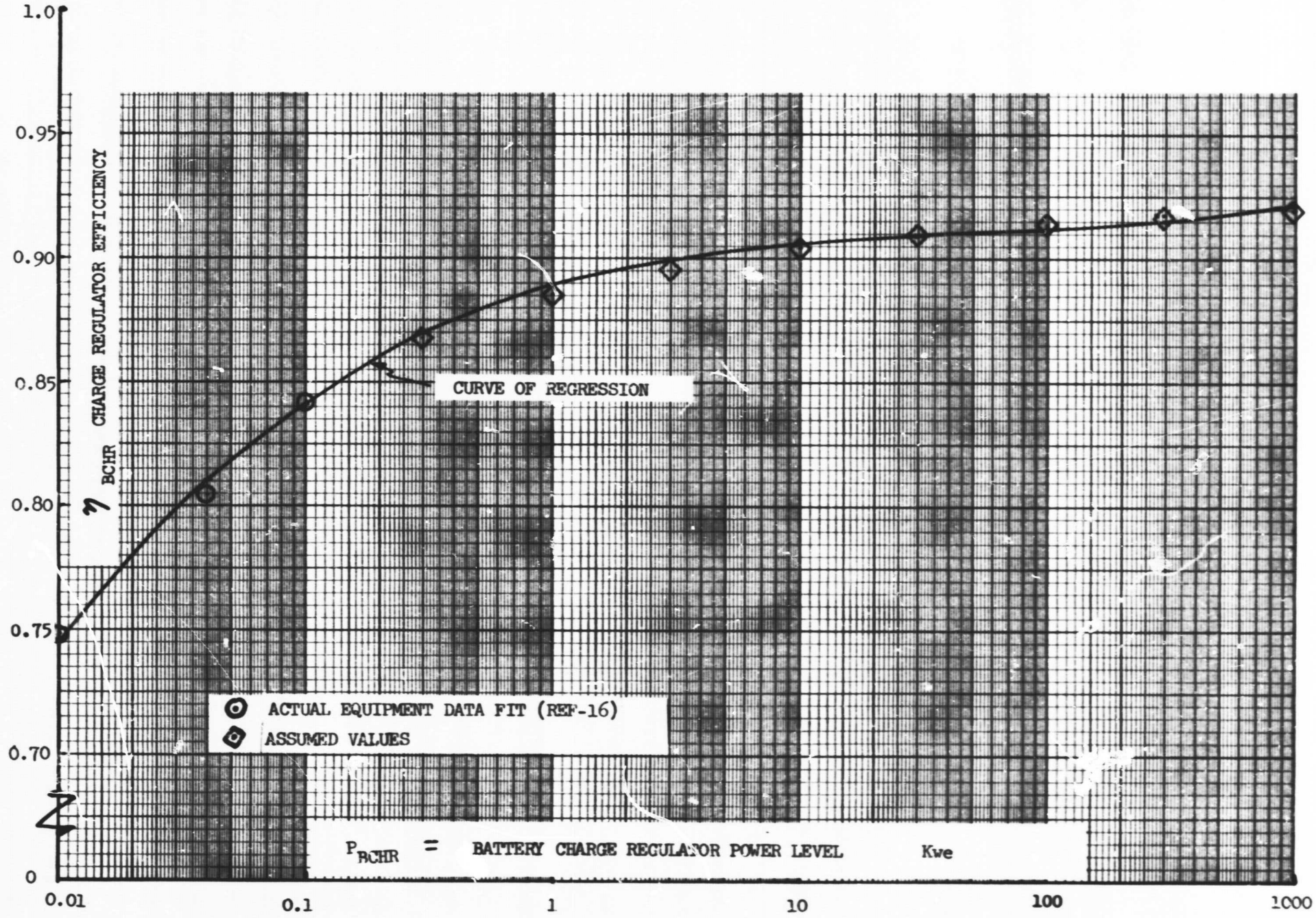

Figure 3-78 Battery Charge Regulator Efficiency

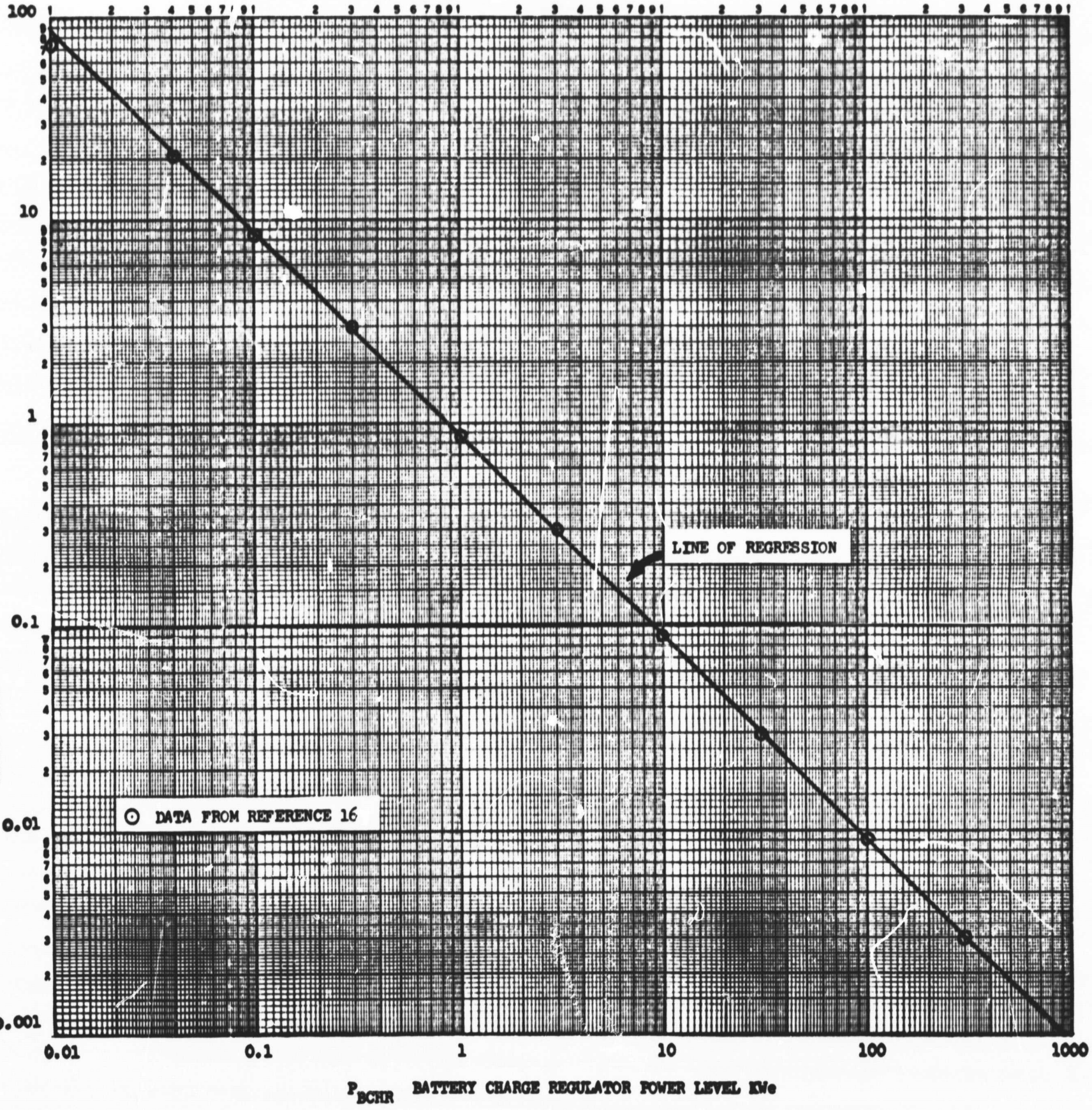

Figure 3-79 Battery Charge Regulator Efficiency

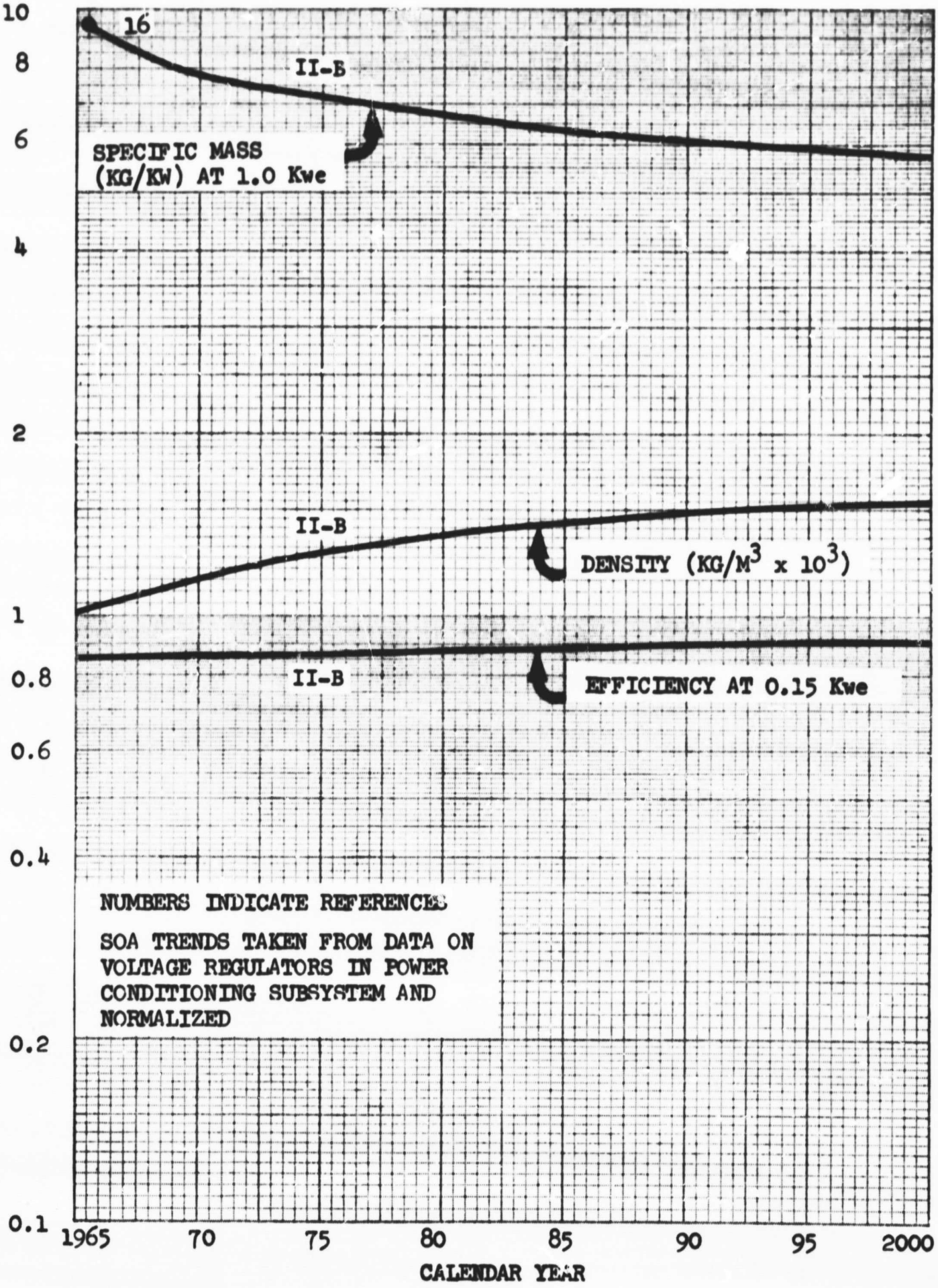

Figure 3-80 Battery Charge Regulator Operational Characteristics (Projected)

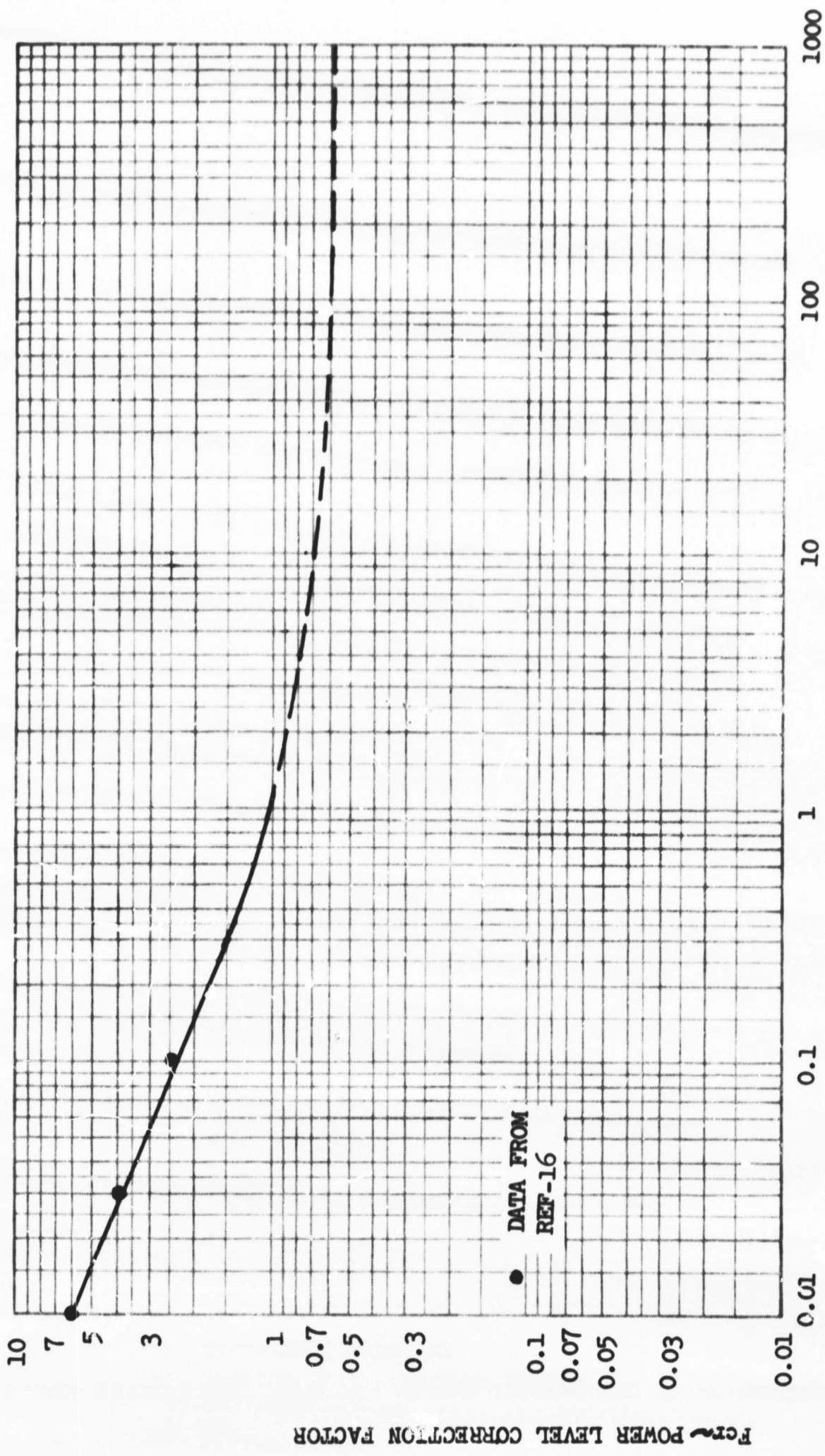

Figure 3-81 Power Level Correction Factor For Battery Charge Regulator Specific Mass

3.1.6 Brayton-Cycle Power Conversion Subsystem

The Brayton-cycle conversion subsystem is attractive for intermediate power levels (2 to as high as 100 kWe) because it offers good cycle efficiencies (estimates range as high as 25 to 30%). In addition, the use of inert gases as the working fluid eliminates corrosion problems, which is important in meeting long-life requirements. A schematic diagram of a typical Brayton-cycle power conversion module is shown in Figure 3-82. One or more modules constitute the Brayton cycle power conversion subsystem. For analytical purposes, each module is divided into five parts, the turbocompressor-alternator unit, the heat source heat exchanger, the recuperator, the radiator heat exchanger, and accessory equipment. The relationship of the major components is shown in Table 3-25.

The most critical component in the Brayton cycle power conversion module is the combined rotating unit (CRU). The CRU consists of a compressor, a turbine, and an alternator mounted on a single rotating shaft. The shaft is supported on gas-lubricated journal and thrust bearings. The major emphasis in Brayton-cycle development programs is on increasing turbine inlet temperature and component efficiencies, and on reducing sensitivity of the gas bearings to thermal distortions of the turbomachinery. The latter problem is coupled to the more general difficulty of packaging the system in an acceptable thermal design, in which the hot turbine is isolated from other system elements to minimize thermal gradients in the vicinity of the bearings.

NASA-Lewis is presently assembling ground test hardware for a 2- to 10-kWe Brayton cycle space power system which could be used either with a 30-ft solar mirror or a plutonium 238 heat source. Tests of the isotopically heated power unit are presently scheduled for 1971 in Lewis' Space Propulsion Facility, now under construction at the Plum Brook Station near Sandusky, Ohio. To date NASA-Lewis has awarded contracts totaling approximately $7 million for various non-nuclear components of the conversion system. A contract ($449,000) has also been awarded by NASA-Lewis to Avco Corporation for the design of an isotope reentry vehicle. Prime contractors include AiResearch Corporation, TRW, Pesco Products, and Gulton Industries.

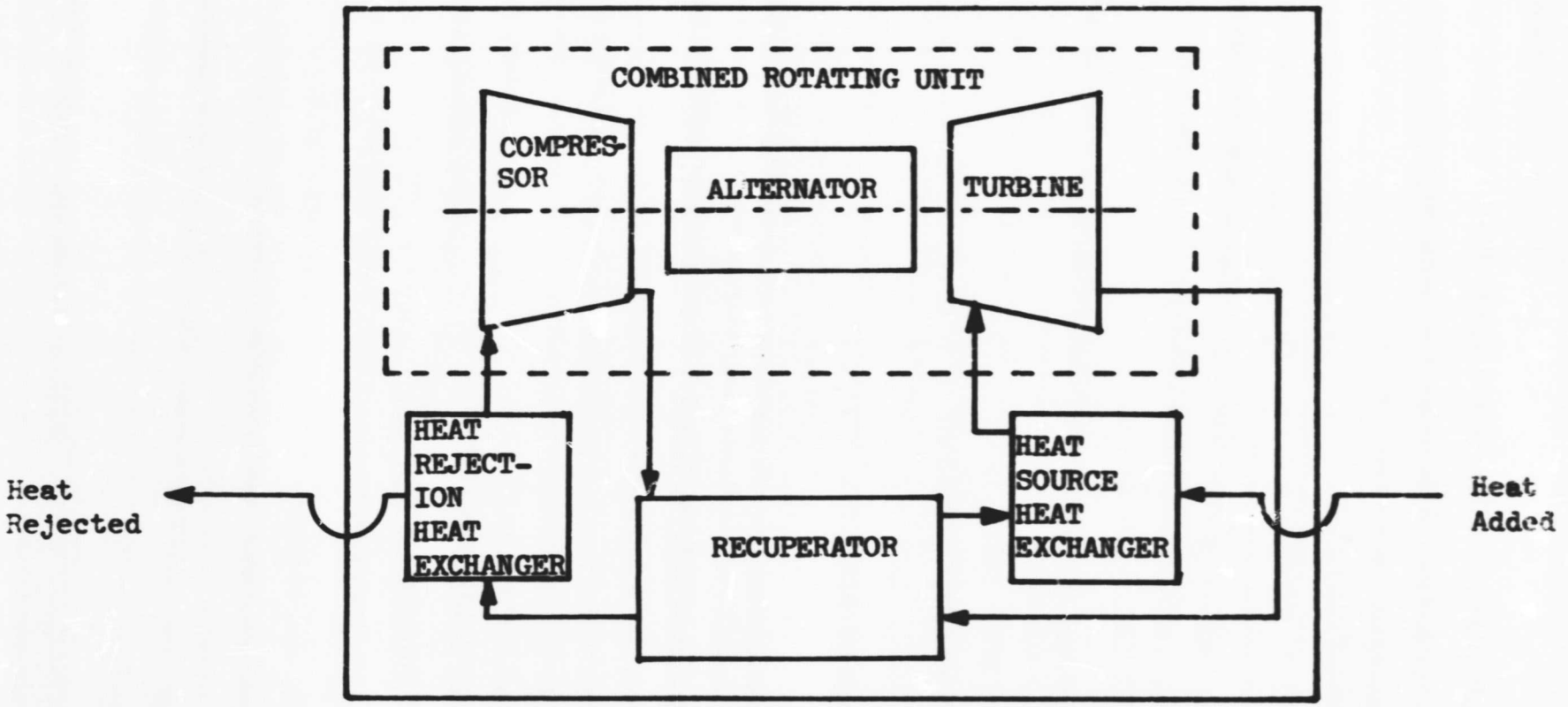

NOTE: 1 or more modules constitute a subsystem

Figure 3-82 Brayton Cycle Power Conversion Module

Table 3-25

BRAYTON-CYCLE POWER CONVERSION SUBSYSTEM BRIEFING CHART

Item	Value
Identification	
Applicable energy source	Solar, isotope, reactor.
Heat rejection subsystems	Gaseous- and liquid-loop radiators, heat pipes
Major components	Combined rotating unit, heat source heat exchanger, heat rejection heat exchanger, recuperator, accessories.
Vehicle — mission application range	
Useful power level	2 to 100 kWe
Duration of mission	Days to years
Types of spacecraft	Manned, unmanned, Earth orbiting, interplanetary
Status	
State of the art	Not available on production basis Efficiency 10 to 35%
Availability of support subsystems	Requires high temperature heat source development
Special problems	Increase life of combined rotating unit bearings.
Subsystem Characteristics	
Range of specific mass	400 to 1,000 kg/kWe
Range of specific radiator area	50 to 70 m^2/kWe
Range of specific volume	0.0875 to 0.0445 m^3/kWe
Range of specific production cost	$6,600 to $3,450/kWe
Range of reliability	0.9 to 0.99 (one year)
Performance Data	
Turbine inlet temperature	900° to 1,400°K
Range of efficiency	10 to 35%

The physical characteristics of the components in the Brayton cycle are computed in the NASA program as a function of the thermal or electrical power which must be transferred or produced during operation. The power levels are determined by calculating the thermodynamic statepoints in the Brayton cycle loop. The statepoints are influenced strongly by the thermodynamic performance of the CRU. Four essential parameters are needed to compute the CRU performance. Compression and expansion ratios are required to compute the adiabatic enthalpy differences across the turbine and compressor. Turbine and compressor efficiencies are then required to find the actual enthalpy differences. All four parameters are interrlated with the performance of the rest of the cycle, and extensive calculations must be performed to ensure that the values used are not only realistic, but optimum, in the sense that they minimize the system mass. Curves of realistic optimum values of efficiencies and the compression ratio are shown in Figures 3-83 and 3-84. The corresponding turbine expansion ratio is found by computing the pressure drops through the various components in the rest of the loop. The density of the working fluid is governed by the system reference pressure at the turbine exit. Optimum values of this pressure are shown in Figure 3-85. The information in Figures 3-83, 3-84, and 3-85 was derived with the use of the Douglas B-21 optimizing computer program. The independent variable in Figures 3-83, 3-84, and 3-85 is the CRU temperature ratio, which is defined as the compressor inlet temperature divided by the turbine inlet temperature (°K/°K). The values shown for a CRU shaft speed of 64,000 rpm were used in this study.

It is usually advantageous to operate at the lowest possible temperature ratio consistent with radiator weight to maximize the Carnot efficiency of the cycle. As a result, the turbine inlet temperature is usually set at an upper value which is limited by material stress capabilities in either the heat source or the turbine wheel. The turbine wheel limited-inlet temperature is projected as a function of calendar year in Figure 3-86.

The most serious limitation to the use of Brayton cycle power conversion subsystems for space vehicles is the life expectancy of the CRU bearings. Consequently, the lifetime of the complete Brayton-cycle subsystem is determined largely by the lifetime of the CRU bearings. A projection of the

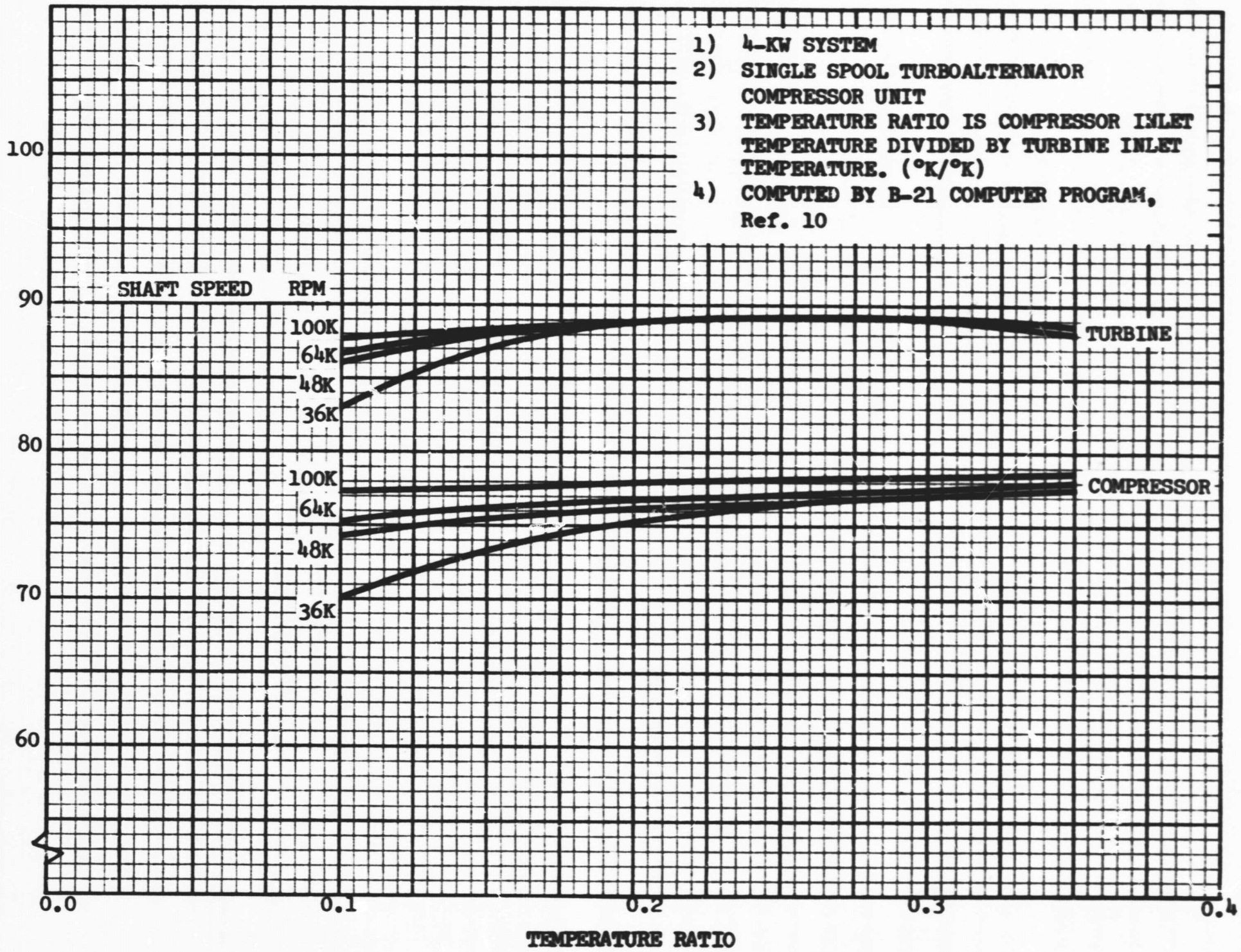

Figure 3-83 Effect of Temperature Ratio on Turbine and Compressor Efficiency

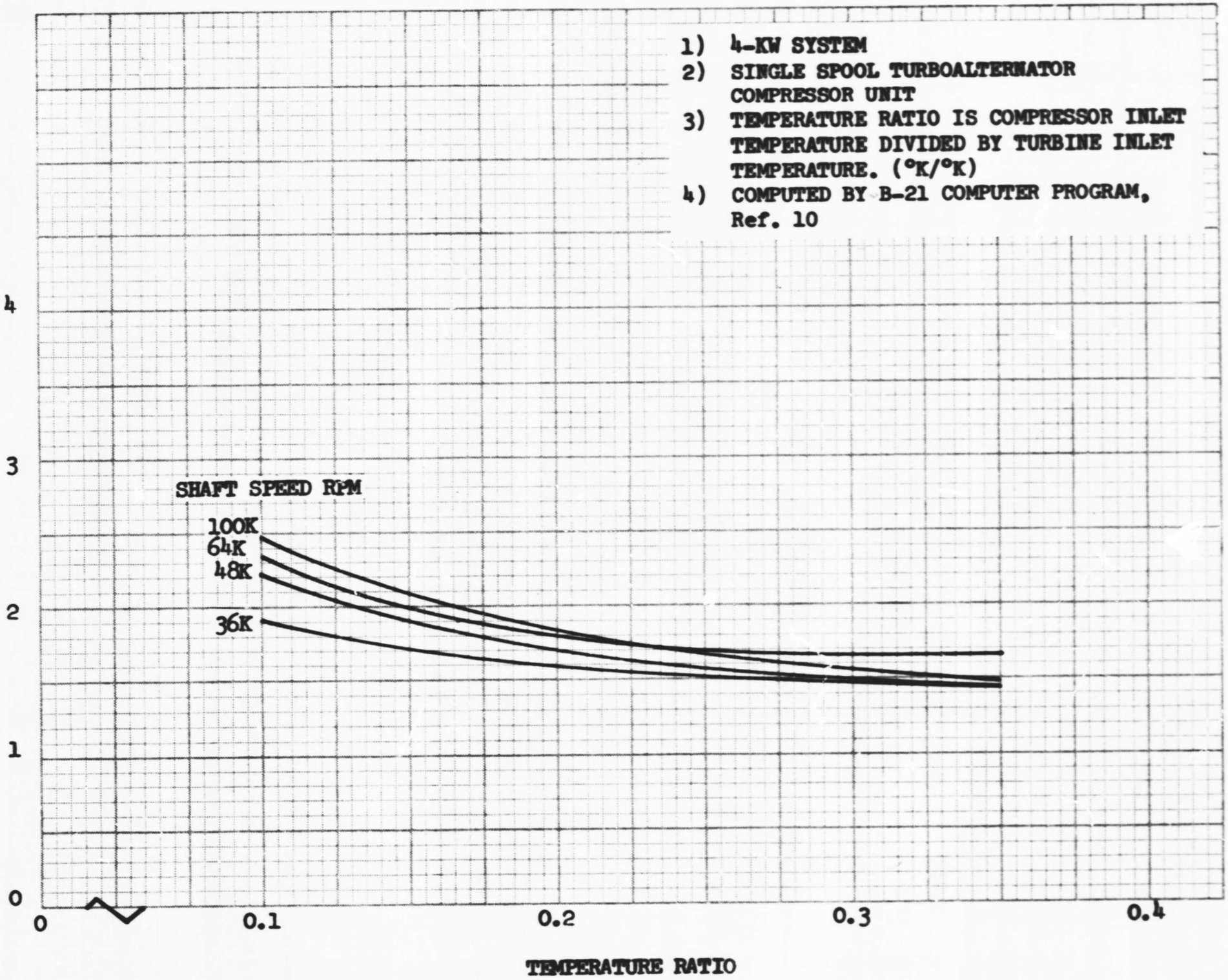

Figure 3-84 BRAYTON CYCLE SUBSYSTEM COMPRESSION RATIOS

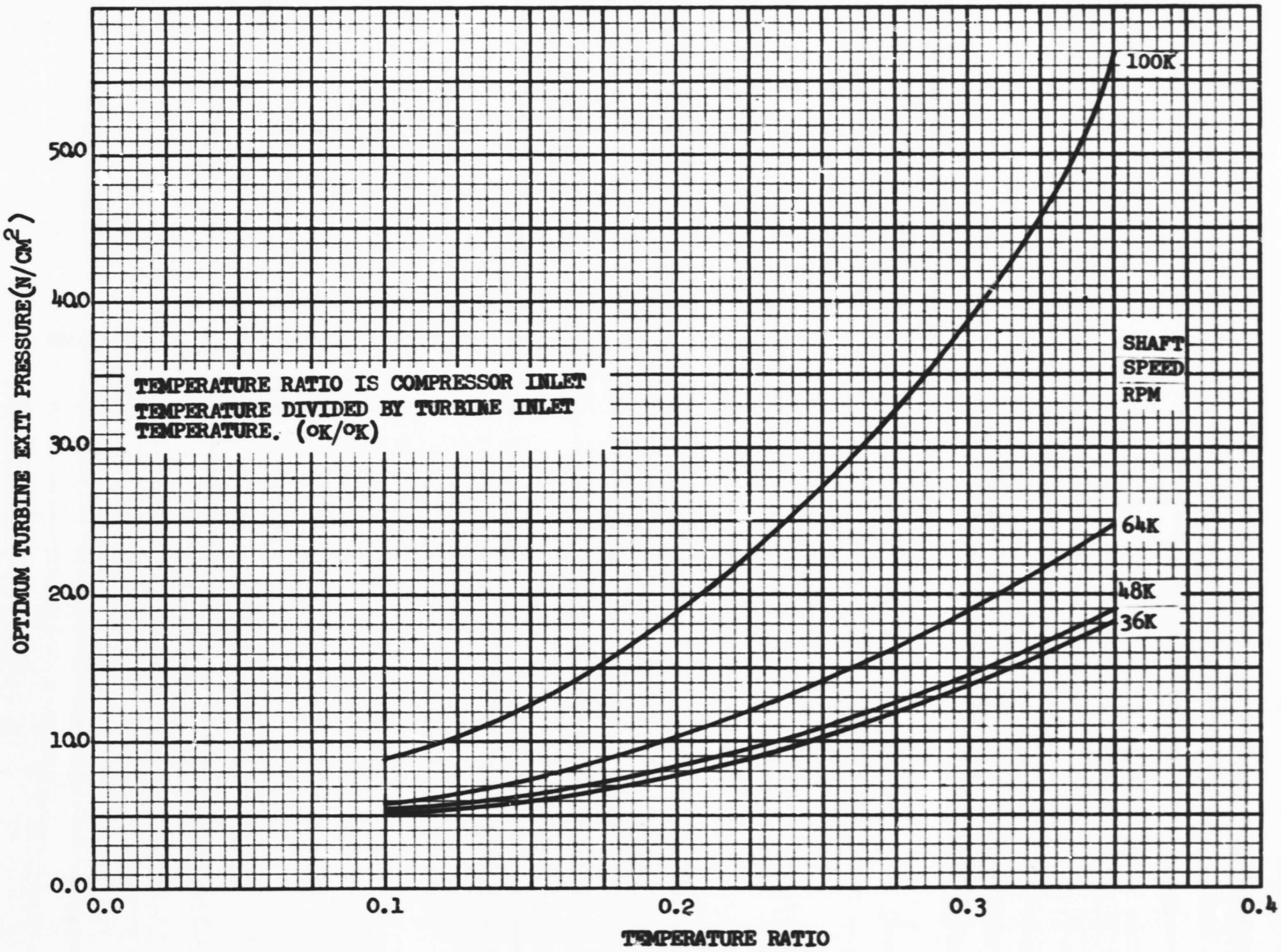

Figure 3-85 . Brayton Cycle Optimum Turbine Exit Pressure (N/CM^2)

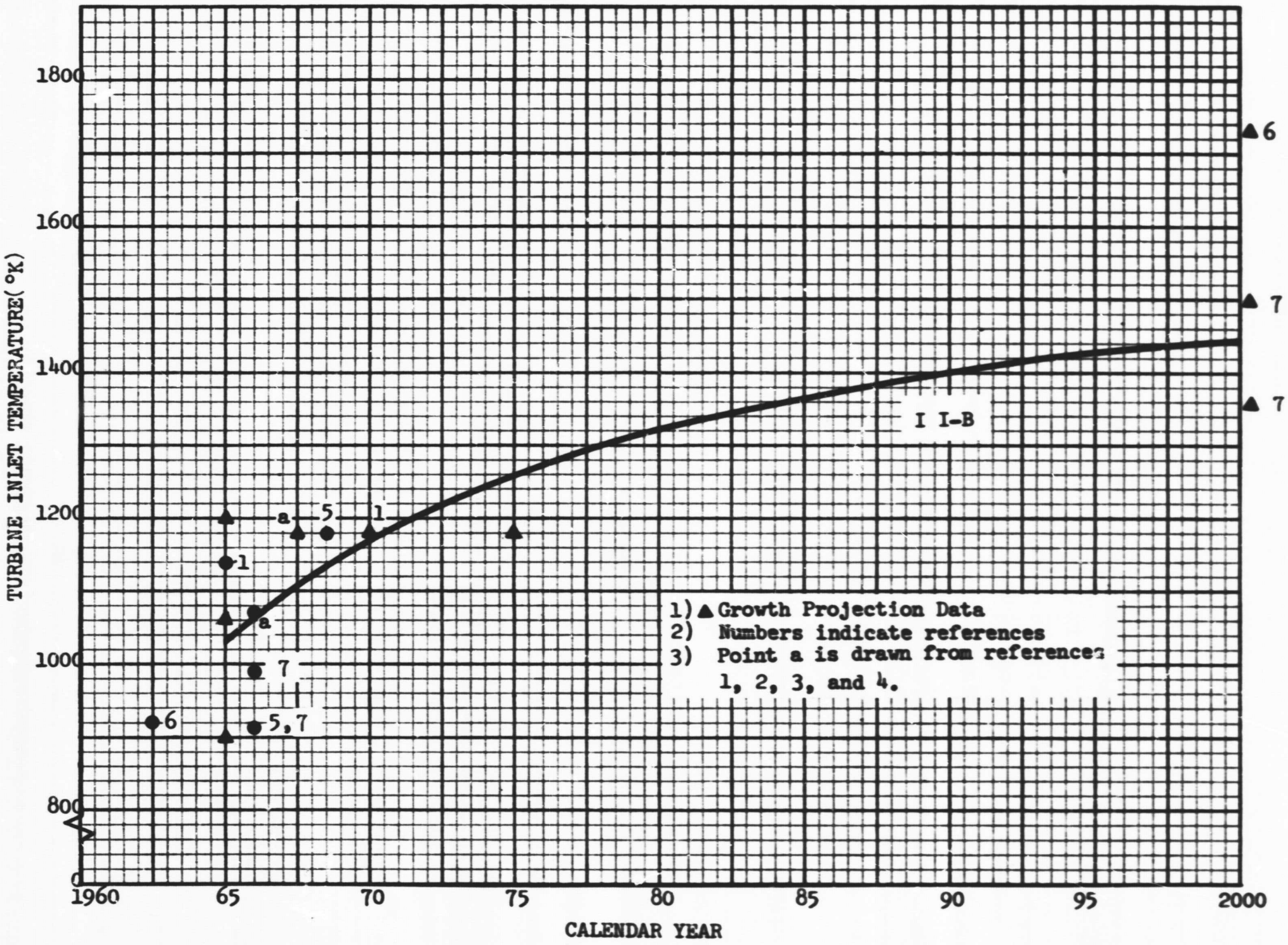

Figure 3-86 Projection of Brayton Cycle Turbine Inlet Temperature

expected improvement in life expectancy of the CRU bearings is shown in Figure 3-87.

Component characteristics, such as specific mass, density, MTBF, lifetimes, and specific production costs, are shown in Figure 3-88 through 3-91. The data presented in the curves are stored in the computer in labeled common arrays for use in designing the power subsystem.

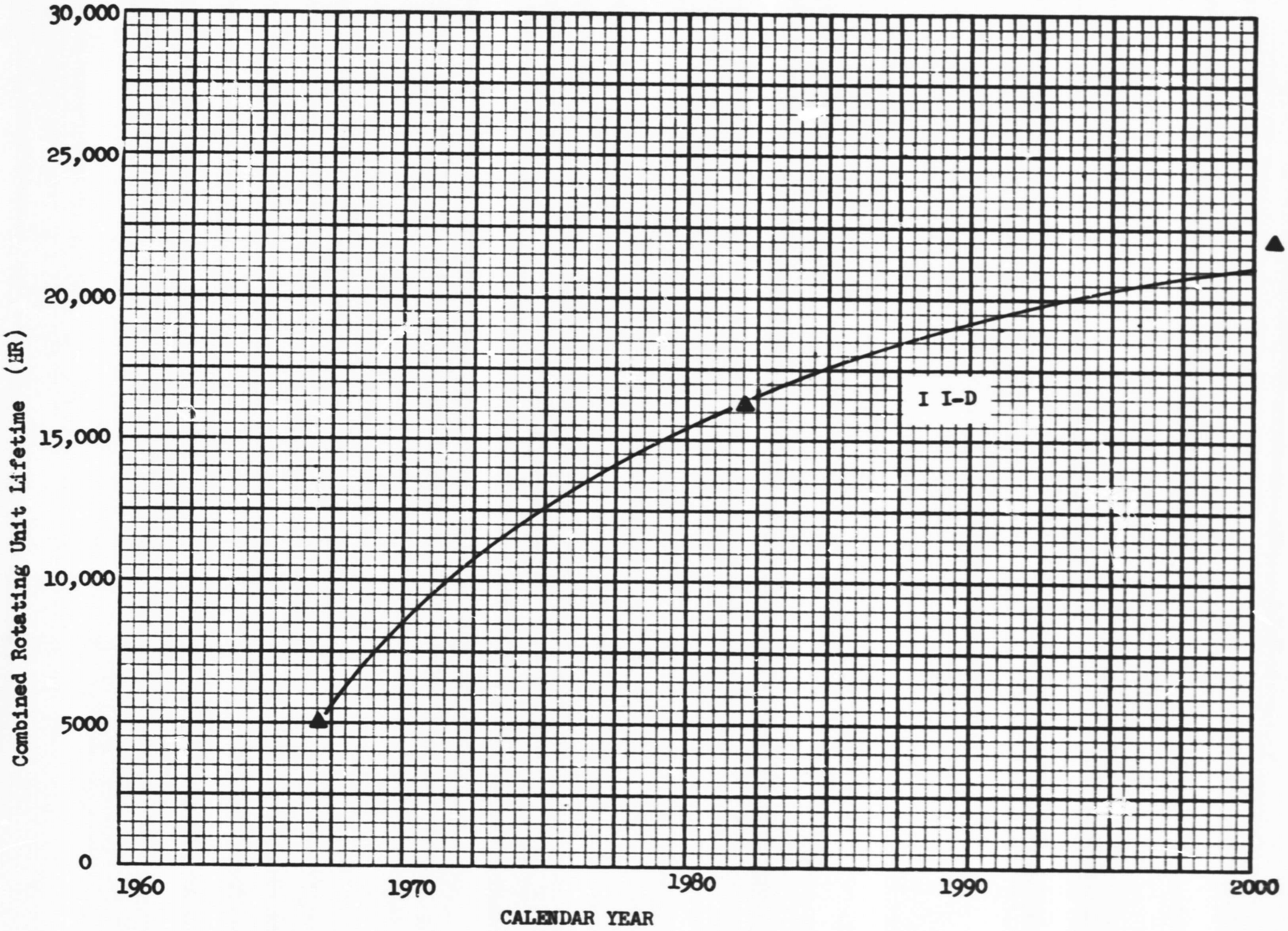

Figure 3-87 Projection of CRU Lifetime

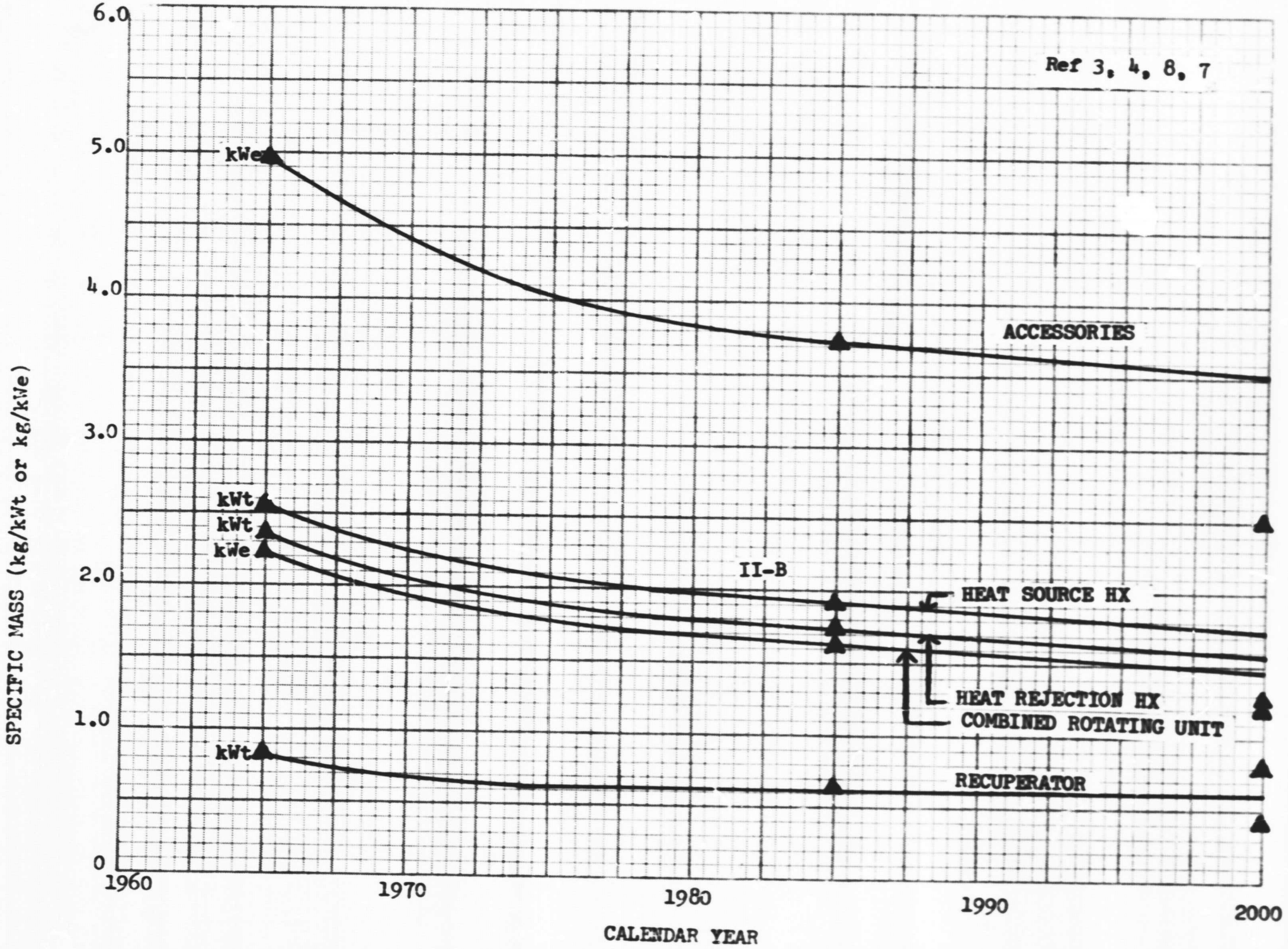

Figure 3-88 Projection of Component Specific Masses For Brayton Cycle Power Conversion Unit

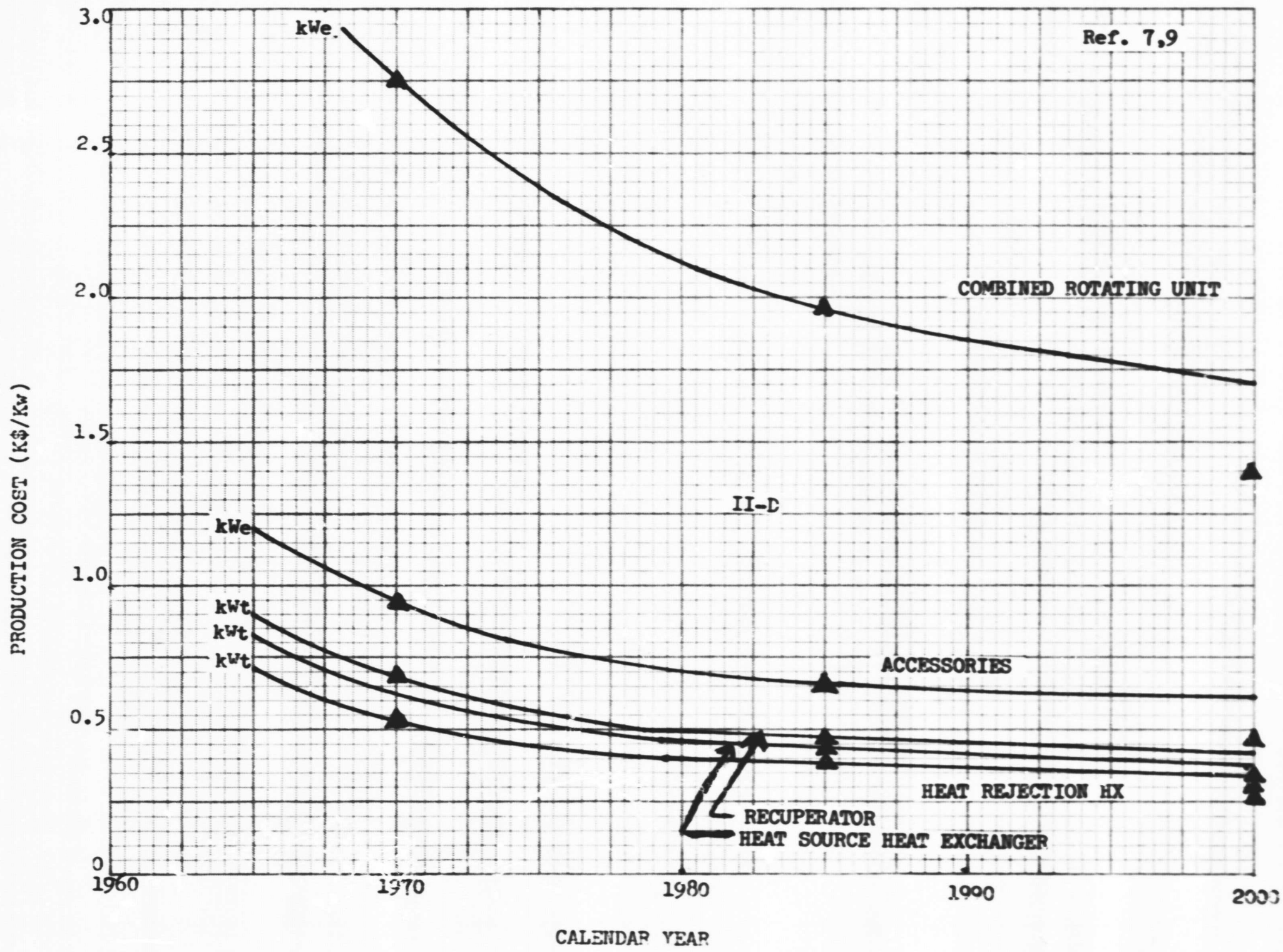

Figure 3-89 Projection of Production Costs For Brayton Cycle Power Conversion Unit Components

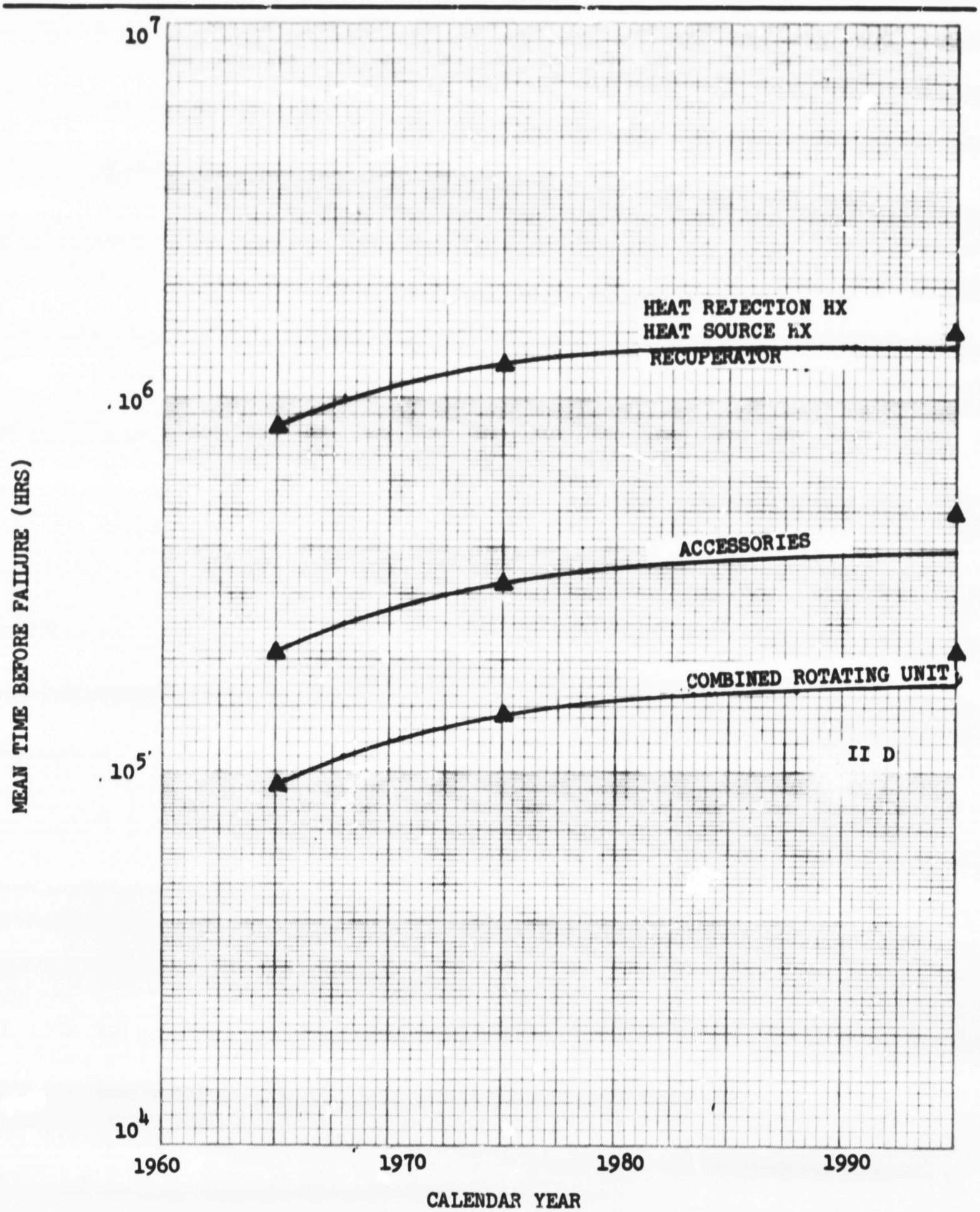

Figure 3-90 Projection of MTBF For Brayton-Cycle Power Conversion Unit Components

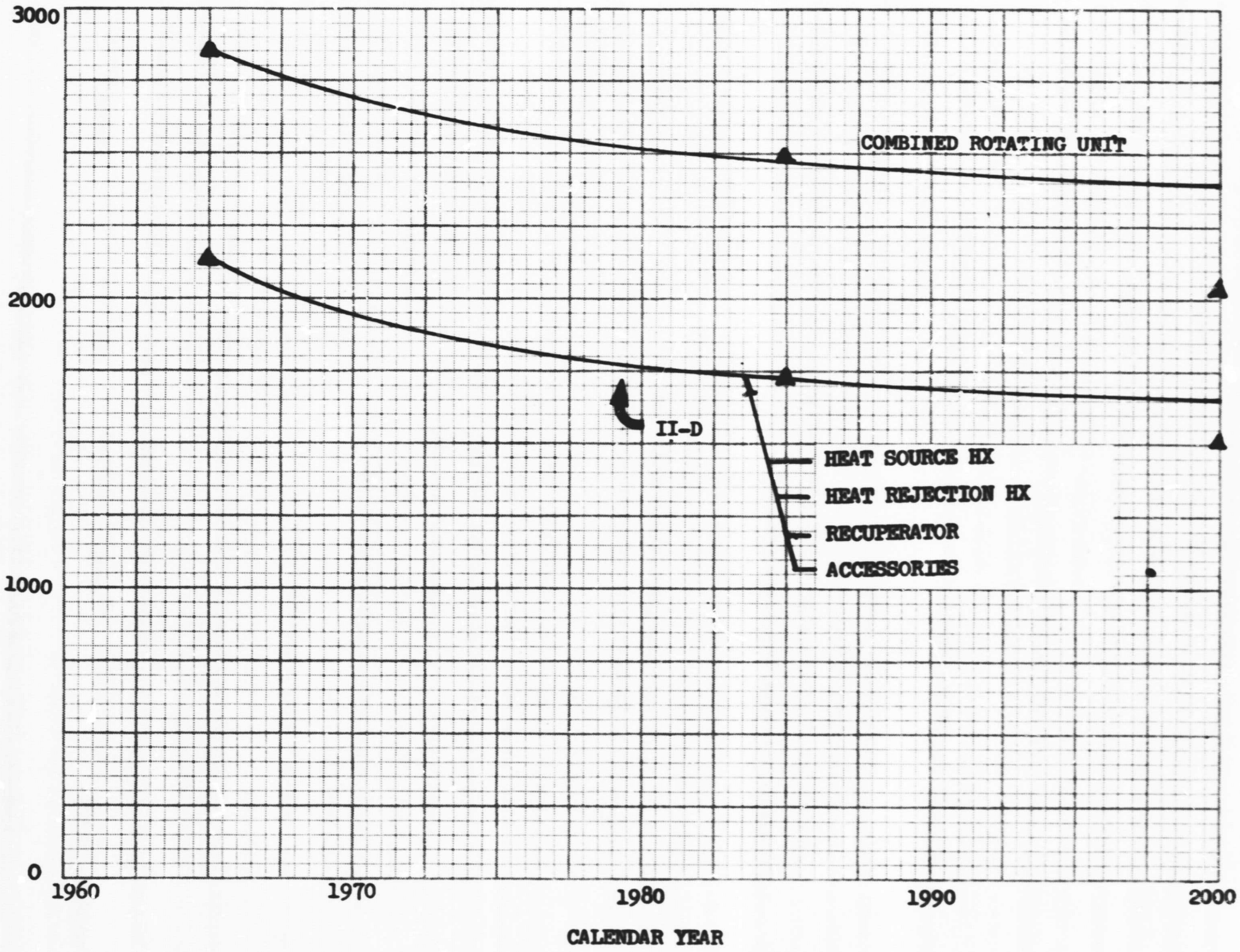

Figure 3-91 Projection of Density for Brayton-Cycle Power Conversion Unit

3.1.7 Rankine Cycle Power Conversion Subsystem

The Rankine cycle power subsystems that have been investigated in the study and are presently under development as a technology can be classified by their working fluids such as mercury, alkali metal, and organic fluid.

3.1.7.1 Mercury and Alkali Metal Rankine Subsystems

The schematic diagram of a typical mercury or alkali metal potassium Rankine cycle power conversion subsystem module is shown in Figure 3-92. The subsystem comprises one or more modules on the line, in standby, or as wearout replacements.

All components of the power conversion subsystems have been grouped in one of the following categories: (1) the boiler, (2) the combined rotating unit, (3) the condenser and subcooler, and (4) the accessory components. The module includes a compact condenser that delivers heat to a noncondensing liquid radiator in the heat rejection subsystem. The condenser is excluded from the power conversion subsystem when direct-condensing radiators are selected. The characteristics of each of the major components are projected separately and used to obtain the characteristics for the mercury and alkali metal Rankine cycle power conversion subsystems. The boiler is normally included in the conversion subsystem, but when the Rankine system is used with a solar concentrator heat source, the boiler becomes part of the heat source subsystem. The combined rotating unit includes the turbine, the alternator, and the bearings and bearing housings. The mercury pump is included with the rotating unit only when it is on the same shaft as the turbo-alternator, in which case its weight and size are inisgnificant. Separate mercury pump-motor components (SNAP-8) usually have significant weight and size and are included in the accessories category. Other components grouped in this category are the mercury loop piping, the structure, the working fluid inventory, the parasitic load and controls, and the startup injection subsystem and controls.

In the Rankine cycle subsystem, heat is added to the working fluid and it is vaporized and superheated in the boiler. The vapor expands in the turbine

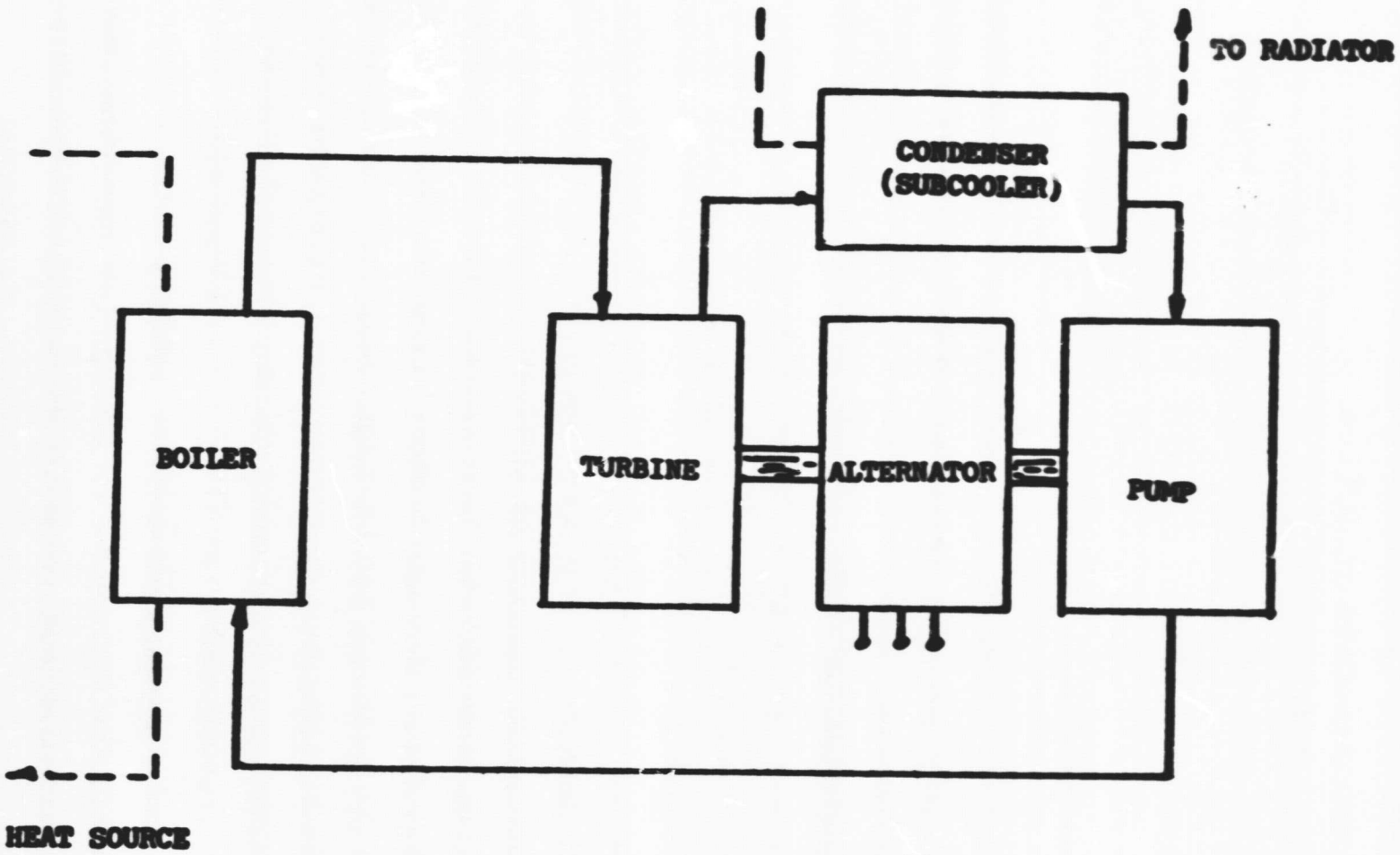

Figure 3-92 Typical Mercury or Alkali Metal Rankine Cycle Module

providing mechanical shaft power to drive the alternator. The vapor is condensed and subcooled in the condenser and flows back to the boiler through the pump. Typical turbine inlet operating temperatures are 980°K for mercury and 1,350°K for alkali metals such as potassium. Mercury systems are normally considered for use in the 2- to 100-kWe power range while potassium systems are planned primarily over the range of 100 kWe to megawatts.

The mercury and alkali metal Rankine power subsystems may receive thermal energy from a solar concentrator, reactor, or isotope heat source. The alkali metal systems are usually planned for use with reactors because of their high power level. Studies have been performed on alkali metal Rankine systems with electrical outputs as low as 5 kWe, with turbine inlet temperatures reduced to provide improved turbine performance. The alkali metal system can be used with a solar concentrator or isotope heat source under these conditions.

The mercury and alkali metal conversion subsystem status, characteristics, and ranges of performance are shown in Tables 3-26 and 3-27. The major component characteristics, performance, and thermodynamic data such as mass, density, failure rate, wearout life, cost, and efficiency are shown in Figures 3-93 through 3-120. The data presented in the curves are stored in the computer program in block data arrays for use in designing the power subsystem.

3.1.7.2 Organic Rankine Conversion Subsystem

The schematic diagram of the organic subsystem is shown in Figure 3-121. The subsystem is similar to the liquid metal Rankine subsystems but differs in several significant areas. The working fluid does not have to be superheated to prevent condensing of vapor in the last stages of the turbine. The organic fluid becomes superheated as it expands because of the shape of the temperature-entropy diagram. The organic subsystem has a regenerator (recuperator) to conserve energy, and as it is presently being developed, has a jet condenser to ensure low-temperature gravity-free condensation. The working fluid mixes with the radiator fluid in the jet condenser and a sufficient amount of radiator fluid is used to condense all of the vapor entering the jet condenser.

Table 3-26

MERCURY RANKINE POWER CONVERSION
SUBSYSTEM BRIEFING CHART

Item	Value
Identification	
Applicable energy source	Solar, isotope, reactor
Heat rejection subsystems	Convective loop and condensing radiator
Major components	Turboalternator, boiler, condenser, and accessory equipment
Vehicle - Mission application range	
Useful power level	1kWe to 100 kWe
Duration of mission	Days to years
Types of spacecraft	Manned, unmanned, Earth orbiting, interplanetary
Status	
State of the art	Prototype in development and performing endurance testing
Availability of support subsystems	Supporting subsystems within current technology levels
Special problems	Boiler wetting, erosion of turbine blades, restart capability in space
Subsystem Characteristics	
Range of specific mass	20 to 50 kg/kWe
Range of specific production cost	125 to 250 kg/kWe
Range of reliability	70 to 95% (1 year)
Range of specific volume	0.5 to 1.5 m^3/kWe
Performance Data	
Turbine temperature	870° to 980°K
Cycle efficiency	6 to 15%

Table 3-27

ALKALI METAL RANKINE POWER CONVERSION SUBSYSTEM BRIEFING CHART

Item	Value
Identification	
Application Energy Source	Solar concentrator isotope, and reactor
Heat Rejection Subsystems	Convective loop and condensing radiator
Major Components	Turboalternator, boiler, condenser, and accessory equipment
Vehicle - Mission Application Range	
Useful power level	5kWe* to multimegawatts
Duration of mission	Days to years
Types of spacecraft	Manned, unmanned, Earth orbiting, interplanetary
Status	
State of the art	Component and technology development phase
Availability of support subsystems	High temperature and isotope and reactor systems not yet available
Special problems	Manufacturing methods for refractory metal subsystems not fully developed
Subsystem Characteristics (1 PCU module)	
Range of specific mass	10 to 30 kg/kWe
Range of specific volume	0.5 to 1.5 m^3/kWe
Range of specific production cost	150 to 300 k$/kWe
Range of reliability	70 to 90% (1 year)
Performance Data	
Turbine inlet temperature	865° to 1,480°K
Cycle efficiency	10 to 23%

*Lower power levels assumed lower range of turbine inlet temperatures (865° to 1,150°K)

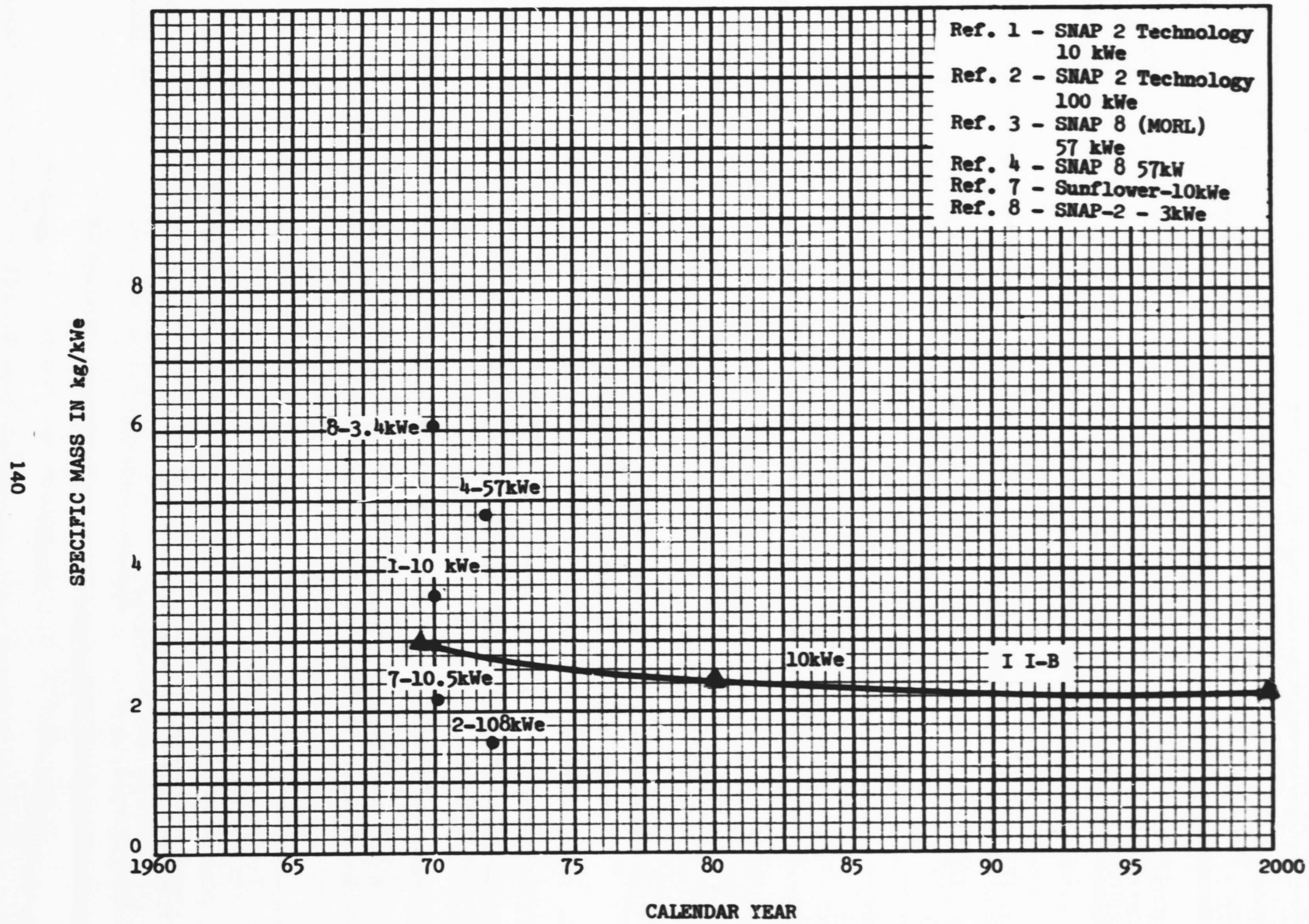

Figure 3-93 Projection-Mercury Rankine Turboalternator (CRU) - Specific Mass

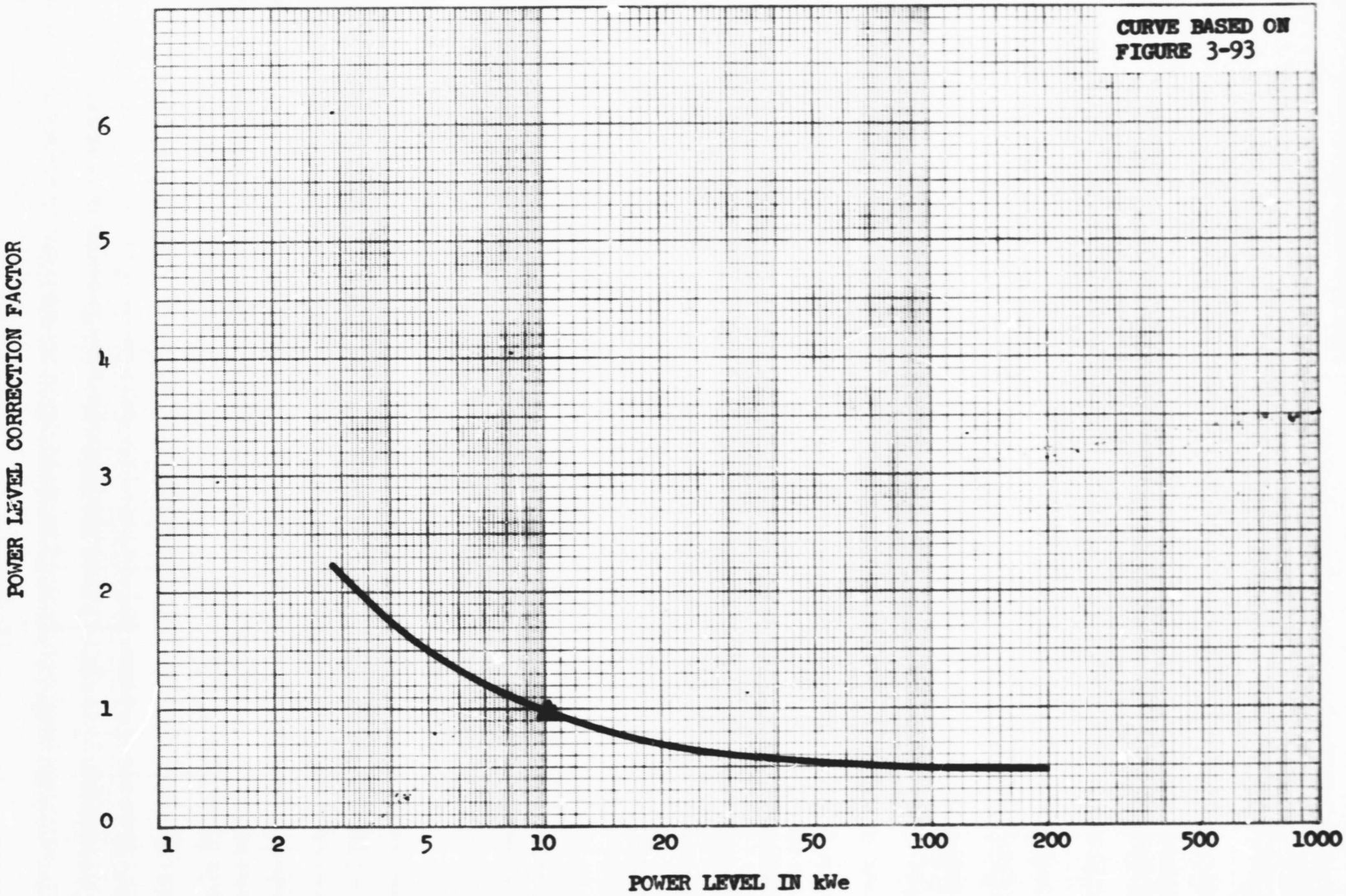

Figure 3-94. Power Level Correction Factor For Mercury Rankine Turboalternator Specific Mass

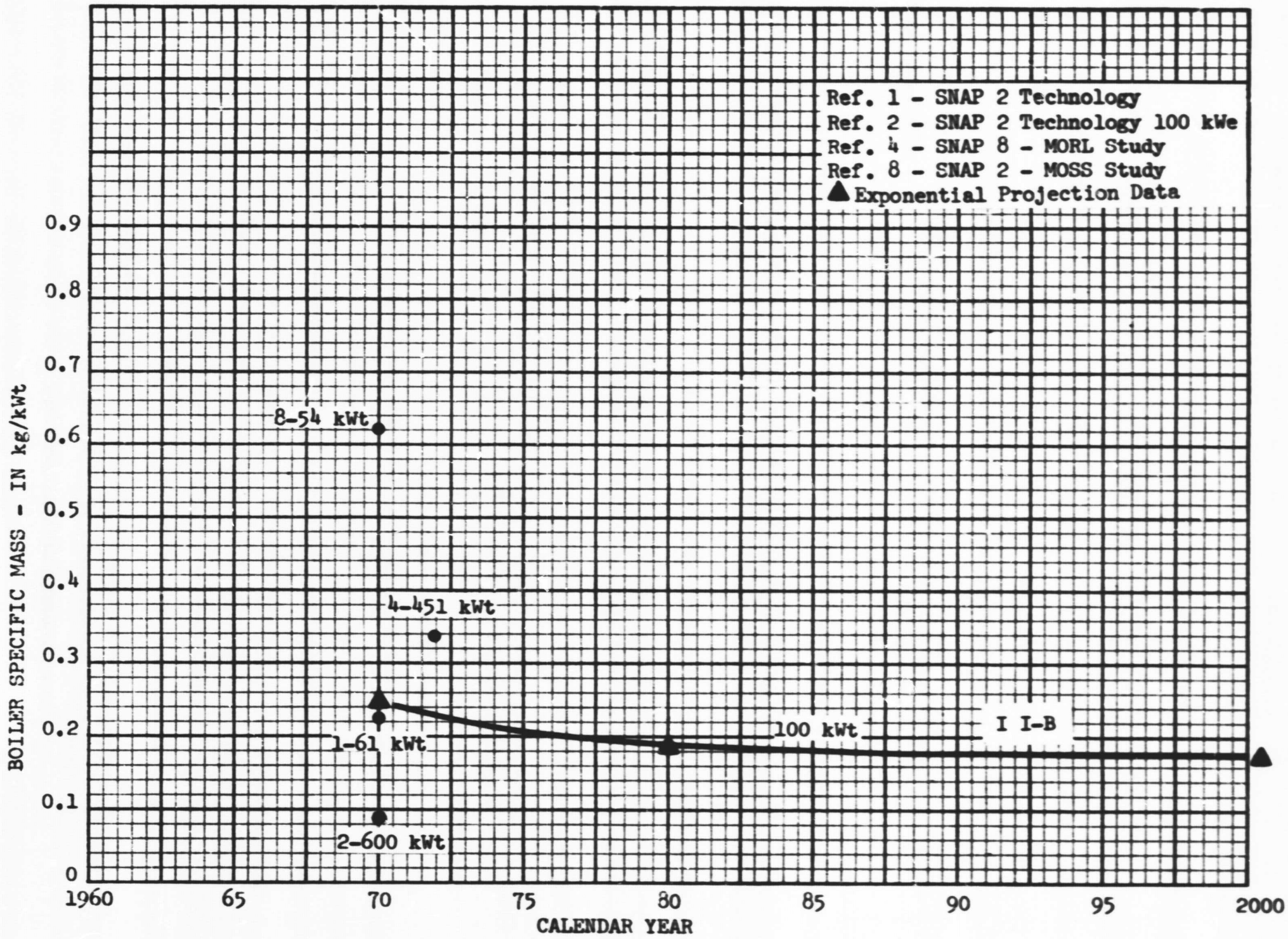

Figure 3-95 PROJECTION - MERCURY RANKINE BOILER SPECIFIC MASS

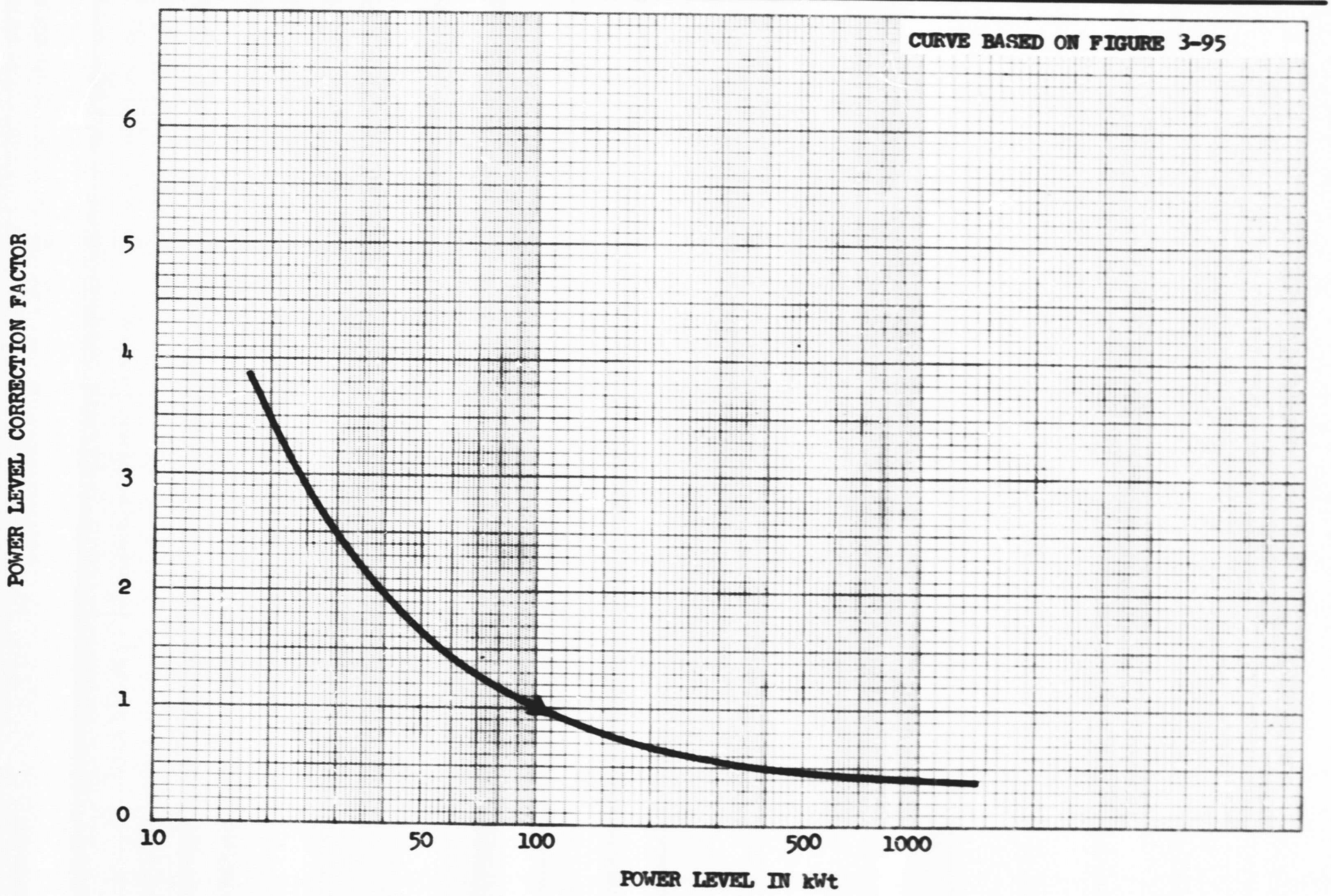

Figure 3-96 Power Level Correction Factor for Mercury Rankine Boiler Specific Mass

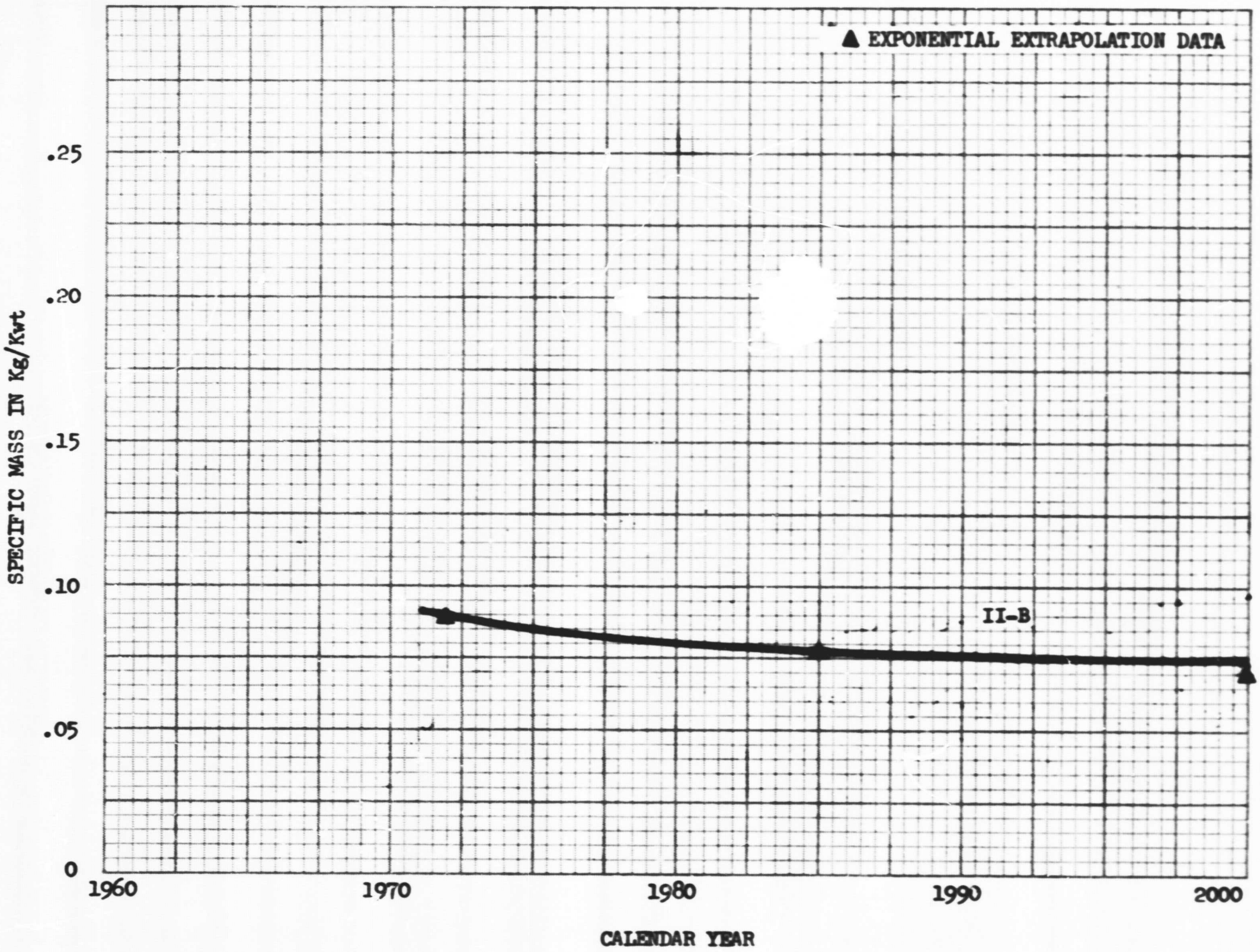

Figure 3-97 Projection Mercury Rankine Condenser Specific Mass

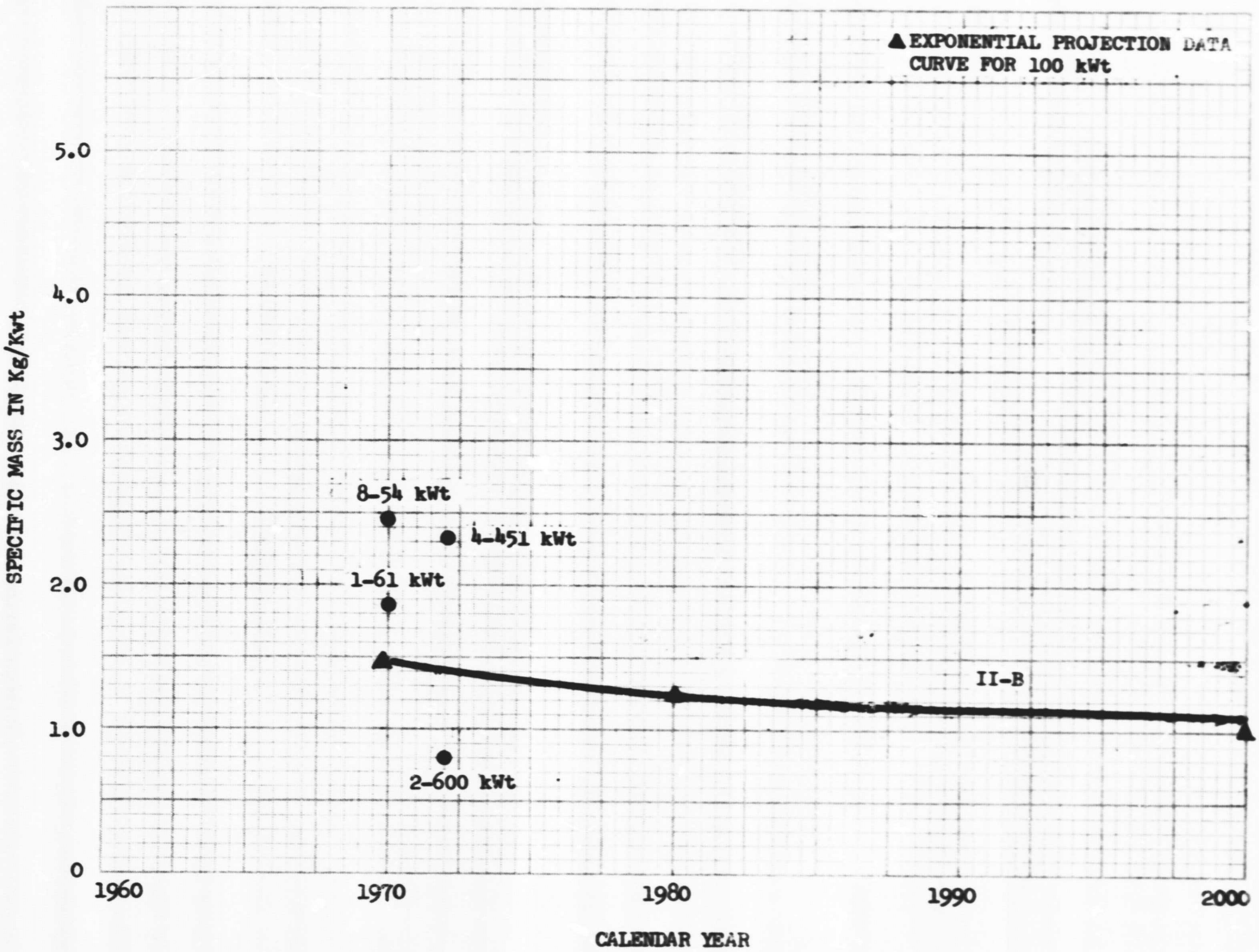

Figure 3-98 Projection Mercury Rankine Accessories Specific Mass

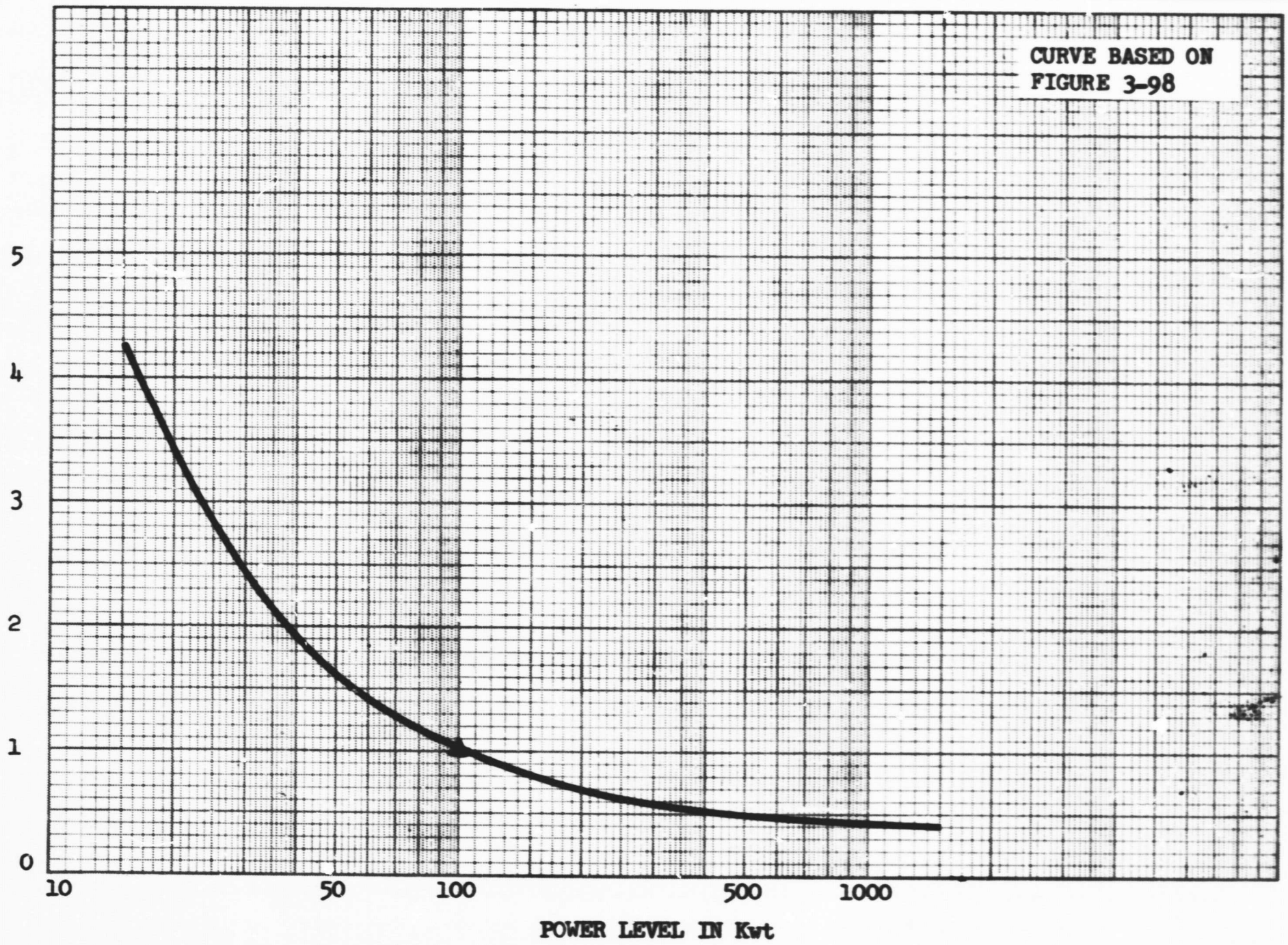

Figure 3-99 Power Level Correction Factor for Mercury Rankine Accessories Specific Mass

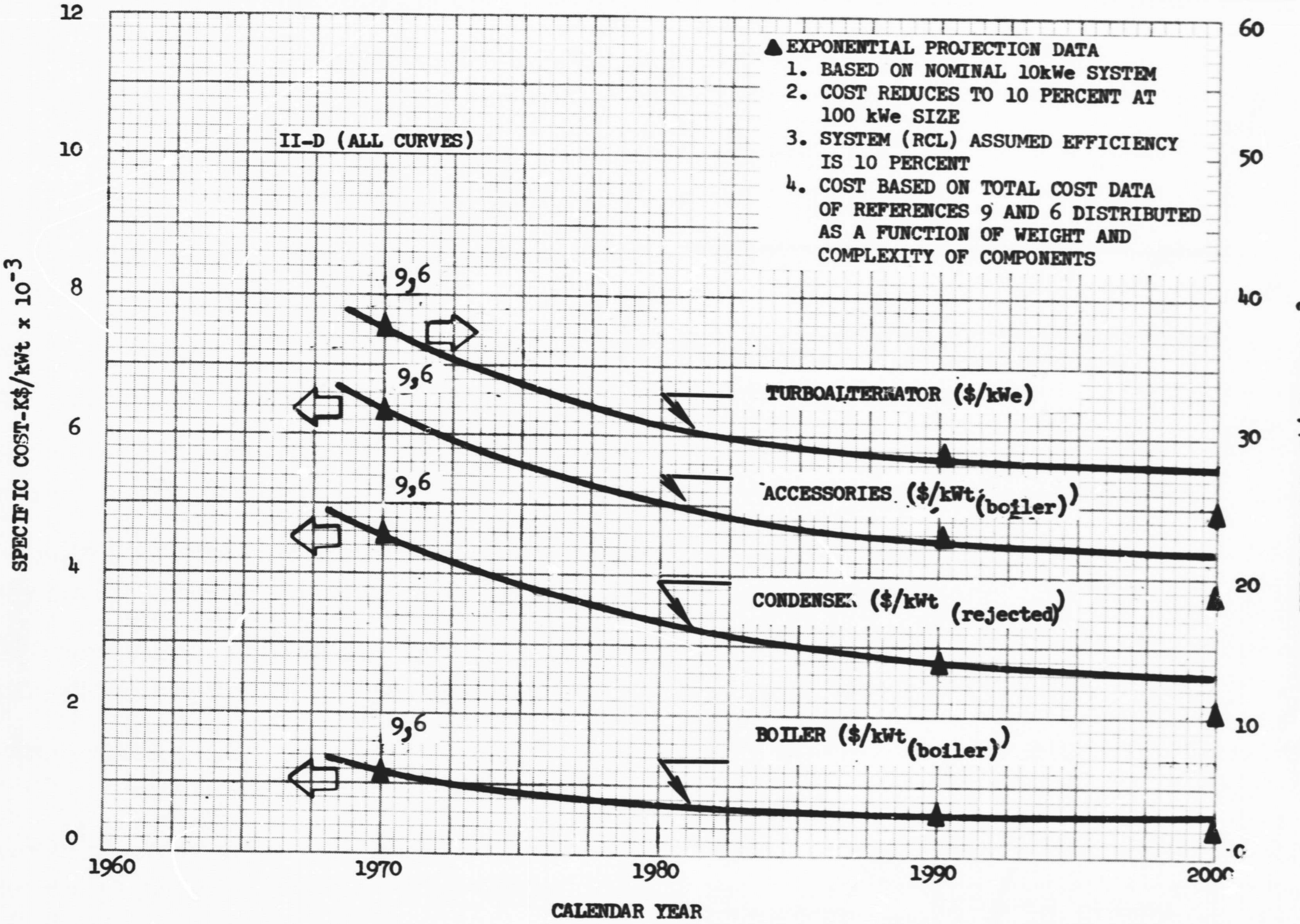

Figure 3-100 Specific Cost of Mercury Rankine Cycle Equipment

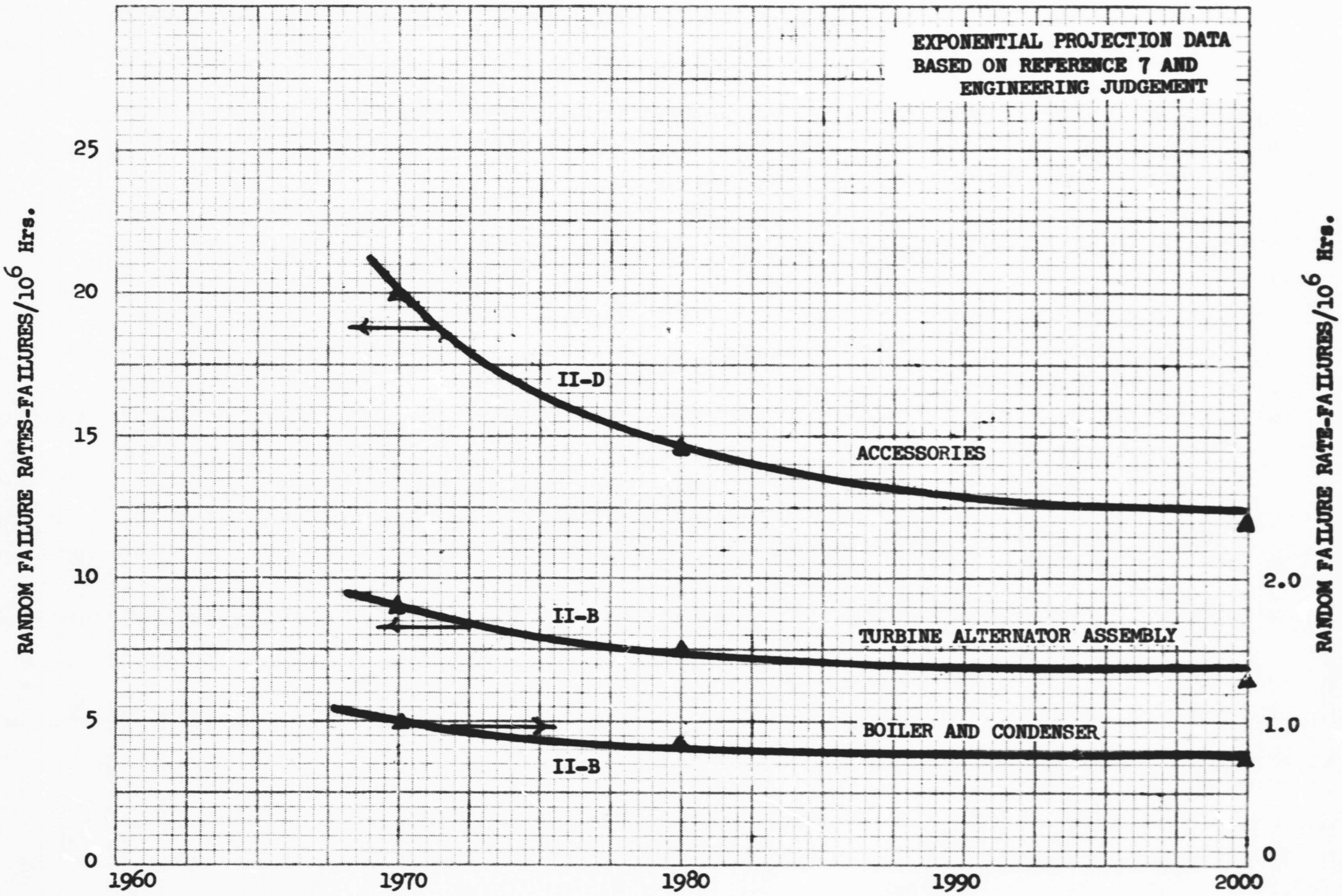

Figure 3-101 Projection of Mercury Rankine Component Failure Rates

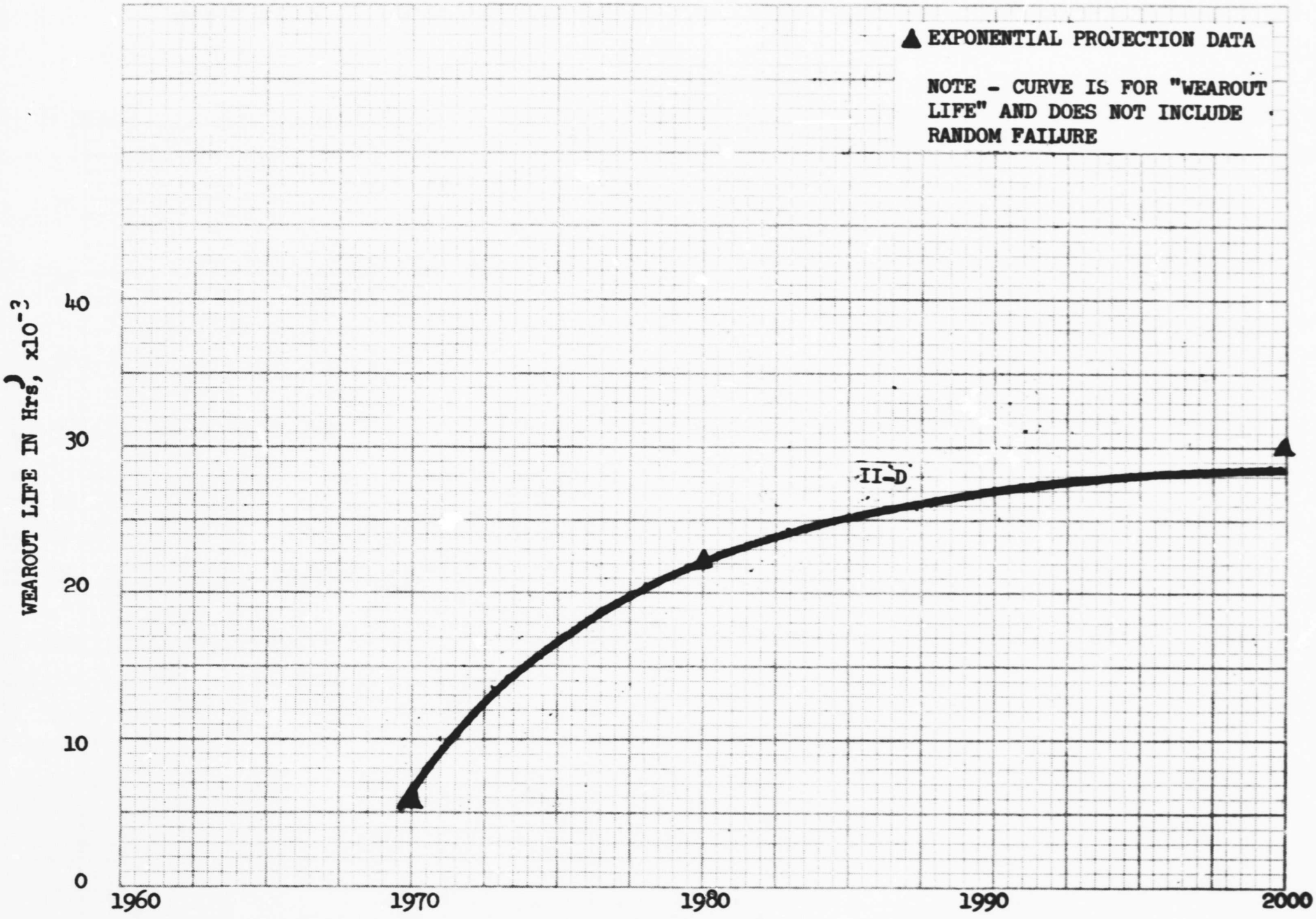

Figure 3-102 Projection of Mercury Rankine Power Conversion Module Wearout Life

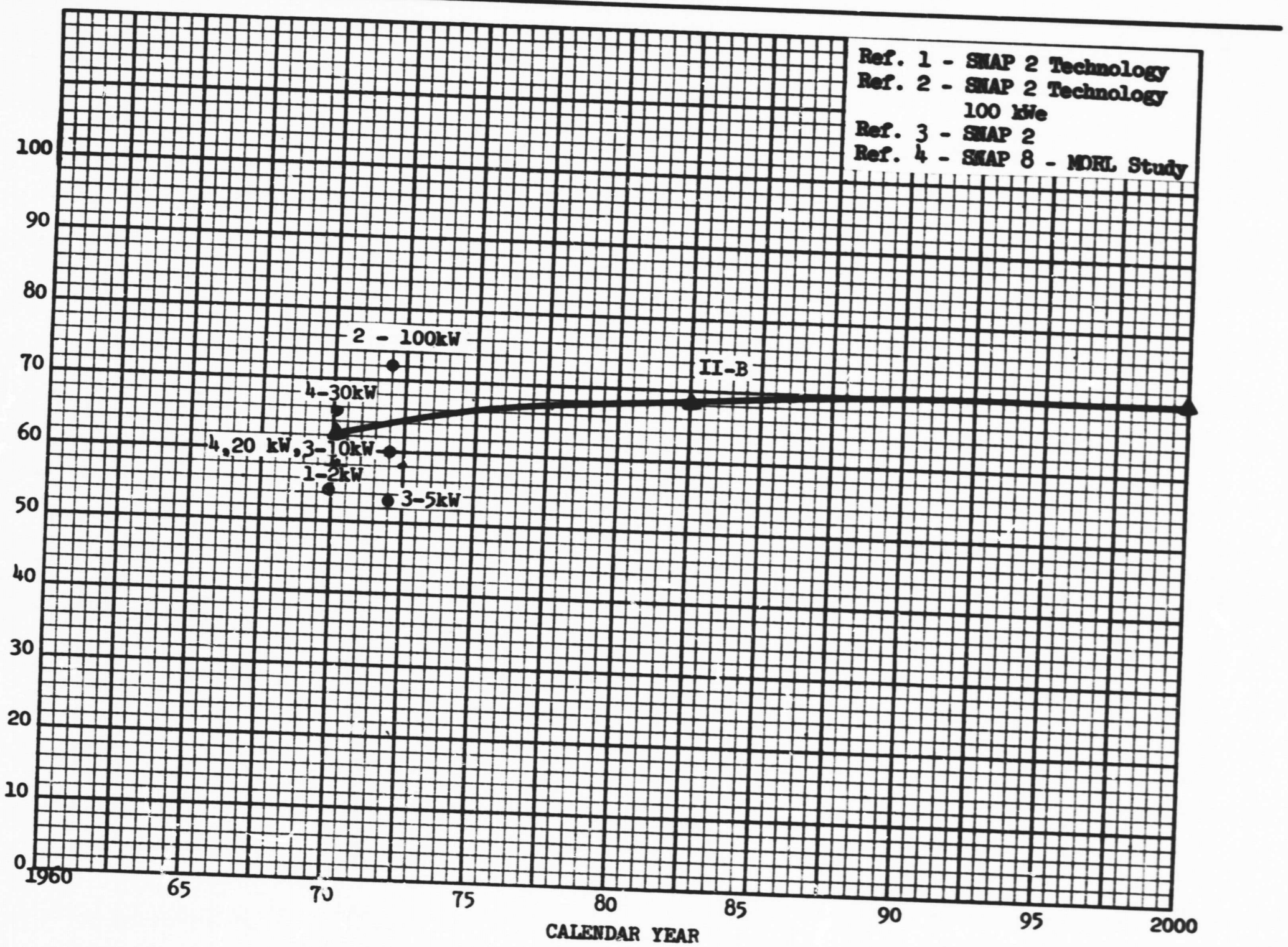

Figure 3-103a PROJECTION - MERCURY RANKINE TURBINE EFFICIENCY

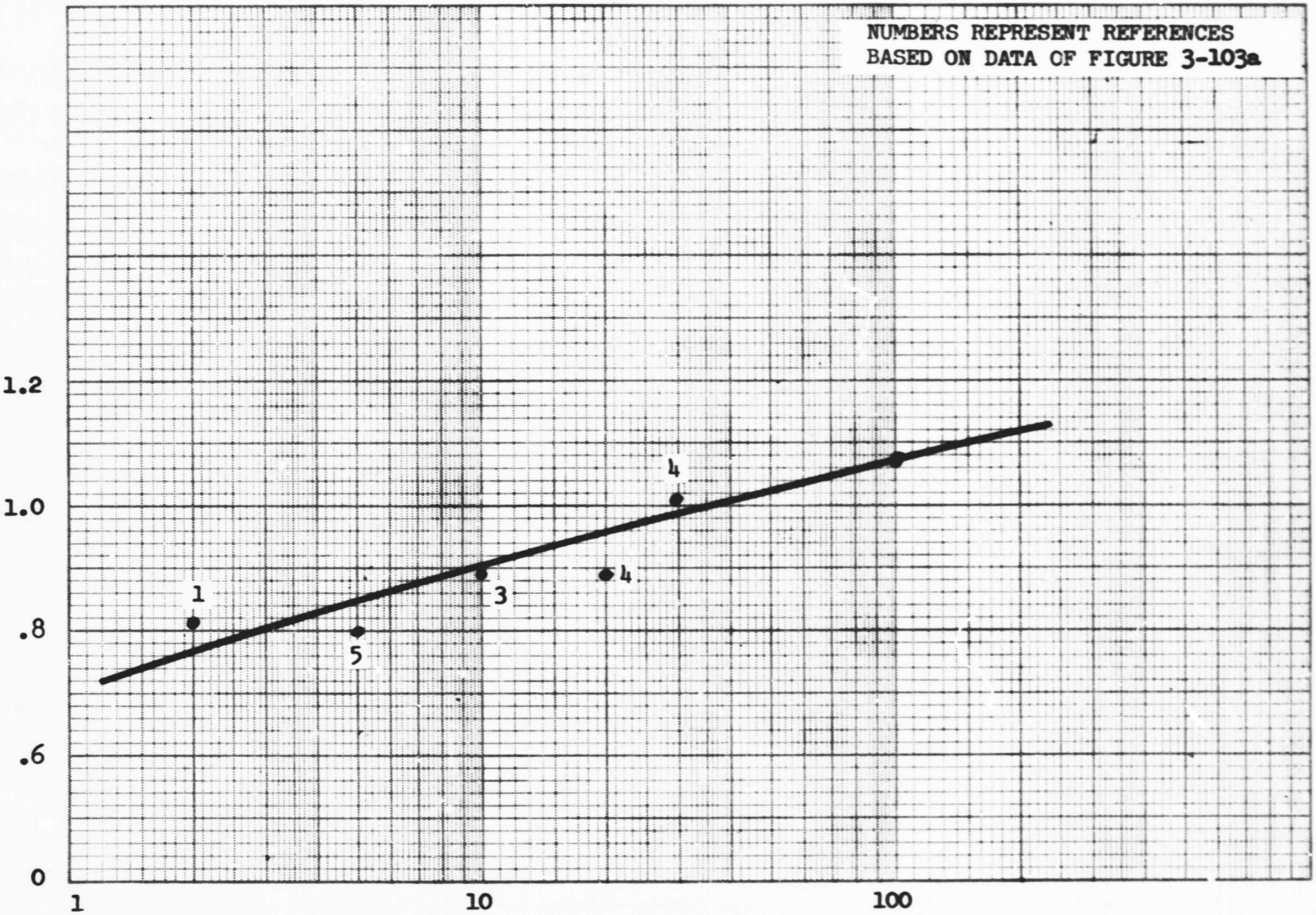

Figure 3-103b Power Level Correction Factor for Mercury Rankine Turbine Efficiency

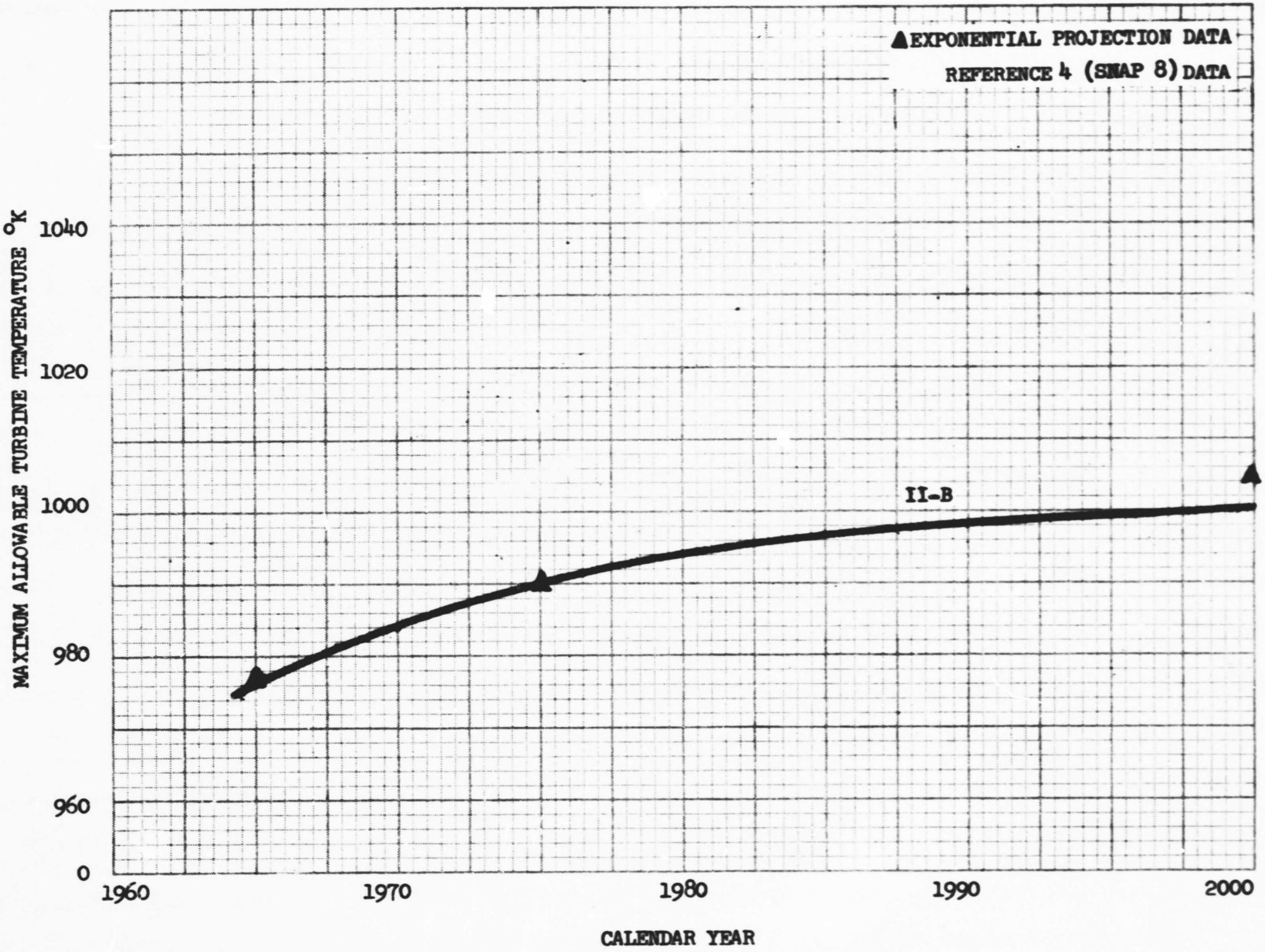

Figure 3-104 Projection of Maximum Turbine Inlet Temperature - Mercury Rankine

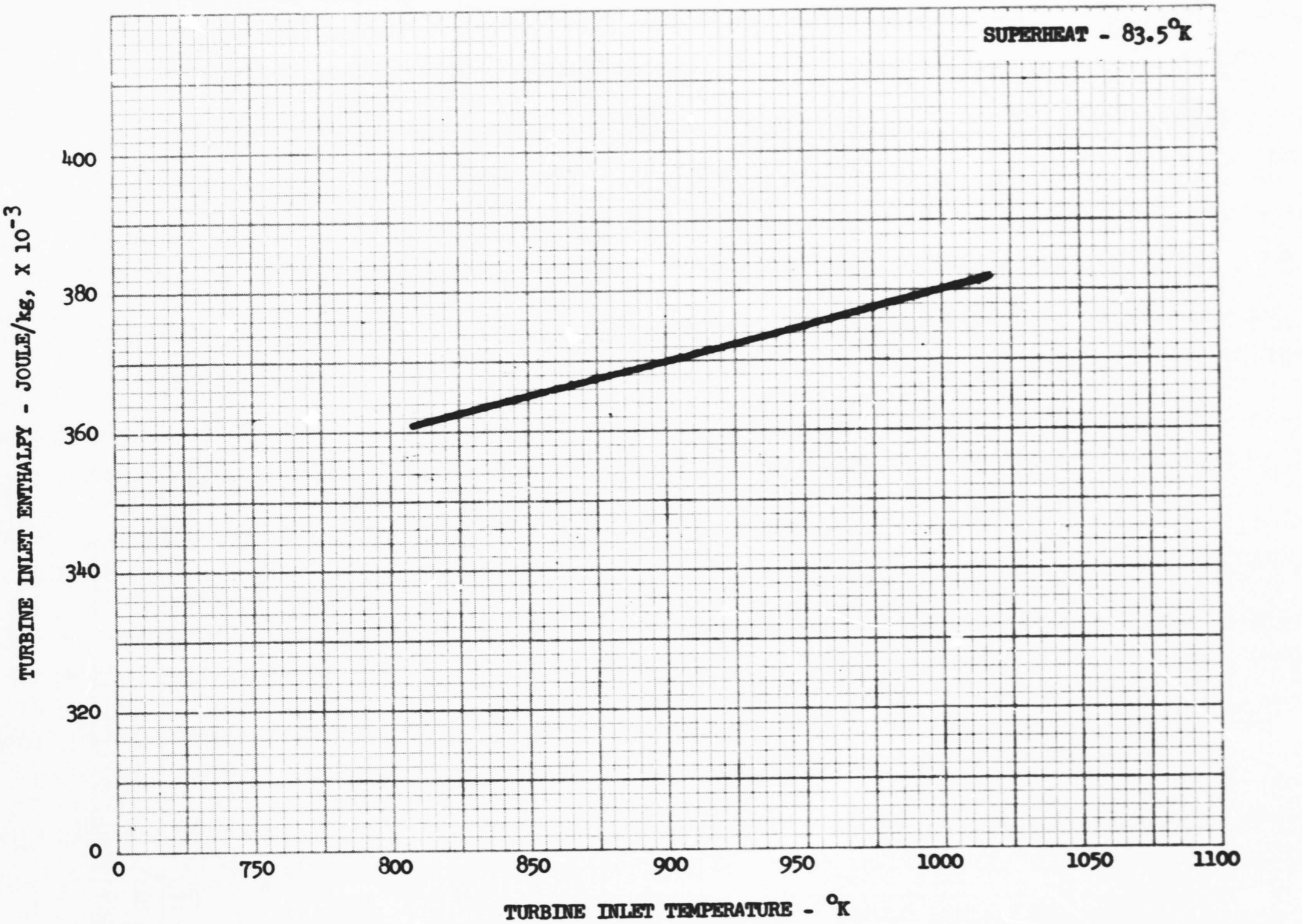

Figure 3-105 Mercury Rankine Turbine Inlet Enthalpy

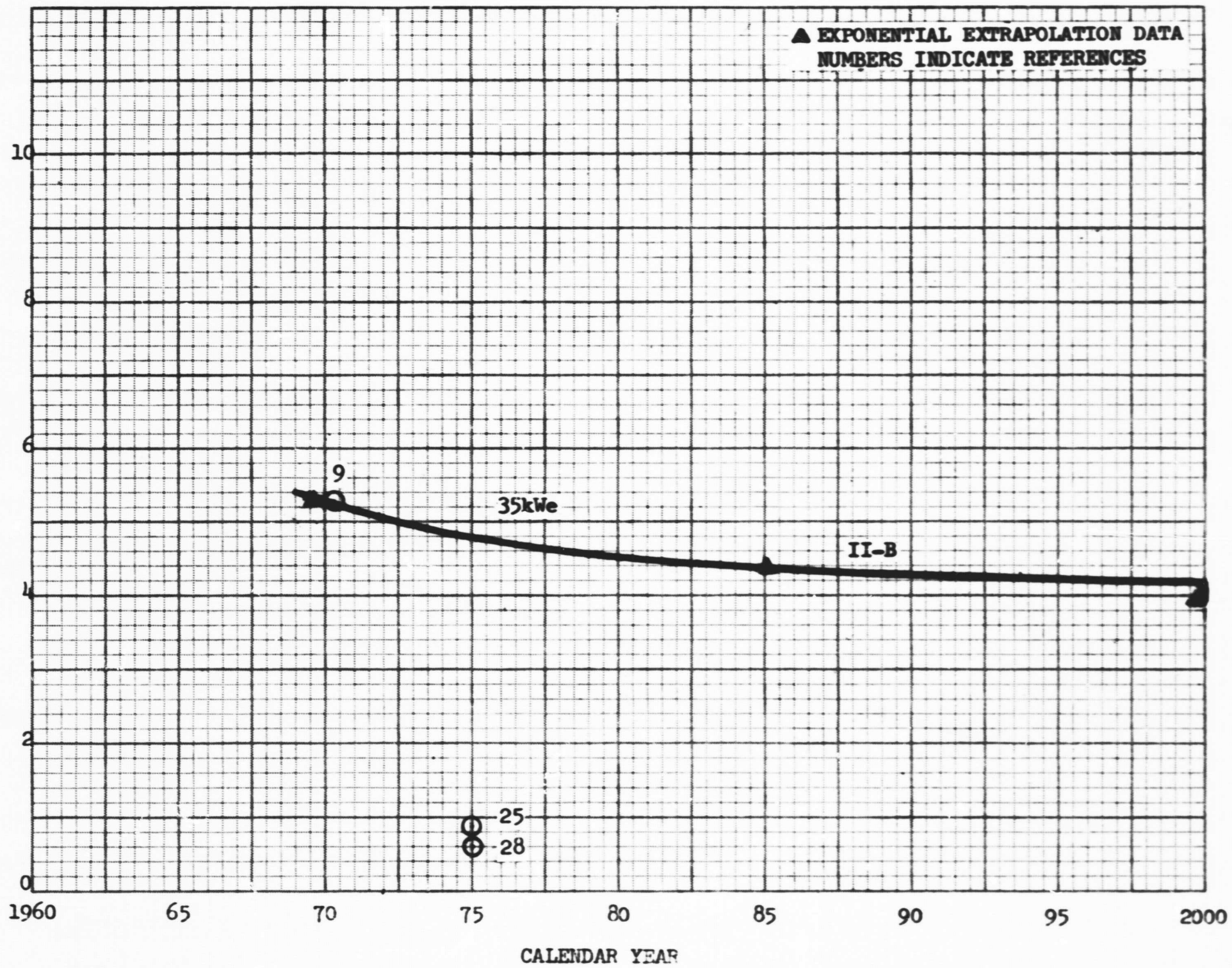

Figure 3-106 Projection of Alkali Metal Rankine Cycle Turboalternator Specific Mass

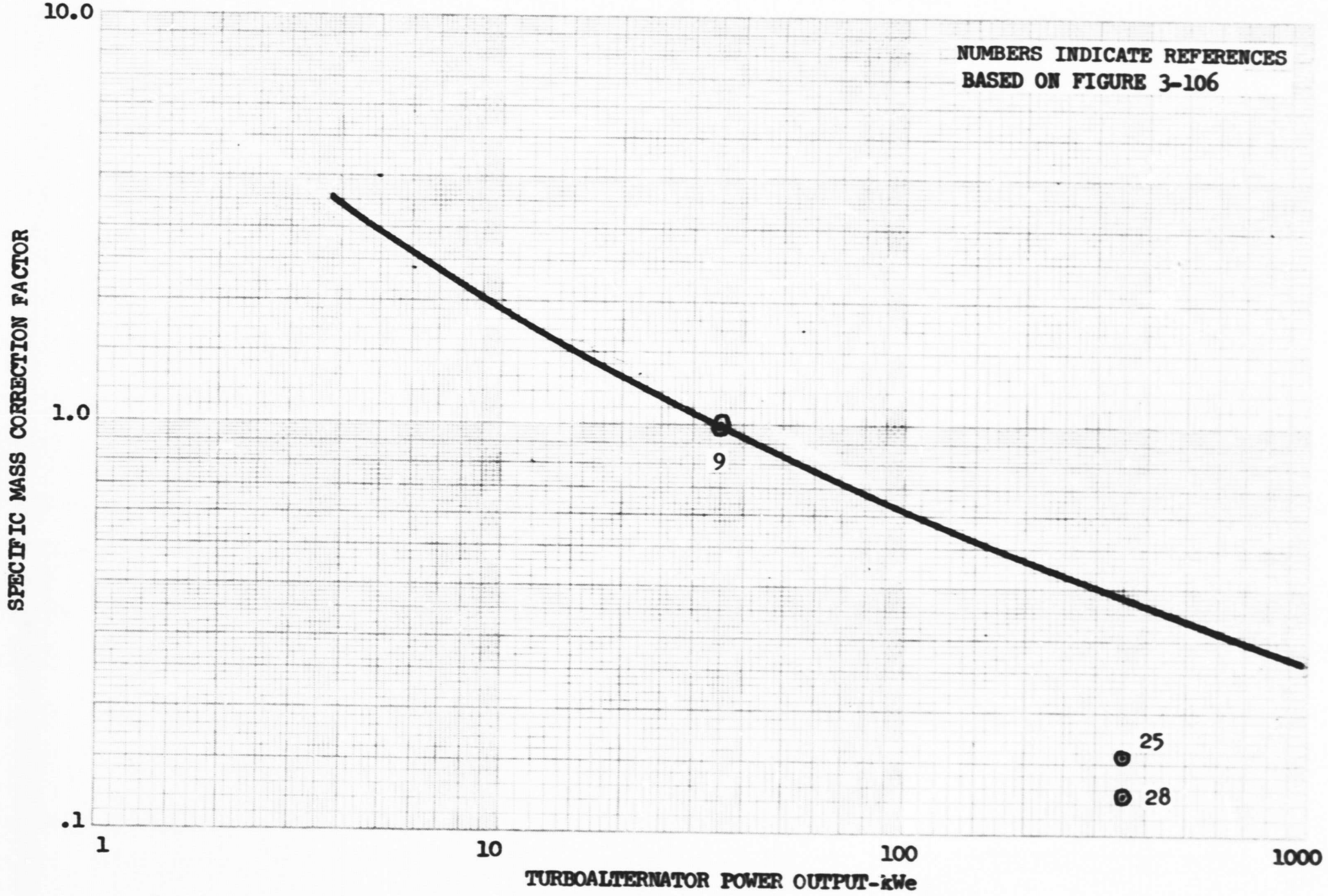

Figure 3-107 Alkali Metal Rankine Cycle Turbcalternator Factor for Specific Mass

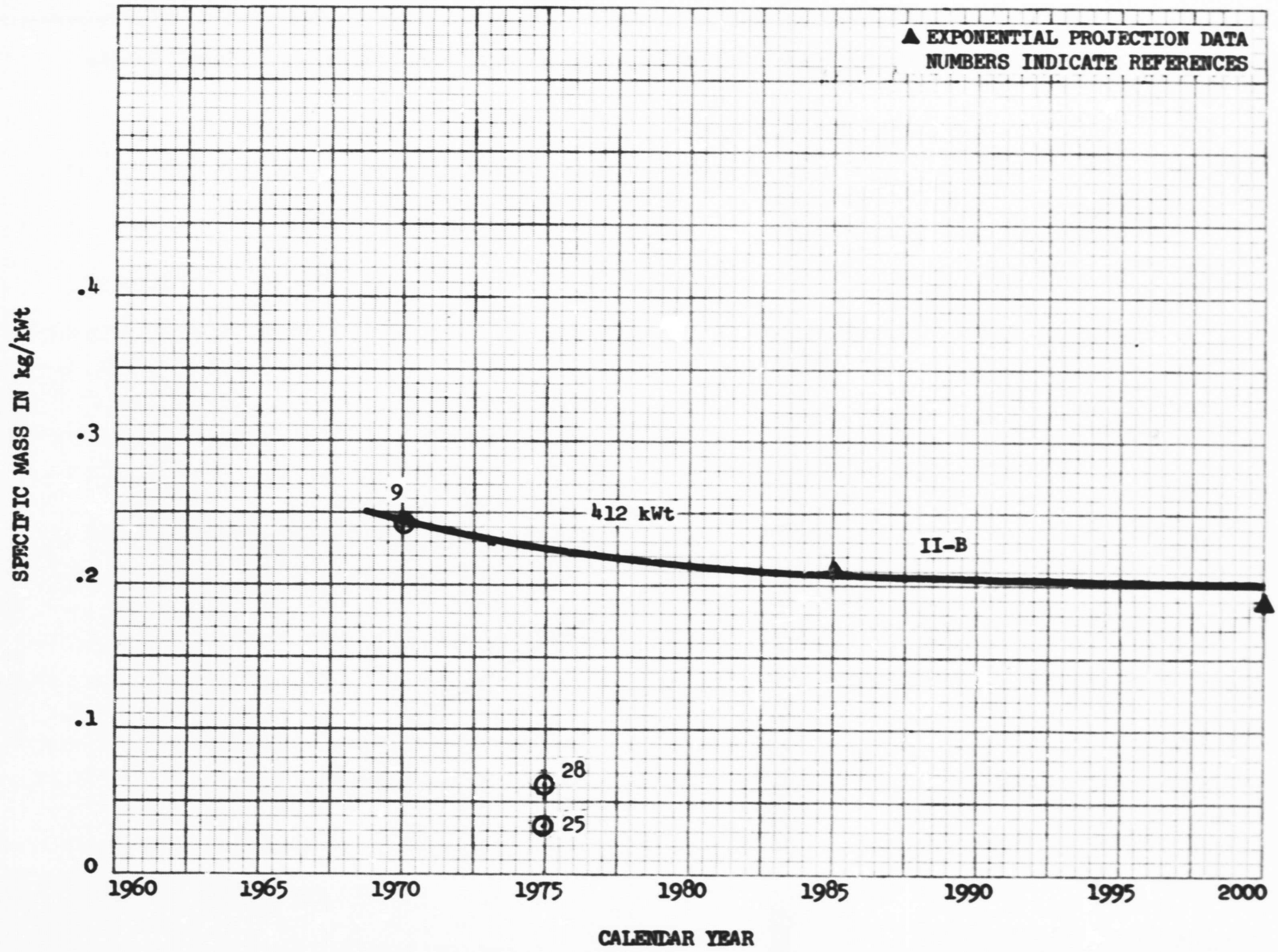

Figure 3-108 Projection of Alkali Metal Rankine Boiler Specific Mass

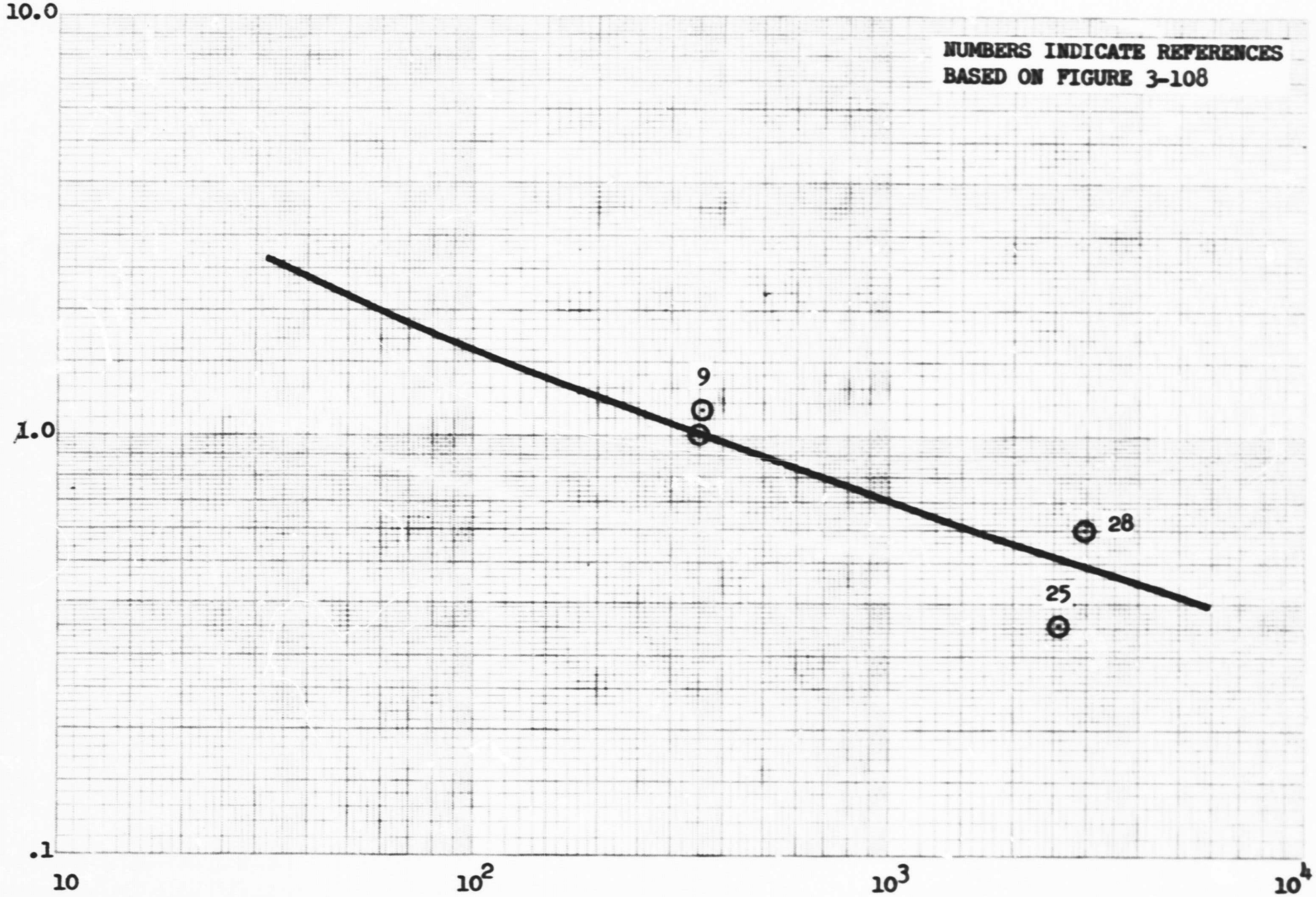

Figure 3-109 Alkali Metal Rankine Boiler Specific Mass Factor

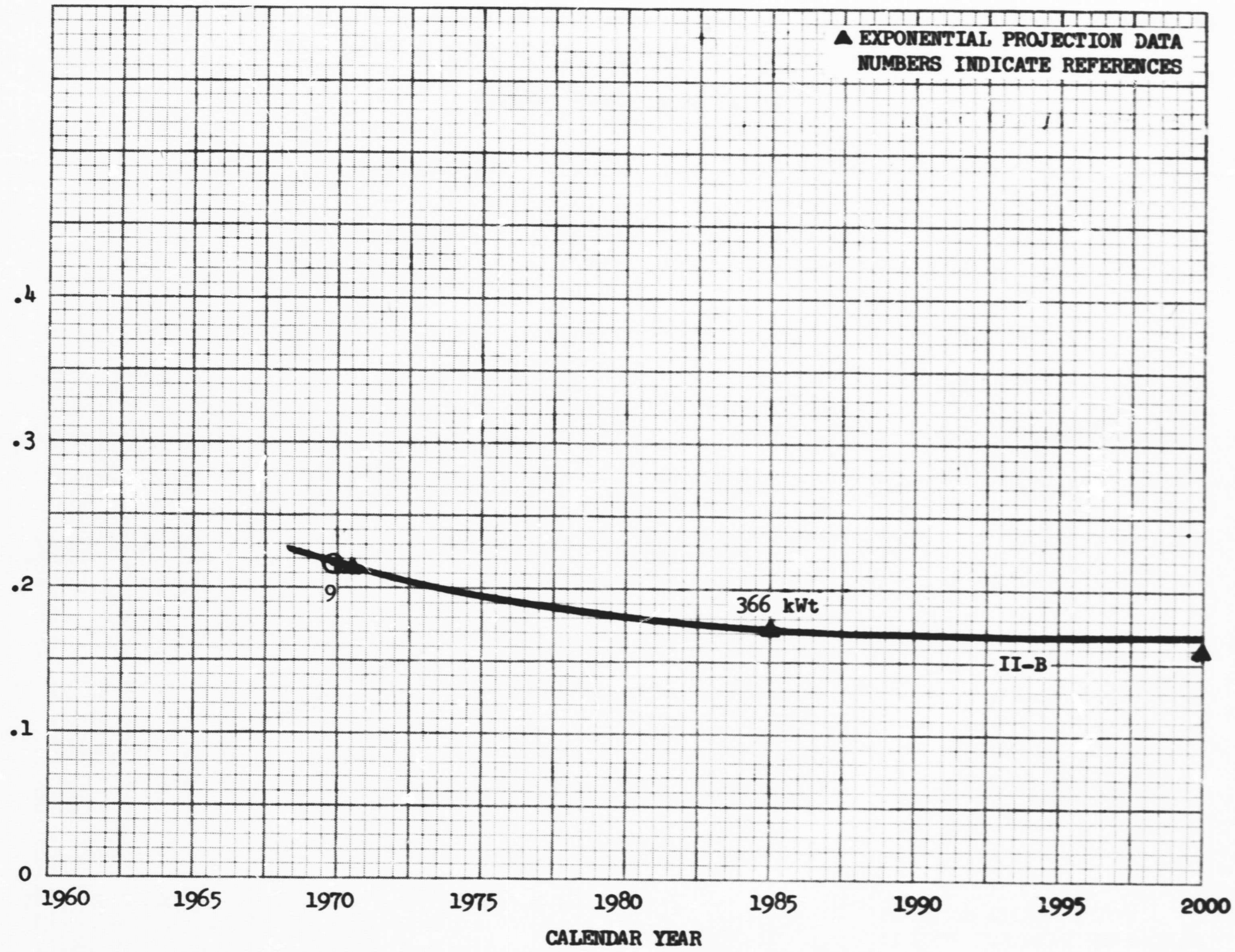

Figure 3-110 Projection of Alkali Metal Condenser Specific Mass

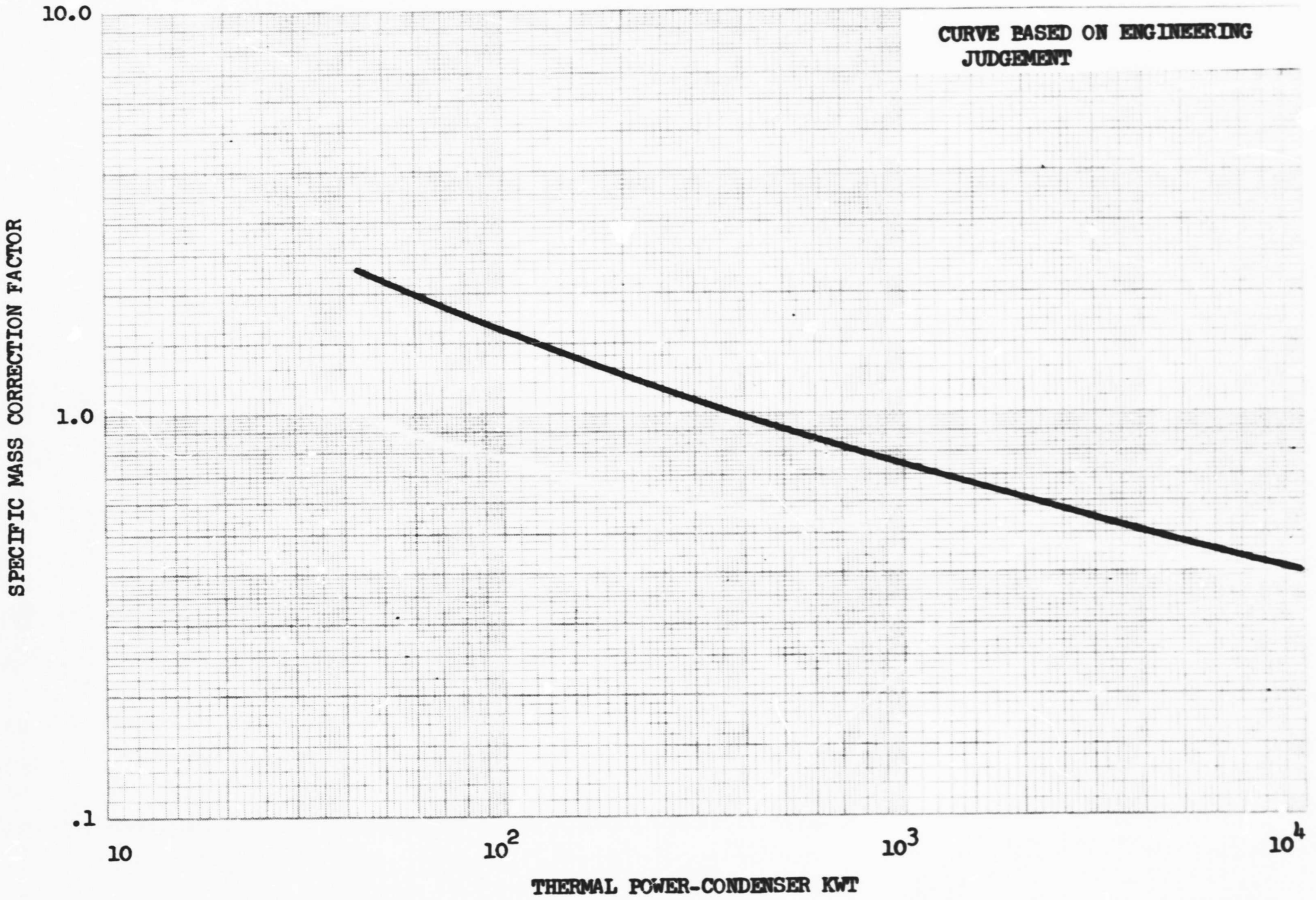

Figure 3-111 Alkali Metal Rankine Condenser Specific Mass Correction Factor

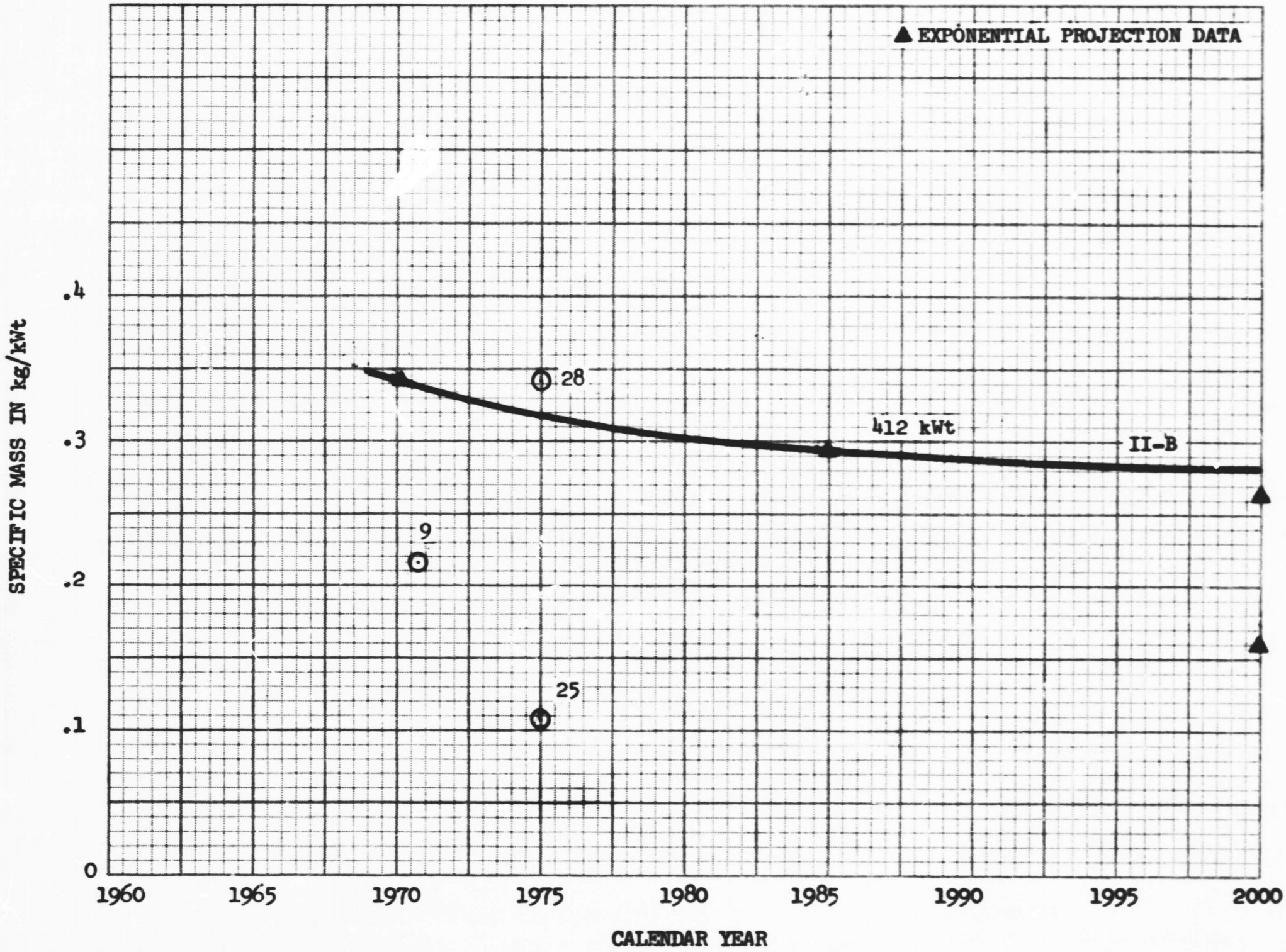

Figure 3-112 Projection Alkali Metal Rankine Accessories Specific Mass

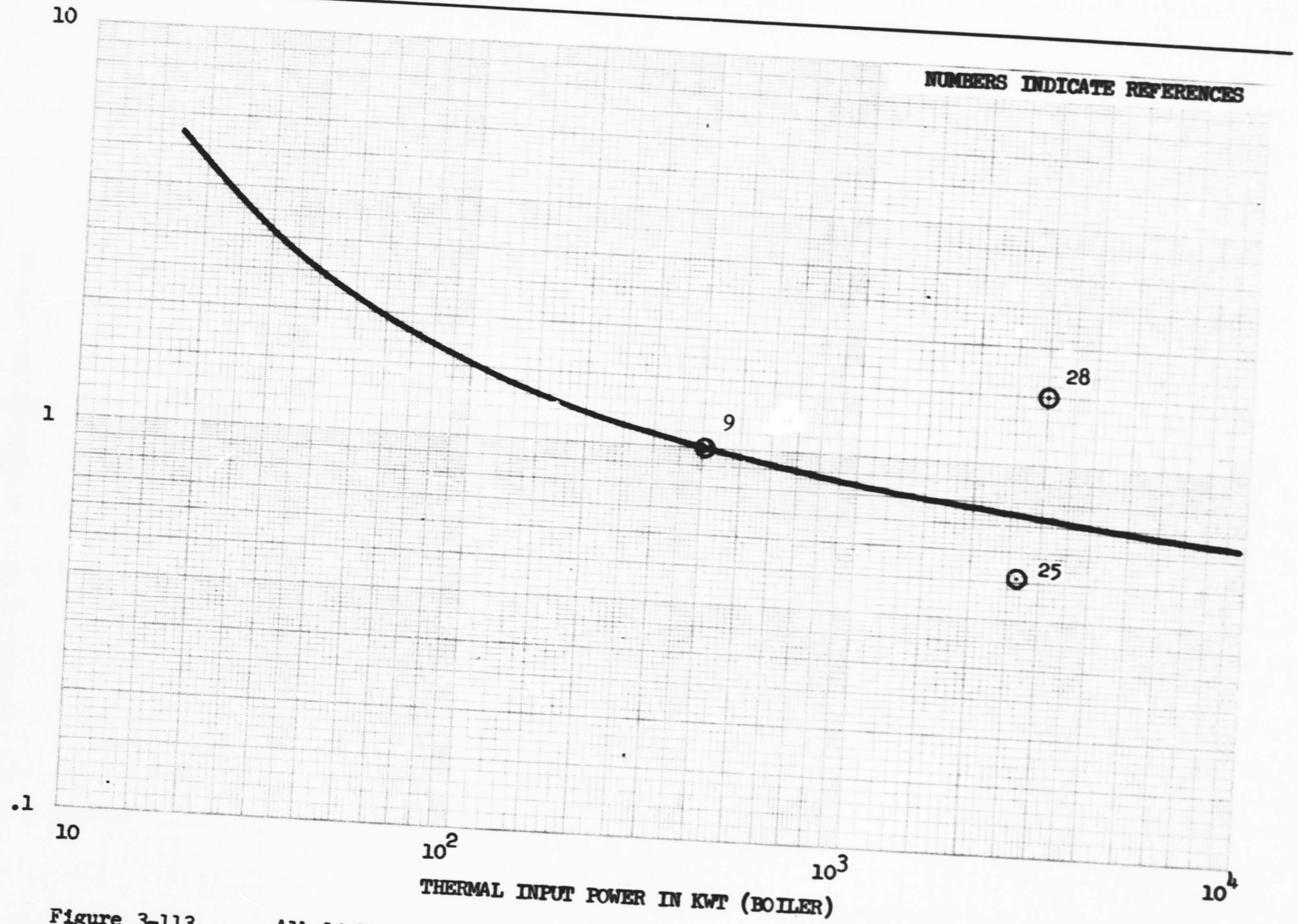

Figure 3-113 Alkali Metal Rankine Accessories Specific Mass Factor

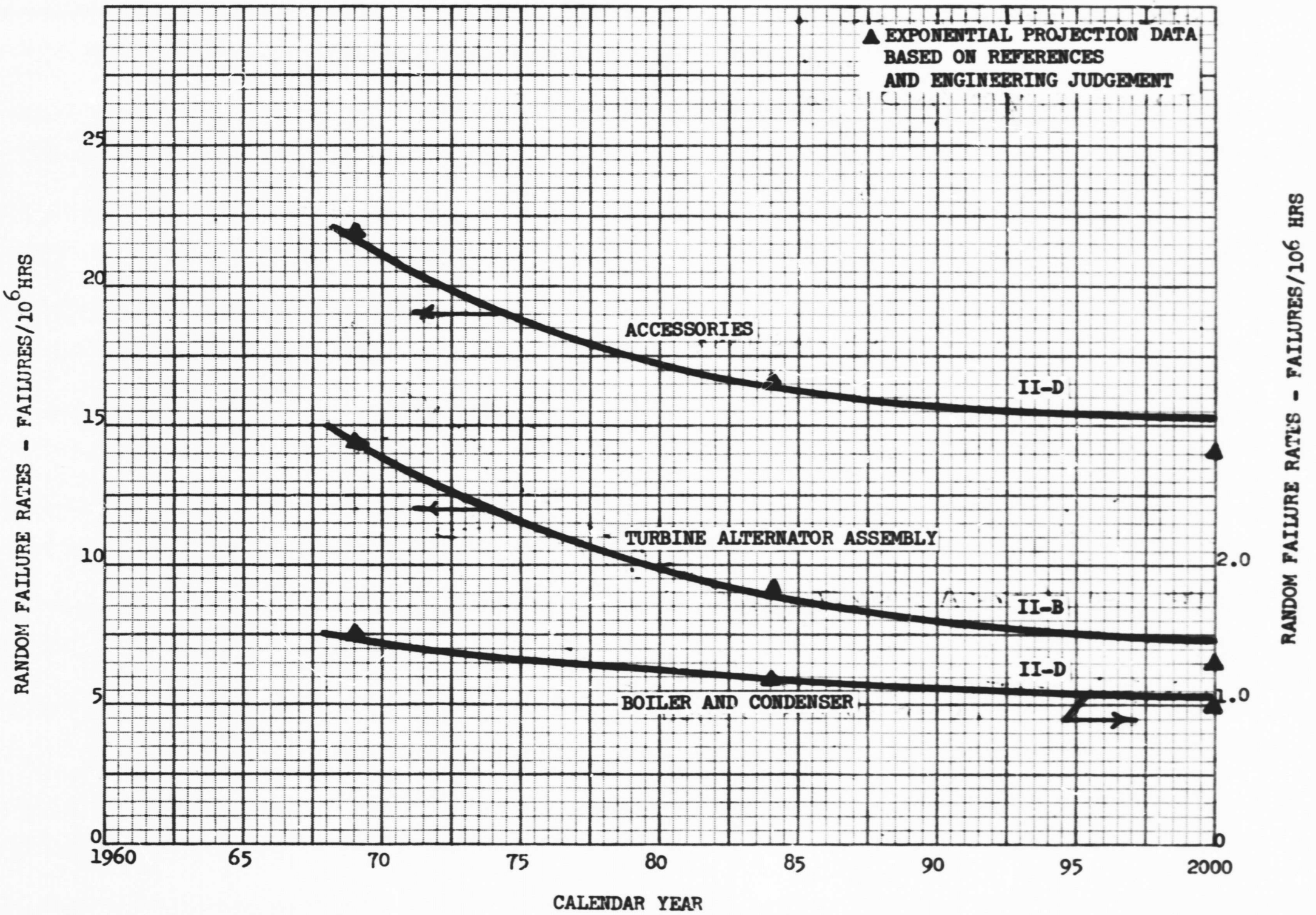

Figure 3-114 Projection of Alkali Metal Rankine Component Failure Rate

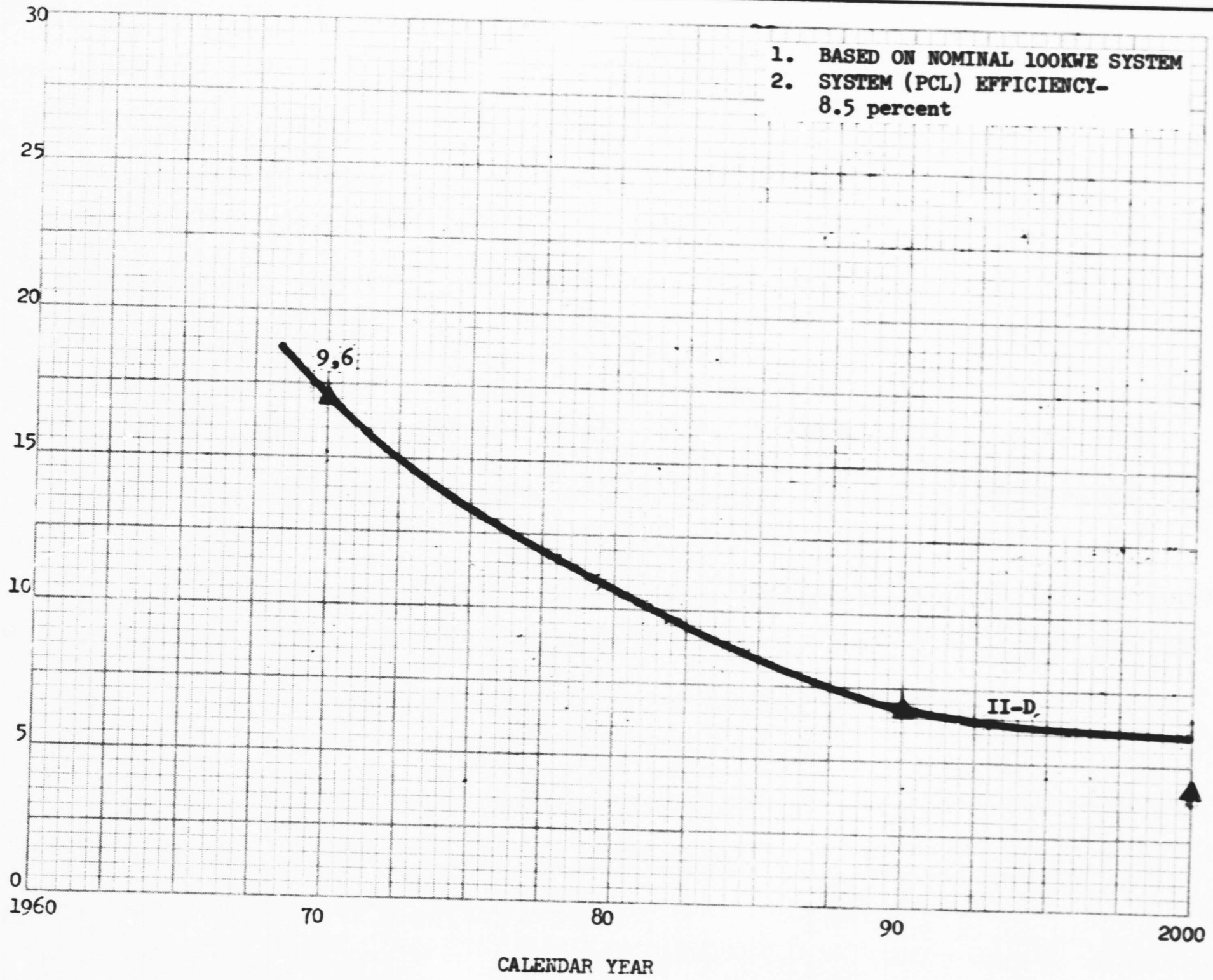

Figure 3-115 Specific Cost of Alkali Metal Rankine Cycle Accessories

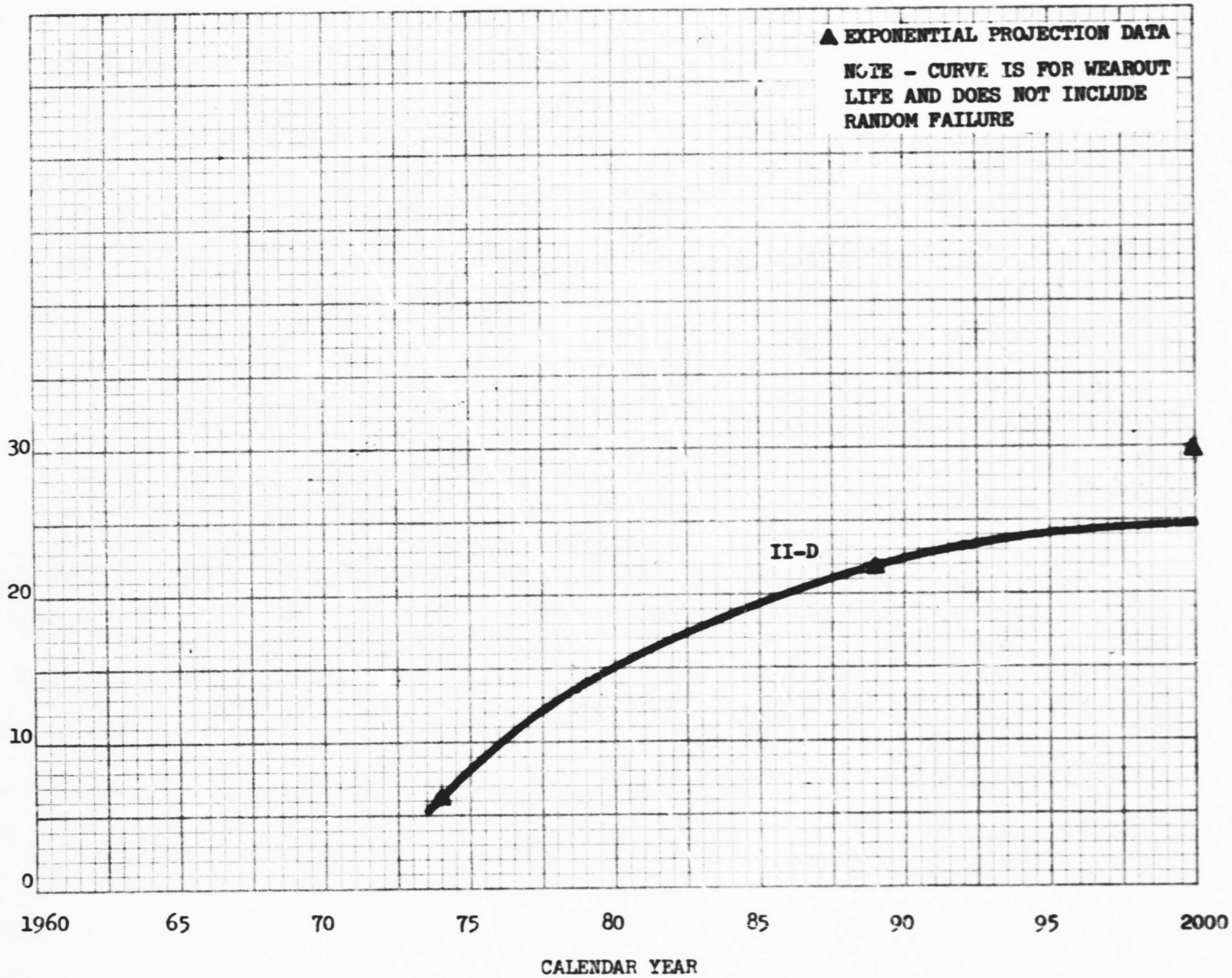

Figure 3-116 Projection of Alkali Metal Rankine Power Conversion Module Wearout Life

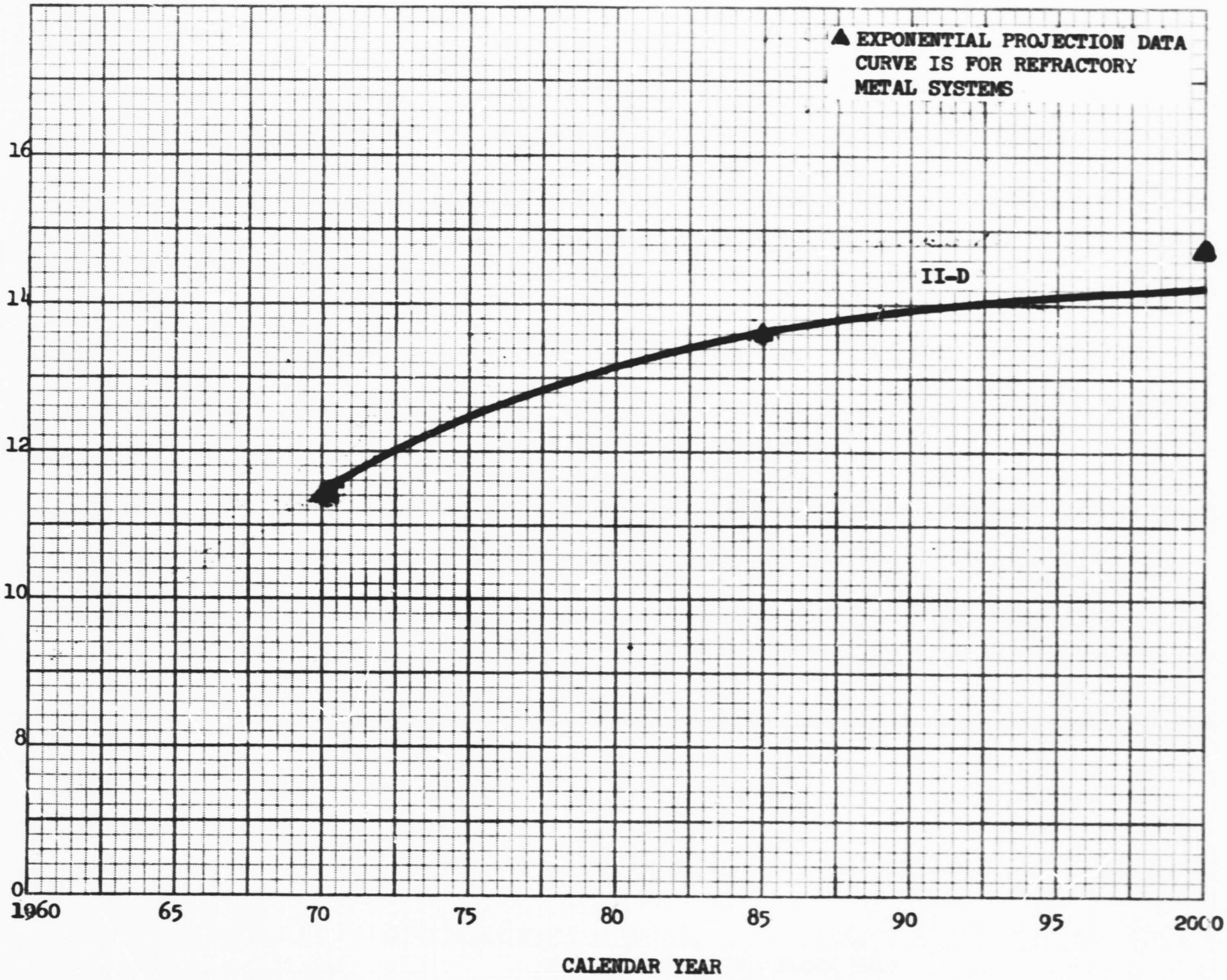

Figure 3-117 Projection of Alkali Metal Rankine Cycle Maximum Turbine Inlet Temperature

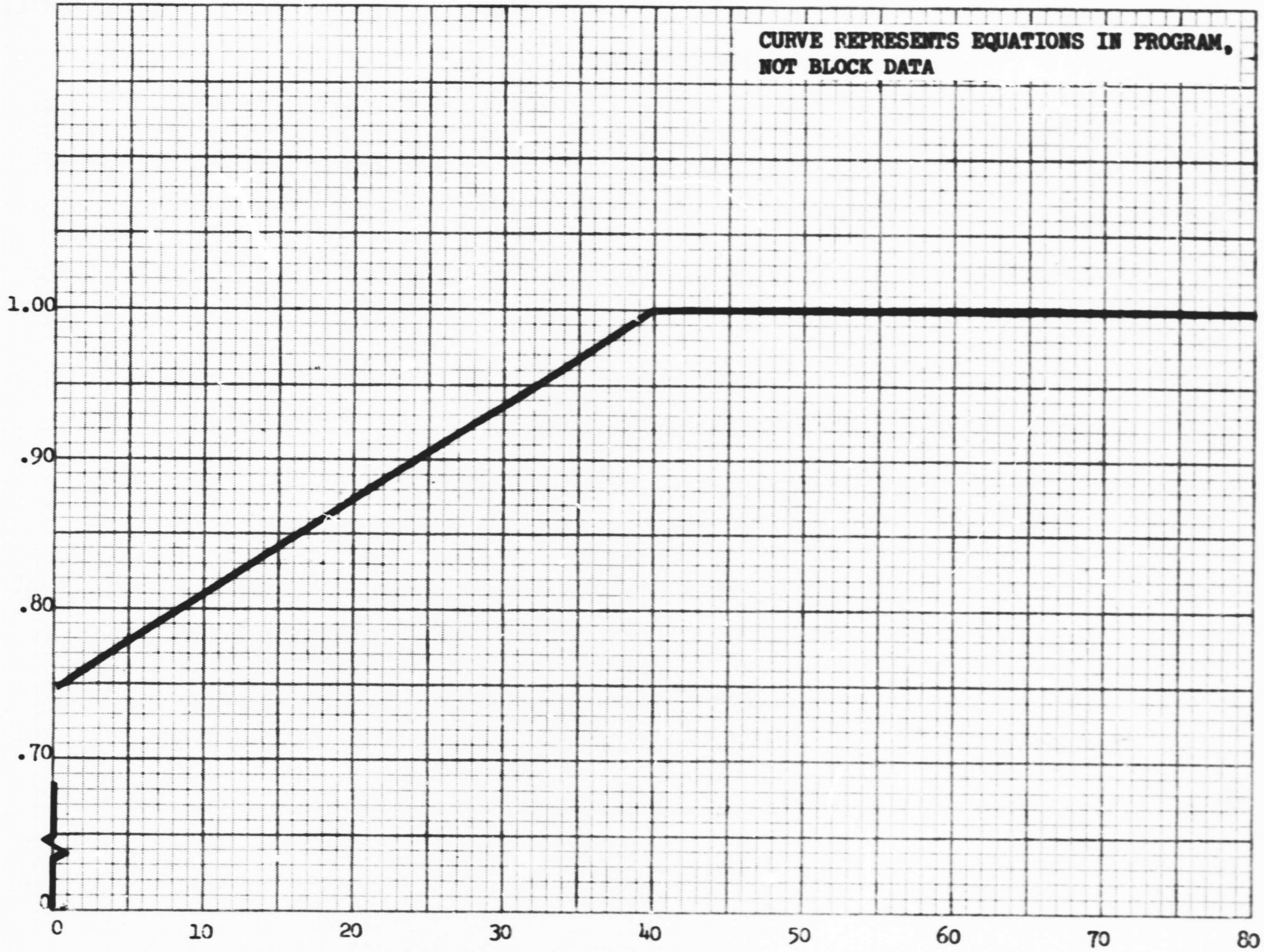

Figure 3-118 Maximum Alkali Metal Turbine Inlet Temperature Factor Versus Power Level

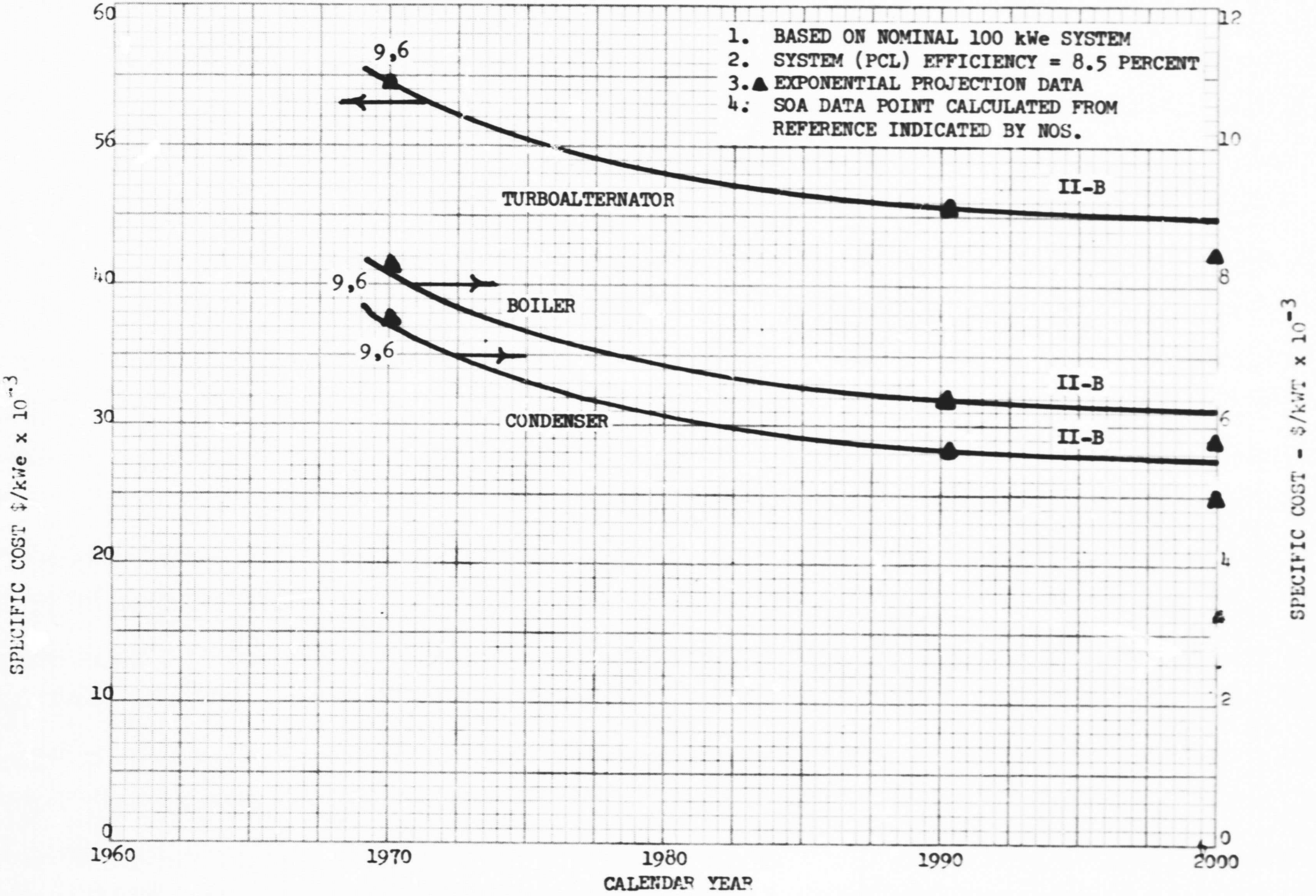

Figure 3-119 Specific Cost of Alkali Metal Rankine Cycle Components

Figure 3-120 Deleted

PRECEDING PAGE BLANK NOT FILMED.

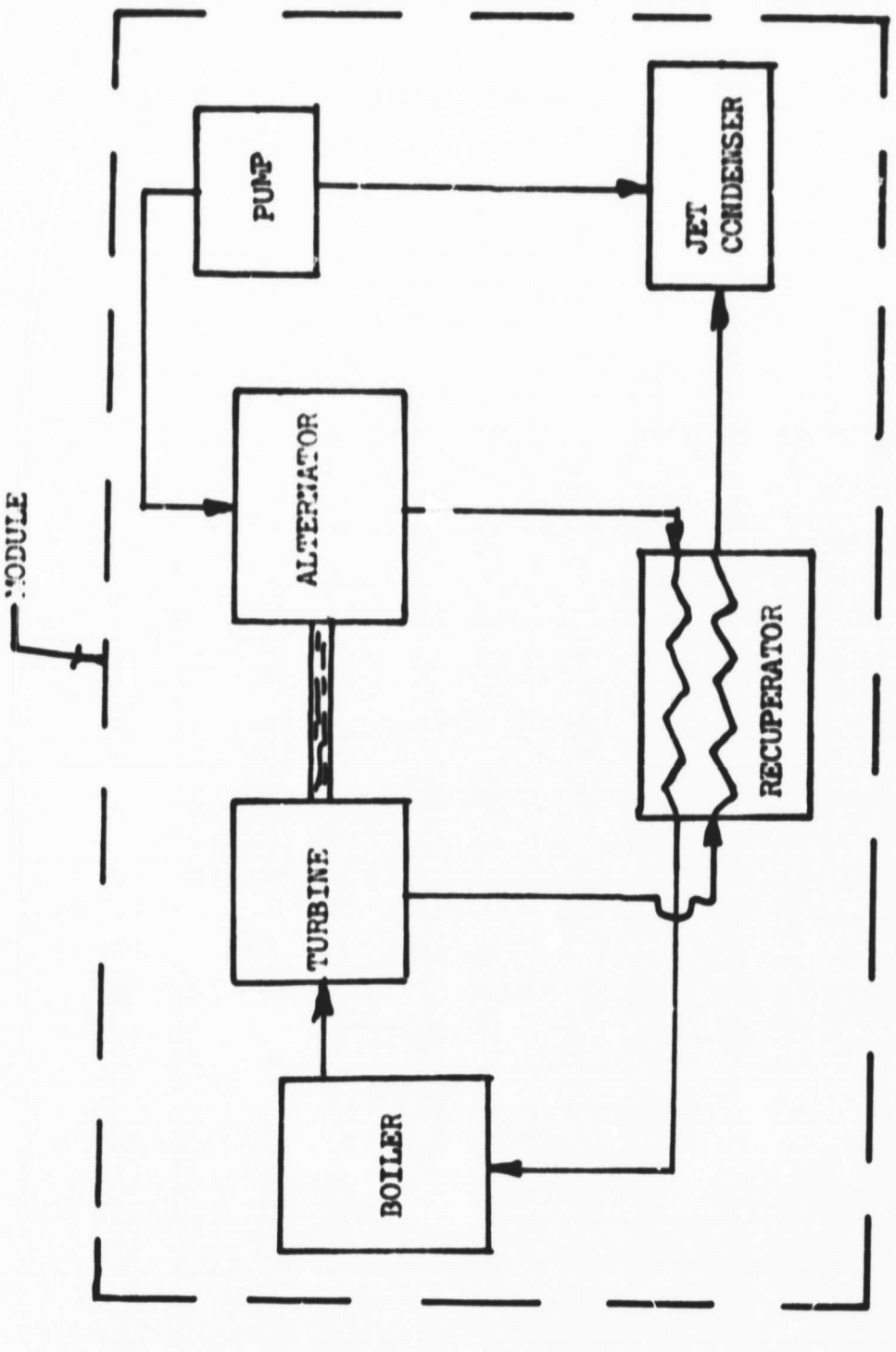

Note: One or modules are used in a subsystem

Figure 3-121 Typical Organic Rankine Cycle Module

The organic Rankine conversion subsystems status, characteristics, and ranges of performance are shown in Table 3-28. The organic subsystem components characteristics and performance such as specific mass, density, failure rates, life, cost, and efficiency are shown in Figure 3-122 through 3-134.

Table 3-28

ORGANIC RANKINE CYCLE CONVERSION
SUBSYSTEM BRIEFING CHART

Item	Value
Identification	
Applicable energy source	Solar, isotope, reactor
Heat rejection subsystem	Convective loop
Major components	Combined rotating unit, boiler, regenerator, jet condenser, accessory equipment
Vehicle - Mission application range	
Useful power level	1kWe to 100 kWe
Duration of mission	Days to years
Types of spacecraft	Manned, unmanned, Earth orbiting, interplanetary
Status (1967)	
State of the art	Prototype unit developed and 2, 700 hour of test time accumulated on unit
Availability of support systems	Supporting subsystems within current technology levels
Special problems	Jet condenser development, fluid degradation
Subsystem Characteristics (1 PCU module)	
Range of specific mass	20 to 30 kg/kWe
Range of specific volume	0.5 to 0.9 m^3/kWe
Range of specific production cost	100 to 200 k$/kWe
Range of reliability	70 to 95% (1 year)
Performance Data	
Turbine inlet temperature	615° to 675°K
Cycle efficiency	12 to 22%

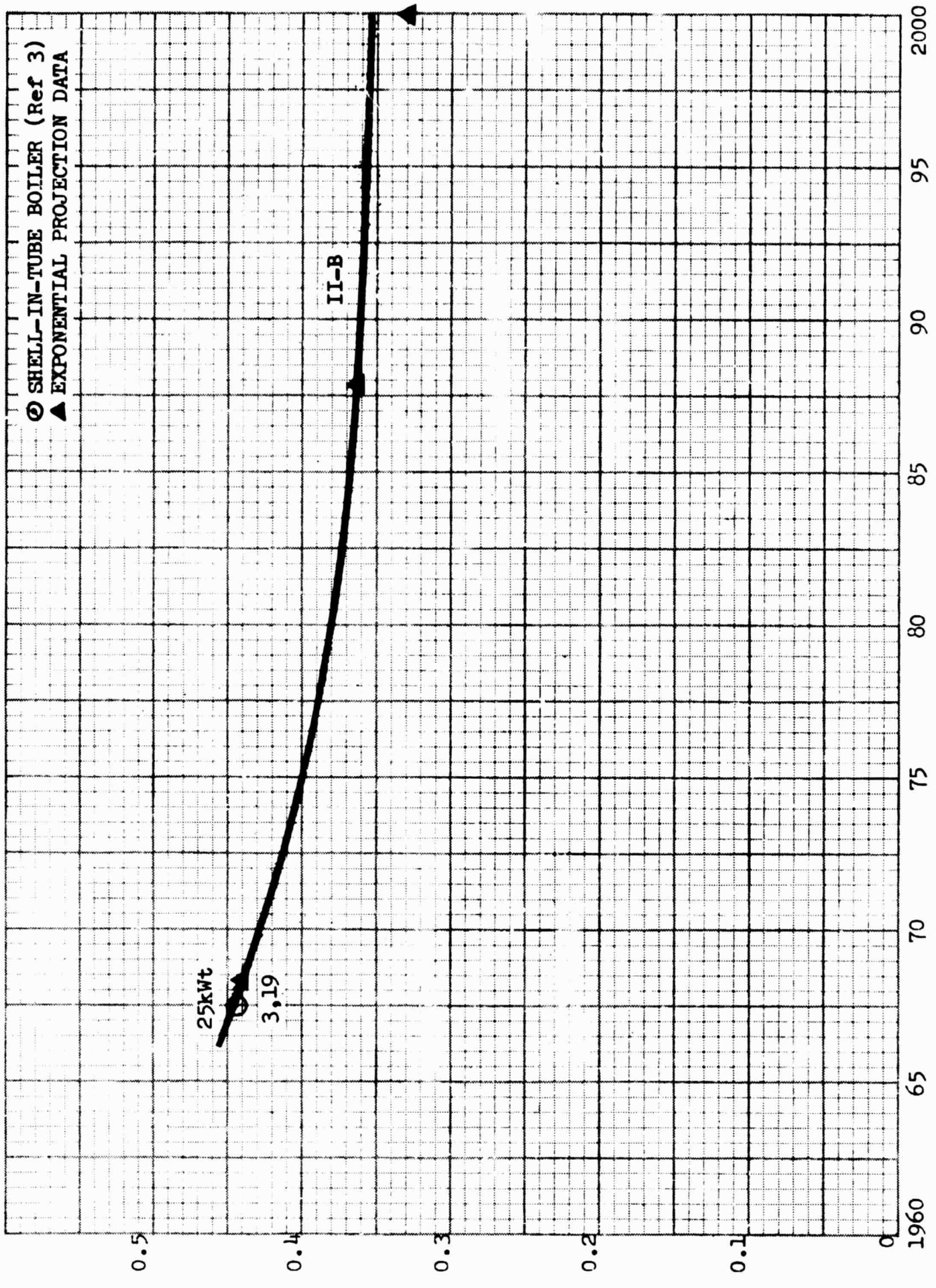

Figure 3-122 Organic Rankine Cycle Boiler Mass

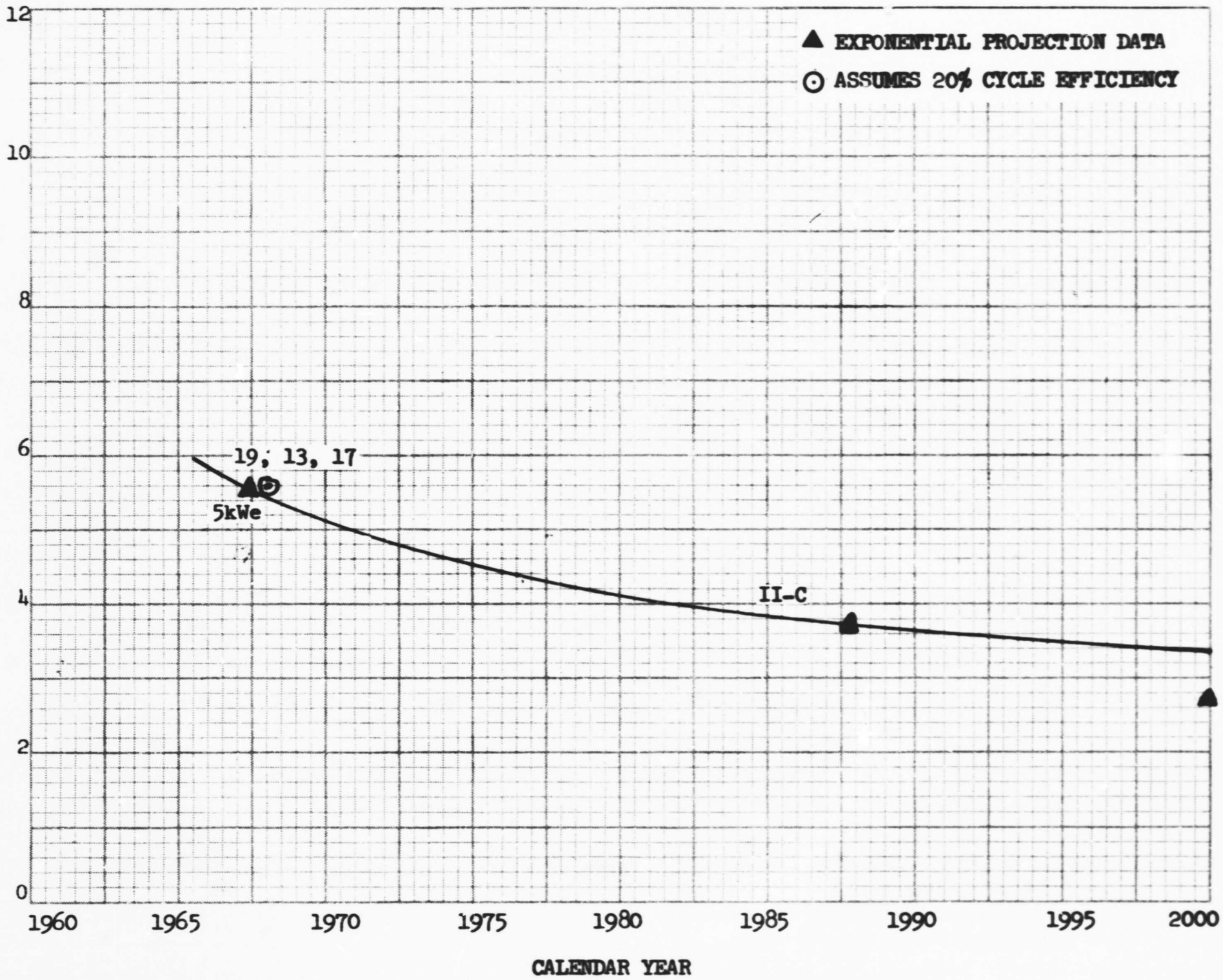

Figure 3-123 Organic Cycle Turbo-Alternator Mass

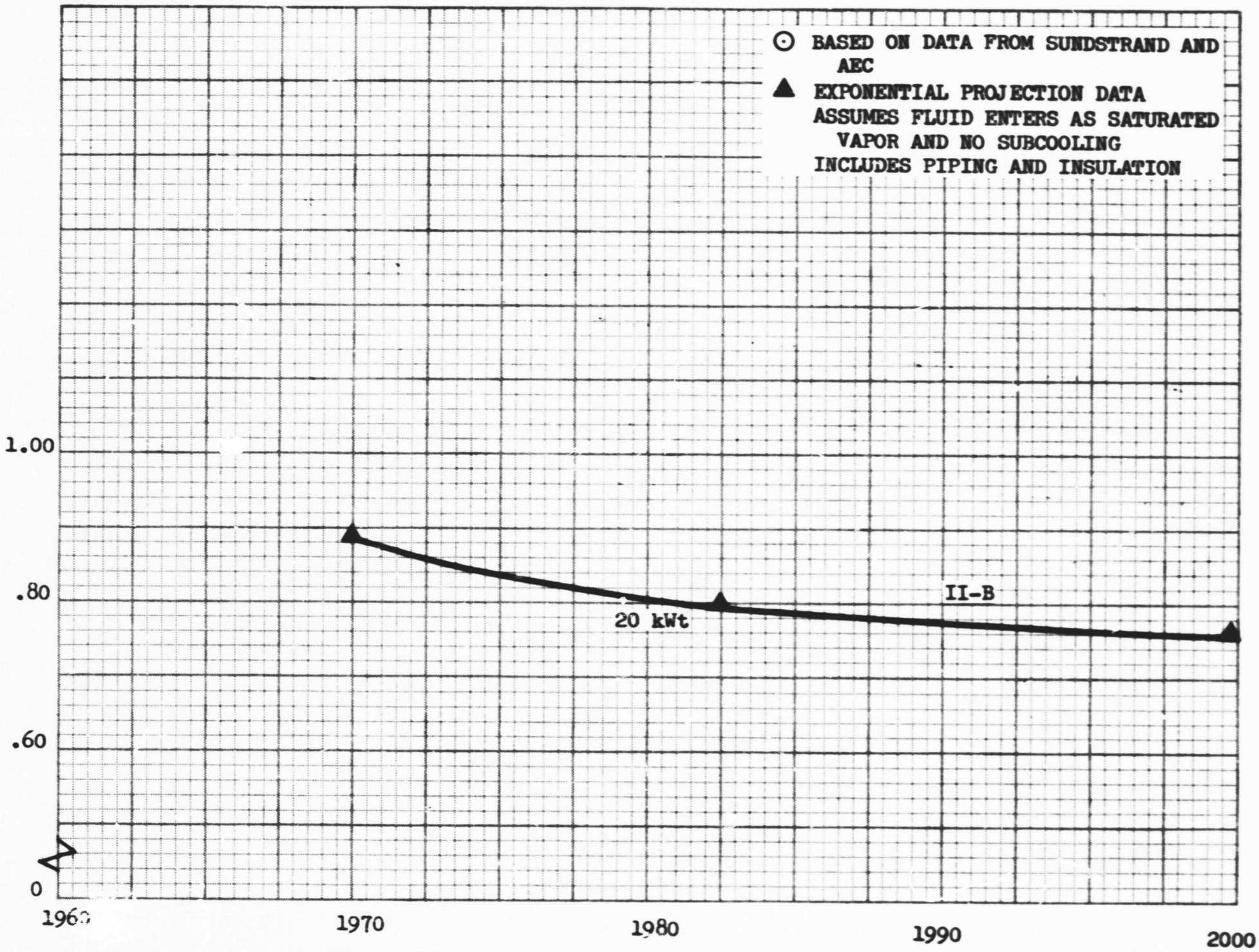

Figure 3-124 Organic Cycle Condenser Mass

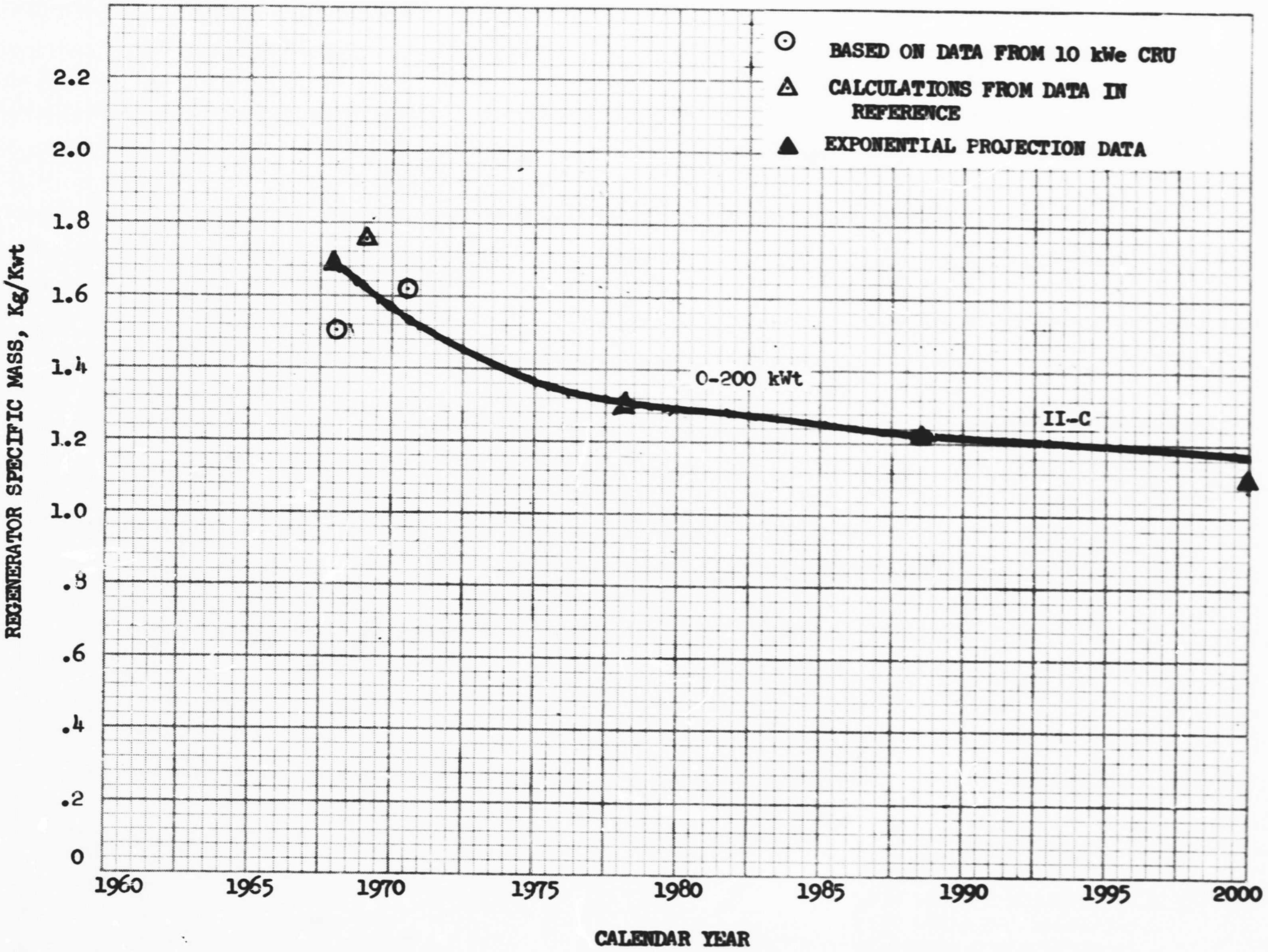

Figure 3-125 Organic Cycle Regenerator Mass

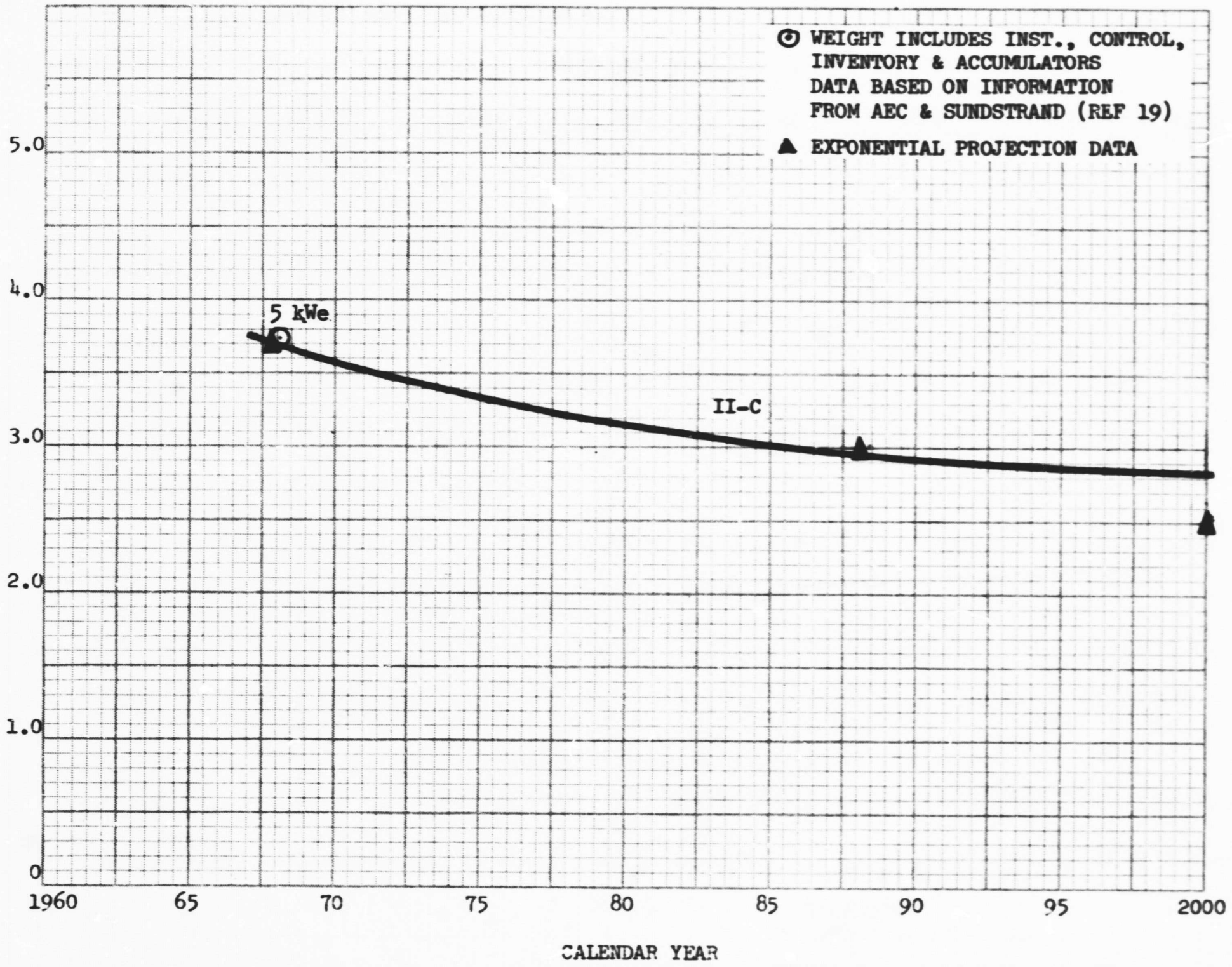

Figure 3-126 Organic Cycle Accessory Mass

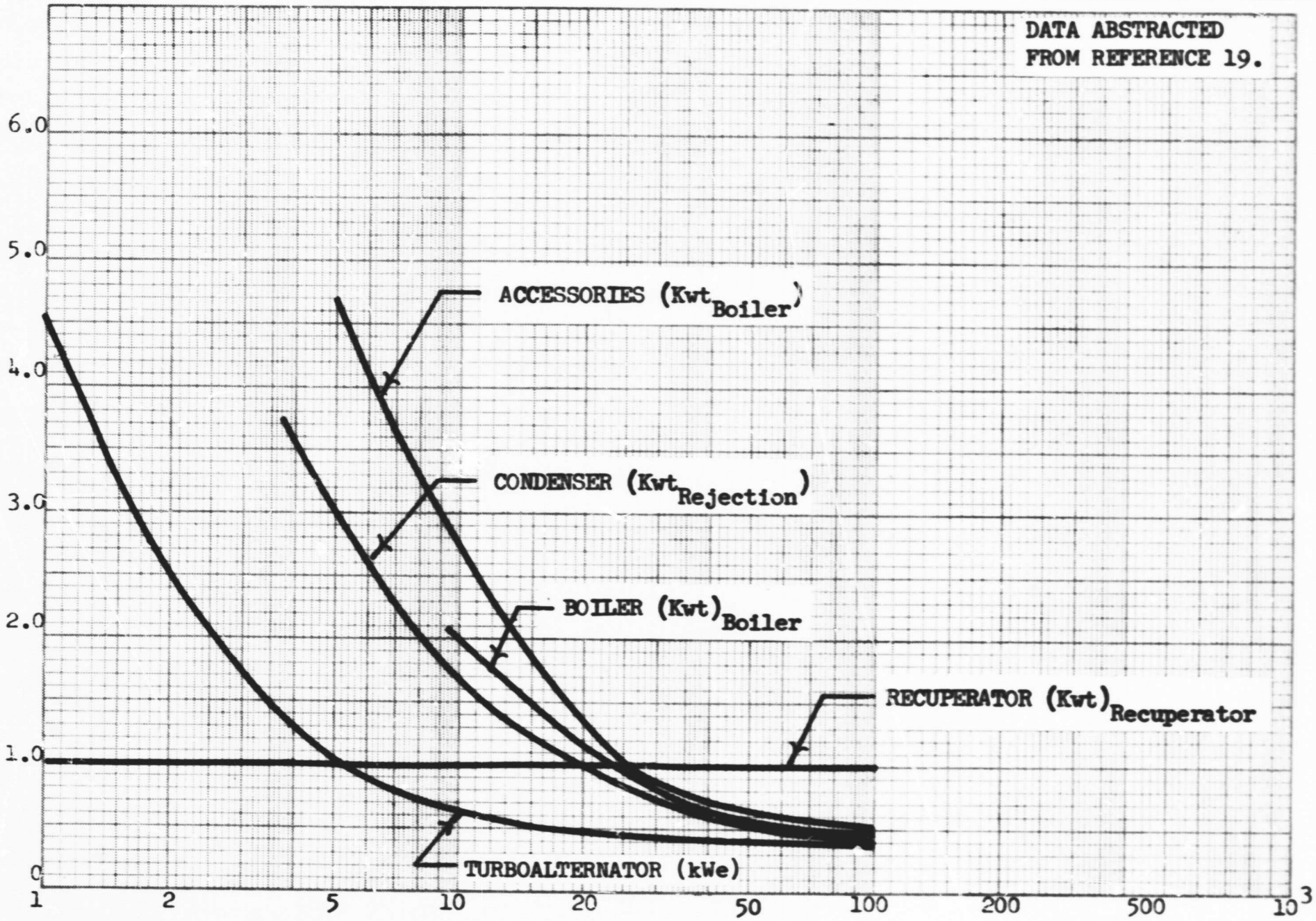

Figure 3-127 Mass Correction Factor For Organic Rankine Cycle Components

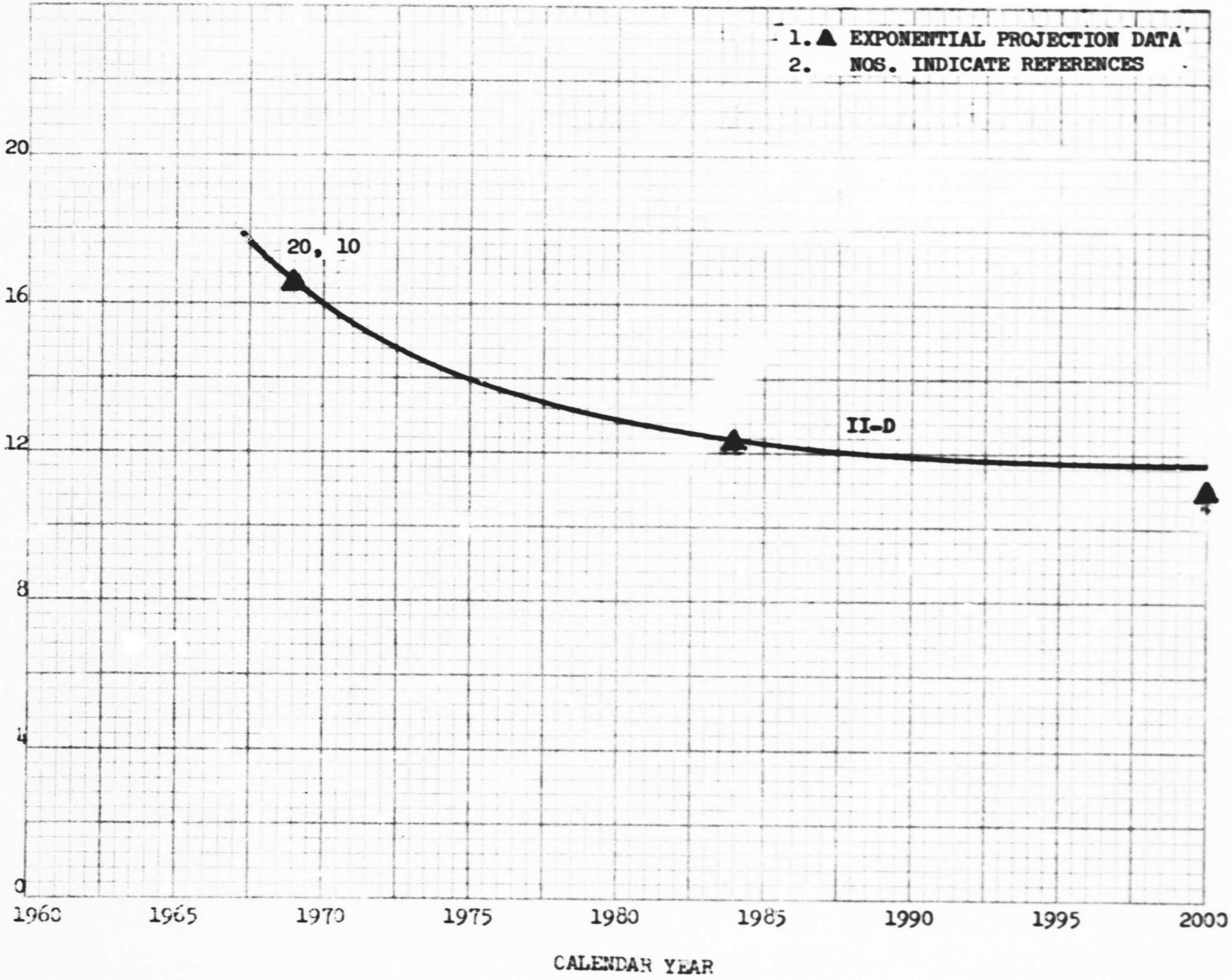

Figure 3-128 Failure Rates of Accessories (Organic Rankine Cycle)

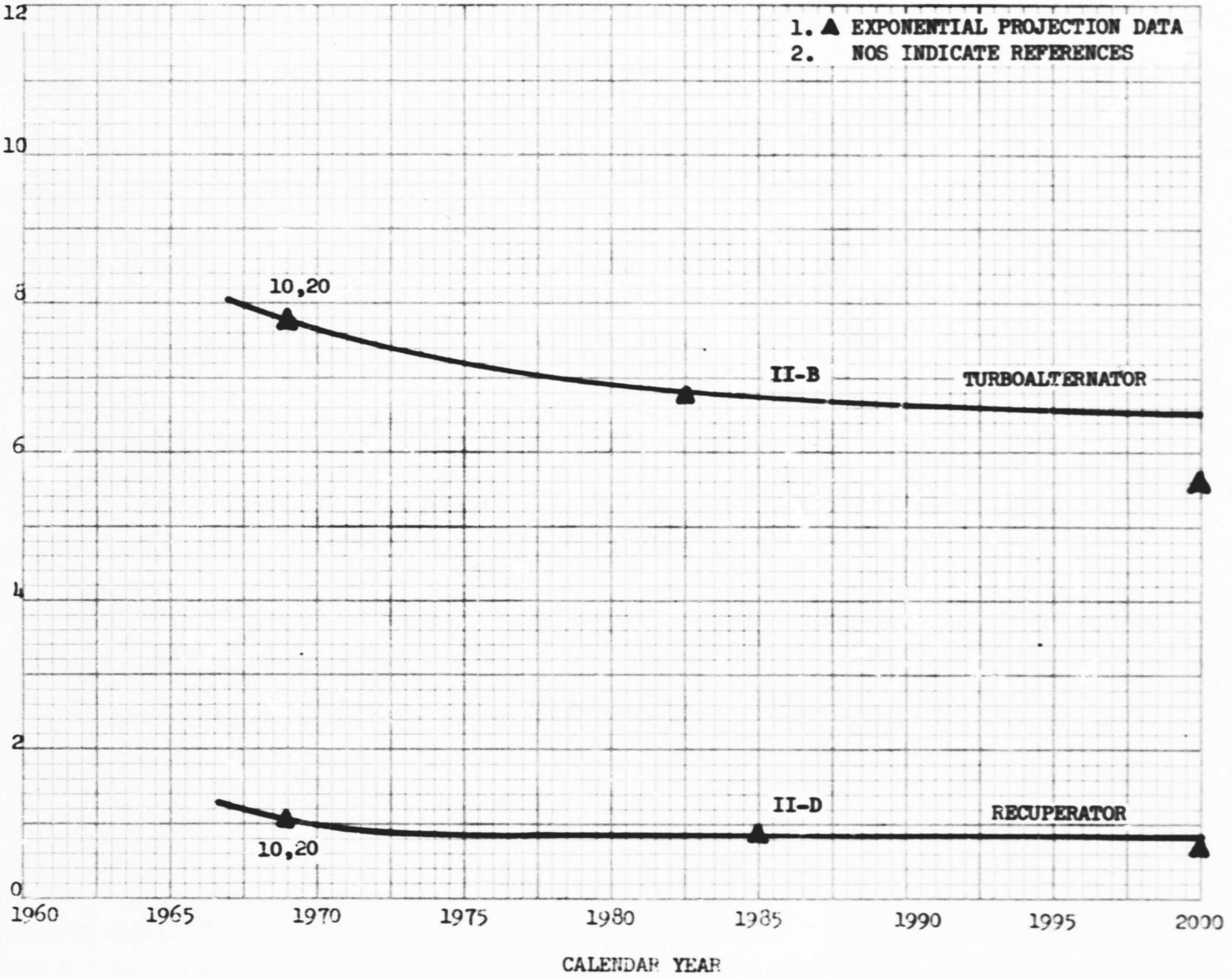

Figure 3-129 Failure Rates of Organic Rankine Cycle Components

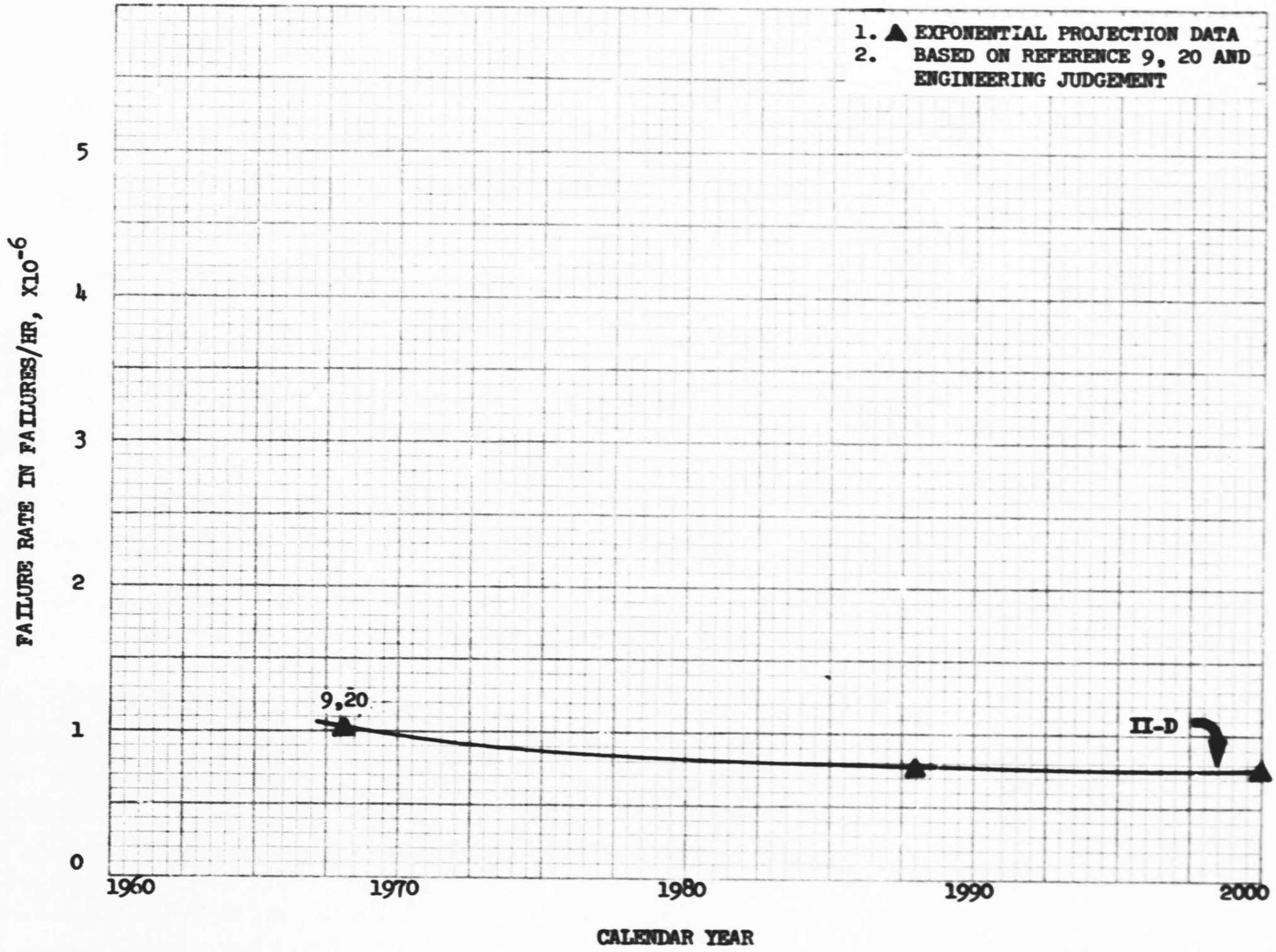

Figure 3-130 Projection Boiler and Condenser Failure Rates - (Organic Rankine)

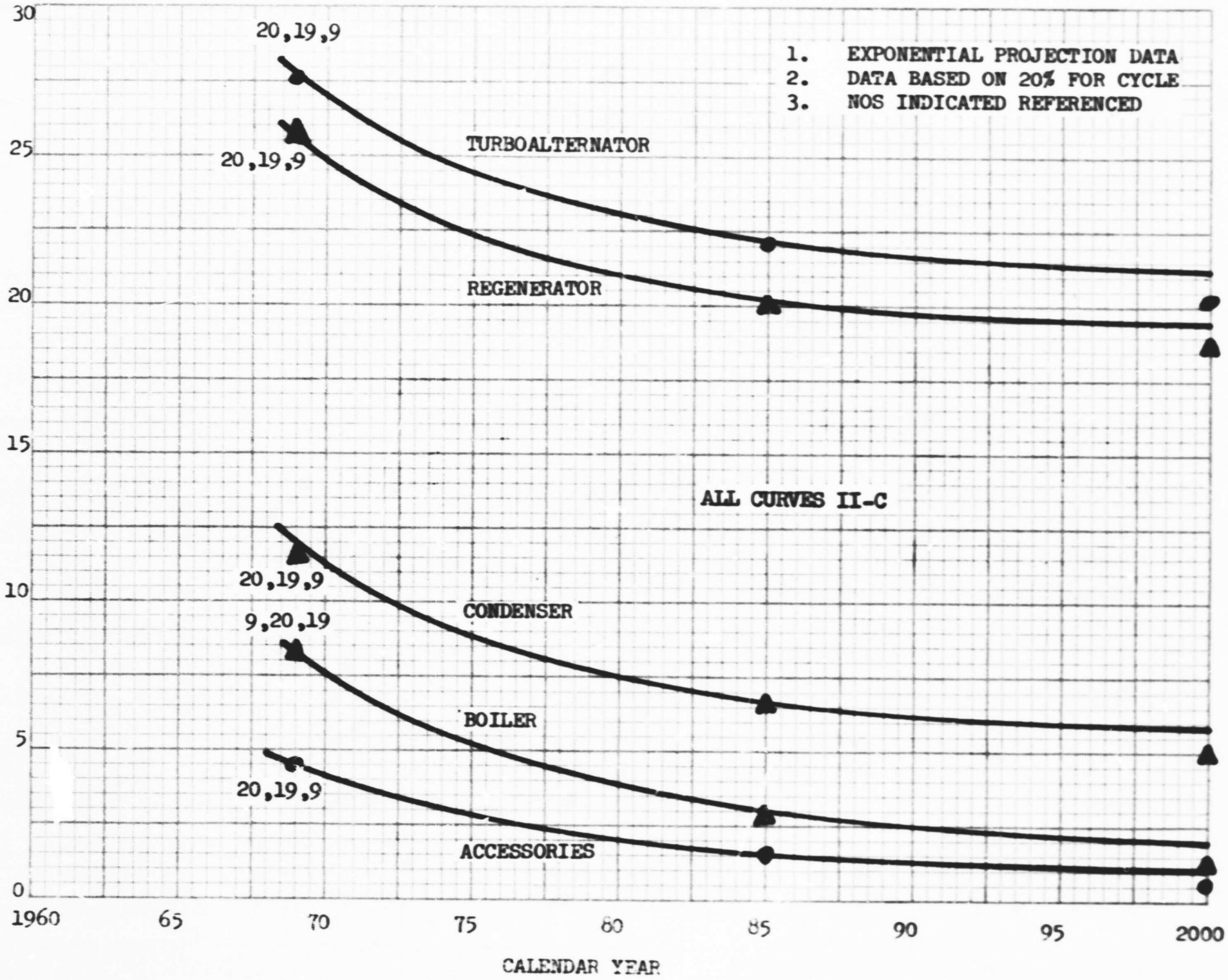

Figure 3-131 Specific Cost Of Component - Organic Rankine Cycle

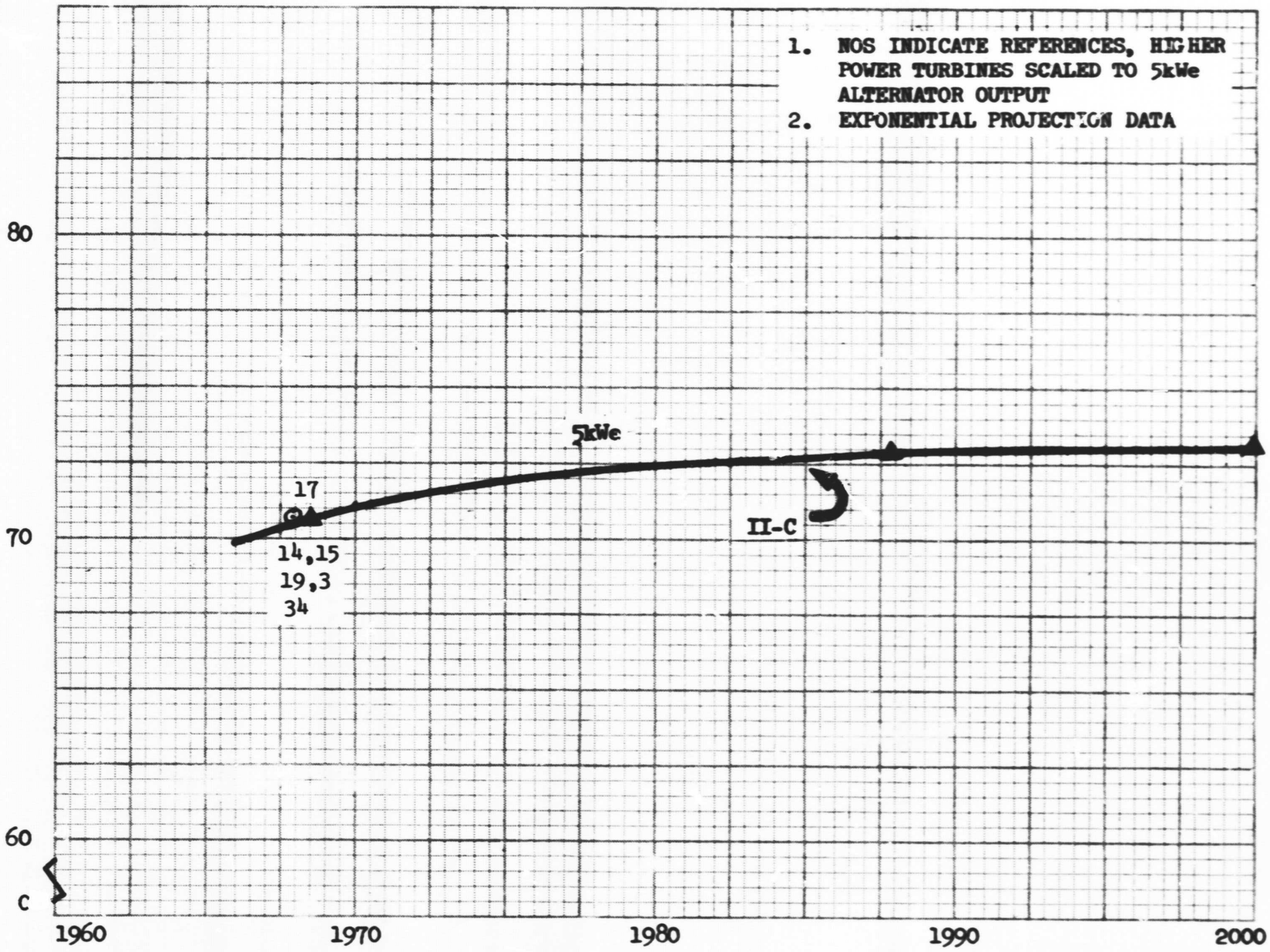

Figure 3-132a Organic Cycle Turbine Efficiency

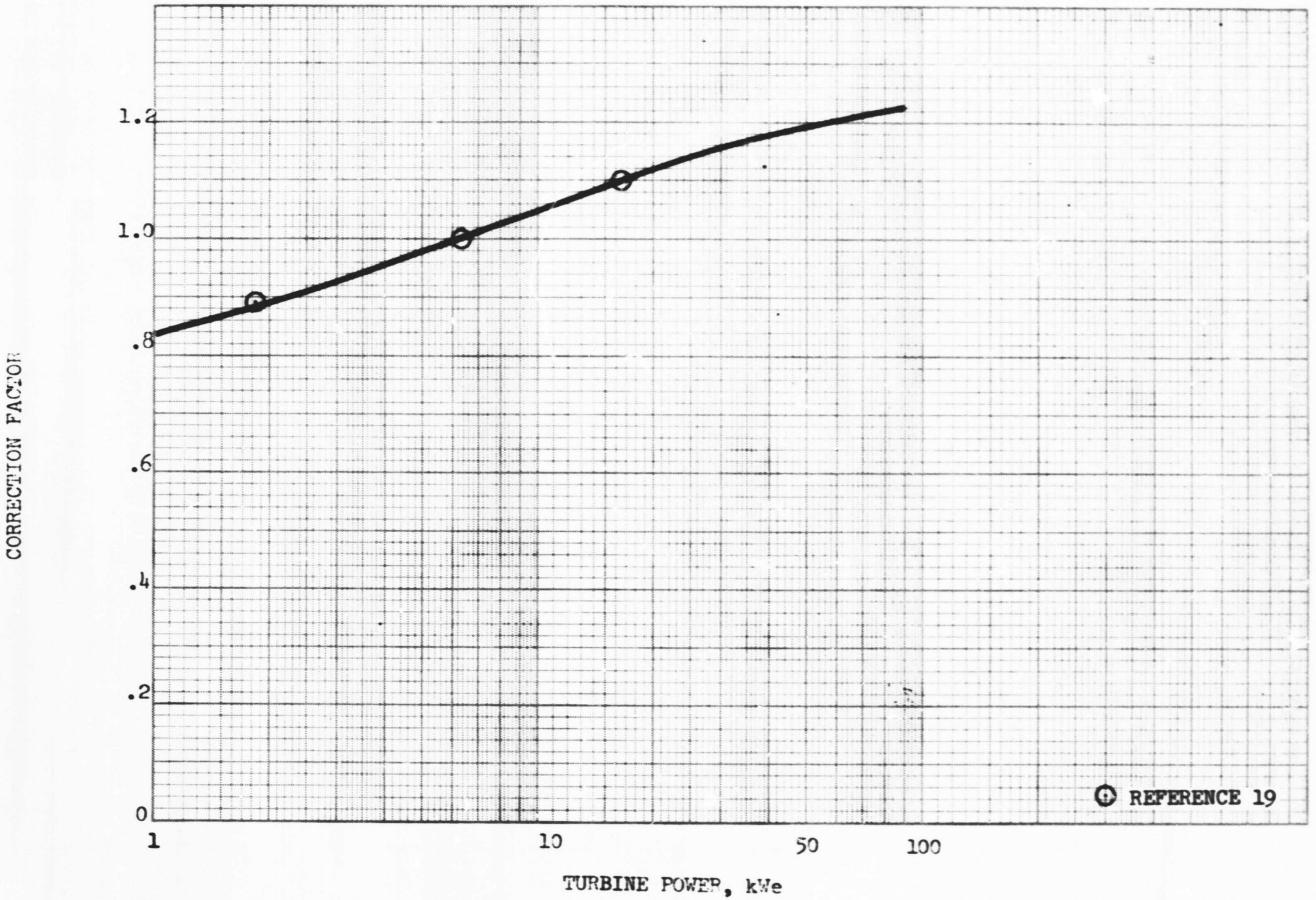

Figure 3-132b Correction Factor For Turbine Efficiency (Organic Rankine Cycle)

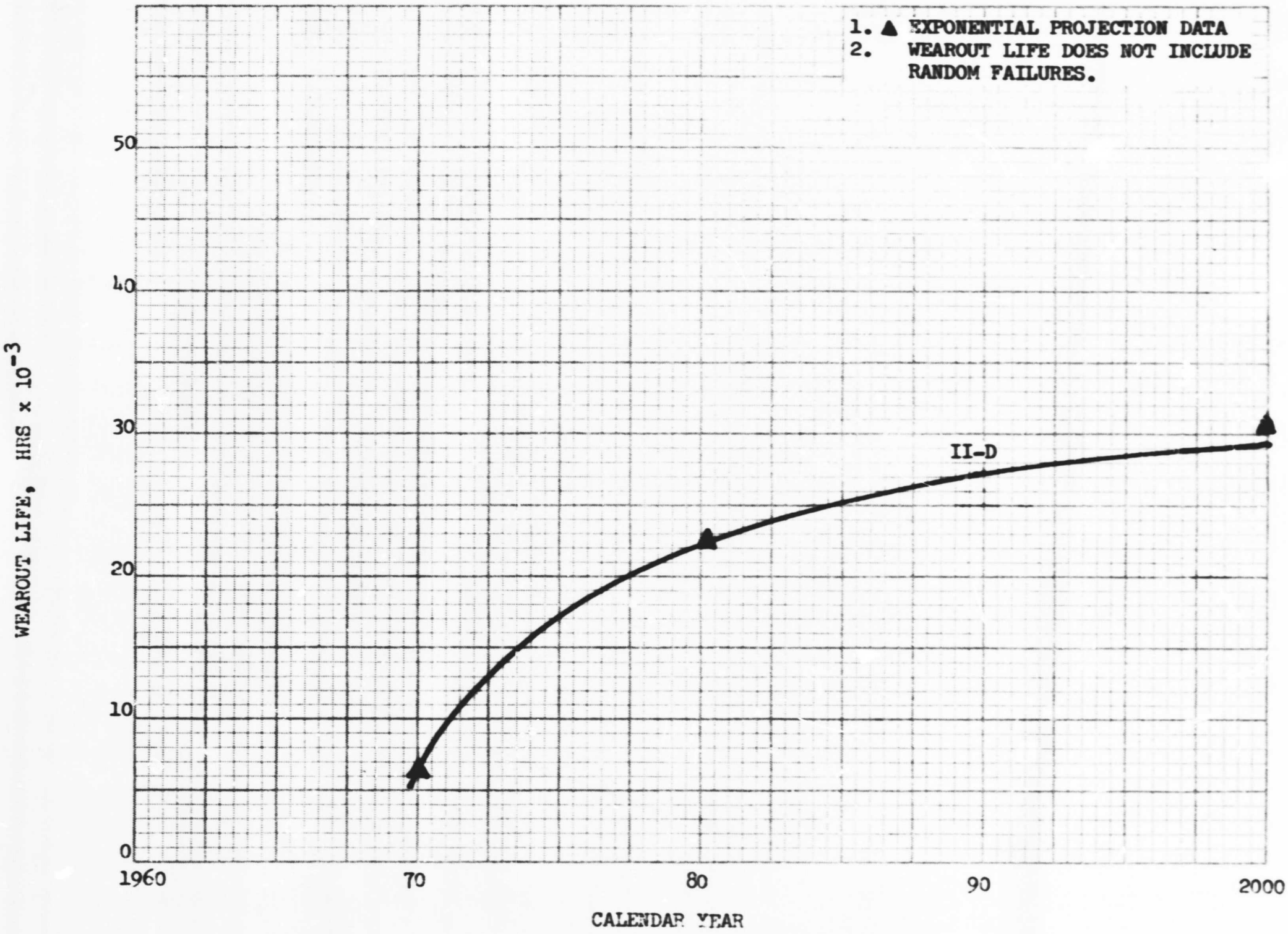

Figure 3-133 Projection of Organic Rankine Cycle Power Conversion Module Wearout Life

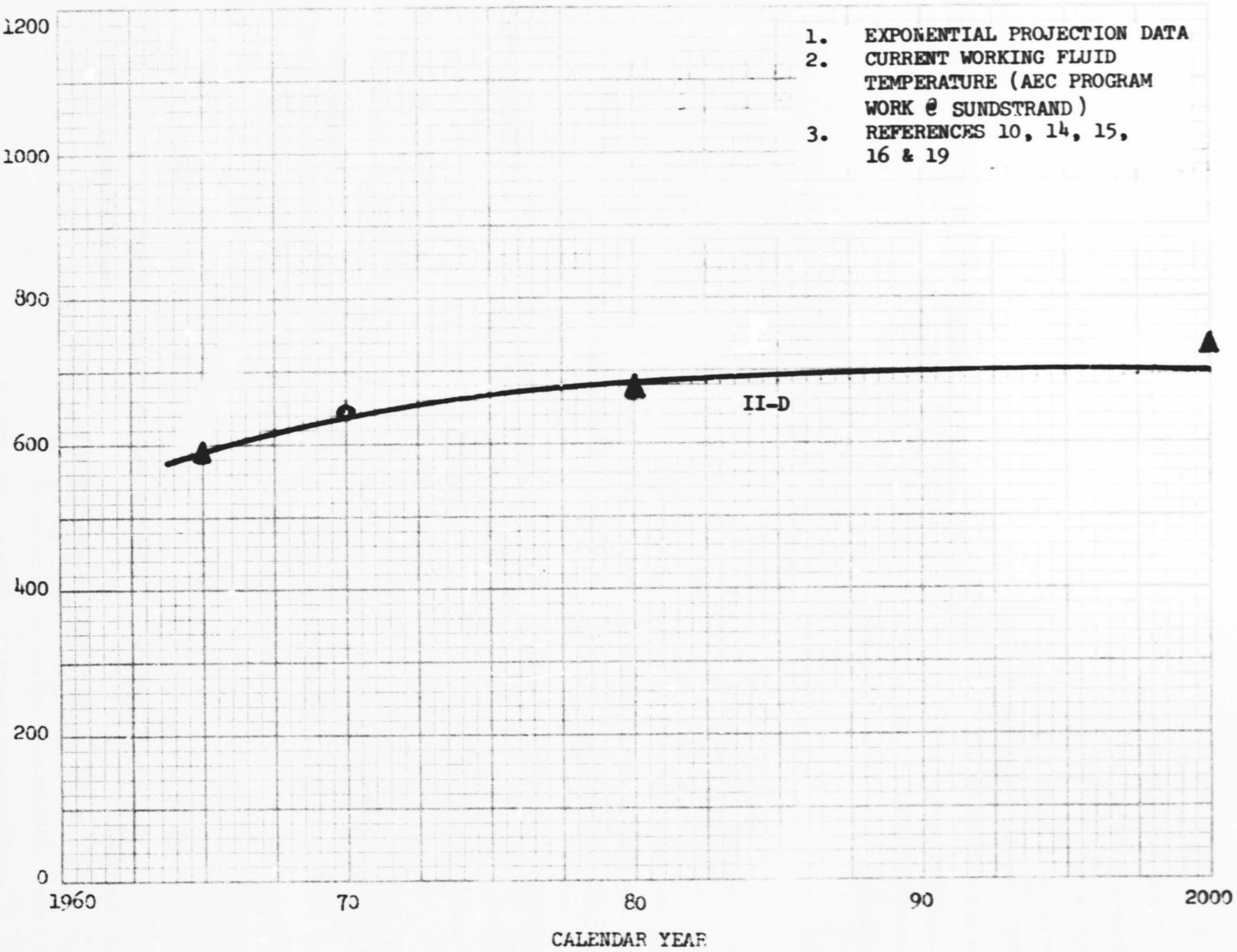

Figure 3-134 Projection Turbine Inlet Temperature Trend (Organic Rankine Cycle)

3.1.8 Chemical Dynamic Power Conversion Subsystem

Various bipropellant and monopropellant reactants such as ethylene oxide, propyl nitrate, hydrogen peroxide, and hydrogen and oxygen have been used for turbine-driven power units and are considered within the current state of the art. Turbine and reciprocating engines that employ hydrogen and oxygen and the hypergolic bipropellants (nitrogen tetroxide and Aerozine) have also been considered for space applications. The space use of chemical dynamic subsystems is typified by the bipropellant-flued pulsed turboalternator that utilizes hydrogen and oxygen or nitrogen tetroxide and Aerozine and is designed for potential use in manned spacecraft and lunar exploration.

The chemical dynamic power conversion subsystem investigated in the study is based primarily on the pulsed-turbine conversion technology. The reactants considered are H_2-O_2 and storable N_2O_4 - Aerozine 50. The power conversion subsystem characteristics of specific mass, density, reliability, and cost are considered to be independent of the reactants used, but the specific fuel consumption rate (mass of reactants for each kilowatt hour) varies with the reactant type.

The power conversion module shown in Figure 3-135 comprises reactant valves, a gas generator, a turbine alternator assembly, a closed-loop lubrication and cooling system with a relatively small radiator, a speed control unit, and structure. The power conversion subsystem is an open-cycle subsystem and the heat rejection requirements other than the heat rejected in the exhaust gas are considered to be negligible, thus the subsystem does not require a main radiator as a supporting subsystem.

The subsystem status, characteristics, and ranges of performance are shown in Table 3-29. The physical and performance characteristics of the subsystem such as specific mass, random failure rate, wearout life, cost, and specific reactant consumption rates are presented for a single power conversion module in Figures 3-136 through 3-141. The current performance characteristics of the power conversion module are based on a single-stage pulsed turbine. The improvement in performance with time is dependent upon the use of a multistage re-entry turbine. The subsystem includes one or more power conversion modules on the line, in standby, or as wearout replacements.

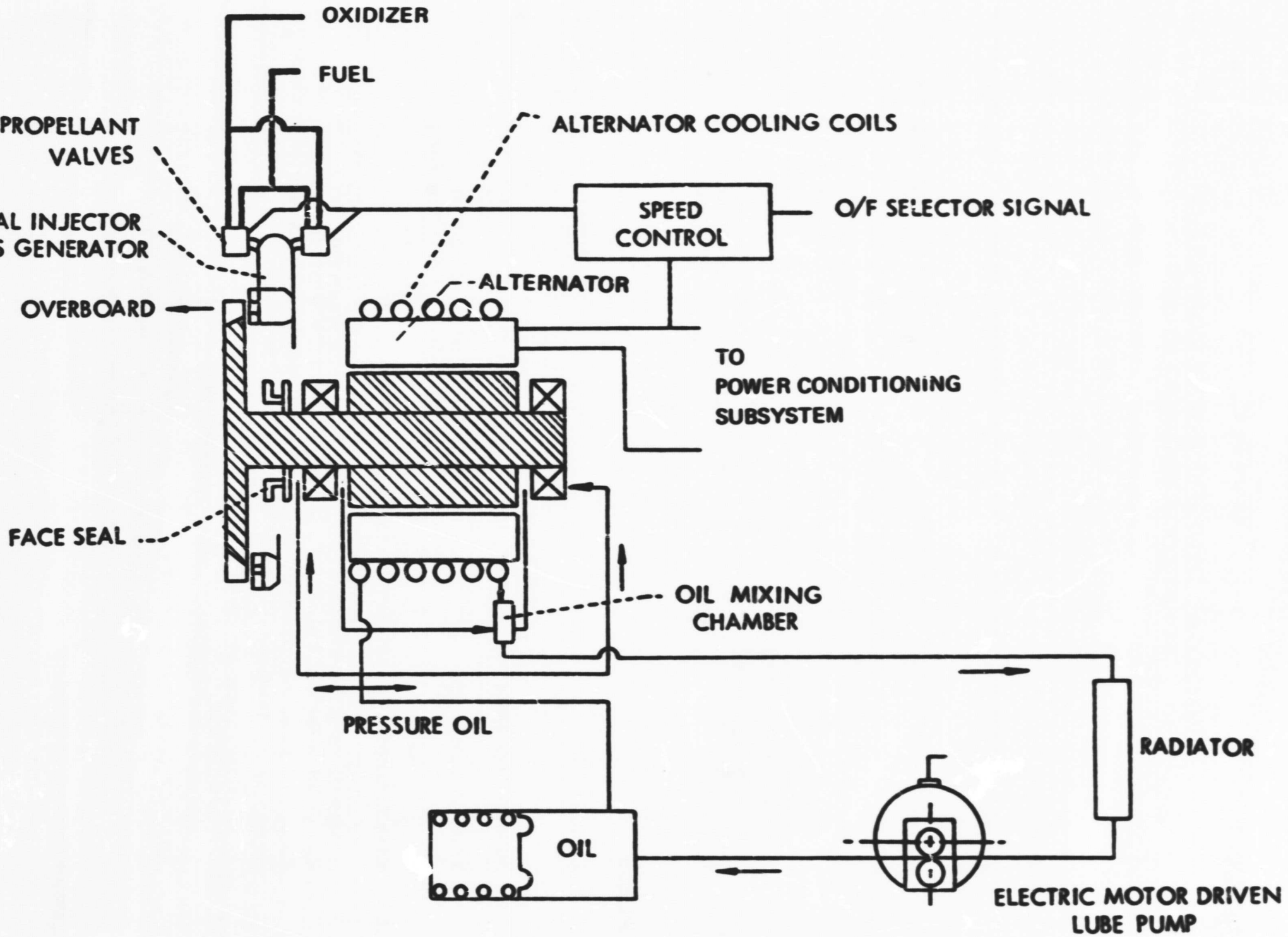

Figure 3-135 Chemical Dynamic Subsystem Module Schematic

Table 3-29

CHEMICAL DYNAMIC POWER CONVERSION
SUBSYSTEM BRIEFING CHART

Item	Value
Identification	
Applicable energy source	Chemical reactants (storable, cryogenic)
Major components	Turbine, alternator, gas generator, valves, and controls
Vehicle - mission application range	Orbiting, interplanetary
Useful power level	1 to 50 kWe
Duration of mission	Hours to days
Types of spacecraft	Manned, unmanned, Earth orbiting, interplanetary (peak and emergency power)
Status	
State of the art	Systems developed - qualification for specific missions required
Supporting subsystems	Within existing technology
Special problems	System development to improve reliability and duration
Subsystem Characteristics	
Range of specific mass	7 to 12 kg/kWe
Range of specific volume	0.2 to 0.6 m^3/kWe
Range of specific production cost	3,000 to 5,000 $/kWe
Range of reliability	90 to 99.9%
Performance Data	
Turbine inlet temperature	800° to 3,000°K
Specific reactant consumption	2 to 5 kg/kWe-hr

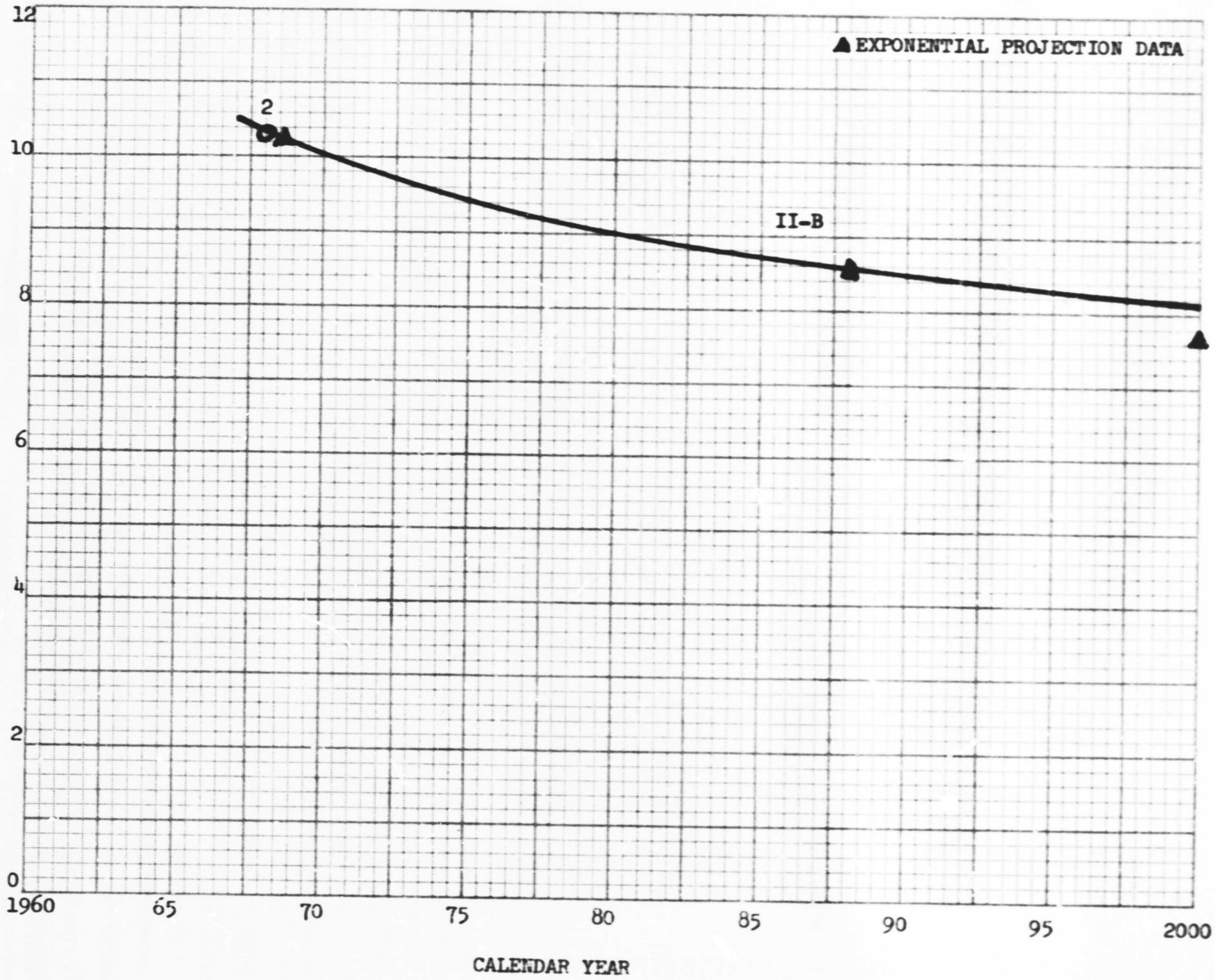

Figure 3-136 Projection, Chemical Dynamic PCU Module Specific Mass

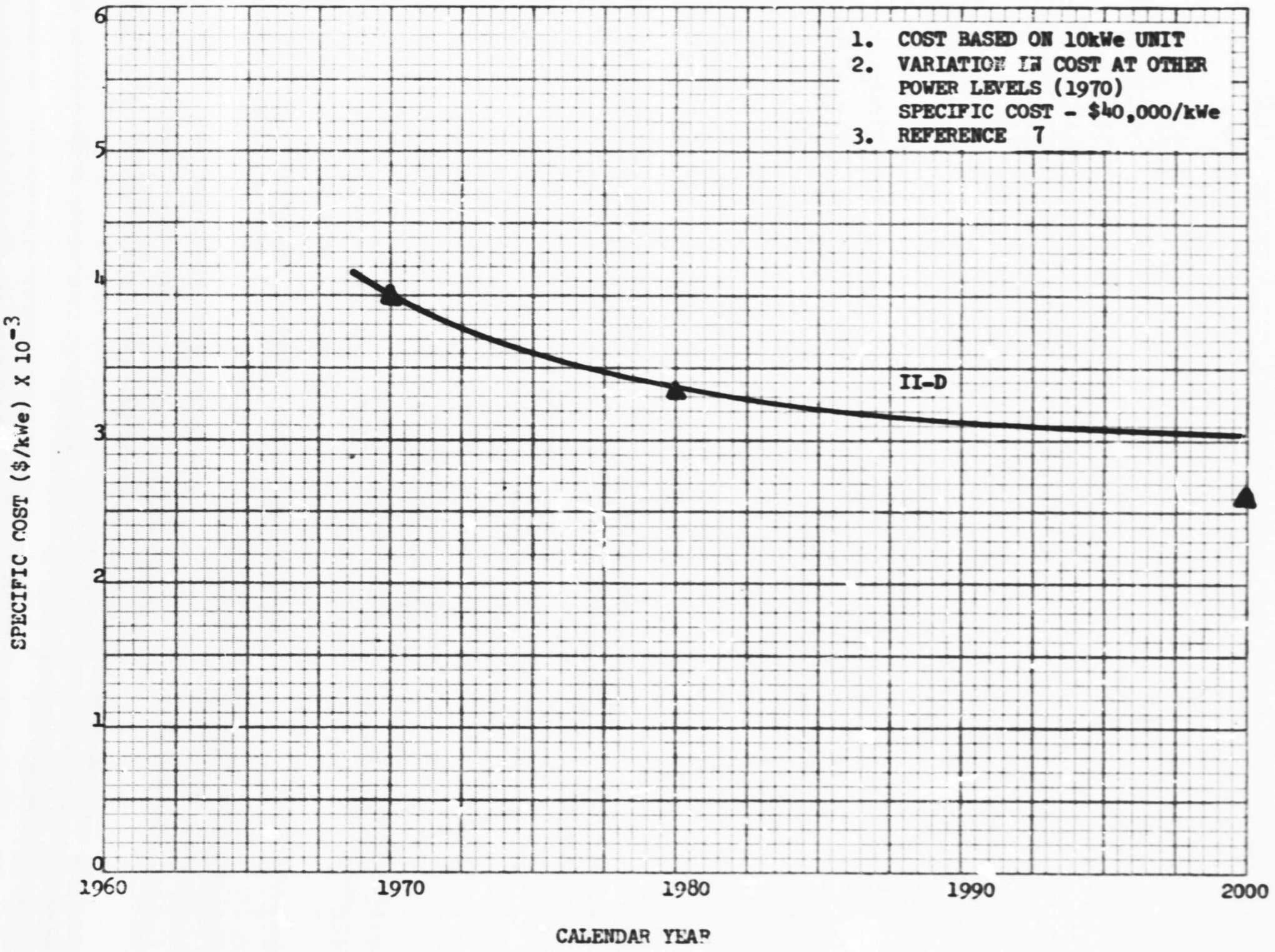

Figure 3-137 Production Cost of Chemical Dynamic Module

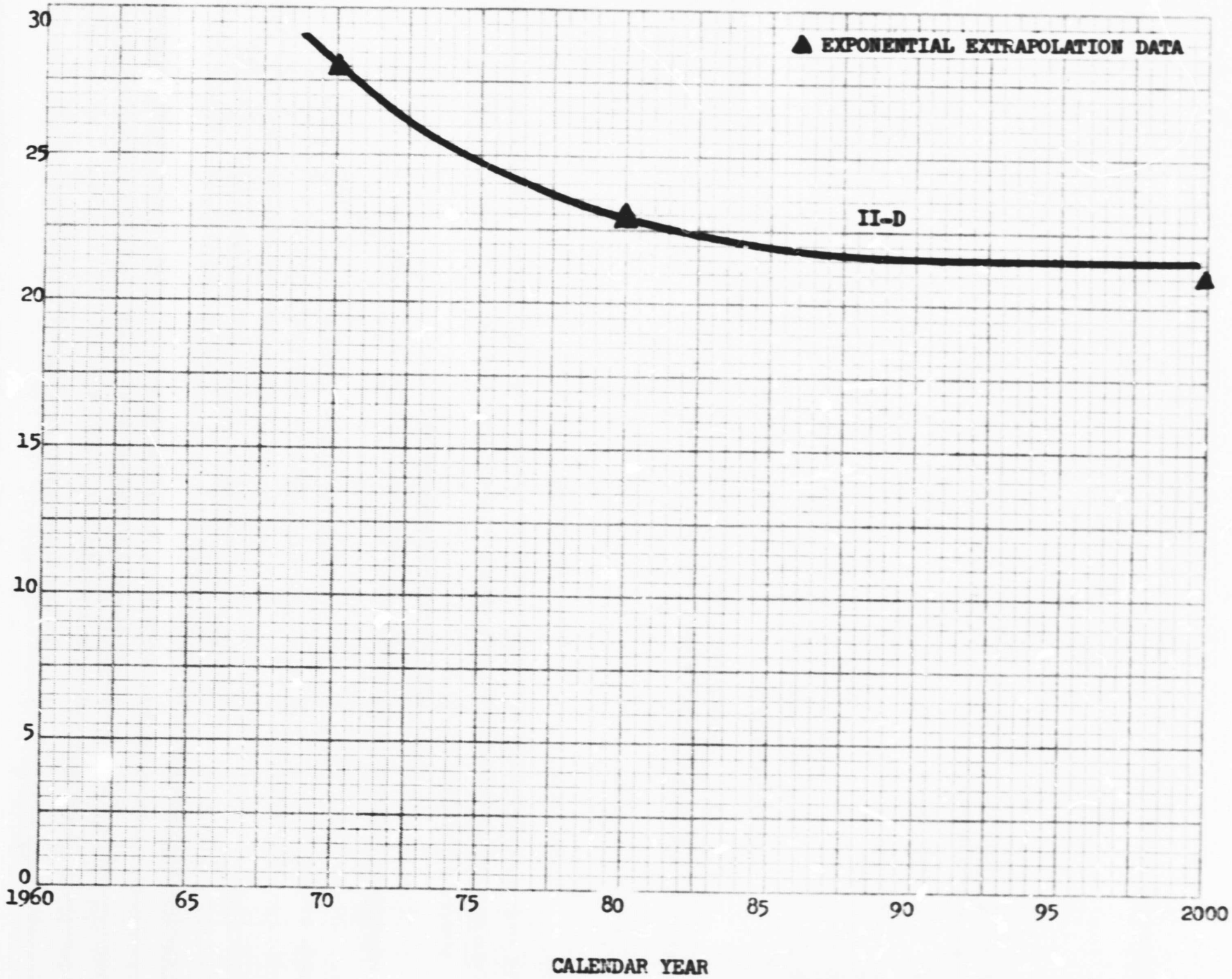

Figure 3-138 Projection of Chemical Dynamic Power Conversion Module Failure Rate

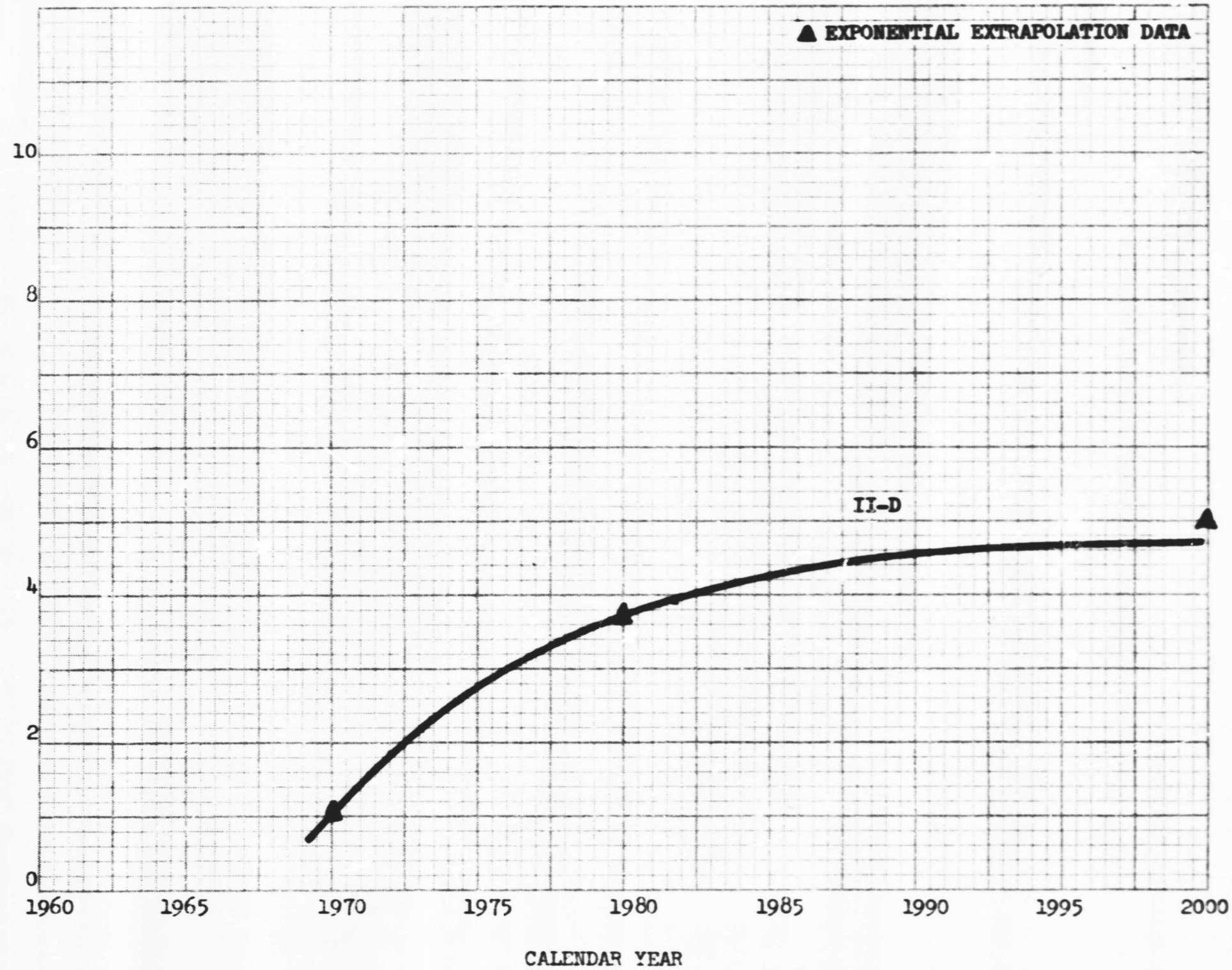

Figure 3-139 Projection of Chemical Dynamic Power Conversion Module Wearout Life

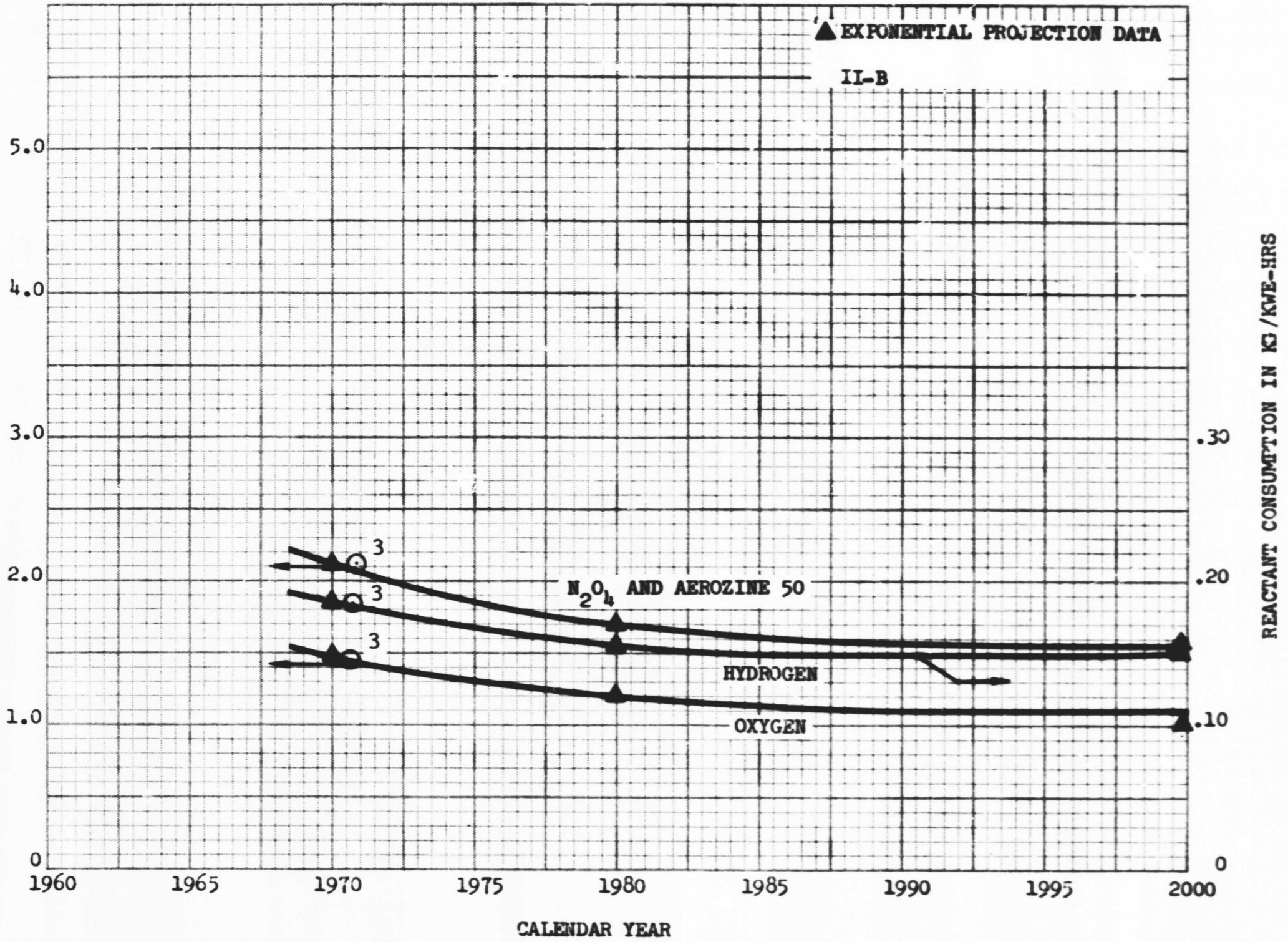

Figure 3-140 Projection of Chemical Dynamic Specific Reactant Consumption

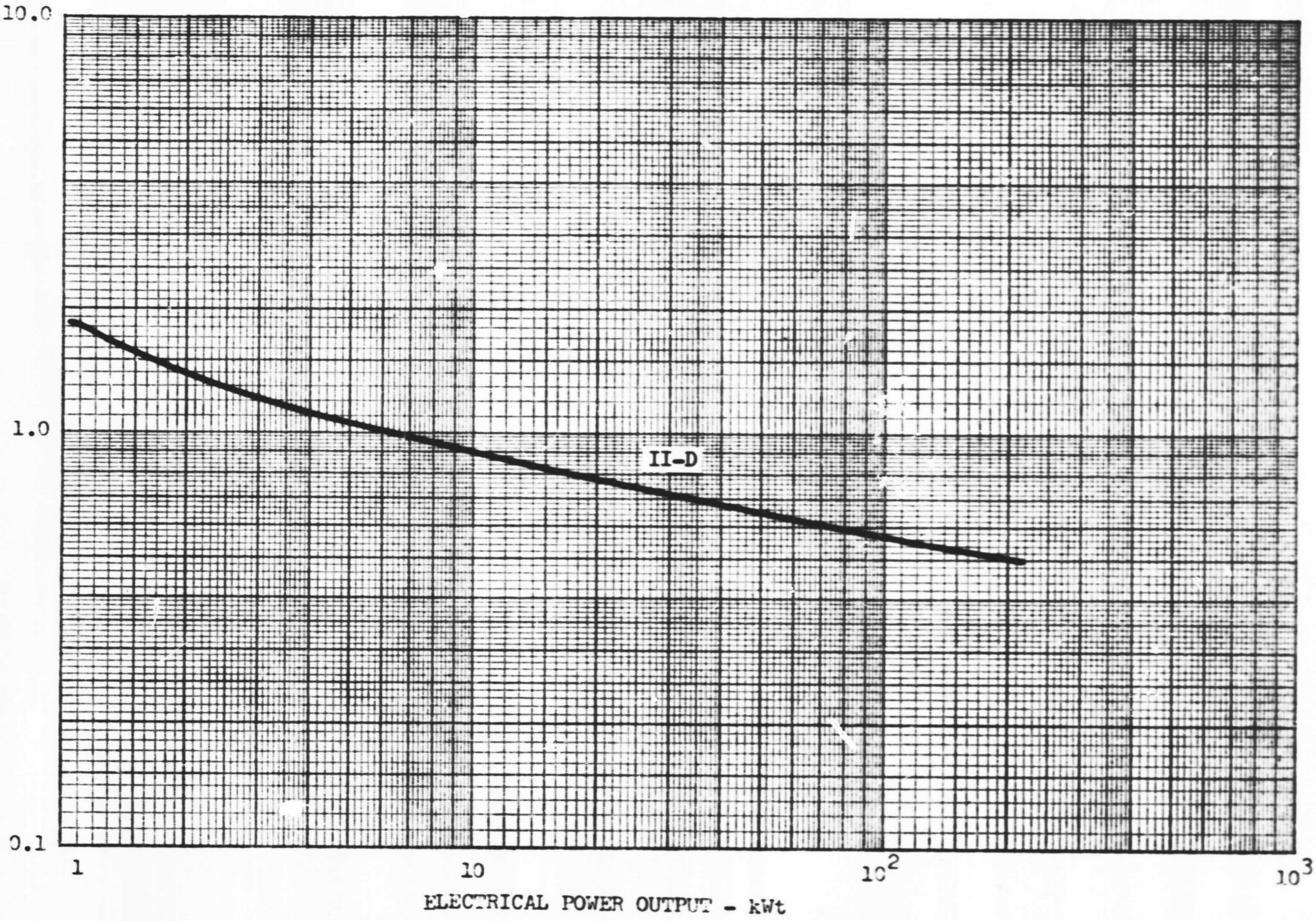

Figure 3-141 Chemical Dynamic Power Conversion Specific Mass Factor

Figure 3-142 Deleted

PRECEDING PAGE BLANK NOT FILMED

3.2 ENERGY SOURCES

Reactors, isotopes, shielding, solar concentractors, and chemical reactants have been analyzed in the study. The parametric and design data for the various energy sources and shield are presented in the following sections.

3.2.1 Nuclear Reactor Subsystem

The reactor energy source can provide thermal power for the Brayton, Rankine, thermionic, or thermoelectric conversion subsystems. The applicability or basic characteristics of space nuclear reactors is summarized in Table 3-30. Power levels from 50 kWt to almost unlimited values are possible. The reactor core can be designed for extended lifetimes of approximately 5 years.

The basic elements of a nuclear reactor consist of (1) the core, (2) the reflector, (3) the control system, (4) the cooling system, and (5) the radiation shield. The basic components of a typical compact space reactor are shown in Figure 3-143. The U-ZrHx reactor (Figure 3-143) uses U-235 fuel alloyed with zirconium, machined into cylindrical rods, hydrated, and then encapsulated by Hastelloy fuel clad. Advanced, high-temperature reactors will use ceramic fuels (UC, UN, UO_2, PuO_2, etc.) without a hydrogen moderator. The U-ZrHx reactor mass and dimensions are shown in Figure 3-144.

The thermal energy produced by the reactor fuel elements is transferred to the power conversion subsystem by a primary heat transfer loop. The primary heat transfer loop coolant is typically liquid metals (NaK or Li) pumped by electromagnetic or centrifugal pumps. The primary loop mass summary is shown in Figure 3-145.

The projected reactor operating temperatures are shown in Figure 3-146. The U-ZrHx reactors are limited to a maximum exit coolant temperature of 1,000°K because of reactivity losses caused by hydrogen leakage at high temperature.

Advanced ceramic fuel reactors are limited by development of stable fuel forms, high-temperature cladding, or coolant-structure interaction.

Table 3-30

NUCLEAR REACTOR HEAT SOURCE SUBSYSTEM BRIEFING CHART*

Item	Value
Identification	
Conversion equipment	Rankine, Brayton, thermionic, thermoelectric
Major components	Core, reflector, coolant, radiation shield, control system
Vehicle-Mission Application Range	
Useful power level	50 to 3,000,000 kWt
Duration of mission	0 to 5 years
Types of spacecraft	Manned-unmanned, orbital, interplanetary
Status	
State of the art	Small U-ZrHx reactors (SNAP-10A, 50 kWt) available
Special problems	Fuel and core material problems at temperature
Component Characteristics	
Range of specific weight	2.0 to 100 kg/kWt
Range of reliability	0.95 to 0.999 (10,000 hr)
Range of specific cost	$500 to $2,000/kWt

*Does not include shield

FUEL ELEMENTS

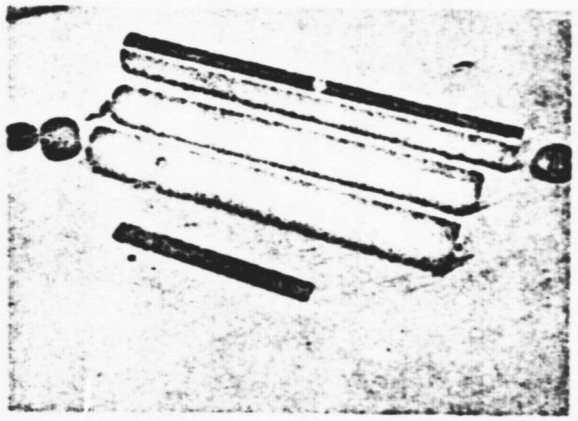

REACTOR CORE

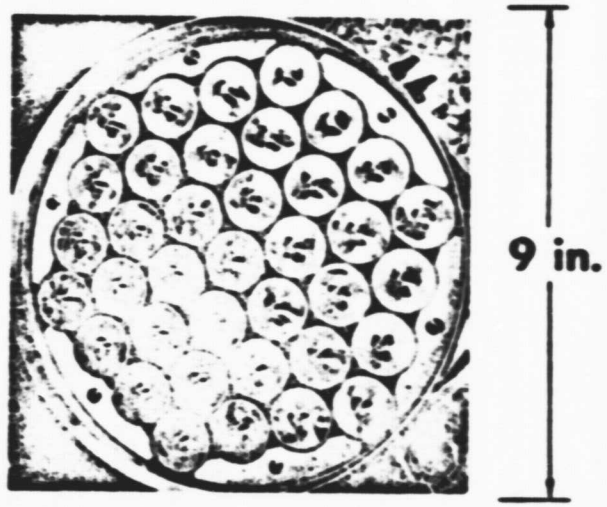

BERYLLIUM REFLECTOR

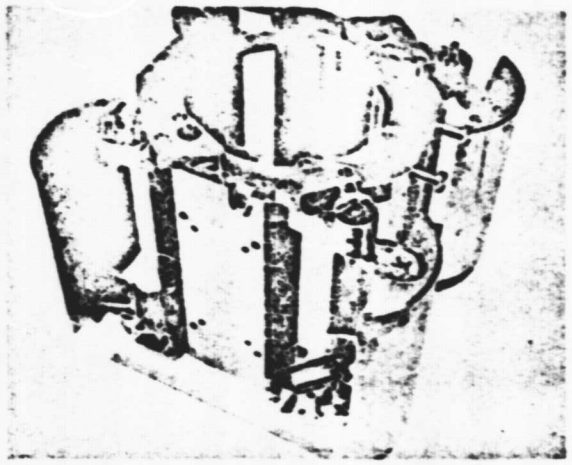

ASSEMBLED REACTOR (Top View)

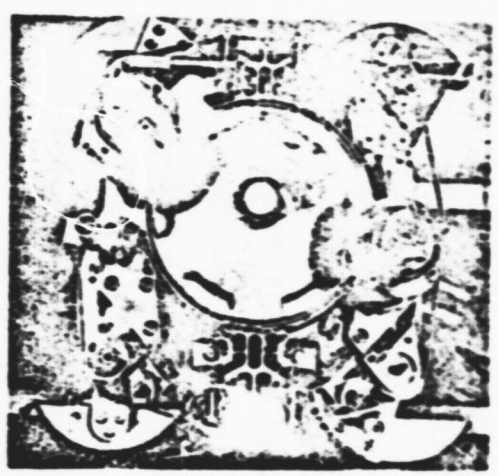

Figure 3-143 U-Z_rH_x (SNAP-8 Type) Reactor Subsystem

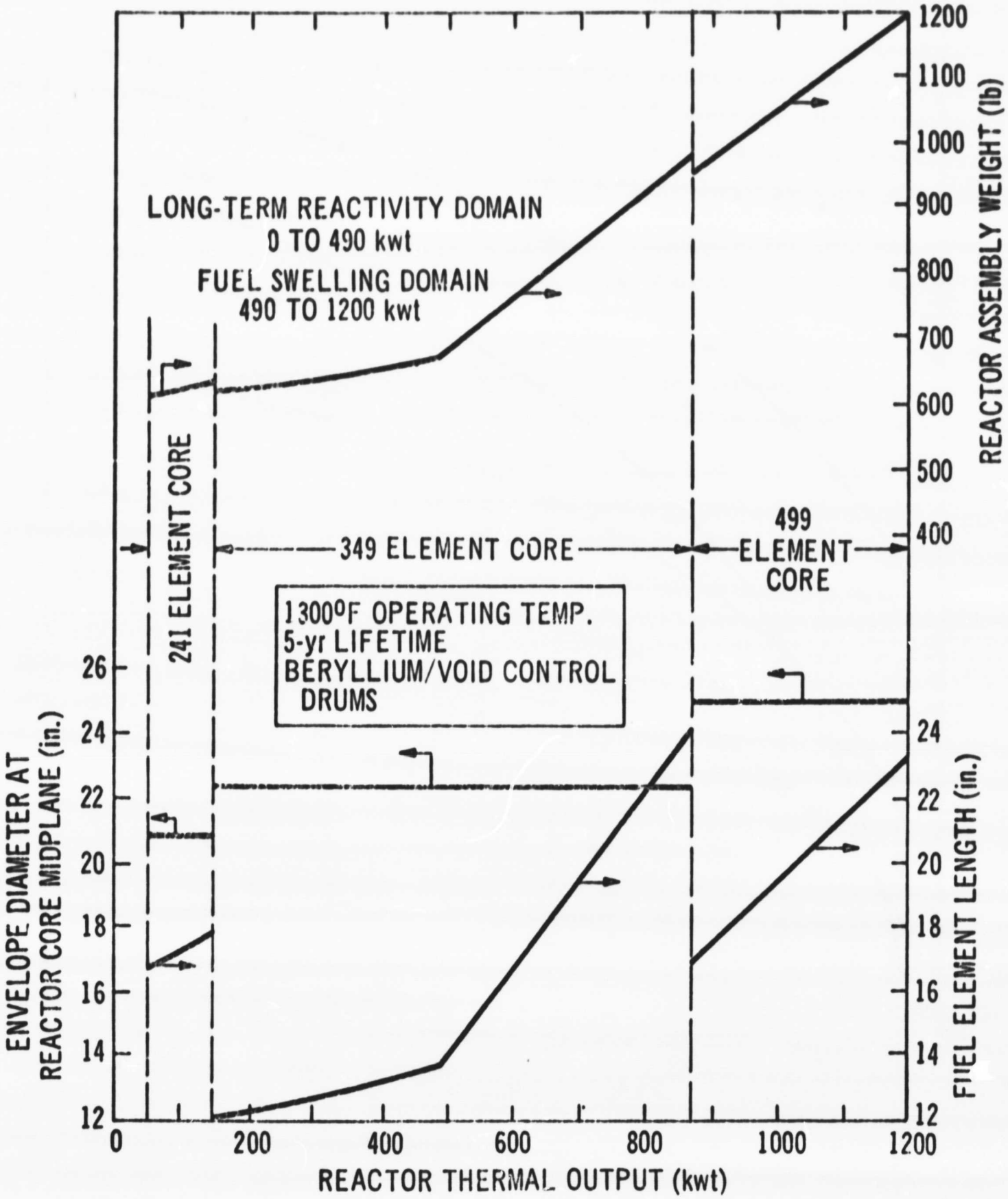

Figure 3-144 Reactor Assembly Data for Minimum Weight Shadow Shielded Configurations (DAC-59213) May 1966

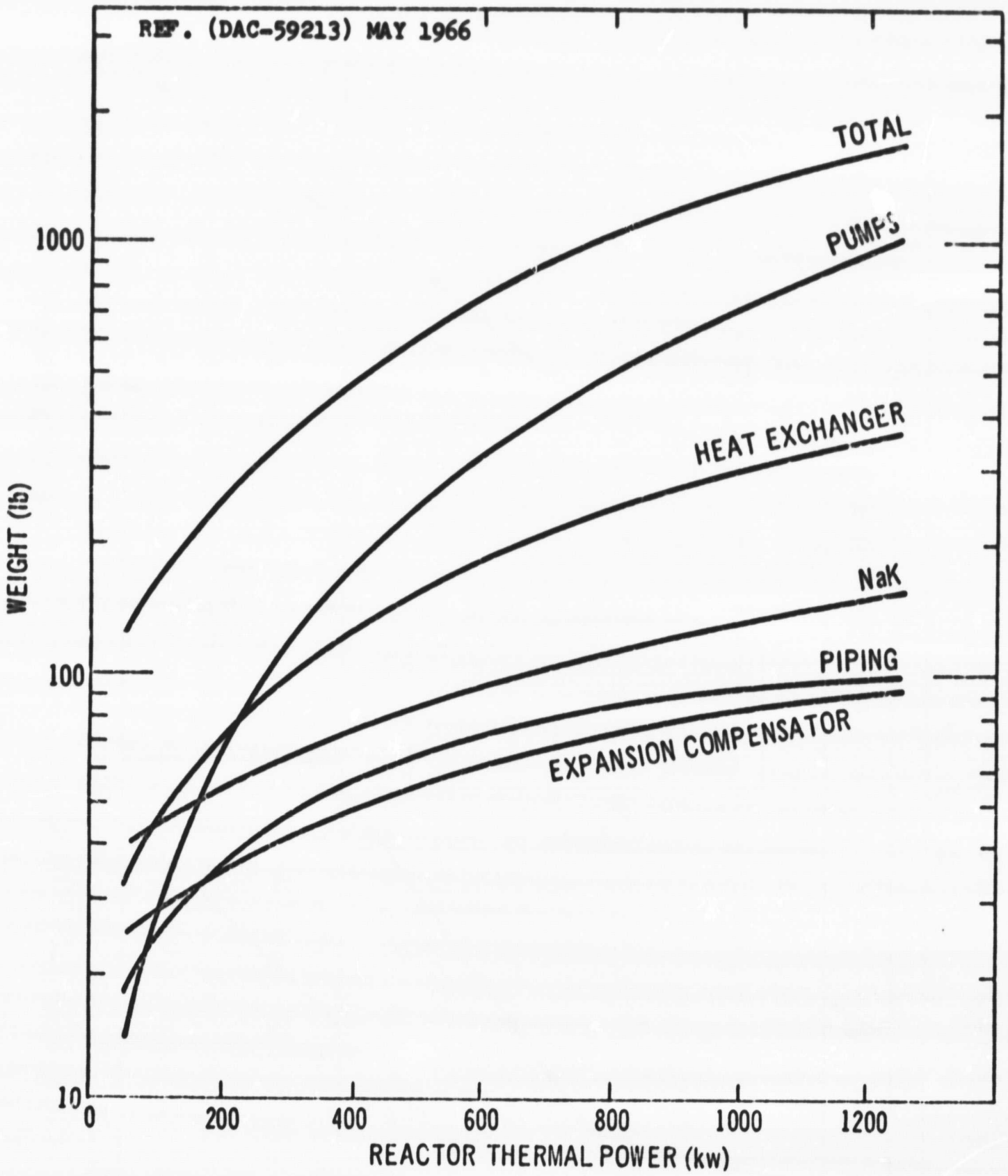

Figure 3-145 Preliminary Coolant Loop Weight vs Reactor Power NaK $\Delta T = 200°F$

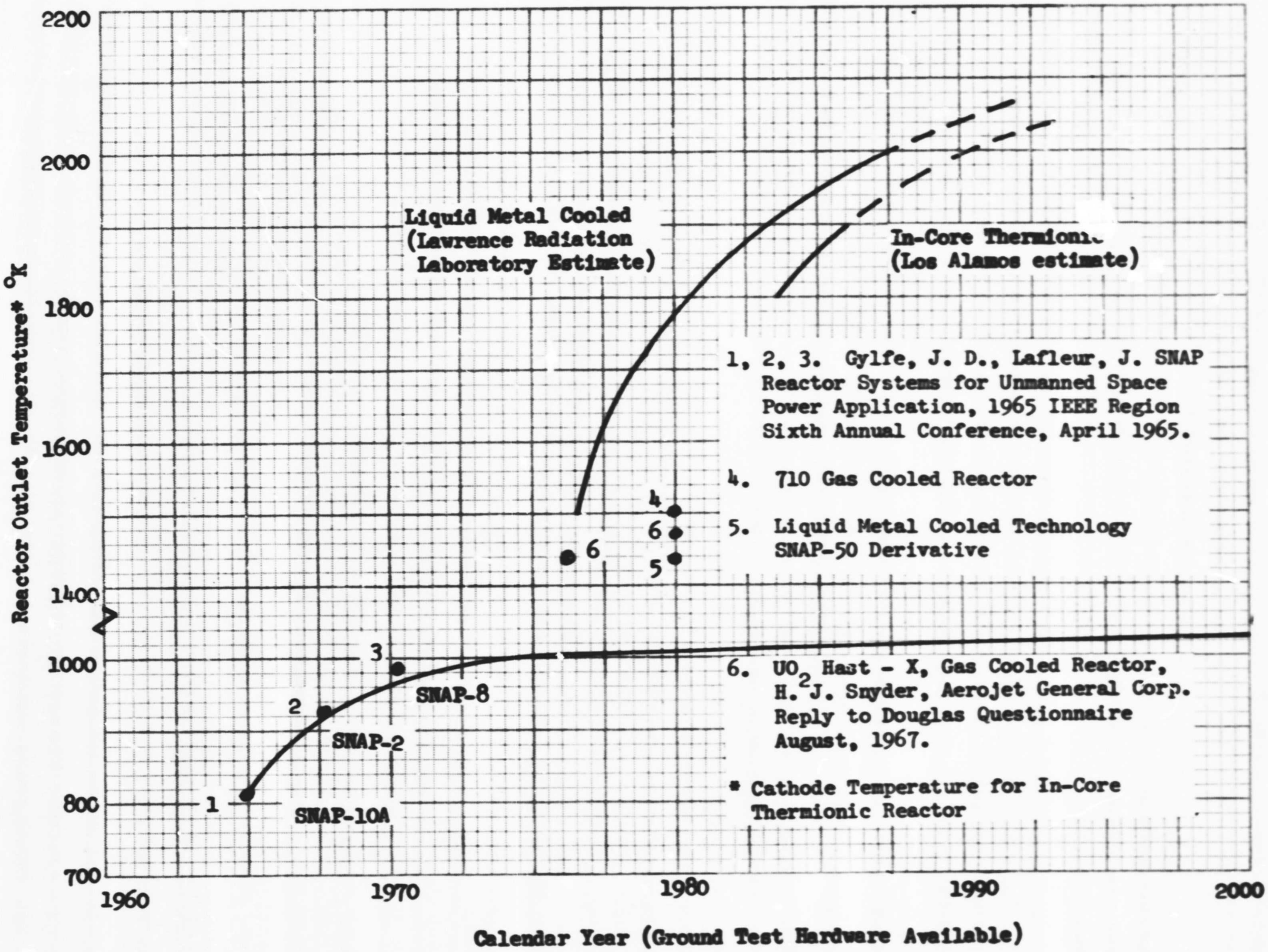

Figure 3-146 Space Power Reactor Outlet Temperature Vs. Calendar Year

Nuclear space reactors may be designed with lifetimes of 5 years by use of a burnable poison and addition of reactivity or nuclear fuel. Present space power system reactors, however, are tested for only 10,000-hour endurance. Reactor reliability is increased by adding redundant control rods and redundant reactivity. The failure rate and lifetime of the reactors are shown in Figure 3-147.

The reactor production costs (Figure 3-148) are based on estimates from development contractors. The present low demand for reactors has not enabled an actual production figure to be established.

3.2.2 Radioisotope Heat Source Subsystem

Isotope heat sources have been designed for operation in space for power ranges from a few watts to 25 kWt. The isotope heat source is inherently a reliable, predictable source of energy unaffected by the environment over the mission lifetime. Major disadvantages are nuclear safety during launch and re-entry in the Earth atmosphere, radiation shielding requirements, and a constant power output that requires a method of dumping excess heat at all times. The major characteristics of the isotope fuel block are given in Table 3-31. Four types of long-life isotopes have been investigated and they include: Sr-90, Co-60, Cm-244, and Pu-238. The first two isotopes are beta and gamma emitters, have large shield requirements, possess higher temperature capability, and are generally available in sufficient quantities. Cm-244 and Pu-238 are alpha particle emitters, possess low shield requirements, but are higher priced, and have limited availability.

The isotope heat source subsystem is shown in Figure 3-149 and is composed of (1) radioisotope fuel, (2) the fuel capsule, (3) the fuel block that transfers heat from the fuel source to the conversion subsystem, (4) the radiation shield, and (5) the thermal control subsystems that keep a constant heat flux to the power conversion system.

The isotope fuels selected for the study are listed in Table 3-32. The selection was based on the following criteria:

1. Atomic Energy Commission production program.
2. Half-life greater than 1 year.
3. Initial power density greater than 5 W/cubic centimeters.

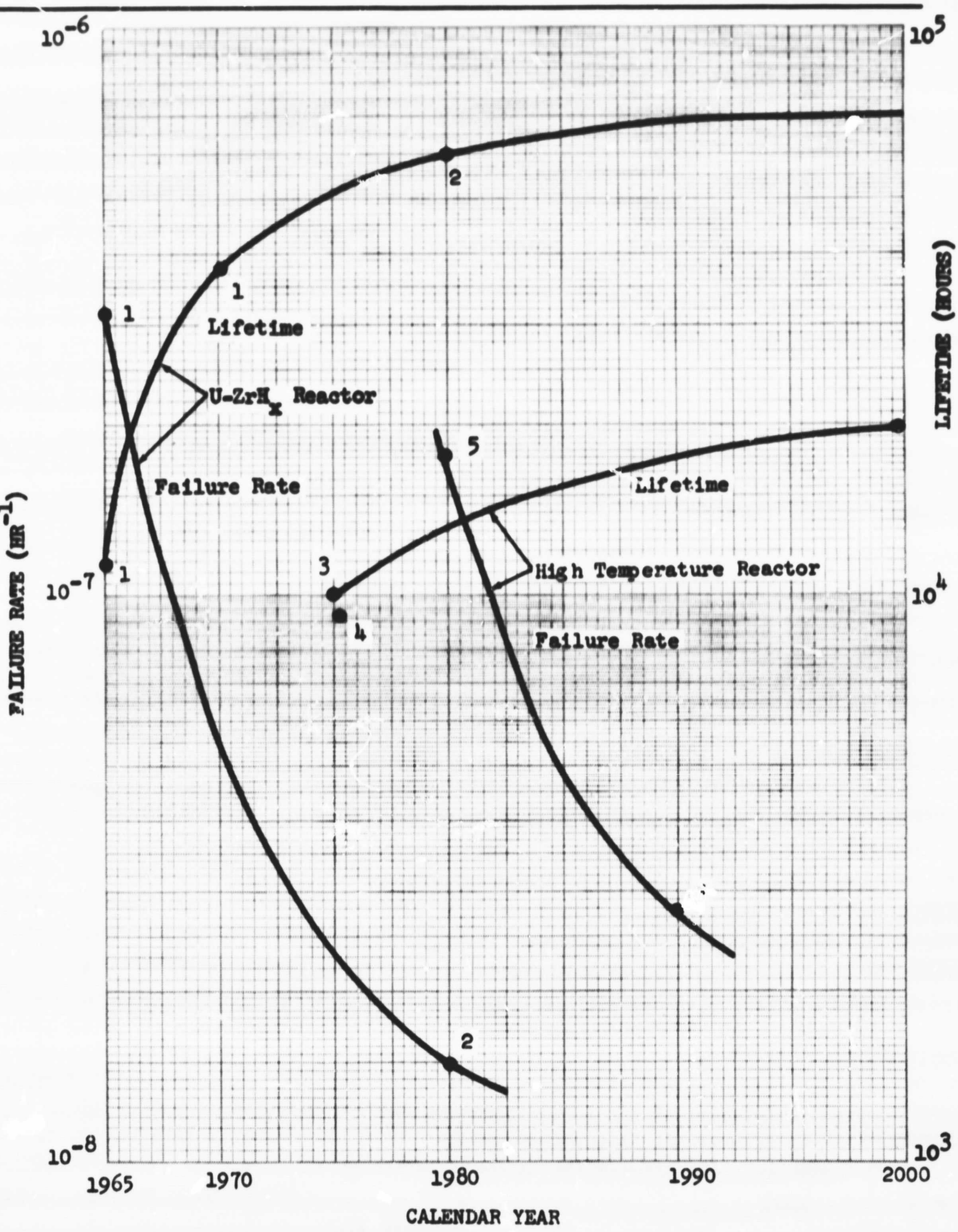

Figure 3-147 Projected Reactor Failure Rate and Lifetime

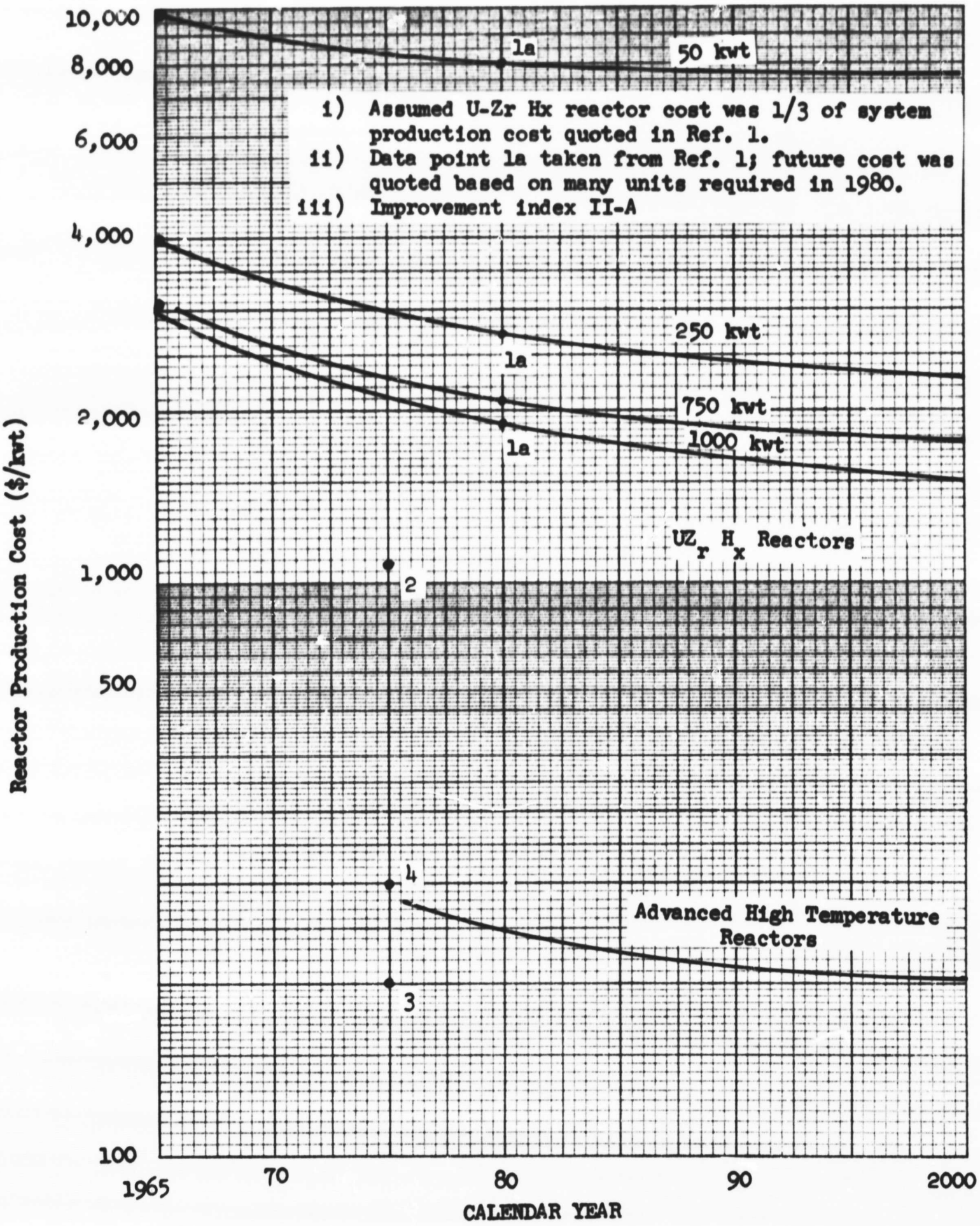

Figure 3-148 Projected Nuclear Reactor Cost

Table 3-31

ISOTOPE HEAT SOURCE SUBSYSTEM BRIEFING CHART*

Item	Value
Identification	
Applicable conversion equipment	Rankine, Brayton, thermoelectric, thermionic
Major components	Fuel capsule, fuel block, thermal control, thermal storage, shield
Vehicle-Mission Application Range	
Useful power level	10 to 50 kWt
Duration of mission	Days to 40 years
Status (1967)	
State of the art	1, 025°K isotope fuel clad temperature 1, 400W fuel block
Special problems	Fuel availability Nuclear safety High-temperature fuel blocks
Subsystem characteristics	
Range of specific weight	1 to 10 kg/kW
Range of specific area	0.5 to 50 W/cm^2
Range of specific volume	0.5 to 30 W/cc
Range of reliability	0.999+ (10, 000 hr)
Range of specific cost	$5 to $2, 000/Wt

*Does not include shield

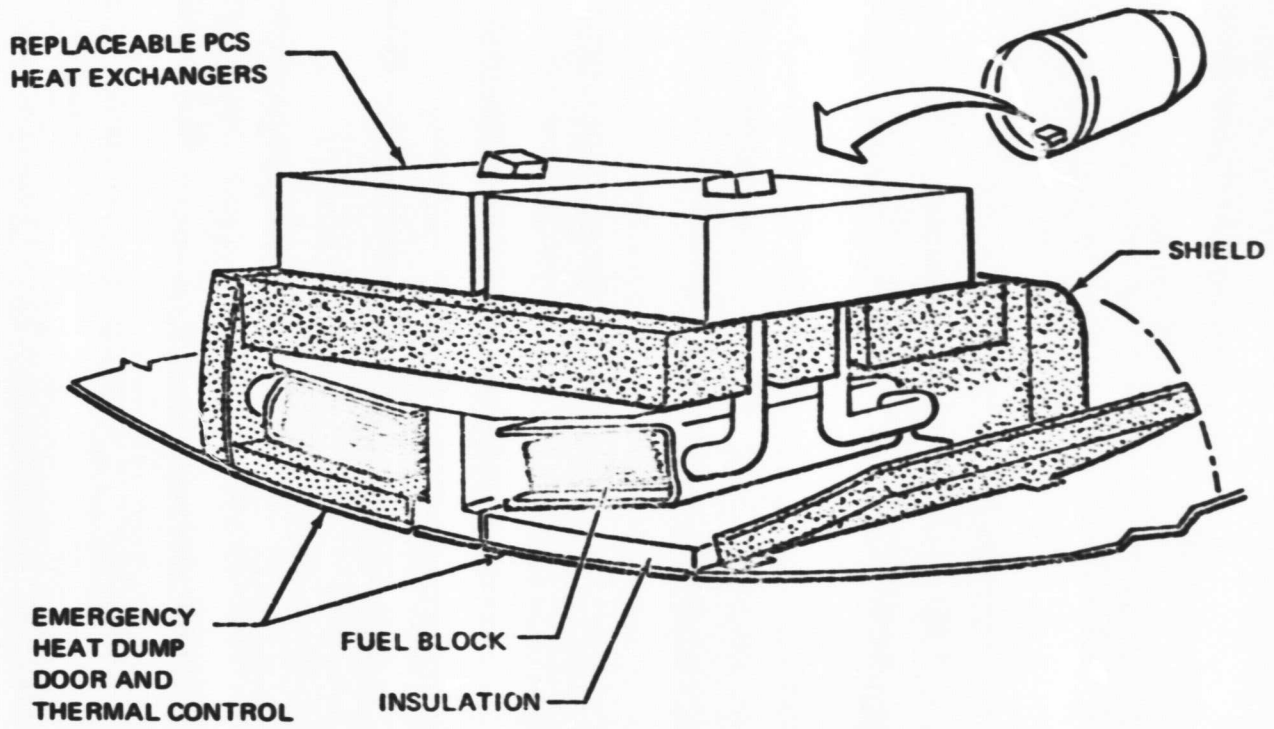

Figure 3-149 Representative Single Source Radioisotope System Installation

Table 3-32 (page 1 of 2)

RADIOISOTOPIC POWER FUEL DATA

Radioisotopes	^{90}Sr-Y	^{238}Pu	^{244}Cm	^{60}Co
Half-life (years)	27.7	87.6	18.4	5.24
Radiation type (a)	β,Y	α,η,Y	α, η,Y	β,Y
Radiation energy (curies/Wt)	148	29.1	29	65
Typical Product Form	$SrTiO_3$	PuO_2	Cm_2O_3	Metal
Density (g/cc) (b)	3.7	10^2	9	8.7
Power (Wt/cc)	0.82	3.6	22.5	27 (j)
Shield thickness (cm) (k)	8	(nil)	3.5(34*)	13
Availability (kWt/yr)				
1967 (c)	9.5	11.5	(i)	130
1970 (c)	170	15 (g)		7500
1980 (d)	770	60		
Present AEC Price ($/$W_{(t)}$) (e)	29.60			32.50
Future Estimated Cost ($/$W_{(t)}$) (f)		1,000.0	400.0	

(a) The symbol Y includes Bremsstrahlung as well as gamma radiation, and, in some cases, is easily shielded.
(b) Practical density of the fuel form.
(c) Scheduled availability from AEC operations.
(d) Based on civilian nuclear power operations.
(e) Based on large orders and does not include conversion, encapsulation or shipping costs.
(f) Based on full-scale production for five to ten years.
(g) Could be increased to 25 kW in 1970, and 180 kW in 1980 at a 50% increase in cost.

(i) Operation now on a developmental basis with cost at 5 kw thermal per year estimated at about $1,110 per thermal watt. Production in the range of 100 kW in 1972 and 400 kW in 1980, estimated at a cost of $480 per thermal watt.
(j) Based on 200 curies/g material with up to 400 curies/g material possible.
(k) Shield thickness in cm of uranium to reduct a 1000 Wt source to 10 mr/hr at 1 meter.
* cm of H_2O for neutron shielding.

Prepared by USAEC
Division of Isotopes Development
March 1966

4. Compatibility with the materials and engineering requirements for space generators.
5. The fuel will be available in adequate quantities and within the time schedule requirements.

The capsule ensures the safe containment of the radioisotope fuel. The capsule must withstand the stresses produced by thermal, chemical, and mechanical forces. With alpha-emitting fuels (Pu-238 and Cm-244), the capsule must also withstand the stresses of the gases evolved or these must be vented. A typical design for an isotope fuel block and a Pu-238 fuel capsule is shown in Figures 3-150 and 3-151 respectively. The required coatings or layers and their function are listed in the figures.

The fuel block contains the fuel capsules and transfers heat from the capsules to the conversion subsystem. The fuel block may be used to achieve a physical transformation of surfaces to obtain optimum heat transfer, e.g., from a cylindrical fuel capsule to a flat-plate surface which radiates to the conversion subsystem heat source heat exchanger (Figure 3-151).

Advanced power conversion systems require isotope heat source temperatures of between 1,200° to 2,200°K. The compatibility and stability of isotope fuel and container materials at these temperatures over the intended mission life has to be demonstrated. The 1,400W Pu-238 fuel block for NSAP-27 will be qualified to approximately 970°K in early 1968. The AEC has initiated a program to develop the Pu-238 technology to a surface temperature of 1,300°K by 1969. The heat source is intended for use with either a Brayton cycle or thermoelectric conversion unit. The total heat source at the end of a 5-year life is 24kWt or 28.6kWt at the start of life. The heat source includes 140 capsules in an intact re-entry vehicle (Reference 1).

The properties of Cm-244 are not as well known, but Oak Ridge expects to qualify the fuel to 1,800°K by 1972 for isotope termionic application (Reference 2). Sr-90 and Co-60 have been subject to fuel studies and their properties at temperatures that are well known. Isotope projected temperature capability is shown in Figure 3-152.

The cost of an isotope heat block may be divided in three parts: (1) fuel cost, (2) encapsulation cost, and (3) system integration and thermal control

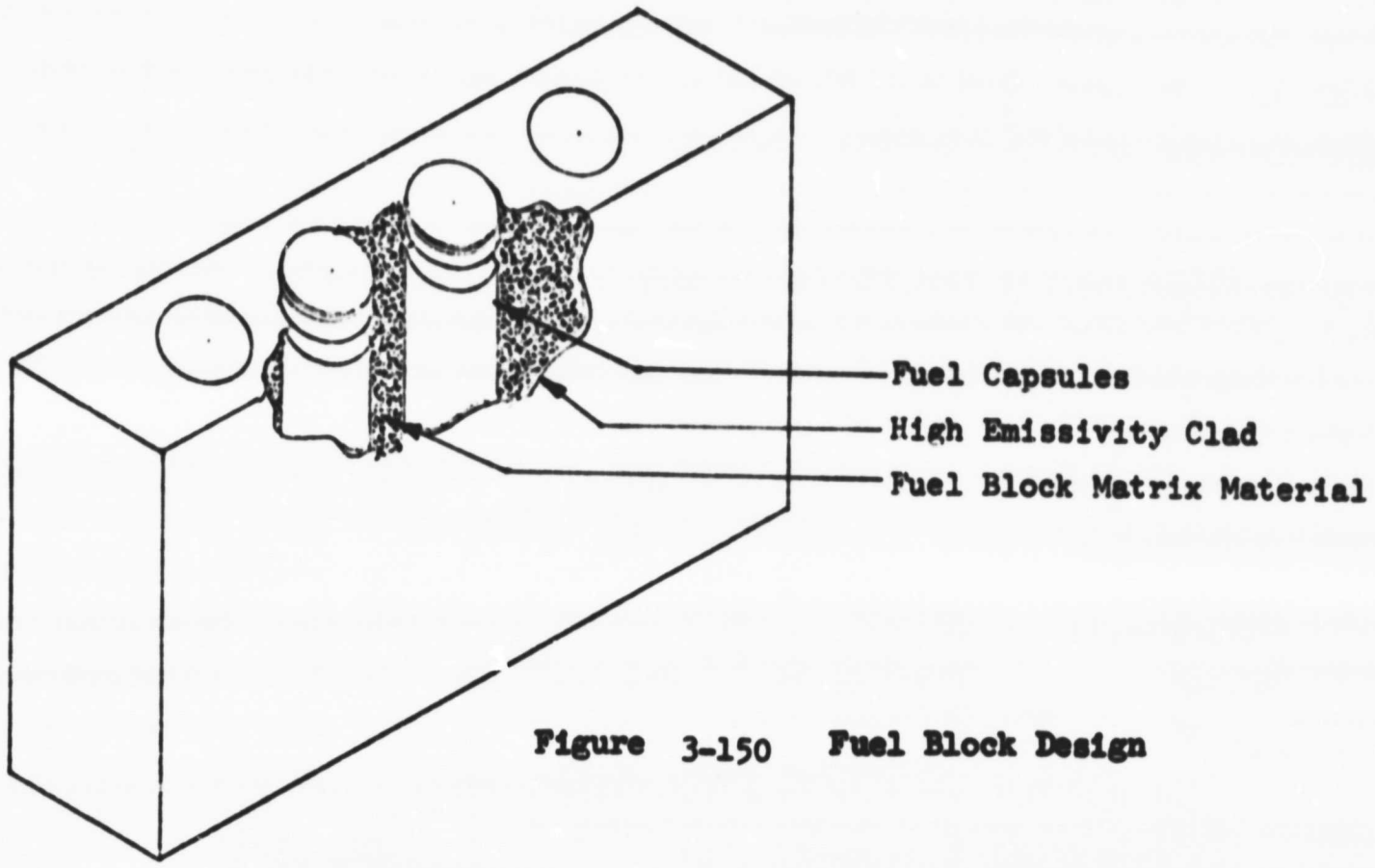

Figure 3-150 Fuel Block Design

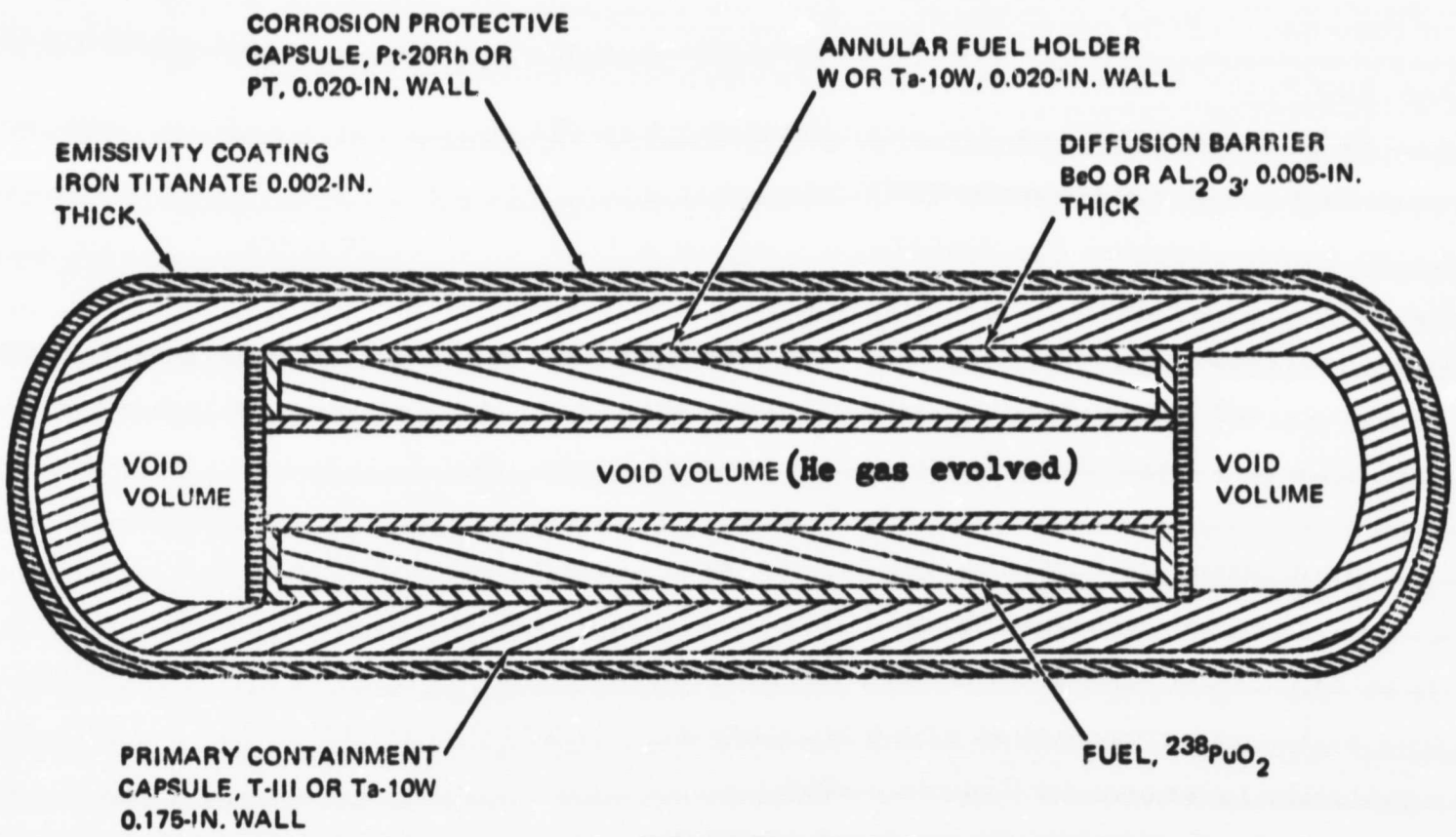

Figure 3-151 Conceptual Design of a $^{238}PuO_2$ Fuel Capsule

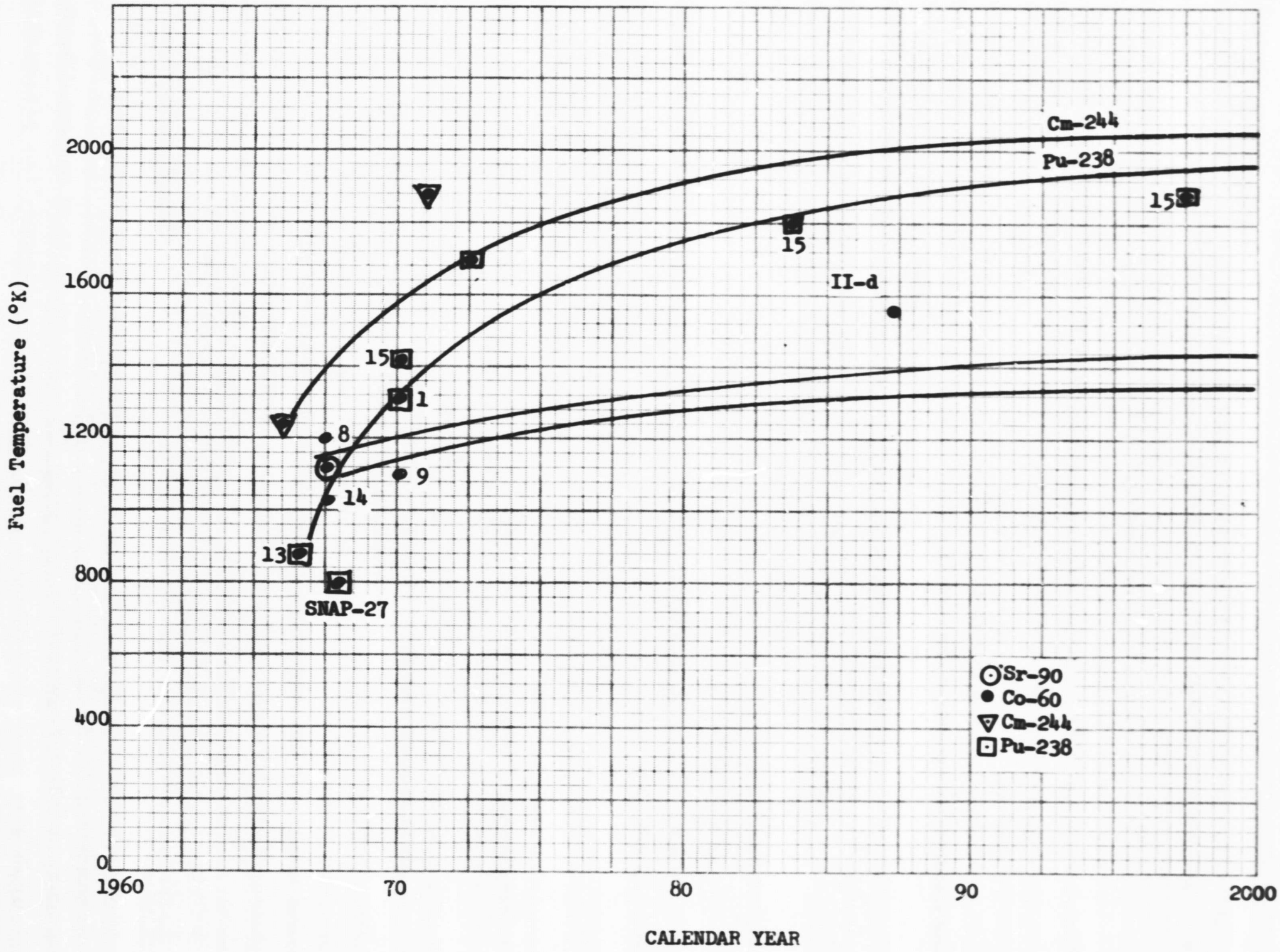

Figure 3-152 Projected Temperature Capability of Isotope Fuels

cost. The cost of isotope is based on production methods and requirements. Enough production of Sr-90 and Co-60 has taken place that actual price per watt has been announced by the AEC. The production of Pu-238 and Cm-244 is still in an exploratory stage and no fixed price has been quoted. A classified analysis of future isotope cost and availability is contained in Reference 3. Figure 3-153 shows projected isotope costs based on unclassified data.

The availability of Pu-238 and Cm-244 isotope fuels is still questionable for high power missions. The availability of these isotopes are discussed in the classified Reference 3. Sr-90 and Co-60 will be available in adequate quantities (100 to 1,000 kWt) throughout the 1970's and beyond on short notice thereby provide no danger of shortage for any contemplated space mission. The projected fuel availability is shown in Figure 3-154.

3.2.3 Shielding (Reactor and Isotope) Subsystem

Shielding must be provided to attenuate the radiation dosage from the reactor and isotope heat sources to meet the exposure limitations of men and payload. The shield materials will differ with the type of radiation emitted by the heat source. The gamma shield material was standardized as depleted uranium alloy (U-8Mo) and the neutron shield material was standardized as lithium hydride enclosed in a stainless steel canister. The major operational characteristics of the nuclear shield subsystem are given in the briefing chart in Table 3-33.

The nuclear shield subsystem attenuates radiation emanating from reactor or isotope heat sources to levels tolerable to the instrument or manned payload. The major components of the nuclear shield are (1) gamma radiation attenuation shield, (2) neutron shield, and (3) shield cooling.

Extensive experience in the SNAP and ANP programs has shown that lithium hydride is an efficient fast neutron shield material with excellent thermal and radiation stability. Its melting point is sufficiently high to permit application in regions close to the reactor, where temperatures as high as 800°K may occur. Additional properties that have led to the selection of natural lithium hydride are its low density (774 kg/m^3) and its low decomposition pressure (25 mm Hg at its melting point of 954°K).

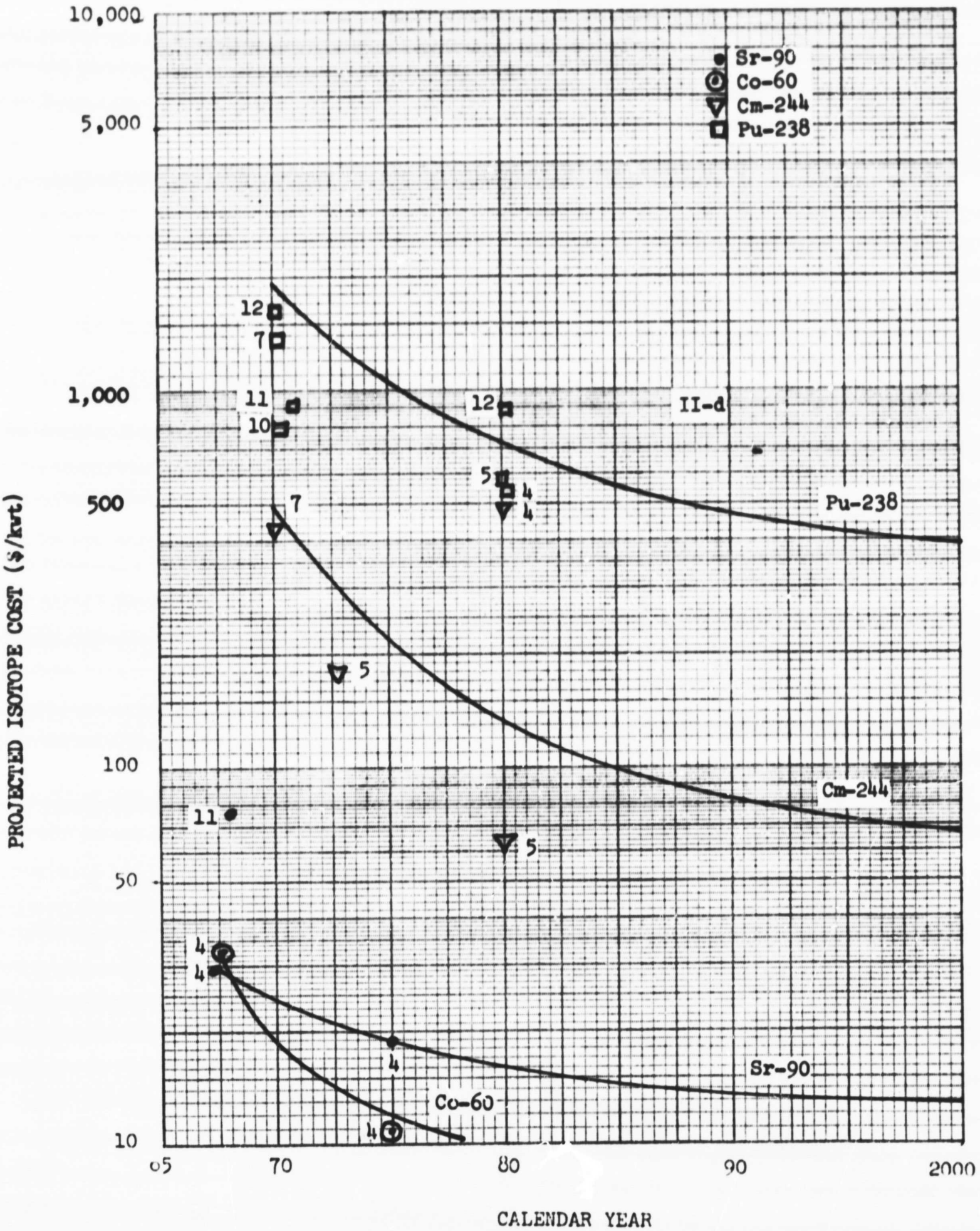

Figure 3-153 Projected Isotope Cost

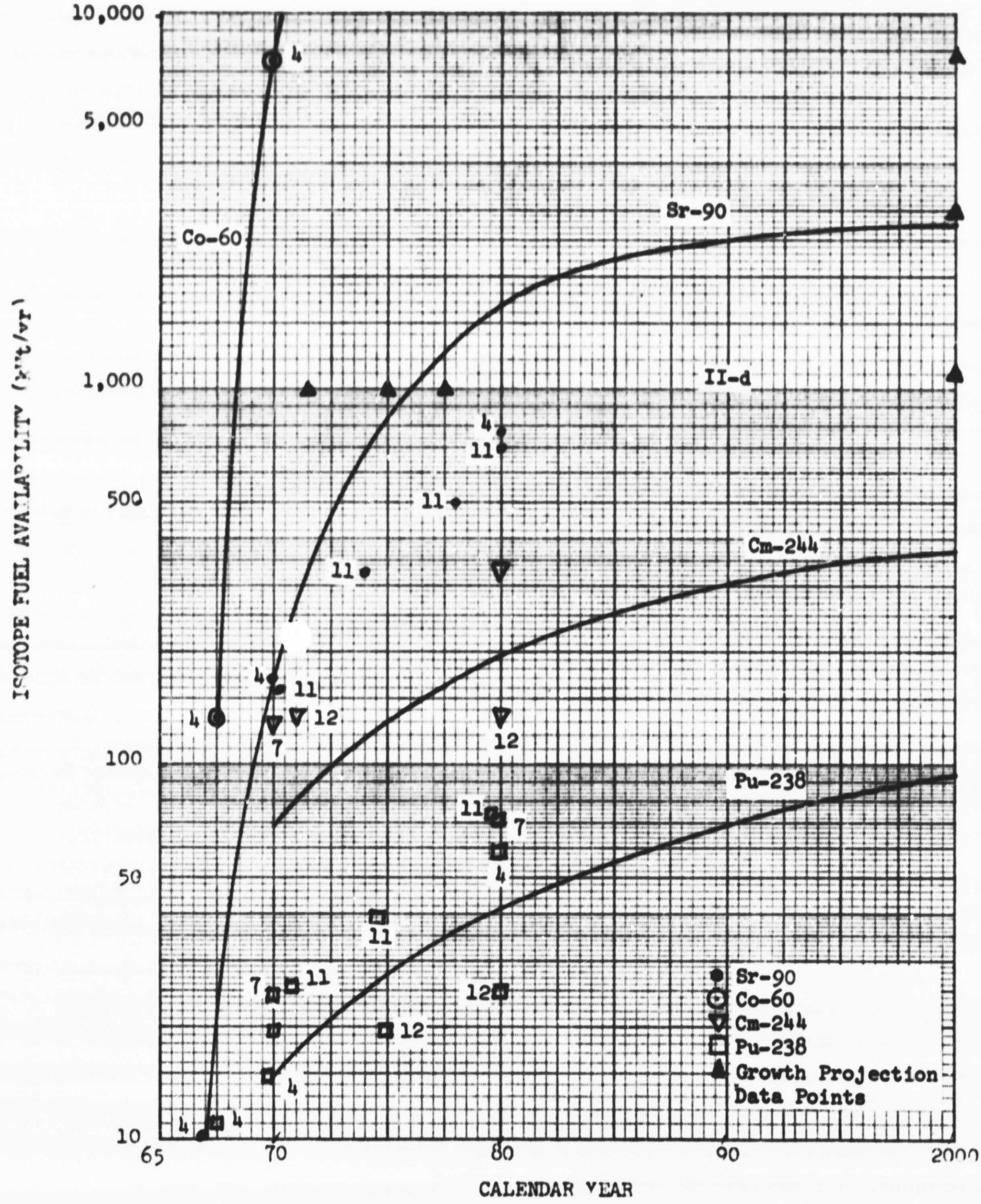

Figure 3-154 Projected Isotope Availability (Preliminary)

Table 3-33

SHIELDING (REACTOR AND ISOTOPE) BRIEFING CHART

Identification	
Applicable energy source	Isotope, reactor
Major components	Gamma shield, neutron shield, shield cooling
Useful power level	50 to 3,000 kWt
Duration of mission	Day to year
Types of spacecraft	Manned, unmanned, Earth orbiting, interplanetary
Status	
State of the art	U-238, LiH. Shielding materials, design techniques available
Availability of support subsystems	No significant problems
Subsystem Characteristics	
Range of specific weight	1 to 10 kg/kWt
Range of specific volume	0.001 to 0.005 m^3/kWt
Range of specific production cost	50 to 200 $/kg
Range of reliability	0.99 to 0.9999 for 1 year
Performance Data	
Operating temperature (maximum)	900°K

The two types of reactor shields used in the study are shown in Figure 3-155. An unmanned instrument shield consists of one block with a U238-8Mo gamma shield and a neutron shadow shield made of LiH cast in a stainless steel container. The gamma shield as a circular plate having a diameter equal to that of the core. The neutron shadow shield is a truncated cone. The cone angle is such that the payload dose plane is completely hidden from the reactor assembly.

Shields for manned applications must attenuate the reactor radiation many more orders of magnitude than required by instrument shields. A typical man-rated shadow shield (Figure 3-155b) consists of two sections, each with a gamma and neutron shield separated by an equipment gallery. The gallery contains the primary loop equipment such as pumps and compensators and the primary-to-secondary loop heat exchanger. The gallery height depends on the size of the primary loop components and will vary from 0.15 to 0.8 m depending on power level. The second section of the shield is used to protect the spacecraft from radiation emanating from the activated primary coolant or from radiation from fission products that could be in the primary loop as a result of fuel element clad failure or activation of loop corrosion products.

The variations in reactor shield weight for unmanned and manned application are given in Figures 3-156 and 3-157 as a function of reactor size, power, level, as well as for the variation in the other parameters listed. The shield mass is calculated by multiplying the reference case shield mass with each of the scale factors which correspond to the input parameters shown in the abscissa. Thus, if the reactor power level is 400 kWt, the neutron dose 10^{13} nvt/hr, and the separation distance 6 m, with the other parameters remaining the same at the reference case, the shield mass is:

$$\text{Mass} = 815\ (0.93)(0.57)(2.7) = 1,168\ \text{kg}$$

A typical isotope shield configuration is illustrated in Figure 3-158. The shield is assumed to have a uniform thickness over the surface and edge of the fuel block facing the spacecraft. The shield thickness versus does rate for neutron and gamma attenuation of the isotope heat source are given in Figures 3-159 to 3-162 for an isotope-payload separation distance of 100 cm.

INSTRUMENT RATED - REFERENCE DESIGN

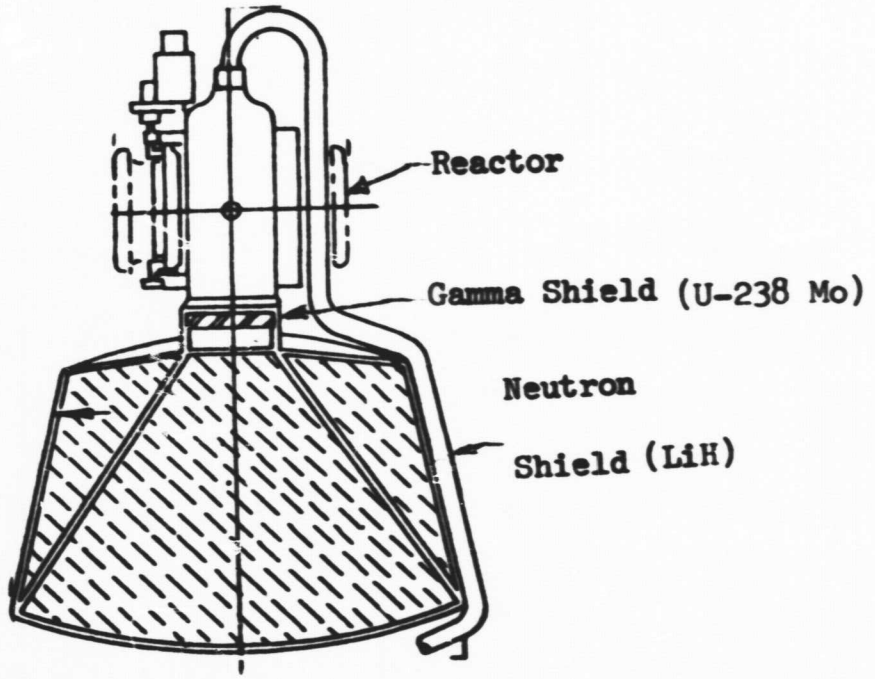

(a)

SHADOW SHIELDED MAN RATED CONCEPT

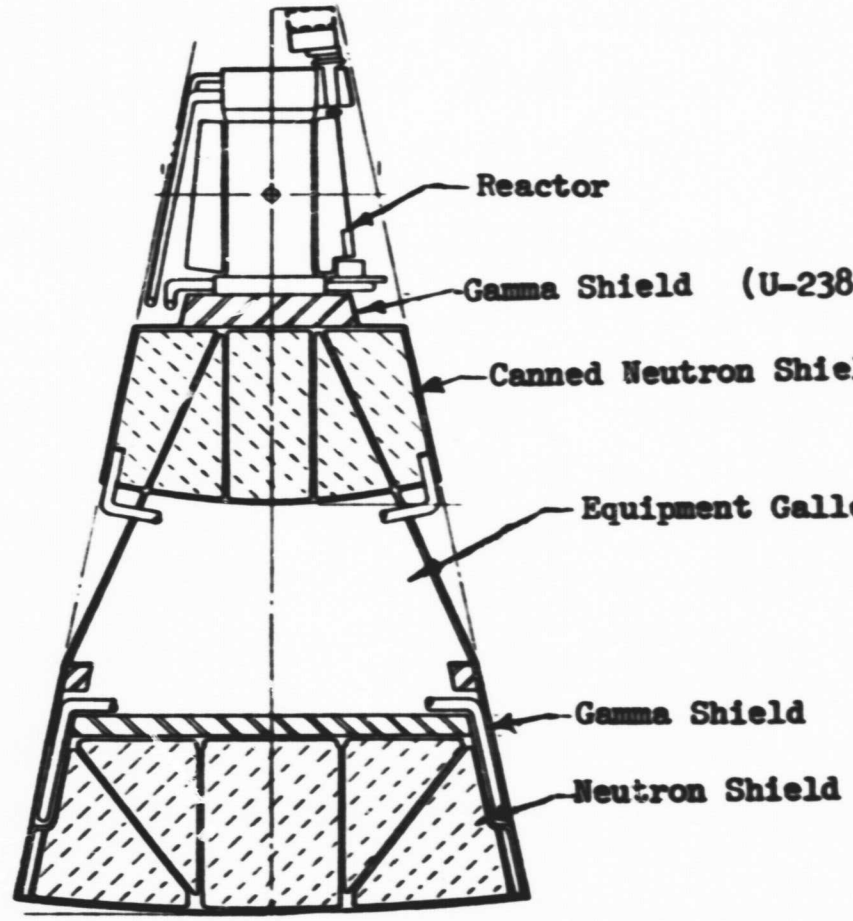

(b)

Figure 3-155 **NUCLEAR REACTOR SHIELD CONFIGURATIONS (Reference 5)**

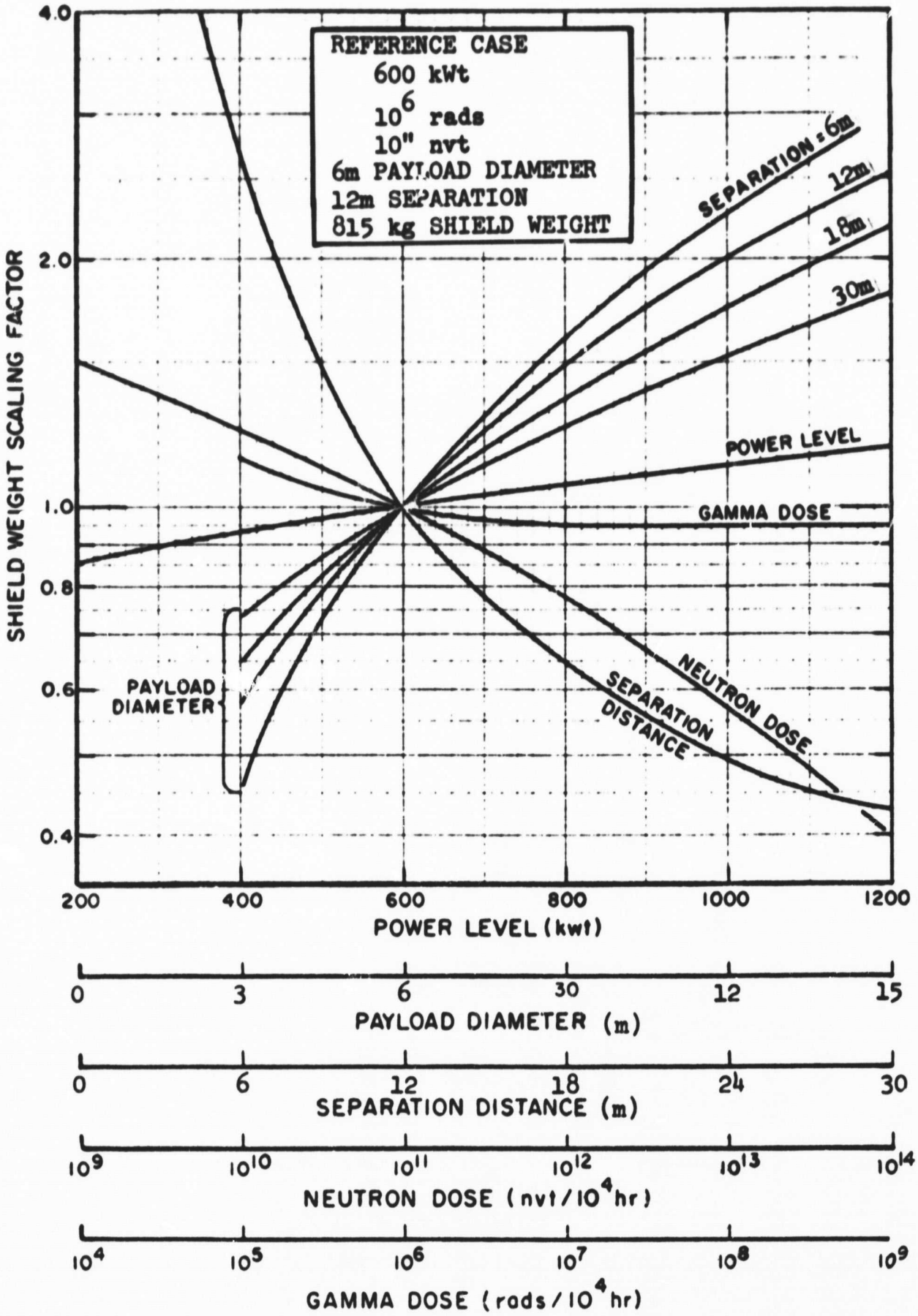

Figure 3-156 **INSTRUMENT SHIELD WEIGHT Vs SYSTEM PARAMETERS (Extracted From Reference 5)**

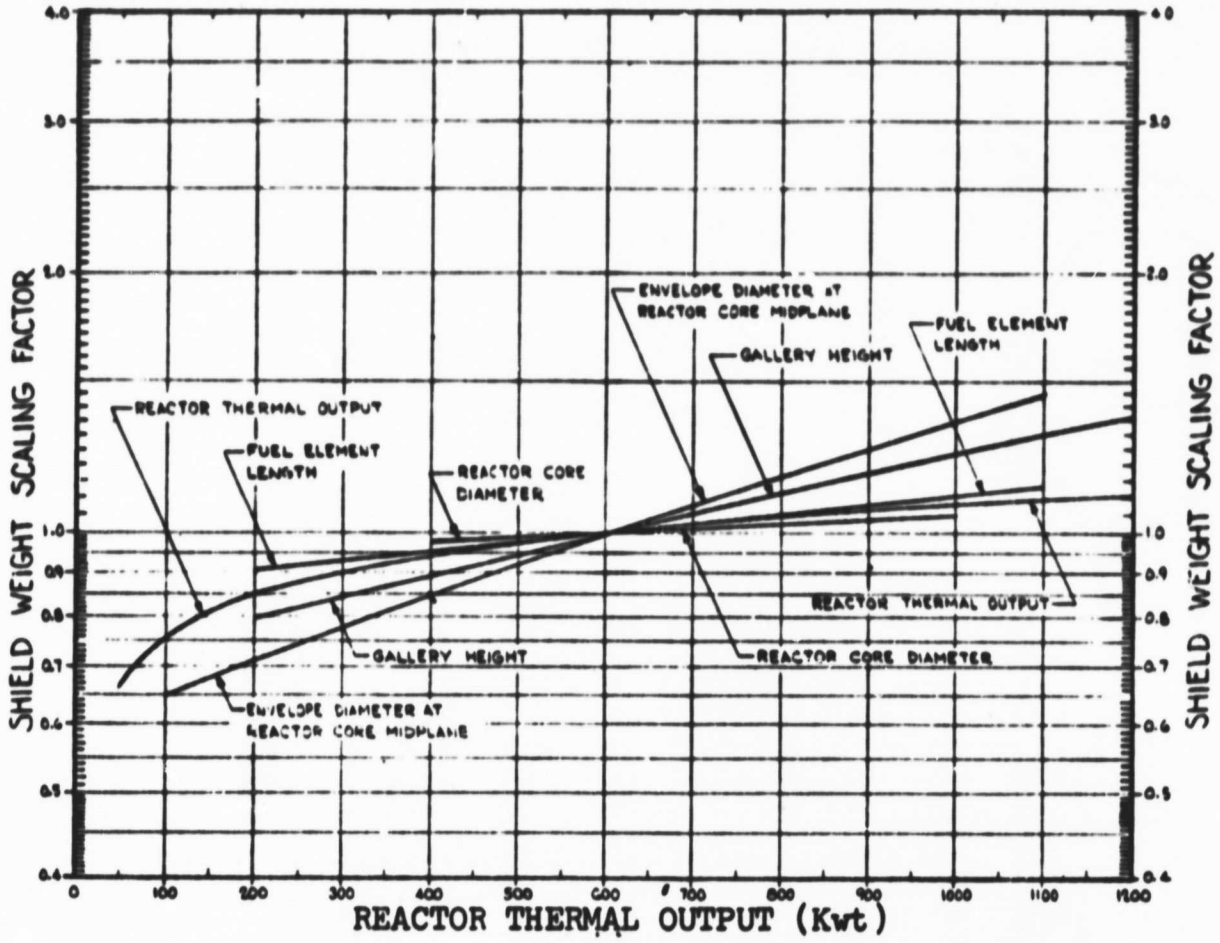

REFERENCE CASE

PARAMETER	VALUE
Reactor Thermal Output	600.0 kWt
Envelope Diameter At Reactor Core Midplane	51 cm
Fuel Element Length	51 cm
Reactor Core Diameter	25.5 cm
Gallery Height	51 cm
Separation Distance	46 m
Dose Plane Diameter	18.4 m
Dose Rate At Dose Plane	4.0 mrem/hr
Shield Weight	1850 kg

AI-66-0125

Figure 3-157 Shadow Shield Weight As a Function of Reactor and Shield Parameters (Extracted from Reference 2)

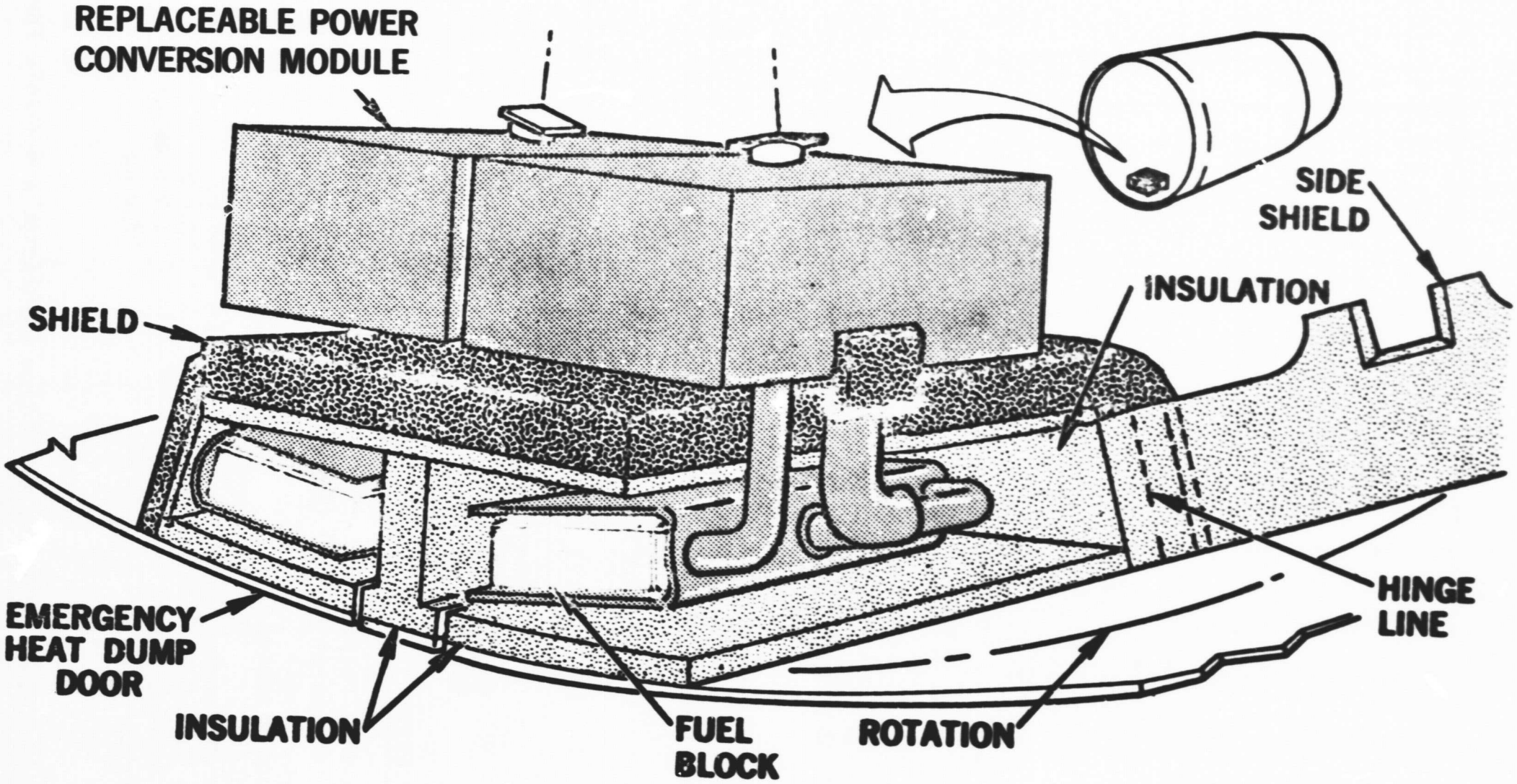

Figure 3-158 Typical Isotope Shield Arrangement

CLASSIFIED
DWG 63-8430

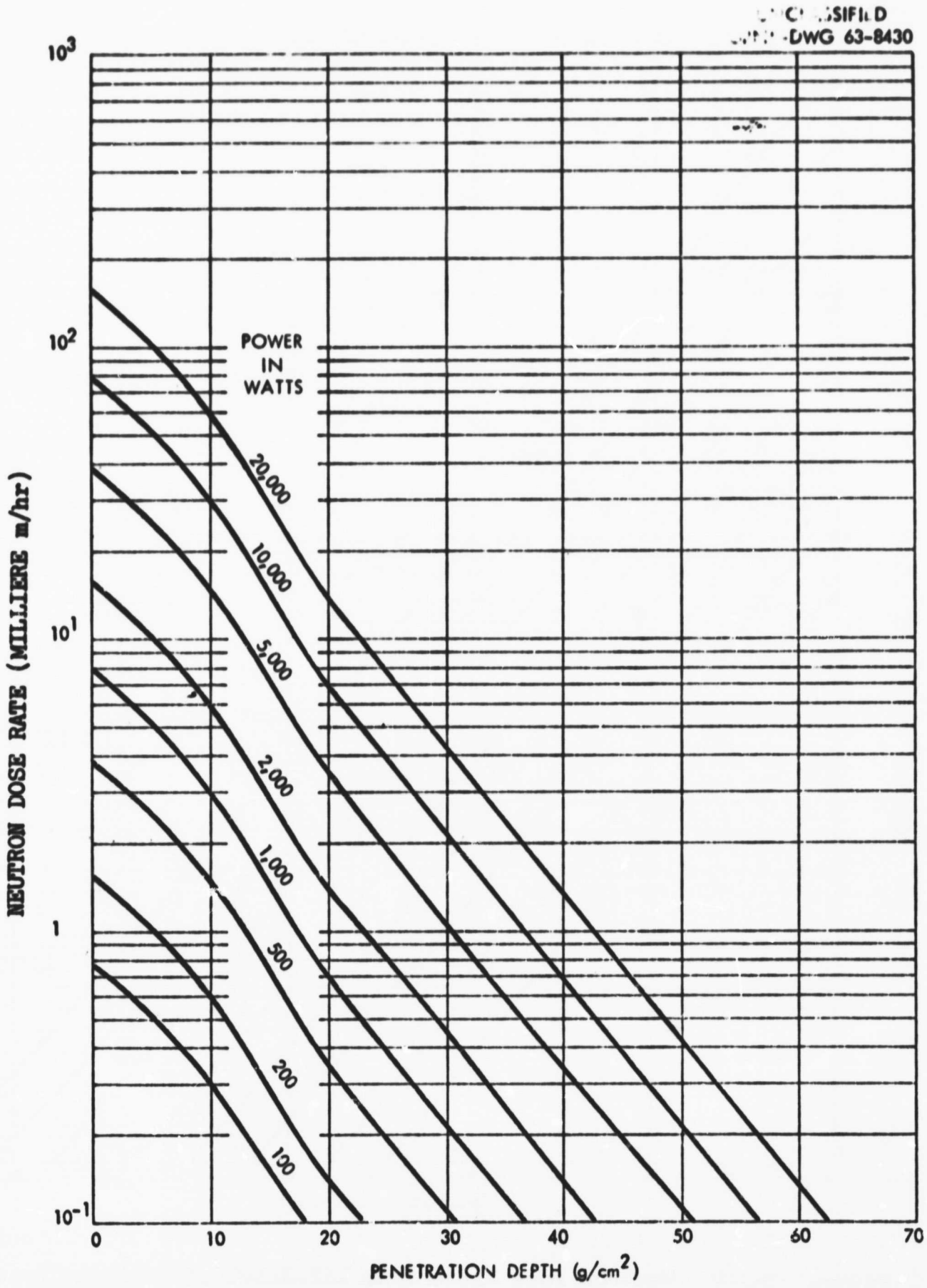

Figure 3-159 Neutron Dose Rates from LiH-Shielded Isotopic Power Sources of Plutonium-238 as a Function of Penetration Depth of Shielding Material. Center of source to dose point separation distance = 100 cm. Abstracted from Ref. 7.

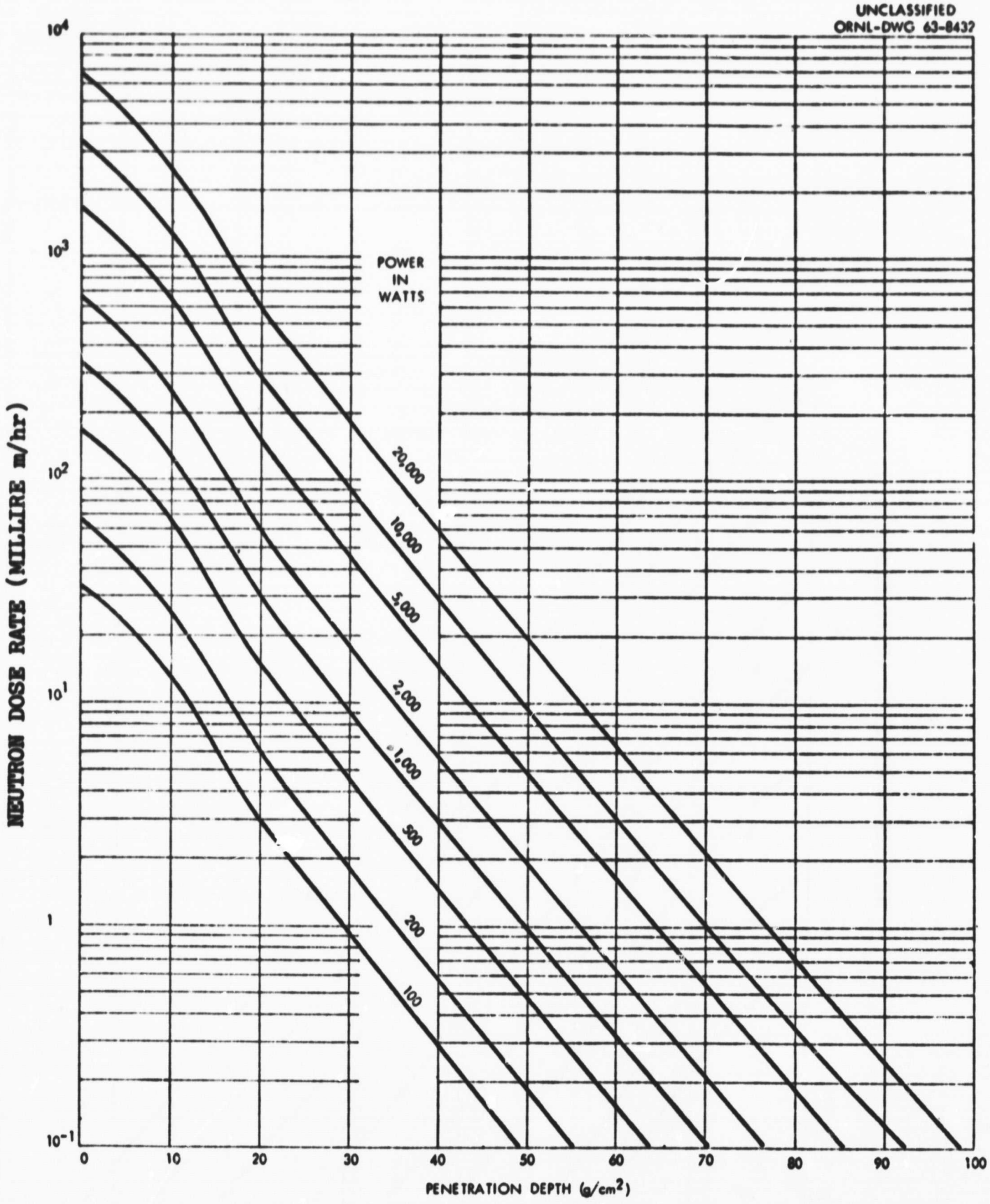

Figure 3-160 Neutron Dose Rates from LiH-Shielded Isotopic Power Sources of Curium-244 as a Function of Penetration Depth of Shielding Material. Center of source to dose point separation distance = 100 cm. Abstracted from Ref. 7.

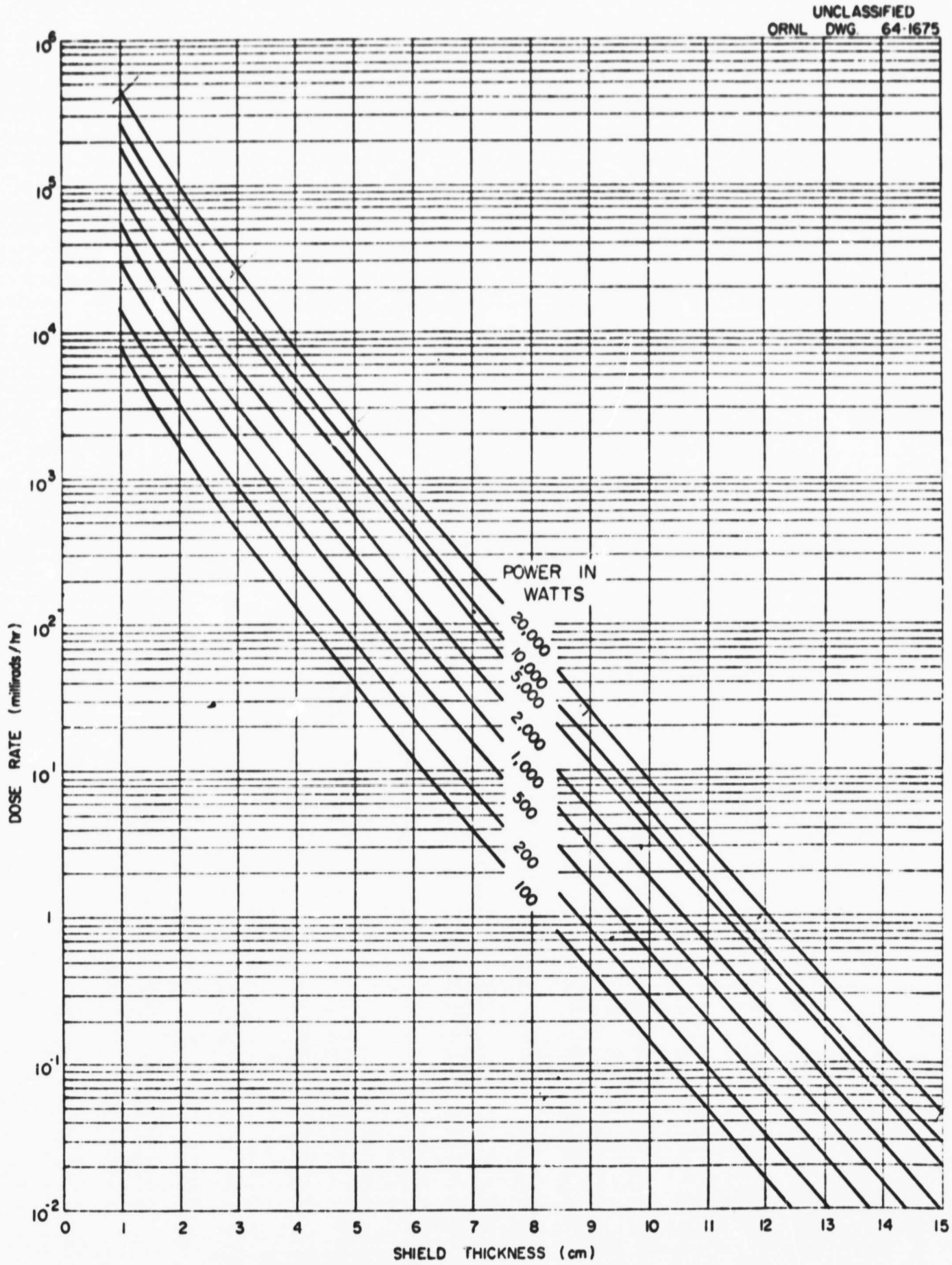

Figure 3-161 Bremsstrahlung Dose Rates from Uranium-Shielded Isotopic Power Sources of Strontium-90 (Strontium Titanate). Center of source to dose point separation distance = 100 cm. Abstracted from Ref. 7.

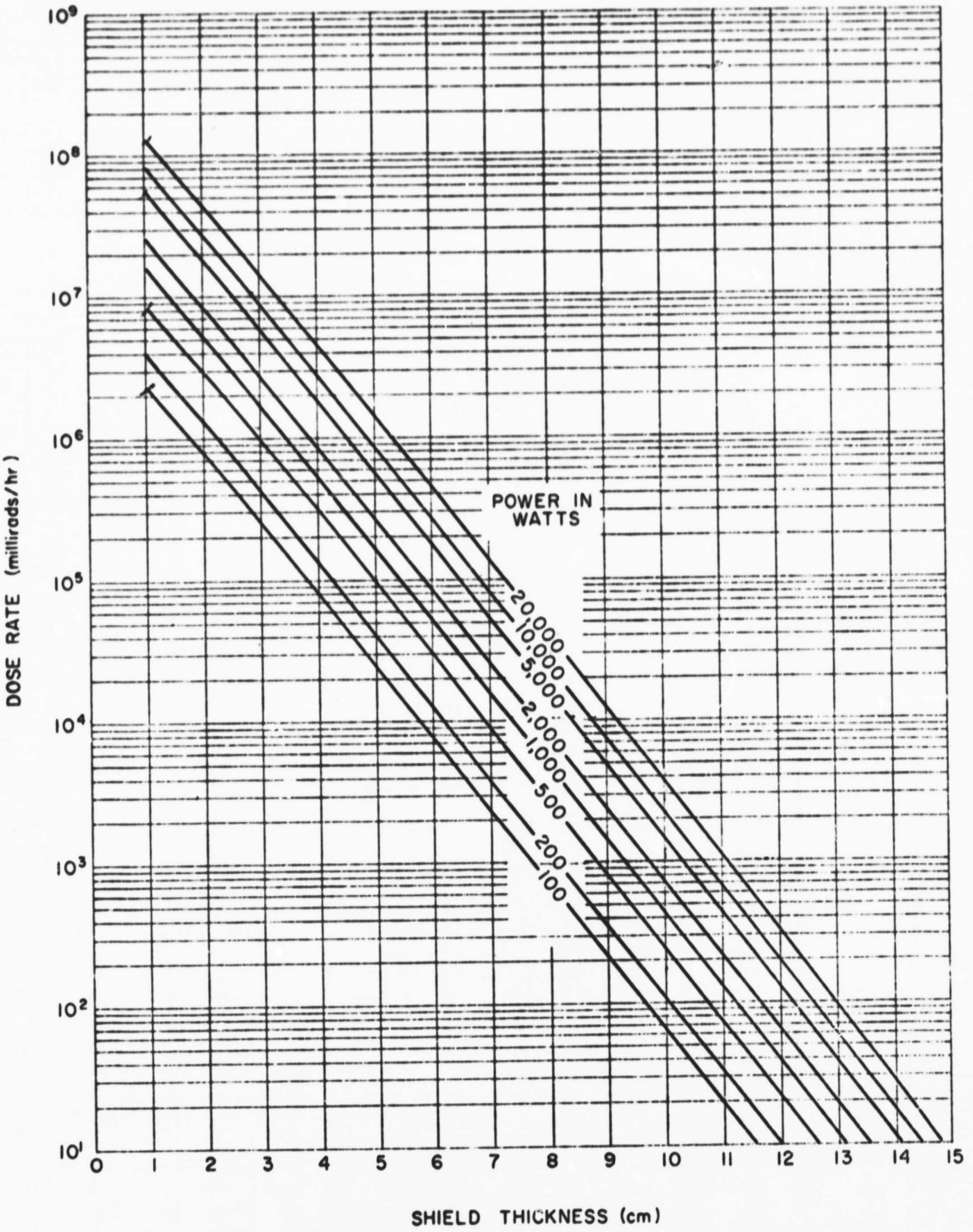

Figure 3-162 Gamma Dose Rates from Uranium-Shielded Isotopic Power Sources of Cobalt-60. Center of source to dose point separation distance = 100 cm. Specific activity of source = 75 curies per gram of cobalt. Abstracted from Ref. 7.

Reliability data for nuclear shields that are used to project reliability trends are given in Figure 3-163. The main failure mode is the meteoroid puncture of the canned LiH neutron shield. High reliability can be reached by segmenting the shield in parts so that the puncture of one will not affect the effectiveness of the others (Reference 3). The specific production cost of the nuclear shields is shown in Figure 3-164

3.2.4 Solar Concentrator Heat Source Subsystem

Several types of solar concentrator subsystems have been under development during the last decade. Solar concentrator efficiencies decrease sharply with higher absorbor temperatures and angular deviation of the concentrator from direct alignment with the sun vector. These facts, coupled with the large volumes required for rigid paraboloid concentrators, the high drag resulting from large deployed areas, and the low radiation resistance of the concentrator surface are the principal limitations for these devices. Every concentrator developed to date, with the exception of the one-piece type, has a folding feature for compactness during launch. The two types of subsystems that have been selected for this study are the one-piece and the folding-petal concentrators.

The concentrator heat source subsystem is shown in Figure 3-165 and consists of the concentrator, the boiler-absorber (receiver), the heat storage material and the accessories. The thermal power output of the solar concentrator is limited by the maximum allowable diameter and the number of concentrators. More than one complete power system operating in parallel thus may be required to meet higher power levels. Redundancy in the concentrator heat source subsystem is obtained by the use of complete standby power systems, each with one solar concentrator subsystem.

The boiler-absorber comprises the basic absorbing shell. Mass penalties are added depending on the amount of heat storage material required for shadow operation and on the number of sets of boiler tubes required in the absorber (dynamic power conversion subsystems only).

The solar concentrator energy source subsystem characteristics and ranges of performance are shown in Table 3-34. The subsystem performance and

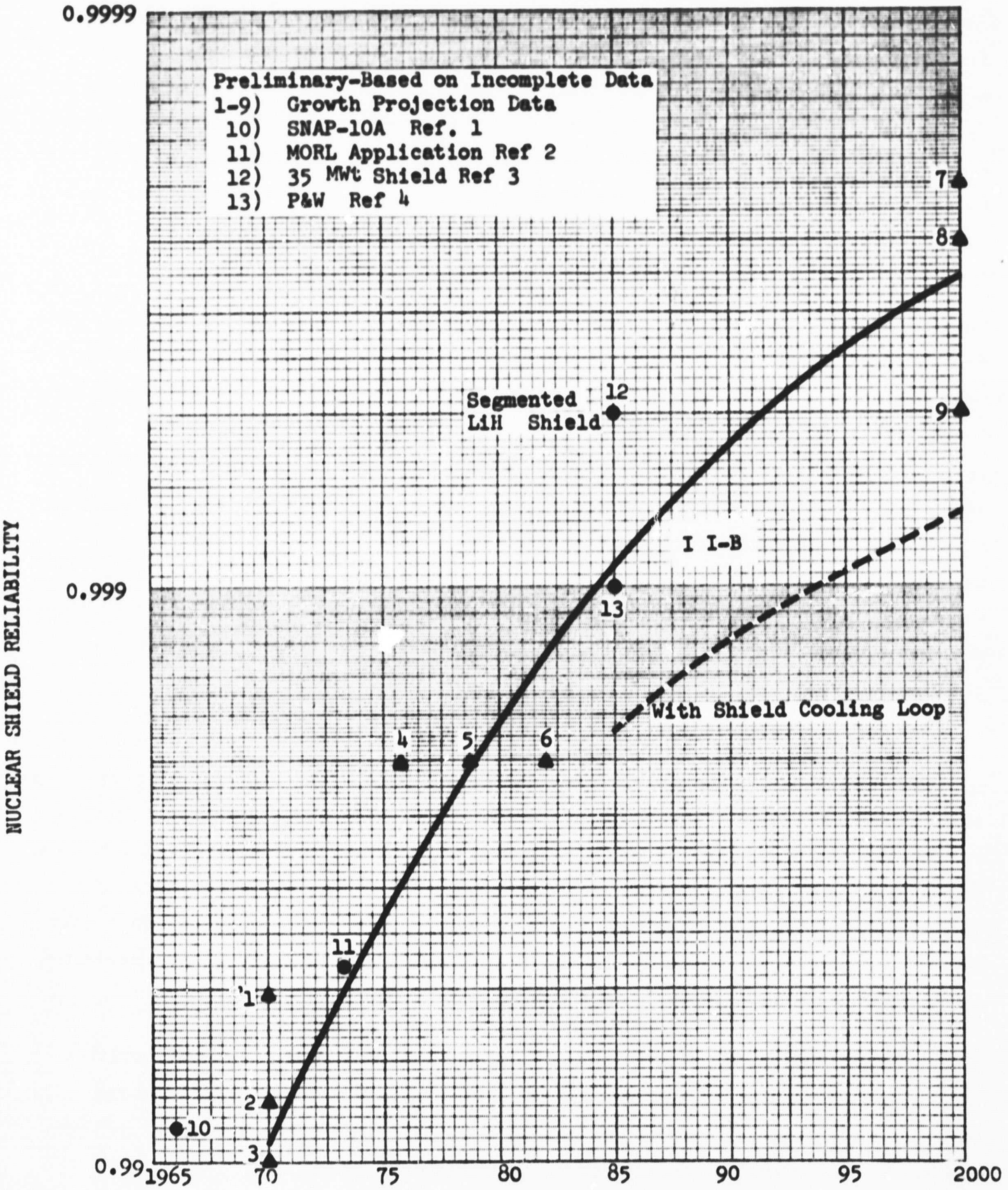

Figure 3-163 Projection-Nuclear Shield Reliability (LiH)

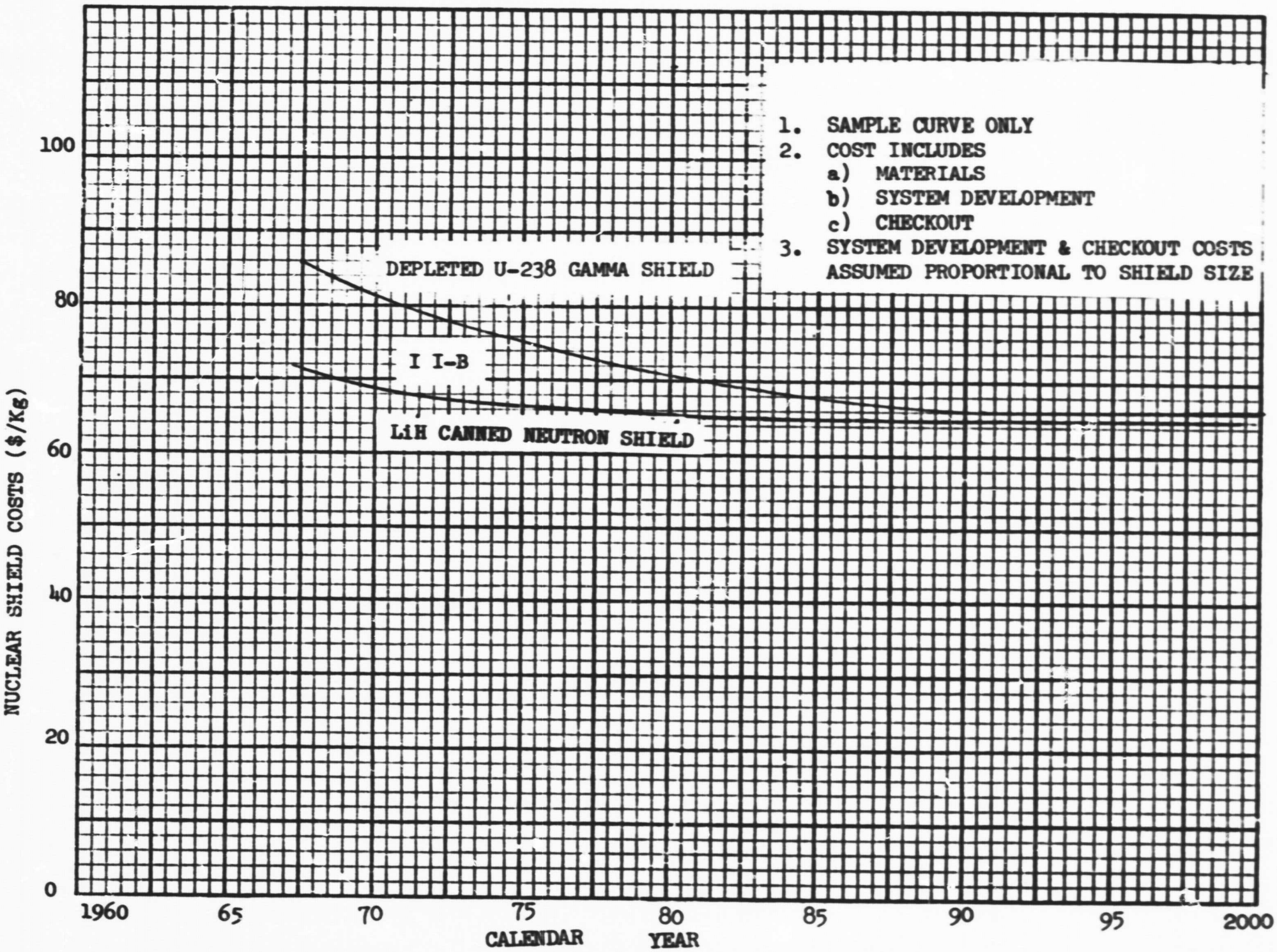

Figure 3-164 Projection - Nuclear Shield Cost

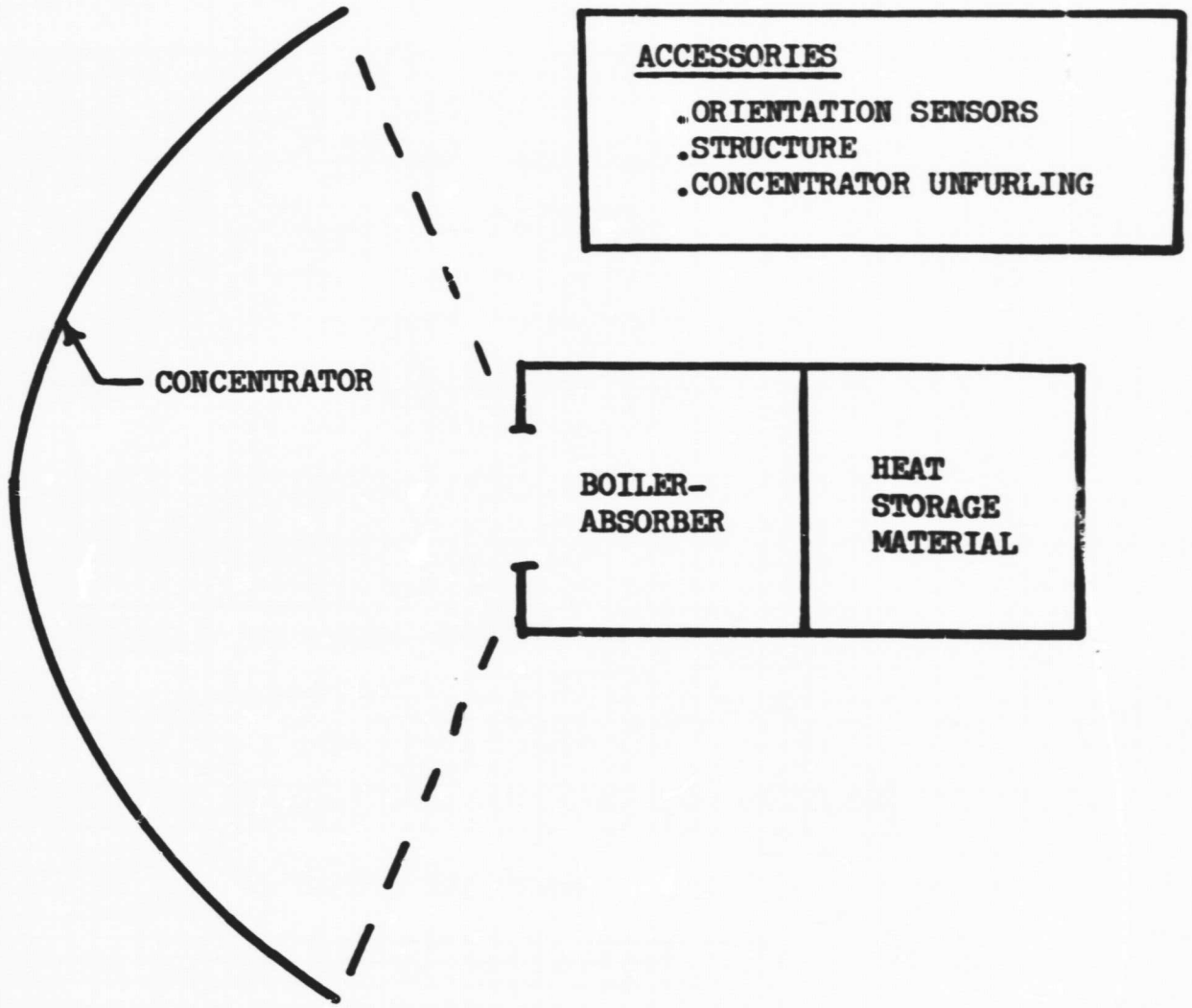

Figure 3-165 Solar Concentrator Heat Source Subsystem

Table 3-34

SOLAR CONCENTRATOR HEAT SOURCE SUBSYSTEM
BRIEFING CHART

Item	Value
Identification	
Conversion equipment	Rankine, Brayton, thermoelectric, thermionic
Major Components	Concentrator, boiler-absorber (receiver), heat storage material, and accessories
Vehicle - mission application range	
Useful power level	4 kWt to 400 kWt
Duration of mission	Days to years
Types of spacecraft	Manned, unmanned, Earth orbiting, interplanetary
Status	
State of the art	One-piece and folding-petal prototype concentrators partially developed. Boiler-absorber development initiated (for Brayton cycle)
Availability of Support Subsystems	
Special Problems	Containment of heat storage material, need development of reliable and accurate orientation components
Subsystem Characteristics	
Range of specific mass	30 to 115 kg/kWe
Range of specific area	0.5 to 1.5 m^2/kWt
Range of specific volume	0.5 to 1.5 m^3/kWt
Range of specific production cost	4,000 to 10,000 $/kWt
Range of reliability	70 to 99% (one year)
Performance Data	
Concentrator-absorber efficiency	60 to 90%

physical characteristics such as specific mass, random failure rate, wear-out life and production cost are presented for the four major component areas in Figures 3-166 through 3-176.

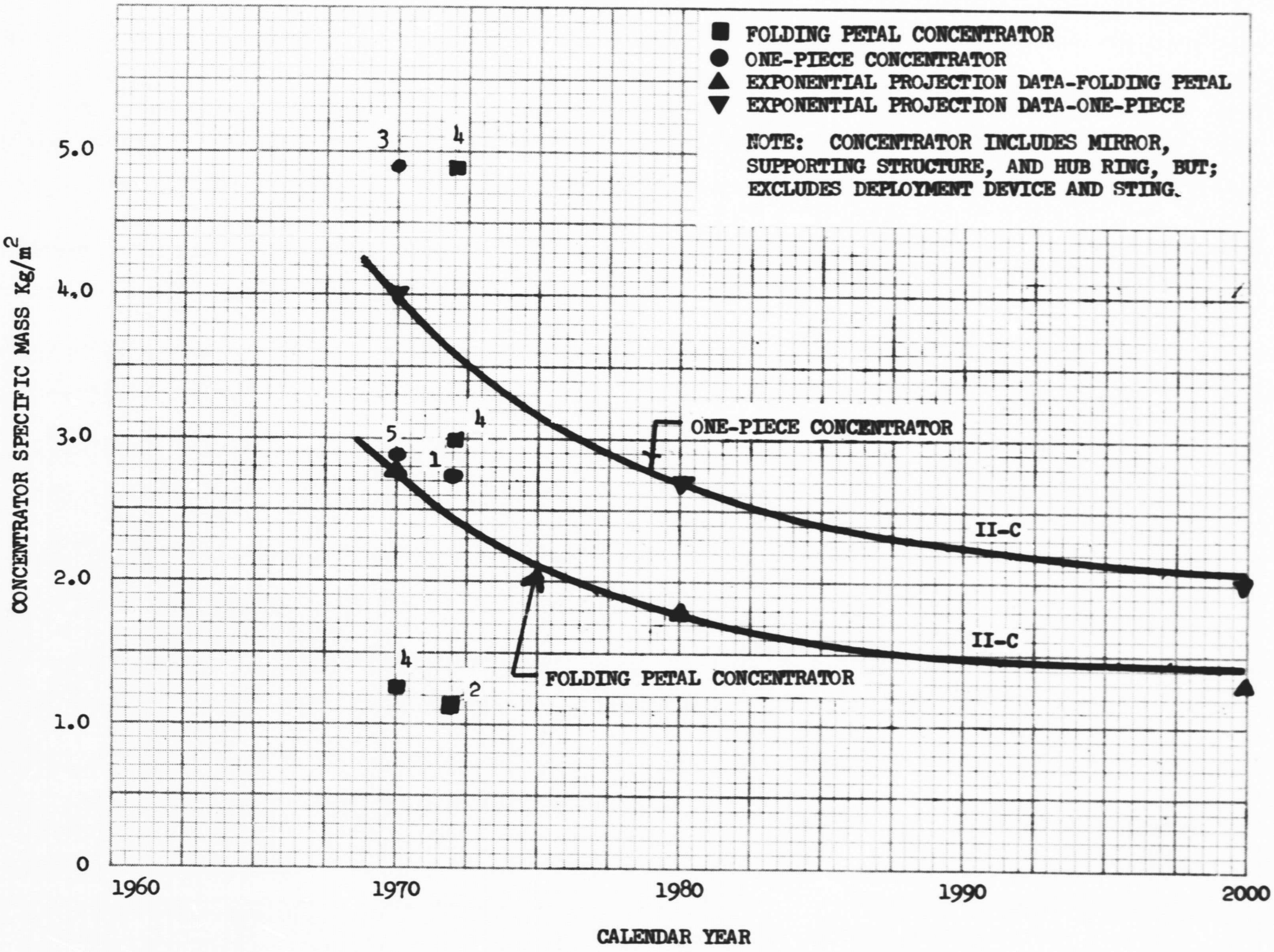

Figure 3-166 — Projection Solar Concentrator Specific Mass

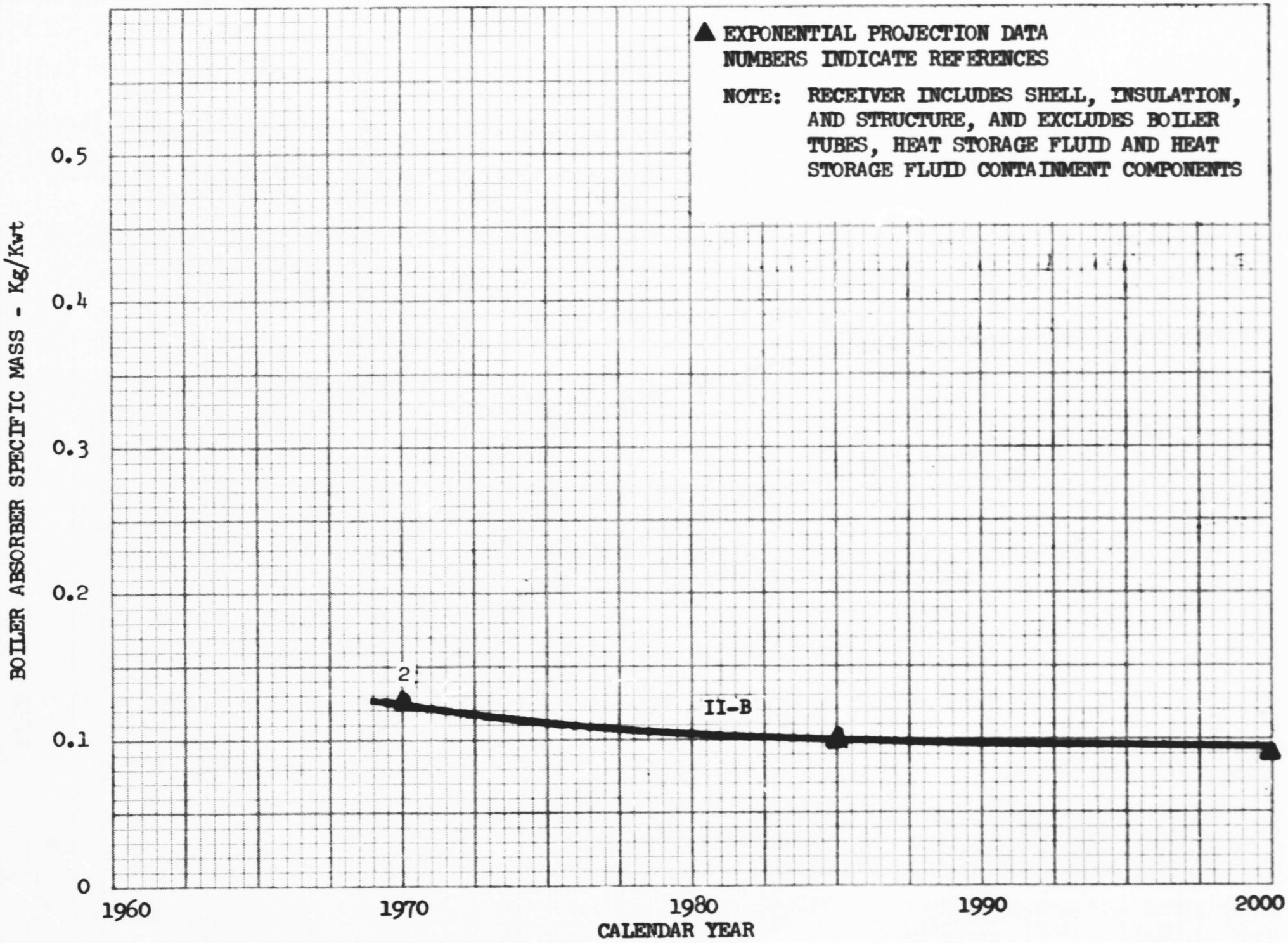

Figure 3-167 Projected Boiler-Absorber Specific Mass

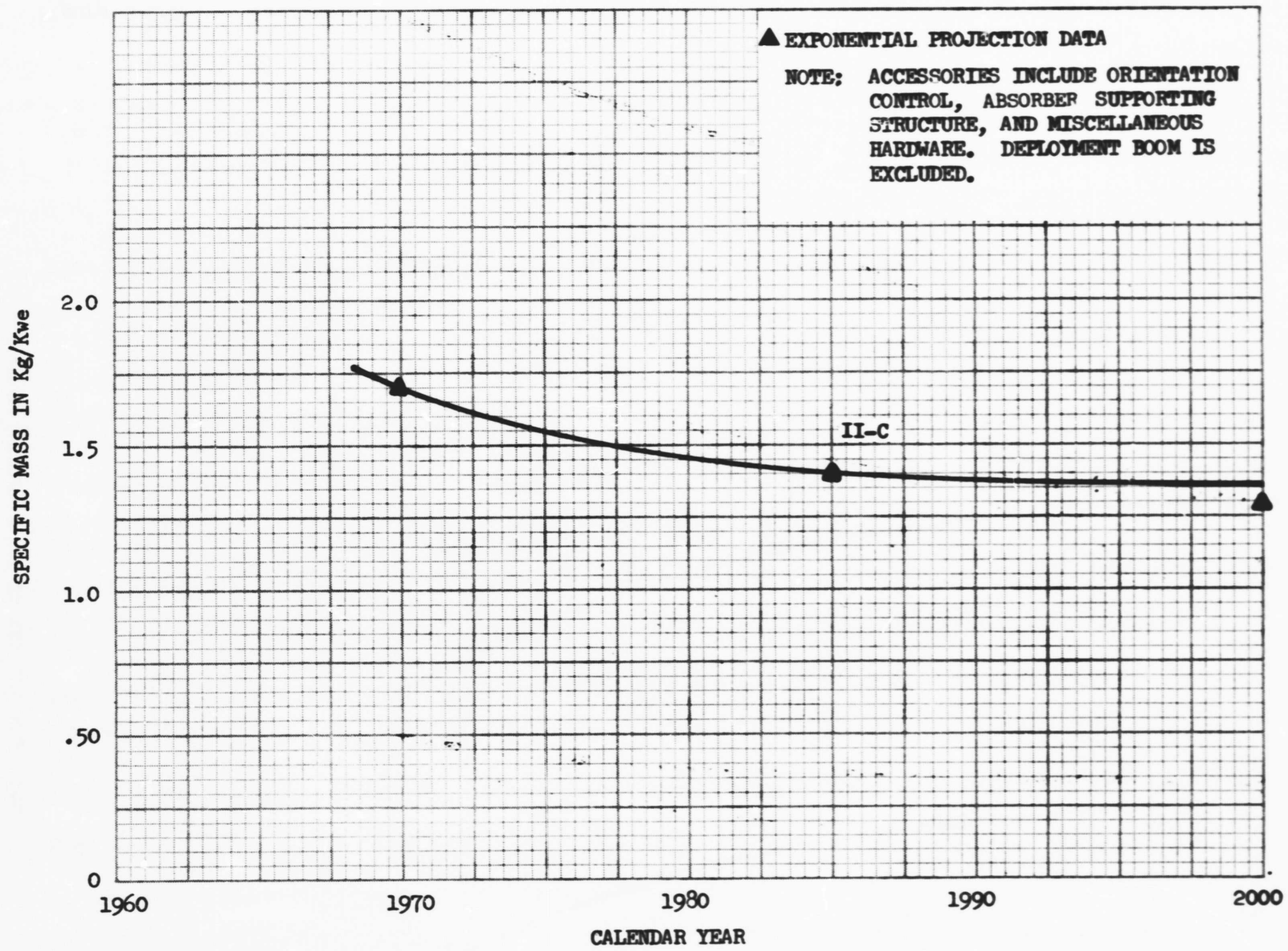

Figure 3-168 — Projection Specific Mass of Solar Concentrator Subsystem Accessories

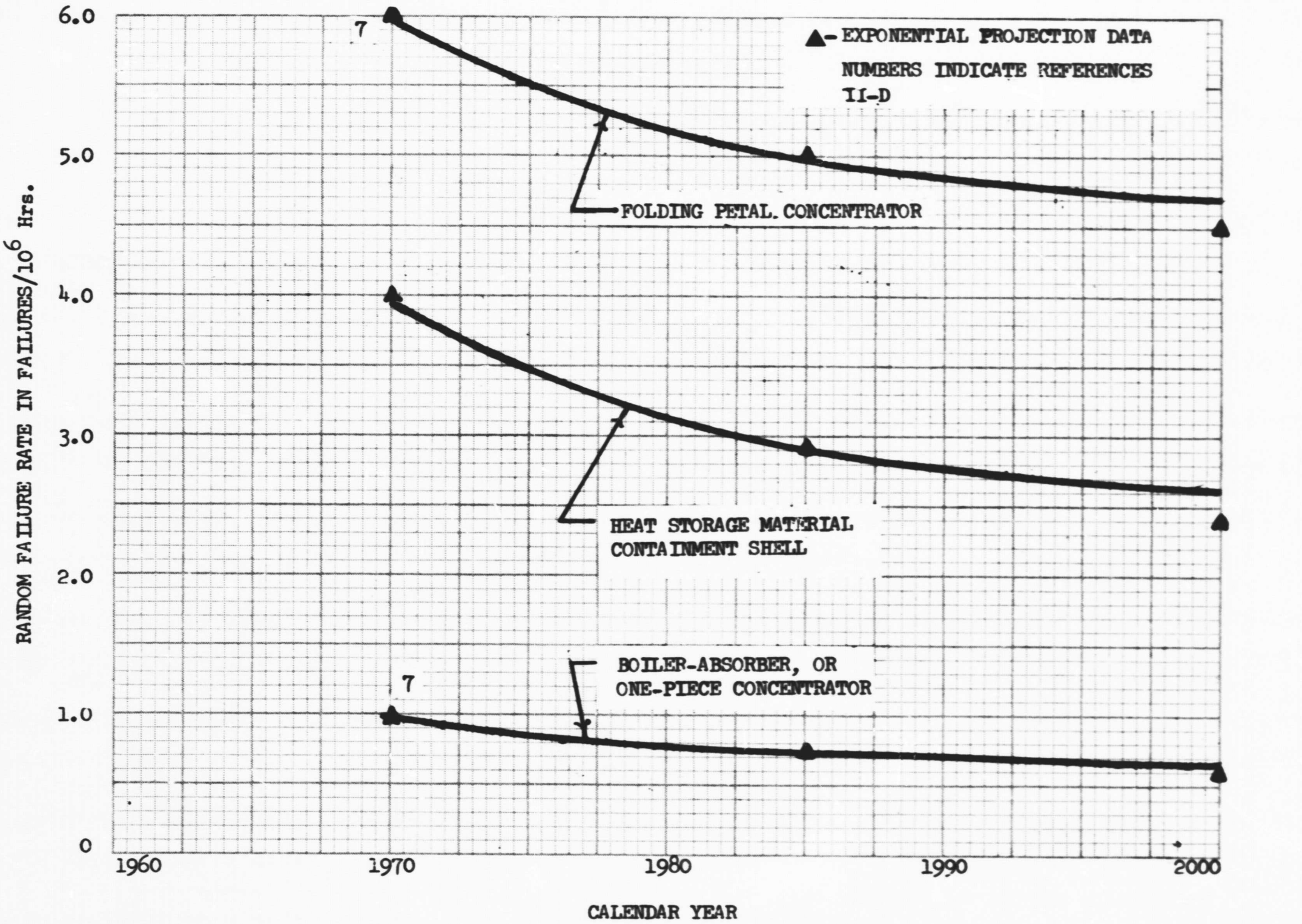

Figure 3-169 Projection of Failure Rate of Solar Concentrator Subsystem Components

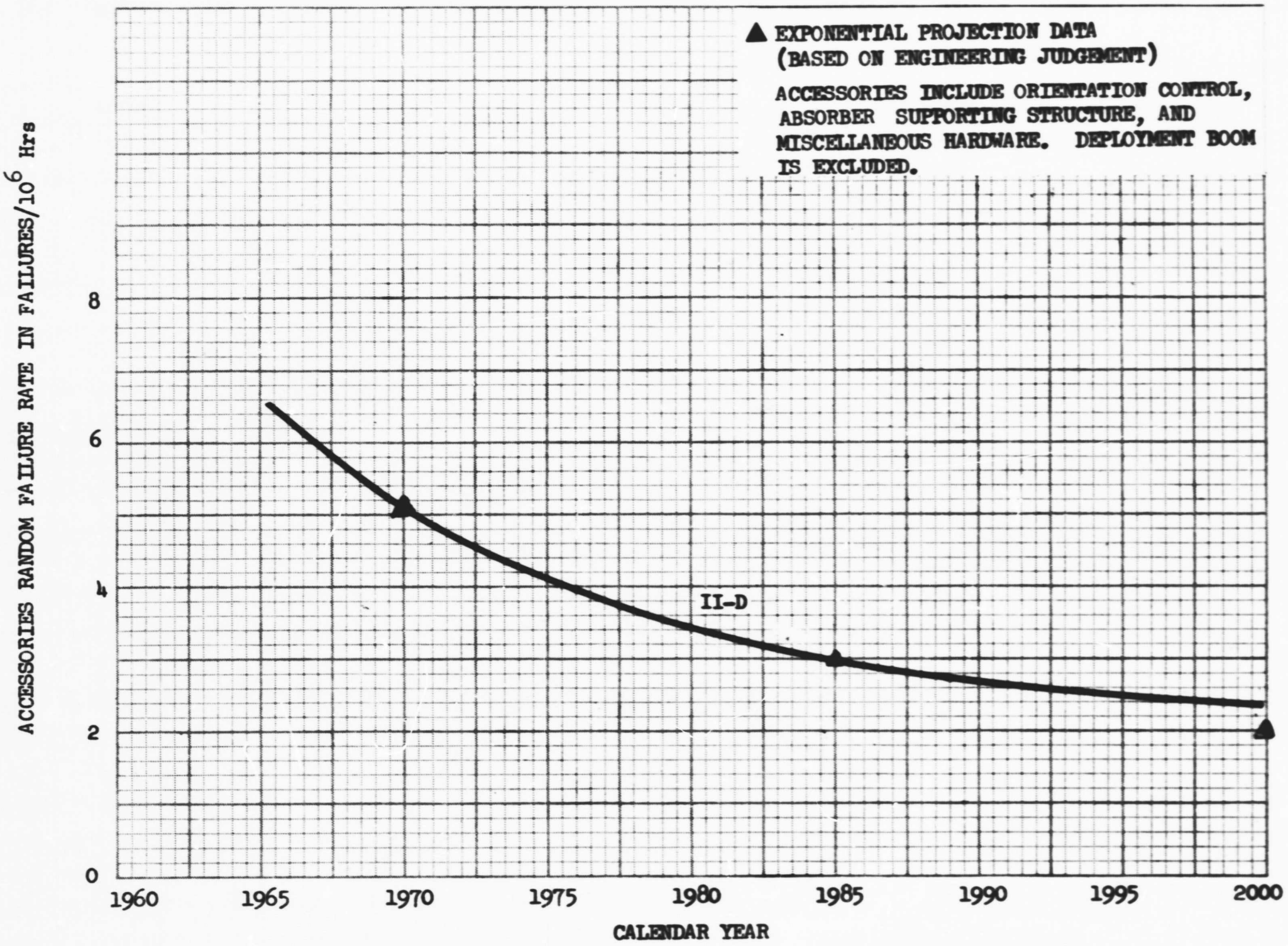

Figure 3-170 Projection of Failure Rate-Solar Concentrator Subsystem Accessories

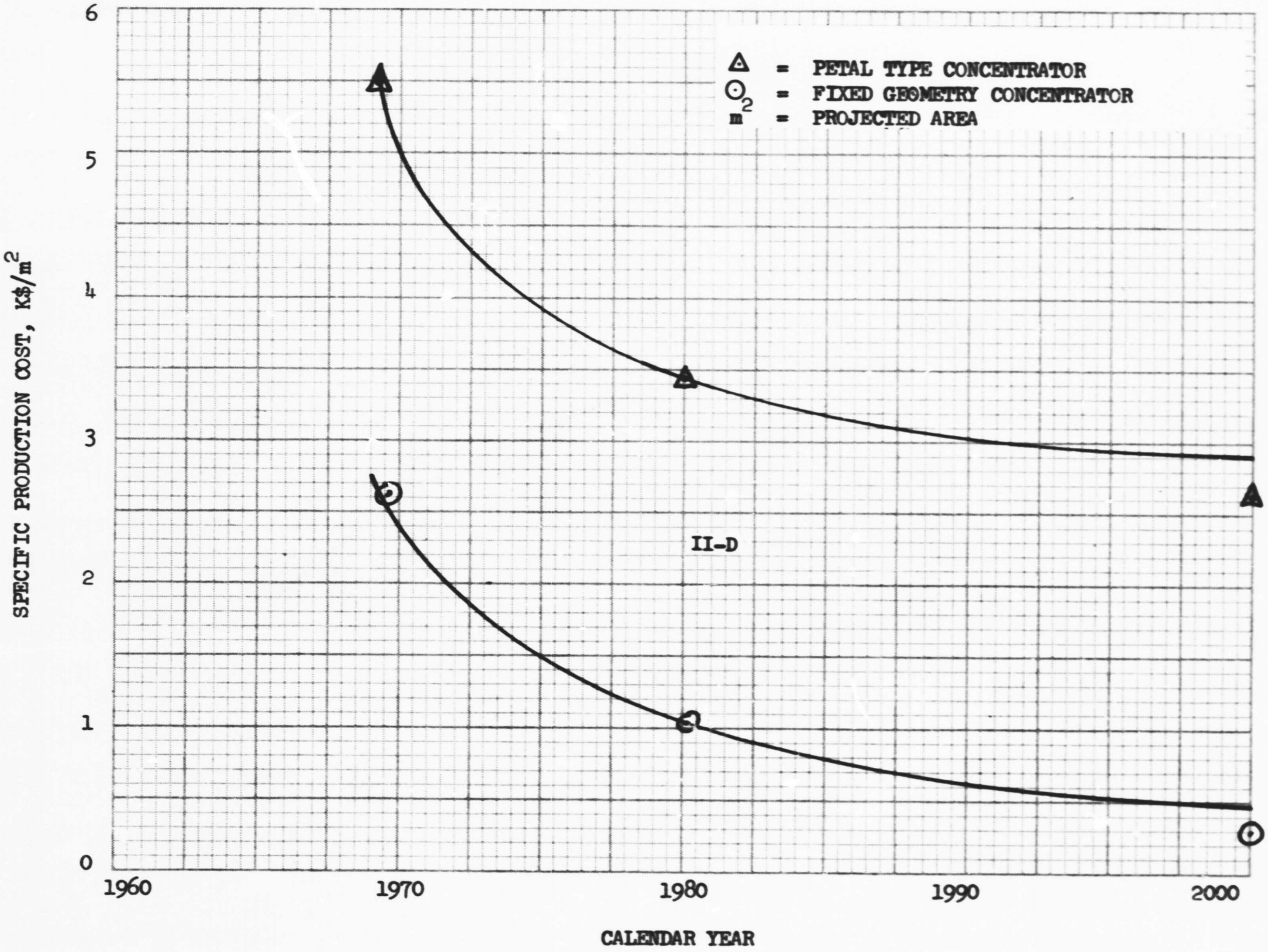

Figure 3-171 — Specific Production Cost of Solar Concentrators

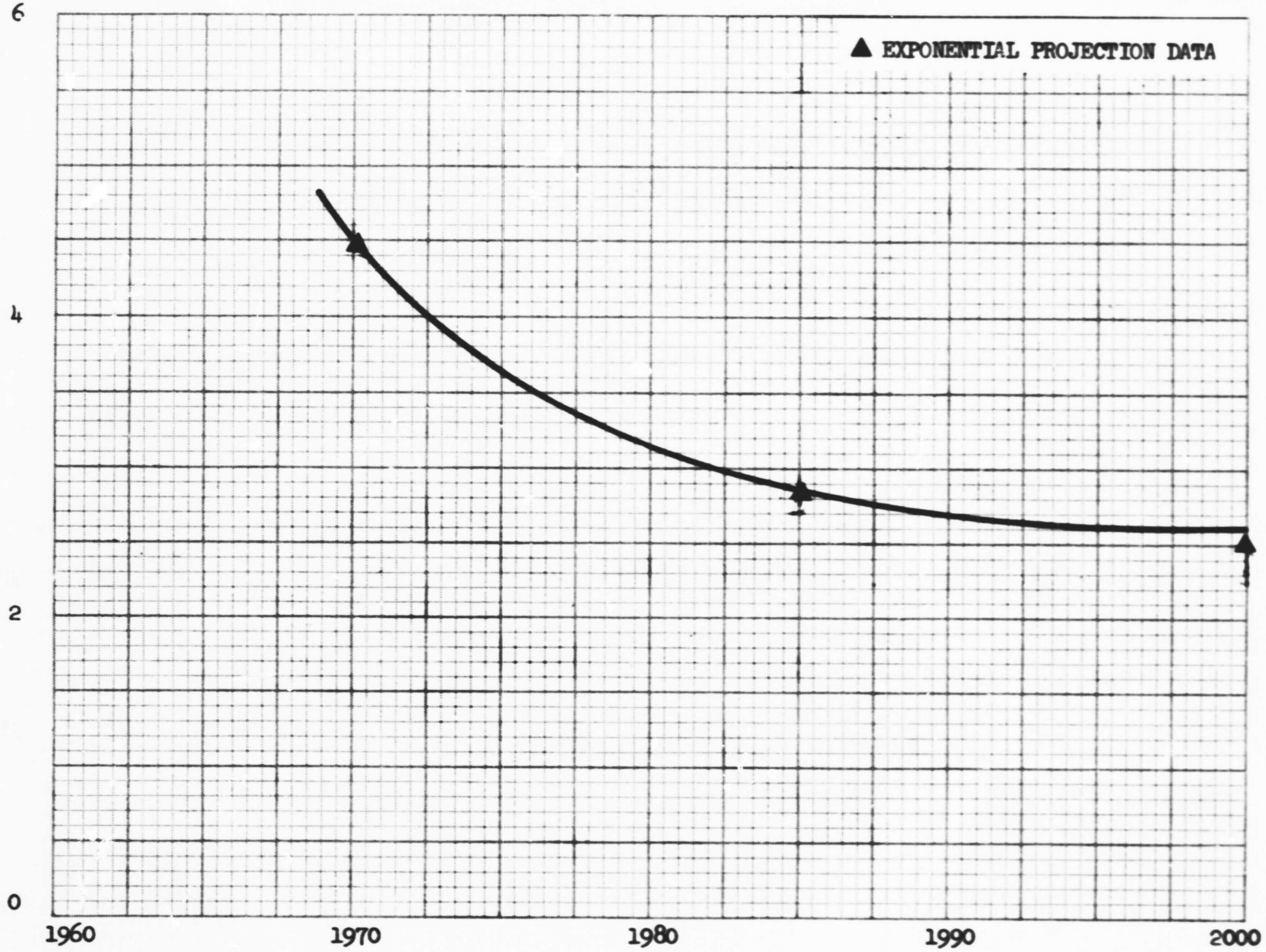

Figure 3-172 Specific Production Cost Solar Boiler Absorber

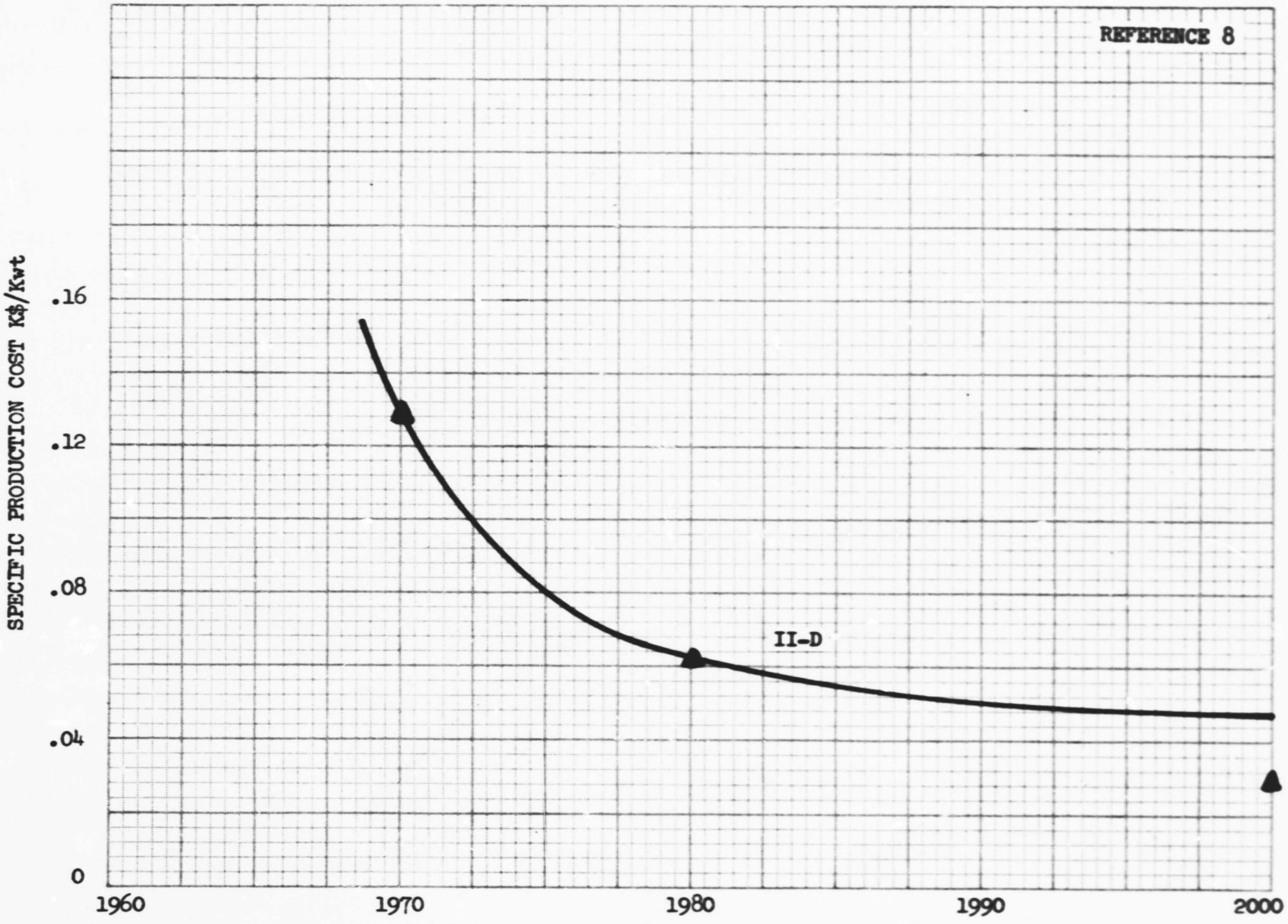

Figure 3-173 Cost of Solar Concentrator Subsystem Accessories

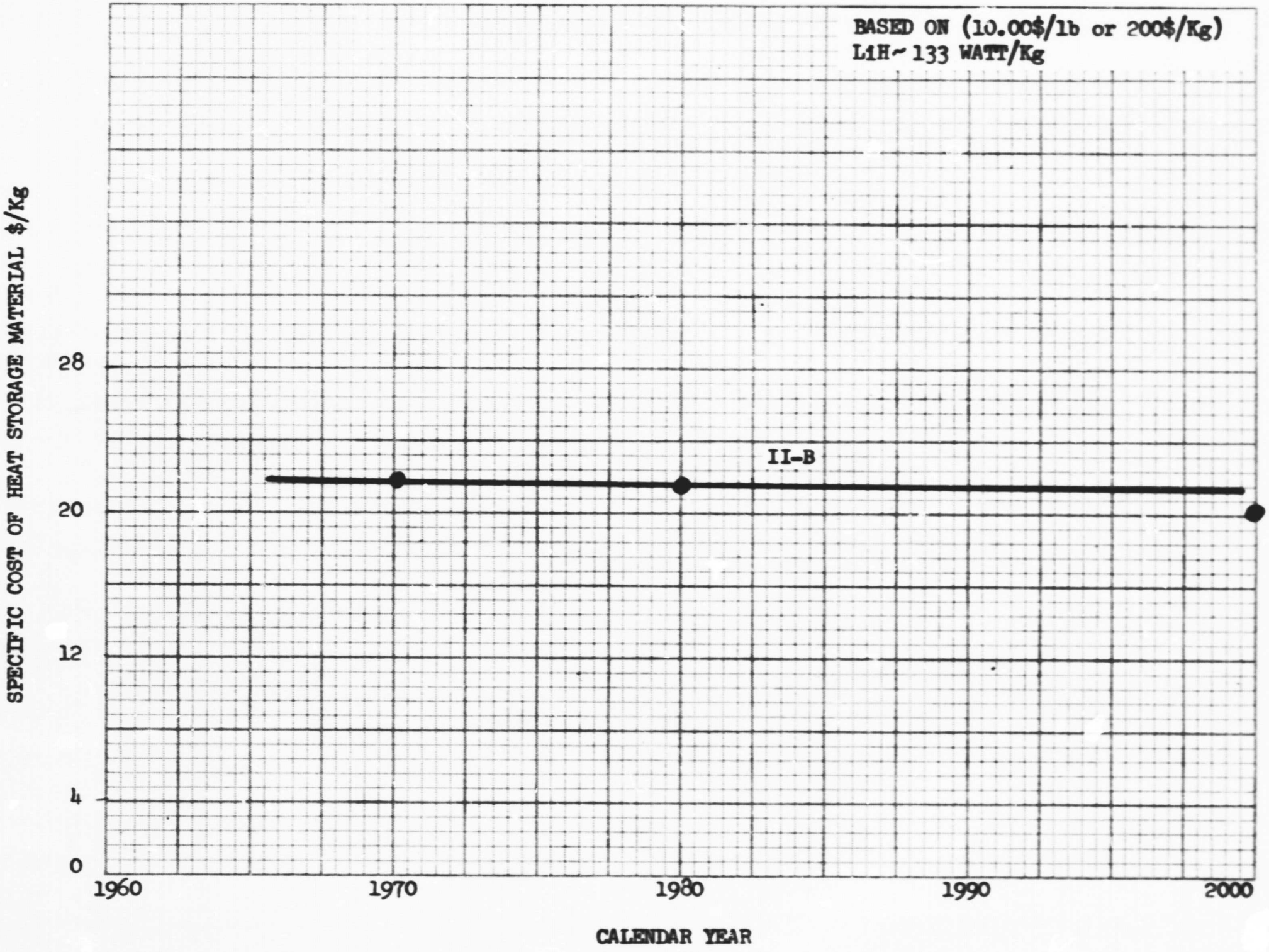

Figure 3-174 — Cost of Heat Storage Material-Solar Heat Source

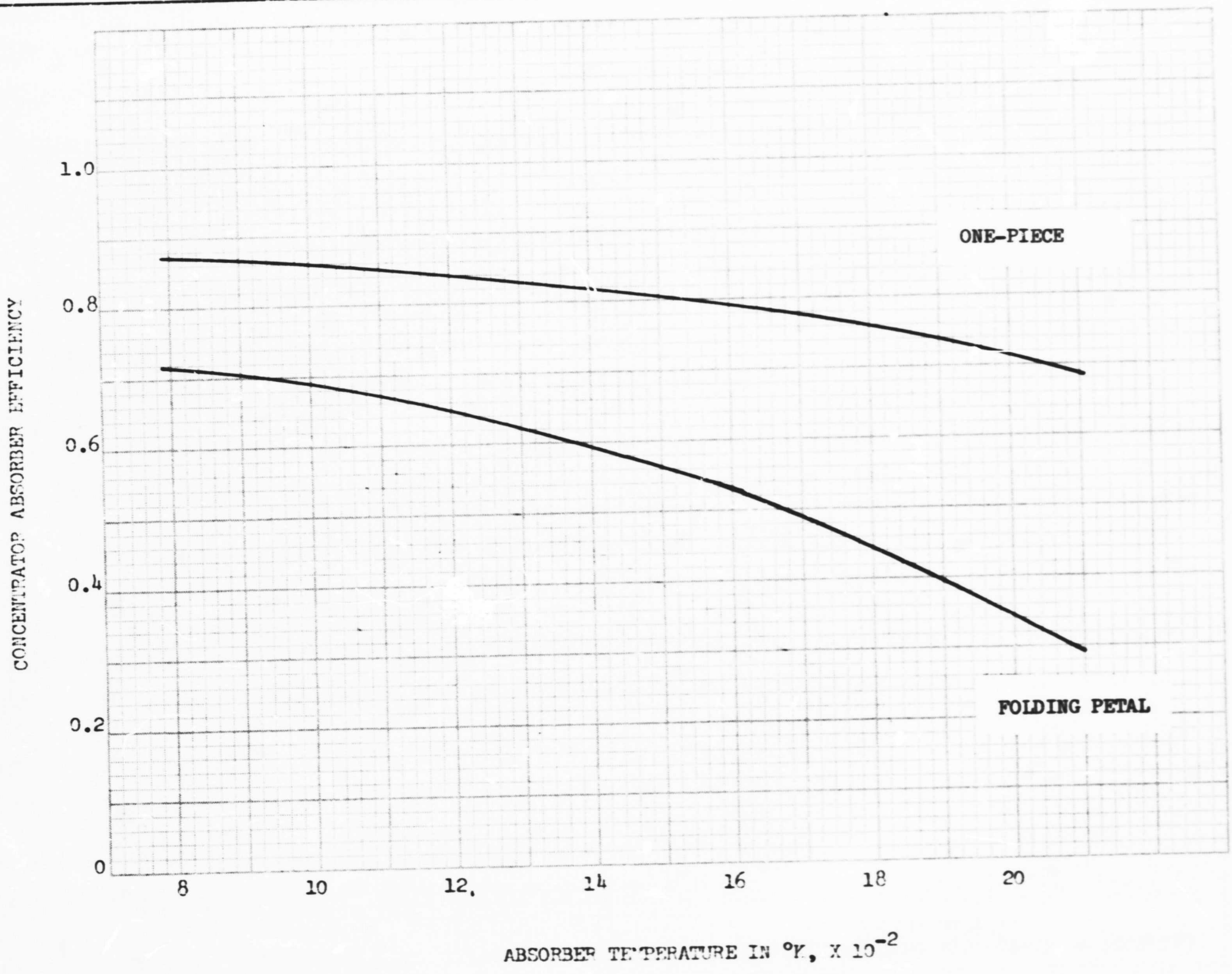

Figure 3-175 Solar Concentrator - Absorber Efficiency versus Temperature

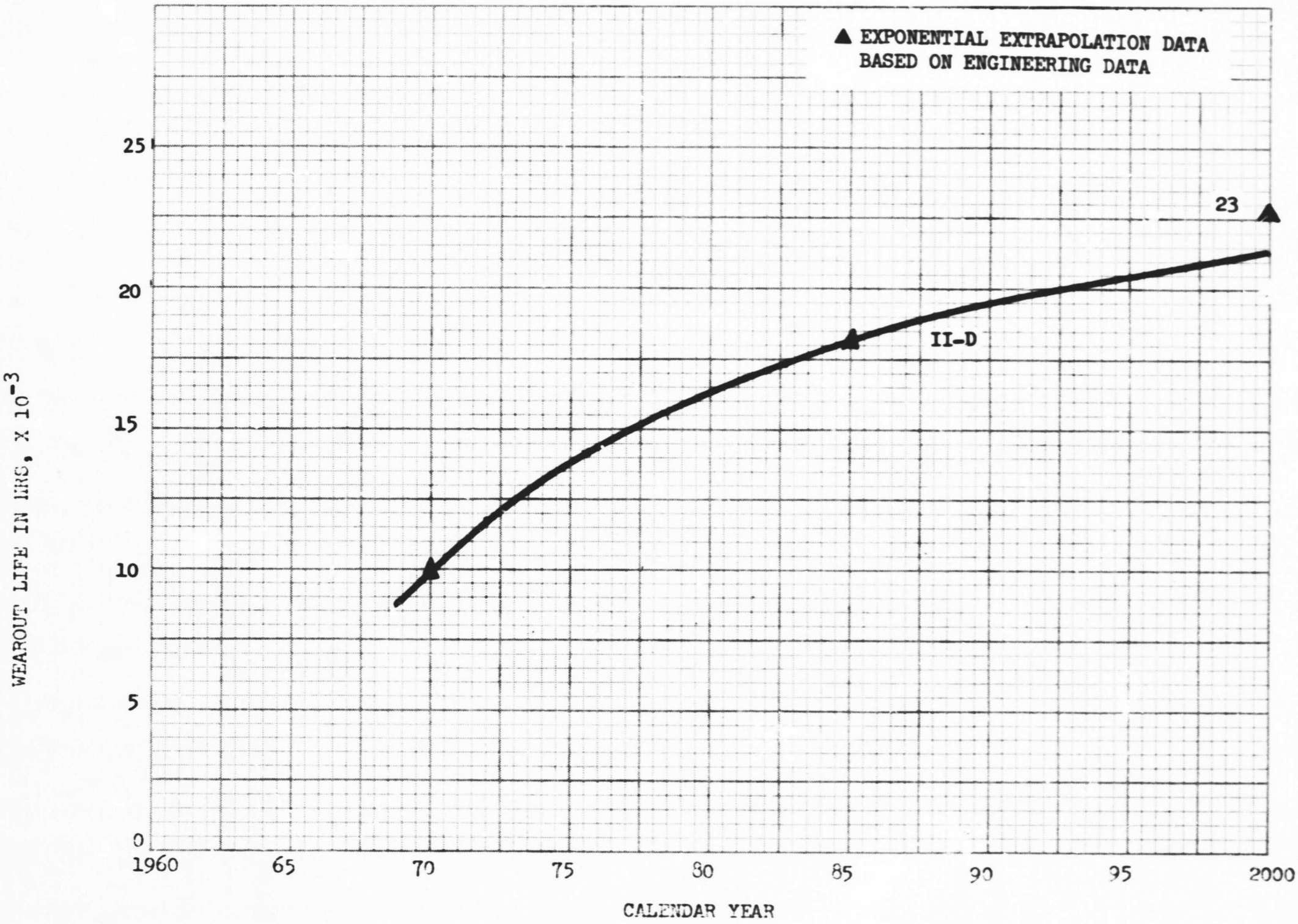

Figure 3-176 Projection of Solar Concentrator Subsystem Wearout Life

3.2.5 Reactant Storage Subsystem

Storable and cryogenic chemical reactants in the liquid or gaseous state are used to supply energy for operation of fuel cells or open-cycle dynamic conversion subsystems. Chemically fueled electrical power systems are generally applicable for mission durations that vary from a few minutes to more than 1,000 hours. Cryogenic storage of hydrogen and oxygen are currently being provided for power systems (fuel cells) used in manned space vehicles, and storable reactant supply systems are provided for power systems (turboalternators) used in missiles. Parametric data for cryogenic storage of hydrogen and oxygen and storable liquid reactants are presented. Significant summary data are shown on the briefing chart of Table 3-35.

3.2.5.1 Cryogenic Reactant Subsystems

Storage of reactants which have low-temperature boiling points can be accomplished by single-phase cryogenic fluid storage at subcritical pressure. Typical cryogenic storage subsystems are shown in Figure 3-177. Cryogenic storage gives high fluid densities at moderate pressures resulting in low reactant storage tankage weight (Figure 3-178) for short duration missions. Standard practice is to change both the supercritical and subcritical fluids to superheated vapor before use. Supercritical storage ensures delivery of a single-phase fluid in the zero-g environment. Subcritical storage subsystems weigh less than supercritical and gaseous storage subsystems, but require more complex equipment to ensure the delivery of single-phase fluids for space electrical power systems.

The curve shown in Figure 3-178 is for power conversion subsystems (fuel cells) that use hydrogen and oxygen in a stoichiometric mixture ratio (O/F=8). The specific weight of the reactant storage may be increased as much as 37% if the mixture ratio is decreased to that required for dynamic conversion subsystems (O/F=2). The specific costs ($/kg) of both storage methods are about the same (Figure 3-179a).

Table 3-35

REACTANT STORAGE SUBSYSTEMS BRIEFING CHART

Item	Value
Identification	
Applicable reactants	Hydrogen, oxygen; N_2O_4, UDMH
Major components	Tanks, insulation, heaters, pipes, controls, valves, support structure
Duration of mission	Short term for cryogenics, long term for storables
Types of spacecraft	Manned, unmanned, Earth orbiting, interplanetary
Status	
State of the art	Cryogenics used for Gemini, storables used for reaction control systems
Special problems	Insulation for long-term storage of cryogens
Subsystem Characteristics	
Range of specific mass	1 to 4.5 kg tank/kg reactant
Range of specific density	51 to 10,000 kg (tank)/m^3
Range of specific production cost	250 to 470 $/kg (reactant)
Range of reliability	0.99 to 0.9999 (up to 90-120 days)

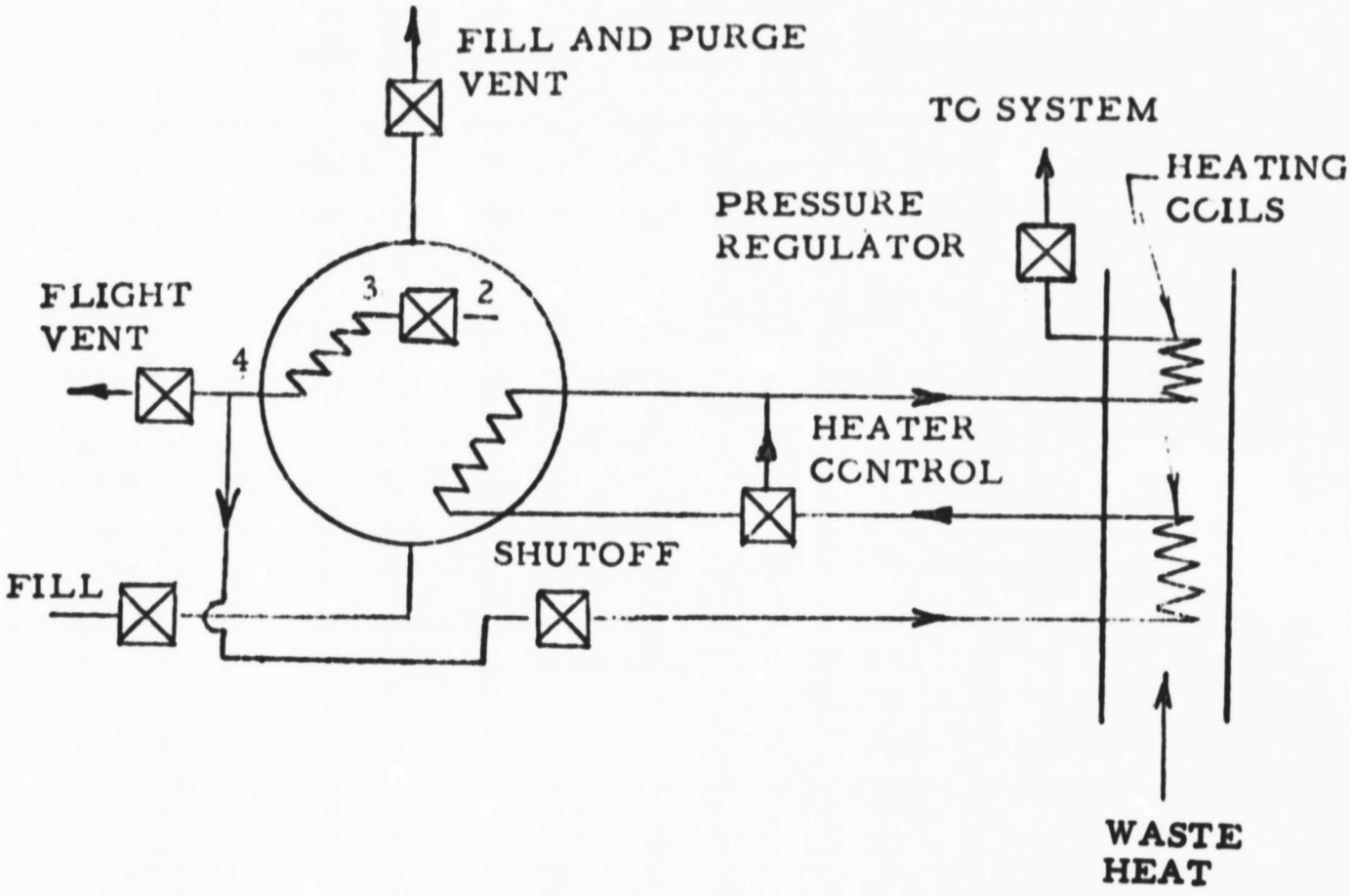

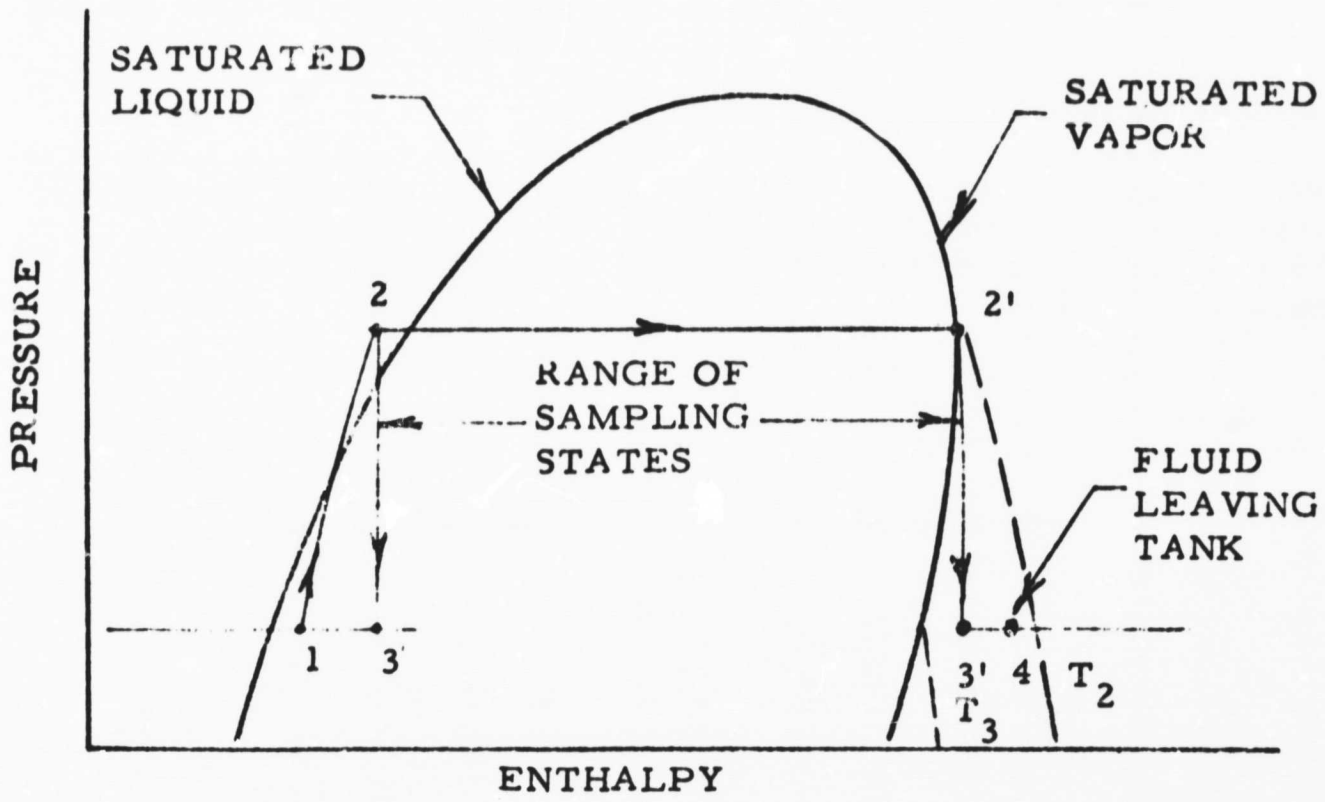

Figure 3-177a Two-Phase (Subcritical) Storage with Vapor Delivery

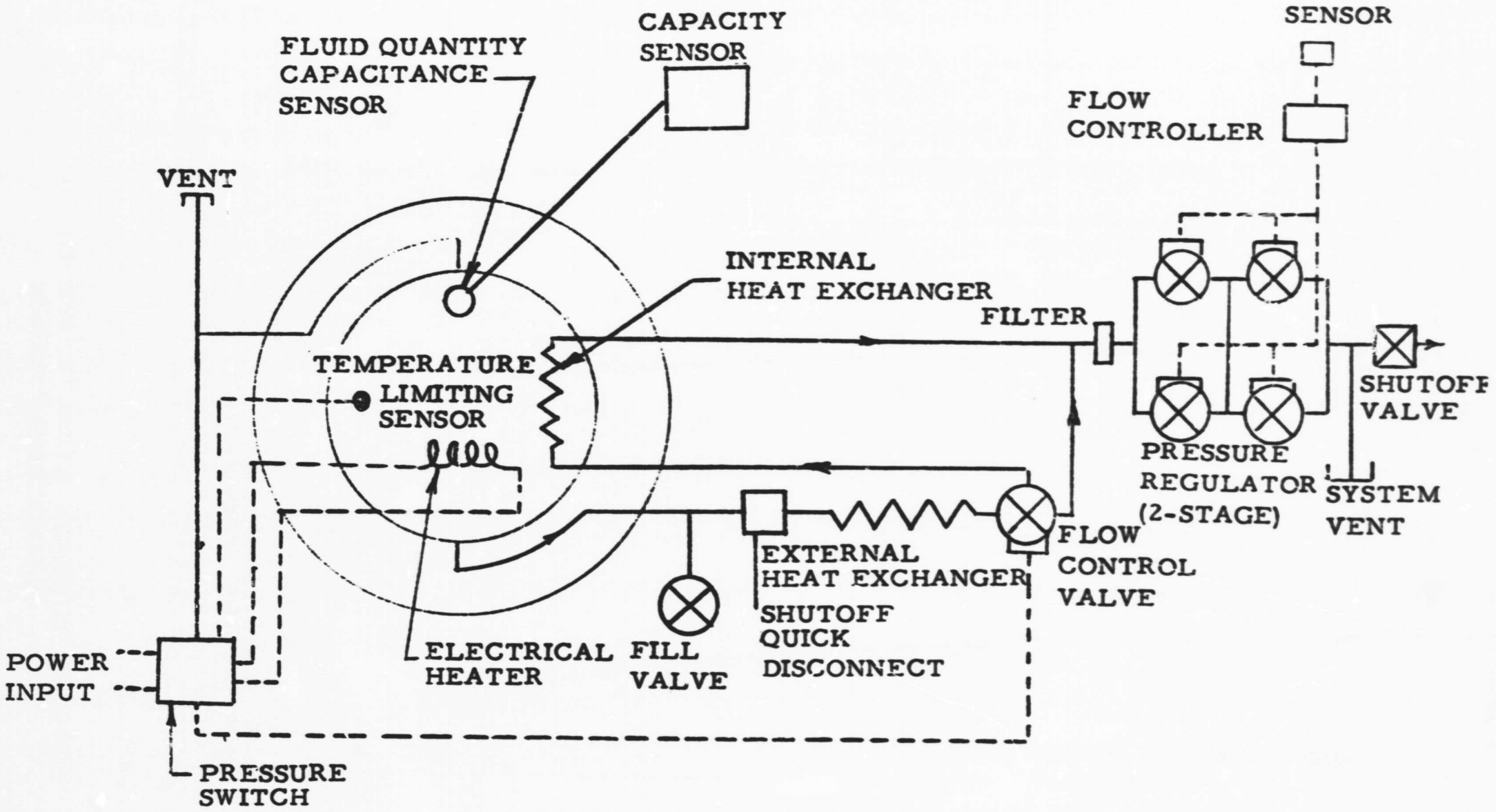

Figure 3-177b Supercritical Cryogenic Fluid Storage

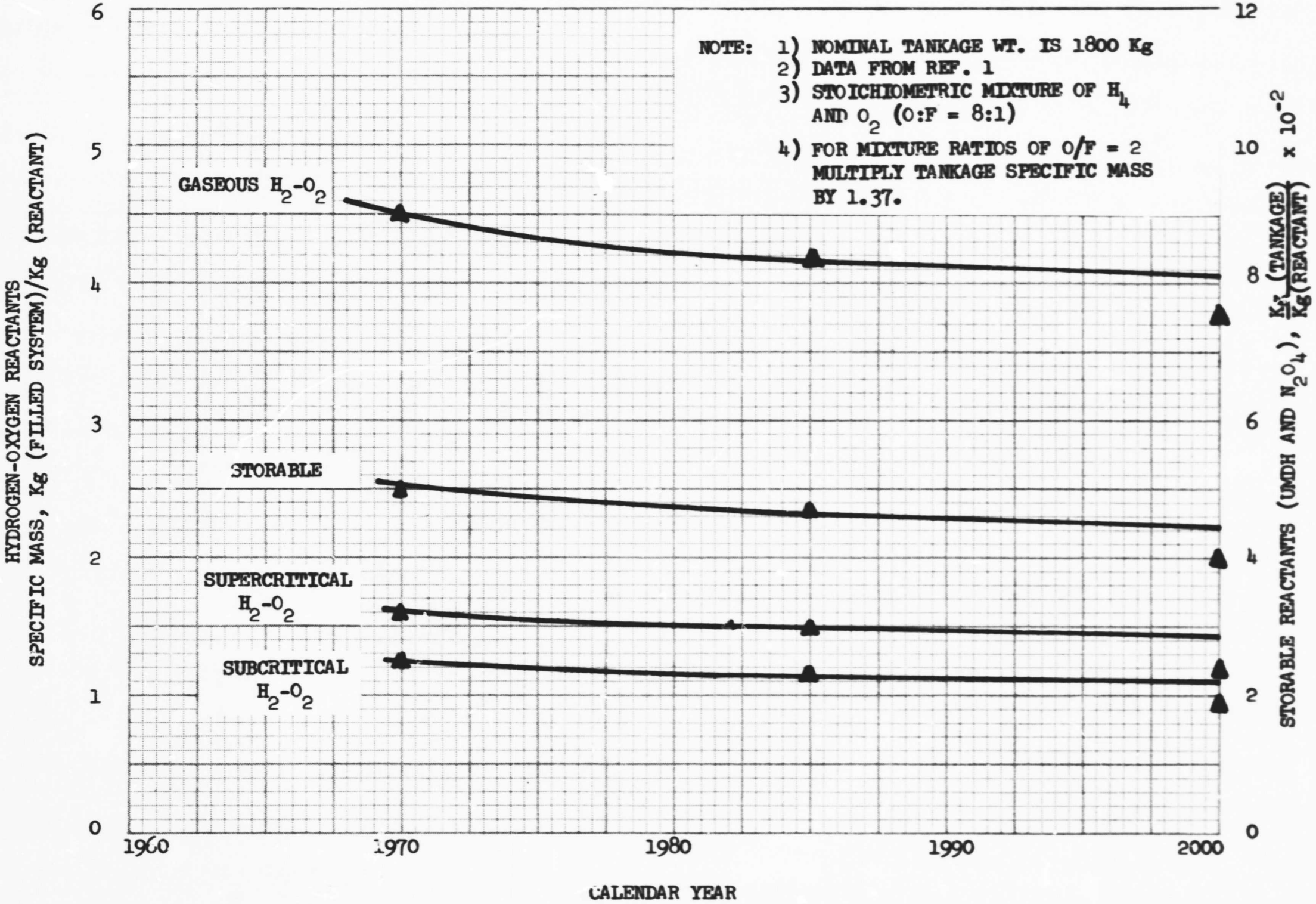

Figure 3-178 Specific Weight Reactant Supply

3.2.5.2 Storable Reactants Subsystems

Reactants can be stored as a gas or as a liquid and a typical high pressure gas storage subsystem is shown in Figure 3-179b. The gaseous storage results in a subsystem insensitive to zero-g effects, requires high pressure containers and constitutes the heaviest supply subsystem (Figure 3-178). Liquid storable reactants are those that do not evaporate, freeze, or otherwise deteriorate when exposed to normal environmental conditions. The reactant selected as representative of the liquid storables is nitrogen tetroxide (oxidizer) and aerozine 50 (fuel). Gaseous reactants considered are gaseous hydrogen and oxygen. The cost of the liquid storable reactant subsystem is given in Figure 3-179a.

Table 3-36 gives a definition of the reactants used for the study. Projected failure rate data for the reactant supply subsystem are shown in Figure 3-179c.

3.3 HEAT REJECTION SUBSYSTEMS

The heat rejection radiator subsystem rejects the power conversion subsystem waste heat to space. The single-phase radiator subsystem shown in Figure 3-180 consists of one or more radiators and tertiary loops. The radiator consists of the radiator tubes, fins, and armor material. The tertiary loop consists of the pump, plumping, expansion compensator, manifolds, and controls. The tertiary loop transports waste heat from the heat exchanger at the power conversion subsystem cold side to the radiator surface which radiates the heat to space. In the tertiary loop the expansion compensator absorbs coolant volume transients, the feed and return piping and manifolds deliver the coolant to the radiator tubes, the pump drives the fluid through the subsystem, and the controls regulate the flow in the loop.

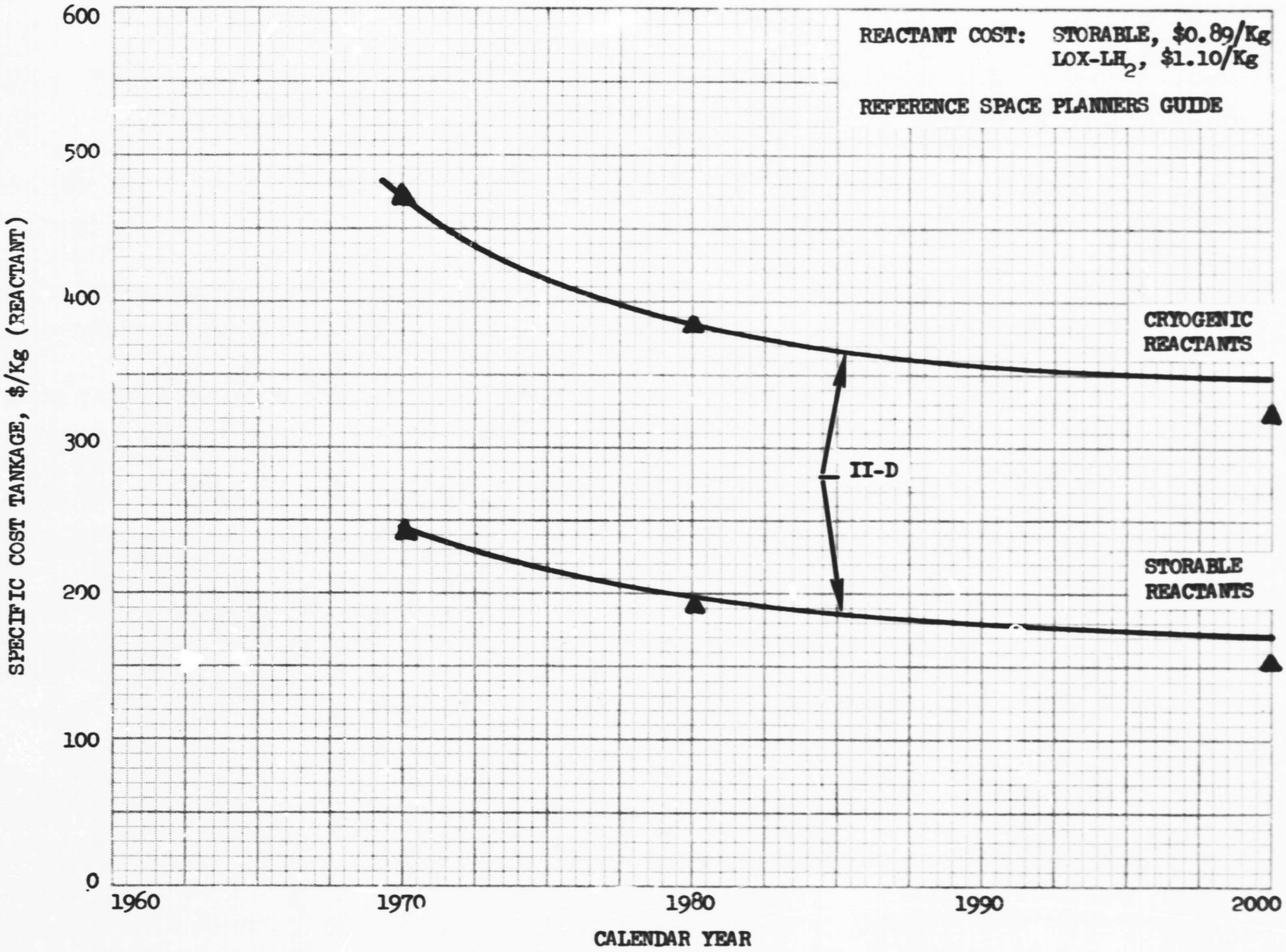

Figure 3-179a Cost of Reactant System Tankage

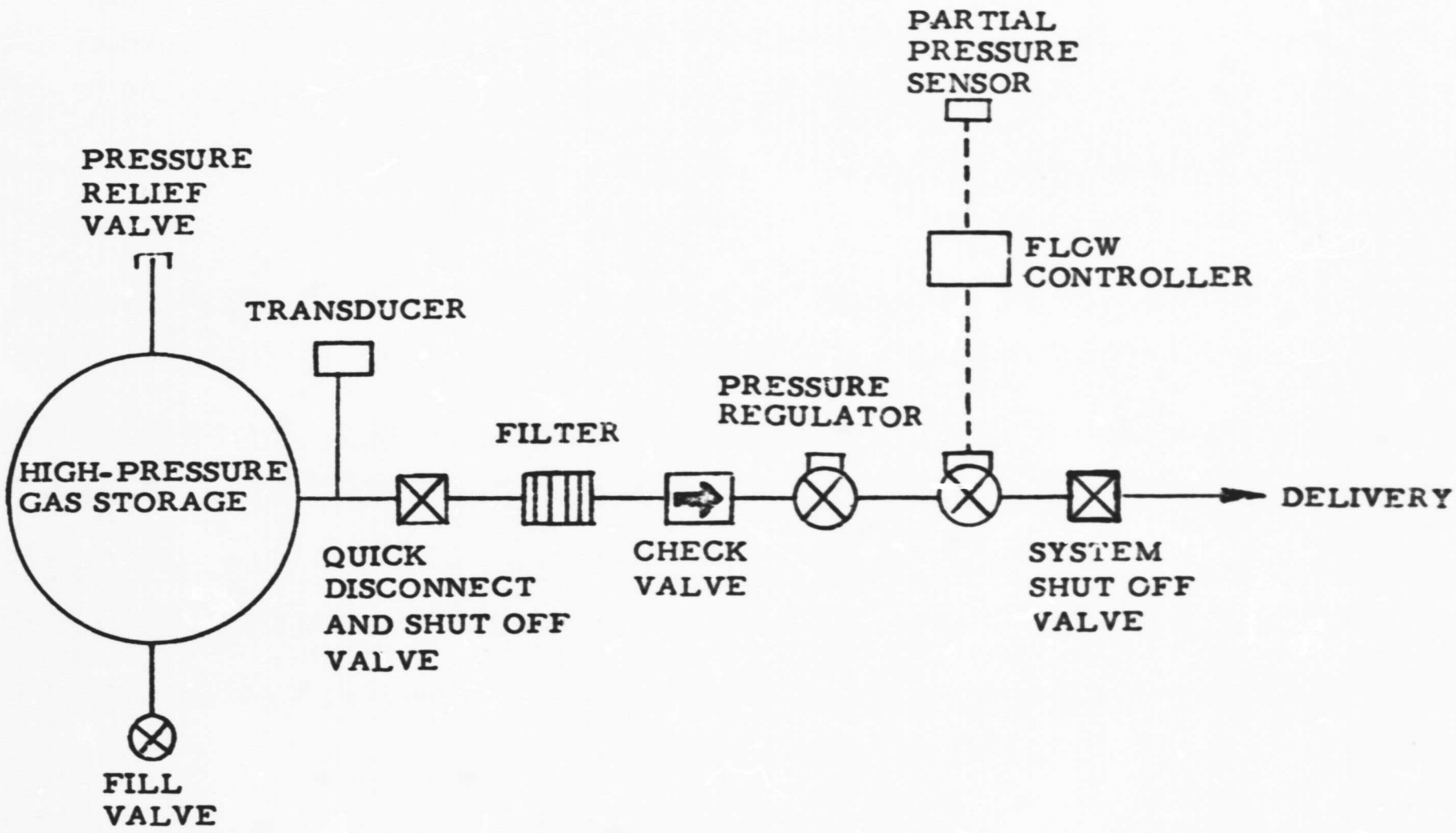

Figure 3-179b High-Pressure Gas Storage - Gas Supply Subsystem Diagram

Table 3-36
CHEMICAL PROPERTIES OF REACTANTS

Chemical	Formula	Specific Density
Aerozine 50% Hydrazine and 50% UDMH	----	0.8
Hydrazine	N_2H_4	0.998
UDMH	$(CH_3)_2N_2H_2$	0.786
Nitrogen tetroxide	N_2O_4	1.43
Liquid oxygen	O_2	1.14
Liquid hydrogen	H_2	0.0711

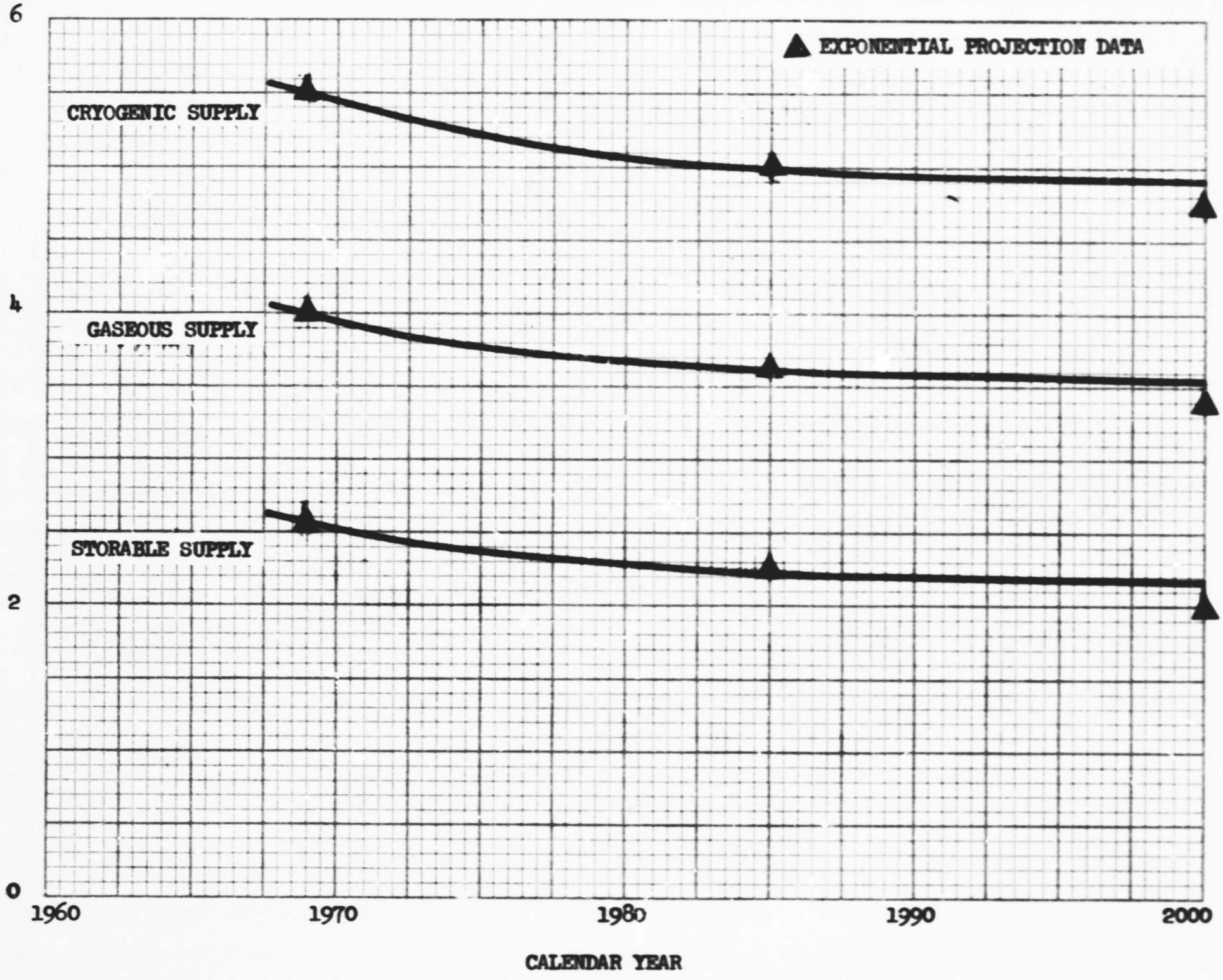

Figure 3-179c Projected Failure Rate for Reactant Supply Subsystems

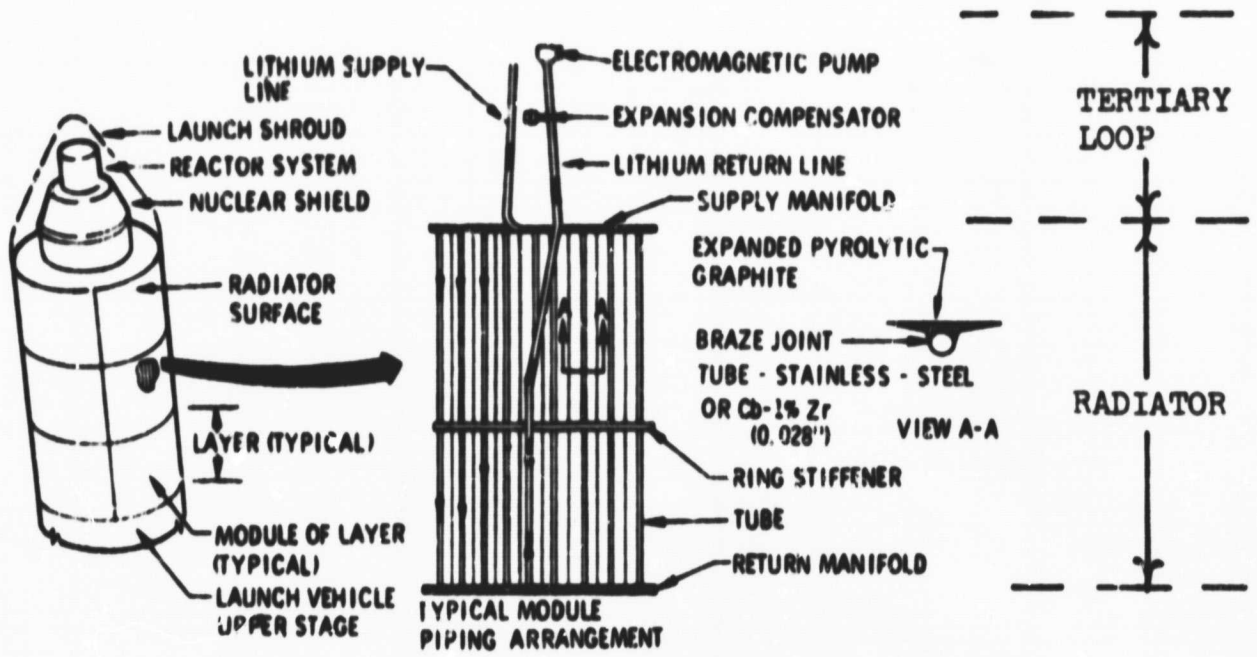

Figure 3-180 Single Phase and Condensing Radiator Configuration

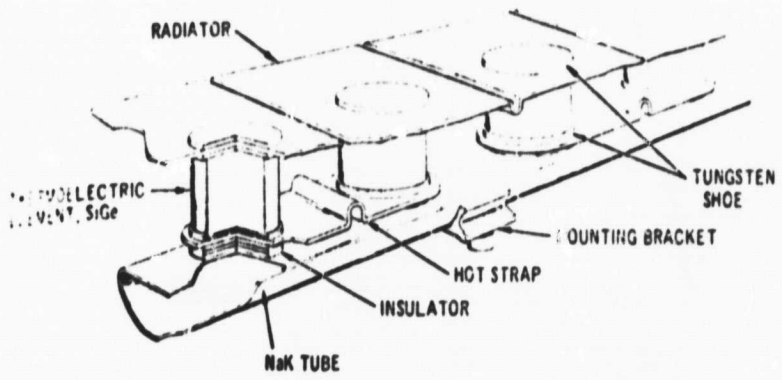

Figure 3-181 Typical Direct Radiating Radiator Configuration

The radiating surface may be a flat plate that rejects heat from both sides or may be a cylinder that can reject heat from only one side. The surface of the vehicle skin is sometimes used as the radiating surface and in this case the power system is not charged for this radiator area mass. The condensing radiator configuration is similar to the single-phase radiator with the exception that the conversion cycle working fluid flows directly through the radiator, thus eliminating the heat sink heat exchanger and the radiator pump. The direct-radiating radiator shown in Figure 3-181 consists of a plate or finned surface that conducts heat from the cold side of a thermionic or thermoelectric converter and rejects it directly to space.

All the radiators are designed to be installed within the cylindrical envelope of the top stage of the launch vehicle. The diameter of the cylinder of the surface and the width of the flat plate radiator is equal to that of the top stage of the booster.

An expanded view of the armored tube designed is also shown in Figure 3-180. The armor fin material must possess good thermal conductivity properties, good resistance to meteoroid penetration, and light weight.

In the direct-radiating module, the thermoelectric or thermionic converter is integral with the radiator tube. Each converter has essentially its own radiator, consisting of platelet finned surfaces.

Both the single-phase and condensing radiators require armor plating to protect the vulnerable areas around the coolant tubes which if punctured by a meteoroid would cause the loss of coolant and subsequent failure of the heat rejection capacity of that coolant loop. The relative armor effectiveness of candidate armor materials is shown in Table 3-37. The merit factor is defined as the armor density times the relative armor thickness and is proportional to armor mass, since thickness is proportional to volume. The armor merit factor shows that expanded pyrolytic graphite is superior at high radiator temperatures. Typical design examples of radiator mass-to-area ratios for power levels of 1,000 to 3,000 kWt are shown in Figure 3-182. The aluminum type radiator is favored below 700°K. The expanded graphite radiators are superior to niobium radiators at temperatures greater than 700°K.

Table 3-37

CANDIDATE RADIATOR ARMOR MATERIAL PROPERTIES (ROOM TEMPERATURE)

Material	Maximum Temperature Capability (°K)	Density (g/cc)	Cratering Coefficient	Dimple Factor	Relative Armor Thickness	Merit Factor	Reference
316 stainless steel	920	7.8	1.9	1.9	1.0	7.8	1
Beryllium	970	1.81	2.28	1.75	1.19	2.16	1
Pyrolytic graphite	1,500	2.12	2.41	1.75	1.62	3.44	1
Expanded pyrolytic graphite	1,500	0.625	1.8	0.5	1.36	0.84	2
Aluminum	1,500	2.7	2.0	1.75	1.57	4.25	3
Niobium	600	8.4	2.0	1.75	1.1	9.25	3

*Merit Factor = Density x Relative Armor Thickness

Table 3-38

HEAT REJECTION SUBSYSTEMS BRIEFING CHART

(Direct radiation, single-phase convective loop, condensing loop)

Identification	
Applicable power conversion systems	Thermionic, thermoelectric, Rankine, Brayton, fuel cell
Major components	Fin-armored-tube module, feed and return piping, pump
	Coolant expansion compensator
Vehicle--mission application range	
Useful power level	Watts to megawatts, thermal
Duration of mission	Short to greater than 10 years
Types of spacecraft	Manned, unmanned, Earth orbiting, interplanetary
Status	
State of the art	Fin armor materials available to a temperature of 1,200°K
Availability of support subsystems	Canned rotor and EM pump development lags other radiator components
Special problems	Coolant containment, two-phase flow stability
Subsystem Characteristics	
Range of specific weight	0.5 to 10 kg/kWt
Range of specific area	0.1 to 1.0 m^2/kWt (temperature dependent)
Range of specific production cost	150 to 250 $/kg
Range of reliability	0.9 to 0.9999 for up to 5 years
Range of temperatures	400° to 1,200°K

The fin-armor-tube weights are dependent on specific design constraints, such as mission duration, reliability, temperature, and power level; therefore, each design must be computed independently within the heat rejection computer subroutine. Figure 3-182 serves only as a guide in the selection of the radiator materials.

The heat rejection subsystem status, characteristics, and range of performance data are presented in Table 3-38. Parametric data for radiator loop canned rotor and electromagnetic pump mass are shown in Figures 3-183 and 3-184. Failure rate data for the radiator loop components are given in Table 3-39. The radiator specific cost in dollars for each kilogram is shown in Figure 3-185.

Table 3-39

SUMMARY OF HEAT REJECTION SUBSYSTEM COMPONENT FAILURE RATE DATA (Reference 4)

Component	Failure Rate	Comment
Piping		
Weld failure	10^{-9}/hr-weld	After process development
Rupture		Design for 0.1 of failure rate due to welding
Pump	10^{-2} to 10^{-3}/year	
Expansion conpensator	10^{-3} to 10^{-5}/year	Based on weld failure
Radiator armored finned-tube	--	Proportional to mission duration, vulnerable area meteoroid flux, and armor thickness

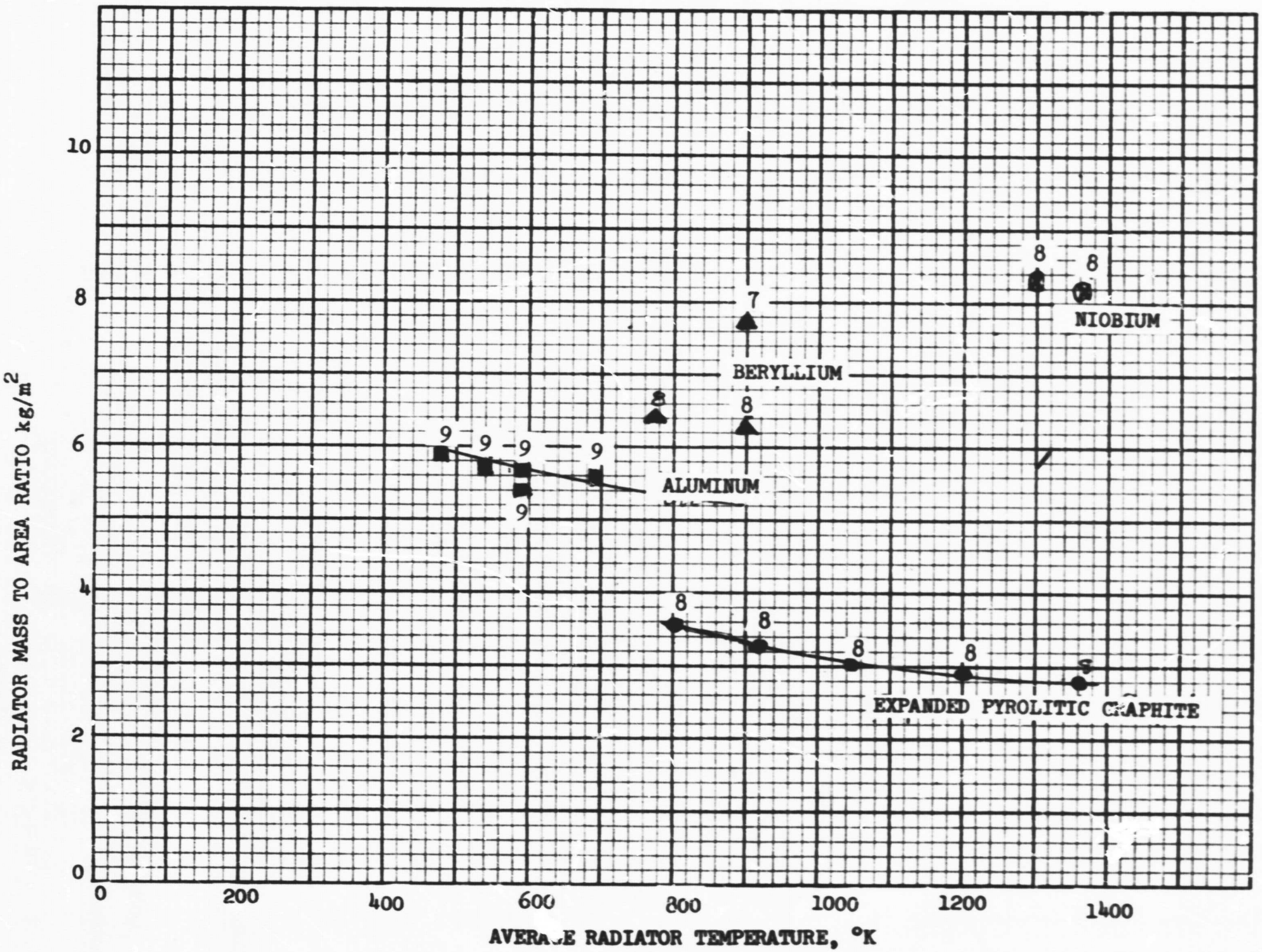

Figure 3-182 **Typical Radiator Mass To Area Ratios (Armored Tube - Fin Module Only)**

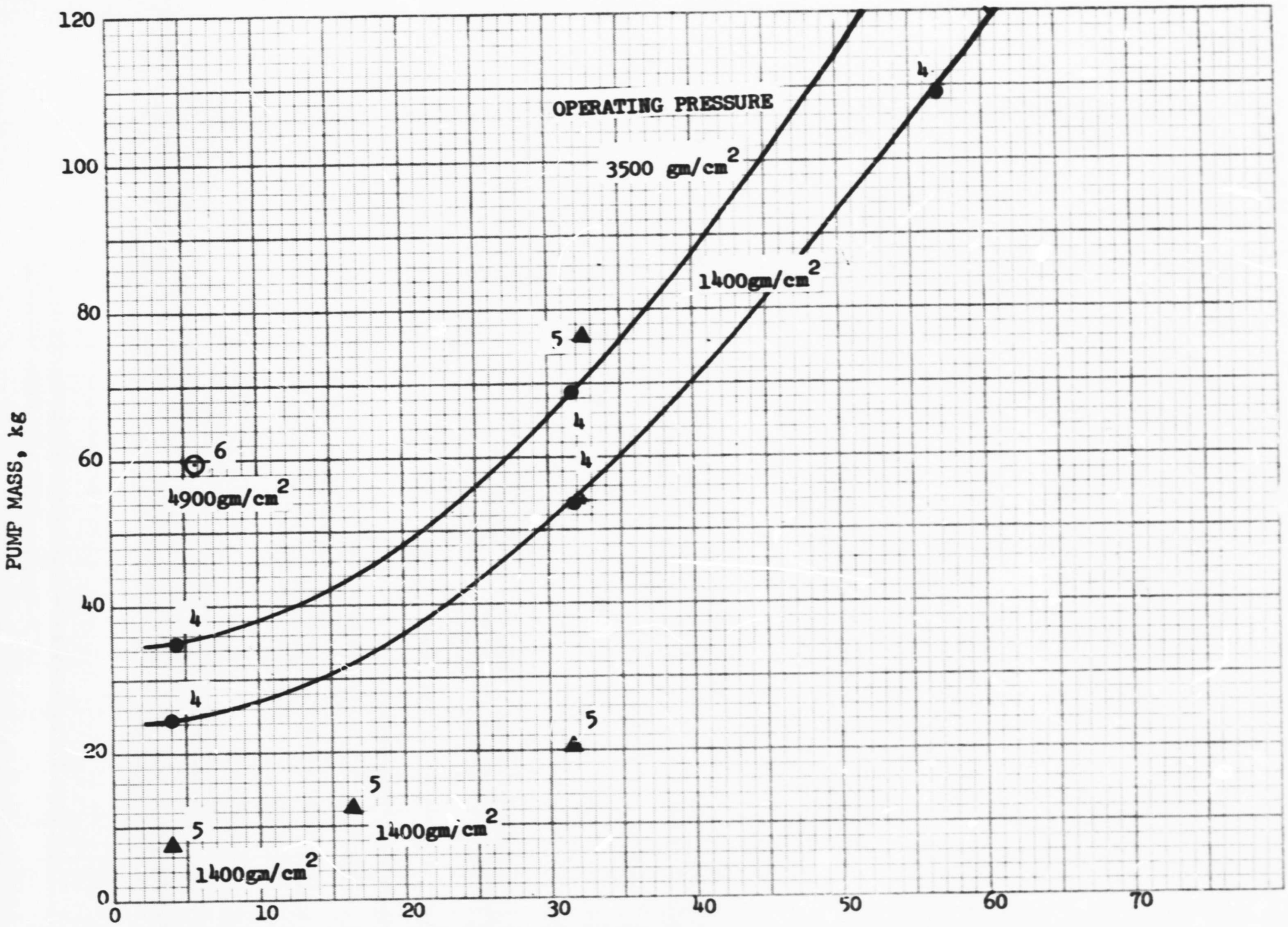

Figure 3-183 Canned Rotor Pump Mass (Lithium Coolant Conditions)

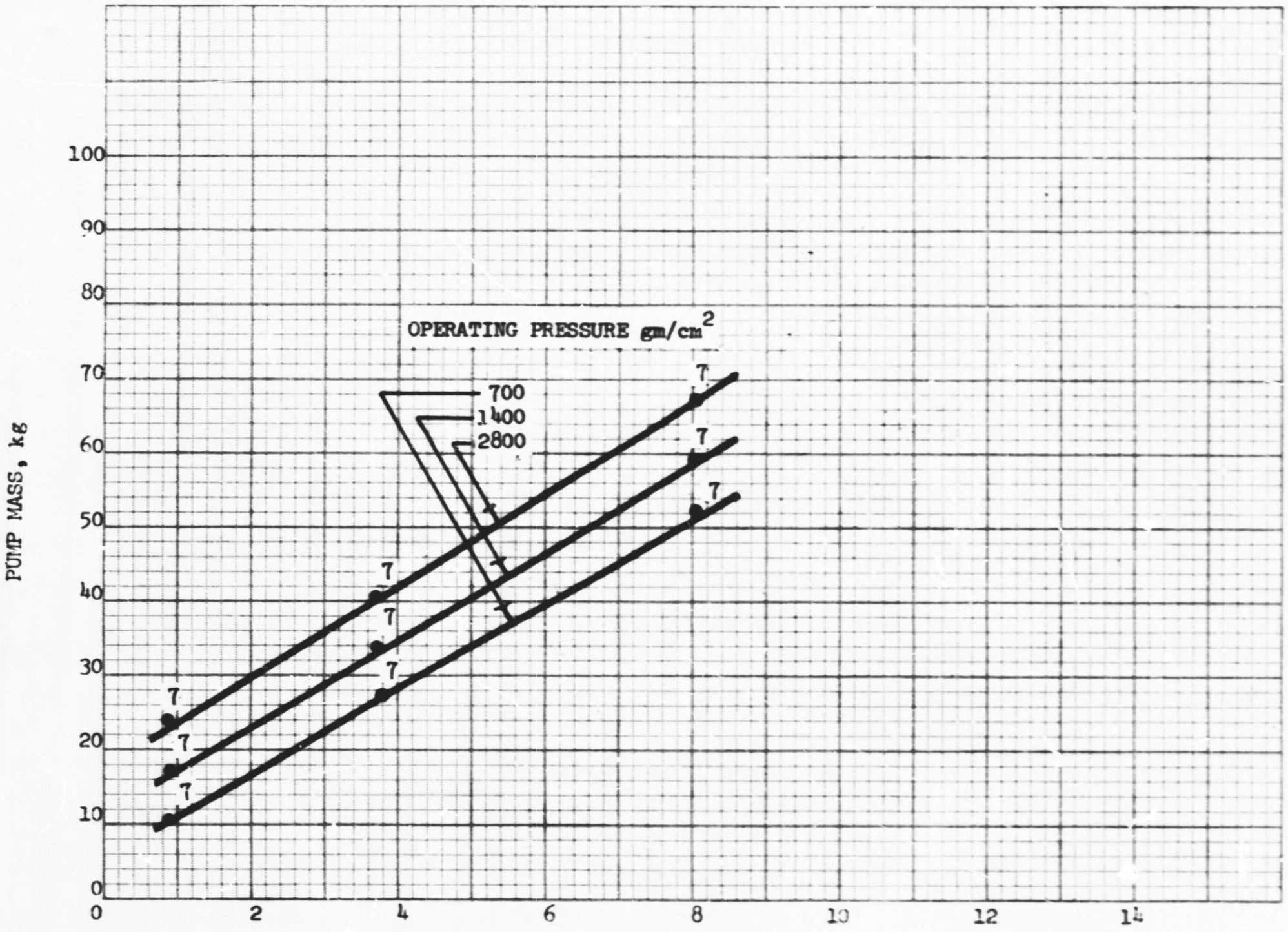

Figure 3-184 Electromagnetic Pump Mass (AC Induction,

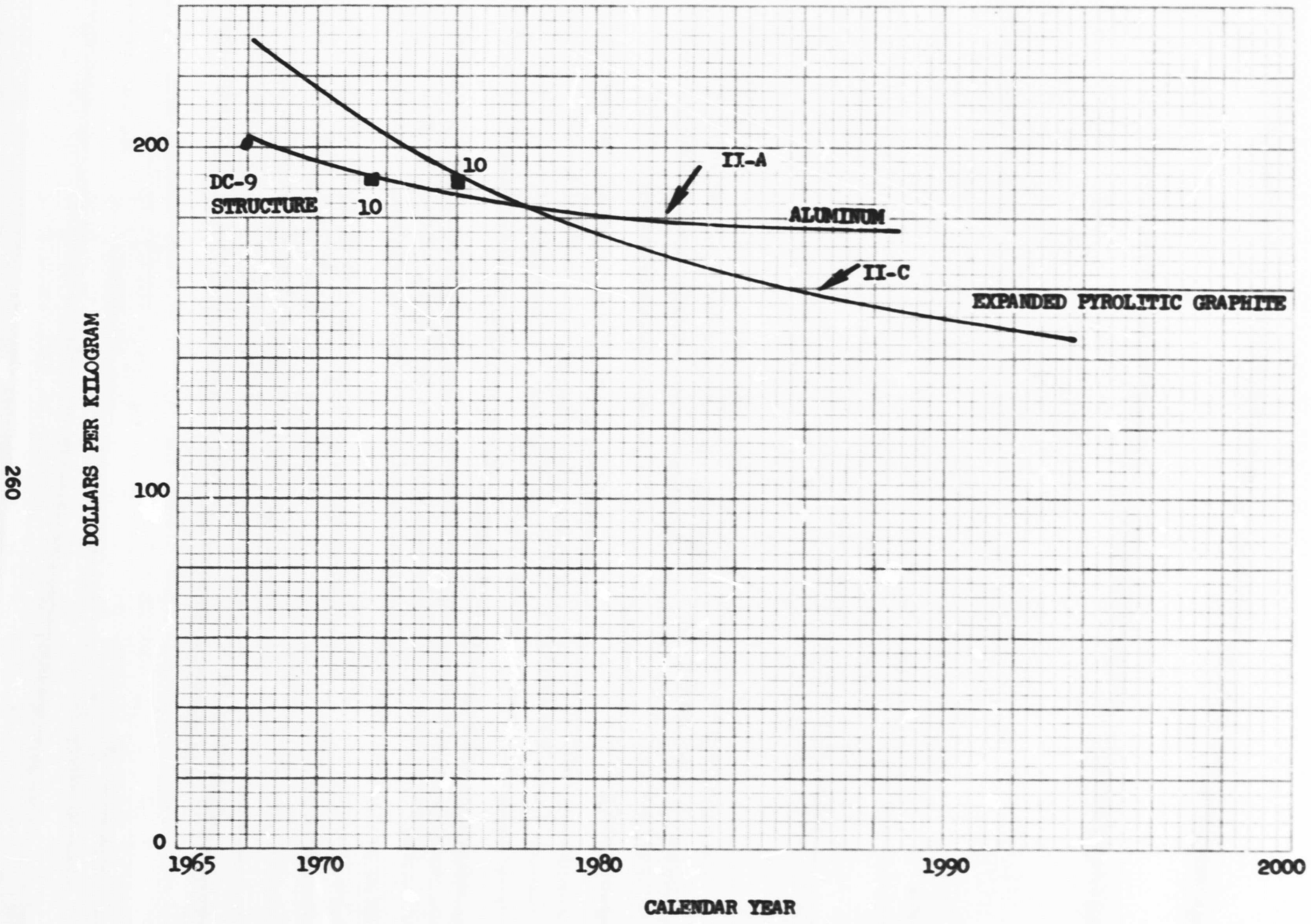

Figure 3-185 Trends in Radiator Structure Production Costs

3.4 POWER CONDITIONING SUBSYSTEMS

The power conditioning subsystem is composed of modules that must condition, convert, and regulate power from the conversion subsystem with minimum loss and maximum reliability to meet the requirements of user subsystems. The design requirements for each of the power conditioning modules must be integrated with all related modules to assure optimum performance at all load demand levels. Schematic diagrams of typical power conditioning subsystems for both ac and dc power sources are shown in Figures 3-186 and 3-187. The physical and operating characteristics of the power conditioning modules are shown in Figures 3-188 through 3-198. The mass, density, efficiency, mean time before failure, and development and production costs can be calculated for each of the power conditioning modules with the parametric information in the figures. Some basic facts concerning the power conditioning subsystem modules are shown in the briefing charts (Tables 3-40 and 3-41).

Table 3-40

POWER CONDITIONING COMPONENTS BRIEFING CHART

Component (1 kW) and Year	Specific Mass (kg/kWe)	Density (kg/m^3)	Efficiency (%)	Mean Time Before Failure (hours)	Specific Cost (k$/kWe)
DC voltage converter and regulator					
1965	13.5	900	85	5×10^5	20
1985	9.4	1,470	89	8×10^5	15.5
DC-AC inverter and regulator					
1965	13.5	900	85	5×10^5	20
1985	9.4	1,470	89	8×10^5	15.5
Transformer					
1965	1.8	2,500	97	10^6	1.0
1985	1.0	2,500	97	10^6	1.0
Rectifier and regulator					
1965	13.5	900	85	5×10^5	20
1985	9.4	1,470	89	8×10^5	15.5

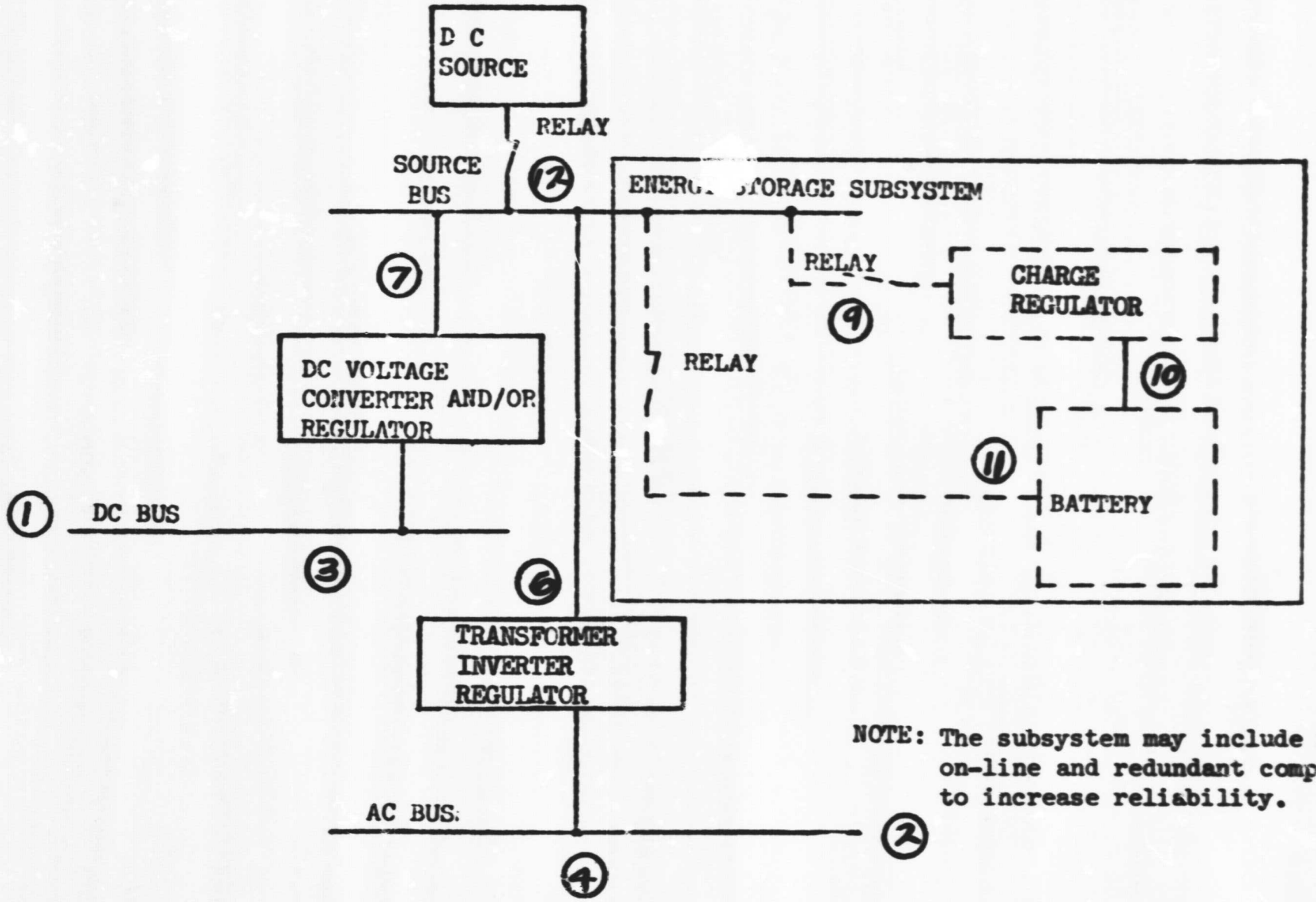

NOTE: The subsystem may include multiple on-line and redundant components to increase reliability.

Figure 3-186 Power Conditioning Subsystem for DC Source

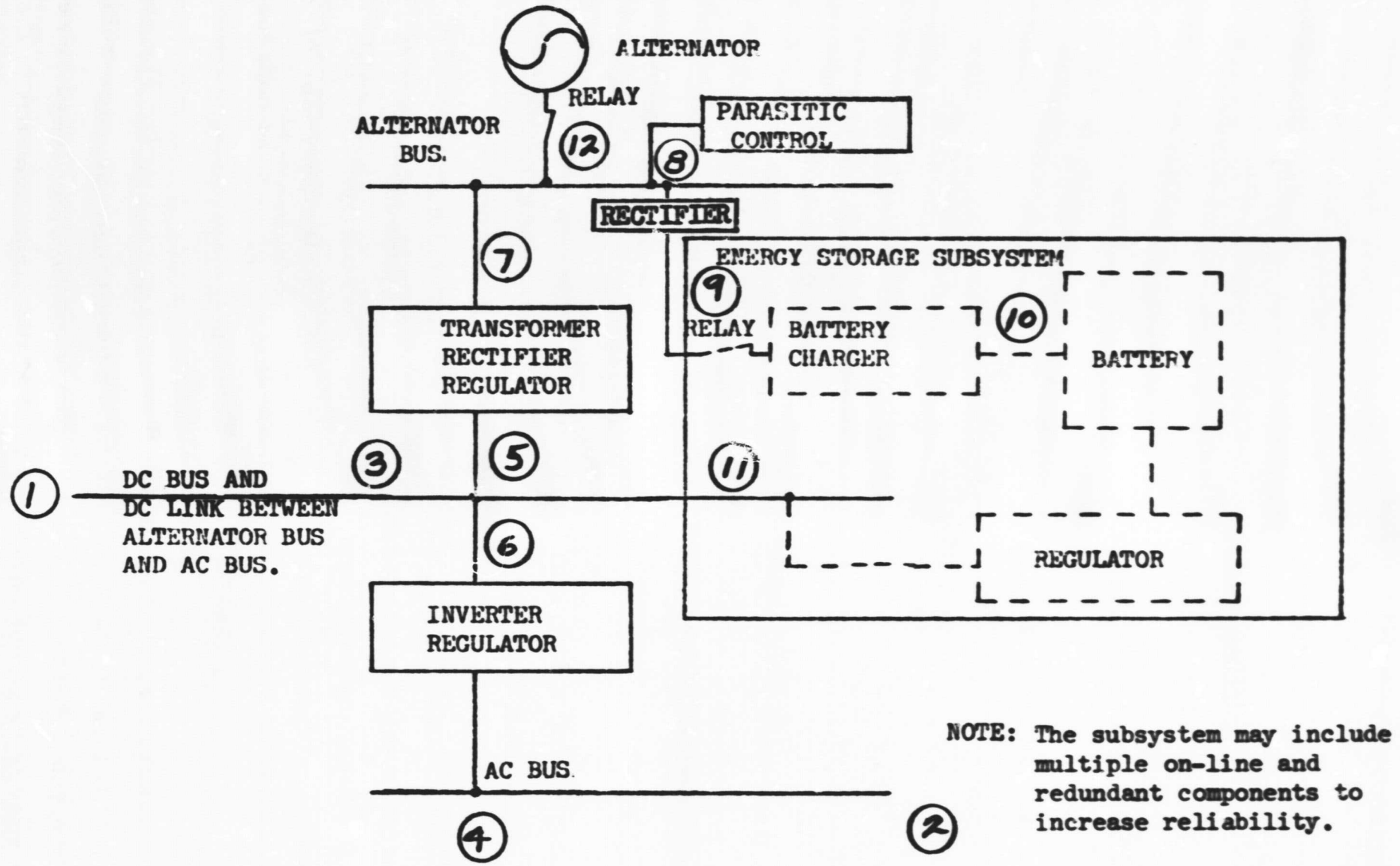

Figure 3-187 Power Conditioning Subsystem for AC Source

Table 3-41

POWER CONDITIONING SUBSYSTEMS BRIEFING CHART

Item	Value
Identification	
Power conditioning cooling subsystem	Convective loop, heat pipe
Major components	Transformers, rectifiers, regulators, inverters, switches
Vehicle – mission application range	All vehicles – all missions
Useful power level	All levels
Duration of mission	Hours to years
Types of spacecraft	Manned, unmanned, Earth orbiting, interplanetary
Status	
Special problems	
Subsystem Characteristics	
Range of specific weight	2.0 to 50 kg/kW
Range of specific volume	0.01 to 0.2 m^3/kW
Range of specific production cost	10,000 to 100,000 $/kW
Range of reliability	0.85 to 0.999% (one year)
Performance Data	
Operating temperature range	Up to 473 °K
Operating efficiency range	50% to 99%

The power conditioning subsystem for a power conversion subsystem with a dc source is shown in Figure 3-186. The energy storage subsystem is closely related to the power conditioning subsystem and is shown on the figure for clarity. The dc-dc voltage converter is omitted if the voltage at the source bus always exceeds the requirements of the dc bus by a sufficient difference. During normal operating conditions, the battery charger operates as a load on the source bus. When the battery supplies energy, the positions of the relays are reversed so that the battery feeds the source bus through the regulator.

The ac power conditioning subsystem is shown in Figure 3-187. The energy storage subsystem is also shown in this figure because of the inter-relationship between the two subsystems. The alternator output is conditioned by rectifying all of the energy to direct current. Part of the direct current is then inverted to supply the alternating current bus. This method (called a dc link)

has been investigated in detail, compared to other types of subsystems, and recommended for use in the MORL space vehicle (Reference 5). The dc link will be used in the ac power conditioning subsystem and has the advantage of permitting the alternator to operate over a wide range of speeds while still supplying power to the ac bus at a constant frequency.

Projections of the specific mass of inverter modules and dc voltage converter modules are shown in Figures 3-188 and 3-189. The projections are shown for maximum power levels of 400 W, 1 kW, and 100 kW. An allowance for the mass of a voltage regulator has been added to the specific mass estimates of the dc voltage converter and the inverter modules. The corresponding values of efficiency, cost, and mean time before failure for the modules are shown in Figures 3-190 through 3-193. The density of the inverter and dc voltage converter module is shown in Figure 3-194.

Projections of specific mass for 0.3-kVA, 10-kVA, and 100-kVA transformers for 400-Hz operation are shown in Figure 3-195. The efficiency and frequency are major input parameters in the design of a transformer. The data shown in Figure 3-195 are for transformers with efficiencies of 97%. A correction factor for conversion from 400 Hz to other frequencies is given in Figure 3-196. The density of the packaged transformer is 2,500 kg/m^3. A typical mean time before failure for transformers is 10^6 hours. A typical installed transformer cost is 1.0 k$/kW.

Estimates of future values for the specific mass of rectifier-regulators are given in Figure 3-197. Cost, failure, and density data for these components are presented in Figures 9-192 through 3-194. The efficiency is given in Figure 3-198.

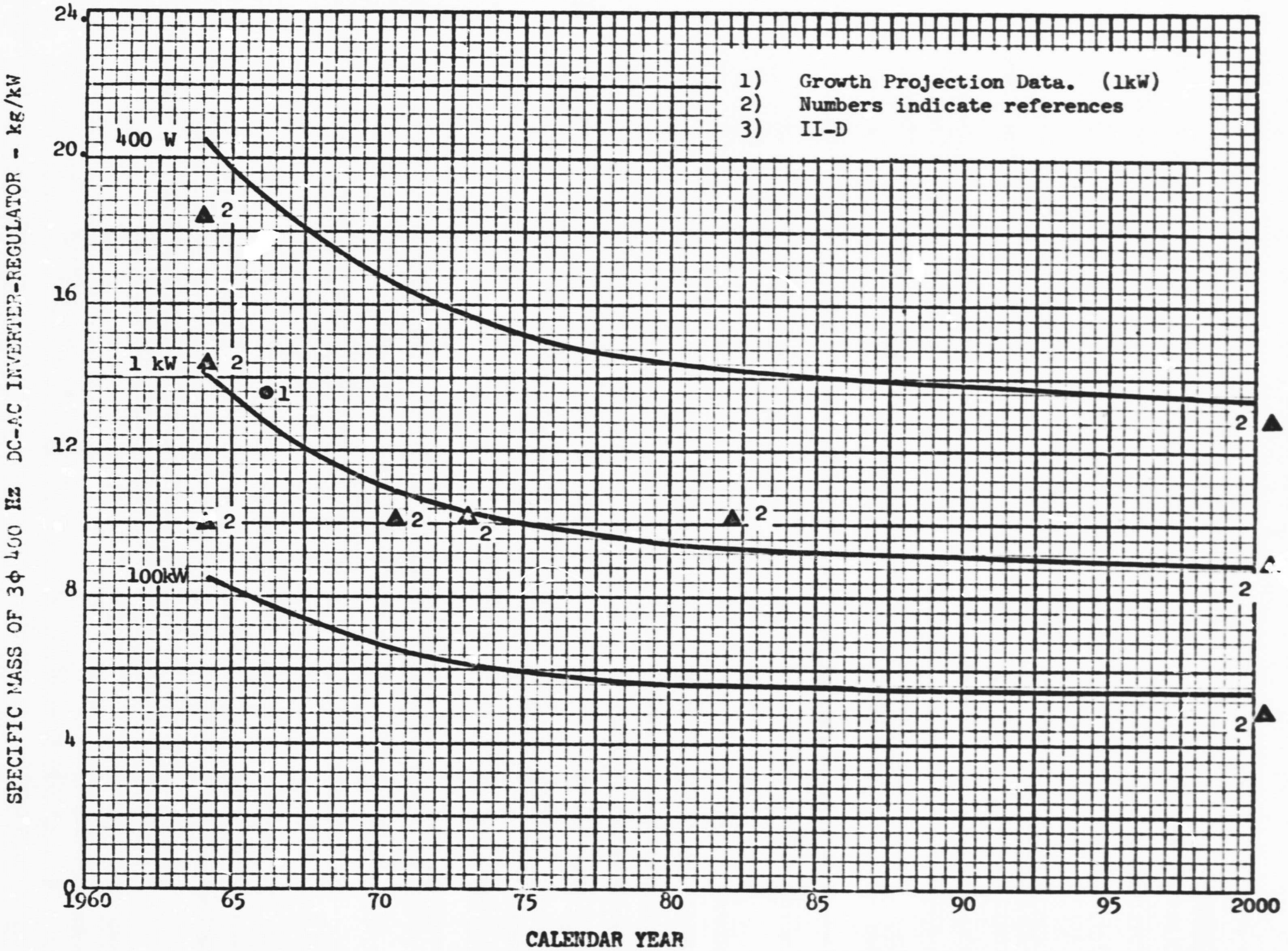

Figure 3-188. Projection of DC - AC Inverter Specific Mass

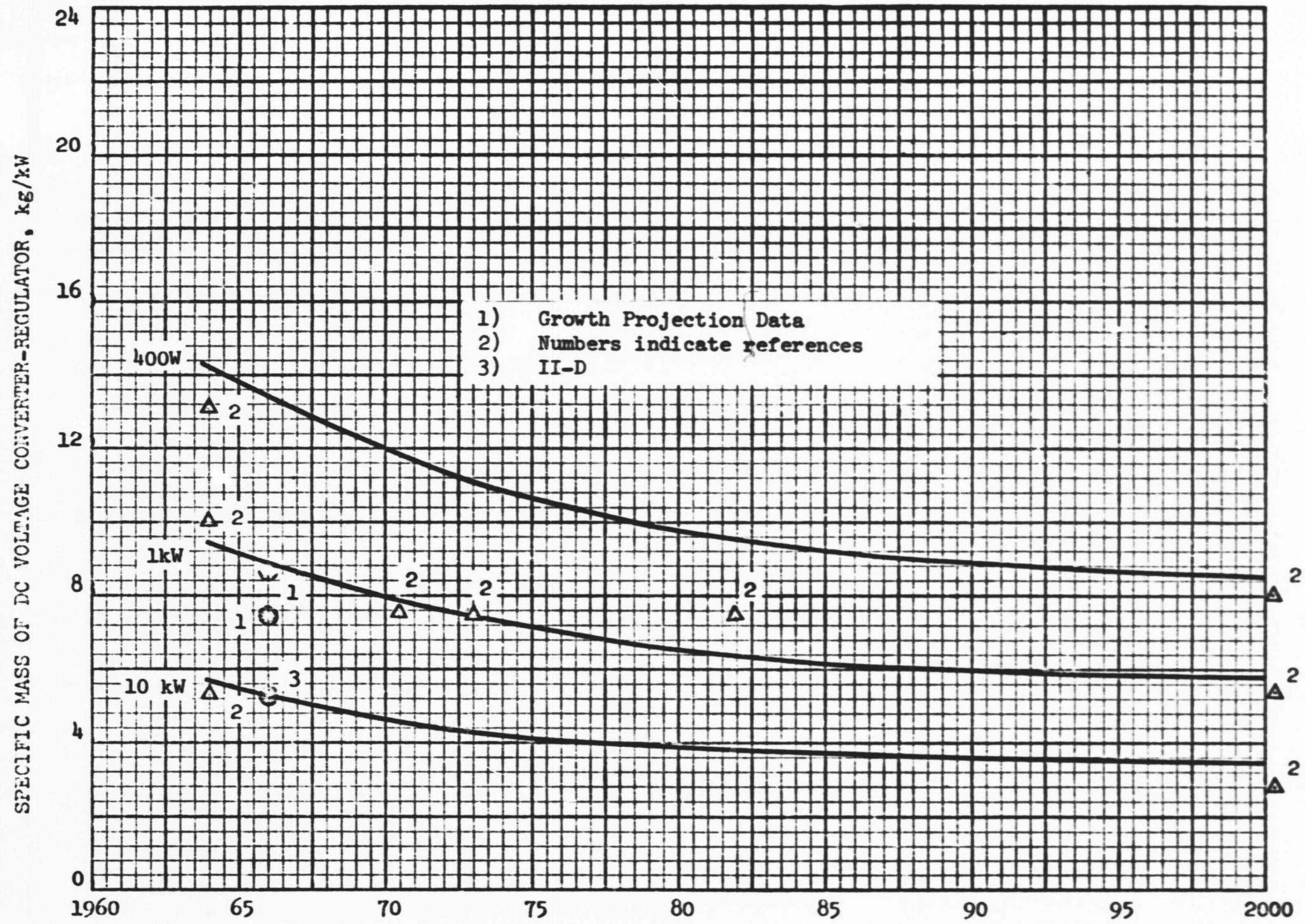

Figure 3-189 Projection of DC Voltage Converter Specific Mass

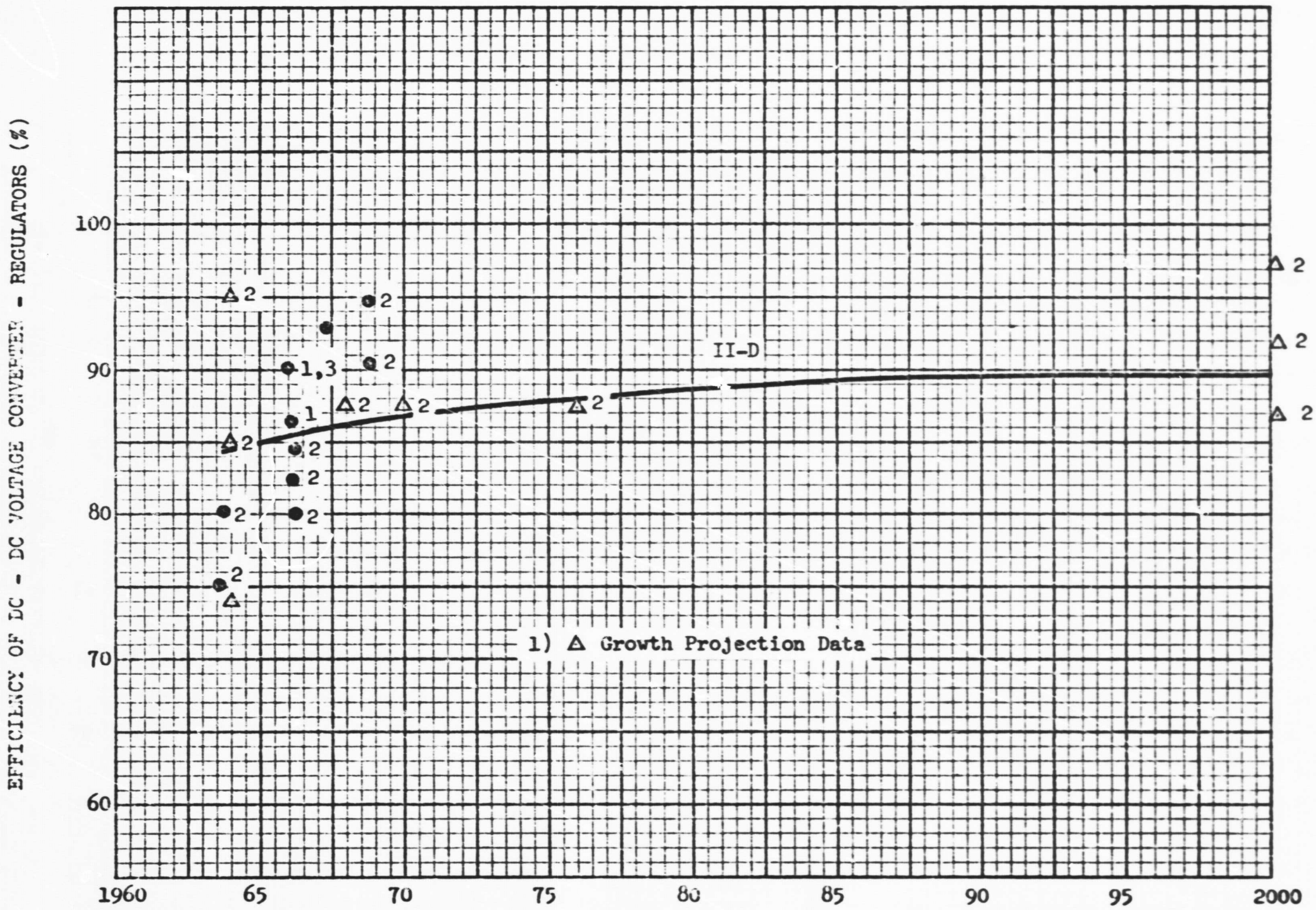

Figure 3-190 Projection of Efficiency of DC Voltage Converters

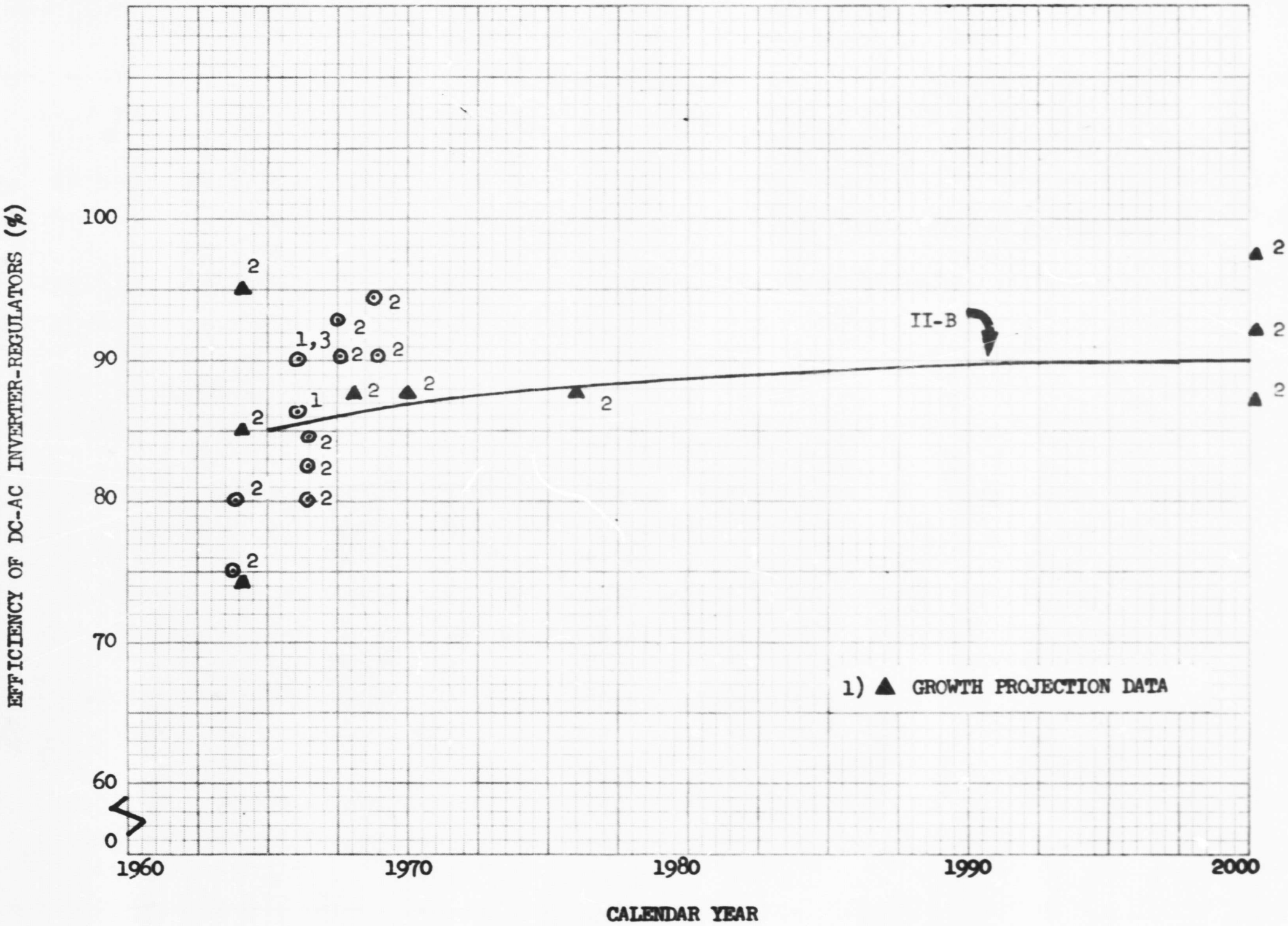

Figure 3-191 Projection of Efficiency of DC-AC Inverters

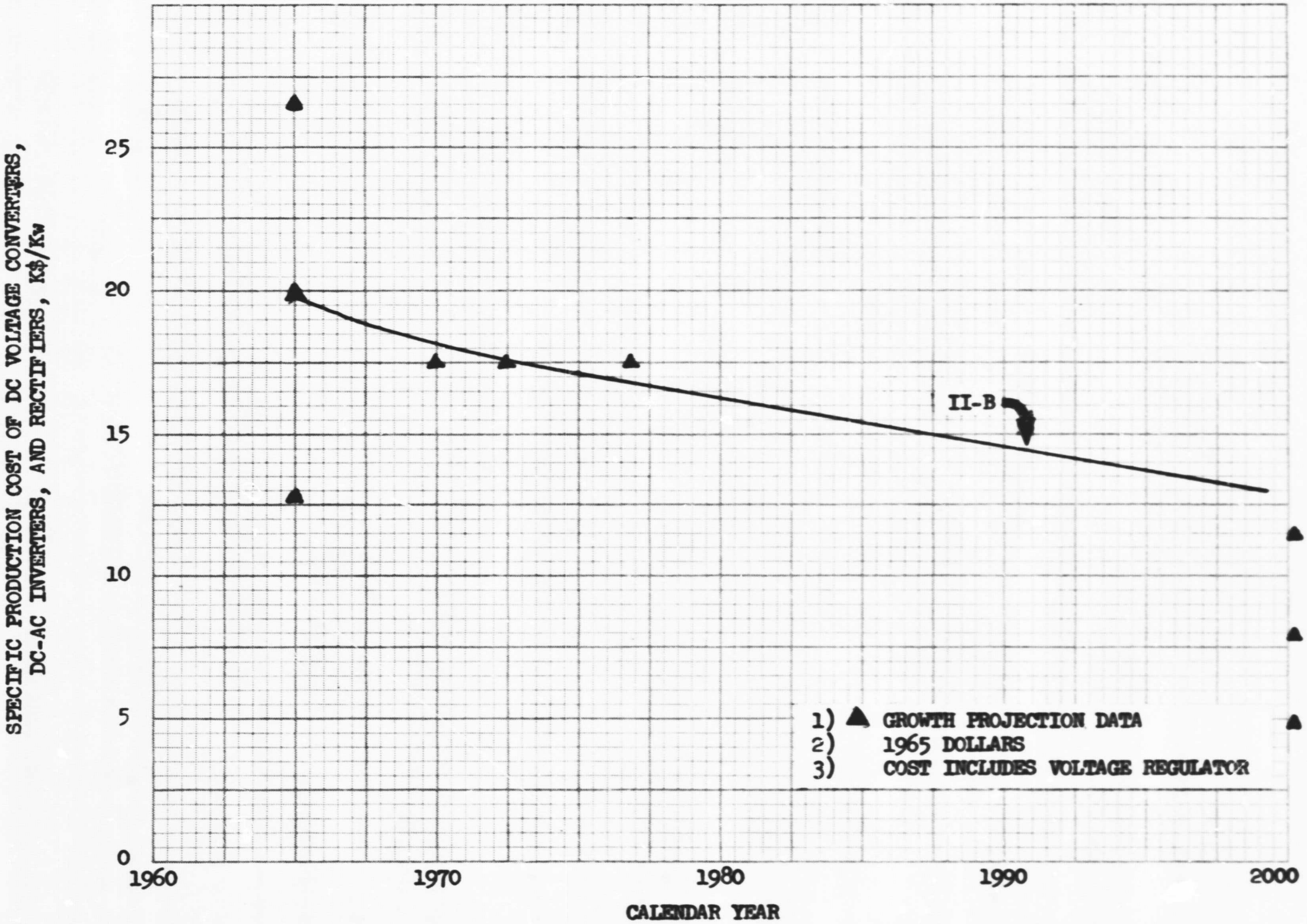

Figure 3-192 Projection of Power Conditioning Equipment Production Costs

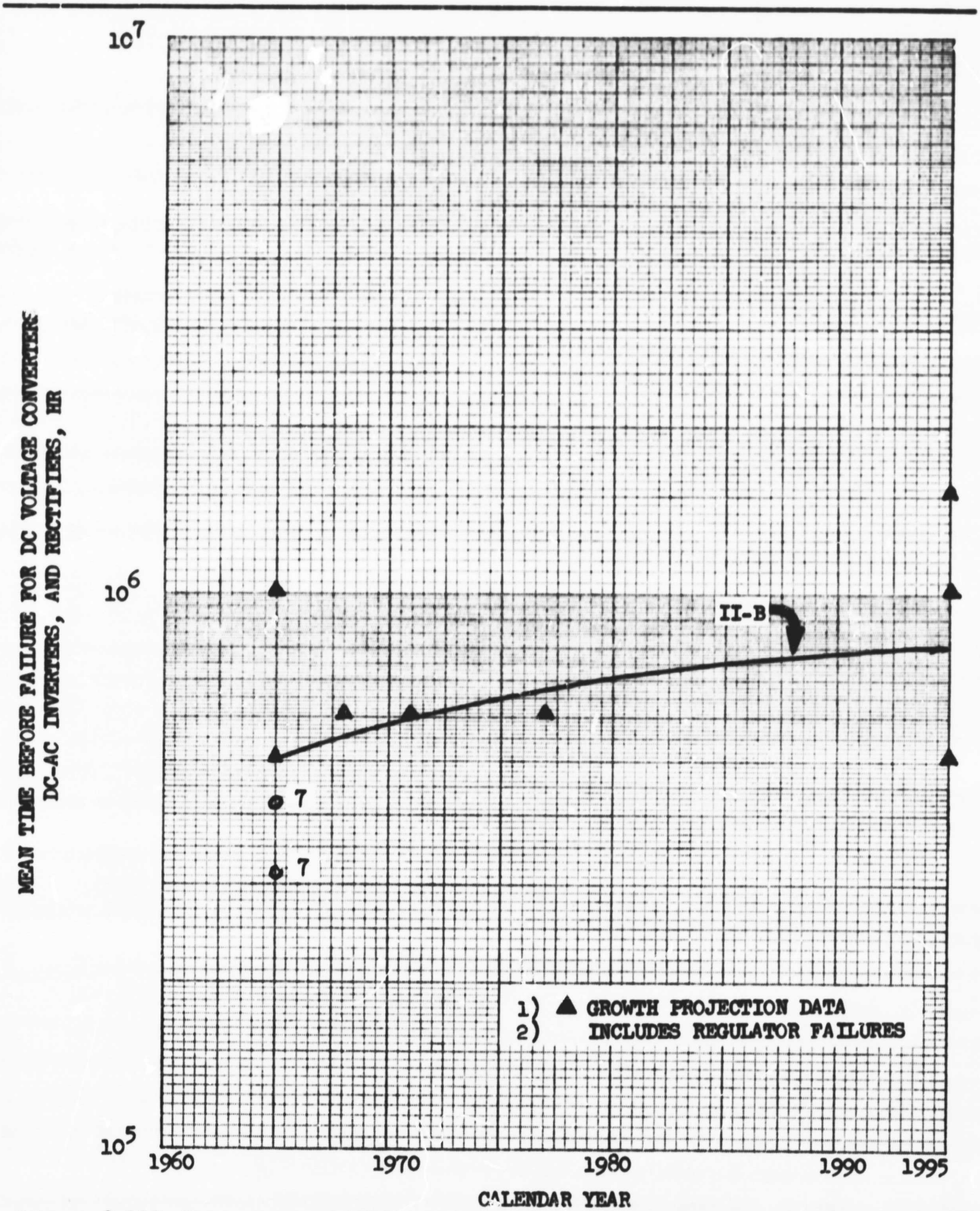

Figure 3-193 Projection of MTBF for Power Conditioning Equipment

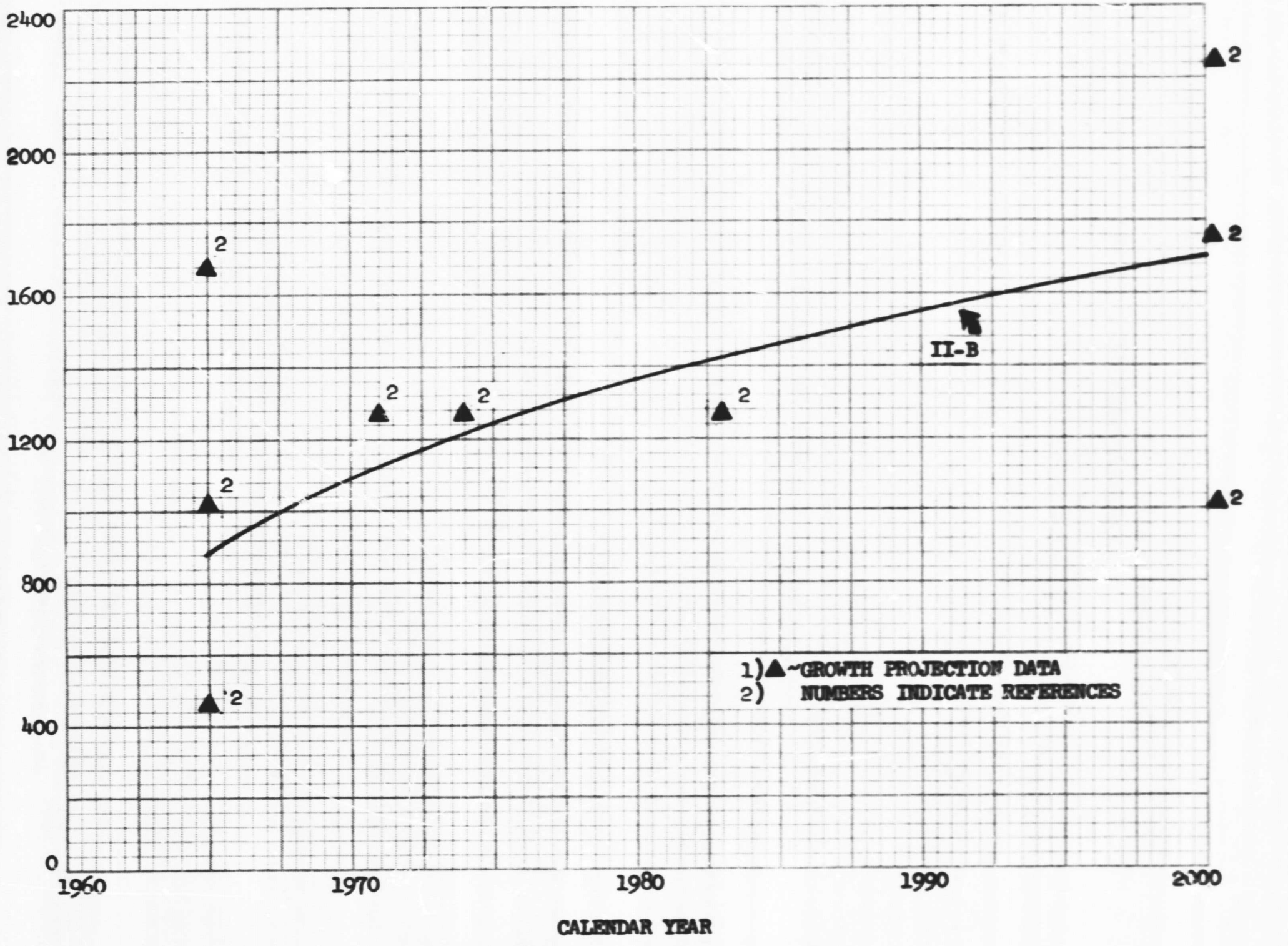

Figure 3-194 Projection of Density of Power Conditioning Equipment

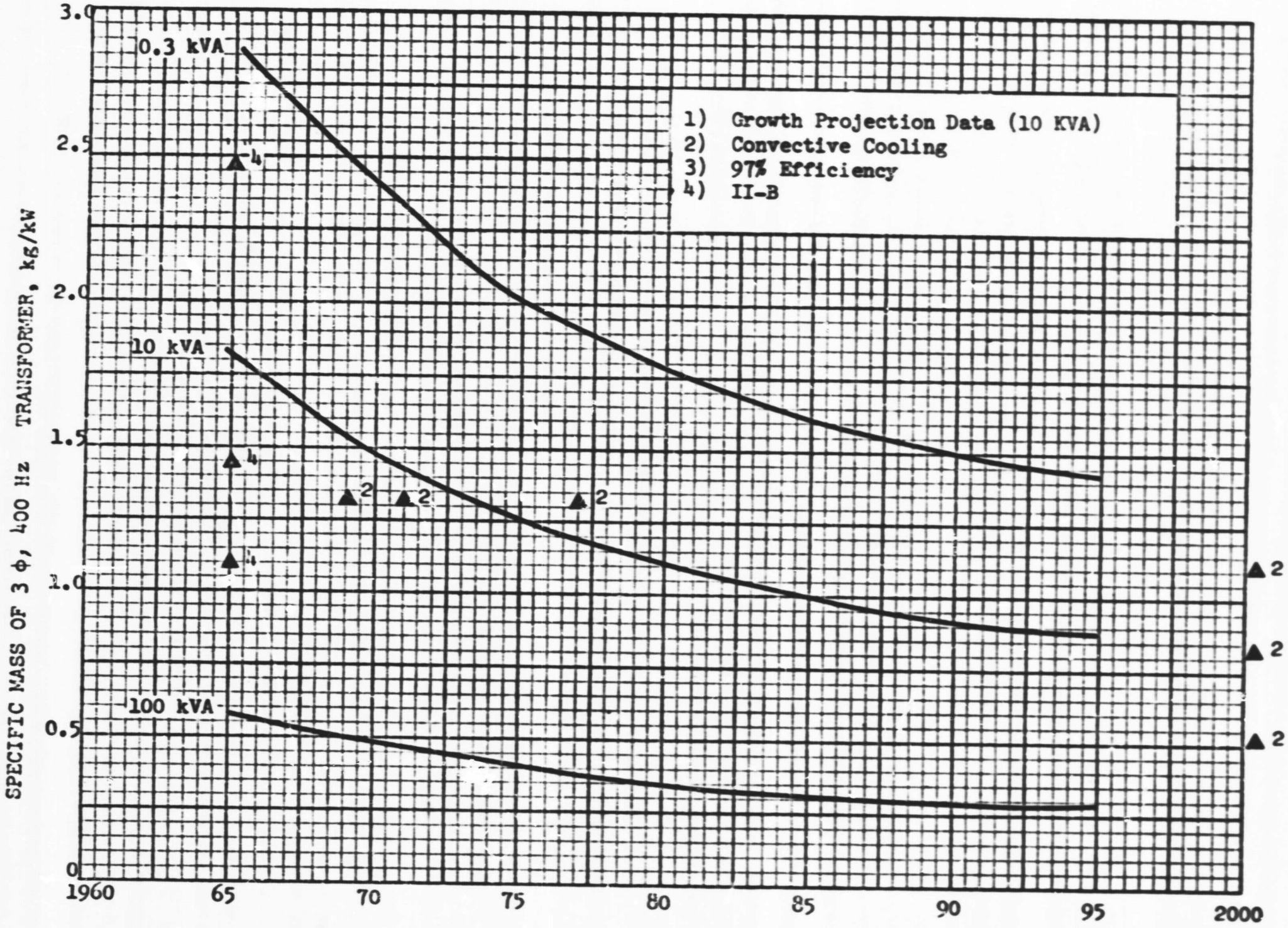

Figure 3-195 Projection of Transformer Specific Mass

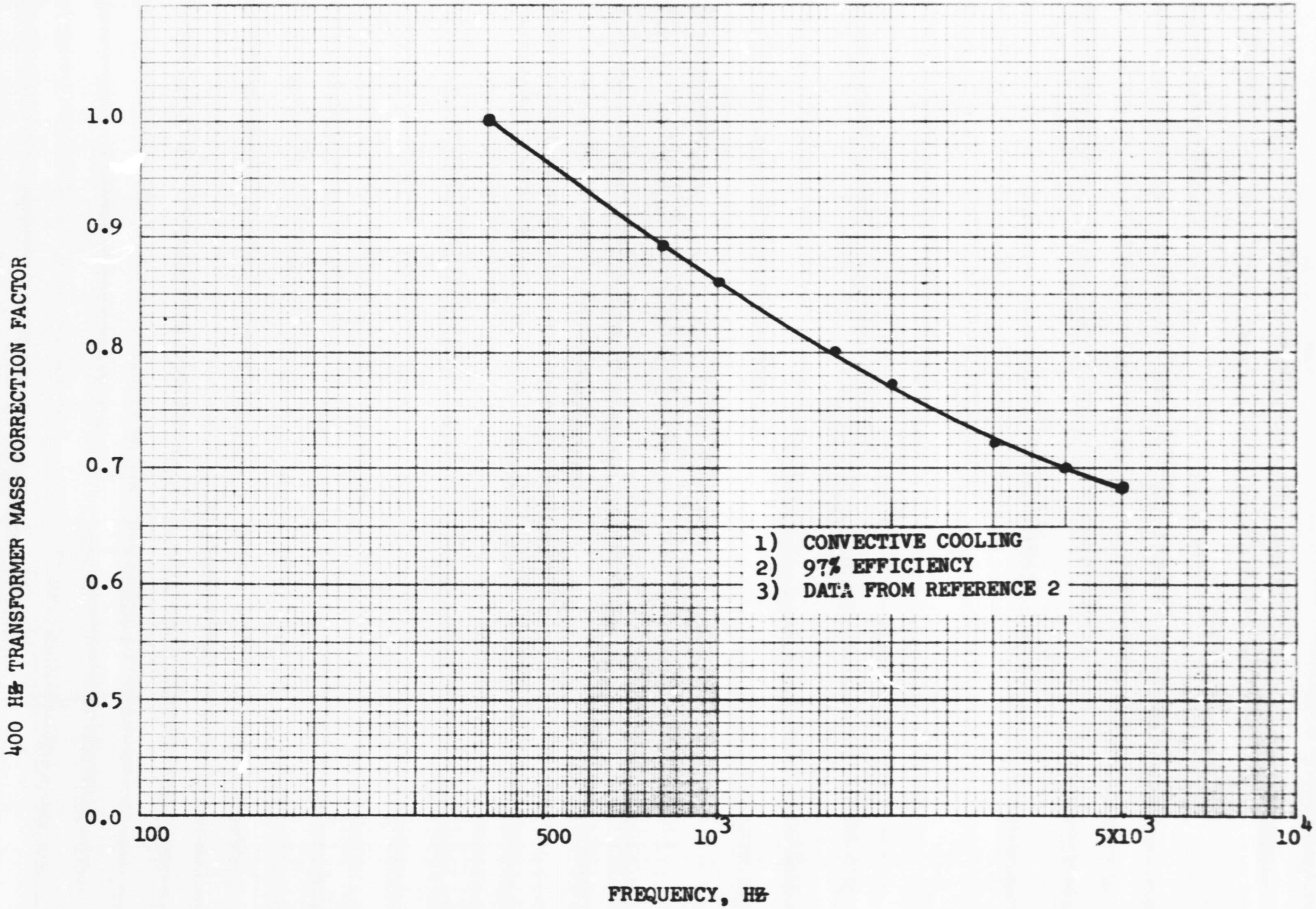

Figure 3-196 Transformer Mass Correction Factor

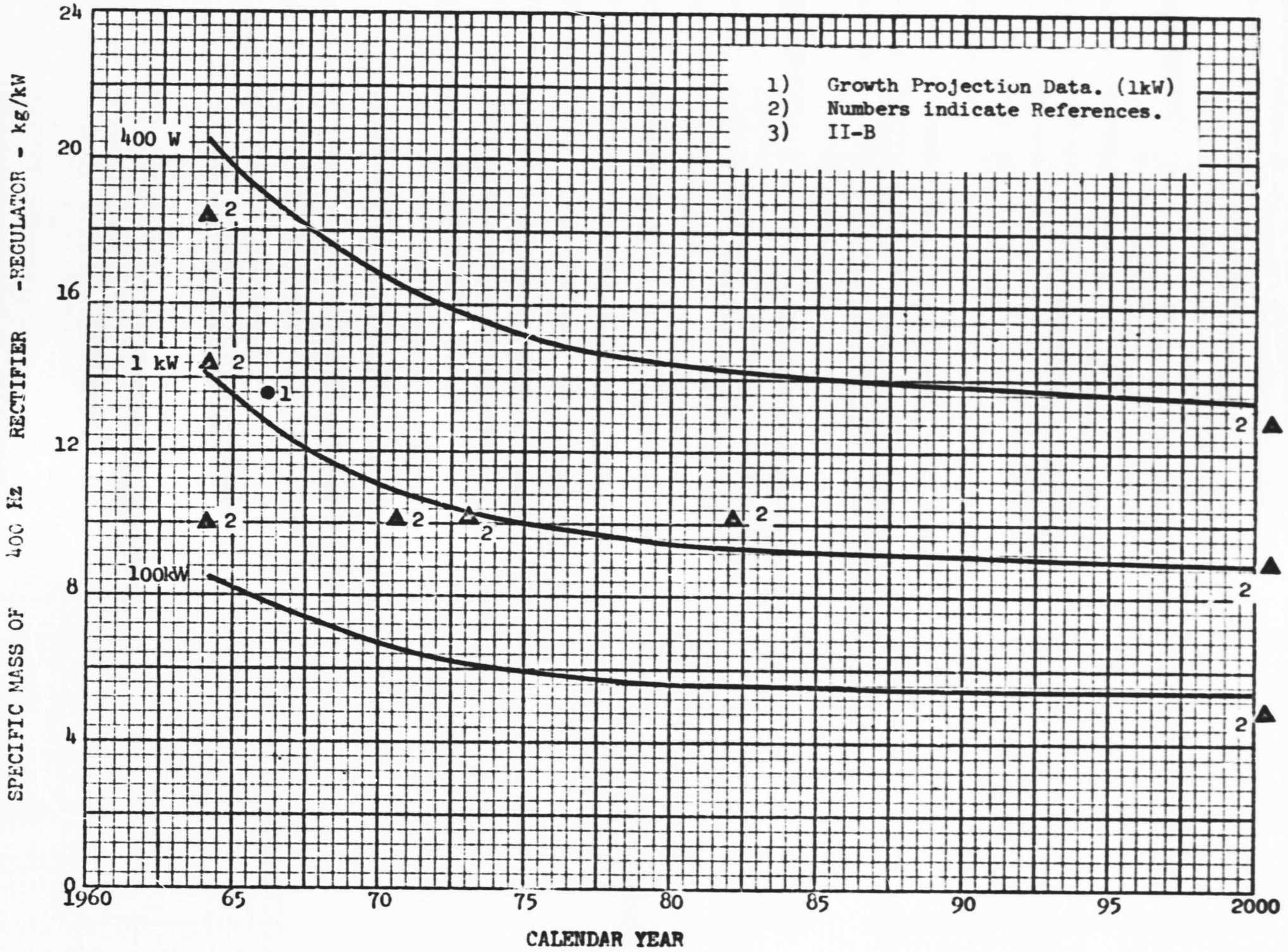

Figur 3-197 Projection of Rectifier Specific Mass

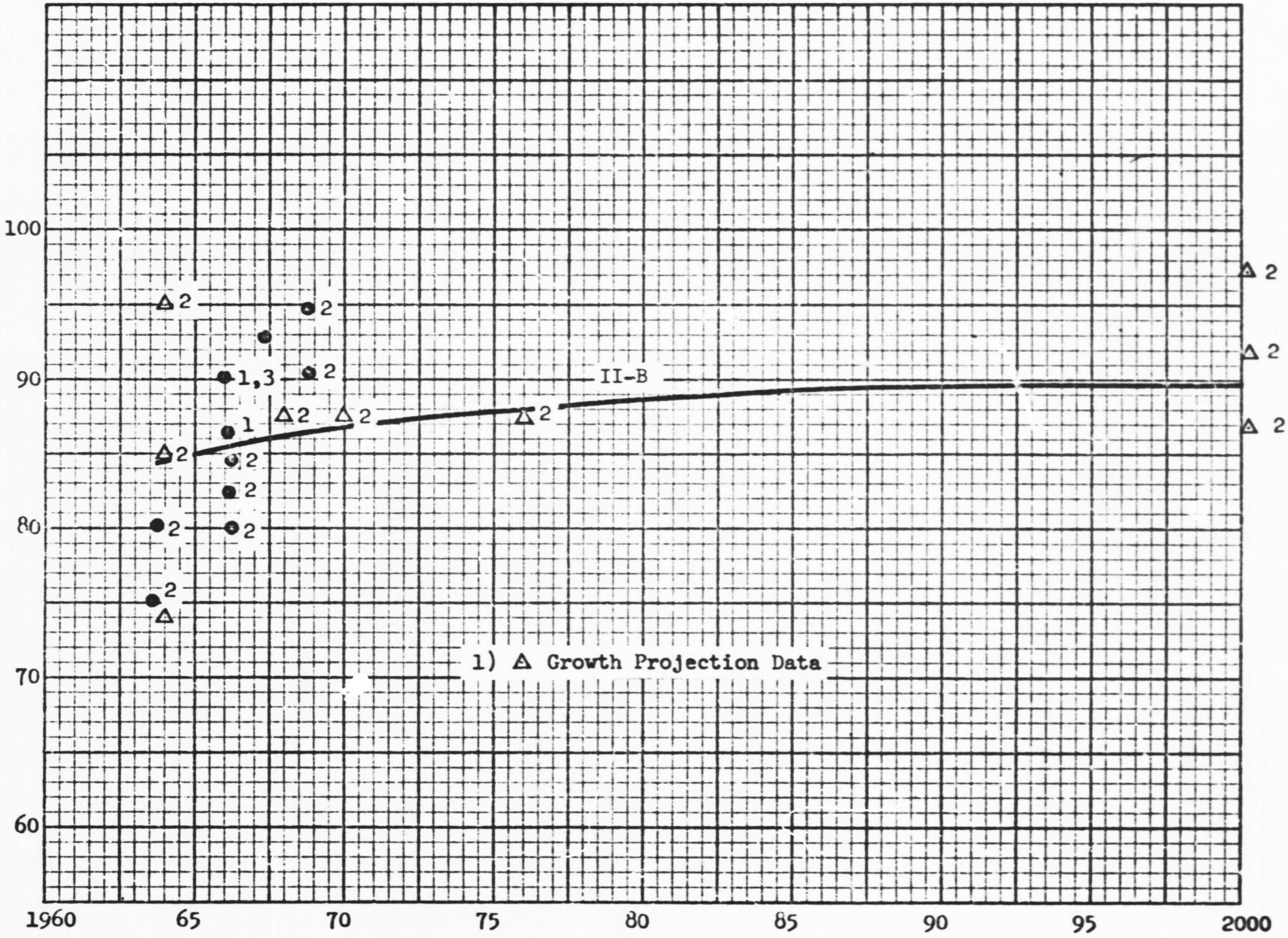

Figure 3-198 Projection of Efficiency of Rectifiers

3.5 POWER DISTRIBUTION SUBSYSTEMS

The power distribution subsystem consists of fuses connected to the power source, protection and/or selector switches, the feeder lines or harness to the loads, connectors, and mounting clamps. Copper wire is presently used for the distribution subsystem but aluminum is being investigated because of the potential lower weight. State-of-the-art characteristics of the power distribution subsystem are shown in Table 3-42. Specifications that govern the design and performance of the distribution subsystem are:

1. Copper wire, MIL-W-5086.
2. Aluminum wire, MIL-W-7072.
3. Installation procedures, MIL-W-5088.

Voltage drop is usually the limiting criterion for the choice of wire size on low voltage (28V) installations. When using higher voltages, the allowable voltage drop is normally within limits when the maximum current rating of the wire is satisfied and in many cases the wire is selected on the basis of minimum wire gage (No. 22) because of fabrication and assembly requirements. There is no economic reason for the use of higher distribution voltages than 115V on spacecraft, except for special subsystem high-voltage requirements that may influence the power conditioning subsystem performance or characteristics. For peak voltages higher than 320V, special consideration must be given to the effects of corona discharge.

Data have been obtained from hardware programs and design studies to determine the power distribution subsystem characteristics. The Apollo, Mercury, MORL, Saturn S-IVB, and military spacecraft programs have been investigated and power distribution subsystem weights are shown in Table 3-43. The weight analysis is based on power level, voltage drop, vehicle dimensions, type of power required (ac or dc), and type of wire. A correlation factor is used to account for the weight of insulation, connectors, and mounting clamps. The factor that will be used in the analysis to correlate the calculated weight to the actual power distribution subsystem weight is shown in Figure 3-199. The weight correlation factor is a function of the type of space vehicle and length-to-diameter ratio of the vehicle.

Table 3-42

POWER DISTRIBUTION SUBSYSTEM BRIEFING CHART

Identification	
Application	Used with all power subsystems
Types	AC, dc, or combined
Major components	Bus bars, feeder lines, harness protection devices, switches, insulation connector, and clamps
Vehicle – Mission Application	
Range	
Useful power level	Watts to MWe
Duration of mission	Days to years
Types of spacecraft	Manned, unmanned, Earth orbiting, or interplanetary
Status	
State of the art	Copper wire
Special problems	Wire vibrates and separates from connector, abrasion of insulation, minimum gage No. 22 wire based on assembly constraints
Subsystem Characteristics	
Range of specific weight	25 to 110 kg/kW
Range of specific production cost	$450 to $900/kg
Range of reliability	0.999 to 0.998* (one year)
Performance Characteristics	
Voltage drop	1/4 to 1% logistic/entry vehicles 1 to 10% orbital/interplanetary vehicles

*Based on Saturn S-IVB hardware design (28-day mission)

The average area of wire for a given voltage drop and total length of wire is determined in the weight analysis. The volume of wire is calculated as the product of 1.3 times the wire area and total length. The factor of 1.3 is an engineering estimate of the volume of insulation, connectors, and clamps. A failure rate of $\lambda = 3 \times 10^{-9}$/hour is used in the study and is based on a reliability analysis of critical circuits on the Saturn S-IVB stage for a 28-day mission. Power distribution costs range from $450 to $900/kg (recurring costs) based on numbers established by cost estimating and a power distribution production cost of $750/kg is used in the study.

Table 3-43
POWER DISTRIBUTION SUBSYSTEM WEIGHTS

Vehicle	Peak Power (kW)	Vehicle Dimension: Length (m)	Vehicle Dimension: Diameter	Specific Weight (kg/kW)	Subsystem Weight (kg)
Mercury (CM)	0.84	2.3	1.4	74.5	62.5
Gemini (CM and SM)	1.8	4.3	1.95	109	196
Apollo (CM)	6	3.55	2.5	58.5	350
Apollo (SM)	6	3.92	4.32	34	204
Apollo (CM and SM)	6	7.47	-	92	554
MORL Brayton	10	12.8	6.6	25.5	255
MORL SNAP-8	20	12.8; 38*	6.6	23	455
Saturn S-IVB	6.8	12.1	6.6	110	750

*Boom length

CM = Command Module
SM = Service Module

NOTE

L* = VEHICLE LENGTH & BOOM LENGTH
CM = COMMAND MODULE
SM = SERVICE MODULE

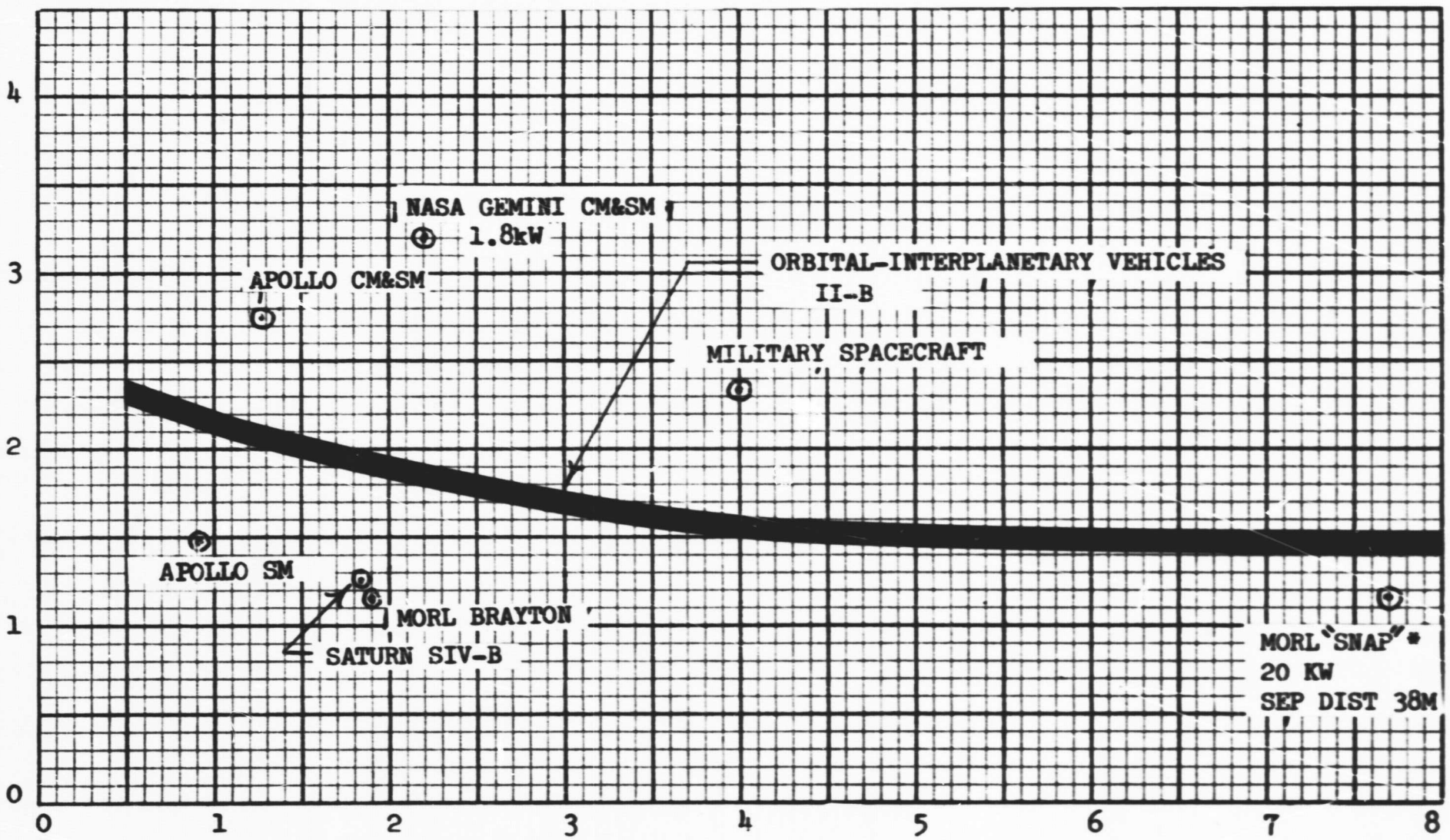

FIGURE 3-199 POWER DISTRIBUTION WEIGHT CORRECTION FACTOR

3.6 POWER SYSTEM INTEGRATION WITH THE SPACE VEHICLE

The major power system integration elements that have been investigated in the study are the interstage or shroud compartment for stowing the power system, the area requirements of the vehicle for comparison with body mounted solar cell area or integrated radiator area, and a boom for deployment of the power system.

3.6.1 Interstage and Shroud

The interstage compartment was sized on the basis of empirical relations for the mass of typical aluminum sheet stringer material used in the construction of the vehicle. The interstage compartment for housing the power system can be either a single cylindrical member or a two piece shroud that separates from the vehicle after the vehicle is in orbit. Separation of the shroud permits the power system to be deployed. Based on existing data, minimum interstage mass is 4.39/m^2 and shroud weight is 9.85 kg/m^2. After the radiator area and volume requirements have been calculated for the power system, the integration subroutine determines the interstage or shroud length that is required to stow the power system. The shroud mass as a function of surface area for several vehicles is shown in Figure 3-200. The weight of the interstage to house the power system is then charged against the power system. The volume constraint was chosen as the governing design parameter; however, the radiator area and body-mounted solar cell area are printed out by the computer program. The diameter of the vehicle is the independent variable and the length of the vehicle is the dependent variable. The length and diameter of the vehicle that are input data to the program are only the dimension of the mission module for manned systems and only the dimensions of the payload compartment for the unmanned systems. The power system volume requirement is then additive to mission or payload module volume in order to obtain the total launch volume. The characteristics and performance data for the vehicle interstage and shroud are shown in Table 3-44.

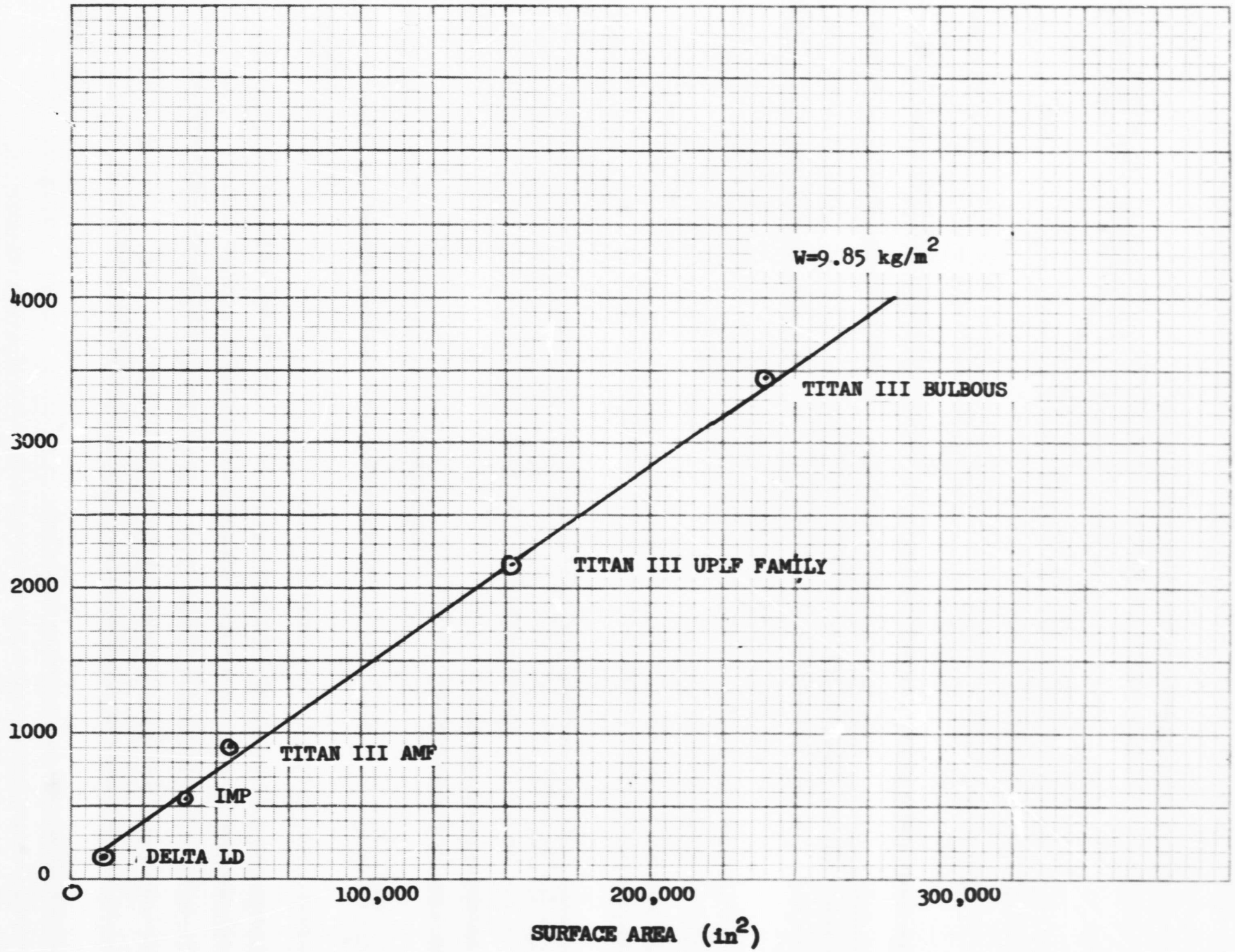

FIGURE 3-200 SPECIFIC MASS OF SHROUD

Table 3-44

VEHICLE INTERSTAGE AND SHROUD
BRIEFING CHART

Identification	
Major components	Aluminum sheet and stringers and explosive-separation devices for shroud
Types of spacecraft	Manned, unmanned, Earth-orbiting, interplanetary
Status	
State of the art	Aluminum material, some plastics
Subsystem Characteristics	
Range of specific weight	Interstage compartment 4.39 kg/m^2 minimum, shroud 9.85 kg/m^2
Range of specific production cost	$300/kg to $600/kg
Reliability	1.0 for interstage, 0.999 for shroud

3.6.2 Deployment Boom

The deployment boom is used for nuclear and isotope power systems to reduce the effect of the heat source nuclear radiation on the crew or payload and on solar cell and solar concentrator power systems to deploy the power system to track the sun. The design of the deployment boom is based on fundamental engineering principles and a typical design concept for a nuclear reactor power system integrated with the MORL vehicle is shown in Figure 3-201. The boom in the computer program is a hollow aluminum cylinder; the aluminum has a yield stress of 4.56×10^8 N/m^2 (66,000 $lb/in.^2$) and a modulus of elasticity of 6.91×10^{10} N/m^2 (10,000,000 $lb/in.^2$).

The boom for the reactor and isotope power system is designed for axial compressive loads with a safety factor of 1.5 and a minimum wall thickness of 0.159 mm (0.0625 in.). Results of studies indicate that a three-section telescopic type boom is deployed and that maximum deployed lengths are approximately 61 m (200 ft.). The inside diameter of the boom for the isotope and reactor power systems was set at 0.305 m (1 ft.).

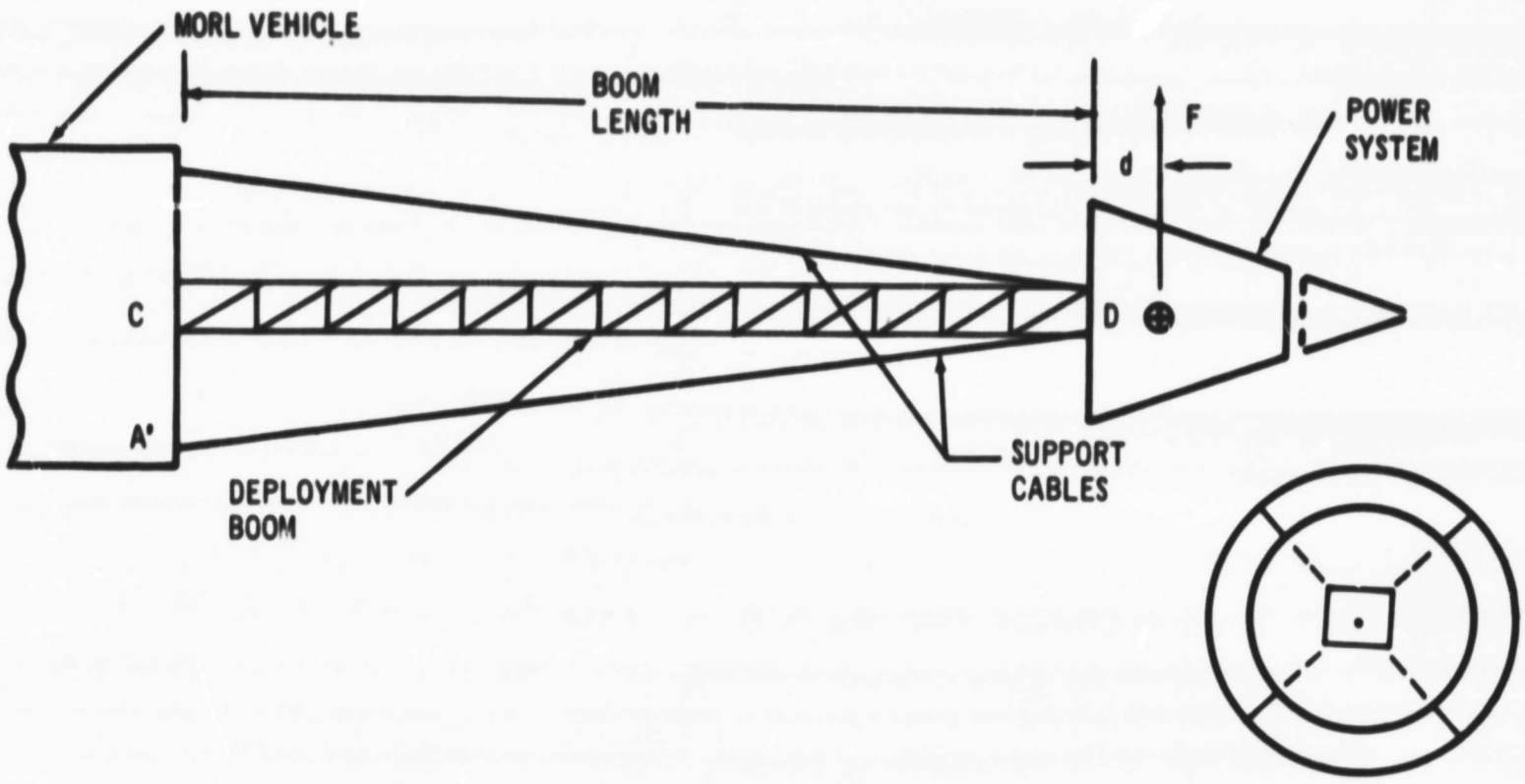

FIGURE 3-201 NUCLEAR REACTOR
POWER SYSTEM DESIGN CONCEPT

The boom for deployed solar cells or solar concentrator power systems was designed for (1) bending stresses, (2) deflection at the end of the beam, (3) transverse shear load, and (4) minimum wall thickness. The bending stress usually governs the design of the boom for these types of power systems. The inside diameter of the boom for the solar concentrator and solar cell power systems was set at 0.71 m (2 ft.).

The characteristics of the boom for deployed power systems are summarized in Table 3-45.

Table 3-45

BRIEFING CHART
DEPLOYMENT BOOM

Identification	
Applicable power systems	Solar, isotope and reactor systems
Major components	Aluminum cylinder, guy wire
Types of spacecraft	Manned, unmanned, Earth orbiting, interplanetary
Status	
State of the art	Aluminum material
	Minimum wall thickness 0.159 mm
	Approximate maximum boom lengths
	Reactor systems 61 m
	Isotope systems 9.1 m
	Solar concentrator system 12.2 m
	Solar cells 1.2 m
Subsystem Characteristics	
Specific production cost	$440/kg
Reliability	0.999

3.7 SUPPORTING DATA

The supporting data that are common to a particular subsystem or component or group of subsystems are presented in this section.

3.7.1 Costing

The cost model, production cost, and development, test, integration, and qualification costs that are used in the study are discussed below.

3.7.1.1 Cost Model

The cost data used in the study consist of the production cost of the component or subsystem plus the cost of developing, testing, integrating, and qualifying (DTI&Q) the power system for the space vehicle. The development and application of a power system to a space vehicle consists of three basic design and cost phases as shown in Figure 3-202. The Phase I effort is the technology development phase and results in the demonstration of the performance, feasibility, and technology readiness of the power system. For example, the SNAP-8 Rankine cycle system, by this definition, is then categorized as a Phase I effort. Because of the lack of sufficient cost data for technology development, this cost is not included in the computer program.

The Phase II effort is defined as the time duration in which the power system is selected and built to specifications for the mission. This phase begins with contract award on authority to proceed (ATP). A 3-year period was assumed for the Phase II effort to develop, test, integrate, and qualify (DTI&Q) the power system for the mission. An example of a system program that is categorized as a Phase II effort is the MOL fuel cells. The DTI&Q costs are determined at the module or subsystem level as a function of power level, mass, or size and appear in the computer program output as DEV COST.

The production costs of the power systems including flight test units are included in the Phase III effort of the program. The production costs are determined at the major component level and the number of on-line, standby, and wearout units (or percent redundancy of components) are used to calculate the total production cost of a subsystem.

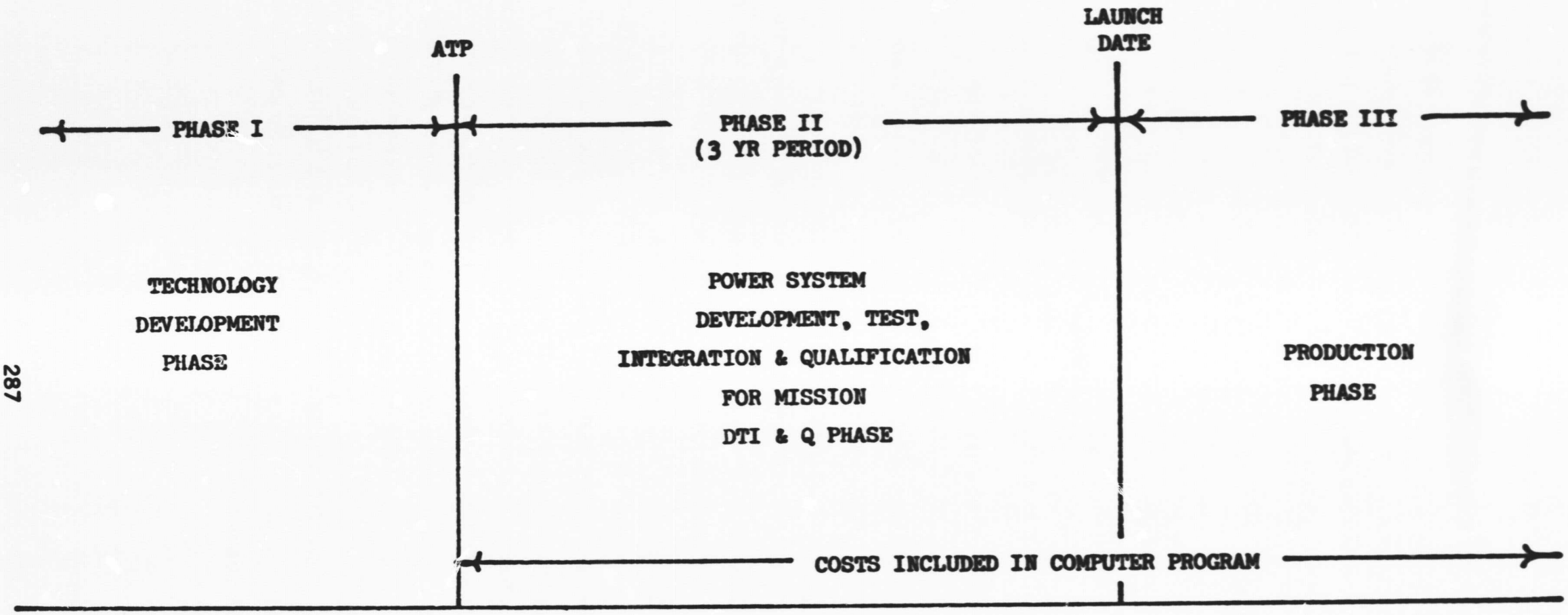

FIGURE 3-202 POWER SYSTEM - MISSION PHASES FOR COSTING MODEL

The total cost of a power system is then calculated as the summation of the DTI&Q costs of the specified subsystem plus the production costs of the major components employed in the total number of subsystems used in the power system. The production cost data is presented in the previous power subsystem sections and qualification costs are presented in Subsection 3.7.1.3.

3.7.1.2 Production Cost

The production cost data is presented in the previous power subsystem sections and is the reoccurring cost of the power system. The production costs are plotted as a function of calendar year.

3.7.1.3 Development, Test, Integration, and Qualification Cost

The DTI&Q costs of the various power subsystems varied considerably, and for some major components or subsystems, little, if any, cost data are available. Where data did not exist, a relative cost comparison which appeared reasonable with respect to the technologies (relative order of complexity, for example) of the various power subsystems was used to estimate the DTI&Q costs. The principal objective in establishing the power subsystem costs is to ensure that a bias in the costs of one power subsystem relative to another did not occur. For example, the DTI&Q power subsystem costs can be determined relative to one another based on the state of the art and relative complexity of the subsystems. The absolute cost will vary because of (1) the quantity of prototype and test subsystems that are delivered, (2) whether or not a flight test is performed, and (3) the scope of the qualification program. Since the absolute cost can vary considerably, the relative cost determinations permits the cost curves to be adjusted up or down when it is deemed necessary to respecify the absolute power subsystem DTI&Q costs. The DTI&Q costs are plotted at the subsystem level (depending on type of power subsystem) as a function of power level, total energy, a physical dimension, or mass. The DTI&Q costs are calculated in the computer program at the subsystem level and then combined together to obtain the total power system DTI&Q costs.

Curves of the DTI&Q costs of the power conversion, heat rejection, power conditioning, power distribution and heat source subsystems and the interstage/shroud structure and deployment boom used in the computer program are shown in Figures 3-203 to 3-207. The Nimbus satellite, the JPL-Boeing 50-kW solar cell arrays, the Gemini fuel cell, and military space stations are typical examples of the cost data that were used in establishing the DTI&Q cost trends.

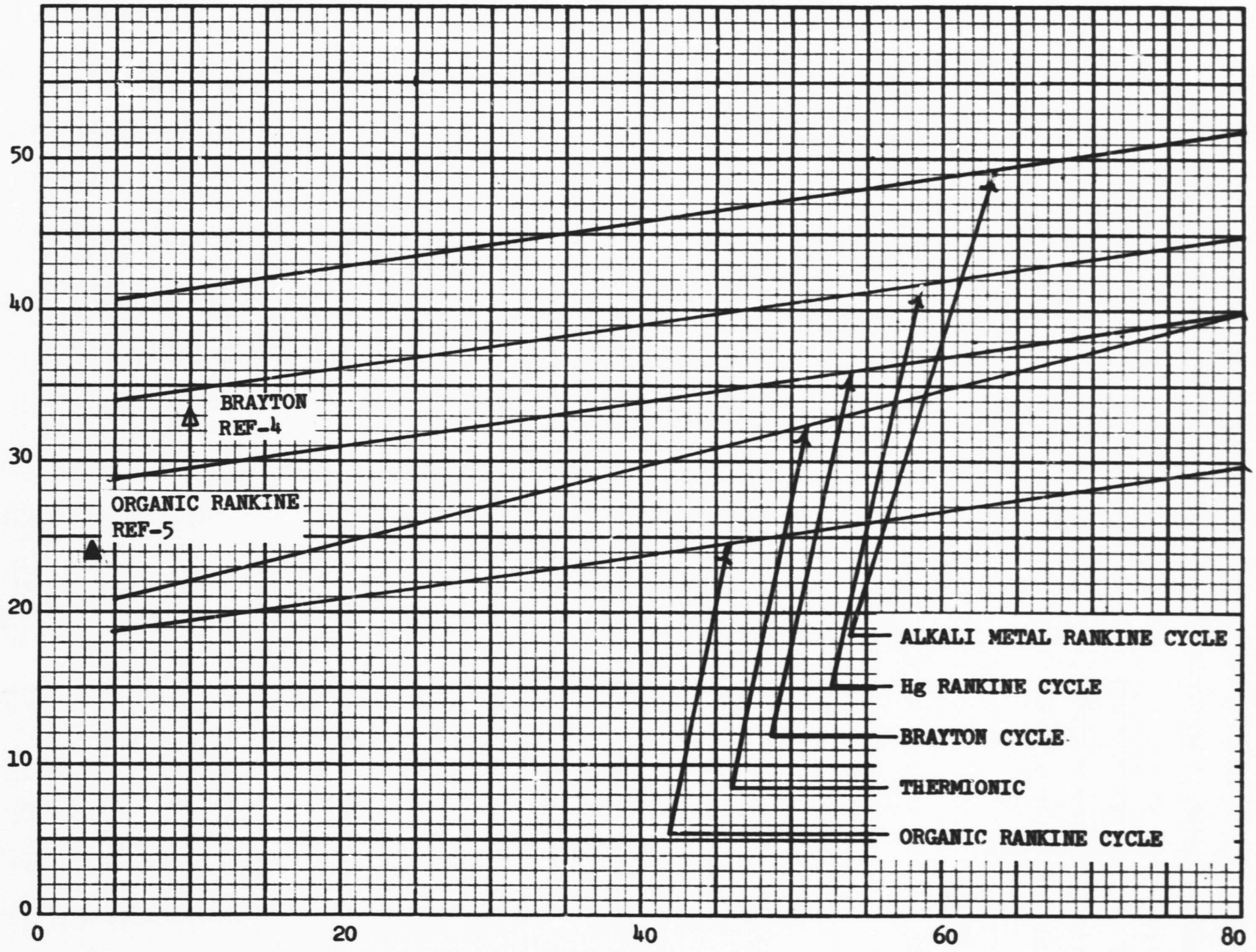

FIGURE 3-203 POWER CONVERSION MODULE DTI&Q COST

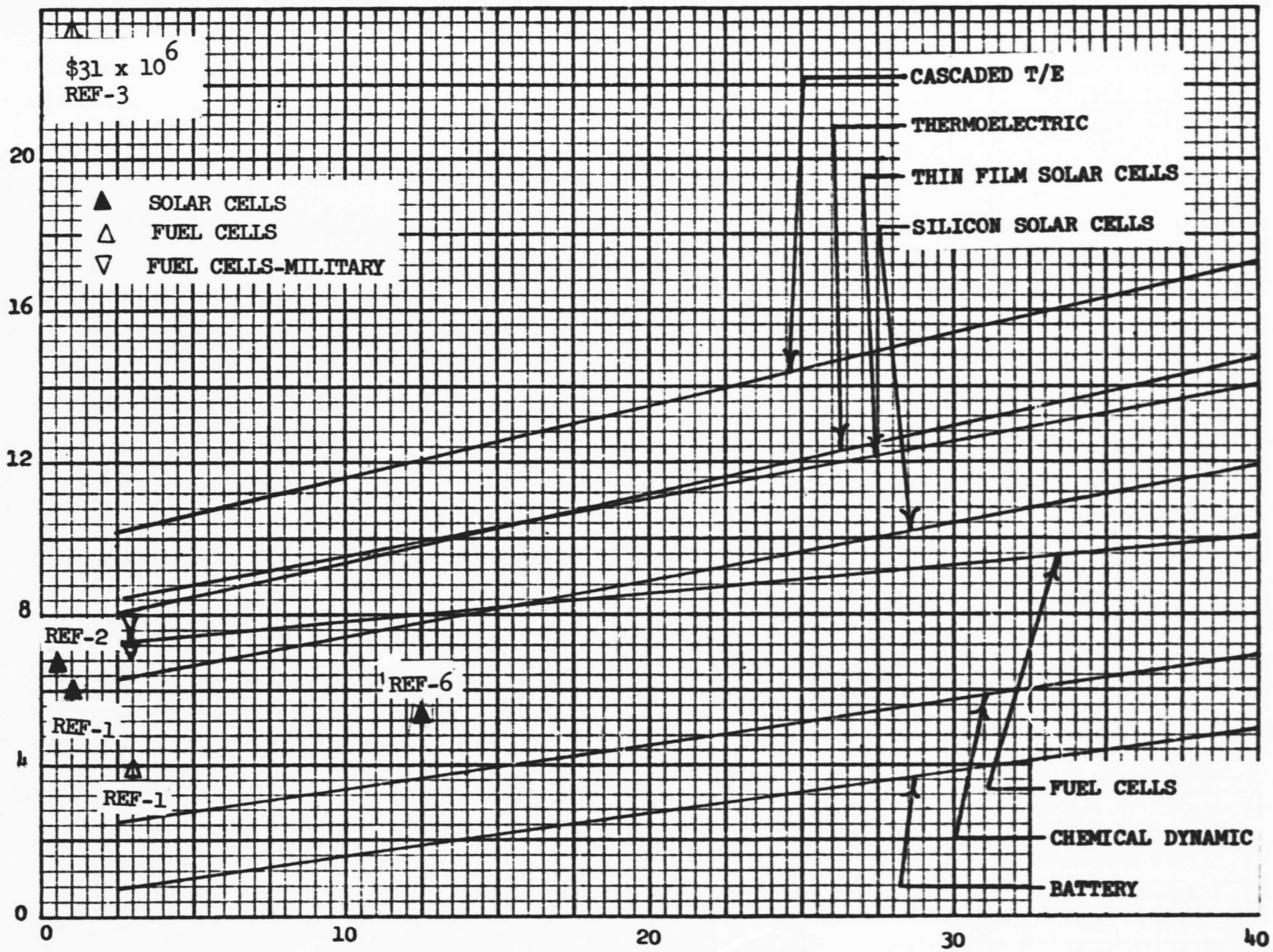

FIGURE 3-204 POWER CONVERSION MODULE DTI&Q COST

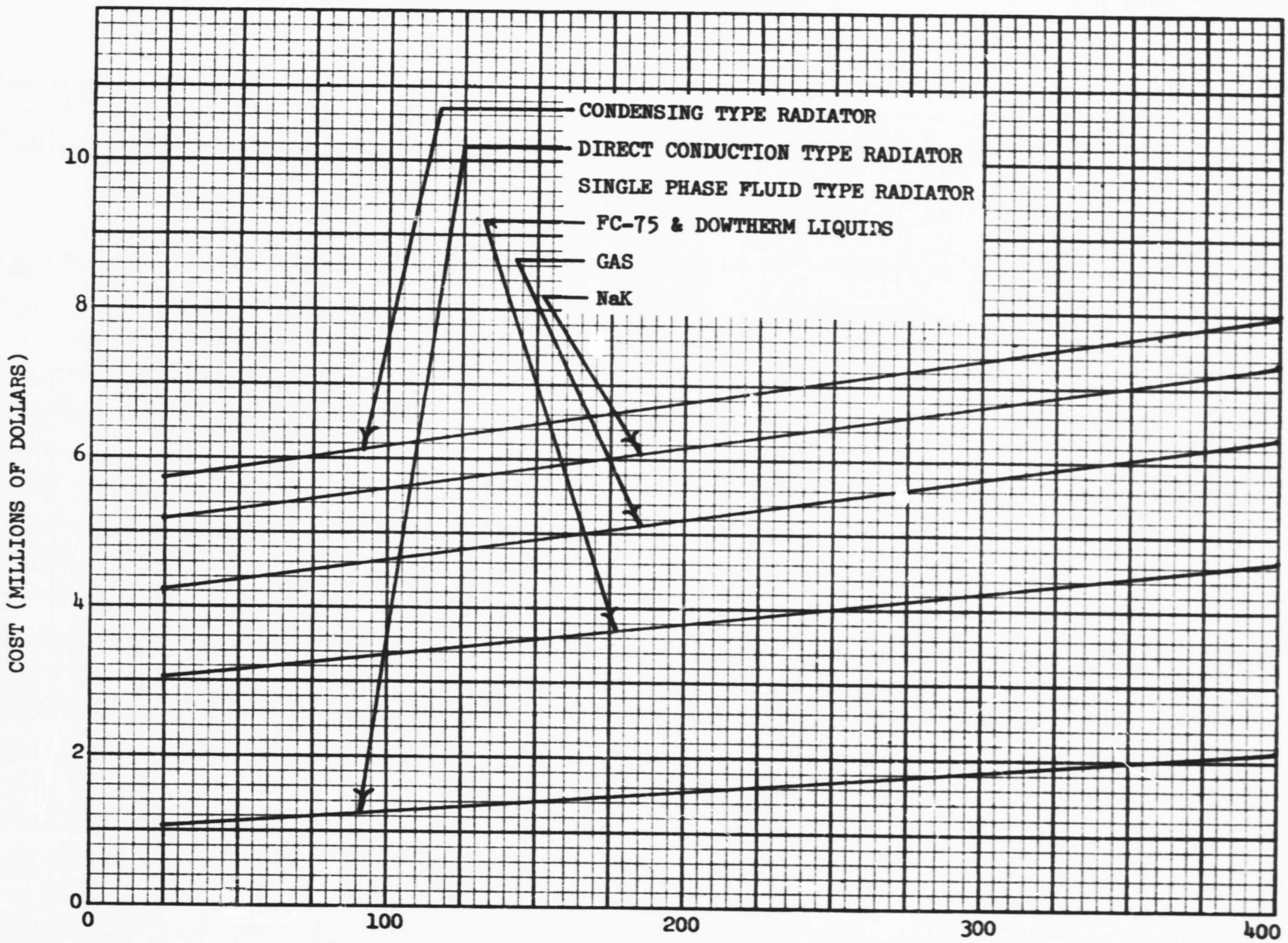

FIGURE 3-205 RADIATOR MODULE DTI&Q COST

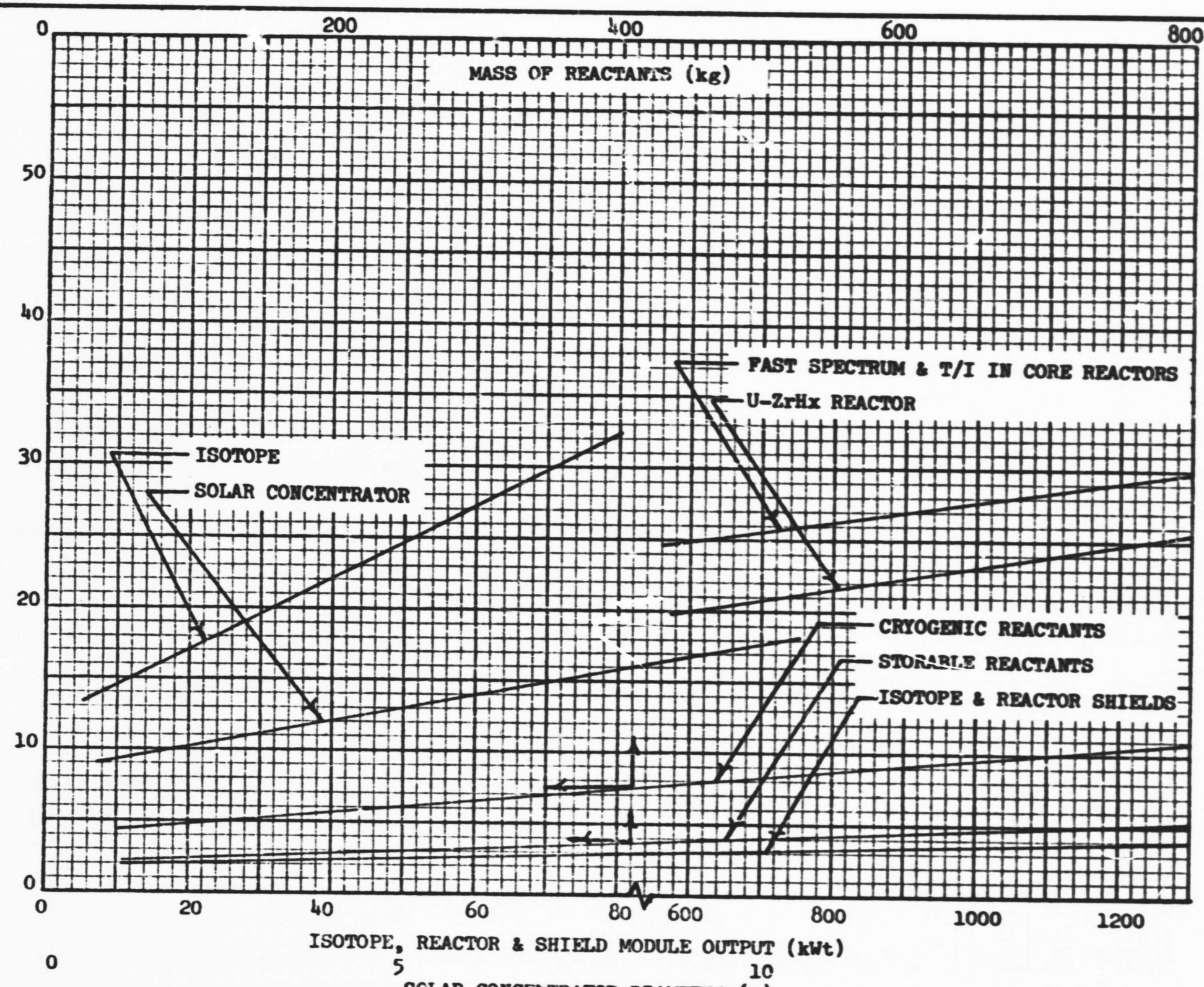

FIGURE 3-206 HEAT SOURCE DTI&Q COSTS

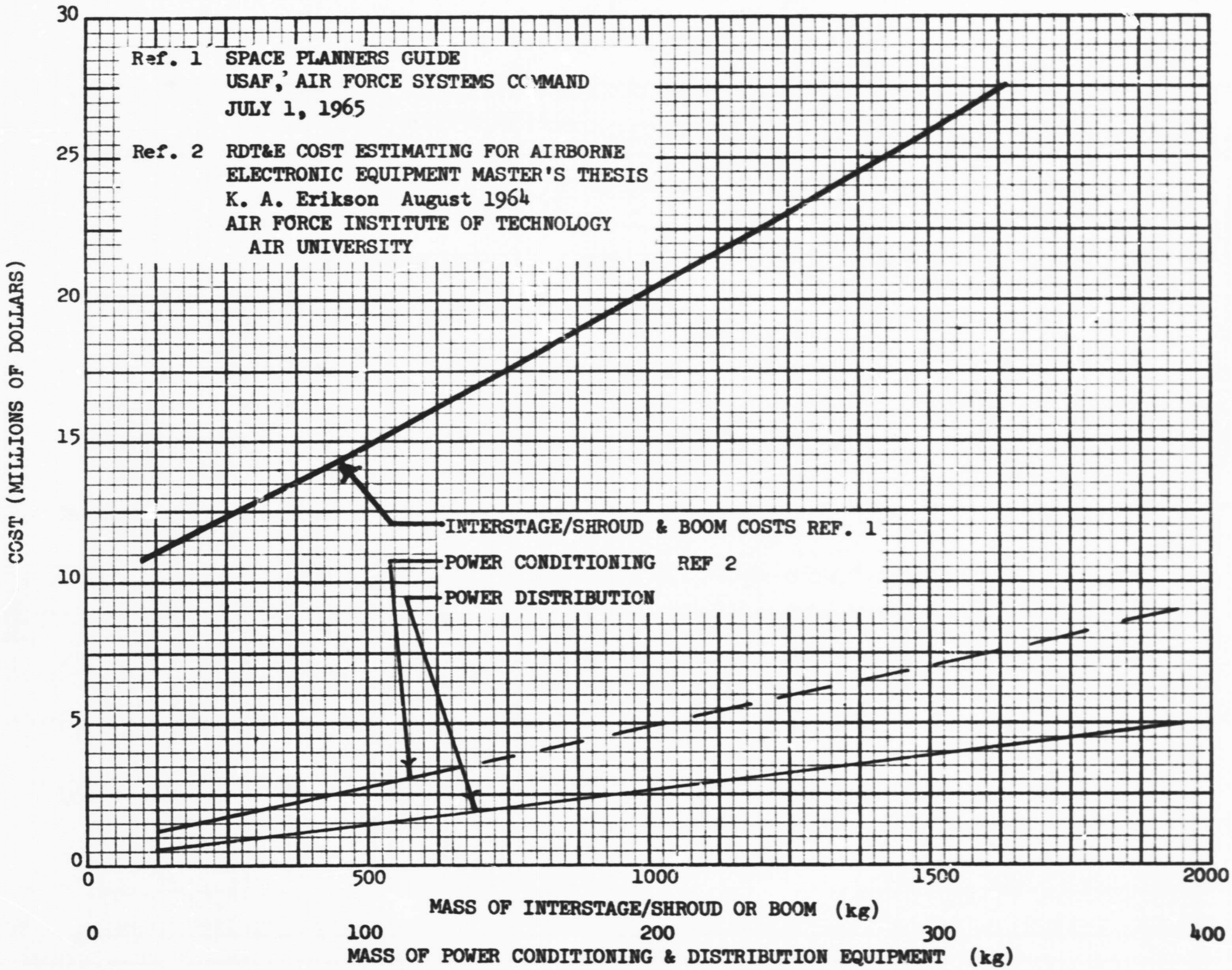

FIGURE 3-207 INTERSTAGE/SHROUD & BOOM AND POWER CONDITIONING DISTRIBUTION EQUIPMENT DTI&O COST

3.8 REFERENCES FOR SECTION 3

3.8.1 Subsection 3.1.1

1. J. V. Goldsmith, Private Communication, JPL, 22 August 1967.
2. F. W. Woodward, Heliotek Division, Textron Electronics Inc., Private Communication, 17 August 1967.
3. T. E. Peterson, Ion Physics Corp., Private Communication, 4 August 1967.
4. K. S. Ling, Centralab Semiconductor, Globe Union Inc., Private Communication, 25 August 1967.
5. R. B. Beltz, H. G. Merch, and A. C. Lee. OGO Solar Array Design, Fabrication and Flight Performance. 1967 Intersociety Energy Conversion Engineering Conference, Miami Beach, Florida, August 1967.
6. H. J. Holbech. A Structural View of Solar Array Development. IECEC, Miami Beach, Florida, August 1967.
7. G. E. Turner and D. R. Tott. Flight Experience With Large Area Solar Array Systems. IECEC, Miami Beach, Florida, August 1967.
8. Large Area Solar Array Design (LASA). The Boeing Co. Second Quarterly Report No. D2-113355-2, March 1967 (JPL Contract No. 951653).
9. J. Miller. Status of the ATM Solar Array. IECEC, Miami Beach, Florida August 1967.
10. Report on the Optimization of the Manned Orbital Research Laboratory (MORL): Volume 27, Laboratory Electrical Power. Douglas Report No. SM-46088, September 1964.
11. Development of a Light Weight Rigid Solar Panel. Electro Optical Systems, EOS Report No. 7017-IDR, 18 May 1966.
12. J. R. Burnett, Electro Optical Systems Inc., Private Communication, 17 July 1967.
13. Manned Mission Photovoltaic Power System Study. RCA-Astronics Division (Contract No. NAS9-5266), RCA Report No. AED-R-3155.
14. R. E. Holmen. Study for Mounting Solar Arrays on the S-IVB Orbital Workshop. Douglas Company Report No. DAC-56583, 20 July 1967.
15. A. Burstein, Hughes Aircraft Co., Private Communication, 17 August 1967.
16. Design and Fabrication of a Deployable Large Area Solar Cell Array Supporting Structure. Ryan Aeronautical Company.

    Report No. 20869 - 1 July 1965
    Report No. 20869 - 2 May 1966
    Report No. 20869 - 3 April 1967

17. W. M. Cottrell, Ryan Aeronautical Co., Private Communication, 17 July 1967.

18. W. Goss, TRW Systems Group, Private Communication, 12 July 1967.

19. H. Majower, Fairchild Hiller Corp., Private Communication, 5 September 1967.

20. Positive Deployable Solar Array Development Program. NASA Contract No. NASf-9658, Fairchild Hiller Corp., Phase I - June 1966, Phase II - March 1967.

21. Thirty Watts/Pound Solar Array Feasibility Study. Fairchild Hiller Corp. Proposal, March 1967.

22. Design Considerations for Large Area Solar Arrays for Manned Space Stations. Hoffman Electronics, August 1963.

23. F. J. Mihrn, Heliotek Division, Textron Electronics Inc., Private Communication, 4 March 1966.

24. L. Schmidt, Hoffman Electrorics, Inc., Private Communication, 22 March 1966.

25. E. Harris and D. Dreyfus. Manned Spacecraft Electrical Power Systems - Requirements, Weight Correlation and Cost Implications. IECEC, Los Angeles, California, September 1966.

26. R. K. Riel, Westinghouse Electric Corp., Private Communication, August 1966.

27. W. M. Goss, TRW Systems Group, Private Communication, 24 June 1966.

28. H. D. Poshay. Aerospace Component Reliability Growth. Douglas Report No. DAC-59067, November 1966.

29. M. J. Mirtich and R. L. Bowman. Effect of Simulated Micrometeoroid Exposure on Performance of N/P Silicon Solar Cells. AIAA Journal, Vol. 5, No. 7, July 1967, Page 1364.

30. R. L. Bowman and M. J. Mirtich. Performance of CdS Solar Cells After Simulated Micrometeoroid Exposure. AIAA Journal, Vol. 6, No. 2, February 1968, Page 378.

31. G. A. Work, TRW Systems Group, Private Communication, 10 January 1968.

32. F. A. Shirland and F. Augustine. Thin-Film Plastic Substrate CdS Solar Cells. Fifth Photovoltaic Specialists Conference, NASA-Goddard Space Flight Center, 19 October 1965.

33. J. M. Deerwester. Reference System Characteristics for Manned Stopover Mission to Mars and Venus. NASA-MAD, July 1967.

34. D. E. Evans, D. E. Pitts and G. L. Kraus. Venus and Mars—Nominal Natural Environment for Advanced Manned Planetary Mission Programs. NASA-MSC, Houston, Texas, NASA SP-3016 (1967), Second Edition.

35. E. F. Koprowski, Douglas Aircraft Company, Private Communication, April 1968.

36. M. Baker, Douglas Aircraft Company, Private Communication, October 1967.

37. A. J. Mosley and A. D. Goedeke. Complete Dose Analysis of the November 12, 1960 Solar Cosmic Ray Event. Third International Space Science Symposium, Washington D.C., 30 April - 9 May 1962.

38. M. B. Baker. Geomagnetically Trapped Radiation. Douglas Report No. SM-47635, October 1964.

39. W. C. Cooley and M. J. Banett. Handbook of Space Environmental Effects on Solar Cell Power Systems. Exotech, Inc., September 1967.

40. J. Vette, Aerospace Corp., Private Communication, July 1967.

41. E. L. Brancato. Radiation Damage in Solar Cells. Presented at ASME Aviation and Space Division Conference, Los Angeles, California.

42. CdS Solar Cells. Harshaw Chemical Co., 4th Photovoltaic Specialists Conference.

43. J. F. Wise (USAF-AFAPL) and R. L. Statler (USNRL). Integral Covers for Solar Cells. 6th Photovoltaic Specialists Conference, March 1967.

44. J. R. Hutenan and F. A. Shirland. The Status of the Clevite CdS Thin Film Solar Cell. Sixth Photovoltaic Specialists Conference, March 1967.

45. I. Stern. Solar Cell Modules Design Experience. RCA-AED—Personal Communication, October 1967.

46. F. A. Shirland. CdS Solar Cell Development. NASA-CR-72382, 29 February 1968.

47. F. A. Blake. Thin-Film Solar Cell Module Development. General Electric Company, MSSD Report No. DIN 68SD4233, 1 April 1968.

48. TRW Space Data. TRW Systems Group, 1967, Second Edition.

49. Dr. A. E. Potter, NASA-Lewis, Private Communication, October 1966.

50. Radiator Design for Space Vehicles. AiResearch Manufacturing Company, 1966.

51. N. Spakowski and K. Kennerad. Environmental Testing of CdS Solar Cells. Sixth Photovoltaic Specialists Conference, Cocoa Beach, Florida, March 1967.

52. CdS—Thin-Film Solar Cells. Clevite Corp., Brochure No. CC 101.

53. S. Gross. Discussion of Power Systems for Solar Probes—Solar Photovoltaic Concepts. First Intersociety Energy Conversion Engineering Conference, Los Angeles, California, September 1966.

54. N/P Silicon Solar Cells. Hoffman Electronics Corp., Technical Information Bulletin No. 3-64, 1964.

55. D. W. Ritchie and J. D. Sandstrom. An Evaluation of Photovoltaic Devices for Future Spacecraft Power Demand. Jet Propulsion Laboratory Technical Report No. 32-1268, May 1968.

56. D. W. Ritchie and J. D. Sandstrom. Multikilowatt Solar Arrays. Presented at the Sixth Photovoltaic Specialists Conference, Cocoa Beach, Florida, March 1967.

57. D. W. Ritchie and J. D. Sandstrom. Jet Propulsion Laboratory, Private Communication, 20 September 1967.

58. W. Cheny and J. A. Zoutendyk. The State-of-the-Art in Solar Cell Arrays for Space Electrical Power. AIAA Journal, Vol. 64, September 1964, Page 738.

59. W. W. Managen. Harshaw Chemical Company, Private Communication, 14 March 1966.

60. F. A. Shirland. Clevite Corporation, Private Communication, 7 March 1966.

3.8.2 Subsection 3.1.2

1. Report on the Design Requirements for Reactor Power Systems for Manned Earth Orbital Applications. Douglas Report DAC-59213, May 1966.

2. G. B. Stafford. Space Power Subsystem Capabilities. AIAA Paper No. 65-468, July 1965.

3. Compact Thermoelectric Converter Development Program. U.S. Atomic Energy Commission Contract No. AT(30-1)-3584, Westinghouse Astronuclear Laboratory.

4. W. C. Flanigan. Research and Investigation on Satellite Attitude Control--Part III Power Sources. AFFDL-TR-64-168, June 1965.

5. State and Trend of Technology, Space. Aerospace Power Division, Wright-Patterson AFB, Ohio, January 1968.

6. S. R. Rocklin. Design and Development of a High Efficiency Cascaded and Segmented Thermoelectric Module. Intersociety Energy Conversion Engineering Conference, August 1967.

3.8.3 Subsection 3.1.3

1. G. N. Hatsopoulos. Thermionic Energy Conversion. Intersociety Energy Conversion Engineering Conference, September 1966.

2. I. M. Houston. Response to Douglas Questionnaire, August 1967.

3. State-of-Art and Technical Forecast Survey. Wright-Patterson Air Force Base Preliminary Projection Report, July 1967.

4. Space Power Systems Advanced Technology Conference. Lewis Research Center Report, NASA-SP-131, August 1966.

5. V. C. Wilson and J. Larence. G. E. Research Laboratory, Final Report Contract AF 33(657)-10132, May 1964.

6. G. Y. Eastman. Proc. Cleveland Thermo Conv. Spec. Conf. October 1964.

7. S. S. Kitrilakis and J. H. Weinstein. Thermo Electron Report 35-64, January 1964.

8. Solar Thermionic Flight Experiment Study. Document No. 65SD4286, May 1965.

9. J. V. Coggi. Weight and Reliability Analysis of a 5 MWe Thermionic In-Core Power Plant. Douglas Report No. DAC-60789, February 1968.

10. A. U. Buatti and J. V. Clausi. Parametric Study of High Power In-Pile Nuclear Thermionic Space Propellants. PWA-2319, March 1964.

11. Studies of Thermionic Materials for Space Power Application. Report No. NASA CR-54980, General Atomics, May 1966.

12. H. B. Finger. Summary Statement on Nuclear Energy Systems for Space Application before the Committee on Astronautical and Space Services. United States Senate, February 1966.

13. P. Rouklove. Analysis of Failures of Thermionic Converters: 1968 ASME Aviation and Space Conference, June 1968.

14. W. E. Loewe. Out-of-Core Thermionic Space Power. Second International Conference on Thermionic Power Generation, Euratom, Stresa, Italy, May 1968.

15. V. C. Wilson and J. Lawrence. Characteristics of a Thermionic Converter With a Fluoride Vapor Deposited Tungsten Emitter Etched to Preferentially Expose the 110 Crystal Planes, Thermionic Conversion Specialist Conference, Palo Alto, California, November 1967.

16. J. Bliaux and M. Clémot. In-Site Thermionic Life Test Sirene 302, Thermionic Specialist Conference, Palo Alto, California, November 1967.

17. T. Speidel. Performance Comparison of Nine RD-502 Cylindrical Diodes With Etched Rhenium Emitters. Thermionic Conversion Specialist Conference, Palo Alto, California, November 1967.

18. M. L. Paquin. Testing of a Calorimeter-Equipped Planer Thermionic Converter, Thermionic Conversion Specialist Conference, Palo Alto, California, November 1967.

19. P. Rouklove. Thermionic Converter and Generator Tests. Thermionic Conversion Specialist Conference, Palo Alto, California, November 1967.

20. J. G. DeSteese and J. S. Holmgrem. A Radially Heated Radioisotope-Powered Thermionic Generator, Thermionic Conversion Specialist Conference, Palo Alto, California, November 1967.

21. S. S. Kitrilakis and F. Rujeh. The Output Characteristics of an Electroetched Rhenium Surface, Thermionic Conversion Specialist Conference, Houston, Texas, November 1966.

22. W. E. Horbough and R. W. Longsdereff. The Development of an Insulated Thermionic-Converter/Heat Pipe Assembly, Thermionic Specialist Conference, Houston, Texas, November 1966.

23. R. M. Williams and W. J. Befano. Electrical Performance of a Rhenium-Niobrium Cylindrical Thermionic Converter, NASA TN D-4533, April 1968.

24. F. A. Ross and T. F. Plunkett. Conceptual Design Analysis of a 5MWE Thermionic Reactor Space Propulsion Plant. Douglas Report SM-46275, February 1965.

25. T. Athanis, P. Brosens and L. Van Someren. Thermionic Converter Life and Failure Investigation. ASME Aviation and Space Conference, June 1968.

3.8.4 Subsection 3.1.4

1. C. Berger. Fuel Cells Incorporating Ion Exchange Membranes, Current State of Development. Presented before the American Chemical Society National Meeting, September 1963.

2. G. B. Stafford. Space Power Subsystem Capabilities. AIAA Paper No. 65-468, July 1965.

3. D. H. Archer, et al. Westinghouse Solid Electrolyte Fuel Cell. Presented before the American Chemical Society National Meeting, September 1963.

4. E. K. Bullock. New Generation Fuel Cell Power Systems for Space Applications. General Electric Company, Paper No. DECO-65-4.

5. D. H. Archer, et al. Cerolyte Fuel Cell, Report No. AFAPL-TR-66-14, March 1966.

6. Ionics Incorporated, Cambridge, Massachusetts, Bulletin FC-102, October 1963.

7. Preliminary Fuel Cell Data for Douglas Aircraft Lunar Landing Bug. Allis-Chalmers, Incorporated, July 1962.

8. General Discussions with Pratt and Whitney Aircraft Company, April 1966.

9. General Discussions with Allis-Chalmers Manufacturing Company, August 1963.

10. General Discussions with Allis-Chalmers Manufacturing Company, July 1966.

11. E. M. Cohn. Primary Hydrogen Oxygen Fuel Cells for Space. Presented at Propulsion and Energetics Panel, 29th Meeting, June 1967.

12. A Report on Fuel Cells. General Electric Company. November 1963.

13. Allis Chalmers Pushes Fuel Cell Efforts. Aviation Week and Space Technology. 23 January 1967.

14. Space Power Systems Advanced Technology Conference. Lewis Research Center, NASA SP-131. 23-24 August 1966.

15. G. C. Szego and J. Edward Taylor. Space Power System Engineering. Progression Astronautics and Aeronautics, Vol. 16.

16. Technological Requirements Common to Manned Planetary Missions. Appendix C. Subsystem Syntheses and Parametric Analyses, NAS2-3918, 1967 (P81).

17. Program Review Document, Space Power Systems and Electric Propulsion Programs. 24 January 1967 (1968 version if available).

3.8.5 Subsection 3.1.5

1. H. Munniks. Electrochimica Corp., Private Communication, 7 August 1967.

2. G. S. Hartmann. Exide Missile and Electronics Division, ESB Inc., Private Communication, 25 August 1967.

3. H. J. Schwartz, et al. Batteries and Fuel Cells. Space Power Systems Advanced Technology Conference, Cleveland, Ohio, (NASA-SP-131), August 1966.

4. Manned Mission Photovoltaic Study. Astro Electronics Division, RCA Report No. AED-R-3155, 9 June 1967.

5. H. N. Seigler. Sealed Cells and Auxiliary Electrodes. 1967 IECEC, August 1967.

6. R. Lutwack. The Heat Sterilizable Battery. 1967 IECEC, Miami Beach, Florida, August 1967.

7. R. Lutwack. Batteries and Space Power Systems. Spacecraft Sterilization Technology Conference, 16-18 November 1965.

8. Studies for the Cost Model of the Astrionics for Launch Vehicles. General Precision Aerospace Report No. C50299-011 (ETO 795), November 1964.

9. H. J. Mandell. Recent Developments in Secondary Batteries. 1966 IECEC, Los Angeles, California, August 1966.

10. G. B. Stafford. Space Power Subsystem Capabilities. AIAA Second Annual Meeting, San Francisco, California, Paper 65-468, July 1965.

11. A. Fleischer. Background Material for the Study of the National Space Power Program: Volume I, Batteries, Primary and Secondary. Interagency Advanced Power Group, November 1964.

12. J. J. Lander. Silver-Zinc Electrodes and Separator Research. Delco-Remy Division, General Motors - Report No. AFAPL-67-107, 31 August 1967.

13. H. D. Poshay. Aerospace Component Reliability Growth. Douglas Report No. DAC-59067, November 1966.

14. W. M. Goss. TRW Systems Inc., Private Communication, 24 June 1966.

15. W. G. Binckley. Power System Configuration Study and Reliability Analysis. Third Quarterly Progress Report, TRW Systems Inc., Report No. E-7441.2-005, April 1967.

16. R. C. Shair. Primary and Secondary Electrochemical Cells for Space Vehicle Power Supplies. Gulton Industries Inc., NASA N64-17997, October 1963.

17. F. C. Arrance and A. G. Ross. Flexible Inorganic Separators for High Rate Batteries. Douglas Report No. A5/TN-010/7, August 1967.

18. F. C. Arrance. Program to Develop an Inorganic Separator for a High Temperature Silver Zinc Battery. Douglas Astropower Laboratory Report No. SM-48461-F, June 1967.

19. C. Berger and F. Arrance. Cycling Characteristics of Ag-Zn Batteries in the Temperature Range 100-150°C. Douglas Astropower Laboratory Report No. SM-46212, May 1964.

20. T. Marces. Douglas Astropower Laboratory, Private Communication, July 1967.

21. W. Goss. TRW Systems, Inc., Private Communication, July 1966.

22. H. T. Francis. Space Batteries Technology Handbook NASA Report No. NASA SP-5004, 1964.

23. Hermetically Sealed Batteries for Space Applications Gulton Industries, Metuchen, New Jersey.

24. Spacecraft Electrical Power System Sizing and Analysis Computations Final Report, Space Technology Laboratories, Redondo Beach, California, Report No. STL 8584-604-RU000, 15 March 1964.

25. B. Lucas and M. Barr. Personal Communication, Eagle-Picher, 9 April 1964.

26. P. Frankel. Space Electric Power Systems Lockheed Report No. LR 17558, February 1964.

27. K. E. Preusse. Personal Communication and Correspondence, Gulton Industries, Metuchen, New Jersey, 11 March 1966.

28. P. J. Rappaport. Performance Ratings of Secondary Batteries Electronics, 19 February 1960.

29. N. D. Wheeler. Survey of Electrochemical Batteries General Electric Company, Electro-Technology, June 1963.

30. W. W. Clark, W. G. Ingling, I. F. Luke, and E. A. Roegers, Jr., Alkaline Battery Evaluation Cook Electric Company, Inland Test Laboratory, Technical Report No. AFAPL-TR-65-42, May 1965.

31. M. Barr. Personal Communication, Eagle-Picher, 17 March 1966 and 12 July 1966.

32. R. C. Shair, J. Liska, and G. Rampel, Silver Cadmium Batteries. Presented at the 18th Annual Power Sources Conference, Atlantic City, New Jersey, May 1964.

33. P. Broad. Personal Communication and Correspondence, Yardney Electric Corporation, New York, 25 March 1966.

34. K. Berger. F. C. Arrance and M. P. Strier, Personal Communication, Douglas Aircraft, Astropower Laboratories, Newport Beach, California, 9 March 1966 and 8 July 1966.

3.8.6 Subsection 3.1.6

1. A. Lowi. Solar Dynamic Power Systems Study--Evaluation. Aerospace Corporation Laboratory Operations Report No. SSD-TRD 63-115, Vol. II, September 1965.
2. P. Frankel. Study for an On-Board Power System for a Manned Orbital Space Station. Lockheed California Company, Burbank, California. Report No. LR 17228, Vols. I and II, November 1963.
3. Solar Brayton Research and Development Program. Garett–PHOENIX Report No. MS 757, October 1964.
4. H. O. Snyder, Jr., J. Munier, and J. E. McCormick. Space Power Conversion System Utilizing the Brayton Cycle and a Direct Coupled Nuclear Reactor. AIAA Report No. 64-454, July 1964.
5. D. T. Bernatowitz. NASA Solar Brayton Studies. NASA-Lewis Report No. TP13-63, September 1963.
6. G. G. McKhann. Preliminary Design of a Pu-238 Isotope Brayton Cycle Power System for MORL. Douglas Report No. SM-48836, Vol. IV, Book 2, September 1965.
7. Project Forecast, Power Generation Report, USAF, SCGF, 64.3, January 1964.
8. A. Pietsch. Reactor Powered Brayton Cycle for Large Space Stations. ASME, Advances in Energy Conversion Engineering, August 1967.
9. G. Stafford. Space Power Subsystem Capabilities. AIAA Paper No. 65-468, July 1965.
10. Secondary Power System Guide Part IV, Generalized B-21 Secondary Power Systems Computer Program for the Brayton Cycle, DAC-59107, June 1966.

3.8.7 Section 3.1.7

1. R. L. Wallerstedt and J. J. Owens. SNAP Mercury "Rankine Program." Conference proceedings, Intersociety Energy Conversion Engineering Conference, 26-28 September 1966, Page 121.
2. 100 kW System Analysis and Design. TRW Technical Memorandum TM-4130, 12 August 1965.
3. F. A. Ross, C. H. Shinbrot, and T. E. Plunkett. Reactor and Power Conversion Design Integration for Manned Earth Orbital Application Douglas Paper No. 4320, 13 August 1967.
4. SNAP-8 Performance Potential Study Final Report. NASA-Lewis Research Center, Contract NASw 1296 (Aerojet 3386), April 1967.
5. TRW Cost Data, Informal. 1966.
6. G. B. Stafford. Space Power Subsystem Capabilities. AIAA Paper No. 65-568, July 1965.

7. Solar Dynamic System Study for Manned Orbiting Space Station (MOSS) Application. TRW ER-5552-1962, Pages 5-3, 5-4.

8. Application of SNAP-2 to Manned Orbital Space Stations. Atomics International, AI-7950, December 1962.

9. R. A. Rackley and E. A. Mock. Potassium Rankine-Cycle Power Plants from 10 kW to 1000 kW. Conference Proceedings, Intersociety Energy Conversion Engineering Conference, 26-28 September 1966, Page 308.

10. G. S. Leighton, Personal Conversation, AEC Germantown, Md., 3 January 1968.

11. Handbook of Instructions for Missile and Space Vehicle Design, AFSCM 80-8; Space Vehicle, Volume II; Space Flight Vehicle Power, Part F. United States Air Force, 20 June 1967.

12. A. W. Adams, Personal Conversation, Sunstrand Aviation Corp., Rockford, Illinois, 22 January 1968.

13. Von Karman Center—Advanced Power System Dept., Verbal Presentation on ORACLE, Aerojet-General Corp. SNAP-8 Division.

14. A. W. Adams and R. E. Nigemann. Organic Rankine Cycle Technology Program--A Status Report, Sunstrand Corp., Aviation Division, Rockford, Ill., 5 January 1968.

15. G. Carver. Personal Contact, Aeroneutronics Aerothermal Laboratories, Ford-Philco Corp., Newport Beach, Calif., 4 January 1968.

16. Organic Rankine Cycle Power Generating Systems, Sunstrand Corp., Aviation Division, Rockford, Ill., B262(50), 5 April 1967.

17. Et al., Multi-Tube Boiler and Condensor Capsule Design Study Report, TRW, Cleveland, Ohio, AF-APL-TR-66-150, March 1967.

18. P. Engle. Trial Report--1.5 kW Solar Dynamic Space Power System, Sunstrand Aviation, Denver, Colo., DCRD-65: 20010, 26 August 1965.

19. G. S. Leighton. Organic Rankine Cycle Guide for Performance Elevation. Space Electric Power Office, U.S. Atomic Energy Commission, 5 December 1967.

20. S. D. Diamond. Preliminary Evaluation of Feher Cycle (Task 1.10), McDonnell Douglas Advanced Biotechnology and Power Dept., Santa Monica, Calif., November 1967.

21. A. E. King, J. B. Fanger, G. S. Leighton. "Electrical Component Technology for 0.25 to 10 Megawatt Space Power," presented at IECEC, 13-17 August 1968, Page 277.

22. R. E. English, et al., "Potassium Rankine Systems Technology," NASA SP-131, August 1966, Page 201.

23. M. A. Zipkin. "Components and System Design for a 400 kW Rankine Cycle Space Power System," presented to 1967 Intersociety Energy Conversion Engineering Conference, August 1967.

24. T. Moss, NASA Lewis Research Center, Personal Communication on Alkali-Metal Power Conversion, July 1968.

25. AiResearch Manufacturing Communication--Weight Breakdown for the Spur System, 1967.

26. State and Trends of Technology, Space, Air Force Aeropropulsion Laboratory, Wright-Patterson AFB Technical Memorandum APIT 68-1, January 1968.

27. M. A. Zipkin, Alkali-Metal, Rankine-Cycle Power Systems for Electric Propulsion, Journal of Spacecraft and Rockets, July 1967, page 852.

3.8.8 Section 3.1.8

1. "Bipropellant Pulsed Energy Turboalternator Power System Development" TRW Equipment, Laboratories, Final Report NASA Contract NAS9-4820, Flugart 1966.

2. State and Trends of Technology, Space, Air Force Aeropropulsion Laboratory, Wright-Patterson AFB Technical Memorandum, APIT 68-1, January 1968.

3. "Bipropellant Fueled Turboalternator Electric Power System," TRW Equipment Laboratories Document (unnumbered) 1967.

4. G. B. Stafford, "Space Power Subsystems Capabilities," AIAA Paper No. 65-568, July 1965.

5. "Pulse Turbine Study for Application to the Maneuverable Spacecraft Program," TRW Equipment Laboratories Brochure June 2, 1967.

6. D. F. Swenski, and J. R. May, Advanced Continuous Duty Power Supply for Space Vehicles, Progress in Astronautics and Aeronautics," Volume 16 (AIAA) 1966.

7. Space Planners Guide, United States Air Force, Air Force Systems Command, July 1965.

3.8.9 Subsection 3.2.2

1. L. Topper. High Temperature Radioisotope Capsule for Large Heat Source. Intersociety Energy Conversion Conference, August 1967.

2. H. S. Gay. Personal Communication, Sandia Corp.

3. Selection of Radioisotopes for Space Power Systems. NASA-TM-X-1212, Lewis Research Center, March 1966 (SRD).

4. Isotope Property Table. Prepared by USAEC Division of Isotope Development, March 1966.

5. C. A. Rohrmann. Radioisotope Heat Sources. HW-76323, October 1963; Revision, January 1967.

6. D. H. Stoddard. Radiation Properties of 244 Cm Produced for Isotope Power Generators. DP-939, November 1964.

7. H. L. Davis. Isotope Cost and Availability. Nucleonics, March 1963.

8. F. D. King and Angerman. Large Scale Co-60 Heat Sources. DP-1066 Vol. II, 1966.

9. Radioisotope Applications in Hydrospace. AGN-8163, February 1966.

10. Systems for Nuclear Power--An Evaluation. USAEC, January 1964.

11. A. J. Streb. Radioisotope Power Systems for Manned Space Stations. AIAA Paper, September 1964.

12. Properties of Radioisotope Heat Sources. Final Report under Contract NAS5-9556, Cook Electric Company, August 1965.

13. E. E. Fowler. AEC Authorizing Legislation Fiscal Year 1966, Part 1, Director of Division of Isotope Development.

14. Savannah River Quarterly Report, DP-1105-1.

15. Power Subsystem State-of-Art and Projection Report. SM-52024, July 1966.

3.8.10 Subsection 3.2.3

1. H. M. Dieckamp, et al. SNAPSHOP, The First Space Test of a Reactor Power Unit. Presented at the XVI International Astronautical Congress Athens, Greece, September 1965.

2. Report on the Design Requirements for Reactor Power Systems for Manned Earth Orbital Applications. Douglas Report No. DAC-59213, May 1966.

3. J. V. Coggi. Weight and Reliability Analysis of a 5 MWe Nuclear Thermionic Space Power System. Douglas Report No. DAC-60789, October 1967.

4. A. U. Buatti, et al. Design Study of a High Power In-Pile Nuclear Thermionic Space Powerplant. NASA CR-54172, July 1964.

5. C. E. Johnson and D. G. Mason. SNAP-8 Reactor and Shield Designs and Operating Experience. AIAA Second Annual Meeting and Technical Demonstration, July 1965.

6. J. W. Larson. Research on Spacecraft and Power Plant Integration Problems. NASA CR-54159, October 1964.

7. E. D. Arnold. Handbook of Shielding Requirements and Radiation Characteristics of Isotopic Power Sources for Terrestrial Marine and Space Applications. ORNL-3576, April 1964.

3.8.11 Subsection 3.2.4

1. Charles H. Castle, and Edward S. Kavalcik, "Development Status of Aluminum Solar Concentrators," Progress in Astronautics and Aeronautics--Volume 16, p 821, Academic Press, 1966.

2. Arnold D. Turring, and Alfred Blav, Solar Dynamic Power Systems from 3 to 100 kW Progress in Astronautics and Aeronautics, Volume 16, p. 703, Academic Press, 1966.

3. Warner L. Stewart, et al., "Brayton Cycle Technology," Space Power Systems Advanced Technology Conference, NASA SP-131, August 1966, p. 110.

4. Gene B. Stafford, "Space Power System Capabilities, AIAA Paper No. 65-468, July 1965.

5. Atwood R. Heath, Jr., and Edward L. Hoffman. "NASA Solar Concentrator Development," Space Power Systems Engineering, Academic Press Inc., N. Y., 1966.

6. A. Lowi, "Solar Dynamic Power System Study," Aerospace Corporation, 1965.

7. Solar Dynamic System Study for Manned Orbiting Space Station (MOSS) Application, TRW Report ER-555-2.

8. Power Subsystems State of the Art and Projection Report, SM-52024, July 1966.

3.8.12 Subsection 3.2.5

1. HIMSD AFSCM 80-8, USAF Handbook of Instructions for Missile and Space Vehicle Design, Volume II--Space Vehicles, December 1966.

2. Analytical Methods for Space Vehicle Atmospheric Control Processes. Report No. ASD-TR-61-162--Part II, November 1962.

3. R. B. Stewart, I. G. Hart, and R. D. McCarty. Interim Thermodynamic Properties for Gaseous and Liquid Oxygen at Temperatures from 55°K to 300°K and Pressures to 300 Atmosphere, N. B. S. Report 7922, 1 October 1963.

3.8.13 Subsection 3.3

1. S. Lieblein and J. H. Diedrich. Material and Geometry Aspects of Space Radiators. NASA TMS-52153, November 1965.

2. J. Madsen, P. P. King, and R. P. Johnston. Experimental Evaluation of Expanded Pyrolytic Graphite for use in Space Radiators. Technical Report AFAPL-TR-67-54, May 1967.

3. Mission Engineering Study of Electrically Propelled Manned Planetary Vehicles. NASA Contract NAS8-20372, ANSO Document No. 6300-216, July 1967.

4. J. V. Coggi. Design Analysis of Segmented Space Radiators. Douglas Report No. DAC-60549, February 1967.

5. Parametric Studies Report Advanced Nuclear Electric Power Generator System Study, PWA 22, June 1963.

6. Research on Spacecraft and Powerplant Integration Problems. GE63SD886, 1963.

7. R. D. Codsfield and R. E. Killen. Comparison of Direct Condensing and Indirect Radiators for Nuclear Rankine Systems. NASA-LR-72318, July 1967.

8. J. V. Coggi and J. Madsen. Evaluation of Expanded Pyrolytic Graphite Radiators for Nuclear Space Power Systems. Douglas Paper 4897, August 1968.

9. Report on the Design Requirements for Reactor Power System for Manned Orbital Operation. Douglas Report No. DAC-59214, May 1966.

3.8.14 Section 3.4

1. W. G. Binckley. Third Quarterly Progress Report, JPL Contract No. 951574. Power System Configuration Study and Reliability Analysis. TRW Systems Report No. E-7441.2-005, 7 January through 6 April 1967.

2. Power Subsystems State of the Art and Projection Report, Douglas Aircraft Co., McDonnell Douglas Corp., SM-52024, July 1966.

3. P. Ramierez, and D. Tollefson. The Application of Modular Concepts for Electric Propulsion Power Conditioning. AIAA Paper No. 66-501, June 1966.

4. AD 460816 Missions and Power Subsystems Studies, Third Quarterly Report (January 1965 to April 1965), Contract AF 33(615)-1604, General Electric Company.

5. W. E. Murray, and R. B. Caldwell. Electrical Power Control Conditioning Subsystems for the Manned Orbital Research Laboratory (MORL), DP 3861, IEEE-6-AES Paper A-43, July 1966.

6. D. Eardes, and M. Eddins. Reliability Engineering Data Series Failure Rates, Avco Corp., Wilmington, Mass., April 1, 1962.

7. Reliability Aspects of Spacecraft Secondary Power Systems, McDonnell Douglas Corp. Report No. DAC 60584, March 15, 1967.

3.8.15 Subsection 3.7.1

1. Space Planners Guide. USAF, Air Force Systems Command, 1 July 1965.

2. Photovoltaic Power Systems On Flight Spacecraft - Nimbus 2. National Aeronautics and Space Administration Contract NAS7-547, Document No. 685D4222, 23 February 1968.

3. PIC Report No. 757 Power Supply for Gemini, January 1967.

4. Preliminary Design of a Pu-238 Isotope Brayton Cycle Power System for MORL; Volume III. Douglas Report No. SM-48834, September 1965.

5. Technical Discussions held with AEC. Aerojet-General Corporation and Sundstrand Aviation Companies, 1967-1968.

6. Baseline Evaluation Review. JPL Contract No. NAS7-100, Large Area Solar Array Design Program, 20 December 1966.